

David G. Lambert
Richard D. Rainbow *Editors*

Calcium Signaling Protocols

Third Edition

METHODS IN MOLECULAR BIOLOGY™

Series Editor

John M. Walker

School of Life Sciences

University of Hertfordshire

Hatfield, Hertfordshire, AL10 9AB, UK

For further volumes:
<http://www.springer.com/series/7651>

Calcium Signaling Protocols

Third Edition

Edited by

David G. Lambert

*Department of Cardiovascular Sciences, Division of Anaesthesia,
Critical Care, and Pain Management, Leicester Royal Infirmary, University of Leicester, Leicester, UK*

Richard D. Rainbow

Department of Cardiovascular Sciences, Leicester Royal Infirmary, University of Leicester, Leicester, UK



Editors

David G. Lambert

Department of Cardiovascular Sciences
Division of Anaesthesia, Critical Care,
and Pain Management
Leicester Royal Infirmary
University of Leicester
Leicester, UK

Richard D. Rainbow

Department of Cardiovascular Sciences
Leicester Royal Infirmary
University of Leicester
Leicester, UK

ISSN 1064-3745

ISSN 1940-6029 (electronic)

ISBN 978-1-62703-085-4

ISBN 978-1-62703-086-1 (eBook)

DOI 10.1007/978-1-62703-086-1

Springer New York Heidelberg Dordrecht London

Library of Congress Control Number: 2012946739

© Springer Science+Business Media, LLC 2013

This work is subject to copyright. All rights are reserved by the Publisher, whether the whole or part of the material is concerned, specifically the rights of translation, reprinting, reuse of illustrations, recitation, broadcasting, reproduction on microfilms or in any other physical way, and transmission or information storage and retrieval, electronic adaptation, computer software, or by similar or dissimilar methodology now known or hereafter developed. Exempted from this legal reservation are brief excerpts in connection with reviews or scholarly analysis or material supplied specifically for the purpose of being entered and executed on a computer system, for exclusive use by the purchaser of the work. Duplication of this publication or parts thereof is permitted only under the provisions of the Copyright Law of the Publisher's location, in its current version, and permission for use must always be obtained from Springer. Permissions for use may be obtained through RightsLink at the Copyright Clearance Center. Violations are liable to prosecution under the respective Copyright Law.

The use of general descriptive names, registered names, trademarks, service marks, etc. in this publication does not imply, even in the absence of a specific statement, that such names are exempt from the relevant protective laws and regulations and therefore free for general use.

While the advice and information in this book are believed to be true and accurate at the date of publication, neither the authors nor the editors nor the publisher can accept any legal responsibility for any errors or omissions that may be made. The publisher makes no warranty, express or implied, with respect to the material contained herein.

Printed on acid-free paper

Humana Press is a brand of Springer

Springer is part of Springer Science+Business Media (www.springer.com)

Preface

In the first and second editions of this volume, a simple observation was made that “the regulation of intracellular Ca^{2+} is a common theme presented in many papers over the last 20 years.” This statement is equally true as a preface for the third edition. Indeed, a crude PubMed search of “calcium AND signaling” starting in 1985 with the seminal paper of Grynkiewicz and colleagues yields >60,000 hits.

The third edition has seen some reorganization; starting with a new editor, Richard Rainbow, and encompasses some of the exciting new molecular techniques that have both enabled new studies of intracellular Ca^{2+} regulation and provided much new information on processes. The third volume is in five parts and comprises 21 chapters; 9 are completely new and the remainder have, in the main, undergone major revision/updating. The five parts are as follows: (1) Theoretical and very simple suspension-based fluorimetric assay, (2) Specialist measurement systems, (3) Measurement of channel activity, (4) Measurement of store release, and the final main section, (5) Specialist measurement techniques which include targeted probes, using G-protein chimeras to force Ca^{2+} signalling for screening, and genetically encoded sensors. Some of the chapters that were left out of this volume can be easily accessed and used to inform rather more basic investigations.

Again compilation of a multiauthor book like this is quite time-consuming, and we are grateful to our authors for their continued patience when things seemed to slow or even stop. Your chapters were in a safe place, and now they can be read. We also acknowledge the help of Professor John M. Walker (series Editor) and David Casey at Springer for keeping us in line.

We would simply end this preface in the same way as for the first and second editions by saying that we hope the third edition will be useful for those contemplating moving into studies of intracellular Ca^{2+} . We hope that you can be tempted to have a try with new technologies and equipment and that you find experimental enquiry in this area as stimulating as we have and still do.

Leicester, UK

*David G. Lambert
Richard D. Rainbow*

Contents

Preface	v
Contributors	ix

PART I GENERAL

1 Fluorescent Measurement of $[Ca^{2+}]_c$: Basic Practical Considerations	3
<i>Alec W.M. Simpson</i>	
2 Measurement of $[Ca^{2+}]_i$ in Whole Cell Suspensions Using Fura-2	37
<i>Anish Patel, Robert A. Hirst, Charlotte Harrison, Kazuyoshi Hirota, and David G. Lambert</i>	

PART II SPECIALIST MEASUREMENT SYSTEMS

3 Confocal Microscopy: Theory and Applications for Cellular Signaling	51
<i>Stephen C. Tovey, Paul J. Brighton, Edward T.W. Bampton, Yan Huang, and Gary B. Willars</i>	
4 Ratiometric Ca^{2+} Measurements Using the FlexStation [®] Scanning Fluorometer	95
<i>Ian C.B. Marshall, Izzy Boyfield, and Shaun McNulty</i>	
5 Measuring Ca^{2+} Changes in Multiwell Format Using the Fluorometric Imaging Plate Reader (FLIPR [®])	103
<i>Ian C.B. Marshall, Davina E. Owen, and Shaun McNulty</i>	
6 Ratiometric $[Ca^{2+}]_i$ Measurements in Adherent Cell-Lines Using the NOVOSTAR Microplate Reader	111
<i>Benjamin D. Hunt and David G. Lambert</i>	

PART III MEASUREMENT OF Ca^{2+} CHANNEL ACTIVITY

7 Whole-Cell Patch-Clamp Recording of Voltage-Sensitive Ca^{2+} Channel Currents in Single Cells: Heterologous Expression Systems and Neurones	123
<i>Jon Brown, Atticus H. Hainsworth, Alessandro Stefani, and Andrew D. Randall</i>	
8 Combined Calcium Fluorescence Recording with Ionic Currents in Contractile Cells	149
<i>Richard D. Rainbow</i>	

PART IV MEASUREMENT OF $\text{Ins}(1,4,5)\text{P}_3$ AND Ca^{2+} RELEASE
FORM INTRACELLULAR STORES

- | | | |
|----|--|-----|
| 9 | Measurement of Phospholipase C by Monitoring Inositol Phosphates
Using [^3H]Inositol Labeling Protocols in Permeabilized Cells | 163 |
| | <i>Alison Skippen, Philip Swigart, and Shamshad Cockcroft</i> | |
| 10 | Single-Cell Imaging Techniques for the Real-Time Detection
of IP_3 in Live Cells | 175 |
| | <i>Carl P. Nelson</i> | |
| 11 | Measurement of Inositol(1,4,5)Trisphosphate Using a Stereospecific
Radioreceptor Mass Assay | 193 |
| | <i>Darren Smart</i> | |

PART V SPECIALIST MEASUREMENT TECHNIQUES

- | | | |
|----|---|-----|
| 12 | Measurement of $[\text{Ca}^{2+}]_i$ in Smooth Muscle Strips Using
Front-Surface Fluorimetry | 207 |
| | <i>Hideo Kanaide and Katsuya Hirano</i> | |
| 13 | Calcium Measurements from Whole Heart Using Rhod-2 | 217 |
| | <i>Bum-Rak Choi</i> | |
| 14 | Measurement of Changes in Endothelial and Smooth Muscle Ca^{2+}
in Pressurized Arteries | 229 |
| | <i>Kim A. Dora and Michael A. Hill</i> | |
| 15 | Single Cell and Subcellular Measurements of Intracellular Ca^{2+}
Concentration | 239 |
| | <i>John G. McCarron, Marnie L. Olson, Susan Chalmers,
and John M. Girkin</i> | |
| 16 | Simultaneous Analysis of Intracellular pH and Ca^{2+}
from Cell Populations | 253 |
| | <i>Raul Martinez-Zaguilan, Linda S. Tompkins,
Robert J. Gillies, and Ronald M. Lynch</i> | |
| 17 | Measurements of Ca^{2+} Concentration with Recombinant Targeted
Luminescent Probes | 273 |
| | <i>Denis Ottolini, Tito Calì, and Marisa Brini</i> | |
| 18 | Chimeric G Proteins in Fluorimetric Calcium Assays:
Experience with Opioid Receptors | 293 |
| | <i>Valeria Camarda and Girolamo Calo'</i> | |
| 19 | Compartmentalizing Genetically Encoded Calcium Sensors | 307 |
| | <i>David A. Williams, Mastura Monif, and Kate L. Richardson</i> | |
| 20 | Measurement of Cytosolic-Free Ca^{2+} in Plant Tissue | 327 |
| | <i>Martin R. McAinsh and Carl K.-Y. Ng</i> | |
| 21 | Measurement of Ca^{2+} -ATPase Activity (in PMCA and SERCA1) | 343 |
| | <i>Danuta Kosk-Kosicka</i> | |
| | <i>Index</i> | 357 |

Contributors

EDWARD T.W. BAMPTON • *MRC Toxicology Unit, University of Leicester, Leicester, UK*

IZZY BOYFIELD • *Neurology & GI Centre of Excellence for Drug Discovery,
GlaxoSmithKline Research and Development Limited, Harlow, Essex, UK*

PAUL J. BRIGHTON • *Division of Reproductive Health, University of Warwick,
Coventry, UK*

MARISA BRINI • *Department of Comparative Biomedicine and Food Science,
Biomedical Sciences University of Padova, Padova, Italy*

JON BROWN • *School of Physiology and Pharmacology, University of Bristol, Bristol, UK*

TITO CALI • *Department of Comparative Biomedicine and Food Science,
University of Padova, Padova, Italy*

GIROLAMO CALO' • *Department of Experimental and Clinical Medicine,
Section of Pharmacology, University of Ferrara, Ferrara, Italy*

VALERIA CAMARDA • *Department of Experimental and Clinical Medicine,
Section of Pharmacology, University of Ferrara, Ferrara, Italy*

SUSAN CHALMERS • *Strathclyde Institute of Pharmacy & Biomedical Sciences,
Strathclyde University, Glasgow, UK*

BUM-RAK CHOI • *Cardiovascular Research Center, Rhode Island Hospital
and Brown Medical School, Providence, RI, USA*

SHAMSHAD COCKCROFT • *Department of Neuroscience, Physiology, and Pharmacology,
University College London, London, UK*

KIM A. DORA • *Department of Pharmacology, University of Oxford, Oxford, UK*

ROBERT J. GILLIES • *Departments of Physiology and Biochemistry,
Texas Tech University Health Sciences Center, Lubbock, TX, USA*

JOHN M. GIRKIN • *Department of Physics, Biophysical Sciences Institute,
Durham University, Durham, UK*

CHARLOTTE HARRISON • *Department of Cardiovascular Sciences, Division of Anaesthesia,
Critical Care, and Pain Management, Leicester Royal Infirmary, University of Leicester,
Leicester, UK*

ATTICUS H. HAINSWORTH • *School of Physiology and Pharmacology, University of Bristol,
Bristol, UK*

MICHAEL A. HILL • *Dalton Cardiovascular Research Centre and Department
of Medical Pharmacology and Physiology, University of Missouri,
Columbia, Missouri, USA*

KATSUYA HIRANO • *Division of Molecular Cardiology, Research Institute
of Angiocardiology, Graduate School of Medical Sciences, Kyushu University,
Fukuoka, Japan*

KAZUYOSHI HIROTA • *Department of Cardiovascular Sciences, Division of Anaesthesia,
Critical Care, and Pain Management, Leicester Royal Infirmary, University of Leicester,
Leicester, UK*

ROBERT A. HIRST • *Department of Cardiovascular Sciences, Division of Anaesthesia,
Critical Care, and Pain Management, Leicester Royal Infirmary, University of Leicester,
Leicester, UK*

- YAN HUANG • *Department of Cell Physiology and Pharmacology, University of Leicester, Leicester, UK*
- BENJAMIN D. HUNT • *Department of Cardiovascular Sciences, Division of Anaesthesia, Critical Care, and Pain Management, Leicester Royal Infirmary, University of Leicester, Leicester, UK*
- HIDEO KANAIDE • *International University of Health and Welfare, Fukuoka, Japan; Division of Molecular Cardiology, Research Institute of Angiocardiology, Graduate School of Medical Sciences, Kyushu University, Fukuoka, Japan*
- DANUTA KOSK-KOSICKA • *Department of Cardiovascular Sciences, Clinical Division of Anaesthesia Critical, Care and Pain Management, University Hospitals of Leicester NHS Trust, Leicester, Leicestershire, UK*
- DAVID G. LAMBERT • *Department of Cardiovascular Sciences, Division of Anaesthesia, Critical Care, and Pain Management, Leicester Royal Infirmary, University of Leicester, Leicester, UK*
- RONALD M. LYNCH • *Department of Physiology, Texas Tech University Health Sciences Center, Lubbock, TX, USA*
- IAN C.B. MARSHALL • *Neurology & GI Centre of Excellence for Drug Discovery, GlaxoSmithKline Research and Development Limited, Harlow, Essex, UK*
- RAUL MARTINEZ-ZAGUILAN • *Department of Physiology, Texas Tech University Health Sciences Center, Lubbock, TX, USA*
- MARTIN R. MCAINSH • *Lancaster Environment Centre, Lancaster University, Lancaster, UK*
- JOHN G. McCARRON • *Strathclyde Institute of Pharmacy & Biomedical Sciences, Strathclyde University, Glasgow, UK*
- SHAUN McNULTY • *Neurology & GI Centre of Excellence for Drug Discovery, GlaxoSmithKline Research and Development Limited, Harlow, Essex, UK*
- MASTURA MONIF • *Department of Physiology, The University of Melbourne, Melbourne, VIC, Australia*
- CARL P. NELSON • *Department of Cardiovascular Sciences, Division of Anaesthesia, Critical Care, and Pain Management, Leicester Royal Infirmary, University of Leicester, Leicester, UK*
- CARL K.-Y. NG • *School of Biology and Environmental Science, University College Dublin, Dublin, Ireland*
- MARNIE L. OLSON • *Strathclyde Institute of Pharmacy & Biomedical Sciences, Strathclyde University, Glasgow, UK*
- DENIS OTTOLINI • *Department of Biomedical Sciences, University of Padova, Padova, Italy*
- DAVINA E. OWEN • *Neurology & GI Centre of Excellence for Drug Discovery, GlaxoSmithKline Research and Development Limited, Harlow, Essex, UK*
- ANISH PATEL • *Department of Cardiovascular Sciences, Division of Anaesthesia, Critical Care, and Pain Management, Leicester Royal Infirmary, University of Leicester, Leicester, UK*
- RICHARD D. RAINBOW • *Department of Cardiovascular Sciences, Leicester Royal Infirmary, University of Leicester, Leicester, UK*
- ANDREW D. RANDALL • *School of Physiology and Pharmacology, University of Bristol, Bristol, UK*
- KATE L. RICHARDSON • *Department of Physiology, The University of Melbourne, Melbourne, VIC, Australia*

- ALEC W.M. SIMPSON • *Department of Cell and Molecular Physiology,
Institute of Translational Medicine, University of Liverpool, Liverpool, UK*
- ALISON SKIPPER • *Department of Neuroscience, Physiology, and Pharmacology,
University College London, London, UK*
- DARREN SMART • *Neurology CEDD, GlaxoSmithKline Pharmaceuticals Ltd., Harlow,
Essex, UK*
- ALESSANDRO STEFANI • *School of Physiology and Pharmacology, University of Bristol,
Bristol, UK*
- PHILIP SWIGART • *Department of Neuroscience, Physiology, and Pharmacology,
University College London, London, UK*
- LINDA S. TOMPKINS • *Department of Physiology, Texas Tech University
Health Sciences Center, Lubbock, TX, USA*
- STEPHEN C. TOVEY • *Department of Pharmacology, University of Cambridge,
Cambridge, UK*
- GARY B. WILLARS • *Department of Cardiovascular Sciences, Division of Anaesthesia,
Critical Care, and Pain Management, Leicester Royal Infirmary, University of Leicester,
Leicester, UK*
- DAVID A. WILLIAMS • *Department of Physiology, The University of Melbourne, Melbourne,
VIC, Australia*

Part I

General

Chapter 1

Fluorescent Measurement of $[Ca^{2+}]_c$: Basic Practical Considerations

Alec W.M. Simpson

Abstract

There is a vast array of dyes currently available for measurement of cytosolic calcium. These encompass single and dual excitation and single and dual emission probes. The choice of particular probe depends on the experimental question and the type of equipment to be used. It is therefore extremely difficult to define a universal approach that will suit all potential investigators. Preparations under investigation are loaded with the selected organic indicator dye by incubation with ester derivatives, by micropipet injection or reverse permeabilization. Indicators can also be targeted to a range of intracellular organelles. Calibration of a fluorescent signal into Ca^{2+} concentration is in theory relatively simple but the investigator needs to take great care in this process. This chapter describes the theory of these processes and some of the pitfalls users should be aware of. Precise experimental details can be found in the subsequent chapters of this volume.

Key words: Fluorescence measurement, Ca^{2+} , Dye loading, Calibration

1. Introduction

It is extremely difficult to write a prescriptive account of how to measure cytosolic free Ca^{2+} ($[Ca^{2+}]_c$) that will suit all potential investigators. The problem arises because of the wide diversity of fluorescent Ca^{2+} indicators that are now available, the variety of cells to be investigated, and the range of detection equipment that can be used. Consequently, this chapter is designed to provide the user with an overview of the technology in order that he or she can move towards developing a protocol that will suit the experimental objectives, cells, and equipment available to the investigator.

The main approaches to measuring $[Ca^{2+}]_c$ before the synthesis of fluorescent Ca^{2+} indicators involved using the Ca^{2+} -activated photoprotein aequorin, Ca^{2+} -selective microelectrodes, or absorbance

indicators (1). The use of aequorin and microelectrodes was generally restricted to large cells (usually from invertebrates) that were easy to handle and manipulate with micropipets. With a few notable exceptions (e.g., injection of hepatocytes and myocytes with aequorin by Cobbold and colleagues (2, 3)), these approaches were not applied to the wide diversity of cells present in mammalian tissues. The use of absorbance dyes did not become widespread since they are not very sensitive to the typical $[Ca^{2+}]_c$ found in cells, and did not offer any real potential for investigating $[Ca^{2+}]_c$ in monolayers or single cells.

The synthesis of quin2 by Tsien (4, 5) in the early 1980s heralded a new era in the measurement of Ca^{2+} by making available fluorescent probes that could be readily introduced into living cells. The most commonly used fluorescent Ca^{2+} indicator has been fura-2, which, along with indo-1, formed the first generation of ratiometric indicators also designed by Tsien and colleagues (6). Subsequently, the fluo-based indicators have been widely used because of their high fluorescence, favorable K_d s, and suitability for 488 laser line excitation.

The Ca^{2+} -binding properties of these indicators are formed by the presence of a tetracarboxylic acid core as found in the Ca^{2+} -chelator EGTA. The original Ca^{2+} indicator quin2 and its successors were designed around an EGTA derivative, BAPTA, also synthesized by Tsien (7). For a compound to act as an intracellular Ca^{2+} indicator, selectivity of the indicator for Ca^{2+} over other physiologically important ions is essential. EGTA already showed a much greater selectivity for Ca^{2+} over Mg^{2+} , Na^+ , and K^+ , but unfortunately, its Ca^{2+} binding is very pH sensitive. Cells undergo physiological changes in pH (8), which in the case of an EGTA-like chelator would affect the reported $[Ca^{2+}]$. Calibrating a pH-sensitive Ca^{2+} indicator is difficult, since small changes in pH of the calibration solutions affect the measured fluorescence and the K_d for Ca^{2+} . The synthesis of BAPTA, a largely pH-insensitive Ca^{2+} chelator, was therefore an important step in the development of fluorescent probes for measuring $[Ca^{2+}]_c$ (7).

Since the introduction of quin2, fura-2, and indo-1, numerous other fluorescent Ca^{2+} indicators have been synthesized, each with varying fluorescence characteristics and K_d s for Ca^{2+} (see ref. 9; Tables 1, 2, and 3). The fundamental properties of these indicators are similar in that the binding of Ca^{2+} produces a wavelength shift in either the excitation or emission fluorescence spectra (6, 9). When there is little or no shift in the excitation spectra, a Ca^{2+} -dependent change in the emission intensity is used to report changes in Ca^{2+} (5, 9). This can arise from Ca^{2+} -dependent changes in the intensity of absorbance or quantum efficiency.

In terms of fluorescence properties, the indicators can be divided into two main groups, those that are excited by near-ultraviolet (UV) wavelengths 330–380 nm (e.g., quin2, fura-2,

Table 1
Single-excitation wavelength indicators

Indicator	Source	UV/V	K _d nM (or μM where indicated)	AM loading	Absorbance -Ca ²⁺ + Ca ²⁺	Emission -Ca ²⁺ + Ca ²⁺	Comments
quin2	MP/TL	UV	60 ^a (115) ^b	✓	352	332	498 High intracellular buffering
Methoxyquin2MF	MP	UV	65 ^a	✓	352	332	498 Methoxyquin2MF ¹⁹ for NMR
Asante Calcium Green	TL	V	135 ^c	✓	517	517	540
Oregon Green 488 BAPTA-1	MP	V	170 ^a	✓	494	494	523 Designed for argon-ion lasers. Used for multiphoton. Dextran conjugate available
Calcium Orange TM	MP	V	185 ^a (380) ^d	✓	549	549	576 See ref. (13)
Calcium Crimson TM	MP	V	185 ^a (221) ^d	✓	590	589	615 See ref. (13)
Calcium Green-1 ^a	MP	V	190 ^a (221) ^d	✓	503	506	534 See ref. (13), Fluorescence lifetime measurements and multiphoton applications. Brighter than fluo-3. Dextran conjugates available
Fluo-2 HighAff ^e	TL	V	235 ^c	✓	490	490	515
Calcium GreenC ₁₈	MP/TL	V	280 ^a (62) ^f	✗	509	509	530 Near-membrane Ca ²⁺ indicator, K _d affected by lipids, ref. (60)
Fluo-4	MP	V	345 ^a	✓	491	494	516 Absorbance peak is close to 488 nm argon-ion laser line. Highly suited to applications using argon-ion lasers. AM ester and Ca ²⁺ -free forms are only weakly fluorescent. Large increase in fluorescence on Ca ²⁺ -binding. Dextran conjugates available

(continued)

Table 1
(continued)

Indicator	Source	UV/V	K _d nM (or μM where indicated)	AM loading	Absorbance -Ca ²⁺ + Ca ²⁺	Emission -Ca ²⁺ + Ca ²⁺	Comments
Asante Calcium NearIR	TL	V	350 ^c	✓	635	635	690
Fluo-3	MP/TL	V	390 ^a	✓	506	506	526
Fluo-2 MedAff ^e	TL	V	400 ^c	✓	490	490	515
Asante Calcium Red	TL	V	400 ^c	✓	Ex 540	650	650
KJM-1	TL	V	500 ^g	✓	560	560	Em 640
Calcium Green-2 TM	MP	V	550 ^a	✓	503	503	536
Rhod-2	MP/TL	V	570 ^a	✓	549	552	571
Oregon Green 488 BAPTA-2	MP	V	580 ^a	✓	494	494	523
X-rhod-1	MP	V	700 ^a	✓	576	580	602
X-rhod-5F	MP	V	1.6 μM	✓	c576	c580	602
Oregon Green 488 BAPTA-6F	MP	V	3 μM	✓	494	494	523

Fluo-5F	MP	V	2.3 μM	✓	491	494	518	518
Magnesium Green ^a	MP	V	6 μM	✓	506	506	531	K_d determined in 0-Mg ²⁺ , indicator will be Mg ²⁺ sensitive
Fluo-4FF	MP	V	9.7 μM ^a	✓	491	494	516	516
Calcium Green-5N ^a	MP	V	14 μM ^a	✓	506	506	532	532
X-rhod-FF	MP	V	17 μM ^a	✓	576	578	602	
Rhod-FF	MP	V	19 μM ^a	✓	548	552	577	Weakly fluorescent in Ca ²⁺ free. Designed to locate in mitochondria
Calcium Orange-5N ^a	MP	V	20 μM	✓	549	549	582	Exhibits fast kinetics suitable for millisecond time resolution. Reference (125). Product discontinued
Orange Green 488	MP	V	20 μM ^a	✓	494	494	521	Designed for Argon-ion lasers
BAPTA-5N								
Fluo-5N	MP	V	90 μM ^a	✓	491	493		
Rhod-5N	MP	V	320 μM ^a	✓	549	551	577	Weakly fluorescent in Ca ²⁺ free

MP produced by Molecular Probes/Invitrogen-Life Technologies Inc., *TL* produced by Teqlabs, *MP/TL* produced by Molecular Probes/Invitrogen-Life Technologies Inc. and Teqlabs Molecular Probes is now a brand of Life Technologies Inc.

^a K_d determined in 100 mM KCl, pH 7.2 at 22°C

^b K_d determined in 100 mM KCl, pH 7.05 at 37°C
^cConditions for K_d determination not defined

^dValues taken from ref. (13)

^eTeqlabs produce LeakRes, NearMem, HighAff, Med Aff, and LowAff variants of many of their probes
^f K_d reported to be 2.30 nM at 0.1 M ionic strength, pH 7.2 at 22°C and 62 nM in the presence of phospholipid vesicles. Reference (60)
^g K_d determined at pH 7.2 and 22°C

Table 2
Dual-excitation indicators

Indicator	Source	UV/V	K_d nM (or μ M where indicated)	AM loading	Absorbance -Ca ²⁺ + Ca ²⁺	Emission -Ca ²⁺ + Ca ²⁺	Comments
Fura Red	MP	V	140	✓	472	436	637
Fura-2	MP/TL	UV	145 ^a (224) ^b	✓	363	335	512
Fura-C ₁₈	MP	UV	150 ^a	✗	365	338	501
Fura-2 LeakRes ^c (Fura PE3)	TL	UV	269 ^d	✓	364	335	502
Bis-fura	MP	UV	370 ^a (250 ^e)	✓	364	335	508
Fura-2 NearMem ^c (FFP-18)	TL	UV	400	✓	364	335	502
Fura-5F	MP	UV	400	✓	363	336	512
Fura-4F	MP	UV	770	✓	366	336	511
							Low quantum yield. Used in combination with single-excitation indicators to obtain ratio values
							Lipophilic near-membrane Ca ²⁺ indicator. K_d may be affected by membrane environment
							Leakage-resistant indicator. Formerly Fura-PE3
							Is brighter and has lower affinity than fura-2. Not available as cell-permeant ester
							Lipophilic near-membrane Ca ²⁺ indicator. K_d affected by membrane environment. Formerly FFP-18

Fura-6F	MP	UV	5.3 μM ^a	✓	364	336	512	505
Fura-FF	MP	UV	5.5 μM ^a	✓	364	335	510	506
BTC	MP	V	7 μM ^a	✓	464	401	533	529
MagFura-2 (FuraProta)	MP	UV	25 μM ^a	✓	369	329	511	508
Magfura-5	MP	UV	28 μM ^a	✓	369	330	505	500
Fura-2 Lowaff ^c (Fura-2FF)	TL	UV	25 μM ^d	✓	364	335	512	505
Fura-FF-C ₁₈	MP	UV	—	✗	337	366	504	495
<hr/>								

MP produced by Molecular Probes/Invitrogen-Life Technologies Inc., TL produced by Teflabs, MP/TL produced by Molecular Probes/Invitrogen-Life Technologies Inc. and Teflabs

Molecular Probes is now a brand of Life Technologies Inc.

^aK_d determined in 100 mM KCl, pH 7.2 at 22°C

^bK_d determined in 100 mM KCl, pH 7.05 at 37°C

^cTeflabs produce LeakRes, NearMem, HighAff, Med Aff, and LowAff variants of many of their probes

^dConditions for K_d determination not defined

^eConditions the same as footnote 'a' except with 1 mM Mg²⁺ present

Table 3
Dual-emission ratiometric indicators

Indicator	Source	UV/V	K_d nM (or μM where indicated)	AM loading	Absorbance -Ca ²⁺ + Ca ²⁺	Emission -Ca ²⁺ + Ca ²⁺	Comments
Indo-1	MP/TL	UV	230 ^a (250 ^b)	✓	346	330	475 401
Indo-1 LeakRes ^c (IndoPE3)	TL	UV	260 ^d	✓	346	330	475 408 Leakage-resistant indicator. Formerly Indo-1PE3
Asante Calcium Red	TL	V	400	✓	Ex488	525	650 Small decrease in 525 nm emission on Ca ²⁺ binding. Single emission when excited at 540 nm
Indo-1 NearMem ^c (FIP18)	TL	UV	450 ^d	✓	346	330	475 408 Lipophilic near-membrane Ca ²⁺ indicator. K_d affected by membrane environment. Formerly FIP-18
Indo-5F	MP	UV	470 ^a	✓	347	331	475 412
Indo-1 LowAff ^c (Indo-1FF)	TL	UV	26 μM	✓	Ex 348	475	408 Formerly Indo-1FF
MagIndo-1	MP	UV	35 μM	✓	349	328	480 390 K_d determined in 0-Mg ²⁺ , indicator will be Mg ²⁺ sensitive

MP produced by Molecular Probes/Invitrogen-Life Technologies Inc., TL produced by Teflabs, MP/TL produced by Molecular Probes/Invitrogen-Life Technologies Inc. and Teflabs Molecular Probes is now a brand of Life Technologies Inc.

^a K_d determined in 100 mM KCl, pH 7.2 at 22°C

^b K_d determined in 115 mM KCl, 20 mM NaCl, 10 mM K-MOPS, pH 7.05, 1 mM Mg²⁺ at 22°C

^cTeflabs produce LeakRes, NearMem, HighAff, Med Aff, and LowAff variants of many of their probes

^dConditions for K_d determination not defined

indo-1, and their derivatives) and those that are excited with visible light at or above 450 nm (e.g., *fluo-indicators*, *Calcium Green*, *rhod*-2; see refs. 9, 10). The fluorophores for the visible indicators tend to be fluorescein and rhodamine derivatives. This is advantageous since a great deal of fluorescence instrumentation has been designed for use with fluorescein- and rhodamine-based dyes.

2. Synthetic Ca^{2+} Indicators

2.1. Single-Excitation Indicators

The first of this family is quin2 (5), Tsien's original fluorescent Ca^{2+} indicator. When excited at 340 nm, an increase in emission intensity peaking at 505 nm is observed on binding Ca^{2+} . Under physiological conditions quin2 has a K_d of 115 nM, making it useful for measuring $[Ca^{2+}]_c$ changes at or close to those found in unstimulated (resting) cells. However, the dye is of little use in monitoring changes in $[Ca^{2+}]_c$ in excess of 1 μM . Poor quantum efficiency has limited the use of this indicator, especially after the introduction of the more fluorescent ratiometric probes. However, quin2 does have some useful properties; like BAPTA, it is a very good buffer of $[Ca^{2+}]_c$, and its use has allowed Ca^{2+} -independent phenomena to be observed (11, 12). Subsequently improved single-excitation indicators have been developed that are more fluorescent and have K_d 's for Ca^{2+} between ~200 nM and 320 μM (9, 10, 13) (see Table 1). These indicators include the fluo derivatives (10), and the Calcium Green and Calcium Orange series of indicators. With these indicators there is little or no shift in either the excitation or emission spectra; however, a marked increase in fluorescence intensity can be observed on Ca^{2+} binding. Calcium Green-2 has a K_d of 550 nM (Table 1) and produces approx 100-fold increase in fluorescence between being Ca^{2+} free and Ca^{2+} saturated. For fluo-3 this increase is reported to be approximately 200-fold. It can of course be problematic if the resting Ca^{2+} signal is so low that cells cannot be readily identified or a reliable calibration achieved. Fluo-4 has a similar K_d to fluo-3 but is more fluorescent with 488 nm excitation and appears to load more readily (9).

2.1.1. Visible Excitation Indicators

The fluo and Calcium Green indicators all have peak excitation spectra at or close to 490 nm (see Table 1), allowing them to be readily used with argon-ion lasers (488 nm excitation). Peak emission lies close to 530 nm. There are Ca^{2+} indicators that can be excited even at longer wavelengths, e.g., rhod-derivatives, the Calcium Crimson and Calcium Orange series, and KJM-1 (Table 1). Rhod-2 is excited at 520 nm, with a peak emission at 580 nm (10), and has been used to measure mitochondrial Ca^{2+} rather than $[Ca^{2+}]_c$ (9, 14). Fura-Red (strictly a ratiometric indicator) when excited at wavelengths close to 480 nm can be used in combination

with fluo-3 to obtain a ratio derived from their respective 530- and 650-nm emission signals. Thus, combinations of visible excitation indicators can be used to obtain ratio measures of $[Ca^{2+}]_c$ (15, 16). Asante Calcium Red (Teflabs) is another Ca^{2+} indicator that can be excited at longer wavelengths. Excitation at 540 nm results in an emission spectra with a peak at 650 nM. A near-infrared derivative, Asanate Calcium NearIR, is also available. Measuring Ca^{2+} with red emitting fluorescent indicators is advantageous as it avoids autofluorescence resulting in a cleaner signal. Also absorbance of excitation and emitted light is much less at longer wavelengths which means that these indicators are better suited to examining Ca^{2+} in tissues.

In general, visible wavelength indicators are attractive because they can avoid problems such as light absorbance by optical elements and cellular autofluorescence. The lower excitation energies of the longer wavelengths also means that photobleaching is reduced. The visibly excited dyes are more suited to the laser-based illumination systems used in confocal microscopy and flow cytometry. The advantage of having a range of indicators that can be excited at different wavelengths is that combinations of ion-indicators can be used together. Thus, Ca^{2+} can be monitored simultaneously with other physiologically important ions such as Na^+ or H^+ (17–19). Moreover, Ca^{2+} can be monitored using indicators in separate domains as with simultaneous measurements of intracellular and extracellular Ca^{2+} (20).

2.1.2. Caged Compounds

Bioactive molecules can be incorporated into physiologically inert (caged) molecules and subsequently released in a controlled manner by photolysis of the chemical “cage.” Introduction of the visible excitation indicators has allowed $[Ca^{2+}]_c$ to be measured during UV-induced flash photolysis of caged compounds such as caged $Ins(1,4,5)P_3$ and Nitr-5 (caged Ca^{2+}) (21–23). This advance has enabled second messengers to be manipulated in a controlled manner while simultaneously monitoring $[Ca^{2+}]_c$.

2.2. Dual-Excitation Indicators

Fura-2 is the archetypal dual-excitation Ca^{2+} indicator (6). In low Ca^{2+} , fura-2 shows a broad excitation spectrum between 300 and 400 nm, with a peak at approx 370 nm. On Ca^{2+} binding, the excitation peak increases in intensity and also shifts further into the UV (Fig. 1). Consequently, if the dye is excited at 340 nm (emission monitored at 510 nm), Ca^{2+} binding will produce an increase in fluorescence, whereas a decrease in the fluorescent signal is observed when the dye is excited at 380 nm (Figs. 1 and 2). When the dye is excited in quick succession at 340 and 380 nm, a ratio of the respective emission signals can be used to monitor $[Ca^{2+}]$. Ratiometric measurements have a number of advantages over single-wavelength probes. The ratio signal is not dependent on dye concentration, illumination intensity, or optical path length. Therefore, spatial variations in these parameters will not affect the

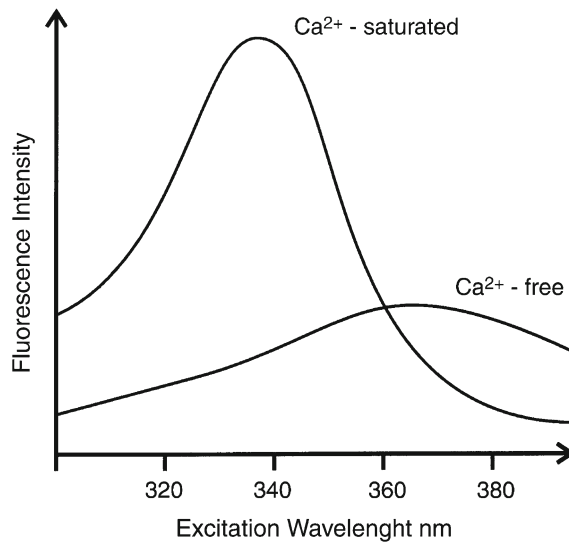


Fig. 1. The Ca^{2+} -free and Ca^{2+} -saturated spectra of fura-2. The two spectra coincide at 360 nm, the isobestic (or isoemissive) point. From this figure it can be seen that when Ca^{2+} binds to fura-2 the fluorescence signal will, increase when the indicator is excited at 340 nm, stay the same when it is excited at 360 nm and decrease when it is excited at 340 nm.

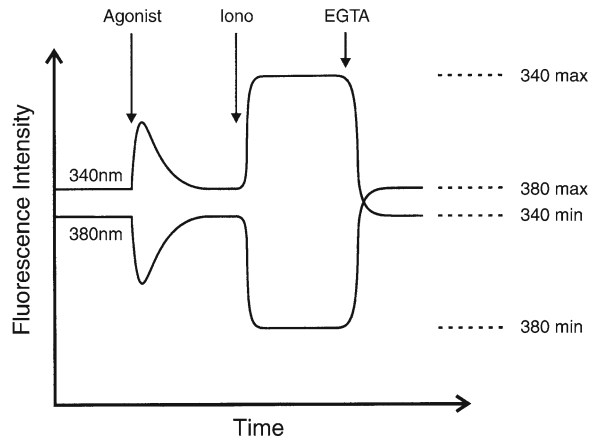


Fig. 2. The typical signals obtained from a fura-2-loaded cell when it is excited at 340 and 380 nm. Agonist stimulation will cause an increase in the 340 nm signal and a decrease in the 380 nm signal. Addition of an ionophore (Iono) in the presence of Ca^{2+} will give $F_{340\text{max}}$ and $F_{380\text{min}}$, whilst subsequent addition of EGTA will give $F_{340\text{min}}$ and $F_{380\text{max}}$. The time taken to reach $F_{340\text{min}}$ and $F_{380\text{max}}$ after the addition of ionophore and EGTA can vary and may be in excess of 30 min. Curve fitting the decay towards R_{min} has been suggested as a strategy to speed up the calibration process (36). The long time period required to obtain R_{min} is not ideal for imaging experiments since the dimensions of the cells may change during the calibration.

estimations of $[Ca^{2+}]_c$. Such factors are especially important if the dyes are to be used for imaging of $[Ca^{2+}]_c$ where illumination intensity and optical properties vary across the field of view (6, 24). Dye leakage and photobleaching frequently lead to a loss of indicator

during an experiment; thus, the active indicator concentration cannot be assumed to be constant (25, 26). Under such conditions, a ratiometric indicator gives a more stable measure of $[Ca^{2+}]_c$ than that could be obtained from a single-excitation indicator. Ratiometric measurements also produce an additional increase in sensitivity.

A further useful property of ratiometric indicators is the presence of an isobestic or isoemissive point. For example, when fura-2 is excited at 360 nm, no Ca^{2+} -dependent change in fluorescence occurs, since at this wavelength the Ca^{2+} -saturated and Ca^{2+} -free excitation spectra coincide (see ref. 6; Fig. 1). If Mn^{2+} is used to quench fura-2 fluorescence, excitation at 360 nm can be used to measure its influx (see ref. 27; Fig. 3). Thus, Mn^{2+} can act as a surrogate for Ca^{2+} in influx studies. Excitation at 360 nm will also reveal the intracellular distribution of fura-2 ((26); see below). If the cytosolic indicator is lost by permeabilizing the plasma membrane (or quenched using Mn^{2+}), the localization of compartmentalized dye will be unveiled (25).

2.3. Dual-Emission Indicators

The Ca^{2+} indicator indo-1 shows a shift and an increase in the peak of its emission spectra when Ca^{2+} binds, whereas the excitation spectra remain unaltered (6). Thus, the dye is excited at a single wavelength between 338 and 350 nm and emission is monitored at 400 and 450 nm, the respective peaks of the Ca^{2+} -bound and Ca^{2+} -free spectra. Indo-1 has a K_d for Ca^{2+} of 250 nM under physiological conditions; Indo-5 F has K_d of 470 nM (Table 3). Another indicator in this class is mag-indo-1. It was originally designed for monitoring Mg^{2+} ; however, because Mg^{2+} generally changes very little, these indicators have been used as low-affinity Ca^{2+} indicators (Table 3). Asante Calcium Red can also be used for emission ratioing. When excited at 488 nm and Ca^{2+} is increased there is small decrease in fluorescence at 525 nm and a large increase at 650 nm. The dual-emission indicators are ideal for simple photometric measurements of Ca^{2+} from cells. They need only a monochromatic light source (which could be via an interference filter) and a beam-splitting dichroic mirror on the emission side to separate the emission signals (400 and 450 nm for indo-1). Two photomultiplier tubes (PMTs) running simultaneously can be used to monitor the emission signals. This arrangement gives the apparatus a very rapid time resolution that is limited by the kinetic properties of the indicators. However, these dyes are not ideal for conventional fluorescence imaging experiments, because either two cameras are required or some method of rapidly changing an emission filter is needed. Aligning the image frames is not easy, and introducing additional optical elements on the emission pathway is not desirable since the amount of light per pixel on the camera is much less than that hitting the photocathode of a PMT tube. However, multispectral cameras now bypass the need for two separate cameras. Also, the current generation of line scanning confocal microscopes

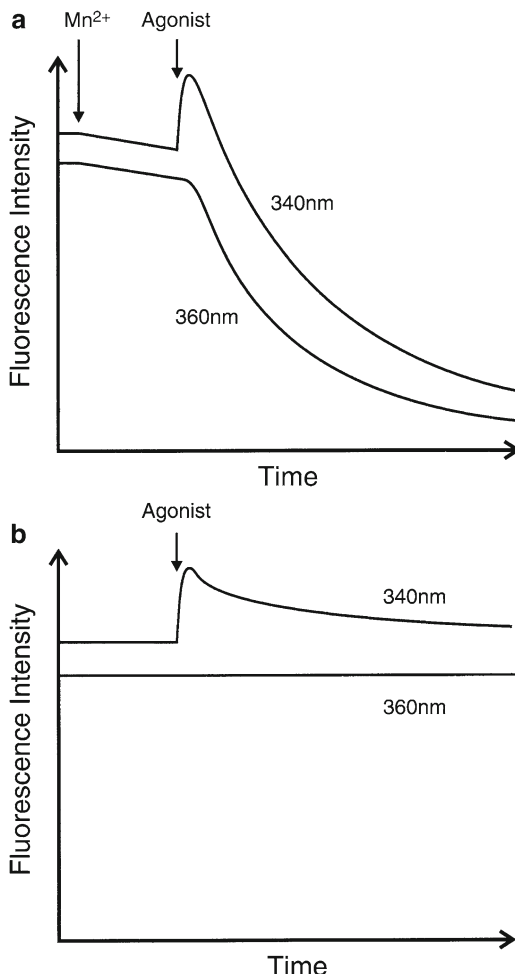


Fig. 3. (a) The effect of Mn^{2+} on fura-2 fluorescence when the dye is excited at 340 and 360 nm. Addition of Mn^{2+} will often initiate a slow quench of fura-2 that is markedly enhanced when the cell(s) is/are stimulated with an agonist. The 360 nm signal represents the Mn^{2+} quench, whilst the 340 nm trace is influenced by the increase in $[Ca^{2+}]_c$ as well as by subsequent Mn^{2+} entry. (b) The control experiment that should be carried out when using Mn^{2+} quench to follow influx. In the presence of Ca^{2+} , whilst the 340 nm signal will reflect changes in $[Ca^{2+}]_c$, the 360 nm signal should not change when the cells are stimulated with an agonist. The exact isobestic point should be determined for each cell type and each fluorescence system.

equipped with optics for resolving separate and variable emission bands are ideally suited for emission ratioing. In addition, Indo-1 is suited for the expanding technology of two- or multiphoton confocal imaging (see Subheading 2.14).

2.4. Loading of Ca^{2+} Dyes

2.4.1. Loading Using Acetoxymethyl Esters

The Ca^{2+} indicators, by their very nature, are charged molecules that cannot cross lipid membranes. However, they can be readily introduced into cells by esterifying the carboxylic acid groups, making them lipophilic and therefore membrane permeant (4).

Fortunately, cells contain many esterases that remove the ester groups, leaving the charged Ca^{2+} indicator trapped inside. Suppliers of the indicators usually sell them as the acetoxymethyl (AM) esters as well as in free acid or salt form. Introducing the dyes into cells involves incubating them with 1–10 μM of the esterified indicator with incubation times varying, usually between 15 min and 2 h. Loading is best achieved in a physiological buffer, but it can also be carried out in serum or culture media, although there will be a certain degree of extracellular esterase activity (28). Some cells may show poor esterase activity; in others, the esterified indicator accumulates in intracellular compartments, where hydrolysis may be incomplete (25, 26, 28–30). As a result, signals from cells may not be entirely derived from the cytoplasm. This “problem” with loading has been used to good effect to actually monitor Ca^{2+} inside organelles (15, 31). The multidrug-resistance transporters (widely expressed in some tumor cells) will remove the esterified indicator directly from the plasma membrane (32), thereby reducing the loading efficiency. Optimization of the loading protocol is discussed in Subheading 2.6.

2.4.2. Microinjection and the Patch Pipet

The introduction of the patch-clamp technique for recording whole-cell and single ion channel currents has provided a great deal of information on the properties of the many selective and nonselective ion channels that are present in the plasma membrane. Some of these channels are Ca^{2+} permeable whereas many others can be regulated by Ca^{2+} . It was therefore extremely useful to combine $[\text{Ca}^{2+}]_c$ measurements with simultaneous recordings of ion channel activity (29, 33). When recordings are made in the whole-cell configuration, the contents of the patch pipet are continuous with the cytoplasm of the cell. This allows the contents of the patch pipet to diffuse out and equilibrate within the cell. Hence, the patch pipet becomes a convenient way of introducing Ca^{2+} indicators and buffers into the cytoplasm of cells, avoiding the hazards of ester loading. Typically, the indicator is introduced at concentrations in excess of 50 μM in the patch pipet. Because the internal volume of the pipet is much larger than that of the cell, the concentration of the dye in the patch pipet will eventually be reflected within the cell.

Microinjection can be used to introduce Ca^{2+} indicators into the cell nucleus as well as into the cytoplasm. Typically the indicators are introduced at concentrations in the order of 1 mM to allow for the small nanoliter volumes that are microinjected. Introduction by patch pipet or microinjection is necessary if either the dextran conjugates of the indicators or other impermeable indicators such as bis-fura-2 are to be used. This fura-2 derivative has a lower affinity for Ca^{2+} (370 nM) and is more fluorescent than fura-2, but unfortunately it is not available as a cell-permeant ester (Table 2).

2.4.3. Reversible Permeabilization

There are a number of ways in which the plasma membrane can be made temporarily permeable to Ca^{2+} indicators. Streptolysin O, electroporation, and ATP4 $-$ have all been used successfully (28, 34–36). The advantage of these techniques is that cytoplasmic loading of poorly or impermeant indicators can be carried out on cell populations. However, the amount of loading may be small and damage to the cells is an inherent risk. Usually millimolar concentrations of the acidic indicator are needed, which is expensive and therefore will tend to limit the loading volume and hence the number of cells that can be loaded in this way.

2.5. Subcellular Localization of the Ca^{2+} Indicators

A number of reports have revealed that the synthetic Ca^{2+} indicators can become localized within intracellular compartments (25, 26, 28–31). In some cases these compartments appear to be mitochondria, or even the endoplasmic reticulum (ER). If signals from the cytosolic indicator can be eliminated, then selective monitoring of organelle Ca^{2+} is possible. However, when one wants to measure $[Ca^{2+}]_o$, obtaining Ca^{2+} -dependent fluorescence from other compartments is clearly a problem. Incomplete hydrolysis can be an additional complication with compartmentalized indicators (25), although in many respects a constant background fluorescence signal is easier to subtract than one that may change with time and with $[Ca^{2+}]$. Experimental approaches that can be used to optimize the cytosolic loading of the indicator are discussed next.

2.6. Optimization of Loading

There are a number of procedures that can increase the loading of the ester into cells, increase the likelihood of the dye being cytoplasmic, and finally, improve the retention of the indicator by the cells. One problem with the esterified indicators is their relatively poor solubility in physiological media. This can be improved by using Pluronic F-127, a nonionic detergent, and by including bovine serum albumin in the loading buffer (36). Pluronic F-127 (25% w/v in dimethyl sulfoxide) is most effective when it is mixed directly with the indicator, before they are added together to the loading buffer. Loading is impaired when the esterified indicator is removed from the plasma membrane by the P-glycoprotein multidrug transporter (32). If this transporter is saturated with another substrate, such as verapamil (10 μM), then introduction of the ester into cells is enhanced.

Compartmentalization of the indicator within cells can be reduced if the loading temperature is decreased from 37°C to room temperature (25, 26). This is most likely mediated through a reduction in endocytosis, a process that will cause the indicators to accumulate in endosomes and topologically related organelles. When reducing the loading temperature, the loading period usually has to be increased. Thus, a balance of optimal temperature and loading period should be found for each cell type.

Once inside a cell, the hydrolyzed indicator should not escape easily; however, rapid decreases in signal intensities during experiments often occur. The cause can be twofold: photobleaching, and transport of the indicators out of the cell. Retention of the indicators can be enhanced by the presence of anion exchange inhibitors such as sulfinpyrazone and probenecid (37, 38). These agents should be present during both the loading period with the ester and afterward during the actual experiment. Fura-2 LeakRes and Indo LeakRes are derivatives of fura-2 and indo-1 that are resistant to leakage. LeakRes (formerly known as PE3) derivatives of other indicators are also available. The LeakRes/PE3 indicators form a zwitterion from a piperazine nitrogen and an adjacent carboxylic acid that apparently enhances their retention (39). Fortunately, they too are available as cell-permeant AM esters.

2.7. Organelle Targeting

Although loading procedures may be designed to optimize the presence of the indicators in the cytosol, selective localization of the indicators may provide useful information about Ca^{2+} regulation in specific organelles or cellular domains (14, 31, 40). Indo-1 has been used to monitor mitochondrial $[\text{Ca}^{2+}]_{\text{m}}$ after the cytosolic dye was quenched using Mn^{2+} (40). The indicator rhod-2 was found to load preferentially into the mitochondria of some cells (14). This probably resulted from the fact that it is highly charged and is readily retained by the polarized mitochondria. The dihydro derivative of rhod-2 also locates preferentially into mitochondria and lysosomes since it can be oxidized within these organelles (9, 10, 14). Fluo-3 has been reported to co-load into the cytosol and mitochondria of endothelial cells such that simultaneous recordings could be made from separate mitochondrial and cytosolic domains identified by confocal microscopy (41).

Low-affinity Ca^{2+} indicators are needed to measure Ca^{2+} in the endoplasmic reticulum ($[\text{Ca}^{2+}]_{\text{ER}}$) since even early conservative estimates suggested that the concentration was likely to be in excess of 5 μM (31, 42–44). The $[\text{Ca}^{2+}]_{\text{ER}}$ is now recognized to be around 500 μM (45); see ref. 46 for a review on organelle Ca^{2+}). At these concentrations, indo-1 and fura-2 will be saturated with Ca^{2+} . Mag-fura-2 (Furaptra) has been used to monitor $[\text{Ca}^{2+}]_{\text{ER}}$ (47). Although it was designed as a Mg^{2+} indicator (48), it is in effect a low-affinity Ca^{2+} indicator (49, 50), given that Mg^{2+} is unlikely to change dramatically. Other low-affinity indicators include fura-2FF, indo-1FF fluo-3FF (31, 39), the “5 N” indicator derivatives produced by Molecular Probes, and the LowAff variants produced by Teflabs (Tables 1, 2, and 3). The problem of loading such indicators selectively into the endoplasmic reticulum is not easily solved, although “normal” loading with esterified indicator at 36°C is reportedly sufficient to locate fura-2 into the mitochondria (41), and Furaptra and fura-2FF into the sarco/ER (29). Screening both cells and loading conditions allowed Hofer and colleagues to

find a cell model where $[Ca^{2+}]_{ER}$ can be monitored (51) by simple loading of the esterified fura-2. Another approach is to load permeabilized cells with indicators, thus allowing the ester greater access to the organelle membranes and the “cytosolic” dye to diffuse out of the cell (47). Unfortunately, cell permeabilization can dramatically change the ultrastructure of the endoplasmic reticulum (52), which is not at all desirable. Information on $[Ca^{2+}]_{ER}$ has also been obtained by isolating the cell nuclei along with the nuclear envelope that is continuous with the endoplasmic reticulum. These isolated nuclei are subsequently loaded with esterified indicators (53) to give measurements of $[Ca^{2+}]$ in the perinuclear endoplasmic reticulum, while incubation of the nuclei with indicator-dextran conjugates allows the $[Ca^{2+}]$ to be monitored in the nucleoplasm.

Injection of dextran-conjugated indicators into the nucleus itself would allow selective measurements of nuclear $[Ca^{2+}]$. This could be combined with another indicator–dextran conjugate that could be injected into the cytoplasm, allowing selective monitoring of Ca^{2+} from the two subcellular regions in an intact cell. For the nucleus and cytoplasm, confocal microscopy offers an alternative approach to monitoring $[Ca^{2+}]$, in that the spatial resolution is such that the cytoplasm and nucleus are separated in single confocal planes. Hence, as long as one can identify the region from which the signal originated, nuclear and cytosolic Ca^{2+} can be monitored by a single, freely diffusible Ca^{2+} indicator (54).

There is continuing evidence for microdomains of $[Ca^{2+}]_c$ within cells (46, 55–58). The Ca^{2+} indicators are, by their nature, Ca^{2+} buffers that can diffuse freely within cells. As such they can act to buffer microdomains, making them harder to resolve. If the Ca^{2+} buffers are made immobile or their diffusion is restricted, more dramatic localized changes in Ca^{2+} should be observed (also see Subheading 2.8). One approach along these lines has been to add a lipophilic tail allowing the indicator to be attached to membranes (59–61). Such indicators include fura C₁₈, Calcium Green C₁₈ (Invitrogen-Life Technologies), and Fura-2 NearMem (FFP18) and Indo-1 NearMem (FIP18) (Teflabs). When injected into the cell, they locate to the cytoplasmic faces of lipid membranes. Thus peri-ER and subplasmalemmal Ca^{2+} can be monitored. It has been reported that when added extracellularly, they can be used to monitor Ca^{2+} efflux (61), although I have found it difficult to obtain sensible data with Calcium Green C₁₈. An elegant refinement of this approach has been to conjugate fura-2 with the specific oligopeptides allowing the indicator to be geranylgeranylated (62). A lipid tail added by prenylation (common to Ras proteins) would allow such indicators to monitor subplasmalemmal Ca^{2+} selectively. Genetically engineered protein indicators for Ca^{2+} allow very selective targeting of Ca^{2+} indicators to cellular organelles. Their potential is discussed more under Subheadings 2.12 and 2.13.

2.8. Indicator Mobility and Buffering of Ca^{2+}

Fura-2 is a relatively high-affinity indicator that will tend to buffer Ca^{2+} . As indicated under Subheading 2.7, restricting the mobility of the Ca^{2+} buffer will also restrict the mobility of Ca^{2+} and potentially aid its detection. In intact cells, Ca^{2+} is not believed to diffuse freely owing to the presence of endogenous Ca^{2+} buffers and stores capable of rapidly sequestering Ca^{2+} (63). Thus, freely mobile indicators such as fura-2 can act to dissipate naturally occurring Ca^{2+} gradients and microdomains of elevated $[\text{Ca}^{2+}]_c$. This is, of course, disadvantageous when the aim is to investigate local changes in $[\text{Ca}^{2+}]_c$. When fura-2 is introduced at high concentrations so that it is the dominant Ca^{2+} buffer, changes in fluorescence actually report the Ca^{2+} flux. At low concentrations when buffering is minimal, fura-2 will reflect more faithfully the actual changes in $[\text{Ca}^{2+}]_c$ (64). Using a slow buffer such as EGTA buffer in combination with a fast Ca^{2+} indicator (fura-2) makes it easier to resolve sites of Ca^{2+} events (58) since Ca^{2+} released by the indicator is effectively “mopped up” by the slower chelator rather than indicator molecules distant from the source of Ca^{2+} .

Tables 1, 2, and 3 list some of the common indicators ranked in order of their K_d values. The lower affinity buffers will of course be better suited to monitoring $[\text{Ca}^{2+}]_c$ without increasing intracellular buffering. A potential problem with using immobile indicators is that if they saturate with Ca^{2+} or photobleach, the ability to monitor $[\text{Ca}^{2+}]$ at a specific location is lost since nonsaturated or unbleached indicator cannot easily replace the impaired dye. As such, this could negate any beneficial effects that localized indicators may confer in the reporting of local changes in $[\text{Ca}^{2+}]_c$. Lower affinity probes may avoid this problem since they would not readily saturate with microdomains of high $[\text{Ca}^{2+}]_c$. All said, dramatic images of elementary Ca^{2+} events can be resolved quite adequately with freely mobile buffers (55).

2.9. Calibration

There are a number of factors that can influence calibration that users of the fluorescent Ca^{2+} indicators need to be aware of. The K_d for Ca^{2+} will vary with temperature, pH, and ionic strength, and for some indicators, the presence of Mg^{2+} will affect the K_d for Ca^{2+} (6, 7, 9, 18, 19, 25, 65). Viscosity also affects the signals (25, 66). It is therefore advisable to calculate the K_d under conditions that mimic, as far as possible, the expected environment in which the dye is to be used. Not all of the published K_d values will relate to the ionic conditions or temperature that may be chosen for experiments; many values have been determined at 22°C and in the absence of Mg^{2+} (see Tables 1, 2, and 3). Apparently, the K_d s of the dextran-conjugated indicators vary from batch to batch (9), so their values would have to be checked. It is, of course, hard to predict precisely what effect the internal cellular environment will have on the Ca^{2+} indicators; however, it is unlikely that the K_d will vary significantly as long as the key parameters outlined above remain constant.

If the K_d is known, all that is required to calibrate a single-excitation wavelength indicator is to determine the maximum and minimum fluorescence values of the indicator (F_{\max} and F_{\min}) when it is Ca^{2+} saturated and Ca^{2+} free, along with any background fluorescence (5). After subtracting the background fluorescence from the signals, $[Ca^{2+}]_c$ can be calculated as follows:

$$[Ca^{2+}]_c = K_d \times (F - F_{\min}) / (F_{\max} - F).$$

When the cells are in suspension, leaked dye will contribute to the background signal particularly if extracellular Ca^{2+} is present, since the extracellular indicator will be saturated with Ca^{2+} . The contribution of the extracellular dye to the signal can be determined either by centrifuging the cells and measuring the fluorescence arising from the supernatant or by adding Mn^{2+} and measuring the instantaneous drop in the signal. This latter approach will only work when using those indicators that are quenched by Mn^{2+} . When adjusting for extracellular dye in this way, the Ca^{2+} -saturated signal from extracellular dye should be subtracted from F_{\max} and from the fluorescence values (F) obtained during the experiment. A fluorescence value equivalent to that from Ca^{2+} -free extracellular dye should be subtracted from F_{\min} . Usually this latter component is small and can be ignored unless the indicator gives a relatively large Ca^{2+} -free signal. A major source of background signals is cellular autofluorescence which is more pronounced when the cells are excited in the UV. The signal from unloaded cells can be used to estimate the background fluorescence, as can certain Mn^{2+} quench protocols as indicated in Fig. 4.

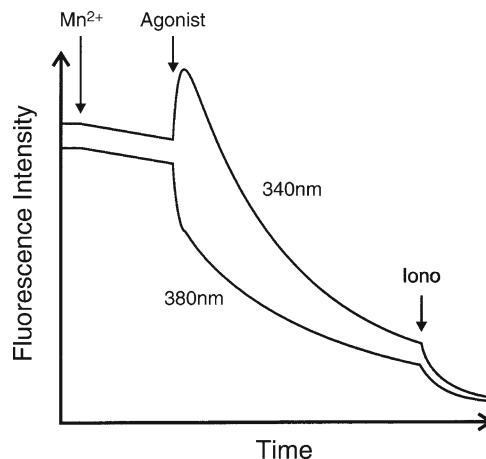


Fig. 4. The effect of adding Mn^{2+} to a cell excited at 340 and 380 nm that is subsequently stimulated by an agonist. The Mn^{2+} quenches both the 340 and 380 nm signals. Usually a steady state is reached when the cytosolic indicator has been quenched. The remaining fluorescence is derived from compartmentalized indicator plus autofluorescence. The intensity values of the 340 and 380 nm signals at this stage represent the background fluorescence. Subsequent addition of an ionophore allows Mn^{2+} to quench the compartmentalized indicator revealing the autofluorescence at 340 and 380 nm.

For single-excitation indicators, optical path length and dye concentration are critical and must remain constant. Consequently in cell suspensions, lysing the cells and determining F_{\max} and F_{\min} work well because the overall dye concentration in the sample chamber does not change, nor does the optical path length. If the measurements are being made on cover slips, then on lysis the dye will diffuse out of the cells and, therefore, out of the focal plane. For such adherent cells, a Ca^{2+} ionophore can be used to estimate F_{\max} . Obtaining F_{\min} , however, is more difficult, since even in the presence of extracellular EGTA, sufficient Ca^{2+} may remain within the cell to affect the estimation of R_{\min} . When calibrating with a suspension, sufficient EGTA must be added to chelate all the 1 mM initial Ca^{2+} that is present in many experiments (with adherent cells the bathing buffer can simply be replaced). This means that there has to be at least a tenfold excess of EGTA to Ca^{2+} in the cuvette (6, 66). When adding EGTA to Ca^{2+} (or vice versa), it should be remembered that 1 mM Ca^{2+} bound to EGTA will liberate 2 mM H^+ . These protons can be removed by adding Tris base or by adding the EGTA as an alkali solution (pH 8.0–9.0). Fluo-3 can be calibrated using the Mn^{2+} -quenched signal to estimate both F_{\min} and F_{\max} (10, 67). In other instances, it may be simpler to normalize the fluorescence signal to F_{\max} . For imaging with a single-wavelength indicator, the normalization has the added benefit that it can be carried out *in situ* on a pixel-to-pixel basis. During calibration of adherent cells, a potential problem is that increased dye leakage may lead to an underestimate of F_{\max} and F_{\min} in relation to the F values obtained prior to the calibration. When using a ratiometric indicator, this would not be such a problem because R_{\max} and R_{\min} values are not affected so dramatically by dye leakage.

With the ratiometric dyes, such as fura-2, the calibration is similar to that for the single-wavelength indicators (6). The maximum and minimum ratio values, R_{\max} and R_{\min} , are required instead of F_{\max} and F_{\min} . Because the ratio is not made with reference to the isobestic point (360 nm) but usually to the 380-nm signal (to improve the SNR ratio) a scaling factor, the $F_{380\max}/F_{380\min}$ ratio is also required. At 360 nm this factor would be equal to 1. Therefore

$$\left[\text{Ca}^{2+}\right]_c = K_d (R - R_{\min}) / (R_{\max} - R) (F_{380\max} / F_{380\min}),$$

where $R = F_{340}/F_{380}$.

With adherent cells, R_{\max} and R_{\min} are best determined *in situ*. R_{\max} is relatively easy to obtain using Ca^{2+} ionophores such as ionomycin and Br-A23187 (see refs. 36, 65). The same problems in obtaining a reliable R_{\min} apply to the ratiometric probes as well as to obtaining F_{\min} with the single-wavelength indicators. Consequently, the calibration protocol is essentially the same as that described above. With fura-2, the Ca^{2+} -saturated signal, determined

by addition of ionophore in the presence of 1–10 mM extracellular Ca^{2+} , will give the $F_{340\text{max}}$ and $F_{380\text{min}}$ (R_{max}). However, problems can arise if the $F_{380\text{min}}$ signal is close to autofluorescence, since dividing by zero or small numbers can play havoc with the software and generate very large erroneous R_{max} values. This is a particular problem when using older 8-bit cameras, since autofluorescence values are likely to be close to zero. R_{min} , which is $F_{340\text{min}}/F_{380\text{max}}$, is obtained by incubating the cells with ionophore in the presence of relatively large amounts of EGTA as outlined above. Note, however, that Br-A23187 is reported to be more effective at transporting Ca^{2+} at acid pH values than ionomycin (36, 65). Figure 2 is a schematic diagram of the 340- and 380-nm signals of fura-2 during agonist stimulation and calibration.

With fura-2, Mn^{2+} quench of the 340- and 380-nm excitation signals can be used to determine the background fluorescence at each wavelength (Fig. 4). Some groups use ionomycin and Mn^{2+} to determine background fluorescence; however, this approach would also quench signals coming from dye trapped inside organelles. To quench the cytosolic signal, it is better to use a maximal concentration of an agonist (or thapsigargin) so that Mn^{2+} rapidly enters the cytosol. Thus, any remaining signal will represent compartmentalized dye and autofluorescence. Ionomycin can be added subsequently to reveal autofluorescence alone, if desired.

When imaging, the calibration should ideally be carried out on a pixel-to-pixel basis (including background subtraction) (68, 69). However, the dimensions of a cell may change between the beginning and the end of an experiment, making perfect calibration virtually impossible. Frequently, the R_{max} and R_{min} values are averages determined for the entire field of view rather than on a pixel-to-pixel basis, although there are analysis packages that allow pixel-to-pixel generation of R_{max} and R_{min} values. I generally use photometric data gained by summing the signal arising from each cell. In this case, it is sufficient to subtract the total background fluorescence originating from each cell.

When calibrating R_{max} and R_{min} on an imaging system, one early problem was that 8-bit cameras only just managed to cover the dynamic range of the indicator. Thus, when the gain and black level are optimized, $F_{340\text{min}}$ may be on scale, but $F_{340\text{max}}$ may saturate the camera and vice versa with the 380-nm signals. It is more than likely that while gain settings may suit some cells in the field of view, for other cells the settings will mean that they are either too bright or too dim. Twelve and 16-bit cameras alleviate this problem. Where possible, cameras should show a linear response to light (24, 69). Confocal microscopes using PMTs should have a very large dynamic range (typically from 10¹ to 10⁶ counts per second for PMTs), but this will depend on the analogue-to-digital converter within the system.

2.10. Calcium Flux Measurements

In addition to providing information on $[Ca^{2+}]_c$, the fluorescent indicators can be used to provide data on Ca^{2+} fluxes. Where influx and efflux are abolished (e.g., by La^{3+}), or where the cells have been permeabilized, the indicators can give kinetic information on the release of Ca^{2+} from intracellular stores (70, 71). When information is required on Ca^{2+} influx, an easy approach is to use the Mn^{2+} quench of fura-2 signals (Fig. 3). If Mn^{2+} is used as a surrogate for extracellular Ca^{2+} , its influx into cells can be followed using fura-2 excited at 360 nm (27). Monochromator-based light sources are best for these experiments since they allow accurate excitation at the isobestic point. If excitation occurs slightly to the right of the isobestic point (i.e., >360 nm), a Ca^{2+} -dependent decrease in fluorescence can be confused with Mn^{2+} entry.

The relative permeability of Ca^{2+} influx pathways to Mn^{2+} may be of interest alone. (72–75). This quench technique can be used to investigate the rapid kinetics of cation entry by stopped flow fluorescence (73). In experiments investigating capacitative or store-operated Ca^{2+} entry, Ba^{2+} and Sr^{2+} have also been used as surrogates for Ca^{2+} . These ions actually behave like Ca^{2+} when they bind to fura-2, and do not quench the signal (74). Barium is also poorly removed from the cell, making it a good indicator of unidirectional fluxes. Interestingly, Sr^{2+} does not appear to enter via store-operated channels but will enter in response to vasopressin, indicating that selective use of permeant cations can be used to distinguish between different influx pathways (75).

The indicators can be used to monitor Ca^{2+} efflux whether it is a release from vesicles, Ca^{2+} stores in permeabilized cells, or extrusion from an intact cell. Efflux can be measured from individual cells by either restricting the extracellular volume (76) or using indicator-dextran conjugates to generate a gel around the cells (20). This restricts the diffusion of Ca^{2+} away, thereby aiding its detection. Alternatively, we have used low concentrations of extracellular fura-2 to monitor Ca^{2+} efflux using cell suspensions (77, 78) where sufficient Ca^{2+} is transported to allow detection by the indicator. With the wide variety of Ca^{2+} indicators now available, it is, of course, possible to combine Ca^{2+} efflux studies using one indicator with measurements of $[Ca^{2+}]_c$ at the same time, using another indicator (20).

2.11. Dextran-Conjugated Indicators

Many of the Ca^{2+} indicators are now available as dextran conjugates (9). They are supplied as 3,000, 10,000, and 70,000 MW dextrans containing poly-(α -D-1,6-glucose) linkages making them resistant to cellular glucosidases. The dextran indicators have a number of useful properties because they

1. Have a restricted mobility.
2. Are not transported out of cells.
3. Remain cytosolic.

4. Are less likely to bind proteins.
5. Can be linked to peptides to allow specific targeting by peptide signal motifs.

2.12. Luminescent Protein Indicators for Ca^{2+}

The reemergence of aequorin as a modern indicator for Ca^{2+} occurred after it was shown that cells could be transfected with aequorin cDNA, allowing specific expression of the photoprotein in intracellular compartments (79, 80). Selective targeting of aequorin to specific organelles or cellular domains such as the mitochondria (79, 80) nucleus (81), endoplasmic reticulum (43, 45), or plasma membrane (82) meant that intracellular, domain-specific, $[Ca^{2+}]$ could be measured. Luminescent probes have a number of advantages including a large signal-to-noise ratio; avoidance of cell and reagent autofluorescence; and requirement of simple photomultiplier technology for the detection of signals. In order to use recombinant aequorin, the apo-protein that is expressed in cells has to be reconstituted into functional aequorin by incubation with a prosthetic agent, coelenterazine (1, 83). Aequorin extracted from the jelly fish already contains the prosthetic group. Coelenterazine is triggered to emit light when Ca^{2+} binds to aequorin and during the luminescent reaction coelenterazine is oxidized to coelenteramide (1, 83). The Apo-aequorin expressed by cells has only to be incubated with coelenterazine for the functional aequorin to be regenerated. This regeneration requires the presence of molecular oxygen and low Ca^{2+} . In the presence of elevated Ca^{2+} the rate of discharge will exceed the rate of regeneration (45). For wild-type aequorin, regeneration can easily be achieved in the presence of 100 nM $[Ca^{2+}]_c$ but regeneration of the luminescent protein in the endoplasmic reticulum presents a number of difficulties (45). Wild-type aequorin is effective for measuring Ca^{2+} in the range of 0.2–50 μM (1). However when $[Ca^{2+}]_c$ exceeds about 10 μM the large consumption of aequorin hampers steady-state measurement of Ca^{2+} . Recombinant aequorin was calculated to have an apparent K_d close to that of wild-type aequorin, around 13–16 μM at room temperature (84). At 37°C the value is around 10 μM (1, 84). In order to measure Ca^{2+} in compartments with a high Ca^{2+} the K_d of the photoprotein for Ca^{2+} was reduced by introducing a point mutation (42). The resulting mutated aequorin has a K_d of around 130 μM . Coelenterazine analogues that undergo a much slower light reaction have been synthesized (83). When used in combination with the mutated aequorin it is possible to measure steady-state $[Ca^{2+}]$ in the order of 700 μM albeit for a few minutes (45). Using *n*-coelenterazine and reduced affinity aequorin subplasmalemmal $[Ca^{2+}]$ has been recorded at around 50 μM (82), the $[Ca^{2+}]_{ER}$ at 700 μM (45), and spikes in mitochondrial $[Ca^{2+}]$ up to around 800 μM (85).

Calibration of aequorin relies on determining its fractional rate of consumption, since it is this rate rather than the light intensity that is proportional to the $[Ca^{2+}]$ (1, 45, 80). In order to monitor Ca^{2+} with any great effect only a small proportion of the total photoprotein must be consumed at any one moment. Also during experimentation the total amount of light emitted has to be recorded so that at each time interval the signal as a proportion of the total amount of signal available can be calculated. This means that when using aequorin, the raw count rate as viewed during the experiment is a poor indicator of the actual $[Ca^{2+}]$. A large spike in counts at the beginning of the experiment may actually be smaller in terms of Ca^{2+} than a small spike towards the end of the experiment. At the end of the experiment any remaining aequorin has to be discharged (by cell lysis in the presence of Ca^{2+}) to establish the total amount of light emitted. The use of recombinant aequorin is ideally suited to photometry. Although it is possible to image Ca^{2+} using aequorin, it has not been used to any great extent for this purpose. Simply there is not enough light emitted for imaging since one molecule of aequorin will emit only one photon. That said, targeting of aequorin allows the average $[Ca^{2+}]$ to be recorded from within restricted domains where it would be difficult to obtain good spatial and temporal resolution using fluorescence imaging techniques. For example, aequorin can be used to measure in a cell population the mean $[Ca^{2+}]$ adjacent to adenylyl cyclase (86).

2.13. Fluorescent Protein Indicators for Ca^{2+}

Many fluorescent protein indicators for Ca^{2+} have now been generated (44, 87–92). For recent reviews see refs. (91, 92). Often referred to as genetically encoded Ca^{2+} indicators (GECIs) or fluorescent Ca^{2+} indicator proteins (FCIPs), these probes have all the targeting advantages that are associated with using aequorin but allow visualization of Ca^{2+} and nondestructive approximation of $[Ca^{2+}]$. Initial probes were based on the observation that Förster (fluorescence) resonance energy transfer (FRET) can take place between the blue- or cyan-emitting mutants of the green fluorescent protein (GFP) and the green- or yellow-emitting GFP mutants (44, 87–93). The CFP and YFP pairing leads to the yellow cameleon (YC) family of probes (44). The fusion protein consists of two GFP mutants separated by calmodulin attached to a calmodulin-binding peptide. When Ca^{2+} binds to the calmodulin, the complex binds to the Ca^{2+} –calmodulin-binding peptide, bringing the GFP mutants sufficiently close for FRET to take place. Thus, when the Cameleon-1 is excited at 380 nm, there is an increase in the 510/445 nm emission ratio on Ca^{2+} binding. Mutation of the calmodulin domain allowed the Ca^{2+} sensitivity to be manipulated: YC2 is effective from 0.1 to 10 μM Ca^{2+} ; YC3, 0.5–100 μM Ca^{2+} ; and YC4, 10–1,000 μM Ca^{2+} (44). These probes have been further improved. YC2.1, 3.1, and 4.1 are much less pH sensitive (94). pH sensitivity limits the applicability, especially for the desired use

of measuring $[Ca^{2+}]_{ER}$. Unfortunately, modifying the probes to decrease their pH sensitivity led to slower maturation of the probe, poor folding at 37°C, and a decreased dynamic range for YC4.1 compared with YC4. Using the “citrine” mutation of EYFP, the GFP variants were further improved to possess greater pH tolerance, increased photostability, decreased sensitivity to halides, and improved protein folding (95). Incorporation of the citrine mutation of YFP into the YC probes generated the citrine cameleon, YC3.3. The Venus cameleon (YC2.12) incorporating the Venus mutant of YFP into YC 2.1 rapidly matures within cells and is effective over $[Ca^{2+}]$ from 0.1 to 10 μM (96). Further cameleons include the CKKp cameleon (YC6.1) and Red Cameleon. The architecture of YC6.1 differs from the other cameleons in that the calmodulin-binding domain of calmodulin-dependent kinase kinase has been inserted in the linker region between the N and C terminal portions of calmodulin. This configuration leads to increased FRET (97).

Other FRET-based Ca^{2+} probes have been developed. Persechini and colleagues (1997) generated the FIP-CA_n series based on BGFP and RGFP (98, 99). The donor and acceptor pairing is separated by a Ca^{2+} -binding domain from smooth muscle myosin light chain kinase (FIP-CB_{SM}) and tethered to variants of N and C terminal inverted calmodulin (CaMCN). The resulting probes bind Ca^{2+} with K_d of 100 nM and 280 nM at 37°C and have a monophasic relationship with Ca^{2+} . They are excited at 380 nm and emission monitored at 440 and 505 nm. The 440/505 nm ratio changes from about 1.5 to 2.5 from Ca^{2+} free to Ca^{2+} saturated. An interesting development from the group is a probe (BSCaM_A) that measures calmodulin rather than Ca^{2+} (100). The design has a calmodulin-binding domain linking the donor and acceptor GFP variants. In BSCaM_A the calmodulin-binding domain derived from neuromodulin binds both apocalmodulin (Ca^{2+} free) and Ca^{2+} -calmodulin allowing the measurement of calmodulin availability. The probe is excited at 430 nm and emission monitored at 530 and 470 nm to give a ratiometric response. Thus when $[Ca^{2+}]_c$ increases the available calmodulin (CaM_A) decreases since calmodulin will bind to target effector molecules. Simultaneous measurement of calmodulin and $[Ca^{2+}]_c$ (the latter with indo-1) allows the relationship between Ca^{2+} -bound and -free calmodulin to be determined.

GFP-based indicators for Ca^{2+} have been developed that do not rely on FRET. These include the Camgaroo, Pericam, and G-CaMP probes (101–103). Tsien and colleagues (101) found that interchanging the N and C terminal portions of GFP variants around amino acids in the region between 142 and 229 (circular permutation) could yield a fluorescent protein. Surprisingly whole protein sequences could be introduced at residue 145 and the resulting chimeric protein was still fluorescent. Camgaroo-1 was constructed by inserting calmodulin between amino acids 145 and

146 of EYFP (101). Ca^{2+} binding can lead to a sevenfold increase in fluorescence of the probe. A desire to improve camgaroo-1 led to the generation of camgaroo-2 containing the Q69M mutation (95). Insertion of this mutation into EYFP resulted in the YFP variant Citrine mentioned above. Consequently camgaroo-2 has many of the improved properties associated with citrine and YC3.3.

The Pericams were constructed from circular permutations of YFP around amino acid 145 and the introduction of calmodulin and M13 domains at that point (104). Three main probes were generated, Flash Pericam, Ratiometric Pericam, and Inverse Pericam. Pericams give a much larger change in fluorescence on Ca^{2+} binding compared with the Cameleons. When excited at 490 nm flash pericam gives an eightfold increase in fluorescence with a K_d for Ca^{2+} of 0.7 μM . Emission peaks at 514 nm. Ratiometric Pericam needs to be excited around 415–418 nm (405 nm for an Ar-ion laser) and 494 nm with emission being monitored at close to 513 nm. Inverse Pericam should be excited around 490–503 nm and emission monitored at about 514 nm. With Inverse Pericam, fluorescence decreases upon Ca^{2+} binding with a K_d of 0.2 μM . The Pericams have been used with great effect to measure $[\text{Ca}^{2+}]_c$ and $[\text{Ca}^{2+}]_m$ in cultured myocytes for example (104). Whilst the Cameleon probes have proved difficult to target to some organelles such as mitochondria, organelle targeting of the Pericam did not appear to be a problem (102, 104). Generally the Pericams fold better than the early Cameleons; Inverse and Ratiometric Pericam do so independently of temperature whereas Flash Pericam folds better at 28–30°C. Since the Pericams are based on EYFP (V68L/Q69K) they show a tendency for pH sensitivity that was eliminated from the later Cameleons. Significantly Ratio Pericam gave a tenfold increase in R_{\max} to R_{\min} compared with under 2 for the early Cameleons. However, replacement of the citrine acceptor with circularly permuted (cp) venus increased the dynamic range of the cameleons by more than threefold, as seen with YC2.12 and YC3.6 (105).

Another handicap of the Cameleons is the potential for interacting with endogenous calmodulin and for the calmodulin domain within the indicator to interact with calmodulin-binding proteins (106–109). Modification of the Ca^{2+} -binding peptide and the calmodulin domain produced the D series of indicators that were unaffected by endogenous calmodulin (106). The original D1 indicator which had a K_d for Ca^{2+} of 60 μM was used to measure $[\text{Ca}^{2+}]$ in the endoplasmic reticulum. This probe was rationally redesigned to produce indicators (D2–D4) with varying dissociation constants for Ca^{2+} and also to increase the emission ratio range by the introduction of circularly permuted venus (D2cpv, D3cpv, and D4cpv; (91, 106, 107)). These latter variants have K_d s for Ca^{2+} of 0.03/3 μM , 0.6 μM , and 64 μM and show 5.3, 5.1, and 3.8 fold changes in emission ratio, respectively. Another approach was to use troponin C as the Ca^{2+} -sensing moiety (92, 108, 109). This has advantages in that troponin expression is restricted to striated

muscle. Consequently there is much less potential for interaction with endogenous binding partners as occurs with calmodulin-based GECIs. The original probe of this type was TN-L15 with an ECFP donor and citrine acceptor (108). This was subsequently modified by manipulation of the TnC domains to reduce the effects of Mg^{2+} and to replace the acceptor with the cp-citrine (109). The resulting probe TN-XL has a dissociation constant for Ca^{2+} of 2.5 μM and fast on-off rates (for a GECI) and shows a fivefold change in ratio from zero Ca^{2+} to saturation. Further modification of the troponin C domain was undertaken to provide a higher affinity probe, TN-XXL with a K_d of 0.8 μM (92).

G-CaMP was based on circularly permuted EGFP (cpEGFP) with M13, cpEGFP, and CaM arranged in series running from the N- to the C-terminus of the chimera (103). The probe is excited around 490 nm with emission peak at about 530 nm. The fluorescence increase on Ca^{2+} binding is monophasic with a K_d of 235 nM. This probe, like many of the early recombinant Ca^{2+} probes, was pH sensitive. As with the other probes it has gone through a number of modifications aimed at reducing its pH sensitivity and increasing its fluorescence (GCaMP1.6) and then improving its thermal stability (GCaMP2; 110, 111). GCaMP3 (90) has further increased baseline fluorescence, increased dynamic range, and a slightly higher affinity for Ca^{2+} (660 nM versus 840 nM for GCaMP2). GCaMP-HS is another refinement of GCaMP2 based on improved folding characteristics (112). It has a higher affinity with a reported K_d of 102 nM compared to 146 nM of GCaMP2. It is important to note that estimates of K_d s are highly dependent upon buffer conditions, especially ionic strength, Mg^{2+} concentration, and temperature (113), hence the different reported K_d s for GCaMP2. When choosing any Ca^{2+} indicator the reported K_d s must be considered with respect to the conditions in which they were determined. The GECIs represent another huge step forward in our ability to monitor intracellular Ca^{2+} . They avoid some of the common problems such as dye leakage, compartmentation, and nonspecific loading associated with the synthetic Ca^{2+} indicators. The targeting advantages of these probes are substantial. They also, by and large, share the same instrumentation for detection as synthetic indicators. The most striking advance with GECIs has been the ability to measure Ca^{2+} either *in vivo* or in tissues (89–92). The application of GECIs to transgenic organisms was not without problems such as inadequate signal and adverse effects on the host organism (see refs. 91, 92). The most recent probes appear to have overcome these issues and are now being used to measure Ca^{2+} during physiological and behavioral responses.

2.14. Detection of Fluorescence Signals

In its simplest form, measurement of $[Ca^{2+}]_c$ using fluorescent indicators requires only an appropriate light source and a PMT detector. A xenon lamp used in combination with interference filters or monochromators can be used to excite the UV and most of the

visible indicators. More sophisticated light sources involving beam-splitting optics are needed for dual-excitation indicators and multiple excitation of indicators used in combination. Photomultipliers are commonly attached to microscopes for photometric detection of $[Ca^{2+}]_c$ in single cells or from the field of view. Conventional imaging using a low-light intensified charge-coupled device (ICCD) camera attached to the fluorescence microscope is common. This technique provides very good photometric data from individual cells within the field of view; however, improved spatial resolution of $[Ca^{2+}]_c$ is provided by confocal microscopy.

A major limitation of conventional imaging has been that even the high numerical aperture objectives that are used to gain sufficient light for detection also collect light from out-of-focus planes. This has a blurring effect on the resulting image. Confocal microscopy avoids this problem by exciting the indicator and collecting the emission via a pinhole or sometimes a narrow slit (114). The geometry is such that light originating from an out-of-focus plane cannot pass through the pinhole. To construct an image, the “confocal spot” has to be scanned over the object in view. This is achieved by generating a series of line scans over the image.

The use of confocal microscopy (usually confocal laser-scanning microscopy [CLSM]) to view fluorescent Ca^{2+} indicators is now widespread. (For reviews of confocal microscopy Ca^{2+} imaging and biphotonics see refs. 114, 115 and also Chapter 3 this publication.) The increased spatial resolution and rapid response time in the line-scan mode have revealed elementary Ca^{2+} release events in excitable and nonexcitable cells (15, 16, 116). The increased resolution provided by these microscopes is particularly advantageous when the indicator has been targeted to a particular domain of the cell (31, 44, 59, 62). In addition to CLSM, there are a number of approaches that can give similar spatial resolution and, in some cases, potentially faster whole-frame data acquisition. Mathematical deconvolution using a series of image planes in the z axis to calculate the blurring effect of the out-of-focus planes is one method (117, 118). Using a calculated point spread function for the objective is another variation on this approach. Other optical methods include the Nipkow disc and a variation described by Wilson (119) that has a greater light throughput. These systems can give confocal-like images without the need to use lasers. The advantage would be that a monochromator-based excitation source could be used, allowing excitation at any desired wavelength or combination of wavelengths. Total internal reflectance fluorescence (TIRF) microscopy allows fast, high-resolution Ca^{2+} imaging that can reveal simultaneously many single-channel Ca^{2+} flux events (120). The limitation of this technique is that images are only acquired within 300 nm of the interface with the plasma membrane.

Two- and three-photon confocal microscopy can also be applied to fluorescence Ca^{2+} indicators (65, 70, 71, 114, 121, 122).

Here the indicator is excited at a longer wavelength and either two or three coincident photons (depending on the dye and excitation wavelength) are able to excite the indicator. For example, indo-1 is normally excited at approximately 350 nm, but can also be excited by light close to 700 nm. The resolution over conventional imaging is enhanced, since statistically the arrival of coincident photons only occurs in a very narrow focal plane. Excitation by longer wavelengths reduces autofluorescence and photobleaching, and therefore the technique has some advantages over other methods. The longer wavelengths allow deeper penetration of the sample in the z axis owing to reduced scatter and absorbance by the tissue and chromophore. The principal handicap at present is the cost of the IR lasers. The current generation of IR femtosecond pulse lasers supplied by Spectra Physics and Coherent can be tuned over the range 700 nm to around 1,000 nm. At the high end of this range absorption of IR by water is a problem.

3. Summary

Over the last two decades the range of fluorescent indicators for Ca^{2+} has increased dramatically, so there are now a host of probes available. Each may offer particular advantages depending on the design of the experiment and the fluorometric equipment available. The synthetic Ca^{2+} indicators allow $[Ca^{2+}]$ determinations in most isolated and cultured cells, and can be used to some extent in tissues. The incubation period with synthetic Ca^{2+} indicators is generally tens of minutes to a few hours at the most. Another highly useful feature of some synthetic probes is their ability to bind Mn^{2+} , Ba^{2+} , and Sr^{2+} allowing the investigation and characterization of Ca^{2+} influx pathways. In comparison, recombinant protein probes require a suitable gene expression system. Plasmid transfection techniques are not readily suited for freshly isolated or quiescent cells; however, viral vectors offer the probes much wider access to cells and tissues. Transgenic cell lines, once generated, provide a very easy and consistent way of measuring Ca^{2+} in a cell of interest and are therefore ideal for screening protocols. Although an early drawback of recombinant probes was access to appropriate molecular biological facilities this is no longer a problem for most contemporary laboratories. Nonetheless, the generation and maintenance of transgenic organisms still require specialist facilities. The synthetic probes offer a fast and reliable approach with well-documented limitations. The recombinant probes open new horizons but also come with their own limitations. There is of course no reason why synthetic and recombinant protein indicators cannot be used in combination as long as appropriate steps are taken with the instrumentation to avoid signal overlap. A variation of this

theme is to use recombinant proteins to target synthetic Ca^{2+} probes as seen with Calcium Green FlAsh (123) and more recently with SNAP-tag-Indo-1 (124).

Careful choice of the indicator is therefore central to achieve a successful outcome. The probe that is chosen will of course depend on the aims of the experiment, on how the indicator will be introduced into the cell(s), and on the excitation source and detection equipment that are available. I hope that this chapter will not only help investigators choose the most appropriate indicator but, in addition, give an insight into what can be achieved using fluorescent Ca^{2+} indicators.

Acknowledgments

I would like to express my thanks to Drs John Quayle and Helen Burrell for reading this manuscript.

References

1. Ashley CC, Campbell AK (eds) (1979) Detection and measurement of free calcium in living cells. Elsevier, Amsterdam
2. Woods NM, Cuthbertson KSR, Cobbold PH (1986) Repetitive transient rises in cytoplasmic free calcium in hormone-stimulated hepatocytes. *Nature* 319:600–602
3. Cobbold PH, Bourne PK (1984) Aequorin measurements of free calcium in single heart cells. *Nature* 312:444–446
4. Tsien RY (1981) A non-disruptive technique for loading calcium buffers and indicators into cells. *Nature* 290:527–528
5. Tsien RY, Pozzan T, Rink TJ (1982) Calcium homeostasis in intact lymphocytes: cytoplasmic free calcium monitored with a new intracellularly trapped fluorescent indicator. *J Cell Biol* 94:325–334
6. Grynkiewicz G, Poenie M, Tsien RY (1985) A new generation of Ca^{2+} indicators with greatly improved fluorescence properties. *J Biol Chem* 260:3440–3450
7. Tsien RY (1980) New calcium indicators and buffers with high selectivity against magnesium and protons: design, synthesis, and properties of prototype structures. *Biochemistry* 19:2396–2404
8. Nuccitelli R, Deamer DW (1982) Intracellular pH: its measurement, regulation and utilization in cellular functions. Alan R Liss, New York
9. Johnson I, Spence MTZ (2010) The molecular probes handbook, a guide to fluorescent probes and labeling technologies, 11th edn. Invitrogen, Carlsbad, CA, USA
10. Minta A, Kao JPY, Tsien RY (1989) Fluorescent indicators for cytosolic calcium based on rhodamine and fluorescein chromophores. *J Biol Chem* 264:8171–8178
11. Hallam TJ, Sanchez A, Rink TJ (1984) Stimulus-response coupling in human platelets. *Biochem J* 218:819–827
12. Simpson AWM, Hallam TJ, Rink TJ (1986) Low concentrations of the stable prostaglandin endoperoxide U44069 stimulate platelet shape change in quin2-loaded platelets without a measurable increase in $[\text{Ca}^{2+}]_i$. *FEBS Lett* 210:301–305
13. Eberhard M, Erne P (1991) Calcium binding to fluorescent calcium indicators: calcium green, calcium orange and calcium crimson. *Biochem Biophys Res Commun* 180: 209–215
14. Hajnoczky G et al (1995) Decoding of cytosolic calcium oscillations in the mitochondria. *Cell* 82:415–424
15. Lipp P, Niggli E (1993) Ratiometric confocal Ca^{2+} measurements with visible wavelength indicators in isolated cardiac myocytes. *Cell Calcium* 14:359–372
16. Lipp P, Niggli E (1993) Microscopic spiral waves reveal positive feedback in subcellular calcium signalling. *Biophys J* 65:772–780
17. Simpson AWM, Rink TJ (1987) Elevation of pH_i is not an essential step in calcium mobilisation

- in fura-2-loaded human platelets. *FEBS Lett* 222:144–148
18. Morris SJ et al (1994) Rapid simultaneous estimation of intracellular calcium and pH. *Methods Cell Biol* 40:183–220
 19. Martinez-Zaguilan R, Parnami G, Lynch RM (1996) Selection of fluorescent ion indicators for simultaneous measurements of pH and Ca^{2+} . *Cell Calcium* 19:337–349
 20. Belan PV et al (1996) A new technique for assessing the microscopic distribution of cellular calcium exit sites. *Pflugers Arch* 433:200–208
 21. Kao JPY, Harootunian AT, Tsien RY (1989) Photochemically generated cytosolic calcium pulses and their detection by Fluo-3. *J Biol Chem* 264:8179–8184
 22. Graham C, Ellis-Davies R (2003) Development and application of caged calcium. *Methods Enzymol* 360:226–238
 23. Ashby MC et al (2002) Localized Ca^{2+} uncaging reveals polarized distribution of Ca^{2+} -sensitive Ca^{2+} -release sites: mechanism of unidirectional Ca^{2+} waves. *J Cell Biol* 158: 283–292
 24. Ryan TA, Milard PJ, Webb WW (1990) Imaging $[Ca^{2+}]_c$ dynamics during signal transduction. *Cell Calcium* 11:145–155
 25. Roe MW, Lemasters JJ, Herman B (1990) Assessment of fura-2 for measurements of cytosolic free calcium. *Cell Calcium* 11:63–73
 26. Malgoroli A et al (1987) Fura-2 measurements of cytosolic free Ca^{2+} in monolayers and suspensions of various types of animal cells. *J Cell Biol* 105:2719–2727
 27. Merritt JE, Jacob R, Hallam TJ (1988) Use of manganese to discriminate between calcium influx and mobilization from internal stores in stimulated human neutrophils. *J Biol Chem* 264:1522–1527
 28. Rink TJ, Cobbold PH (1987) Fluorescence and bioluminescence measurement of cytoplasmic free calcium. *Biochem J* 248:313–328
 29. Almers W, Neher E (1985) The Ca^{2+} signal from fura-2-loaded mast cells depends strongly upon the method of loading. *FEBS Lett* 192:13–18
 30. Steinberg SF, Belizikian JP, Al-Awqati Q (1987) Fura-2 fluorescence is localised to mitochondria in endothelial cells. *Am J Physiol* 253:C744–C754
 31. Golovina VA, Blaustein MP (1997) Spatially and functionally distinct Ca^{2+} stores in sarcoplasmic and endoplasmic reticulum. *Science* 275:1643–1648
 32. Homolya L et al (1993) Fluorescent cellular indicators are extruded by the multidrug resistance protein. *J Biol Chem* 268: 21493–21496
 33. Neher E (1989) Combined fura-2 and patch clamp measurements in rat peritoneal mast cells. In: Sellin LC, Libelius R, Thesleff S (eds) *Neuromuscular junction*. Elsevier, Amsterdam
 34. Steinberg TH et al (1987) ATP $^{4-}$ permeabilizes the plasma membrane of mouse macrophages to fluorescent dyes. *J Biol Chem* 262:8884–8888
 35. Di Virgilio F, Fasolato C, Steinberg TH (1988) Inhibitors of membrane transport system for organic anions block fura-2 excretion from PC12 and N2A cells. *Biochem J* 256: 959–963
 36. Kao JPY (1994) Practical aspects of measuring $[Ca^{2+}]_c$ with fluorescent indicators. *Methods Cell Biol* 40:155–181
 37. Di Virgilio F, Steinberg TH, Silverstein SC (1990) Inhibition of fura-2 sequestration and secretion with organic anion transport blockers. *Cell Calcium* 11:57–62
 38. Di Virgilio F et al (1988) Fura-2 secretion and sequestration in macrophages. *J Immunol* 140:915–920
 39. TELFLabs Fluorescent ion indicator handbook (2011). Texas Fluorescence Labs Inc., 9415 Capitol View Drive, Austin, TX 78747
 40. Miyata H (1991) Measurement of mitochondrial free Ca^{2+} concentration in living single rat cardiac myocytes. *Am J Physiol* 261: H1123–H1134
 41. Donnadieu E, Bourguignon LYW (1996) Ca^{2+} signalling in endothelial cells stimulated by bradykinin: Ca^{2+} measurement in the mitochondria and the cytosol by confocal microscopy. *Cell Calcium* 20:53–61
 42. Kendall JM, Dormer RL, Campbell AK (1992) Targeting aequorin to the endoplasmic reticulum of living cells. *Biochem Biophys Res Commun* 189:1008–1016
 43. Montero M et al (1995) Monitoring dynamic changes in free Ca^{2+} concentration in the endoplasmic reticulum of intact cells. *EMBO J* 14:5467–5475
 44. Miyawaki A et al (1997) Fluorescent indicators for Ca^{2+} based on green fluorescent proteins and calmodulin. *Nature* 388:882–887
 45. Alvarez J, Montero M (2002) Measuring $[Ca^{2+}]_c$ in the endoplasmic reticulum with aequorin. *Cell Calcium* 32:251–260
 46. Laude A, Simpson AWM (2009) Compartmentalized signalling: Ca^{2+} compartments, microdomains and the many facets of Ca^{2+} signalling. *FEBS J* 276:1800–1816
 47. Hofer AM, Machen TE (1993) Technique for *in situ* measurement of calcium in intracellular

- inositol 1,4,5-trisphosphate-sensitive stores using the fluorescent indicator mag-fura-2. *Proc Natl Acad Sci USA* 90:2598–2602
48. Raju B et al (1989) A fluorescent indicator for measuring cytosolic free magnesium. *Am J Physiol* 256:C540–C548
 49. Konishi M et al (1991) Myoplasmic Ca^{2+} transients in intact frog skeletal muscle fibres monitored with the fluorescent indicator furaptra. *J Gen Physiol* 97:271–302
 50. Ogden D et al (1995) Analogue computation of transient changes of intracellular free Ca^{2+} concentration with the low affinity Ca^{2+} indicator furaptra during whole-cell patch clamp recording. *Pflugers Arch* 429:587–591
 51. Hofer AM et al (1998) Free $[\text{Ca}^{2+}]$ dynamics measured in agonist-sensitive stores of single living intact cells: a new look at the refilling process. *EMBO J* 17:1986–1995
 52. van de Put FMM, Elliott AC (1996) Imaging of intracellular calcium stores in individual permeabilized pancreatic acinar cells. *J Biol Chem* 271:4999–5006
 53. Gerasimenko OV et al (1995) ATP-dependent accumulation and inositol trisphosphate- or cyclic ADP-ribose mediated release of Ca^{2+} from the nuclear envelope. *Cell* 80:439–444
 54. Minamikawa T, Takahashi A, Fujita S (1995) Differences in features of calcium transients between the nucleus and the cytosol in cultured heart muscle cells: analyzed by confocal microscopy. *Cell Calcium* 17:165–176
 55. Cheng H, Lederer WJ, Cannell MB (1993) Calcium sparks, elementary events underlying excitation-contraction coupling in heart muscle. *Science* 262:740–744
 56. Rizzuto R et al (1993) Microdomains with high Ca^{2+} close to IP_3 -sensitive channels that are sensed by neighbouring mitochondria. *Science* 262:744–747
 57. Berridge MJ (1997) The AM and FM of calcium signalling. *Nature* 386:759–760
 58. Zenisek D et al (2003) Imaging calcium entry sites and ribbon structures in two presynaptic cells. *J Neurosci* 23:2538–2548
 59. Etter EF, Kuhn MA, Fay FS (1994) Detection of changes in near-membrane Ca^{2+} concentration using a novel membrane-associated Ca^{2+} indicator. *J Biol Chem* 269:10141–10149
 60. Etter E et al (1996) Near membrane Ca^{2+} transients resolved using the Ca^{2+} indicator FFP18. *Proc Natl Acad Sci USA* 93:5368–5373
 61. Lloyd QP, Kuhn MA, Gay CV (1995) Characterization of calcium translocation across the plasma-membrane of primary osteoblasts using a lipophilic calcium-sensitive fluorescent dye, calcium green-C-18. *J Biol Chem* 270:22445–22451
 62. Horne JH, Meyer T (1997) Elementary calcium release units induced by inositol trisphosphate. *Science* 276:1690–1692
 63. Clapham DE (1995) Calcium signalling. *Cell* 80:259–268
 64. Neher E, Augustine GJ (1992) Calcium gradients and buffers in bovine chromaffin cells. *J Physiol* 450:273–301
 65. Williams DA, Fay FS (1990) Intracellular calibration of the fluorescent calcium indicator fura-2. *Cell Calcium* 11:75–83
 66. Poenie M (1990) Alteration of intracellular fura-2 fluorescence by viscosity: a simple correction. *Cell Calcium* 11:85–91
 67. Merrit JE et al (1990) Use of fluo-3 to measure Ca^{2+} in platelets and neutrophils. *Biochem J* 269:513–519
 68. Tsien RY, Harootunian AT (1990) Practical design criteria for a dynamic ratio imaging system. *Cell Calcium* 11:93–109
 69. Moore EDW et al (1990) Ca^{2+} imaging in single living cells: theoretical and practical issues. *Cell Calcium* 11:157–179
 70. Toescu EC, Petersen OH (1994) The thapsigargin-evoked increase in $[\text{Ca}^{2+}]_i$ involves an InsP_3 -dependent Ca^{2+} release process in pancreatic acinar cells. *Pflugers Arch* 427:325–331
 71. Wilcox RA, Strupish J, Nahorski SR (1995) Measurement of Ca^{2+} fluxes in permeabilised cells using $^{45}\text{Ca}^{2+}$ and fluo-3. *Methods Mol Biol* 41:215–227
 72. Broad LM, Cannon TR, Taylor CW (1999) A non-capacitative pathway activated by arachidonic acid is the major Ca^{2+} entry mechanism in A7r5 smooth muscle cells stimulated with low concentrations of vasopressin. *J Physiol* 517:121–134
 73. Sage SO, Reast R, Rink TJ (1990) ADP evokes biphasic Ca^{2+} influx in fura-2-loaded human platelets. *Biochem J* 265:675–680
 74. Hatae J, Fujishiro N, Kawata H (1996) Spectroscopic properties of fluorescence dye fura-2 with various divalent cations. *Jpn J Physiol* 46:423–429
 75. Byron KL, Taylor CW (1995) Vasopressin stimulation of Ca^{2+} mobilization, two bivalent cation entry pathways and Ca^{2+} efflux in A7r5 rat smooth muscle cells. *J Physiol* 485:455–468
 76. Tepikin AV (1992) Acetylcholine-evoked increase in the cytoplasmic Ca^{2+} concentration and Ca^{2+} extrusion measured simultaneously in single mouse pancreatic acinar cells. *J Biol Chem* 267:14073–14076
 77. Zolle O, Lawrie AM, Simpson AWM (2000) Activation of the particulate and not the soluble guanylate cyclase leads to inhibition of Ca^{2+} extrusion through localised elevation of cGMP. *J Biol Chem* 275:25892–25899

78. Green AK, Zolle O, Simpson AWM (2002) Atrial natriuretic peptide attenuates Ca^{2+} oscillations in rat hepatocytes by modulating plasmamembrane Ca^{2+} fluxes. *Gastroenterology* 123:1291–1203
79. Rizzuto R et al (1992) Rapid changes of mitochondrial Ca^{2+} revealed by specifically targeted recombinant aequorin. *Nature* 358:325–327
80. Robert V et al (2000) Recombinant aequorin as a tool for monitoring calcium concentration in subcellular compartments. *Methods Enzymol* 327:440–456
81. Brini M et al (1994) Nuclear targeting of aequorin – a new approach for measuring nuclear Ca^{2+} concentration in intact-cells. *Cell Calcium* 16:259–268
82. Marsault R et al (1997) Domains of high Ca^{2+} beneath the plasma membrane of living A7r5 cells. *EMBO J* 16:1575–1581
83. Shimomura O, Musik B, Kishi Y (1989) Semi-synthetic aequorins with improved sensitivity to Ca^{2+} ions. *Biochem J* 261:913–920
84. Brini M et al (1995) Transfected aequorin in the measurement of cytosolic Ca^{2+} concentration ($[Ca^{2+}]_c$). *J Biol Chem* 270:9896–9903
85. Montero MT et al (2000) Chromaffin-cell stimulation triggers fast millimolar mitochondrial Ca^{2+} transients that modulate secretion. *Nat Cell Biol* 2:57–61
86. Cooper DMF (2002) Calcium-sensitive adenylyl cyclase/aequorin chimeras as sensitive probes for discrete modes of elevation of cytosolic calcium. *Methods Enzymol* 345:105–112
87. Demaurex N, Frieden M (2001) Measurements of free luminal ER Ca^{2+} concentration with targeted “cameleon” fluorescent proteins. *Cell Calcium* 34:109–119
88. Miyawaki A (2003) Fluorescence imaging of physiological activity in complex systems using GFP-based probes. *Curr Opin Neurobiol* 13:591–596
89. Miyawaki A (2003) Visualization of the spatial and temporal dynamics of intracellular signaling. *Dev Cell* 4:295–305
90. Tian L et al (2009) Imaging neural activity in worms, flies and mice with improved GCaMP calcium indicators. *Nat Methods* 6:875–881
91. Palmer A et al (2011) Design and application of genetically encoded biosensors. *Trends Biotechnol* 29:144–152
92. Manck M, Griesbeck O (2008) Genetically encoded calcium indicators. *Chem Rev* 108:1550–1564
93. Miyawaki A, Tsien RY (2000) Monitoring protein conformations and interactions by fluorescence resonance energy transfer between mutants of green fluorescent protein. *Methods Enzymol* 327:472–500
94. Miyawaki A et al (1999) Dynamic and quantitative Ca^{2+} measurements using improved cameleons. *Proc Natl Acad Sci USA* 96:2135–2140
95. Griesbeck O et al (2001) Reducing the environmental sensitivity of yellow fluorescent protein. *J Biol Chem* 276:29188–29194
96. Nagai T et al (2002) A variant of yellow fluorescent protein with fast and efficient maturation for cell-biological applications. *Nat Biotechnol* 20:87–90
97. Truong T et al (2001) FRET-based *in vivo* Ca^{2+} imaging by a new calmodulin-GFP fusion molecule. *Nat Struct Biol* 8:1069–1073
98. Persechini A, Lynch JA, Romoser VA (1997) Novel fluorescent indicator proteins for monitoring free intracellular Ca^{2+} . *Cell Calcium* 22:209–216
99. Romoser VA, Hinkle PM, Persechini A (1997) Detection in living cells of Ca^{2+} -dependent changes in the fluorescence emission of an indicator composed of two green fluorescent protein variants linked by a calmodulin-binding sequence. *J Biol Chem* 272:13270–13274
100. Black DJ, Tran Q-K, Persechini A (2004) Monitoring the total available calmodulin concentration in intact cells over the physiological range in free Ca^{2+} . *Cell Calcium* 35:415–425
101. Baird GS, Zacharias DA, Tsien RY (1999) Circular permutation and receptor insertion within green fluorescent proteins. *Proc Natl Acad Sci USA* 96:11241–11246
102. Nagai T et al (2001) Circularly permuted green fluorescent proteins engineered to sense Ca^{2+} . *Proc Natl Acad Sci USA* 98:3197–3202
103. Nakai J, Ohkura O, Imoto K (2001) A high signal-to-noise Ca^{2+} probe composed of a single green fluorescent protein. *Nat Biotechnol* 19:137–141
104. Robert V et al (2001) Beat-to-beat oscillations of mitochondrial $[Ca^{2+}]$ in cardiac cells. *EMBO J* 20:4998–5007
105. Nagai T et al (2004) Expanded dynamic range of fluorescent indicators for Ca^{2+} by circularly permuted yellow fluorescent proteins. *Proc Natl Acad Sci USA* 101:10554–10559
106. Palmer AE et al (2004) Bcl-2-mediated alterations in endoplasmic reticulum Ca^{2+} analyzed with an improved genetically encoded fluorescent sensor. *Proc Natl Acad Sci USA* 101:17404–17409
107. Palmer AE et al (2006) Ca^{2+} indicators based on computationally redesigned calmodulin-peptide pairs. *Chem Biol* 13:521–530
108. Heim N, Griesbeck O (2004) Genetically encoded indicators of cellular calcium dynamics based on troponin C and green fluorescent protein. *J Biol Chem* 279:14280–14286

109. Mank M et al (2006) FRET-based calcium biosensor with fast signal kinetics and high fluorescence change. *Biophys J* 90:1790–1796
110. Ohkura M et al (2005) Genetically encoded bright Ca^{2+} probe applicable for dynamic Ca^{2+} imaging of dendritic spines. *Anal Chem* 77:5861–5869
111. Tallini YN et al (2006) Imaging cellular signals in the heart *in vivo*: cardiac expression of the high-signal Ca^{2+} indicator GCaMP2. *Proc Natl Acad Sci USA* 103:4753–4758
112. Muto A et al (2011) Genetic visualization with an improved GCaMP calcium indicator reveals spatiotemporal activation of the spinal motor neurons in zebrafish. *Proc Natl Acad Sci USA* 108:5425–5430
113. Hires SA, Tian L, Looger LL (2008) Reporting neural activity with genetically encoded calcium indicators. *Brain Cell Biol* 36:69–86
114. Schild D (1996) Laser scanning microscopy and calcium imaging. *Cell Calcium* 19:281–296
115. Parker I, Marriott G (2003) Biophotonics, part A. Methods in enzymol, vol 360. Academic, San Diego
116. Berridge MJ (1997) Elementary and global aspects of calcium signalling. *J Physiol* 499: 291–306
117. Agard AD (1984) Optical sectioning microscopy: cellular architecture in three dimensions. *Annu Rev Biophys Bioeng* 13:191–219
118. Monck JR et al (1992) Thin-section ratiometric Ca^{2+} images obtained by optical sectioning of fura-2-loaded mast cells. *J Cell Biol* 116:745–759
119. Juskaitis R et al (1996) Efficient real-time confocal microscopy with white-light sources. *Nature* 383:804–806
120. Demuro A, Parker I (2005) “Optical patch-clamping”: single-channel recording by imaging Ca^{2+} flux through individual muscle acetylcholine receptor channels. *J Gen Physiol* 126:179–192
121. Zhang ZX et al (1997) Continuous wave diode laser induced two-photon fluorescence excitation of three calcium indicators. *Jpn J Appl Phys* 36:L1598–L1600
122. Konig K, Simon U, Halbhuber KJ (1996) 3D resolved two photon fluorescence microscopy of living cells using a modified confocal laser scanning microscope. *Cell Mol Biol* 42:1181–1194
123. Tour O et al (2007) Calcium Green FlAsH as a genetically targeted small-molecule calcium indicator. *Nat Chem Biol* 3:423–431
124. Bannwarth M et al (2009) ACS Chem Biol 4:179–190
125. Escobar AL et al (1997) Kinetic properties of DM-nitrophen and calcium indicators: rapid transient response to flash photolysis. *Pflugers Arch* 434:615–631

Chapter 2

Measurement of $[Ca^{2+}]_i$ in Whole Cell Suspensions Using Fura-2

Anish Patel, Robert A. Hirst, Charlotte Harrison, Kazuyoshi Hirota, and David G. Lambert

Abstract

Use of Fura-2 in whole cell suspensions to measure changes in intracellular Ca^{2+} is probably one of the simplest, yet most widely used protocols described in this volume. Whole cell suspensions are loaded with Fura-2 and then placed into a cuvette-based fluorimetric system (measuring 510 nm emission at alternating 340/340 nm excitation). Cells can be stimulated with agonists and antagonists to enable temporal response profiling and concentration-response curves to be constructed. The protocol can be used for a wide range of cells including those transfected with Ca^{2+} -signaling proteins, e.g., receptors and channels. Loading characteristics and the need for agents to retain loaded dye (e.g., probenecid) need to be determined empirically. Calibration of whole cell suspensions to convert the fluorescent signal into Ca^{2+} is simply performed using Triton-X lysis (to determine R_{max}) and EGTA chelation (to determine R_{min}).

Key words: Fura-2, Whole cell suspensions, Cuvette-based measurement system

1. Introduction

An elevation in intracellular calcium concentration ($[Ca^{2+}]_i$) acts to trigger a range of cellular events including neurotransmitter release, muscle contraction, and oocyte fertilization (1, 2). The pattern of elevation in $[Ca^{2+}]_i$ and response to that elevation are dependent on the agonist and the cell type.

The introduction of the calcium-sensitive dye Fura-2 (3) revolutionized the measurement of $[Ca^{2+}]_i$ in whole cell suspensions, populations of adherent cells, single cells, and in subcellular regions (see ref. 4). Fura-2 is a ratiometric dye in that when Ca^{2+} binds, the excitation spectrum shifts rightward. In the presence of Ca^{2+} , maximum Fura-2 fluorescence (at 510 nm emission) is observed at a wavelength of 340 nm and in Ca^{2+} -free conditions at 380 nm. Therefore, it follows that the concentration of free intracellular

Ca^{2+} is proportional to the ratio of fluorescence at 340/380. The Grynkiewicz equation describes this relationship (3):

$$[\text{Ca}^{2+}]_i (\text{nM}) = K_d \times [(R - R_{\min}) / R_{\max} - R] \times Sfb,$$

where K_d (for Ca^{2+} binding to Fura-2 at 37°C) = 225 nM, $R = 340/380$ ratio, $R_{\max} = 340/380$ ratio under Ca^{2+} -saturating conditions, $R_{\min} = 340/380$ ratio under Ca^{2+} -free conditions, and $Sfb =$ ratio of baseline fluorescence (380 nm) under Ca^{2+} -free and -bound conditions. The K_d for Ca^{2+} binding to Fura-2 decreases with decreasing temperature.

As noted in Chapter 1, Fura-2-free acid is Ca^{2+} sensitive but membrane impermeant. To effect cell loading, cells are incubated with Fura-2 pentaacetoxymethyl (AM) ester; this form of the dye is Ca^{2+} insensitive. Once inside the cell, esterase enzymes sequentially cleave the AM groups to leave Fura-2-free acid trapped inside the cell, where it is able to bind Ca^{2+} .

In this chapter the authors describe the use of Fura-2 to measure $[\text{Ca}^{2+}]_i$ in suspension of several different cell types (see ref. 4). The technique is quite straightforward and involves incubating cells with Fura-2/AM, a postincubation period to allow full de-esterification, and extensive washing.

In cell suspensions, an estimate of global changes in $[\text{Ca}^{2+}]_i$ can only be made. This is useful in combination with the currently available pharmacological agents to study sources of Ca^{2+} (intracellular vs. extracellular) in a given response and to screen for Ca^{2+} -mobilizing drugs and receptors. However, detailed information regarding subcellular localization requires more sophisticated measurements using standard subcellular imaging (see Chapter 6) or confocal microscopy (see Chapters 4 and 5).

2. Materials

2.1. Cell Culture

1. Undifferentiated SH-SY5Y human neuroblastoma cells (gift from Dr. J. L. Beidler, Sloane Kettering Institute, Rye, NJ).
2. Culture medium for SH-SY5Y cells: Minimum essential medium supplemented with 10% fetal calf serum (FCS), 2 mM glutamine, 100 IU/mL penicillin, 100 IU/mL streptomycin, and 2.5 µg/mL fungizone (see Note 1).
3. NG108-15 neuroblastoma X glioma hybrid cells (see Note 2).
4. Culture medium for NG108-15 cells: Dulbecco's minimum essential medium supplemented with 10% FCS, 2 mM glutamine, 100 IU/mL penicillin, 100 IU/mL streptomycin, 2.5 µg/mL fungizone, and HAT (hypoxanthine [0.1 mM], aminopterin [0.4 µM], thymidine [16 µM]) (see Note 1).

5. Chinese hamster ovary (CHO) cells expressing the recombinant δ opioid receptor (gift from Dr. L. A. Devi, Department of Pharmacology, New York University, NY).
6. Culture medium for CHO cells: HAMS F12 medium supplemented with 10% FCS, 100 IU/mL penicillin, 100 IU/mL streptomycin, 2.5 μ g/mL fungizone, and 100 μ g/mL genetin (see Notes 1 and 3).
7. HEK293 cells (human embryonic Kidney) expressing recombinant human urotensin II receptor (UT): These were cultured in minimal essential media containing 10% fetal bovine serum, 100 IU/mL penicillin and 100 μ g/mL streptomycin, 2.5 μ g/mL of fungizone, 2 mM L-glutamine, and 400 μ g/mL of geneticin (see Notes 1 and 3).

2.2. Buffers

1. Krebs HEPES buffer (for loading and washing): 143.3 mM Na^+ , 4.7 mM K^+ , 2.5 mM Ca^{2+} , 1.3 mM Mg^{2+} , 125.6 mM Cl^- , 25 mM HCO_3^- , 1.2 mM $H_2PO_4^-$, 1.2 mM SO_4^{2-} , 11.7 mM glucose, and 10 mM HEPES, pH 7.4 titrated with 10 M NaOH.
2. Nominally Ca^{2+} -free Krebs HEPES buffer, pH 7.4, as in item 1, omitting Ca^{2+} and adding 0.1 mM EGTA. This should be made in plastic beakers as glass leaches significant amounts of Ca^{2+} .
3. Low Na^+ Krebs HEPES buffer, pH 7.4, for depolarization: 43.3 mM Na^+ , 2.5 mM Ca^{2+} , 1.3 mM Mg^{2+} , 125.6 mM Cl^- , 25 mM HCO_3^- , 1.2 mM $H_2PO_4^-$, 1.2 mM SO_4^{2-} , 11.7 mM glucose, and 10 mM HEPES. With this buffer, 100 mM K^+ is added (see Note 4).
4. Cell harvest buffer: 10 mM HEPES-buffered 0.9% saline plus 0.05% EDTA, pH 7.4 (with 10 M NaOH).

2.3. General Reagents

1. Fura-2/AM (Sigma, Dorset, UK). Make up as a stock (1 mM) solution by dissolving in dimethylsulfoxide and storing aliquots (10 μ L) at -20°C until required.
2. Triton X-100 (Sigma). Make a stock (4%) solution in warmed water.
3. EGTA (Sigma). Make a stock (90 mM) solution in 1 M NaOH.
4. Probenecid (Sigma). Dissolve at 50 mg/mL (175 mM) stock in 1 M NaOH. Use at 2.5 mM in buffer (see Note 5).

3. Methods

3.1. Tissue Culture and Monolayer Harvesting

1. Maintain confluent monolayers (75 cm^2) of cells in the appropriate media.
2. Split one flask of confluent cells using trypsin (0.5 g/L)-EDTA (2 g/L, 5 mL) solution as supplied (see Note 1) into the

required number of experimental flasks, each containing 20 mL of supplemented media. After 2 days of incubation (37°C, 5% CO₂ incubator), remove the media and replace with 25 mL of fresh supplemented media.

3. Culture cells (feed 24 h before use with fresh medium) until confluent (use cells as soon as confluent—some cells require use slightly subconfluent to prevent stripping from the flask—this should be determined empirically).
4. On the day of the experiment, remove medium and add 5 mL of harvest buffer to cell monolayer.
5. Remove 5 mL of harvest buffer immediately, and add a further 5 mL of fresh harvest buffer and incubate at 37°C for ~5 min.
6. Gently tap the side of the flask to dislodge the adherent cell monolayer. Check under a microscope.
7. When all the cells are in suspension, transfer it to a centrifuge tube. Rinse the cells out of the flask by adding approx 15 mL of experimental buffer. Transfer this to the centrifuge tube.
8. Sediment at 500 × g in a low-speed centrifuge for 3–5 min.
9. Remove supernatant, dislodge the pellet, and resuspend the cells into 30 mL of fresh experimental buffer. Invert the tube three times and resediment at 500 × g for 3–5 min.
10. Repeat step 9 once more, and finally resuspend the pellet in 2 mL of experimental buffer.

3.2. Fura-2 Loading and Measurement of Intracellular Calcium

Optimal Fura-2 loading time and de-esterification time may vary depending on the cell type used, and hence it is recommended that these times should be adjusted accordingly. The protocol used by the authors in a range of cell types is as follows:

1. Incubate cell suspensions with 5 μM of Fura-2/AM in 2 mL (10 μL of 1 mM Fura-2/AM) for 30 min at 37°C in the dark.
2. Resuspend in Krebs/HEPES buffer to a total of 30 mL.
3. Incubate a further 20 min at room temperature in the dark to allow for de-esterification of the Fura-2/AM.
4. Sediment the cells (500 × g for 3 min) and resuspend in 30 mL of Krebs/HEPES.
5. Sediment (500 × g for 3 min) and resuspend in buffer allowing 2 mL per determination (see Note 6).
6. Place cell suspensions (2 mL) in a quartz cuvette containing a magnetic stirrer and place in the cuvette holder, which is maintained at 37°C with a water jacket.
7. Simultaneously monitor and, if possible, display 340 and 380 excitation intensity (at 510 emission). Signal sampling should be set according to the kinetics of the changes in [Ca²⁺]_i; the authors routinely make one ratio measurement per second (see Note 7).

8. Following establishment of stable 340 and 380 recordings, add compounds to be tested (see Note 8).
9. Maintain stock of loaded cells on ice (see Note 9).
10. Calibrate the fluorescence signal as follows (see Note 10):
 - (a) Add 0.1% Triton X-100 (50 μ L) to the cuvette to produce cell lysis and liberate Fura-2 into a Ca^{2+} -containing buffer. Under these conditions, Fura-2 saturates with Ca^{2+} and maximum fluorescence ratio (R_{max}) is determined (see Note 11).
 - (b) 4.5 mM EGTA (150 μ L), pH > 8.0, to chelate Ca^{2+} and determine minimum fluorescence ratio (R_{min}) (see Note 12).
 - (c) Substitute R_{max} , R_{min} , and the derived Sfb along with measured R values from cell suspensions into the Grynkiewicz equation (3) and estimate $[Ca^{2+}]_i$. This can be accomplished using a spreadsheet-type program, although the authors use FLDM software associated with the fluorimeter (see Note 7).

3.3. Examples of $[Ca^{2+}]_i$ Measurements Made in Cell Suspensions

3.3.1. Carbachol Stimulation in SH-SY5Y Cells

SH-SY5Y cells express a homogenous population of M_3 muscarinic receptors that are coupled to phospholipase C and increased $[Ca^{2+}]_i$. The authors have shown that this $[Ca^{2+}]_i$ is biphasic, with a peak phase mediated by release from intracellular stores and a plateau phase resulting from Ca^{2+} entry across the plasma membrane (4, 5). A typical experiment is described below:

1. Cells are harvested (see Subheading 3.1, steps 4–10).
2. Suspensions are loaded with Fura-2 as described in Subheading 3.2.
3. Following de-esterification and washing, cells are placed into a cuvette and 340/380 nm fluorescence monitored.
4. Stocks of loaded cells are kept on ice.
5. As can be seen in Fig. 1, the response to 10 μ M carbachol was biphasic (Fig. 1a). Also shown for comparison is a typical 340/380 nm recording (Fig. 1b) and the derived 340/380 ratio (Fig. 1c).

3.3.2. K^+ Stimulation in NG108-15 Cells

The authors have previously reported a nifedipine-sensitive increase in $[Ca^{2+}]_i$ in NG108-15 cells in response to depolarization with high K^+ (6). A typical experiment is described next:

1. Cells are harvested (see Subheading 3.1, steps 4–10).
2. Suspensions are loaded with Fura-2 as described in Subheading 3.2.

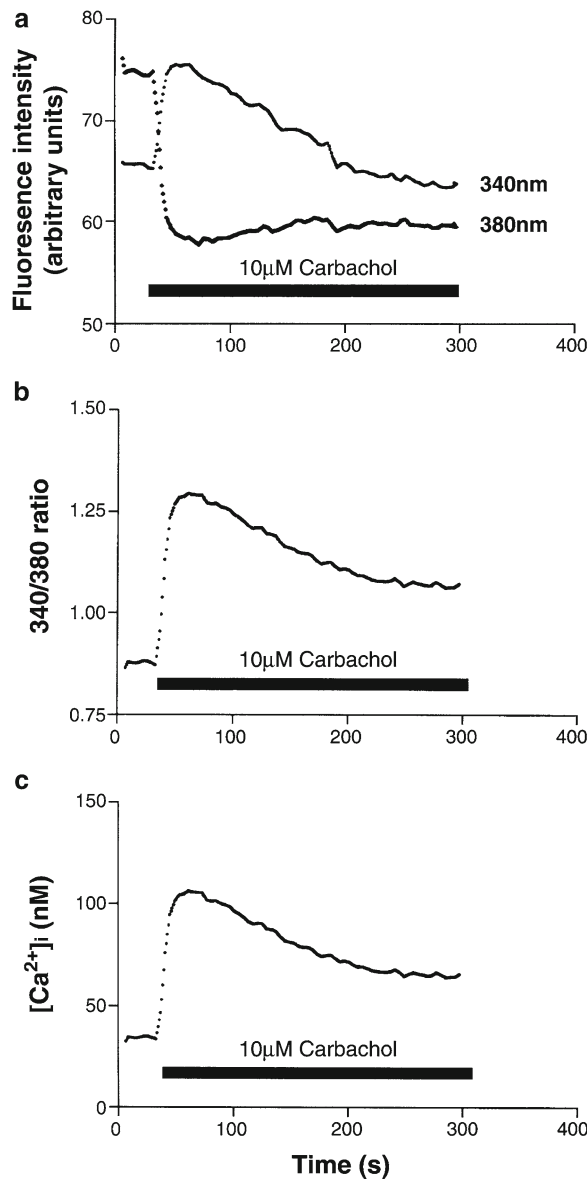


Fig. 1. Carbachol increases $[Ca^{2+}]_i$ in suspensions of SH-SY5Y cells. (a) Emission at 340 and 380 nm excitation. Note the antiparallel movement of both traces. (b) Derived 340/380 ratio and (c) $[Ca^{2+}]_i$ after calibration. In these studies R_{max} , R_{min} , and Sfb were 4.61, 0.64, and 2.39, respectively. Autofluorescence at 340nm and 380nm were 1.67 and 3.18 arbitrary units $\leq 2\%$ of cell signal.

3. Following de-esterification and washing in low Na⁺ buffer (Subheading 2.2, item 3), cells are placed into a cuvette and 340/380 nm fluorescence monitored.
4. Cells are challenged with 100 mM K⁺.

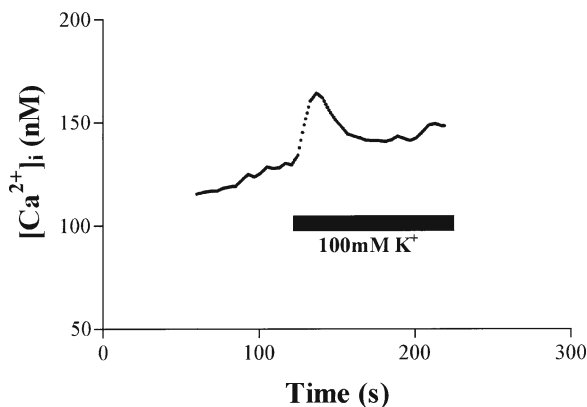


Fig. 2. K^+ depolarization (100 mM, bar) of NG108-15 cells results in a monophasic increase in $[Ca^{2+}]_i$. Representative trace modified from ref. (6).

5. Stocks of loaded cells are kept on ice.

6. As can be seen in Fig. 2, depolarization with K^+ produces a monophasic increase in $[Ca^{2+}]_i$. This response is mediated by L-type, voltage-sensitive Ca^{2+} channels (6).

3.3.3. D-[Pen^{2,5}]enkephalin and Adenosine Triphosphate Stimulation in CHO Cells

CHO cells have been shown to express low levels of the multidrug-resistance efflux pump, P-glycoprotein (7). It is possible that this pump is responsible for extrusion of Fura-2 from the cell and, hence, increasing baseline measurements. Probenecid is an organic anion transport inhibitor, originally developed to prevent excretion of penicillin from the kidney, that has been shown to block efflux of Fura-2 (7, 8). The authors have noted that with the use of CHO cells expressing recombinant opioid receptors (and endogenous purinergic receptors (9)), high rates of Fura-2 leakage can be reduced by inclusion of probenecid (Fig. 3a). A typical experiment is described below.

1. Cells are harvested (see Subheading 3.1, steps 4–10).
2. CHO cell suspensions are loaded, washed, and then de-esterified in the presence of 2.5 mM probenecid as noted in Subheading 3.2.
3. Cells are challenged with either 1 μ M DPDPE or 100 μ M adenosine triphosphate (ATP).
4. Between determinations, the stock of loaded cells is kept on ice.
5. As can be clearly seen in Fig. 3a, Fura-2 leakage was significantly reduced in the presence of probenecid. However, the peak phase response to ATP was also reduced. Careful characterization of the effects of probenecid on the signaling process under study should always be made (see Note 5).

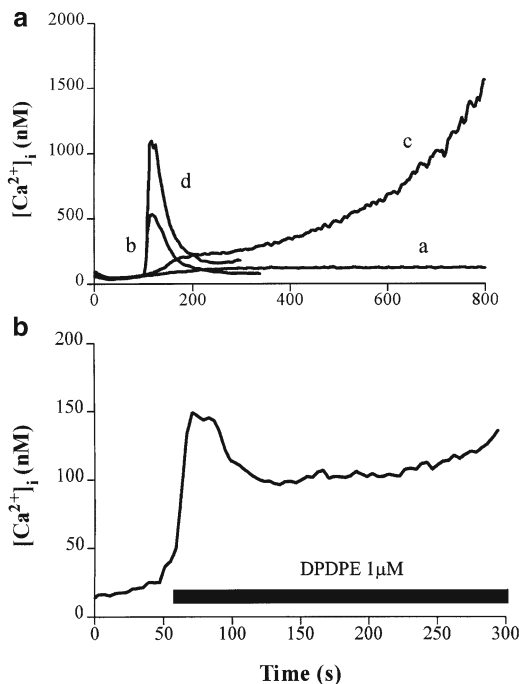


Fig. 3. (a) Representative time course showing effects of 2.5 mM probenecid in CHO cells expressing the recombinant δ opioid receptor. Probenecid reduced fura-2 leakage in unstimulated cells (a) when compared to unstimulated control (c) and reduced the peak and plateau phases of 100 μ M ATP-stimulated (b) when compared to stimulated control (d). (b) 1 μ M DPDPE increased $[Ca^{2+}]_i$ in CHO cells expressing the recombinant δ opioid receptor. Probenecid was not included in this experiment.

3.3.4. Urotensin II Stimulation in HEK Cells

HEK cells are also very amenable to use in this simple fluorimetric protocol with Fura-2. We have not found it necessary to use probenecid with these cells. A typical experiment is described below for cells expressing the recombinant human urotensin II receptor. Cells are stimulated with the endogenous ligand urotensin II, which *in vivo* is involved in cardiovascular physiology (10).

1. Cells are harvested (see Subheading 3.1, steps 4–10).
2. HEK cell suspensions are loaded, washed, and then de-esterified as noted in Subheading 3.2.
3. Cells are challenged with increasing concentrations of Urotensin II.
4. Between determinations, the stock of loaded cells is kept on ice.
5. Figure 4 shows a typical data set for time course and concentration–response experiments.

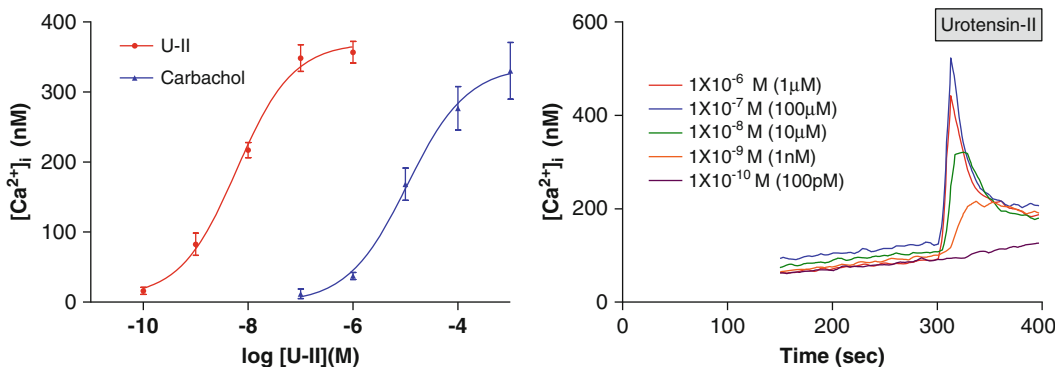


Fig. 4. U-II induced a concentration-dependent increase in intracellular calcium. (Left) Representative temporal calcium responses at each U-II concentration investigated. The duration of U-II stimulation is indicated by the bar. (Right) Concentration-response curve showing the maximum calcium response at each U-II concentration investigated. Carbachol is added for comparison (which activated muscarinic receptors in these cells). Data are presented as mean \pm SEM of $n=5$ experiments and are unpublished.

4. Notes

1. All tissue culture media and reagents are supplied by Life Technologies, Paisley, Scotland.
2. From European Collection of Animal Cell Cultures (Web site <http://www.biotech.ist.unige.it/cldb/cname-dh.html>).
3. Where geneticin (G418) or similar is included in cells expressing recombinant receptors and so on as a selection agent, only the stock cultures should be treated. Experimental cultures should be free of selection medium as G418 may inhibit phospholipase C-mediated responses.
4. For varying levels of K^+ , adjust Na^+ accordingly.
5. Probenecid is insoluble at millimolar concentrations in Krebs HEPES buffer. Therefore, a stock solution was made at 50 mg/mL (175 mM) in 1 M NaOH. This was then diluted in Krebs HEPES buffer prior to addition of $CaCl_2$ (2.5 mM). The Krebs HEPES buffer containing probenecid (NaOH) was set at pH 7.4 by the addition of HCl (10 M, ~100 μL). Caution should be used when using probenecid to reduce Fura-2 leakage as the authors have shown that agonist-induced increases in $[Ca^{2+}]_i$ could be inhibited by this agent (see Fig. 2).
6. One confluent 75-cm² flask of SH-SY5Y cells is sufficient to give five determinations (i.e., resuspend in 10 mL of buffer). For larger number of determinations, load more flasks. However, remember that as the loaded cells stand they leak Fura-2, leading to a time-dependent increase in basal. This can be overcome to some extent by sedimenting and resuspending

aliquots of the loaded suspension periodically. Some cells leak Fura-2 more than others, notably CHO cells (see below).

7. The authors routinely use a Perkin-Elmer LS50B fluorimeter (Beaconsfield, UK) equipped with the software FLDM. Files are saved to disk and 340/380 ratios can be converted to $[Ca^{2+}]_i$ following calibration. It is always advisable to be familiar with the software that controls the configuration and experimental settings of the fluorimeter. Different software packages are available, and for information and troubleshooting the reader is advised to consult the software supplier.
8. For drugs make up 40 times more concentrated so that when 50 μL is added to 2 mL of buffer + cells, the desired concentration is achieved. Additions are made as swiftly as possible to avoid light entering the fluorimeter. All agents used should be tested for fluorescence properties. This can be accomplished by adding to a cuvette containing nominally Ca^{2+} -free buffer (containing several micromolar Ca^{2+}) and Fura-2-free acid (0.5 μM).
9. The authors have noted that de-esterified cells that extrude Fura-2 should be maintained on ice between experiments as this reduces the loss of Fura-2. In addition, care should be taken to ensure that Fura-2-loaded cells are used for experiments immediately after de-esterification.
10. For cells loaded from a single batch of cells, the authors make a single calibration (i.e., they do not calibrate each cuvette of cells), normally the last cuvette used. This needs to be checked for all cell lines and they recommend a comparison of individually calibrated data with all data calibrated from the first and last run of the batch.
11. Addition of Triton X-100 causes complete cell lysis and an increase in 340 and a decrease in 380 nm fluorescence. A globular residue remains in the cuvette, and, therefore, the reusable quartz cuvette should be thoroughly rinsed between experiments using deionized water.
12. Autofluorescence is an important issue for many cell types. This is the fluorescence produced from unloaded cells and can be determined in two ways. First, place an aliquot of unloaded cells into the fluorimeter and measure the fluorescence at 340 and 380 nm (FLDM software has this capability). The main drawback with this method is that the density of unloaded cells should be identical to the density of cells used for Ca^{2+} measurements. The second method is to add 0.1 mM Mn^{2+} to the lysed cell suspension after determination of R_{min} . In this protocol, the quenching properties of Mn^{2+} are utilized. In the authors' studies using SH-SY5Y, NG108-15, and CHO cells, they have found the autofluorescence to be negligible when

compared to the signal from loaded cells and, therefore, do not routinely subtract autofluorescence (e.g., see Fig. 1). However, they recommend that whenever using a new cell line, autofluorescence should be assessed.

References

1. Clapham D (1995) Calcium signalling. *Cell* 80:259–268
2. Berridge MJ (1993) Inositol trisphosphate and Ca^{2+} signalling. *Nature* 361:315–325
3. Grynkiewicz G, Poenie M, Tsien RY (1985) A new generation of Ca^{2+} indicators with greatly improved fluorescence properties. *J Biol Chem* 260:3440–3449
4. Lambert DG, Wojcikiewicz RJH, Safrany ST, Whitham EM, Nahorski SR (1992) Muscarinic receptors, phosphoinositide metabolism and intracellular calcium in neuronal cells. *Prog Neuropsychopharmacol Biol Psychiatry* 16: 253–270
5. Cobbold PH, Rink RJ (1987) Fluorescence and bioluminescence measurement of cytoplasmic free calcium. *Biochem J* 248:313–328
6. Hirota K, Lambert DG (1997) A comparative study of L-type voltage sensitive Ca^{2+} channels in rat brain regions and cultured neuronal cells. *Neurosci Lett* 223:169–172
7. Brezden CB, Hedley DW, Rauth AM (1994) Constitutive expression of P-glycoprotein as a determinant of loading with fluorescent calcium probes. *Cytometry* 17:343–348
8. Edelman JL, Kajimura M, Woldemussie E, Sachs G (1994) Differential effects of carbachol on calcium entry and release in CHO cells expressing the m3 muscarinic receptor. *Cell Calcium* 16:181–193
9. Iredale PA, Hill SJ (1993) Increases in intracellular calcium via activation of an endogenous P(2)-purinoceptor in cultured CHO-k1 cells. *Br J Pharmacol* 110:1305–1310
10. McDonald J, Batuwangala M, Lambert DG (2007) Role of urotensin II and its receptor in health and disease. *J Anesth* 3:378–389

Part II

Specialist Measurement Systems

Chapter 3

Confocal Microscopy: Theory and Applications for Cellular Signaling

**Stephen C. Tovey, Paul J. Brighton, Edward T.W. Bampton,
Yan Huang, and Gary B. Willars**

Abstract

The development of confocal microscopy and the commercial availability of confocal microscopes have provided many laboratories with an extremely powerful approach to examine cellular structure and function. Allied with the development of suitable tools, it is now possible to interrogate a wide range of structural and functional aspects on both fixed and live cells. Here we describe the basic principles underlying confocal microscopy and provide methodological accounts of how it can be used to study aspects related particularly (but not exclusively) to the expression, activation, and regulation of signaling by G-protein-coupled receptors. Specifically we provide detailed protocols for examining: the cellular expression and distribution of proteins by immunocytochemistry; cytoplasmic and organelle Ca^{2+} signaling using fluorescent indicators; second messenger generation using fluorescently tagged biosensors; and ligand/receptor internalization using fluorescently tagged peptide agonists and receptors.

Key words: Confocal microscopy, Fluorescence, Immunofluorescence, Ca^{2+} indicators, Biosensors, Phospholipase C, Receptor internalization, Fluorescent ligand, Green fluorescent protein

1. Introduction

The main aim of this chapter is to introduce some of the basic principles behind the technique of confocal microscopy. Subsequently, we describe how recent advances in this technology, allied with the continued development of Ca^{2+} -sensitive chemical and genetically encoded fluorescent probes, have provided us with methodologies for unraveling the complexities of Ca^{2+} signaling at the cellular and subcellular level. Specifically we provide detailed methodologies for the study of Ca^{2+} signaling within the cytosol and within subcellular compartments using Ca^{2+} -sensitive fluorescent indicators in conjunction with confocal microscopy. In addition, the chapter describes a number of confocal-based

methodologies that can be used to study other aspects of intracellular signaling, such as immunofluorescent labeling, use of fluorescently tagged biosensors for measuring phospholipase C (PLC) activity, and use of fluorescently tagged ligands and receptors for measuring ligand and receptor internalization. It should be noted that several excellent texts are available that cover the principle and practice of confocal microscopy in relation to biological systems in far greater depth than is possible here (1–3).

1.1. History of Confocal Microscopy

Marvin Minsky, a postdoctoral fellow at Harvard University, originally developed the concept of the confocal microscope in the early 1950s. Subsequently, in 1957, Minsky filed a patent for his invention (patented in 1961). This original design was not sufficiently sensitive for fluorescence and was ill-suited to biological samples as the stage rather than the light beam moved, leading to vibration artifacts. It was not until the late 1970s and early 1980s that other scientists took advantage of his invention and developed the first single-beam laser scanning confocal microscope (LSCM) for use in biological research (1). Over the past twenty years the increase in commercially available confocal microscopes has led to them becoming commonplace in many life science departments throughout the world. The definition of confocal imaging (and hence confocality) is the illumination and detection of a single point within a specimen at a resolution close to the theoretical diffraction-limited maximum (1). Thus, a confocal microscope allows the nonintrusive optical sectioning of biological specimens in a technique known as “optical slicing” allowing thin optical sections to be obtained from “thick” samples. This is achieved by the positioning of two pinholes at appropriate points in the light path. The first is required to produce a sharp intense point of illuminating light (minimizing scatter from excitation light), whilst the second acts to process transmitted light from the specimen. Confocal microscopes are routinely used in the fields of biological research, chemical analysis, and materials testing. In biological research the confocal microscope has been used extensively to study three-dimensional structures in both fixed and live material.

The advent of confocal imaging technology has proven particularly useful in the field of fluorescence, where a wide variety of fluorescent tags and fluorescent indicators are available for the study of biological systems. The main advantage of a confocal microscope over a conventional fluorescence microscope is the ability to visualize a thin optical section within a cell or a tissue by virtue of rejecting the out-of-focus light originating from excited fluorophores throughout the rest of the sample. This is obviously of great utility for the study of intracellular Ca^{2+} signals, and the parallel development of both fluorescent Ca^{2+} indicators and confocal techniques has enabled the detection of Ca^{2+} release in defined regions of the cell at spatial and temporal resolutions that were previously unimaginable.

1.2. Principles of Confocal Microscopy

The main benefit of a confocal microscope is the improvement it gives in both horizontal and vertical resolution over conventional fluorescence microscopes. The way in which a confocal microscope achieves this increased resolution (by rejecting out-of-focus light) inevitably means that a powerful source of illumination is required. Typically, the source of illumination is a laser, hence the term LSCM, as lasers represent a bright, stable, and easy-to-focus source of light with minimal divergence. The requirement for a high-intensity light source is also one of the main drawbacks of confocal microscopy, as it exacerbates problems such as cytotoxicity of live material and photobleaching of fluorophores. Added to this, conventional continuous-wave gas lasers (such as Ar, Kr/Ar, or He/Ne) only produce excitation light within a restricted range of the visible spectrum, thereby reducing the fluorescent indicators available for use compared to conventional fluorescence microscopy. However, it should be pointed out that most lasers have more than one excitation line. For example, a Kr/Ar laser can have several lines, including 458, 488, 568, and 647 nm. In addition, recent advances in laser technology (i.e., the development of diode-pumped solid state (DPSS) and diode-based lasers) have resulted in many modern commercial instruments being equipped with three to five laser systems, each controlled by high-speed acousto-optic tunable filters (AOTFs) to allow precise regulation of wavelength selection and flexible control of laser intensity. It should also be noted that UV lasers are available for confocal microscopes, but they remain expensive and require expensive optics (e.g., UV-corrected objectives).

The LSCM works by repeatedly scanning a laser beam across the sample and collecting light emitted from the sample through a pinhole aperture. As described above, it is this pinhole aperture that is responsible for giving confocality, in that it is responsible for rejecting the out-of-focus light arising from the rest of the sample (Fig. 1). The narrower the pinhole is, the thinner the section and the more confocal the image; conversely if the pinhole is fully open then confocality is lost. The pinhole also dictates that light can only be collected from a single point within a sample at any given time, so in order to achieve a reconstructed two-dimensional (2D) image of the sample the laser beam must be scanned across the specimen (so-called point scanning) with a detector recording the single point outputs as a 2D array. The transmitted light (photons) collected through the pinhole aperture is normally detected by one or more photomultiplier tubes (PMTs) and converted into a flow of electrical signals. High-end confocal microscope systems are usually equipped with several PMTs, and/or detectors such as avalanche photodiodes (APDs) with increased quantum-efficiency, that enable simultaneous imaging of different fluorophores in multi-labeled specimens. Images can then be recreated on a computer screen or a cathode ray tube and subsequently collated and stored as a digital image or a

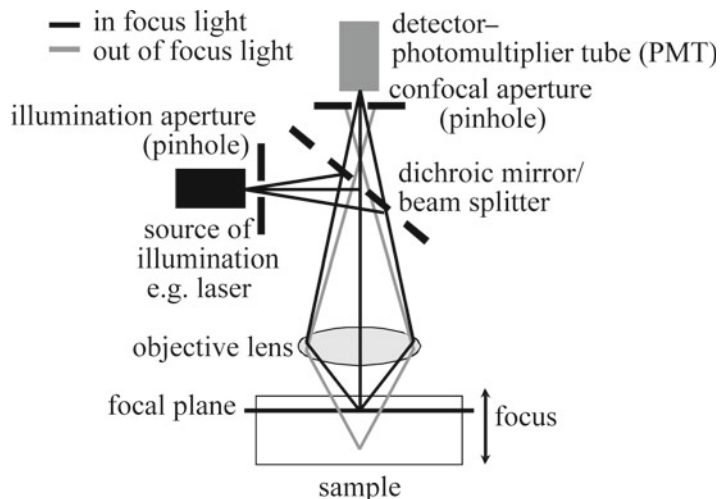


Fig. 1. Simplified light path of a standard LSCM. Illuminating laser light is reflected onto the objective lens by a dichroic mirror. The objective lens focuses the excitation light onto the sample. In-focus fluorescence that is emitted by the sample passes through the dichroic mirror and is detected by a PMT. Out-of-focus fluorescence light is rejected by the confocal aperture. Any illuminating light reflecting back from the sample is reflected away from the detector by the dichroic mirror.

series of digital images. Recent advances in laser systems, filters, photodetectors, computer technology, data storage, and fluorophores have all aided progress in the field of confocal imaging.

At present there are two main types of commercially available confocal microscopes that can be categorized by the way in which the excitation light is scanned onto the sample.

1.2.1. Standard Scanning

This group of confocal microscopes are the most common and are generally considered to have the best spatial resolution, but they are only capable of relatively modest scan rates (i.e., have limited temporal resolution). This group includes, for example, LSCMs such as the Zeiss LSM 710, Leica TCS SP5, Nikon C2, and Olympus Fluoview FV1000. In this case, scanning is usually achieved by the use of two vibrating, mechanically driven mirrors to guide the laser beam across the sample in both the vertical and horizontal direction in a raster pattern. With these confocal microscopes the speed of scanning is governed entirely by the mechanical movement of a pair of computer-controlled galvanometric mirrors, leading to a limitation in the time resolution that can be achieved (typically 0.5–5 Hz). For most applications this is not a problem, but when studying small but fast subcellular Ca^{2+} release events or even the rapid onset of a whole-cell Ca^{2+} wave, then it is often desirable to achieve a greater temporal resolution. This can be achieved by reducing the scan area or employing a line scan, in which a particular region of the sample is repeatedly and rapidly

scanned in one dimension (1D) only, meaning the movement of only one mirror is required. Although this method provides high temporal resolution, information may be lost as the image is spatially restricted. Alternatively many high-end confocal systems incorporate tandem scanners which combine a conventional scanner for high resolution with a rapidly oscillating resonant scanner for high-speed video-rate imaging (30 Hz or higher). In addition, acousto-optical deflectors (AODs), as used in LSCMs such as the Noran Oz and more recently VisiTech Eye, also enable video-rate confocal imaging (50 Hz or much higher). Here an AOD device replaces the mirror responsible for horizontal scanning and the laser beam is rapidly scanned across the sample by nonmechanical deflection through an arrangement of static prisms and AODs arranged in two dimensions (4–7). The disadvantage of employing resonant scanners or AODs is that the increase in temporal resolution they achieve tends to result in a decrease in the signal-to-noise ratio and consequently a loss of spatial resolution.

1.2.2. Spinning Disk

Spinning disk confocal microscopes that use multiple pinholes (or slits such as the Olympus DSU) to construct the confocal image are an alternative to the standard LSCM. Commercial systems based on Yokogawa Electric Corporation's CSU-X1 spinning disk technology include the Perkin Elmer UltraVIEW VoX, Andor Revolution® XD, Leica SD AF, and Zeiss cell observer® SD.

In these machines, the light beam is scanned across the specimen using a rapidly rotating disk containing thousands of pinholes arranged in a spiral pattern (Nipkow disk). In this manner, all parts of the sample are illuminated “quasi-simultaneously” and emitted light returns through the pinholes, thereby rejecting the out-of-focus blur from the rest of the sample. Each hole effectively behaves like an individual confocal microscope and because so many points are scanned simultaneously, these systems offer advantages when it is essential to acquire data as rapidly as possible. Initially, spinning disk systems used illumination light very inefficiently but this has been overcome by using an array of microlenses to focus illumination light upon the pinholes.

This type of system has the advantage of working with both lasers and other light sources, such as mercury arc lamps, potentially reducing the cost of the light source and removing some of the problems commonly associated with the use of lasers. It also allows the use of real-time color imaging with direct viewing (through an eyepiece or ocular) as the emitted light does not need to be de-scanned as with other confocal microscopes. This is because the “quasi-simultaneous” illumination effectively produces a multipoint scanning pattern that allows the image to be formed in real time and focused onto a charge-coupled device (CCD) or highly sensitive QE electron multiplying CCD (EMCCD) camera for acquisition.

1.3. Applications of Confocal Microscopy with Relation to Ca^{2+} Signaling

1.3.1. Fluorescent Ca^{2+} Indicators

Confocal microscopy provides an incredibly powerful and versatile tool for measuring changes in intracellular $[\text{Ca}^{2+}]$ ($[\text{Ca}^{2+}]_i$). However, there are many points to consider before using a confocal microscope to monitor changes in $[\text{Ca}^{2+}]_i$. One such consideration is whether to use a fluorescent Ca^{2+} dye or a specifically targeted genetically encoded Ca^{2+} indicator (GECI) as the sensor; this will depend on both the desired application and the type of confocal setup that is available (lasers/filters/detectors, etc.) as well as the cell type under study. Added to this are the obvious considerations regarding confocal instrumentation and whether spatial or temporal resolution is of paramount importance (or indeed both). It should also be remembered that confocal microscopes are still relatively expensive to purchase, run, and maintain, and hence cost may also be a consideration.

One of the main uses of confocal microscopes in the Ca^{2+} -signaling field has been the study of global and subcellular (including organelle) Ca^{2+} signals using fluorescent indicators sensitive to changes in $[\text{Ca}^{2+}]$. Most of these Ca^{2+} indicators are based on the Ca^{2+} chelators, EGTA and BAPTA, which have been modified to incorporate fluorescent reporter groups (8,9). The utility of such indicators was greatly enhanced by the development of AM-ester forms of the indicators that can be passively loaded into cells (8). Two main classes of Ca^{2+} indicators have evolved, these being single-wavelength (non-ratiometric) and dual-wavelength (ratiometric) indicators. In the former case, increases in $[\text{Ca}^{2+}]$ are determined by changes in the fluorescence intensity of the indicator (e.g., fluo-3 or fluo-4) at a single wavelength which occurs in the absence of any spectral shift. Generally there is an increase in fluorescence upon binding Ca^{2+} , although a decrease is seen with the visible-light excitable fura-2 analogue fura red. As an example, the Ca^{2+} -bound form of fluo-3 is ~40 times brighter than the Ca^{2+} -free form (9). The main drawback with single-wavelength indicators is their very reliance on the measurement of fluorescence at a single wavelength as an index of $[\text{Ca}^{2+}]$. This means that care must be taken when calculating $[\text{Ca}^{2+}]$ from raw fluorescence levels as this can be influenced by aspects other than changes in $[\text{Ca}^{2+}]$. This may occur, for example, as a consequence of alterations in cell thickness (e.g., in contractile cells such as cardiac myocytes), loss of indicator from the cell (due to leakage or active extrusion), or photobleaching. Photobleaching is the irreversible damage of Ca^{2+} indicator molecules following exposure to the light used for excitation, resulting in a loss of fluorescence related to the duration of exposure to the source of excitation. In the case of dual-wavelength Ca^{2+} indicators, such as fura-2 and indo-1 (8), changes in $[\text{Ca}^{2+}]$ still lead to changes in excitation/emission intensity, but additionally the Ca^{2+} -free and Ca^{2+} -bound forms have distinct spectra. With fura-2, Ca^{2+} -dependent spectral shifts occur in the excitation spectra, whereas for indo-1 significant

shifts are seen in the emission spectra. With dual-wavelength indicators, the Ca^{2+} -free and Ca^{2+} -bound forms of the indicator have spectral peaks at different wavelengths and this allows a ratio to be calculated at any given time during an experiment. This ratio is independent of the indicator concentration and therefore minimizes some of the artifacts that can arise when using single-wavelength indicators. Despite the obvious advantages of dual-wavelength (ratiometric) indicators, the most popular indicators for confocal Ca^{2+} imaging are undoubtedly single-wavelength indicators from the fluo, calcium-green, or oregon green 488 BAPTA family (i.e., those excited by a standard 488 nm laser line). In the main, this is because most single-wavelength indicators have excitation maxima in the visible part of the spectrum, making them compatible with the standard laser lines on most confocal microscopes. Conversely, both fura-2 and indo-1 are excited in the UV part of the spectrum, leading to comparatively weak emission along with the added expense of a UV laser for excitation and microscope objectives optically corrected for UV light. Ratiometric measurements with visible wavelength indicators have been made using simultaneous loading of fluo-3 and fura-red and exploiting the reciprocal changes in fluorescence emission upon Ca^{2+} binding (10, 11). Alternatively, ratiometric measurements with fluo-3 have been achieved by co-loading with a spectrally distinct Ca^{2+} -insensitive dye such as celltracker orange (12). Methods utilizing two dyes, however, have the drawback that reproducible measurements can only be performed if both dyes load the cells at the same rate to achieve a reproducible ratio of dye concentrations. In order to maintain the ratio of dye concentrations it also requires both dyes to be equally affected by photobleaching, diffusion, and transportation out of the cell or into organelles.

The original single-wavelength Ca^{2+} -sensitive indicator was quin-2 (13, 14) but this was superseded by a variety of indicators based on either fluorescein (fluo-3, fluo-4, fluo-8, calcium green) or rhodamine-like chromophores (calcium orange, calcium crimson, rhod-2). The number of single-wavelength indicators seems to increase annually and careful consideration should be given to the choice of indicator for particular experimental purposes. Firstly, the likely amplitude (i.e., concentration) of Ca^{2+} signals should be considered. For example, for low-amplitude Ca^{2+} signals, the affinity of the Ca^{2+} indicator should not be too low; otherwise the signals will be undetectable. Conversely, higher affinity indicators may resolve small signals but saturate with larger signals. The *in vitro* K_d values of most commercially available Ca^{2+} indicators can be found on the Molecular Probes Web site (<http://www.invitrogen.com/site/us/en/home/brands/Molecular-Probes.html>). One of the main advantages of an indicator such as fluo-3 is that it has a low level of fluorescence at resting cytoplasmic $[\text{Ca}^{2+}]$ and exhibits a large increase in fluorescence upon binding Ca^{2+} , thus ensuring a large

dynamic range for detecting Ca^{2+} signals of varying size (15). Conversely, indicators such as calcium green and fluo-4 were designed to have a higher level of fluorescence at resting $[\text{Ca}^{2+}]_i$, allowing them to be used in cells where subcellular regions need to be identified and clearly defined (e.g., the dendrites and dendritic spines of neurons). The penalty for this increased resting fluorescence is a decrease in the dynamic range of the indicator, restricting the amplitude of Ca^{2+} signals that can be visualized. The main difficulties associated with the use of single-wavelength dyes are poor indicator loading, dye compartmentalization, dye leakage or extrusion, and, especially in the case of confocal imaging, photobleaching. By definition, having increased confocality means that the signal is being collected from a much smaller volume and hence fewer molecules of fluorophore are available for imaging. In addition, a high-intensity light source is required to maintain an adequate signal for detection. Both of these issues mean that photobleaching can be a major difficulty during confocal imaging of Ca^{2+} . To counteract this, dyes including calcium orange and oregon green 488 BAPTA have been developed that are less prone to photobleaching, although many of these have other drawbacks such as a poor dynamic range (15). The advent of green fluorescent protein (GFP) and related fluorescent proteins has led to a desire to image Ca^{2+} in cells transfected with GFP-tagged proteins of interest. This type of experiment requires a degree of caution as the spectral properties of GFP (and its many variants) can overlap with many common Ca^{2+} indicators leading to possible spectral interference and resultant artifacts (16), although there is now a range of monomeric red fluorescent proteins available that are spectrally distinct from many of the Ca^{2+} indicators. Furthermore, Ca^{2+} imaging in cells transfected with, for example, enhanced GFP (eGFP)-tagged proteins is possible by using 488 nm-excited dyes with a sufficiently large Stokes shift to isolate emission from GFP (i.e., fura-red) or alternatively red-shifted fluorescent Ca^{2+} indicators such as x-rhod-1.

1.3.2. Protein-Based Fluorescent Ca^{2+} Indicators

As discussed in the previous section, the use of synthetic, small-molecule fluorescent indicators has greatly increased our understanding of Ca^{2+} signals at the single-cell level. However, with the exception of rhod-2 that preferentially localizes to the mitochondria and mag-fluo-4/fluo-5N that have been used to measure endoplasmic reticulum (ER) Ca^{2+} levels (17), dyes are either difficult to or cannot be targeted to specific intracellular organelles or indeed specific regions within a tissue/organism. The Ca^{2+} -sensitive chemiluminescent protein aequorin, isolated from the marine jellyfish *Aequorea victoria*, has previously been genetically modified to allow targeting to specific intracellular organelles where it can act as a specific sensor for Ca^{2+} (18). However, aequorin signals are weak and difficult to measure at the single-cell level (19, 20). This leads to the development of a variety of GECIs based on

another protein isolated from *Aequorea victoria*, namely, GFP and its genetically engineered mutants (e.g., the blue-shifted cyan fluorescent protein (CFP) and the red-shifted yellow fluorescent protein (YFP)). GFP has the advantage of being excited in the visible spectrum and also of being bright enough to be of use in confocal microscopy. Two main categories of GFP-based GECIs have been developed: (1) those where Ca^{2+} binding to a Ca^{2+} -responsive element affects FRET (Fluorescence or Förster Resonance Energy Transfer) between two fluorescent proteins, e.g., cameleons (21–24), and (2) those where the Ca^{2+} -responsive element is inserted into a single fluorescent protein and Ca^{2+} binding modulates the protonation state of the chromophore, e.g., camgaroos, (25, 26), Pericams (27), G-CaMPs (28–30), “Case” sensors (31), and grafted EF-hands (32) (covered in detail in refs. 19, 20, 33). The majority of these sensors are based on the Ca^{2+} binding properties of the protein calmodulin (CaM) or portions thereof, and rely on the fact that when CaM binds Ca^{2+} it undergoes a conformational change. The early cameleons were based on a fusion protein of CaM and its target peptide M13 (peptide from skeletal muscle myosin light chain kinase). The fusion protein was tagged at the C-terminus of CaM with CFP and the N-terminus of M13 with YFP (21, 22). Upon binding Ca^{2+} , CaM undergoes a conformational change that brings the two fluorophores closer together allowing FRET to occur (see Note 1). Hence, an increase in FRET corresponds to an increase in $[\text{Ca}^{2+}]_i$ (21, 22). At a similar time to the development of cameleons another sensor, FIP-CB_{SM}, based on a similar principle was developed (34). In this case the probe is based on the M13 peptide tagged at either end with blue and green varieties of GFP. As $[\text{Ca}^{2+}]$ increases, Ca^{2+} -bound CaM binds to the M13 peptide leading to a conformational change and a decrease in FRET (34). Further genetic exploitation of GFP led to the development of the camgaroos, pericams, G-CaMPs, “Case” sensors, and grafted EF-hands (25–32). The original camgaroo sensor was constructed by inserting the sequence encoding CaM at position Tyr145 of YFP. The binding of Ca^{2+} to this sensor leads to a conformational change in the CaM that causes a sevenfold increase in the brightness of YFP (25). Pericams are the result of further genetic modifications of YFP, in which case a circularly permuted variant of YFP (cpYFP) was created, with the original carboxy and amino terminals fused by a linker peptide. The YFP was then cleaved elsewhere in its sequence, creating new carboxy and amino terminals that were then fused to CaM and the M13 peptide, respectively, in effect making a “YFP sandwich” (27). Subtle mutations in the YFP sequence have led to the generation of several varieties of pericam: flash pericam that becomes brighter upon binding Ca^{2+} ; inverse pericam that becomes less bright; and ratiometric pericam in which there is a spectral shift upon binding Ca^{2+} (27). A similar approach was used to construct G-CaMP and “Case” sensors with insertion

of CaM and M13 peptide into a circularly permuted form of GFP (cpGFP). GEICs have been successfully used to measure Ca^{2+} signals after subcellular targeting to the ER (21, 23, 35), nucleus (21), Golgi (26), mitochondrial-matrix (24, 36, 37), and plasma membrane (24, 38–41). Targeting of GECIs to specific proteins can also allow Ca^{2+} measurements to be made in specific micro- or nanodomains associated with specific proteins. GECIs have also been functionally expressed in a tissue-dependent manner in zebrafish (42) and mice (43, 44), as well as non-vertebrate but genetically tractable systems including plants (45), nematodes (46), and flies (41, 47–49). GECIs also allow extended time-lapse experiments in cells where synthetic indicator-leakage may be a problem and they can also be used in controlled “inducible” expression systems. However, drawbacks to using GECIs include the need to transfet with plasmid DNA, smaller signals upon binding of Ca^{2+} , and an increased susceptibility to photobleaching compared to many synthetic Ca^{2+} -sensitive fluorescent indicators. A further drawback of many GECIs is that the CaM part of the probe has the potential to influence Ca^{2+} signaling through buffering or adverse effects on endogenous CaM (19, 20). However, for cameleons this problem has been solved by the generation of CaM/M13 mutants (the “D family” of cameleons) that do not bind wild-type CaM (23, 24). Other CaM-based indicators such as G-CaMPs and pericams would doubtlessly benefit from similar mutations. Alternatively, GECIs such as TN-XLL, where troponin C replaces CaM as the Ca^{2+} -responsive element, have been used in cells, such as neurons, with high endogenous CaM levels (39, 41). There is an ever-expanding number of GECIs available, with many of the original sensors superseded by improved versions. As with synthetic Ca^{2+} indicators, the sensor of choice will depend on both experimental criteria (e.g., K_d for Ca^{2+} ; brightness; ratiometric) and the equipment available (i.e., image splitter or motorized filter wheels for FRET). A discussion of the practicalities and a detailed methodology of using genetically encoded Ca^{2+} indicators can be found later in this chapter (Subheading 3.6) and elsewhere (33, 50).

1.3.3. Measurement of Organelle $[\text{Ca}^{2+}]$ with GECIs

As with measurement of cytosolic $[\text{Ca}^{2+}]$, the most important initial consideration in selecting a sensor to measure organelle $[\text{Ca}^{2+}]$ is the likely concentration range within the organelle and thus the desired K_d of the sensor to give the widest linear dynamic range. Different Ca^{2+} sensitivities have been obtained, mainly by selective mutation of the CaM module to alter its binding affinity. The most widely studied organelles are the ER, mitochondria, and Golgi apparatus. For the ER, the estimated resting $[\text{Ca}^{2+}]$ is 60–400 μM but only 1–50 μM post-mobilization (21). The probe of choice here is the FRET-based D1ER, which consists of a truncated enhanced CFP and a citrine fluorescent protein joined by a linker and hinge containing modified calmodulin and M13 sequences.

Table 1

Recommended protein Ca^{2+} sensors for use in selected organelles. K'_d is the calculated apparent dissociation constant (see Note 24) and n is the calculated Hill coefficient taken from the cited literature. Note that D3 is also suitable for measurements of $[\text{Ca}^{2+}]$ in the cytoplasm and nucleus

Organelle	Targeting motif	Ca^{2+} sensor	Sensor K'_d (μM)	n	References
Mitochondria	2 repeats of the mitochondrial targeting sequence of subunit IV of cytochrome c oxidase	Ratiometric pericam	1.7	1.1	(27)
Endoplasmic reticulum	Calreticulin signal sequence and KDEL retention motif	D1ER	0.58 and 56.46	1.18 and 1.67	(21, 23)
Golgi apparatus	N-terminal 81 aa of human galactosyltransferase type II	D3	1.5	1.1	(26)

A calreticulin signal sequence at the N-terminus of CFP and a KDEL retention sequence at the C-terminus of citrine ensure ER retention. This probe has a biphasic $[\text{Ca}^{2+}]$ response with K'_d values of 0.8 and 60 μM (23). For measurement of mitochondria $[\text{Ca}^{2+}]$, either mitoD3 (a FRET-based probe) or ratiometric pericam is recommended (27). In addition to being ratiometric, the latter also has the advantage of a greater level of response than the small changes associated with FRET probes. However, it does show some pH sensitivity, which must be considered. The ratiometric pericam can also be combined with fura-red to allow concomitant cytoplasmic $[\text{Ca}^{2+}]$ measurements. We have used this to demonstrate the heterogeneity of mitochondrial $[\text{Ca}^{2+}]$ responses in neurons, which relate to their spatial distribution (51). For Golgi, the FRET-based probe D3, targeted to the Golgi by the N-terminal 81 amino acids of human galactosyltransferase type II, has been used successfully (26). The characteristics of these probes are summarized in Table 1. For a more complete coverage of different probes and their uses the reader is referred to an earlier review (50).

1.4. Applications of Confocal Microscopy to Other Aspects of Cell Signaling

1.4.1. Protein-Based Fluorescent Indicators to Measure Signaling

A wide variety of proteins alter their subcellular localization in response to activation and such movement can be either monitored in real time using genetically encoded, fluorescently tagged recombinant proteins or in end-point assays by immunocytochemistry (using epitope-tagged or native proteins) to derive indices of activation. A few examples include the movement of some PKC (Protein Kinase C) isoforms from the cytosol to plasma membrane on activation, the movement of nuclear factor of activated T-cells (NFAT) from the cytosol to the nucleus, and the recruitment of

β -arrestin to activated GPCRs. Furthermore, state-dependent interactions between proteins can be monitored by techniques such as FRET to determine activation state and roles in signaling. For example, FRET between CFP-ERK (extracellular signal-regulated kinase) and MEK-YFP (ERK kinase) is reduced following ERK activation and translocation from the cytosol to the nucleus (52). More complex FRET techniques exist allowing further sophistication in the imaging of signaling activity including, for example, three-chromophore, two-stage FRET that has been used to demonstrate trimerization of TRAF2 (53). Here, excitation of CFP results in FRET to YFP, which in turn results in FRET to a monomeric red fluorescent protein (mRFP).

1.4.2. Confocal Imaging of Phospholipase C Activity

A number of fluorescently tagged protein biosensors have also been developed for the real-time imaging of PLC (Phospholipase C) activity (54–58). Similar to some of the proteins described above, the cellular distribution of these biosensors is influenced by the levels of the second messengers, inositol 1,4,5-trisphosphate ($\text{Ins}(1,4,5)\text{P}_3$) and diacylglycerol (DAG), such that alterations in the cellular distribution of the biosensors provide an index of PLC activity. Before the advent of these biosensors, studies were restricted to population-based assays which, although providing information about PLC activity, gave no spatial information and only limited temporal resolution. The biosensors are fusions of a fluorescent reporter molecule (usually GFP or a derivative) with a protein domain that interacts with an intracellular signaling molecule. Thus, the $\text{Ins}(1,4,5)\text{P}_3$ biosensor is a fusion of the pleckstrin-homology (PH) domain of PLC $\delta 1$ with eGFP (eGFP-PH_{PLC $\delta 1$}) (54, 56). This enhanced form of GFP (eGFP or quite often now simply GFP) is a mutated form of GFP that has an excitation maximum at 488 nm, making it brighter when used with the standard 488 nm laser line available on most confocal microscopes. Under resting conditions eGFP-PH_{PLC $\delta 1$} is localized to the plasma membrane by the virtue of its high affinity for the membrane lipid phosphatidylinositol 4,5-bisphosphate (PtdIns(4,5)P₂). Upon activation of PLC, PtdIns(4,5)P₂ is hydrolyzed to $\text{Ins}(1,4,5)\text{P}_3$ and DAG. $\text{Ins}(1,4,5)\text{P}_3$ competes with PtdIns(4,5)P₂ for PH_{PLC $\delta 1$} . Furthermore, the plasma membrane concentration of PtdIns(4,5)P₂ may fall substantially. The result is a translocation of the fusion protein from the membrane to the cytosol (54, 56) and thus an increase in cytosolic fluorescence corresponds to an increase in PLC activity (Fig. 2a). Translocation of tagged PH_{PLC $\delta 1$} may report primarily $\text{Ins}(1,4,5)\text{P}_3$ generation rather than PtdIns(4,5)P₂ depletion (57) although this is a little controversial and the relative contributions may be context dependent. More selective biosensors have been developed including a fluorescently tagged Tubby domain from the tubby protein (a transcriptional regulator) that is selective for PtdIns(4,5,)P₂. FRET-dependent $\text{Ins}(1,4,5)\text{P}_3$ biosensors have also been developed based on the binding domain of the $\text{Ins}(1,4,5)\text{P}_3$ receptor.

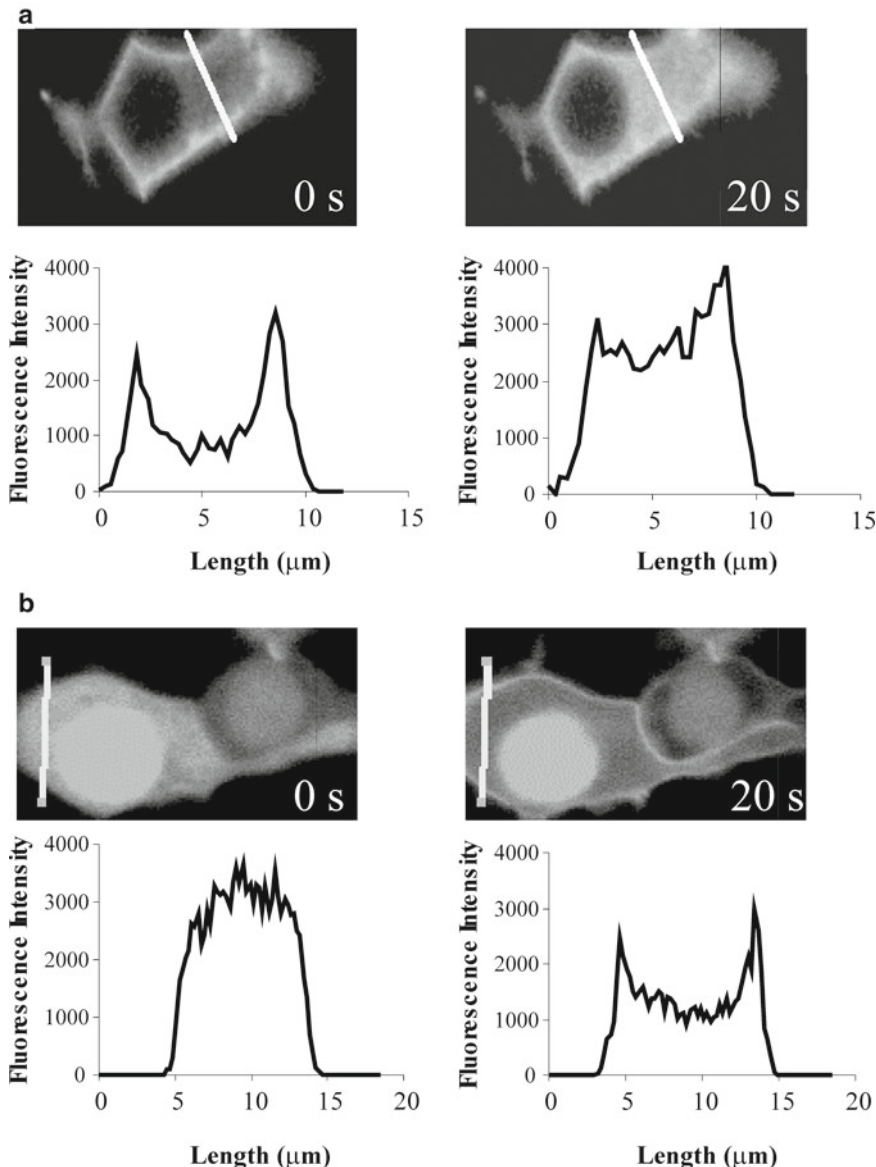


Fig. 2. (a) HEK293 cells stably expressing the human muscarinic M₃ receptor transfected with eGFP-PH_{PLCδ1}. At rest (0 s), the biosensor is located in the plasma membrane, but after stimulation with 100 μM methacholine (20 s), the biosensor becomes cytoplasmic corresponding to the production of Ins(1,4,5)P₃. The change in distribution can be seen clearly in the profiles that represent fluorescence intensity along the lines shown. (b) HEK293 cells stably expressing the human muscarinic M₃ receptor transfected with eGFP-PKCγ(C1₂). At rest (0 s), the biosensor is clearly located homogeneously across the cell but after stimulation with 100 μM methacholine (20 s), the biosensor is recruited to the plasma membrane as DAG is produced. The change in distribution can be seen clearly in the profiles that represent fluorescence intensity along the lines shown.

These include LIBRA (luminous inositol trisphosphate-binding domain for ratiometric analysis) (59), fretino (particularly fretino-2; FRET-based indicator for inositol trisphosphate) (60), FIRE (particularly FIRE-1; fluorescent InsP₃-responsive element)

(61), and IRIS-1 (IP_3R -based IP_3 sensor 1) (62). In addition to providing specificity for $\text{Ins}(1,4,5)\text{P}_3$, the dependence on intramolecular FRET removes both the need to co-express proteins and the possible effect of differential expression levels on FRET signals. There can be problems associated with the use of such probes including their ability to act as a sponge or a sink for the molecule of interest.

In addition to the $\text{Ins}(1,4,5)\text{P}_3$ biosensors, the other limb of the PLC signaling pathway can also be monitored by confocal microscopy using a DAG biosensor, which is a fusion of the tandem C1 domains (C1_2) of $\text{PKC}\gamma$ with eGFP (eGFP– $\text{PKC}\gamma(\text{C1}_2)$) (55, 58). Under resting conditions eGFP– $\text{PKC}\gamma(\text{C1}_2)$ has a homogeneous distribution across the cell nucleus and cytoplasm, but upon activation of PLC and production of DAG it is recruited to the plasma membrane through binding of $\text{PKC}\gamma(\text{C1}_2)$ to DAG. Hence, a decrease in cytosolic fluorescence and an increase in plasma membrane fluorescence is an index of DAG formation and therefore PLC activation (Fig. 2b).

Probes also exist for other parts of the phosphoinositide signaling pathway, for example $\text{PtdIns}(3,4,5)\text{P}_3$ (63). The activity of other signaling pathways can be monitored using a variety of biosensors. Thus, cAMP can be monitored using fluorescently tagged protein kinase A (PKA) subunits in which cAMP-evoked dissociation reduces intermolecular FRET (20), although difficulties such as the reassociation with endogenous subunits can lead to loss of signal and limit their usefulness. Improvements in the detection of cAMP have led to a probe that is dependent upon intramolecular FRET between CFP and YFP located at the N- and C-terminals, respectively, of an exchange protein activated by cAMP (Epac 1; guanine nucleotide exchange factor for Rap1), which has been mutated to enhance cytosolic location and abolish catalytic activity (64). Here, cAMP binding separates the fluorophores and reduces FRET. Such probes can also be targeted to specific subcellular domains including the plasma membrane (65). Intracellular cGMP can be monitored using an N-terminally truncated, catalytically inactive, cGMP-dependent protein kinase tagged with an N-terminal eCFP and a C-terminal eYFP (cygnet-2; cyclic GMP indicator using energy transfer) or pH-resistant eYFP variant, Citrine (cygnet-2.1) in which FRET is decreased by cGMP (66).

Confocal microscopy has provided important insights into the activity and regulation of a wide variety of signaling pathways, including many associated with GPCR-mediated signaling. It is clear that current and future developments in the probes themselves and the techniques for measurement (e.g., fluorescence recovery after photobleaching (FRAP), fluorescence lifetime imaging (FLIM), fluorescence correlation spectroscopy (FCS), total internal reflection fluorescence microscopy (TIRFM), and multiphoton confocal microscopy) will enable evermore complex interrogation of signaling pathways.

*1.4.3. Determination**of GPCR or Ligand**Internalization by Confocal*
Microscopy

Internalization of plasma membrane GPCRs is a typical response to agonist activation, allowing cells to regulate their sensitivity and responsiveness to subsequent agonist exposures. The current model of GPCR regulation is that, following agonist activation, most types of GPCRs undergo phosphorylation. Their subsequent internalization is required for dephosphorylation and recycling of resensitized receptors back to the plasma membrane or alternatively their proteolytic degradation. Measurements of internalization have been, and continue to be, instrumental in revealing such aspects of receptor regulation. Methods for determining internalization have historically involved the use of radioligands. This has typically involved the measurement of cell surface receptors, using a radioligand, both before and after a period of agonist exposure to induce internalization. This of course relies on the ability to both remove the agonist that was used to mediate internalization and to measure surface receptors in the absence of further changes caused by processes such as recycling or further internalization. This can be achieved by, for example, washing to remove the agonist with subsequent binding at a low temperature to block further internalization. For relatively low-affinity agonists their removal is easily achieved by washing with physiological buffers. However, for high-affinity ligands (e.g., many peptides that have nM affinities) removal from the receptor can be more problematic, requiring acidic conditions to cause full dissociation. High-affinity ligands often internalize with their receptors and this has also been exploited to measure receptor internalization. Thus, radiolabeled high-affinity agonists can be internalized and following removal of the surface-bound activity this can be used as a measure of receptor internalization. Despite the relative ease of quantification, these techniques do not allow real-time measurement of receptor internalization, nor do they allow the subcellular localization and trafficking of receptors to be determined. Confocal microscopy offers an alternative means to examine GPCR internalization and although quantification can be problematic it provides the prospect of visualizing internalization and other trafficking events at the single-cell level. For example, using dual-label confocal immunocytochemistry, the subcellular localization of receptors can be determined and used to provide information on their trafficking events. As an alternative to visualizing receptors through antibodies and associated fluorophores, the receptors can be tagged directly with fluorophores such as GFP or its variants. Although tagging may itself influence receptor function and trafficking, this approach not only has the potential to allow the subcellular localization of receptors, but it can also permit the real-time visualization of their movement including internalization. A detailed discussion on the use of GFPs to assess internalization can be found elsewhere (67). An alternative to GFP-tagging of the receptor is to generate a version of the GPCR incorporating an N-terminal epitope tag such as VSV. An antibody labeled with the pH-sensitive dye CypHer-5, that recognizes the

epitope tag, is then used to label the receptor prior to agonist stimulation. At typical extracellular pH values of 7.4 the dye has little fluorescence but within the acidified endosome the dye fluoresces strongly under red light, thereby identifying internalized receptors within this compartment (68). Conventional confocal imaging or a high-content screening platform can then be used to assess receptor internalization.

In a similar way to which radiolabeled high-affinity agonists can be used to determine receptor internalization, fluorescently labeled agonists and confocal microscopy can also be used. It must be remembered however that ligands may dissociate from their receptor as they move into and through the endocytic pathway and may also recycle and/or degrade independently (69), providing important considerations in the interpretation of data collected using this technique. Choosing a fluorophore can be difficult, as there is a wide range that can be conjugated to both non-peptide and peptide ligands. The choice may be limited by the confocal system (e.g., the laser lines and filters available, see Note 2), the ligand(s) and/or receptor(s) under investigation, and the photo-bleaching and pH sensitivity of the fluorophore (see Note 3). It goes beyond the remit of this chapter to discuss the relative merits of all those available. However, GE Healthcare (<http://www.GEhealthcare.com>) supply a range of CyDye, eGFP, and other conjugates, and Molecular Probes (<http://www.invitrogen.com>) supply Alexa Fluor and BODIPY fluorophores and both companies provide further information on their Web sites. There are also numerous reviews detailing the uses and benefits of different fluorescent labels (e.g., (70, 71)).

Although potentially providing real-time visualization of internalization, confocal images exploring internalized receptor or ligand are extremely difficult to quantitate and a cautionary approach to interpreting the data is required. Furthermore, photo-bleaching, quenching, differences in the power of the laser, focal drift, pixilation of images, and other difficulties such as defining the plasma membrane add to the problems of quantification. However, with sensible experimental design and careful analysis, quantification of receptor and/or ligand internalization using confocal microscopy can be achieved. Advances in the analysis packages, particularly on high-content screening platforms, have also helped considerably. For many, the nature of the investigation means that the images taken of internalization in their own right provide suitable documentation (see Fig. 3). Many others have applied different, sometimes complex, methods to quantify internalization of fluorescently labeled receptor or ligand. A comprehensive discussion of these methods is beyond the remit of this chapter and the reader is referred elsewhere (72–76) and we present a relatively simple method below that we have applied to receptor internalization.

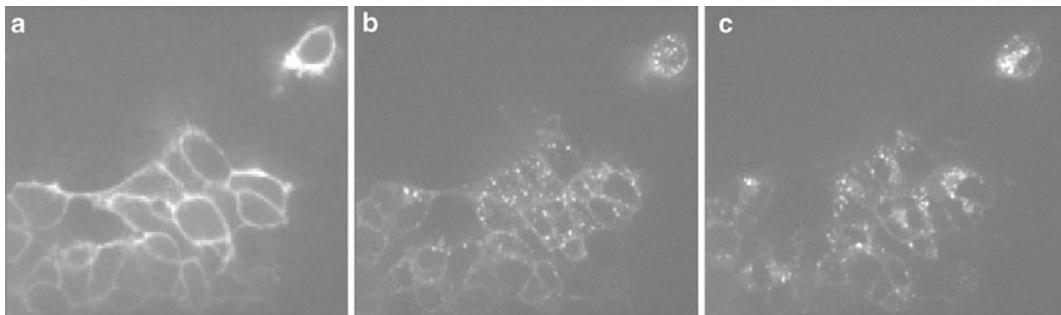


Fig. 3. HEK293 cells stably expressing human NMU1 were cultured on glass coverslips and mounted onto the stage of an UltraVIEW confocal microscope. The temperature was maintained at 37°C and 10 nM Cy3B-pNmU-8 added at 0 s. With excitation at 568 nm, confocal fluorescent images were collected intermittently over a 12-min period. (a) Shows membrane localization of fluorescence 180 s following addition of Cy3B-pNmU-8. (b, c) Images at 300 s and 600 s, respectively, showing internalization in the form of punctate regions of fluorescence.

2. Materials

All chemicals can be obtained from Sigma-Aldrich (Poole, UK) unless otherwise stated, whilst all microscope slides and coverslips are available from VWR International Ltd. (Poole, UK). All cell culture reagents can be obtained from Invitrogen Ltd. (Paisley, UK). All solutions and reagents should be prepared with milli-Q or equivalent grade water (ddH₂O). When dealing with cells in culture, it is imperative that care should be taken to ensure that all reagents are sterile filtered prior to use.

2.1. Cells, Culture Media, and Ligands

1. Key, of course, is the availability of cells expressing either native or recombinant receptors of interest.
2. Appropriate cell growth media: This will obviously vary both between and within laboratories. Below we describe studies using HEK293 cells expressing recombinant human neuromedin U receptor 1 (NMU1) or the human muscarinic M₃ receptor for which we have used Eagle's minimum essential medium with Glutamax-1 and Earle's salts supplemented with fetal calf serum (10%), nonessential amino acids (1%), 50 U/mL penicillin, and 50 µg/mL streptomycin. We also describe studies using HEK293 cells with the stable expression of C-terminally eGFP-tagged human glucagon-like peptide-1 receptor (GLP-1R) (77), which we culture in Dulbecco's modified Eagle's medium (DMEM, containing 4.5 g/L glucose) supplemented with 10% FBS and 200 µg/mL of geneticin (G418, Invitrogen, Paisley, UK) for continual selection. For HeLa cells (used in these studies for the examination of mitochondrial Ca²⁺ signaling) we generally use DMEM, supplemented with 10% fetal calf serum, 50 U/mL penicillin, and 50 µg/mL streptomycin.

Culture the cells in a humidified atmosphere (95% O₂, 5% CO₂, 37°C), replace the culture medium every third day, and passage them at ~80% confluence.

3. Ligands appropriate for the receptors of interest.

2.2. Immuno-fluorescence

1. Prepare a stock solution of poly-D-lysine hydrobromide at 1 mg/mL (1%) in ddH₂O. Store aliquots at -20°C. On the day of use, dilute the stock solution 1:100 in ddH₂O and sterile filter prior to coating coverslips.
2. 10× Phosphate-buffered saline (PBS): 101 mM Na₂HPO₄, 17.6 mM KH₂PO₄, 26.8 mM KCl, 1.37 M NaCl. To prepare 1 L of 10× PBS, dissolve 14.4 g Na₂HPO₄, 2.4 g KH₂PO₄, 2 g KCl, and 80 g NaCl in 800 mL ddH₂O and adjust to pH 7.2. Make up to 1 L with ddH₂O and store at room temperature. Dilute to 1× for use.
3. 4% Paraformaldehyde solution: Add 4 g of paraformaldehyde to 100 mL of 1× PBS (see Note 4).
4. 100% Methanol (cooled to -20°C) (see Note 5).
5. Triton X-100: Prepare a stock solution of 20% Triton X-100 in 1× PBS. Rotate in a tube overnight at 4°C to dissolve. Dilute the stock solution to 0.2% as required.
6. Blocking buffer: 3% bovine serum albumin (BSA) in 1× PBS (see Note 5).
7. Antibodies: For general advice on dealing with antibodies see Note 6.
8. Antibody solutions: Antibodies should be used at the concentration recommended by the manufacturer or alternatively at a concentration determined empirically by the user (see Note 6). Primary antibodies should be dissolved in an appropriate blocking buffer (see above for a typical example). To reduce nonspecific labeling, fluorescently labeled secondary antibodies should be prepared in a blocking buffer containing serum from the host animal (e.g., a goat anti-rabbit secondary antibody should be prepared in 1× PBS containing 10% goat serum).
9. Commercially available mountants: Vector Shield (Vector laboratories, Peterborough, UK), Citifluor (Citifluor Ltd, London, UK), or ProLong Gold (Invitrogen, Paisley, UK).

2.3. Single-Cell Confocal Ca²⁺ Imaging and the Determination of Ligand or GPCR Internalization by Confocal Microscopy

1. Krebs-HEPES buffer (KHB): 10 mM HEPES, 4.2 mM NaHCO₃, 10 mM glucose, 1.18 mM MgSO₄·7H₂O, 1.18 mM KH₂PO₄, 4.69 mM KCl, 118 mM NaCl, 1.29 mM CaCl₂; pH 7.4. To prepare 1 L of KHB, dissolve 2.38 g HEPES, 0.35 g NaHCO₃, 2.10 g glucose, 0.29 g MgSO₄·7H₂O, 0.16 g KH₂PO₄, 0.35 g KCl, 6.92 g NaCl, 0.19 g CaCl₂ in 800 mL ddH₂O and adjust to pH 7.3 with 5 M NaOH. Make up to 1 L with ddH₂O and store at 4°C.

2. Stock solutions (1 mM) of the acetoxyethyl (AM) ester form of fluorescent Ca^{2+} indicators (e.g., fluo-4) should be prepared in high-quality anhydrous dimethylsulfoxide (DMSO), then dispensed into 20 μL aliquots, and stored, well sealed, at -20°C (see Notes 7 and 8).
3. Fluorescent ligand. Here we have used porcine neuromedin U (pNmU-8) coupled to cy3B (Cy3B-pNmU-8): Cy3B is obtained as the Cy3B-NHS ester (GE Healthcare) and attached to the N-terminus of porcine NmU-8 as per the manufacturer's instructions. Following conjugation the product is purified by high-performance liquid chromatography and tested for biological activity (see Note 9). There is now a wide range of commercially available fluorescent ligands or alternatively a number of companies that will produce such labeled ligands to order.
4. Reagents for calibration of the $[\text{Ca}^{2+}]$ if required. Ionomycin at a suitable stock concentration (e.g., 1 mM) in DMSO such that 1–5 μM ionomycin can be used for calibration. To make a stock 0.5 M EGTA solution, dissolve 19 g EGTA in 80 mL ddH₂O and adjust pH to 8.0 with concentrated (10 M) NaOH (EGTA will not dissolve until the pH is raised to 7.5–8.0). Once dissolved and pH 8.0 achieved, adjust volume to 100 mL with ddH₂O. Stock 2.5 M CaCl₂ is made by dissolving 36.75 g CaCl₂·2H₂O in 100 mL ddH₂O.

2.4. Measurement of Organelle $[\text{Ca}^{2+}]$

1. Extracellular medium (EM): 121 mM NaCl, 5.4 mM KCl, 1.6 mM MgCl₂, 6 mM NaHCO₃, 25 mM HEPES, 1.8 mM CaCl₂, 9 mM glucose: pH 7.4. To make 1 L of EM, dissolve 7.07 g NaCl, 0.4 g KCl, 0.33 g MgCl₂·6H₂O, 0.5 g NaHCO₃, 5.96 g HEPES in 800 mL ddH₂O and adjust pH to 7.4 with 5 M NaOH. Make up to 1 L with ddH₂O. Make stock solutions of 1.67 M glucose (dissolve 30 g glucose in 100 mL ddH₂O) and 2.5 M CaCl₂ (dissolve 36.75 g CaCl₂ in 100 mL ddH₂O) and add 600 μL stock glucose and 72 μL stock CaCl₂ (if required) per 100 mL of EM just prior to use. Some experiments may require zero extracellular Ca^{2+} (e.g., examining store-operated Ca^{2+} entry (SOCE)). Addition of glucose only as needed lengthens storage of the EM. Alternative buffers such as the KHB described above may also be used but this may be dependent upon the cell type.
2. High-quality DNA preparations encoding the probe of interest; e.g., prepared by a kit, such as MaxiPrep Plus (QIAGEN, Crawley, UK), PureLink™ HiPure (Invitrogen, Paisley, UK), or JetStar (Genomed, Löhne, Germany).
3. HEPES-buffered saline (HBS) for calcium phosphate transfection: To make 1 L dissolve 5 g HEPES, 8 g NaCl, 1 g glucose, 3.7 g KCl in 800 mL ddH₂O and add 10 mL of Na₂HPO₄ stock solution (0.94 g Na₂HPO₄·7H₂O in 50 mL ddH₂O).

Adjust to pH 7.1 with 5 M NaOH and make up to 1 L with ddH₂O. Sterile filter, aliquot into 50 mL tubes, and store frozen at -20°C, keeping one working aliquot at 4°C.

4. Reagents for calibration of the [Ca²⁺] (see Subheading 2.4, item 4).

3. Methods

3.1. Indirect Immunofluorescence Protocol for Adherent Cells

One technique that is routinely used to examine the subcellular distribution of proteins is indirect immunofluorescence labeling. Adherent cells can be fixed and permeabilized to allow antibodies targeted against specific cellular proteins access to the cell interior. Specific binding of the primary antibody to its target protein can then be detected using a secondary antibody coupled to a fluorophore. Common fluorophores include fluorescein isothiocyanate (FITC), tetramethyl rhodamine isothiocyanate (TRITC), and Texas Red or any of the AlexaFluor range (Invitrogen, Paisley, UK), all of which can be visualized using the standard laser lines on most commercially available confocal microscopes.

3.1.1. Preparation of Coverslips

1. Coverslips should be of an appropriate thickness (typically 170±10 µm) for optimal confocal resolution. Coverslips may be stringently cleaned with either acetone or 100% ethanol prior to use and then sterilized by either autoclaving or flaming. Alternatively, for most purposes, coverslips can be sterilized in 70% ethanol and then rinsed in sterile 1× PBS prior to use.
2. To aid cell adhesion, coverslips may be coated with a variety of substances such as fibronectin, gelatin, or poly-D-lysine to provide a substratum for adherence and growth. For example, poly-D-lysine is prepared as a 0.01% solution in sterile ddH₂O (see Subheading 2.2, item 1). Depending on size, coverslips can then be coated with between 100 and 500 µL of poly-D-lysine solution. Following a 20-min incubation at room temperature, the poly-D-lysine should be aspirated, coverslips rinsed with sterile 1× PBS, and allowed to air-dry in a tissue culture hood for 20 min prior to the plating of cells.

3.1.2. Immunofluorescence Labeling

1. Cells in the appropriate growth medium should be seeded onto poly-D-lysine-coated 22 mm diameter borosilicate glass coverslips contained in 6-well multi-dishes. Cells should then be returned to the incubator for 24–48 h to allow adequate adhesion.
2. Fixation: On the day of experimentation, the growth medium should be removed and the cells washed once with 1× PBS at room temperature. The cells may then be fixed using either 4%

paraformaldehyde at room temperature (cross-linking fixation) or 100% methanol cooled to -20°C (protein precipitation fixation) (see Note 5).

- (a) Paraformaldehyde fixation: Immerse coverslips in 4% paraformaldehyde at room temperature for 30 min. Wash the coverslips once with 1× PBS. Aspirate the PBS and then permeabilize the cells by addition of 0.2% Triton X-100 in 1× PBS for 5 min at room temperature. Wash the coverslips three times for 5 min each in 1× PBS. Then proceed to the blocking step (step 3).
- (b) Methanol fixation and permeabilization: Immerse coverslips in -20°C methanol for 10 min. Wash the coverslips three times for 5 min each with 1× PBS at room temperature. Then proceed to the blocking step (step 3).
3. Blocking: All coverslips should be incubated with blocking buffer (3% BSA in 1× PBS) for 45–60 min at room temperature. This step is essential for producing a low level of background staining (see Note 5). Coverslips should then be washed once in 1× PBS for 5 min.
4. Staining: The primary antibody should be diluted as appropriate in blocking buffer (for example, 3% BSA in 1× PBS). It should be noted that when using a high concentration of antibody it is recommended that the solution is centrifuged for 20 min at $\geq 12,000 \times g$ at 4°C. This removes aggregated material, thereby reducing nonspecific background staining. The time and temperature for incubation with primary antibody will vary depending upon the antibody, but a good starting point is to incubate the coverslips with primary antibody overnight at 4°C with mild agitation (e.g., a rocking platform).
5. Following incubation, aspirate the primary antibody and wash the coverslips three times for 5 min each in 1× PBS at room temperature.
6. Incubate all coverslips with the appropriate concentration of fluorescently labeled secondary antibody in an appropriate blocking buffer (see Subheading 2.2, item 8) for 45–60 min at room temperature in the dark.
7. Aspirate the secondary antibody and wash each coverslip three times for 5 min each with 1× PBS at room temperature in the dark.
8. At this stage the cell nucleus can be counterstained as a cell marker. When using an FITC-conjugated secondary antibody this may be achieved by a 5-min incubation with 2% propidium iodide (PI). It should be noted that PI cannot be used as a counterstain when using either TRITC- or Texas Red-conjugated secondary antibodies, but other counterstains such as Hoescht or DAPI may be used if a UV laser is available.

9. Coverslips can then be mounted onto standard microscope slides using a commercially available mountant (see Subheading 2.2, item 9). Vector Shield (Vector Labs, Peterborough, UK), Citifluor (Citifluor Ltd, London, UK), or ProLong Gold (Invitrogen, Paisley, UK), each contains anti-photobleaching agents that help preserve the lifetime of many common fluorophores. Slides can be stored for short term (several weeks) in the dark at room temperature or alternatively, coverslips can be sealed onto microscope slides using clear nail varnish and stored in the dark at 4°C for several months.
10. Slides are then ready for viewing. For example, the detection of a FITC-conjugated secondary antibody can be achieved by excitation with the 488 nm laser line on most commercially available confocal microscopes. In our case, standard 2D images are taken (512×512 pixels) using an Olympus Fluoview or PerkinElmer UltraVIEW confocal microscope using a $60\times$ oil-immersion objective lens, with images collected using PMTs or a CCD camera, respectively. Care should be taken when interpreting subcellular staining patterns. For example, it is wise to use a counterstain to mark the position of the cell nucleus and if a protein is thought to be localized to a specific subcellular compartment, then this should be confirmed by co-localization studies with a known marker protein. Adequate controls should also be included, for example, incubation with a blocking peptide to the primary antibody should remove specific staining. A more detailed description of the controls and potential pitfalls surrounding immunofluorescence labeling can be found elsewhere (78, 79).

3.2. Dual-Label Immunofluorescence in Adherent Cells

The dual-labeling immunofluorescence procedure represents an extension of the method discussed in Subheading 1. In this scenario, the main concern is the selection of both primary and secondary antibodies to allow visualization of two different cellular proteins. It is essential that the primary antibodies have been raised in different species. Most commonly, one antibody is a mouse monoclonal antibody and the other is a polyclonal antibody raised in rabbit. If primary antibodies from the same species were to be used, then the secondary antibodies would bind indiscriminately making an interpretation of the labeling impossible. That said, if there is no alternative and the isotype of the mouse monoclonal antibodies are known (usually these are quoted on the supplied datasheet) and differ (IgM, IgG₁, IgG_{2a}, IgG_{2b}, or IgG₃), then isotype-specific antibodies may be used in combination. These are available from companies such as Molecular Probes/Invitrogen. To ensure that there is really no cross-reactivity, controls are essential, staining singly with both primary antibodies and with the opposite isotype-specific secondary antibody in each case as well as the cognate secondary, before doing dual staining. The main consideration with the secondary antibodies is the choice of fluorophore.

It is essential that the fluorophores present on the two different secondary antibodies both excite and emit in different parts of the spectrum in order to reduce bleed through of light from one channel to the other. The most common combination is probably FITC and Texas Red that absorb maximally at blue and green wavelengths but emit green and red light, respectively. This combination of fluorophores has previously been used to show, for example, the subcellular co-localization of type II ryanodine receptors and type II $\text{Ins}(1,4,5)\text{P}_3$ receptors in atrial myocytes (6). It should also be noted that care must be taken to select the appropriate laser line for illumination and the appropriate filters for detecting emission (see Note 2).

1. Steps 1–3 of the previous single-label immunofluorescence protocol should be followed, i.e., fixation, permeabilization, and blocking.
2. Staining: The primary antibodies should be diluted as appropriate in blocking buffer (for example, 3% BSA in 1× PBS) and added as a mixture to the coverslips of cells. Coverslips should be incubated with the primary antibody solution overnight at 4°C with mild agitation.
3. Following incubation, aspirate the primary antibody solution off and wash the coverslips three times for 5 min each in 1× PBS at room temperature.
4. Incubate all coverslips with an appropriate concentration of the first fluorescently labeled secondary antibody in an appropriate blocking buffer (see Subheading 2.2, item 8) for 45–60 min at room temperature in the dark.
5. Aspirate the first secondary antibody and wash each coverslip three times for 5 min each with 1× PBS at room temperature in the dark.
6. Incubate all coverslips with an appropriate concentration of the second fluorescently labeled secondary antibody in an appropriate blocking buffer (see Subheading 2.2, item 8) for 45–60 min at room temperature in the dark.
7. Aspirate the second secondary antibody and wash each coverslip three times for 5 min each with 1× PBS at room temperature in the dark.
8. Coverslips can then be mounted onto standard microscope slides using an appropriate anti-photobleaching mountant as described in Subheading 2.2, item 9.

3.3. Real-Time Confocal Imaging of Intracellular Ca^{2+} Transients in Adherent Cells

Advances in confocal imaging technology and the concomitant development of fluorescent Ca^{2+} indicators over the past 10 years or so have greatly enhanced our understanding of both the spatial and temporal aspects of agonist-evoked Ca^{2+} signals at the single-cell level (3–5). Indeed, there are now a wide variety of fluorescence-based Ca^{2+} indicators available. Several excellent resources exist to

aid in the selection of appropriate Ca^{2+} indicators (e.g., Molecular Probes handbook of fluorescent indicators at <http://www.invitrogen.com/site/us/en/home/References/Molecular-Probes-The-Handbook.html>) and there are also several excellent reviews outlining the advantages and disadvantages of many of these indicators (15, 80). The method described below is for single-cell Ca^{2+} imaging in HEK293 cells loaded with the AM ester form of fluo-4 (fluo-4 AM) using either an Olympus Fluoview or PerkinElmer UltraVIEW confocal microscope.

1. Plate cells onto 25 mm diameter borosilicate glass coverslips coated with 0.01% poly-D-lysine in 6-well multi-dishes (2 mL of cells/well). Cells should be seeded at a density that gives ~80% confluence on the day of experimentation. Cells are then returned to the incubator for between 24 and 48 h to ensure adequate adhesion.
2. On the day of experimentation, aspirate off the growth medium and wash the cells once with KHB at room temperature.
3. Aspirate off the KHB and replace with fresh KHB containing 2 μM fluo-4 AM and 0.02% pluronic F-127. The cells should then be placed in the dark at room temperature for 45 min to allow adequate loading of the Ca^{2+} -sensitive indicator (see Notes 7 and 8).
4. After loading, wash the cells once with KHB. Add 1 mL KHB to each coverslip and incubate in the dark for ~45 min at room temperature to allow adequate de-esterification of the indicator (see Notes 7 and 8).
5. Cells on coverslips can then be mounted into a chamber on the stage of an inverted microscope (e.g., Olympus IX50) and maintained at 37°C using a Peltier thermal heating device and, if required, by keeping perfusion buffers in a heated water bath (see Note 10).
6. Cells can then be imaged using a 60 \times oil-immersion objective lens and fluo-4 excited using the 488 nm laser line with emitted fluorescence collected at wavelengths >505 nm.
7. Images (256 \times 256 pixels) are typically collected (by PMT or CCD) as a time series, with the rate of image capture dependent on the type of experiment and the capabilities of the confocal microscope being used (see Note 11).
8. Online image analysis can then be performed using software provided by the confocal microscope manufacturer (e.g., Fluoview software for the Olympus Fluoview and PerkinElmer imaging suit for the UltraVIEW). Alternatively, images can be exported for off-line analysis using other image analysis packages such as NIH image (Image J) (see <http://rsb.info.nih.gov/nih-image/download.html>). Raw fluorescence data can

be exported to Microsoft Excel and expressed as either the change in fluo-4 fluorescence relative to basal fluo-4 fluorescence (F/F_o) or alternatively the raw fluorescence data can be converted into changes in $[Ca^{2+}]$ using the following formula:

$$[Ca^{2+}] = K'_d \left((f - f_{min}) / (f_{max} - f) \right)$$

where f is the fluorescence intensity of fluo-4 at any given time point during the experiment and f_{min} and f_{max} are the minimal and maximal fluorescence intensities of fluo-4, reflecting the calcium-free and the calcium-saturated forms of the indicator. The values of f_{min} and f_{max} are usually determined at the end of each experiment by the addition to the perfusion chamber of a calcium ionophore such as A23187 or ionomycin (1–5 μM) in the presence of either 10 mM EGTA or 10 mM CaCl₂ (for f_{min} and f_{max} , respectively). The K_d for fluo-4 as determined *in vitro* is ~345 nM, although this may differ in a cellular context. For example, the apparent K_d (K'_d) for fluo-3 inside HeLa cells has been determined as ~810 nM versus 395 nM *in vitro* (15) (see Notes 12 and 24).

3.4. Confocal Imaging of PLC Activity in Adherent Cells Using Protein Biosensors

The methodology below describes the use of two genetically engineered biosensors that can be used to detect the generation of Ins(1,4,5)P₃ and DAG, the second messengers produced upon activation of PLC. The use of these biosensors has enabled PLC activity to be determined at the single-cell level, both visually and in real time (54–58). Alternatively, the use of the biosensors in co-transfection experiments has allowed us to examine proteins that modulate PLC activity. For example, we have successfully used co-transfection of the biosensors with RGS proteins (regulators of G-protein signaling) to determine the impact of RGS proteins on Gα_q-mediated PLC signaling at the single-cell level. Details of the biosensor constructs can be found in Note 13.

1. Plate cells (e.g., HEK293 cells stably expressing the recombinant human muscarinic M₃ receptor) in standard growth media into 6-well multi-dishes containing 25 mm diameter borosilicate glass coverslips coated (where required) with an appropriate substratum (e.g., 0.01% poly-D-lysine as described in Subheading 3.1.1). Ideally, cells should be seeded at a density that gives a confluence of ~30–50% on the day of transfection. Cells should then be returned to the incubator for 24 h to allow adequate cell adhesion.
2. The next day cells should be transfected with DNA encoding the appropriate biosensor. Cells can be routinely transfected using any one of several commercially available transfection reagents as per the manufacturer's instructions. Suitable transfection reagents include, for example, Fugene 6 (Roche Diagnostics, Lewes, UK), Lipofectamine 2000 (Invitrogen Ltd, Paisley, UK), or Genejuice (Merck-Chemicals Ltd., Nottingham, UK).

3. Transfection of adherent cells using Fugene 6: Add 100 µL of serum-free growth medium to a sterile tube. Add 3 µL of transfection reagent directly into the medium and mix gently. Incubate at room temperature for 5 min.
4. To a fresh sterile tube add 1 µg of the appropriate biosensor DNA (see Note 13).
5. After the 5-min incubation is complete, add the mixture of medium and transfection reagent dropwise onto the DNA. Gently mix using a pipette and incubate at room temperature for 15 min.
6. The DNA/Fugene 6 complex should then be added dropwise to a single well of a 6-well multi-dish (containing ~2 mL of fresh media, e.g., change the media on the cells prior to transfection). Cells should then be returned to the incubator for between 24 and 48 h prior to experimentation. For certain cell types it may be necessary to remove the transfection reagent after 8 h to reduce any cytotoxic effects.
7. On the day of experimentation, remove the growth medium and wash the cells once with 2 mL of KHB at room temperature.
8. Coverslips can then be used as the base of a perfusion chamber and mounted on the stage of an inverted microscope. The temperature is maintained by a Peltier thermal heating device and, if required, by keeping perfusion buffers in a heated water bath.
9. The biosensors can then be visualized using a 60× oil-immersion objective lens, by exciting eGFP using the 488 nm laser line with emitted fluorescence collected at wavelengths >505 nm by PMT or CCD. Typically images (256 by 256 pixels) collected every 1 s are sufficient for detecting the movement of the eGFP-tagged biosensors.
10. Changes in eGFP fluorescence in response to cellular stimulation can then be expressed as absolute changes in cytosolic eGFP fluorescence or changes in cytosolic fluorescence in relation to the initial basal level of cytosolic eGFP fluorescence (F/F_0). Changes in the subcellular distribution of eGFP fluorescence can also be determined by measuring pixel intensity across a cell (see Fig. 2).

3.5. Determination of Ligand or GPCR Internalization by Confocal Microscopy

In this section we describe a confocal method to monitor the internalization of (pNmU-8), with the fluorophore Cy3B (GE Healthcare) conjugated to its N-terminus (Cy3B-pNmU-8). This neuropeptide binds with high affinity to both mammalian forms of its cognate GPCRs (NMU1 and NMU2), resulting in internalization of both ligand and receptor. Here we describe a method to visualize internalization of Cy3B-pNmU-8 with the human NMU1 expressed as a recombinant protein in HEK293 cells. We also

describe a method for assessing ligand-induced internalization of an eGFP-tagged GLP-1R.

1. Receptor-expressing cells (e.g., HEK293 expressing recombinant human NMU1 used here for studying ligand internalization or cells with stable expression of a C-terminally eGFP-tagged human GLP-1R used here to study receptor internalization) should be cultured and plated on poly-D-lysine-coated coverslips as described in Subheading 3.3, steps 1 and 2.
 2. Cells should then be returned to the incubator for 24–48 h to allow adequate cell adhesion. On the day of experimentation, mount a coverslip onto the stage of the confocal microscope (e.g., a PerkinElmer UltraVIEW). Here the coverslip forms the bottom of a chamber to which 250 μ L of KHB should be added. Buffer is added at the required temperature, with the temperature maintained using a Peltier heated coverslip holder (see Note 14). Cells are imaged using a 60 \times oil-immersion objective lens.
- 3.5.1. Ligand Internalization*
1. Prior to addition of the fluorescently labeled ligand, obtain a phase image of the cells that can be used subsequently to compare or overlap with the fluorescence image to help with identification of the subcellular localization of the ligand. It is also important to consider the specificity of binding of the fluorescent ligand and any possible contribution of nonspecific binding to cellular fluorescence (see Note 15).
 2. Add directly to the bath 250 μ L of KHB containing the fluorescently labeled ligand at twice the required final concentration (20 nM Cy3B-pNmU-8) (see Note 16). The temperature of this addition should be equivalent to the bath temperature. Great care should be taken not to move the chamber or dislodge cells from the coverslip (see Note 17). As an alternative, ligands can be added through a perfusion system (see Note 18).
 3. Visualization of the fluorescent ligand can be achieved using an appropriate excitation wavelength and suitable filter set (see Note 2). For example, on a PerkinElmer UltraVIEW confocal system, Cy3B is excited at 568 nm using a Kr/Ar laser with emitted fluorescence collected with a broadband RGB emission filter. The intensity of excitation is minimized, using the lowest possible laser setting where images can be seen clearly (see Note 3).
 4. To avoid photobleaching (see Note 3) of Cy3B, fluorescent images of cells should be collected intermittently (e.g., 2–3 images every 30 s) over the period of time during which internalization occurs. The time course required will depend upon the receptors and the expression system. Alternatively surface-bound fluorescence can be removed by washing following an initial period of internalization (see Note 19).
 5. The images can then be analyzed to assess internalization (Fig. 3; see Note 20).

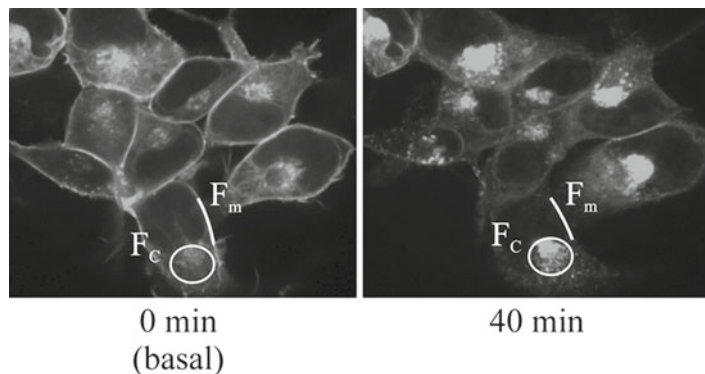


Fig 4. HEK293 cells stably expressing the human GLP-1R containing a C-terminal eGFP tag were cultured on glass coverslips and mounted onto the stage of an UltraVIEW confocal microscope. The temperature was maintained at 37°C and images taken before (0 min) and at various time points after bath addition of 100 nM GLP-1. Shown here is an image after 40 min of GLP-1 stimulation. F_c represents the cytosolic (predominantly endosomal) fluorescence while F_m is the plasma membrane fluorescence. Internalization is calculated as described in Note 20.

3.5.2. Receptor Internalization

1. Visualization of the eGFP-tagged receptor can be achieved using an appropriate excitation wavelength and suitable filter set (see Note 2). For example, on a PerkinElmer UltraVIEW confocal system, eGFP is excited at 488 nm using a Kr/Ar laser with emitted fluorescence collected above 505 nm. The intensity of excitation is minimized, using the lowest possible laser setting where images can be seen clearly (see Note 3).
2. For determining receptor internalization, images are captured before the ligand is added (basal, 0 min) and then at various times after ligand addition (e.g., at 2.5, 5, 10, 20, 30, 40, 50, and 60 min). Ligand can be added by either perfusion or by direct addition to the bath (see Subheading 3.5.1, step 4). We tend to use direct bath addition for peptides as these can be expensive and can stick to the perfusion tubing.
3. The images can then be analyzed to assess internalization (Fig. 4; see Note 20).

3.6. Measurement of Organelle $[Ca^{2+}]$

1. Plate cells (e.g., HeLa) onto 28 mm borosilicate glass No. 0 or 1 coverslips located in 6-well multi-dishes and leave for 24 h to adhere. Cells should be plated to achieve 30–40% confluence on the day of transfection.
2. Transfect cells with plasmid encoding the required probe. A range of transfection reagents (see Subheading 3.4, step 2) are available which all work well, although in our experience simple calcium phosphate transfection is perfectly adequate and results in lower toxicity. Alternatively, stable cell lines may be obtained by subsequent selection with increasing concentrations

of G418 or other appropriate antibiotic for selection (typically 600–1,000 µg/mL G418 works well in selecting stable transformants in the HeLa cell line; optimization of killing-curves for any other cell line is recommended) and/or fluorescence-activated cell sorting (FACS) with single cell selection to obtain clonal cell lines.

3. For calcium phosphate transfection, for each well for transfection, put 86 µL HBS into a tube, add 5.1 µg of the required plasmid DNA, and mix each tube thoroughly. Add 5.1 µL 2.5 M CaCl₂ to each tube and vortex immediately to mix. Leave for 20 min. Meanwhile remove and replace media on cells with 1.4 mL fresh media and return to incubator. After 20 min, add the transfection mixture dropwise to wells while rocking back and forth and place back into the incubator (must be a 5% CO₂ incubator). Change media the following day.
4. Wait at least 48 h after transfection before imaging. Although expression may be observable by 24 h, in our experience expression is maximal after 48 h and better results are obtained.
5. Wash cells twice with EM (this is particularly important if a zero Ca²⁺ EM is being used), taking care not to dislodge the cells. Transfer coverslip into imaging chamber and seal. Add EM to chamber and place into heated stage on microscope. The temperature is maintained by a Peltier thermal heating device and, if required, by keeping perfusion buffers in a heated water bath. We use a Zeiss Axiovert inverted microscope attached to the Zeiss LSM 510 confocal imaging system.
6. Focus cells using brightfield and switch to fluorescence to select for transfected cells. Choose cells that are in the middle range of brightness: too low may give poor resolution of any changes and too high may cause buffering of Ca²⁺. If there are concerns about buffering of Ca²⁺ by the probe, try to image cells of varying brightness and compare the data. Typically, using a 63× oil immersion lens we can obtain images every second (however, see Note 21).
7. For ratiometric pericam, real-time confocal images are collected by sequential excitation at 405 nm and 488 nm with emissions collected between 505 nm and 545 nm. Ratiometric images can be calculated off-line using appropriate software (e.g., GraphPad Prism, San Diego, USA, or Image J with the appropriate plug-ins) using data from whole cells or regions of interest (ROI). Typically, upon binding Ca²⁺ the fluorescence intensity from the 405 nm excitation will go down and that at 488 nm will increase resulting in an increase in the 488/405 nm ratio (see Fig. 5a). For FRET probes using the CFP–YFP pairing (such as D1ER), excitation at 405 nm with emissions collected at 485 nm (CFP signal) and 535 nm (FRET signal) should be employed (see Note 22). The first reading gives the

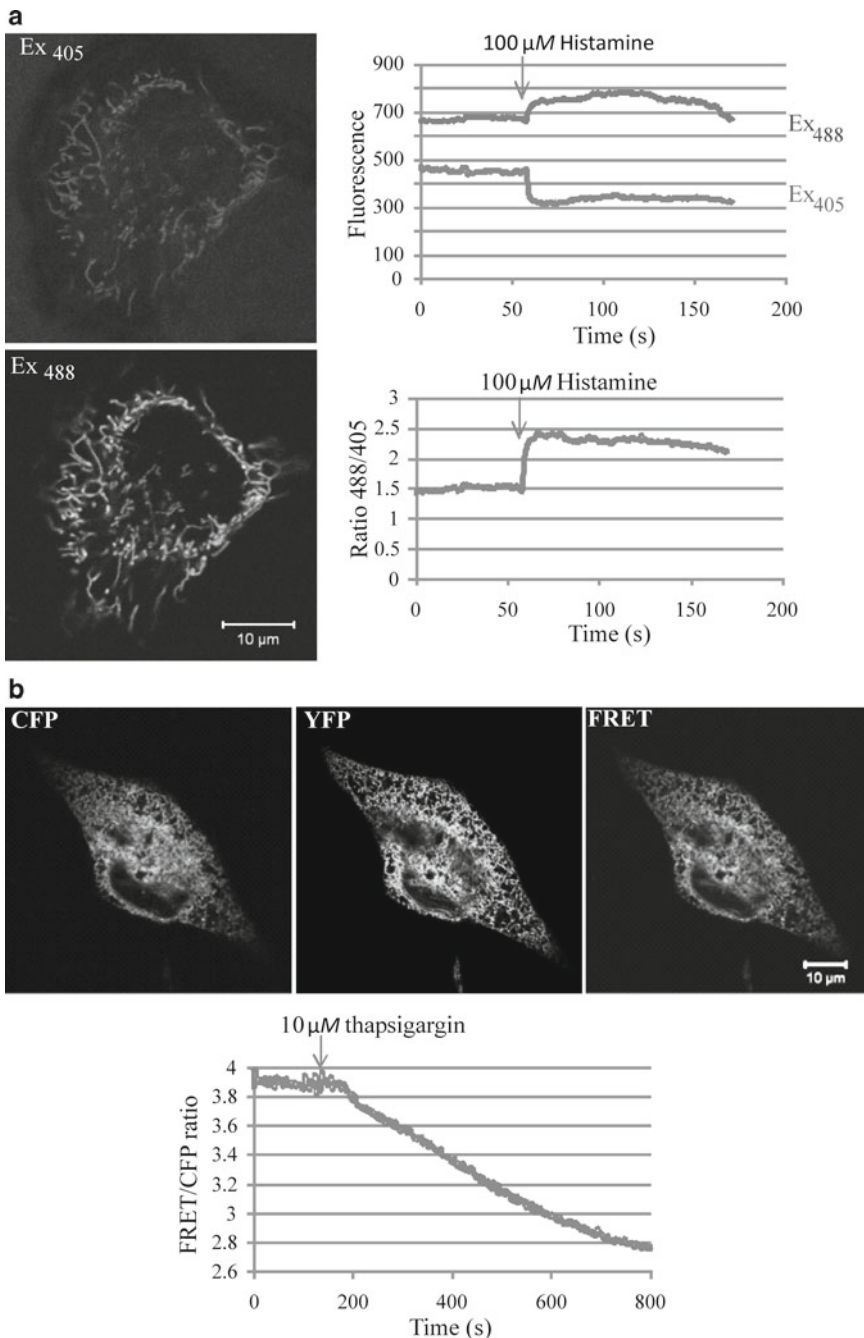


Fig. 5. (a) HeLa cell expressing mitochondrially targeted ratiometric pericam, showing clear mitochondrial localization. Mitochondrial Ca^{2+} levels were increased upon stimulation of the cells with histamine, which causes release from the ER into the cytoplasm, which mitochondria then buffer by Ca^{2+} uptake. Note that the individual traces for excitation at 405 nm and 488 nm move in opposite directions to give a ratio that increases with increasing $[\text{Ca}^{2+}]$. (b) HeLa cell expressing D1ER, showing clear ER localization. Upon depletion of the ER Ca^{2+} with thapsigargin (THG) the ratio of FRET signal to CFP signal declines, indicative of the loss of ER Ca^{2+} .

baseline CFP fluorescence and the second gives the FRET measure. Typically the FRET signal increases upon Ca^{2+} binding and the signal in the CFP channel decreases. Thus, the FRET ratio (FRET/CFP) rises with increasing $[\text{Ca}^{2+}]$ and falls if Ca^{2+} is depleted (see Fig. 5b). It is also possible to measure the direct YFP fluorescence as a control (see Note 22).

8. Collect images for at least 20 s to obtain baseline measurements and to ensure no change in the focal plane. Add reagents to perturb $[\text{Ca}^{2+}]$. This can be done manually, adding a 2× solution dropwise without touching the chamber in between measurements. Alternatively a perfusion system may be used (see Note 23).
9. Relative fluorescent changes are often quoted for a given experiment and these are often sufficient. However, it is possible to convert ratio data to molar values using the following equation:

$$[\text{Ca}^{2+}] = K'_d [(R - R_{\min}) / (R_{\max} - R)]^{(1/n)},$$

where K'_d is the apparent dissociation constant (see Note 24), R is the recorded ratio, R_{\min} is the minimum ratio under Ca^{2+} -free conditions, R_{\max} is the maximum ratio under saturating levels of Ca^{2+} , and n is the Hill coefficient. Published values for K'_d and n are summarized in Table 1. R_{\min} and R_{\max} must be calculated at the end of the experiment to calibrate the probe being used. One simple method to determine these values is to use the Ca^{2+} ionophore, ionomycin, with or without extracellular Ca^{2+} . For R_{\min} add 1–5 μM ionomycin in the presence of 10 mM EGTA and without Ca^{2+} (to chelate the remaining Ca^{2+}), and then change the EM to one with 10 mM Ca^{2+} to determine R_{\max} (however, see Note 25).

4. Notes

1. FRET is a phenomenon characterized by the transfer of energy from one excited fluorophore (the donor, e.g., CFP) to another fluorophore (the acceptor, e.g., YFP). To enable FRET to work the donor fluorophore must have an emission spectrum that overlaps considerably with the excitation spectrum of the acceptor fluorophore. For FRET to occur the donor and acceptor fluorophores must be in close proximity to one another; hence FRET has been used extensively to study protein–protein interactions. A detailed discussion of FRET and its use in biological systems is covered elsewhere (81).
2. As discussed in Subheading 1.2, confocal microscopes routinely have lasers that produce excitation light in the visible spectrum.

Hence, care should be taken when selecting a fluorophore or Ca^{2+} -sensitive fluorescent indicator to ensure that it is capable of being used with the instrumentation available. A further consideration is that of dichroic mirrors and emission filters. A wide variety of optical filters and filter blocks are available from companies such as Omega Optical Inc. (Brattleboro, VT, USA; <http://www.omegafilters.com>) and Chroma Corp. (Rockingham, VT, USA; <http://www.chroma.com>). These include dual- and triple-coated dichroic mirrors that are suitable for use in dual-labeling experiments. Some high-end confocal microscopes are equipped with acousto-optical beam splitters (AOBS) or other similar devices. AOBS are acousto-optical crystals that act as tunable deflection devices for light. AOBS is tunable to channel any laser line onto the sample and simultaneously transmit very efficiently the emitted light to the detector increasing spectral flexibility.

3. The photobleaching of fluorophores describes the process in which the fluorophore's structure is altered as a result of absorption of excitation light causing it to progressively lose its fluorescence. This problem is often exacerbated with many fluorophores by the need for high-excitation light to obtain detectable fluorescence emission. The problem of photobleaching can be minimized by keeping both laser intensity and exposure times to a minimum. Some fluorophores are also extremely sensitive to changes in pH and are more susceptible to photo-bleaching in a low pH environment. Although this can be exploited experimentally, whereby loss of fluorescence is indicative of receptors/ligands entering the low pH environment of endosomes and lysosomes, the use of a pH-insensitive fluorescent conjugate, for example, some of the Cy-Dyes (GE Healthcare), Alexa Fluor and BODIPY (Invitrogen), will limit this problem.
4. Paraformaldehyde should be weighed out in a fume hood whilst wearing gloves and a protective mask. Paraformaldehyde is insoluble at room temperature and as such the solution should be placed in a shaking water bath maintained at 60°C until the paraformaldehyde dissolves. The paraformaldehyde solution should then be cooled to room temperature prior to use (this may be achieved rapidly by placing the solution on ice). The paraformaldehyde solution is relatively unstable and should preferably be made fresh on the day of experimentation.
5. Methanol is generally thought to be the quickest and easiest option for fixation, but it is also the most destructive and in general gives poor structural preservation. Methanol solubilizes and precipitates proteins, often leading to the loss of membrane-bound antigens. Methanol treatment also results in the permeabilization of cells, removing the need for a permeabilization step (as is required for paraformaldehyde

fixation). Paraformaldehyde works by cross-linking proteins and is generally considered to be the method of choice when the maintenance of cellular structure is of importance (for example in highly structured cells such as cardiac myocytes and neurons). After fixation and permeabilization cells should be incubated in an appropriate blocking buffer to reduce background staining. The addition of 0.2% Triton to the blocking buffer may also help to minimize background staining.

6. Upon receipt of any antibody it is vital to ensure that the datasheet is read thoroughly and that stock antibody solutions are kept at the appropriate temperature (usually either 4°C or -20°C). Preferably, antibodies should be aliquoted into suitable volumes for storage to prevent repetitive freeze/thaw cycles that can lead to loss of antibody function and the formation of inactive antibody aggregates. Secondary antibodies labeled with fluorophores for indirect immunofluorescence studies should be kept in lightproof containers at 4°C unless otherwise stated in the supplier's instructions. The supplier's instructions should be the starting point for determining the appropriate dilution of primary antibody. More detailed discussion on determining the concentration of antibody for use empirically is beyond the scope of this chapter, but several other excellent resources cover this topic (78, 79).
7. Most common fluorescent indicators used for confocal Ca²⁺ imaging are polycarboxylate anions that are lipophilic and hence not cell permeant. This problem has been overcome by the addition of "protective" AM ester groups to mask the charged carboxyl groups present on the indicator. This makes the AM ester form of, for example, fluo-4 uncharged and consequently cell permeant. Once inside the cell, endogenous nonspecific esterases cleave off the protecting lipophilic AM ester-groups leaving the original hydrophilic Ca²⁺-sensitive form of fluo-4 trapped inside the cell. It should also be noted that the esterified form of the indicator is also free to cross other cellular membranes, such as those of intracellular organelles like the mitochondria, where esterase activity may result in compartmentalization. The loading of fluo-4 AM into cells is usually aided by the addition of a mild nonionic surfactant such as pluronic F-127 (0.02%). The pluronic acts as a dispersing agent for the AM esters, aiding their solubility. Pluronic can be added directly to aqueous solutions although it is relatively insoluble and particulate matter should be removed by centrifugation. Alternatively, make a 20% stock solution of pluronic in DMSO (gentle warming to 40°C may assist in dissolving the detergent) and dilute 1:1,000 into aqueous solution. Serum proteins such as BSA (0.5–1%) can also improve loading efficiency, probably by acting as hydrophobic carriers for the

AM esters. It should be noted that as an alternative to AM ester loading, the hydrophilic free acid form of fluo-4 may be introduced into cells by invasive procedures such as microinjection through a patch pipette (80).

8. In some instances there is significant dye loss from cells during and after loading. It is believed that this loss occurs by an extrusion mechanism that expels organic anions and as such can be blocked effectively by inhibitors such as probenecid and sulfinpyrazone (82). For example, sulfinpyrazone can be used at 100–250 μM to aid the loading of dyes such as fura-2 AM. It should be noted that the loading time mentioned in the methodology (Subheading 3.3, step 3) is for HEK293 cells and follows basic guidelines issued by the manufacturers. Different cell types may require different loading conditions, with possible variables being the concentration of indicator used and the time of loading. Temperature (e.g., 37°C) can not only increase the rate of loading, but it can also increase the rate of active extrusion and the degree of compartmentalization. In general, the latter issue of compartmentalization means that indicator loading at 37°C is not recommended.
9. Any potential impact of the fluorescent moiety on ligand binding and/or efficacy should be addressed. Dependent upon the nature of the fluorophore, this can be assessed in competition binding and/or functional assays and compared to the properties of the unlabeled ligand. For example, we have demonstrated that the addition of Cy3B to pNmU-8 did not affect potency based on functional assays using recombinantly expressed human NMU1 or NMU2.
10. The temperature at which Ca^{2+} imaging experiments are performed depends entirely upon the user. Carrying out experiments at 37°C is obviously more physiological, but also increases the risk of dye extrusion and compartmentalization. Typically, in our imaging experiments cells are loaded and de-esterified at room temperature, but experiments are performed at 37°C, with the temperature maintained by a Peltier heated coverslip holder. Typically, agonists are added to cells using a pump-driven perfusion system with flow rates of 1–5 mL/min. Agonists can then be washed out by perfusion with KHB.
11. Rate of confocal capture: As discussed in the introduction the rate of image capture will be dependent upon the confocal microscope. Previously, elementary Ca^{2+} release events (Ca^{2+} puffs) have been visualized using fluo-3 in a variety of cell types with a Noran Ozconfocal microscope recording a 256×256 pixel area at 7.5 Hz (an image every 133 ms) (83). Using the same system, rapid onset Ca^{2+} sparks have been visualized in cardiac myocytes recording a 512×115 pixel area at 30 Hz (6, 84).

Using either an Olympus Fluoview or PerkinElmer UltraVIEW confocal microscope, we more routinely measure whole cell Ca^{2+} transients (256×256 pixels) at a frequency of 1–2.5 Hz.

12. *In vitro* K_d values for most fluorescent Ca^{2+} indicators are available from Molecular Probes (<http://www.invitrogen.com>), as are a variety of *in vitro* calibration kits that attempt to mimic cellular environments (e.g., high concentrations of KCl). Ideally the fluorescent indicator chosen should be calibrated *in vivo* as described elsewhere (15), and the f_{\min} and f_{\max} calculated at the end of each experiment. Detailed discussion on the various problems with obtaining *in vivo* calibrations, not least the difficulty of obtaining accurate values for f_{\min} and f_{\max} , can be found elsewhere (15).
13. The original eGFP-tagged constructs for detecting $\text{Ins}(1,4,5)\text{P}_3$ (eGFP–PH_{PLC61}) and DAG (eGFP–PKC γ (C1₂)) production are described by Stauffer et al. (54) and Oancea et al. (55), respectively. These constructs were obtained for use from Stefan Nahorski (University of Leicester, UK), but were originally gifts from Tobias Meyer (Duke University Medical Center, North Carolina, USA). It should be noted that the success of this technique does appear to be receptor and cell dependent. No movement of the eGFP–PH_{PLC} δ_1 construct was seen upon stimulation of the endogenous muscarinic M₃ receptor in wild-type HEK293 cells. This suggests that this technique is a relatively insensitive way of examining cellular signaling compared to the use of Ca^{2+} indicators, where a robust increase in Ca^{2+} can be measured in these cells upon muscarinic M₃ receptor activation.
14. Ligand binding and subsequent internalization are, of course, temperature dependent. Internalization can be substantially reduced by lowering the temperature to <16°C. For receptor/ligand combinations where internalization is extremely rapid, making initial visualization of plasma membrane located fluorescence difficult, the temperature can be kept low (<16°C), using for example a Peltier device, to allow initial image capture, followed by an increase in temperature during the monitoring of internalization.
15. As with many ligands, the binding of a fluorescently labeled ligand may include a nonspecific component. Indeed many fluorophores are lipophilic and have the possibility of anchoring within the plasma membrane. Such lipophilic properties of the fluorescently labeled ligand and any nonspecific binding can be determined by pretreating cells with maximal concentrations of other agonists or antagonists for the receptor of interest prior to the addition of the fluorescent ligand. If parental cells are available that do not express the receptor under study, these can also provide excellent controls for nonspecific binding.

For example, we have established that parental HEK293 cells that do not express NmU receptors show no detectable fluorescence following the addition of Cy3B-pNmU-8. Furthermore, cellular associated fluorescence following addition of Cy3B-pNmU-8 is blocked in cells expressing NmU receptors by the pre-addition of a supra-maximal concentration (1 μ M) of unlabeled NmU.

16. The concentration of ligand used depends on a number of parameters including its affinity for the receptor, level of receptor expression, fluorescence intensity of the fluorophore, and sensitivity of the confocal system. For example, we have used a concentration of Cy3B-pNmU-8 (10 nM) that will give maximal receptor occupancy. Binding to the cells is easily visible and requires a laser intensity that does not result in rapid and extensive photobleaching (see Note 3).
17. It is common to lose some cells during washing. The strength at which cells adhere to the coverslip is affected by factors including cell type, presence of a substratum (e.g., poly-d-lysine), and amount of time the cells have been left to adhere. Generally, for fluorescence confocal microscopy, cell loss before the experiment has no adverse effect on the experimental outcome because investigations are made at the single-cell level. This can, however, influence the number of cells in the field of view. It is desirable to have a good number of cells (e.g., >5) per field of view. However, cell loss and particularly cell movement can affect later quantification and vigilance throughout an experiment is required.
18. The rate of perfusion required will depend on the bath volume. As an example, we have successfully used a rate of 5 mL/min with a bath volume of ~0.5 mL and have found this suitable for addition and removal of agonists or test agents in functional studies such as the measurement of $[Ca^{2+}]_i$. Bath applications are preferred if the ligand is either likely to stick to tubing or is in short supply/expensive. Some peptide ligands can be extremely “sticky” and can adhere to tubes and plasticware. This has the potential to affect the final concentration of ligand that reaches the cells. In addition, ligand may leach out of tubing onto cells during subsequent experiments. The inclusion of a carrier protein will help considerably. For NmU-8, we routinely use 0.01% BSA in the buffer.
19. Following a period of binding and/or internalization it may also be possible to remove ligand bound to the outer surface of the plasma membrane to allow, for example, easier visualization of sub-plasmalemmal fluorescence and potential recycling of fluorophore from intracellular sites back to the plasma membrane. High-affinity ligands such as Cy3B-pNmU-8 require an acid wash to promote dissociation from the receptor. This may

be problematic if the acidity changes cellular morphology or influences activity within the endocytic pathway.

20. Direct comparison of images collected immediately after the addition of the fluorescent ligand and following a period to allow internalization will permit a qualitative assessment of internalization (Fig. 3). This may be adequate if experimental paradigms are being investigated that may, for example, block internalization. In addition, internalization can be assessed using analysis software. Such software is an integral part of the confocal microscope and permits a variety of online and off-line analysis tools that can measure changes in fluorescence. For example, an ROI within a cell can be selected and changes in fluorescence determined as a function of time. An increase in cytosolic fluorescence will be indicative of ligand/receptor internalization. However, internalization most often results in the formation of sparsely distributed punctate spots and the measurement of increases in cytosolic fluorescence may be a relatively insensitive method for assessing internalization. An area of membrane can also be selected as the ROI and the loss of membrane-associated fluorescence determined as an index of internalization. Alternatively, a measure of both membrane fluorescence and cytosolic fluorescence can be derived and used to provide an index of internalization as described. This may be particularly useful when determining receptor internalization, when you can be certain that the fluorescent tag (e.g., a C-terminal eGFP tag) will not dissociate from the receptor into the extracellular space. We have used this to assess ligand-induced internalization of the recombinantly expressed GLP-1R containing a C-terminal eGFP-tag (77). To do this, the full sets of images from an experiment are examined and an ROI drawn within the cytosol of a cell along with a line as an ROI over the area representing the plasma membrane. Internalization in each cell can then be quantified using the formula $1 - (F_{m_t} / F_{c_t}) / (F_{m_b} / F_{c_b})$, where F_m is membrane fluorescence, F_c is the cytosolic fluorescence (in the case of internalized receptors, most probably predominantly the endosomal compartment), t is time, and b is basal. This should be performed for a significant number of cells. When measuring changes in fluorescence, special consideration should be given to the possible contribution of photobleaching (see Note 3). The potential contribution of photobleaching can be assessed by performing the experiment under identical conditions of laser illumination but in which internalization is blocked either chemically or by low temperature. Such experiments can be used to set experimental parameters that minimize photobleaching and can provide data that can be subtracted from experimental data to assess internalization in the absence of an influence of photobleaching. GPCR internalization can be

blocked by a variety of methods including hypertonic sucrose, phenylarsine oxide (PAO), and concanavalin A. Internalization is also essentially blocked at temperatures below 16°C. This can be achieved with a Peltier unit and is a relatively simple method for confocal microscopy. When examining fluorescent ligands it must be remembered that the technique as described determines the localization of fluorescent ligand. At any one time this may reflect a dynamic equilibrium between extracellular ligand and ligand located within different subcellular compartments. Further it may not wholly reflect receptor trafficking (69).

21. Using a high numerical aperture (NA) lens allows excellent spatial resolution of events in the cell, if accompanied by sufficient image averaging, but this is at the expense of speed of acquisition. If very fast events need to be recorded there are various tricks that can be used with a traditional LSCM. By selecting a smaller ROI and/or reducing the image averaging, along with reductions in pixel dwell time, it is possible to obtain several images per second if faster dynamics are needed (at the expense of spatial resolution). For very fast imaging of events in different areas of the cell, small ROIs can be selected in the relevant areas and scanning only done in those areas.
22. Although many confocal microscopes have a 457 nm line for excitation of CFP, this is at the edge of the excitation spectrum for YFP and so can result in direct excitation of the YFP and thus obscure any FRET. CFP can be excited using a 405 nm laser line, which has essentially no crossover with the YFP excitation range. However, if a laser line of 430 nm is available this may also be used. To remove all cross talk, cells can be transfected with plasmids containing only CFP or YFP and spectral unmixing employed (85). Briefly, cells can be transfected with plasmids containing only YFP and measure F_{DA}/F_{AA} (a) and F_{DD}/F_{DA} (b) or CFP and measure F_{DA}/F_{DD} (c) and F_{AA}/F_{DD} (d), where F_{DA} is the intensity of fluorescence upon donor excitation in acceptor emission channel, F_{DD} donor excitation/donor emission, and F_{AA} acceptor excitation/acceptor emission. Each channel's cross talk is then corrected by subtracting the intensity of the other channel's multiplied by the cross talk coefficients (a-d). For example the CFP signal is given by $F_{DD} - b \times F_{AA}$ and the FRET signal by $F_{DA} - \alpha \times F_{AA} - c \times F_{DD}$. It is also possible to measure the direct YFP fluorescence by excitation at 514 nm and emission at 535 nm as a control for photo-bleaching; however, as this requires extra scanning time, this slows down the acquisition rate and increases risk of photo-damage and is not routinely necessary. Occasional measurement of YFP fluorescence can, however, be used to correct for any photobleaching. A correction factor is given by $F_{AA}^0/F_{AA}t$ (YFP fluorescence at the start of experiment over fluorescence

intensity at a given time point). Multiply this correction factor by the F_{DA} (fluorescence intensity of the FRET channel).

23. It is possible to add drugs manually, but great care must be taken not to perturb the focal plane. By adding a larger volume dropwise, adequate mixing can be achieved; alternatively gentle pipetting up and down may be done to ensure complete mixing, but this must be done without touching the side or bottom of the chamber as this will disturb the focal plane. It is also essential to pre-warm the drug solution, as thermal variations can also affect the focal plane. If drugs need to be added in and washed out for addition of further drugs, a perfusion system is essential (see Note 18).
24. Two measures for dissociation constant may be found in the literature. K_d , measured in solution using the calcium indicator, is the absolute dissociation constant. K'_d , which is measured in the cellular context, is the apparent dissociation constant and reflects any effects of other proteins, etc. and it is this which is generally used where it has been calculated and which has been quoted.
25. Ionomycin and high $[Ca^{2+}]$ are toxic to cells, which may therefore die before probe saturation. This will give an underestimate of R_{max} and thus an overestimate of the $[Ca^{2+}]$. This has been noted for the ER probe in HeLa and MCF7 cells. An alternative protocol to determine R_{max} in the ER of such cells is to permeabilize cells for 5 min with 25 μM digitonin (to permeabilize the plasma membrane), and then add 10 mM Ca^{2+} , 1 mM ATP, and 1 mM Mg^{2+} to activate the SERCA pump. This should give rise to a plateau (R_{max}), before decaying as the cell dies.

Acknowledgements

The Wellcome Trust (grant 061050), BBSRC (Biotechnology and Biological Sciences Research Council; grants 91/C15897 and 01/A4/C/07909), GlaxoSmithKline, and the Medical Research Council (MRC) are thanked for financial support.

References

1. Sheppard CJR, Shotton DM (1997) Confocal laser scanning microscopy. BIOS Scientific Publishers Limited, Oxford, UK
2. Sheppard CJR (1999) Confocal microscopy – principles, practice and options. In: Mason WT (ed) Fluorescent and luminescent probes for biological activity. Academic, London, UK, pp 303–309
3. Lipp P, Bootman MD (1999) High resolution confocal imaging of elementary calcium signals in living cells. In: Mason WT (ed) Fluorescent and luminescent probes for biological activity. Academic, London, UK, pp 337–343
4. Berridge MJ (1997) Elementary and global aspects of calcium signaling. J Physiol 499: 291–306

5. Bootman MD, Berridge MJ, Lipp P (1997) Cooking with calcium; the recipes for composing global signals from elementary events. *Cell* 91:367–373
6. Lipp P, Laine M, Tovey SC, Burrell KM, Berridge MJ, Li W, Bootman MD (2000) Functional InsP_3 receptors that may modulate excitation-contraction coupling in the heart. *Curr Biol* 10:939–942
7. Kirchhefer U, Hanske G, Jones LR, Justus I, Kaestner L, Lipp P, Schmitz W, Neumann J (2006) Overexpression of junction causes adaptive changes in cardiac myocyte Ca^{2+} signaling. *Cell Calcium* 39:131–142
8. Grynkiewicz G, Poenie M, Tsien RY (1985) A new generation of Ca^{2+} indicators with greatly improved fluorescence properties. *J Biol Chem* 260:3440–3450
9. Minta A, Kao JP, Tsien RY (1989) Fluorescent indicators for cytosolic calcium based on rhodamine and fluorescein chromophores. *J Biol Chem* 264:8171–8178
10. Lipp P, Niggli E (1993) Ratiometric confocal Ca^{2+} -measurements with visible wavelength indicators in isolated cardiac myocytes. *Cell Calcium* 14:359–372
11. Lohr C (2003) Monitoring neuronal calcium signalling using a new method for ratiometric confocal calcium imaging. *Cell Calcium* 34: 295–303
12. Skokos D, Shakhar G, Varma R, Waite JC, Cameron TO, Lindquist RL, Schwickert T, Nussenzweig MC, Dustin ML (2007) Peptide-MHC potency governs dynamic interactions between T cells and dendritic cells in lymph nodes. *Nat Immunol* 8:835–844
13. Tsien RY (1980) New calcium indicators and buffers with high selectivity against magnesium and protons: design, synthesis, and properties of prototype structures. *Biochemistry* 19:2396–2404
14. Tsien RY, Pozzan T, Rink TJ (1982) Calcium homeostasis in intact lymphocytes: cytoplasmic free calcium monitored with a new, intracellularly trapped fluorescent indicator. *J Cell Biol* 94:325–334
15. Thomas D, Tovey SC, Collins TJ, Bootman MD, Berridge MJ, Lipp P (2000) A comparison of fluorescent Ca^{2+} indicator properties and their use in measuring elementary and global Ca^{2+} signals. *Cell Calcium* 28:213–223
16. Bolsover S, Ibrahim O, O’luanaigh N, Williams H, Cockcroft S (2001) Use of fluorescent Ca^{2+} dyes with green fluorescent protein and its variants: problems and solutions. *Biochem J* 356: 345–352
17. Tovey SC, Sun Y, Taylor CW (2006) Rapid functional assays of intracellular Ca^{2+} channels. *Nat Protoc* 1:259–263
18. Rizzuto R, Pinton P, Carrington W, Fay FS, Fogarty KE, Lifshitz LM, Tuft RA, Pozzan T (1998) Close contacts with the endoplasmic reticulum as determinants of mitochondrial Ca^{2+} responses. *Science* 280:1763–1766
19. Rudolf R, Mongillo M, Rizzuto R, Pozzan T (2003) Looking forward to seeing calcium. *Nat Mol Cell Biol* 4:579–586
20. Pozzan T, Mongillo M, Rudolf R (2003) Investigating signal transduction with genetically encoded fluorescent probes. *Eur J Biochem* 270:2343–2352
21. Miyawaki A, Llopis J, Heim R, McCaffrey JM, Adams JA, Ikura M, Tsien RY (1997) Fluorescent indicators for Ca^{2+} based on green fluorescent proteins and calmodulin. *Nature* 388:882–887
22. Miyawaki A, Griesbeck O, Heim R, Tsien RY (1999) Dynamic and quantitative Ca^{2+} measurements using improved cameleons. *Proc Natl Acad Sci USA* 96:2135–2140
23. Palmer AE, Jin C, Reed JC, Tsien RY (2004) Bcl-2-mediated alterations in endoplasmic reticulum Ca^{2+} analyzed with an improved genetically encoded fluorescent sensor. *Proc Natl Acad Sci USA* 101:17404–17409
24. Palmer AE, Giacomello M, Kortemme T, Hires SA, Lev-Ram V, Baker D, Tsien RY (2006) Ca^{2+} indicators based on computationally redesigned calmodulin-peptide pairs. *Chem Biol* 13:521–530
25. Baird GS, Zacharias DA, Tsien RY (1999) Circular permutation and receptor insertion within green fluorescent proteins. *Proc Natl Acad Sci USA* 96:11241–11246
26. Griesbeck O, Baird GS, Campbell RE, Zacharias DA, Tsien RY (2001) Reducing the environmental sensitivity of yellow fluorescent protein – mechanism and applications. *J Biol Chem* 276:29188–29294
27. Nagai T, Sawano A, Park ES, Miyawaki A (2001) Circularly permuted green fluorescent proteins engineered to sense Ca^{2+} . *Proc Natl Acad Sci USA* 98:3197–3202
28. Nakai J, Ohkura M, Imoto K (2001) A high signal-to-noise Ca^{2+} probe composed of a single green fluorescent protein. *Nat Biotech* 19:137–141
29. Ohkura M, Matsuzaki M, Kasai H, Imoto K, Nakai J (2005) Genetically encoded bright Ca^{2+} probe applicable for dynamic Ca^{2+} imaging of dendritic spines. *Anal Chem* 77:5861–5869
30. Tian L, Hires SA, Mao T, Huber D, Chiappe ME, Chalasani SH, Petreanu L, Akerboom J, McKinney SA, Schreiter ER, Bargmann CI, Jayaraman V, Svoboda K, Looger LL (2009) Imaging neural activity in worms, flies and mice with improved GCaMP calcium indicators. *Nat Methods* 6:875–881

31. Souslova EA, Belousov VV, Lock JG, Stromblad S, Kasparov S, Bolshakov AP, Pinelis VG, Labas Y, Lukyanov S, Mayr LM, Chudakov DM (2007) Single fluorescent protein-based Ca^{2+} sensors with increased dynamic range. *BMC Biotechnol* 7:37
32. Zou J, Hofer AM, Lurtz MM, Gadda G, Ellis AL, Chen N, Huang Y, Holder A, Ye Y, Louis CF, Welshhans K, Rehder V, Yang JJ (2007) Developing sensors for real-time measurement of high Ca^{2+} concentrations. *Biochemistry* 46:12275–12288
33. McCombs JE, Palmer AE (2008) Measuring calcium dynamics in living cells with genetically encodable calcium indicators. *Methods* 46:152–159
34. Romoser VA, Hinkle PM, Persechini A (1997) Detection in living cells of Ca^{2+} -dependent changes in the fluorescence emission of an indicator composed of two green fluorescent protein variants linked by a calmodulin-binding sequence. A new class of fluorescent indicators. *J Biol Chem* 272:13270–13274
35. Ishii K, Hirose K, Iino M (2006) Ca^{2+} shuttling between endoplasmic reticulum and mitochondria underlying Ca^{2+} oscillations. *EMBO Rep* 7:390–396
36. Arnaudeau S, Kelley WL, Jr Walsh JV, Demaurex N (2001) Mitochondria recycle Ca^{2+} to the endoplasmic reticulum and prevent the depletion of neighbouring endoplasmic reticulum regions. *J Biol Chem* 276:29430–29439
37. Filippin L, Magalhaes PJ, Di Benedetto G, Colella M, Pozzan T (2003) Stable interactions between mitochondria and endoplasmic reticulum allow rapid accumulation of calcium in a subpopulation of mitochondria. *J Biol Chem* 278:39224–39234
38. Emmanouilidou E, Teschemacher AG, Pouli AE, Nicholls LI, Seward EP, Rutter GA (1999) Imaging Ca^{2+} concentration changes at the secretory vesicle surface with a recombinant targeted cameleon. *Curr Biol* 9:915–918
39. Heim N, Griesbeck O (2004) Genetically encoded indicators of cellular calcium dynamics based on troponin C and green fluorescent protein. *J Biol Chem* 279:14280–14286
40. Nagai T, Yamada S, Tominaga T, Ichikawa M, Miyawaki A (2004) Expanded dynamic range of fluorescent indicators for Ca^{2+} by circularly permuted yellow fluorescent proteins. *Proc Natl Acad Sci USA* 101:10554–10559
41. Mank M, Reiff DF, Heim N, Friedrich MW, Borst A, Griesbeck O (2006) A FRET-based calcium biosensor with fast signal kinetics and high fluorescence change. *Biophys J* 90:1790–1796
42. Higashijima S, Masino MA, Mandel G, Fetcho JR (2003) Imaging neuronal activity during zebrafish behaviour with a genetically encoded calcium indicator. *J Neurophysiol* 90:3986–3997
43. Hasan MT, Friedrich RW, Euler T, Larkum ME, Giese G, Both M, Duebel J, Waters J, Bujard H, Griesbeck O, Tsien RY, Nagai T, Miyawaki A, Denk W (2004) Functional fluorescent Ca^{2+} indicator proteins in transgenic mice under TET control. *PLoS Biol* 2:763–775
44. Ji G, Feldman ME, Deng KY, Greene KS, Wilson J, Lee JC, Johnston RC, Rishniw M, Tallini Y, Zhang J, Wier WG, Blaustein MP, Xin HB, Nakai J, Kotlikoff MI (2004) Ca^{2+} -sensing transgenic mice – postsynaptic signaling in smooth muscle. *J Biol Chem* 279:21461–21468
45. Iwano M, Shiba H, Miwa T, Che FS, Takayama S, Nagai T, Miyawaki A, Isogai A (2004) Ca^{2+} dynamics in a pollen grain and papilla cell during pollination of *Arabidopsis*. *Plant Physiol* 136:3562–3571
46. Kerr R, Lev-Ram V, Baird G, Vincent P, Tsien RY, Schafer WR (2000) Optical imaging of calcium transients in neurons and pharyngeal muscle of *C. elegans*. *Neuron* 26:583–594
47. Reiff DF, Thiel PR, Schuster CM (2002) Differential regulation of active zone density during long-term strengthening of *Drosophila* neuromuscular junctions. *J Neurosci* 22:9399–9409
48. Fiala A, Spall T, Diegelmann S, Eisermann B, Sachse S, Devaud J-M, Buchner E, Galizia CG (2002) Genetically expressed cameleon in *Drosophila melanogaster* is used to visualize olfactory information in projection neurons. *Curr Biol* 12:1877–1884
49. Reiff DF, Ihring A, Guerrero G, Isacoff EY, Joesch M, Nakai J, Borst A (2005) In vivo performance of genetically encoded indicators of neural activity in flies. *J Neurosci* 25:4766–4778
50. Palmer AE, Tsien RY (2006) Measuring calcium signaling using genetically targetable fluorescent indicators. *Nat Protoc* 1:1057–1065
51. Young KW, Bampton ETW, Pinon L, Bano D, Nicotera P (2008) Mitochondrial Ca^{2+} signalling in hippocampal neurons. *Cell Calcium* 43:296–306
52. Fujioka A, Terai K, Itoh RE, Aoki K, Nakamura T, Kuroda S, Nishida E, Matsuda M (2006) Dynamics of the Ras/ERK MAPK cascade as monitored by fluorescent probes. *J Biol Chem* 281:8917–8926
53. Li IT, Pham E, Truong K (2006) Protein biosensors based on the principle of fluorescence resonance energy transfer for monitoring cellular dynamics. *Biotechnol Lett* 28:1971–1982
54. Stauffer TP, Ahn S, Meyer T (1998) Receptor induced transient reduction in plasma membrane $\text{PtdIns}(4,5)\text{P}_2$ concentration monitored in living cells. *Curr Biol* 8:343–346

55. Oancea E, Teruel MN, Quest AFG, Meyer T (1998) Green fluorescent protein (GFP)-tagged cysteine-rich domains from protein kinase C as fluorescent indicators for diacylglycerol signalling in living cells. *J Cell Biol* 140:485–498
56. Nash MS, Young KW, Willars GB, Challiss RA, Nahorski SR (2001) Single cell imaging of graded $\text{Ins}(1,4,5)\text{P}_3$ production following G-protein-coupled-receptor activation. *Biochem J* 356:137–142
57. Nahorski SR, Young KW, Challiss RAJ, Nash MS (2003) Visualizing phosphoinositide signalling in single neurons gets a green light. *Trends Neurosci* 26:444–452
58. Oancea E, Meyer T (1998) Protein kinase C as a molecular machine for decoding calcium and diacylglycerol signals. *Cell* 95:307–318
59. Tanimura A, Nezu A, Morita T, Turner RJ, Tojo Y (2004) Fluorescent biosensor for quantitative real-time measurements of inositol 1,4,5-trisphosphate in single living cells. *J Biol Chem* 279:38095–38098
60. Sato M, Ueda Y, Shibuya M, Umezawa Y (2005) Locating inositol 1,4,5-trisphosphate in the nucleus and neuronal dendrites with genetically encoded fluorescent indicators. *Anal Chem* 77:4751–4758
61. Remus TP, Zima AV, Bossuyt J, Bare DJ, Martin JL, Blatter LA, Bers DM, Mignery GA (2006) Biosensors to measure inositol 1,4,5-trisphosphate concentration in living cells with spatiotemporal resolution. *J Biol Chem* 281:608–616
62. Matsuya T, Michikawa T, Inoue T, Miyawaki A, Yoshida M, Mikoshiba K (2006) Cytosolic inositol 1,4,5-trisphosphate dynamics during intracellular calcium oscillations in living cells. *J Cell Biol* 173:755–765
63. Varnai P, Rother KI, Balla T (1999) Phosphatidylinositol 3-kinase-dependent membrane association of the Bruton's tyrosine kinase pleckstrin homology domain visualized in single living cells. *J Biol Chem* 274:10983–10989
64. Ponsioen B, Zhao J, Riedl J, Zwartkruis F, van der Krogt G, Zaccolo M, Moolenaar WH, Bos JL, Jalink K (2004) Detecting cAMP-induced Epac activation by fluorescence resonance energy transfer: Epac as a novel cAMP indicator. *EMBO Rep* 5:1176–1180
65. DiPilato LM, Cheng X, Zhang J (2004) Fluorescent indicators of cAMP and Epac activation reveal differential dynamics of cAMP signalling within discrete subcellular compartments. *Proc Natl Acad Sci USA* 101:16513–16518
66. Honda A, Adams SR, Sawyer CL, Lev-Ram V, Tsien RY, Dostmann WR (2001) Spatiotemporal dynamics of guanosine 3',5'-cyclic monophosphate revealed by a genetically encoded, fluorescent indicator. *Proc Natl Acad Sci USA* 98:2437–2442
67. Kallal L, Benovic JL (2000) Using green fluorescent proteins to study G-protein-coupled receptor localization and trafficking. *Trends Pharmacol Sci* 21:175–180
68. Milligan G (2003) High-content assays for ligand regulation of G-protein-coupled receptors. *Drug Discov Today* 8:579–585
69. Koenig JA, Kaur R, Dodgeon L, Edwardson JM, Humphrey PPA (1998) Fates of endocytosed somatostatin sst_2 receptors and associated agonist. *Biochem J* 336:291–298
70. Daly CJ, McGrath JC (2003) Fluorescent ligands, antibodies, and proteins for the study of receptors. *Pharmacol Ther* 100:101–118
71. Miyawaki A, Sawano A, Kogure T (2003) Lighting up cells: labelling proteins with fluorophores. *Nat Cell Biol* (Suppl.): S1–S7
72. Awaji T, Hirasawa A, Kataoka M, Shinoura H, Nakayama Y, Sugawara T, Izumi S, Tsujimoto G (1998) Real-time optical monitoring of ligand-mediated internalization of $\alpha(1\beta)$ -adrenoceptor with green fluorescent protein. *Mol Endocrinol* 12:1099–1111
73. Go WY, Roettger BF, Holicky EL, Hadac EM, Miller LJ (1997) Quantitative dynamic multi-compartmental analysis of cholecystokinin receptor movement in a living cell using dual fluorophores and reconstruction of confocal images. *Anal Biochem* 247:210–215
74. Maamra M, Finidori J, Von Laue S, Simon S, Justice S, Webster J, Dower S, Ross R (1999) Studies with a growth hormone antagonist and dual-fluorescent confocal microscopy demonstrate that the full-length human growth hormone receptor, but not the truncated isoform, is very rapidly internalized independent of Jak2-Stat5 signaling. *J Biol Chem* 274:14791–14798
75. Sneddon WB, Syme CA, Bisello A, Magyar CE, Rochdi MD, Parent J-L, Weinman EJ, Abou-Samra AB, Friedman PA (2003) Activation-independent parathyroid hormone receptor internalization is regulated by NHERF1 (EBP50). *J Biol Chem* 278:43787–43796
76. Böhme I, Beck-Sickinger AG (2009) Illuminating the life of GPCRs. *Cell Commun Signal* 7:16
77. Huang Y, Wilkinson GF, Willars GB (2010) Role of the signal peptide in the synthesis and processing of the glucagon-like peptide-1 receptor. *Br J Pharmacol* 159:237–251
78. Harlow E, Lane D (1988) Antibodies – a laboratory manual. Cold Spring Harbor Laboratory, Cold Spring Harbor, NY, USA
79. Mongan LC, Grubb BD (2004) Immunocytochemical identification of G-protein-coupled receptor expression and

- localization. In: Willars GB, Challiss RAJ (eds) Methods in molecular biology, vol 259, 2nd edn, Receptor signal transduction protocols. Humana, Totowa, NJ
80. Kao JPY (1994) Practical aspects of measuring $[Ca^{2+}]$ with fluorescent indicators. In: Nuccitelli R (ed) A practical guide to the study of calcium in living cells. Academic, San Diego, CA, pp 155–180
81. Bader JE, Beck-Sickinger AG (2004) Fluorescence resonance energy transfer to study receptor dimerization in living cells. In: Willars GB, Challiss RAJ (eds) Methods in molecular biology, vol 259, 2nd edn, Receptor signal transduction protocols. Humana, Totowa, NJ
82. Di Virgilio F, Steinberg TH, Silverstein SC (1990) Inhibition of Fura-2 sequestration and secretion with organic anion transport blockers. *Cell Calcium* 11:57–62
83. Tovey SC, de Smet P, Lipp P, Thomas D, Young KW, Missiaen L, De Smedt H, Parys JB, Berridge MJ, Thuring J, Holmes A, Bootman MD (2001) Calcium puffs are generic $InsP_3$ -activated elementary calcium signals and are down-regulated by prolonged hormonal stimulation to inhibit cellular calcium responses. *J Cell Sci* 114:3979–3989
84. Mackenzie L, Bootman MD, Laine M, Berridge MJ, Thuring J, Holmes A, Li WH, Lipp P (2002) The role of inositol 1,4,5-trisphosphate receptors in Ca^{2+} signalling and the generation of arrhythmias in rat atrial myocytes. *J Physiol* 541:395–409
85. Gordon GW, Berry G, Liang XH, Levine B, Herman B (1998) Quantitative fluorescence resonance energy transfer measurements using fluorescence microscopy. *Biophys J* 74: 2702–2713

Chapter 4

Ratiometric Ca²⁺ Measurements Using the FlexStation® Scanning Fluorometer

Ian C.B. Marshall, Izzy Boyfield, and Shaun McNulty

Abstract

The FlexStation® Scanning Fluorometer is a fluorescence plate reader that can measure intracellular Ca²⁺ concentration using both single-wavelength and dual-wavelength fluorescent probes. The FlexStation uses a Xenon flashlamp and monochromators for both excitation and emission light to allow the use of a wide range of fluorescent indicators. The system incorporates a fluid transfer system for addition of test compounds from a source plate to the cell plate during data acquisition. Both plates are contained within a temperature-controlled unit that can be controlled accurately between room temperature and 45°C. The FlexStation can be configured to read a range of plate sizes. In this chapter generic methods for assessing intracellular Ca²⁺ on the FlexStation using ratiometric dyes are described.

Key words: Calcium, Flexstation, High throughput

1. Introduction

Many commercial organizations currently use the Fluorometric Imaging Plate Reader (FLIPR®: Molecular Devices, Sunnyvale, California, USA) to conduct high-throughput measurements of intracellular Ca²⁺ concentration (see Chapter 7), taking advantage of its rapid kinetics, reliability, and compatibility for automation. For the majority of industrial applications, the primary limitation of FLIPR (i.e., its requirement for single-wavelength fluorescent probes using visible light excitation) is not a significant issue. Indeed, visible light probes offer certain benefits over their UV-excited ratiometric counterparts such as reduced sample autofluorescence and higher absorbance, thereby allowing relatively low concentrations of dye to be used. However, under certain circumstances researchers may prefer to conduct high-throughput experiments with ratiometric dyes, particularly when issues of dye leakage, photobleaching, or signal-to-noise ratio become a concern.

The most commonly used dual-wavelength ratiometric dye for Ca^{2+} measurements is fura-2 (1). The fluorescence emission from fura-2 (measured at greater than 510 nm) varies with Ca^{2+} concentration depending on the excitation wavelength used. When excited at 340 nm, fura-2 emission increases with increasing Ca^{2+} concentration. However, when excited at 380 nm, fura-2 emission decreases with increasing Ca^{2+} concentration. The ratio of emissions following excitation at 340 nm and 380 nm is a more reliable indicator of Ca^{2+} concentration than emission from single-wavelength dyes because it is less affected by differences in dye concentration (as may occur during loading), photobleaching, and illumination intensity and offers an improved signal:noise ratio. Consequently, fura 2 lends itself to more accurate calibration of intracellular free Ca^{2+} concentration within cells compared to single-wavelength dyes.

The FlexStation[®] Scanning Fluorometer (Molecular Devices, Sunnyvale, California, USA; Fig. 1) is a fluorescence plate reader that can measure intracellular Ca^{2+} concentration using both single-wavelength and dual-wavelength fluorescent probes. The FlexStation uses a Xenon flashlamp and monochromators for both excitation and emission light to allow the use of a wide range of

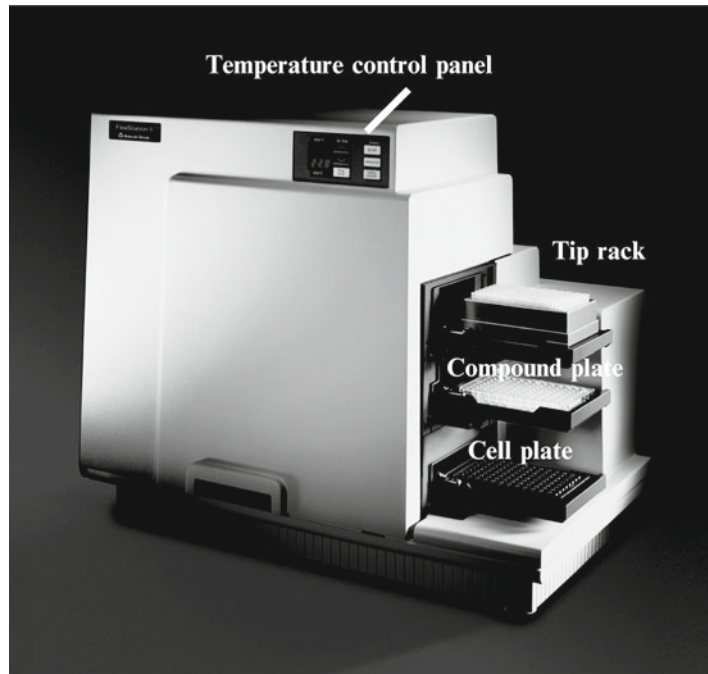


Fig. 1. The FlexStationTM scanning fluorometer (Molecular Devices, Sunnyvale, California, USA). Critical components of the system are *marked*.

fluorescent indicators (excitation range 250–850 nm; emission range 375–850 nm). This flexibility in choosing specific wavelengths also allows the FlexStation to perform excitation and emission scans for characterizing new fluorescent markers. The system incorporates a fluid transfer system for addition of test compounds from a source plate to the cell plate during data acquisition. Both plates are contained within a temperature-controlled unit that can be controlled accurately between room temperature and 45°C. The FlexStation can be configured to read 6-, 12-, 24-, 48-, 96-, and 384-well plates although fluid transfer is currently limited to 96- and 384-well plate format. In contrast to FLIPR, each well is read individually, thereby reducing temporal resolution across the plate. To offset this limitation, compounds are added to the cell plate one column at a time and responses are monitored for the duration of the experiment in each column.

The time interval between successive Ca²⁺ measurements may be a deciding factor in assessing whether the FlexStation is an appropriate tool for ratiometric Ca²⁺ measurements in a particular study, and it is therefore important for the user to understand fully how the instrument collects ratio pairs during a typical experiment. Once compounds have been added to a single column of the plate, the wells are excited first with 340 nm light and emission is measured down all wells of the column with 0.1-s time resolution between wells. The excitation wavelength is then switched to 380 nm and emission is measured back up the column, again with a time resolution of 0.1 s. The excitation wavelength is then switched back to 340 nm for the next set of time-points until the column has been imaged across the full time-course of the experiment. Compounds are then added to the next column of the plate and the cycle is repeated. In practice, this means that the shortest time interval between 340 nm and 380 nm recordings in a single well varies between 2.2 and 0.75 s depending on whether the well lies at the top or bottom of the column. Also, the shortest time between successive 340 nm recordings within a single well is approximately 3 s in a 96-well plate. For very rapid Ca²⁺ transients, this method for collecting 340:380 nm pairs may be unsuitable since peak Ca²⁺ responses are liable to be underestimated. However, slower and more sustained Ca²⁺ transients can be measured without significantly underestimating the peak Ca²⁺ response and with the additional advantages of compensating for uneven dye loading and photobleaching. Here, we describe generic methods for assessing intracellular Ca²⁺ on the FlexStation using ratiometric dyes. These methods are best used as a starting point to which additional modifications relevant to the researchers' particular cell system can be made.

2. Materials

1. Suitable cell cultures are necessary which may include Human Embryonic Kidney (HEK293) cells and Chinese Hamster Ovary (CHO) cells.
2. Tyrodes Buffer (145 mM NaCl, 2.5 mM KCl, 10 mM HEPES, 10 mM glucose, 1.2 mM MgCl₂, 1.5 mM CaCl₂).
3. Fura-2 acetoxymethyl ester (Molecular Probes, Eugene, OR) dissolved in dimethyl sulfoxide (DMSO) to provide a 2 mM stock solution. Aliquots should be stored at -20°C and used once after thawing (see Note 1).
4. Probenecid (Sigma, Poole, UK) dissolved in 1 M NaOH (5 ml) and diluted 1:1 with Tyrodes buffer to give a 250 mM stock (see Note 2).
5. Pluronic F-127 (Molecular Probes, Eugene, OR) dissolved in DMSO at 20% (w/v) (see Note 3).
6. 75 cm² culture flasks (Nunc, Denmark).
7. Cell plates: 96-well black walled, clear base plates with or without poly-D-lysine coating (Corning Inc, High Wycombe, UK).
8. Compound plates: 96-deepwell clear V-bottom polypropylene plates (Greiner, Stonehouse, UK).
9. Disposable 200 µl non-sterile polypropylene tips (Molecular Devices Corporation, Sunnyvale, California, USA).
10. Embla Plate Washer (Molecular Devices).

3. Methods

3.1. Preparation of Cells for Ca²⁺ Measurements

1. HEK293 cells are typically grown in 75 cm² flasks in minimum essential medium (MEM) supplemented with nonessential amino acids, 10% fetal calf serum, and 2 mM L-glutamine at 37°C under 5% CO₂. CHO cells are grown in Hams-F12 medium supplemented with 10% fetal bovine serum at 37°C under 5% CO₂.
2. Cells are typically seeded into black-walled, clear-based 96-well plates at a density of 25,000 cells per well (minimum volume 100 µl) and cultured overnight (see Note 4) prior to use.

3.2. Preparation of Agonist/Antagonist Plates

1. Prepare agonists and antagonists in clear 96-deepwell plates as follows. Make up agonists at four times and antagonists at six times their final maximum assay concentrations by dissolving first in appropriate solvent and then diluting in Tyrodes buffer.

2. Apply highest required concentrations of compounds to the end column of plates and perform serial dilutions across the plates as required. Half- or quarter-log dilutions can be performed either manually or using robotics (e.g., Biomek 2000, Beckman Coulter). The final concentrations used are commonly 0.1 nM to 10 µM. For compounds dissolved in DMSO, the final concentration of DMSO applied to cells should not exceed 1%.

3.3. Loading Cells with Fura-2

1. Equal volumes of fura-2 stock and Pluronic F-127 stock are mixed to provide an adequate volume for cell loading.
2. Make up loading medium by adding fura 2:pluronic F-127 mixture to cell culture medium to give a final fura 2 concentration of 2 µM.
3. Remove medium from cell plate and replace with 100 µl loading medium per well. Incubate for between 30 and 120 min at either room temperature or 37°C (see Note 5). Probenecid (2.5 mM) can be included in the loading medium and/or wash medium if required (see Note 2).
4. Wash cells three times with Tyrodes buffer using an Embla Plate Washer and leave in 125 µl Tyrodes for antagonist studies or 150 µl for single-addition agonist studies as appropriate. Add 25 µl of buffer or antagonist as appropriate from the antagonist plate (this step can be done using a Biomek FX robotic system, Beckman Coulter) and incubate for 30 min to allow antagonists to bind and to allow cells to de-esterify intracellular fura-2 am dye (see Note 6).
5. Wash cells three times with Tyrodes buffer using the Embla Plate Washer and incubate in 150 µl Tyrode solution (see Note 7).
6. Transfer the cell plate, agonist plate, and tip rack to the appropriate drawers in the FlexStation prior to experimentation.

3.4. Setting Up the FLEXStation for Fura-2 Ratiometric Measurements

1. Open SoftMax Pro® Software and choose the FLEX option under Set-Up.
2. Set the number of wavelengths to 2 and choose excitation wavelengths of 340 nm and 380 nm in LM1 and LM2.
3. For maximum time resolution, set the Readings speed to fast (under Sensitivity) and set Timing Interval to match the minimum interval (3.1 s at highest resolution).
4. Set other parameters as appropriate, including length of experiment, wells to read, compound addition parameters, and assay plate type (see Note 8).
5. Once parameters have been set, click Read to initiate compound addition and data capture.

3.5. Data Analysis

1. Data are automatically stored to disk at the end of the capture. Data may be analyzed using the extensive data calculation and analysis capabilities of SoftMax Pro or off-line by exporting fluorescence values and time-points as an ASCII file.
2. Ratio measurements can be converted to intracellular $[Ca^{2+}]$ using the following Eq. 1:

$$[Ca^{2+}] = K_d (R - R_{min}) / (R_{max} - R) (F_{380max} / F_{380min}), \quad (1)$$

where K_d is the dissociation constant of Fura-2, R_{min} and R_{max} are the 340/380 ratios of the Ca^{2+} -free and Ca^{2+} -bound forms of the dye, respectively, and F_{380max} and F_{380min} are the fluorescence emission intensities of Ca^{2+} -free and Ca^{2+} -bound dye, respectively, following excitation at 380 nm. R_{min} , R_{max} , F_{380max} , and F_{380min} are determined empirically within the plate by incubating cells either with 10 μM ionomycin (to achieve R_{max} and F_{380min}) or with ionomycin and 10 mM EGTA (to achieve R_{min} and F_{380max}).

4. Notes

1. Fura 2 AM is insoluble in aqueous solution. A concentrated stock in DMSO should be divided into small aliquots suitable for individual experiments and stored frozen at $-20^{\circ}C$ until use. It is essential to mix the DMSO stock well to avoid the formation of particulates which can become compartmentalized during dye loading.
2. Probenecid is an inhibitor of inorganic anion transporters that are able to extrude the hydrolyzed form of fura 2 from the cytosol. It is advisable to compare dye loading in the presence and absence of probenecid to determine whether inorganic anion transporters present a potential problem in the particular cells under investigation.
3. Pluronic F-127 is a nonionic detergent that is commonly used to improve dispersion of fura 2 AM in aqueous solution. For best results, it should be mixed with fura 2 AM before addition to the aqueous buffer.
4. Weakly adherent cell lines can be used in the FlexStation by using poly-D lysine-coated plates. Suspension cultures can also be used in the FlexStation. However, for these cells it is advisable to centrifuge cells to the bottom of the plate following loading in order to generate a monolayer of cells at the bottom of the well.
5. Optimal dye loading conditions (e.g., concentration of dye, loading time/temperature, and inclusion of probenecid) should be determined empirically for each cell line.

6. Since the ester and free acid forms of fura 2 have different spectral properties and sensitivities to Ca²⁺, it is important to assist removal of nonhydrolyzed ester from the cytosol following loading (i.e., de-esterification). Therefore, a 30-min incubation period is recommended following dye loading to allow both hydrolysis of fura 2 AM and diffusion of fura 2 AM from the cytosol into the wash buffer.
7. The protocol for the Embla Plate Washer should be optimized for each assay. Adjustments can be made to aspiration and dispensation heights, dispensation speed, strength of the vacuum, and number of washes per cycle in order to minimize cell disruption. After the final wash step, cells should typically be allowed to recover for an additional 20 min before running on the FlexStation.
8. The parameters for the integrated FlexStation pipettor require optimization for each assay. The dispensation height of the pipettor and the speed of dispensation should be adjusted to ensure optimal delivery of the compounds to the specific plates being used. Optimal delivery should not cause cell disruption but should allow adequate mixing of the compounds in the well. To assist adequate mixing of compounds, the volume of agonist added to the well is typically 25% of the final well volume. The optimal dispenser speed may vary according to how well cells adhere to the bottom of the well. Cells can be checked following dispensation using the plate viewer.

Reference

1. Grynkiewicz G, Poenie M, Tsien RY (1985) A new generation of Ca²⁺ indicators with greatly improved fluorescence properties. *J Biol Chem* 260:3440–3450

Chapter 5

Measuring Ca²⁺ Changes in Multiwell Format Using the Fluorometric Imaging Plate Reader (FLIPR®)

Ian C.B. Marshall, Davina E. Owen, and Shaun McNulty

Abstract

The Fluorometric Imaging Plate Reader (FLIPR) has made a significant contribution to drug discovery programs. The key advantage of FLIPR over conventional plate readers is the ability to measure fluorescence emission from multiple wells (96 wells or 384 wells) simultaneously and with high temporal resolution. Consequently, FLIPR has been used extensively to record dynamic intracellular processes such as changes in intracellular Ca²⁺ ion concentration, membrane potential, and pH. Since FLIPR is used to measure a functional response in cells, it is rapidly able to distinguish full agonists, partial agonists, and antagonists at a target of interest, making the system a valuable screening tool for interrogation of compound libraries. Automated FLIPR systems for ultra high throughput have also become available that employ integrated plate stackers, washers and specialized stages to allow users to shuttle cell and compound plates from incubators or storage magazines onto the FLIPR system itself. In this chapter generic methods for assessing intracellular Ca²⁺ on the FLIPR are described.

Key words: Calcium, Fluorometric imaging plate reader, High throughput

1. Introduction

The Fluorometric Imaging Plate Reader (FLIPR: Molecular Devices, Sunnyvale, California, USA) (see Fig. 1) has made a significant contribution to drug discovery programs in the pharmaceutical industry since the first commercial instruments were introduced seven years ago (1). The key advantage of FLIPR over conventional plate readers is the ability to measure fluorescence emission from multiple wells (96 wells or 384 wells) simultaneously and with high temporal resolution. Consequently, FLIPR has been used extensively to record dynamic intracellular processes such as changes in intracellular Ca²⁺ ion concentration, membrane potential, and pH. Since FLIPR is used to measure a functional response in cells, it is rapidly able to distinguish full agonists, partial agonists,



Fig. 1. The Fluorometric Imaging Plate Reader (FLIPR; Molecular Devices, Sunnyvale, California, USA).

and antagonists at a target of interest, making the system a valuable screening tool for interrogation of compound libraries. Typically, FLIPR can be used to screen over 150 compound plates per day in a high throughput screening environment equating to over 50,000 compounds at a single concentration in a 384-well system.

Since FLIPR is an excellent tool for monitoring changes in intracellular Ca^{2+} concentration, it is ideally suited to the characterization of ligand-gated ion channels or G protein-coupled receptors (GPCRs) linked to phospholipase C and Ca^{2+} mobilization. However, GPCRs that normally signal through adenylyl cyclase

(i.e., receptors coupled to G_i or G_s) can also be studied using FLIPR in recombinant systems through the use of promiscuous “adaptor” (2) and chimeric G-proteins (3, 4) that artificially couple these receptors to the Ca²⁺ release machinery.

The FLIPR system uses an argon-ion laser to illuminate each well of a 96- or 384-well plate simultaneously. The laser has two excitation peaks (488 nm and 510 nm) making the system compatible for a number of nonratiometric Ca²⁺ indicator dyes including fluo 3, fluo 4, and Calcium Green-1. Emitted light from the whole plate is collected through a highly sensitive, cooled charge coupled device (CCD) camera. Patented excitation optics in conjunction with restricted depth of field of the CCD camera reduces the contribution of background fluorescence due to extracellular dye. Successive measurements can be taken at 1 s intervals across the whole plate for measurement of transient responses or can be taken over tens of minutes for responses demonstrating longer time courses. During acquisition, a robotic multiwell pipettor adds test compounds to the plate as required, allowing measurements to be taken before and after compound addition. A large number of experimental parameters can be controlled by the user (e.g., laser parameters, camera parameters, time of agonist addition, mixing parameters) in order to permit optimization of assays for different cells and dye loading protocols. In order to minimize experimental variability due to inconsistent environmental conditions, the FLIPR system contains a heated stage maintaining the assay and reagent microplates at a constant temperature during experiments.

Recently the FLIPR³ system has been launched which offers additional sensitivity and capability to measure luminescence (e.g., some bright luciferase, and aequorin). Automated FLIPR systems for ultra high throughput have also become available that employ integrated plate stackers, washers and specialized stages to allow users to shuttle cell and compound plates from incubators or storage magazines onto the FLIPR system itself.

Here we describe generic methods that can be used to study agonist and antagonist properties of test compounds in recombinant cell systems using standard FLIPR formats. These methods are best used as a starting point to which additional modifications relevant to the researchers particular model system should be made to optimize signal-to-noise ratios.

2. Materials

1. Human Embryonic Kidney (HEK293) cells and Chinese Hamster Ovary (CHO) cells. These are typical cell lines used successfully in FLIPR experiments designed to investigate recombinantly expressed targets (see Note 1).

2. Tyrodes Buffer (145 mM NaCl, 2.5 mM KCl, 10 mM HEPES, 10 mM glucose, 1.2 mM MgCl₂, 1.5 mM CaCl₂).
3. Fluo 3 or Fluo 4 acetoxyethyl ester (Molecular Probes, Eugene, OR) dissolved in dimethyl sulfoxide (DMSO) to give a 2 mM stock solution. Aliquots should be stored at -20°C and used once only after thawing (see Note 2).
4. Probenecid (Sigma, Poole, UK) dissolved in 1 M NaOH (5 ml) and diluted 1:1 with Tyrodes buffer to give a 250 mM stock (see Note 3).
5. Pluronic F-127 (Molecular Probes, Eugene, OR) dissolved in DMSO at 20% (w/v) (see Note 4).
6. 75 cm² Culture flasks (Nunc, Denmark).
7. Cell plates: 96-well black walled, clear base plates with or without poly-D-lysine, or suitable alternative coatings (Corning Inc, High Wycombe, UK).
8. Compound plates: 96-deepwell clear V-bottom polypropylene plates (Greiner, Stonehouse, UK).
9. Black disposable 200 µl nonsterile polypropylene tips (Molecular Devices Corporation, UK).
10. Embla Plate Washer (Molecular Devices Corporation, Sunnyvale, CA).

3. Methods

3.1. Preparation of Cells for Ca²⁺ Measurements

1. HEK293 cells are typically grown in 75 cm² flasks in minimum essential medium (MEM) supplemented with nonessential amino acids, 10% fetal calf serum, and 2 mM L-glutamine at 37°C under 5% CO₂. CHO cells are grown in Hams-F12 medium supplemented with 10% fetal bovine serum at 37°C under 5% CO₂.
2. Seed cells into black walled, clear based 96-deepwell plates at a density of 25,000 cells per well (minimum volume 100 µl) and culture overnight prior to experimentation (see Note 1).

3.2. Preparation of Agonist/Antagonist Plates

1. Prepare agonists and antagonists in clear 96-deepwell plates as follows. Make up agonists at four times and antagonists at six times their final maximum concentrations by dissolving first in appropriate solvent and diluting in Tyrodes buffer.
2. Apply highest required concentrations of compounds to end column of plates and perform serial dilutions across the plates as required. Half- or quarter-log dilutions can be performed either manually or using robotic systems (e.g., Biomek 2000,

Beckman Coulter). The final concentration ranges used are commonly between 0.1 nM and 10 μM. For compounds dissolved in DMSO, the final concentration of DMSO applied to cells should not exceed 1%. Adequate experimental controls must be established to investigate potential solvent effects for each experimental system used.

3.3. Loading Cells with Fluorescent Indicator

1. Mix equal volumes of fluorescent indicator (fluo 3/fluo 4) and Pluronic F-127 stocks.
2. Prepare loading medium by adding dye–pluronic F-127 mixture to cell culture medium or Tyrodes buffer to obtain a final concentration of 6 μM (Fluo-4) or 12 μM (Fluo-3).
3. Add 50 μl loading medium per well. Incubate for 30–120 min at either room temperature or 37°C (see Note 5). Probenecid (2.5 mM) can be included in the loading medium and/or wash medium if required ensuring adequate dye loading (see Note 3).
4. Wash the cells four times with 200 μl Tyrodes buffer using an Embla Plate Washer and leave in 125 μl Tyrodes (see Note 6) for antagonist studies or 150 μl for agonist studies requiring a single compound addition.
5. Add 25 μl of buffer or antagonist as appropriate from the antagonist plate (this step can be done using a Biomek FX robotic system, Beckman Coulter) and incubate for 30 min.

3.4. Measurement of Ca²⁺ on the FLIPR

1. Transfer the cell plate, agonist plate, and tip rack to the appropriate positions on the FLIPR imaging platform.
2. A signal test should be undertaken to establish effective dye loading and confirm robust cell plating by establishing basal fluorescence prior to experimental initiation. During this process, the CCD camera captures an image of the plate before addition of agonists and the mean fluorescence reading for each well is displayed on the monitor. The signal test allows the user to determine whether cells have loaded with dye uniformly across the plate and also if preincubated antagonists have elicited any agonist effect on the cells. An optimal signal test should give an average fluorescence intensity value of 8,000–12,000 fluorescence intensity units (FIU) per well (see Note 7).
3. If the fluorescence intensity value is too low to obtain a good signal-to-noise ratio, adjust FIU output if necessary by altering the laser output, the camera aperture or the image exposure length. Typically, the camera aperture is set to F2, the camera exposure to 0.4 s and the laser output is adjusted between 300 and 800 mW to achieve optimal fluorescence intensity.
4. Adjust FLIPR run protocol as required to control data acquisition parameters and compound additions. During the run the

FLIPR will automatically transfer agonists to the cell plate using an integrated robot and images will be captured before and after the addition of agonist (see Note 8).

5. Once parameters are set, initiate the experimental run.

3.5. Data Analysis

1. Following completion of the FLIPR acquisition, data are automatically stored on the PC. For permanent storage of data files, it is recommended that data is transferred via networked connections to a secure server or recordable CD.
2. For each well, fluorescent readings are extracted and tabulated versus time within an ASCII text file. Data can then be exported to another system for analysis of results and curve fitting. Typically data are analyzed using an iterative curve-fitting package (e.g., GraphPad Prism) and curves are fitted using a four-parameter logistic equation.
3. Agonist potencies are typically reported as EC_{50} values (concentration yielding half-maximal effect) or pEC_{50} (where $pEC_{50} = -\log[EC_{50}]$) and intrinsic activity (maximal effect as a proportion of the maximal effect of a reference agonist).
4. Antagonist potencies are typically reported as IC_{50} values (molar concentration yielding 50% inhibition of a reference agonist stimulation) or K_B as follows:

$$K_B = IC_{50} / \left(1 + \left([agonist] / EC_{50} \right) \right),$$

where $[agonist]$ is the molar agonist concentration used and EC_{50} is the molar potency of the agonist.

4. Notes

1. Weakly adherent cell lines can be used in the FLIPR by using poly-D lysine coated plates. Suspension cultures can also be used in FLIPR. However, for these cells it is advisable to centrifuge cells to the bottom of the plate following loading in order to generate a monolayer of cells at the bottom of the well.
2. Fluo3 AM and Fluo 4 AM are insoluble in aqueous solution. Concentrated stocks in DMSO should be divided into small aliquots suitable for individual experiments and stored frozen at -20°C until use. It is essential to mix the DMSO stock well to avoid the formation of particulates which can become compartmentalized during dye loading.
3. Probenecid is an inhibitor of inorganic anion transporters that are able to extrude the hydrolyzed form of dyes from the cytosol. During assay development, it is advisable to compare dye loading in the presence and absence of probenecid to determine

whether inorganic anion transporters are a problem in the particular cells under investigation.

4. Pluronic F-127 is a nonionic detergent that is commonly used to improve dispersion of acetoxyethyl ester forms of fluorescent indicators in aqueous solution. For optimum results, pluronic should be mixed with dye before addition to the aqueous buffer.
5. Optimal dye loading conditions (e.g., concentration of dye, loading time/temperature, and inclusion of probenecid) should be determined empirically during assay development for each cell line utilized.
6. The protocol for the Embla Plate Washer should be optimized for each assay. Adjustments can be made to aspiration and dispensation heights, dispensation speed, the strength of the vacuum and the number of washes per cycle in order to minimize cell disruption. After the final wash step, cells should typically be allowed to recover for 20 min before running on the FLIPR.
7. Assays should be optimized to give suitable basal FIU (8–12,000) and a robust agonist-induced response (typically 8–25,000 FIU over basal). To achieve this, a number of parameters can be adjusted including cell density, choice of dye, dye concentration and loading conditions. Responses should be less than 40,000 FIU to avoid camera saturation (the CCD camera saturates at ~65,000 FIU).
8. The parameters for the integrated FLIPR pipettor require optimization for each assay. The dispensation height of the pipettor and the speed of dispensation should be adjusted to ensure optimal delivery of the compounds to the specific plates being used. Optimal delivery should cause no cell disruption but should allow adequate mixing of the compounds in the well. To assist adequate mixing of compounds, the volume of agonist added to the well is typically 25% of the final well volume. The optimal dispenser speed may vary according to how well cells adhere to the bottom of the well. Cells can be checked following dispensation using the plate viewer.

References

1. Shroeder KS, Neagle BD (1996) FLIPR: a new instrument for accurate, high throughput optical screening. *J Biomol Screen* 1:75–80
2. Milligan G, Marshall F, Rees S (1996) G₁₆ as a universal G protein adapter: implications for agonist screening strategies. *Trends Pharmacol Sci* 17:235–237
3. Conklin BR, Farfel Z, Lustig KD, Julius D, Bourne HR (1993) Substitution of three amino acids switches receptor specificity of G_q to that of G_{ia}. *Nature* 363:274–276
4. Coward P, Chan SDH, Wada HG, Humphries GM, Conklin BR (1999) Chimeric G-proteins allow a high-throughput signalling assay of Gi coupled receptors. *Anal Biochem* 270:242–248

Chapter 6

Ratiometric $[Ca^{2+}]_i$ Measurements in Adherent Cell-Lines Using the NOVOfstar Microplate Reader

Benjamin D. Hunt and David G. Lambert

Abstract

The control of free ionized intracellular calcium concentration ($[Ca^{2+}]_i$) is an established mechanism of cellular activation, regulating a diverse range of cellular events. Consequentially, experimental measurement of $[Ca^{2+}]_i$ is a potent technique for the medical science laboratory. The NOVOfstar microplate reader is a versatile system, which may be easily configured to measure $[Ca^{2+}]_i$. Moreover, the relatively low cost of this system makes it an attractive one for researchers adhering to a modest budget, whilst allowing medium throughput to be achieved.

These methods serve as a starting point for researchers wishing to measure intracellular calcium concentration in adherent cell-lines using the NOVOfstar plate reader. Briefly, adherent cells are seeded into well plates 1 day prior to calcium determinations being made. On the day of the experiment, autofluorescence values of individual wells of cells are determined prior to the cells being loaded with the fluorophore, fura-2. $[Ca^{2+}]_i$ determinations are acquired by activating a predefined program within the NOVOfstar software; full parameters are provided within this chapter for this purpose. Fluorescence ratio values may be easily calibrated to give absolute intracellular calcium concentrations (nM). Calibration involves determining experimental fluorescence at calcium-saturating and calcium-free conditions; ionomycin and EGTA are used to produce these two conditions respectively. Finally, mathematical calculation of absolute intracellular calcium concentration is described by use of the Grynkiewicz equation.

Key words: NOVOfstar, Fura-2, Calcium, Ratiometric, Calibration, Adherent, Cell-line, CHO

1. Introduction

The NOVOfstar microplate reader (BMG Labtech, Fig. 1) is a versatile user-programmable instrument capable of measuring fluorescence, luminescence, or absorbance in standard microplates of up to 384 wells. The system consists of a thermostatically controlled stage (room temperature to 45°C) accommodating sample and reagent plates, which are served by an integrated robotic pipettor arm. Liquid reagents may be precisely transferred between the reagent and sample plates or from one of three reagent reservoirs.



Fig. 1. The NOVOstar microplate reader.

Multiwavelength detection of up to eight excitation/emission pairs is facilitated by a Xenon flashlamp and user-customizable filter wheels. The flexibility of this system makes it appropriate for a wide range of applications including but not limited to ELISAs, cell-viability assays, intracellular pH measurement, and luciferase reporter assays. High temporal resolution (up to 20 ms) makes this system suitable for capturing fast kinetic events such as intracellular calcium mobilization. The relatively low-cost and high-versatility of the NOVOstar microplate reader makes it an attractive system for research groups adhering to a modest budget while allowing medium throughput to be achieved.

The principal limitation of the NOVOstar plate reader is its ability to record measurements from only one well at any given time. Consequentially, measurements must be made in one of two reading modes (see Note 1). For fast kinetic events (such as calcium mobilization) recordings are best made with the NOVOstar microplate reader programmed in “well mode,” meaning that the entire program of injections and recordings is completed for each well in sequence. This ensures that fast Ca^{2+} transients are recorded with high temporal resolution, thus reducing the possibility of underestimating the peak response. However, this reading mode has the undesirable effect of increasing the interval between loading of cells with the fluorescent probe and making fluorometric determinations for subsequent wells. The possible ramifications of this effect may be reduced by randomizing the read direction of wells on the plate between repeat experiments, staggering loading of cells by use of microplates with detachable columns of wells, or use of an anion transport inhibitor such as probenecid if time-dependent leak of the probe is characterized as a problem for the cell-line of choice (1).

Dual wavelength fluorescent probes are often utilized in the measurement of $[Ca^{2+}]_i$ as the data obtained may be easily calibrated to give absolute Ca^{2+} concentrations. Moreover, the ratio of fluorescent emission at the two wavelengths is generally considered to be a more reliable indicator of $[Ca^{2+}]_i$ when compared with single-wavelength fluorescent probes. Fura-2 is by far the most widely utilized dual fluorescent probe in use (2, 3). The fura-2 molecule is commonly purchased featuring pentacetoxy-methyl ester (AM) modifications which facilitate the species' passage across the cellular membrane. Endogenous esterases within the cytosolic compartment then cleave these modifications from the molecule, thus largely preventing it leaving the cell. Fura-2 exhibits a calcium-dependent excitation spectral shift: when calcium-unbound, fluorescence emission at 510 nm is predominantly achieved by excitation at 380 nm. However, when calcium-bound, fluorescence emission of Fura-2 at 510 nm is predominantly achieved by excitation at 340 nm. The calculated ratio of fluorescence emission at the two excitation wavelengths (340:380) is considered to be a reliable indicator of $[Ca^{2+}]_i$. Moreover, these values may be easily calibrated to give absolute calcium concentrations by use of the Grynkiewicz equation (2). These methods focus on the measurement of $[Ca^{2+}]_i$ in Chinese Hamster Ovary cells seeded in 96-well culture plates. It is expected that these methods should be easily adaptable for other adherent cell-lines or culture plate sizes.

2. Materials

1. Adherent cell-lines in mid-log phase. Suitable cell-lines include Chinese Hamster Ovary (CHO) or human embryonic kidney (HEK-293) cells.
2. Krebs-HEPES buffer (freshly made): 143.3 mM Na^+ , 4.7 mM K^+ , 2.5 mM Ca^{2+} , 1.3 mM Mg^{2+} , 125.6 mM Cl^- , 25 mM HCO_3^- , 1.2 mM $H_2PO_4^-$, 1.2 mM SO_4^{2-} , 11.7 mM D-glucose, and 10 mM HEPES, pH 7.4 titrated with 10 M NaOH.
3. Wash fluid: 0.5 M NaOH (see Note 2).
4. System fluid: 50% ethanol (see Note 3).
5. Pluronic F-127 (Sigma Aldrich): Dissolve in dimethylsulfoxide to give a stock concentration of 2% (w/v), (see Note 4).
6. Fura-2/AM (Sigma Aldrich): Dissolve in dimethylsulfoxide to a concentration of 1 mM. Store in the dark at -20°C in 10 μ L aliquots until required (see Note 5).
7. EGTA (Sigma Aldrich, Dorset, UK): Produce a 360 mM stock in Krebs-HEPES buffer.

8. Ionomycin (Sigma Aldrich): Dissolve in dimethylsulfoxide to a working concentration of 160 μ M. An intermediate concentration of 1 mM may be produced for storage. Keep all aliquots at -20°C until use (see Note 6).

3. Methods

3.1. Preparation of Cell Cultures

1. CHO cells are typically grown in T75 flasks and maintained in D-MEM/F-12 (1 \times) liquid 1:1 supplemented with 10% fetal calf serum, penicillin (100 IU/mL), streptomycin (100 μ g/mL), and fungizone (2.5 μ g/mL) at 37°C/5% CO₂ (see Note 7).
2. Trypsinise cells and resuspend in approximately 10 mL, disperse any conglomerates by thorough pipetting.
3. Quantify the cell density by use of a hemocytometer and adjust to the required seeding density by tenfold serial dilution in Sterilin tubes (see Note 8).
4. Seed the cells in the culture plate by use of a multiwell pipettor and incubate overnight at 37°C/5% CO₂.

3.2. Instrument Setup

1. Configure the NOVOSTAR light guides in bottom reading mode (see Note 9).
2. Prepare wash fluid and place in reagent position 1.
3. Connect the system fluid reservoir to the instrument.
4. Switch on the instrument, set the reader configuration to “fluorescence intensity,” and prime the pipettor pump with system fluid.
5. Define the set point for the thermostatically controlled stage.
6. Prepare pharmacological agents in the reagent plate and maintain on ice, 50 μ L at 3 \times final concentration in Krebs-HEPES buffer is recommended.

3.3. Loading Cells with Fura-2

1. Remove media from wells and rinse monolayers three times with 200 μ L Krebs-HEPES buffer, final volume 50 μ L/well.
2. Place the sample plate into the NOVOSTAR instrument and initiate a previously configured protocol to determine autofluorescence values for individual wells (see Table 1—column a).
3. Prepare loading buffer by mixing volumes of pluronic F-127 and Fura-2 stocks.
4. Dilute above mixture with Krebs-HEPES buffer to give final concentrations of 0.02% and 4 μ M for pluronic F-127 and Fura-2, respectively. Supplement loading and subsequent buffers with 1 mM probenecid if indicated.

Table 1

Recommended programmable parameters for establishment of run protocols within the NOVOstar plate reader software. Protocols are provided for (a) determination of autofluorescence, (b) $[Ca^{2+}]_i$ measurement, and (c) calibration run

	(a)	(b)	(c)
<i>Basic parameters</i>			
Test name	<user defined>	<user defined>	<user defined>
Measurement plate	<user defined>	<user defined>	<user defined>
Reagent plate	<empty>	<user defined>	<empty>
Positioning delay (s)	0.5	0.5	0.5
No. of kinetic windows	1	2	3
Measurement start time (s)	0.0	0.0	0.0
No. of intervals	2	8	8
No. of flashes per well and interval	5	5	10
Interval time (s)	1.26	1.26	1.46
Fluorescence intensity	<selected>	<selected>	<selected>
No. of multichromatics	2	2	2
<i>Kinetic windows (interval 1/interval 2/interval 3)</i>			
Start time (s)	n/a	0.0/19.7/-	0.0/12.0/187.2
No. of intervals	n/a	8.0/39.0/-	8.0/120/120
No. of flashes	n/a	5/5/-	10/10/10
Interval time (s)	n/a	1.26/1.26/-	1.46/1.46/1.46
<i>Concentrations/volumes/shaking (volume 1/volume 2)</i>			
Shaking mode	n/a	Orbital	Orbital
Shaking width (mm)	n/a	2	3
Additional shaking	n/a	No shaking	No shaking
Volume (μL)	n/a	25	5/10
Pump to use	n/a	Pump 1	Pump 1/pump 1
Pump speed ($\mu L/s$)	n/a	10	200/200
Shaking time (s)	n/a	2	5/5
<i>Pipettor options (volume 1/volume 2)</i>			
Source		Reagent microplate (1:1)	Reagent position 2/reagent position 3
Aspirate depth (mm)	n/a	10.0	<user defined>
Dispense depth (mm)	n/a	0.0	5.0
Use air gap	n/a	<selected>	<selected>
Preaspiration volume (μL)	n/a	0	10
Mix volume (μL)	n/a	0	10
Mix cycles	n/a	0	2
Wash reagent volume (μL)	n/a	50	50
Soak time (s)	n/a	5	5
Wash cycles	n/a	3	3
Reuse wash reagent	n/a	<deselected>	<deselected>
Rinse cycles	n/a	3	3

(continued)

Table 1
(continued)

	(a)	(b)	(c)
<i>Injection timing (volume 1/volume 2)</i>			
Volume 1 injection start time (s)	n/a	19.7	12.0/187.0
Time-optimized measurement	n/a	<deselected>	<deselected>
<i>Multichromatic (1/2)</i>			
Excitation filter	340-10/380-10	340-10/380-10	340-10/380-10
Emission filter	510-10/510-10	510-10/510-10	510-10/510-10
Gain	<user defined>	<user defined>	<user defined>

5. Remove buffer from the wells of the reagent plate and replace with loading buffer (50 µL/well). Incubate in the dark for 30 min at 37°C/5% CO₂.
6. Remove loading buffer from wells and rinse the monolayers three times with 200 µL Krebs-HEPES buffer. Incubate in the dark at room temperature for 20 min.
7. Rinse the monolayers a further three times with 200 µL Krebs-HEPES buffer, final volume 50 µL.

3.4. Making [Ca²⁺]_i Determinations

1. Transfer the sample and reagent plates to the defined positions on the stage of the NOVOSTar. Allow sufficient time for the plates to reach the defined temperature.
2. The gain setting for the photomultiplier tube must be optimized to allow an appropriate signal to noise ratio (see Note 10).
3. The run protocol should be defined prior to the start of the experiment. Recommended settings are given in Table 1—column b. Consideration should be given to the effects of hydrodynamic forces generated during injection of reagents into the well (see Subheading 4).
4. Initiate the run protocol.

3.5. Calibration Run

1. Place stocks of ionomycin and EGTA in reagent positions 2 and 3.
2. Define a separate run protocol for conducting calibrations, three calibrations are recommended, which are evenly spaced across the plate. Recommended settings are given in Table 1—column c.
3. Initiate the run protocol. R_{\max} is given from incubation with the calcium ionophore, ionomycin (final concentration, 10 µM). R_{\min} is given from subsequent addition of the calcium chelator, EGTA (final concentration, 40 mM).

3.6. Data Manipulation and Analysis

1. Data are automatically stored as a Microsoft Excel workbook (.xls). A second macro-enabled Microsoft Excel workbook can be easily produced to reduce the length of time taken to manipulate experimental data, although some manual data entry/scrutiny will still be necessary.
2. Subtract autofluorescence values from experimental fluorescence and calibration values.
3. Calculate 340:380 nm ratios for all experimental and calibration data. This might not be necessary for the entire time-course depending on requirements; identify specific time-points or maxima/minima in advance if required.
4. Calculate absolute $[Ca^{2+}]_i$ by use of the Grynkiewicz equation:

$$[Ca^{2+}]_i = K_d \left[\frac{R - R_{\min}}{R_{\max} - R} \right] \beta$$

where, K_d for fura-2/ Ca^{2+} binding at 37°C is 225 nM, R is the 340:380 ratio, R_{\max} is the 340:380 ratio under Ca^{2+} -saturating conditions, R_{\min} is the 340:380 ratio under zero- Ca^{2+} conditions, and β is the Ca^{2+} -free: Ca^{2+} -saturating ratio at 380 nm.

3.7. Effects of Injection Variables on Shear Stress-Induced Calcium Mobilization

The effects of injection variables on cellular assays in fluid-handling systems, such as the NOVOstar plate reader, are poorly characterized at present. Despite this, optimizing these variables is a critical stage of methodological development for studies utilizing such a system. Figure 2 demonstrates how the reliability of data generated in high- or medium-throughput systems may be called into doubt if experimental protocols are not thoroughly scrutinized during development. The concentration-response curve (CRC) shown was generated in Chinese Hamster Ovary cells stably transfected

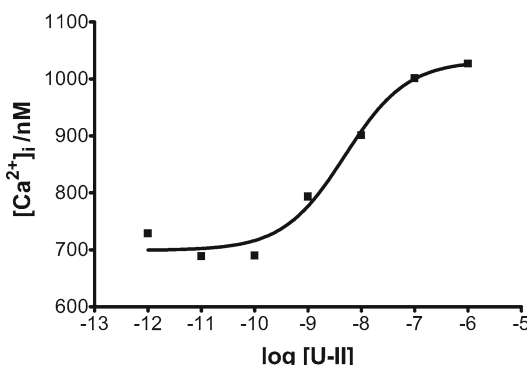


Fig. 2. A calibrated CRC to urotensin-II in CHO_h UT cell-line. Data are elevated on a baseline of approximately 700 nM.

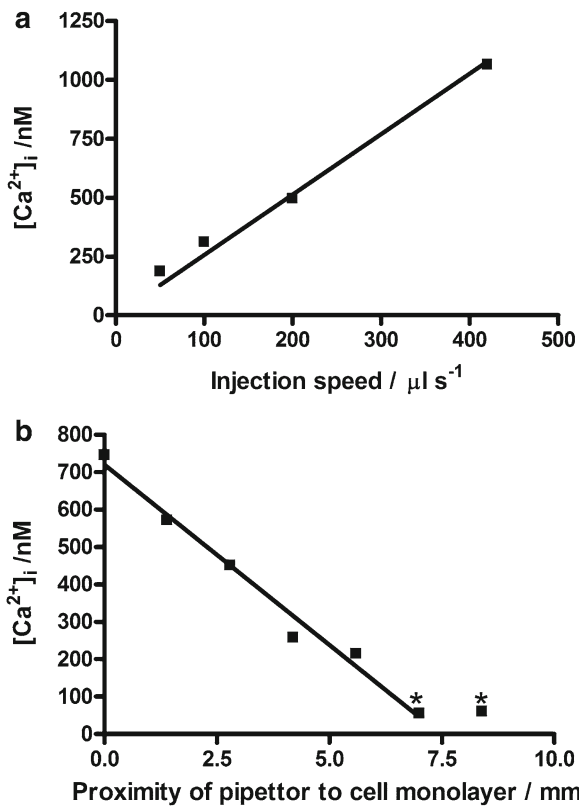


Fig. 3. Effect of (a) injection speed at a fixed pipettor depth of 2 mm (b) pipettor depth at a fixed injection speed of 100 $\mu\text{L/s}$, on magnitude of injection artifact. Data points marked “Asterisk” indicates that no injection artifact was generated.

with the recombinant human urotensin-II receptor (UT). Although the CRC is textbook-perfect with respect to its EC_{50} and R^2 values, the data are clearly erroneous due to the curve’s elevation on a baseline of approximately 700 nM. Such an error would not have been instantly evident if fluorescence ratios had of been plotted, highlighting the importance of data calibration to absolute $[\text{Ca}^{2+}]$ when at all possible.

Figure 3 demonstrates the cause of the above error to be rooted in shear stress generation, resulting from the injection of fluids into the experimental wells. The magnitude of shear stress-induced calcium transients is directly proportional to the speed of injection but inversely so to the proximity of the pipettor to the cell monolayer. The NOVOSTAR microplate reader allows users to program injection speed within the range of 420–1 $\mu\text{L/s}$ and the proximity of the pipettor from the cell monolayer to any depth within the well. The authors strongly suggest that both of these variables are rigorously optimized prior to production of experimental data. Moreover, the

authors suggest that pharmacological agents be dispersed within experimental wells by use of the shaking function as opposed to the pipettor mixing function, again to reduce shear stress.

4. Notes

1. The NOVOstar plate reader must be configured in one of two reading modes, which dictate how data are acquired. *Plate mode*: for slow and sustained kinetics. All experimental wells are read quickly in one cycle and then the cycle is repeated up to 250 times. *Well mode*: for fast kinetic events. Each experimental well is measured in turn for a predetermined length of time; all injections for a given well occur during that time.
2. Wash fluid is used to clean the pipettor needle between injections; 0.5 M NaOH is recommended.
3. System fluid is used to flush the pipettor needle after the washing stage; 50% ethanol is recommended.
4. Pluronic F-127 is a nonionic detergent which aids dispersion of fura-2 in aqueous solution.
5. Fura-2 is readily photobleached; therefore, care must be taken to limit its exposure to light. This applies to fura-2 stocks as well as cells during loading and deesterification. Simple measures include switching off fluorescent strip lighting and closing window blinds during handling.
6. Ionomycin is a calcium ionophore isolated from *Streptomyces conglobatus* and purchased as a free acid. It is used to raise intracellular calcium concentration for R_{max} determination.
7. Substances used to select for expression of recombinant proteins (such as G418 or hygromycin-B) should *not* be included in experimental media.
8. Chinese Hamster Ovary cells are typically seeded at a density of 30,000 cells/well in 96-well plates.
9. Bottom reading mode indicates that fluorescence is measured from beneath the well plate. This mode must be selected if the pipettor is in use during the experimental run.
10. Three individual test wells of Fura-2 loaded cells (of the same type and seeding density) should be used to determine the appropriate gain setting. Add 10 μ M (final concentration) ionomycin to each of the three wells and measure the fluorescence after 1 min (Ex: 340/380, Em: 510 nm). The software will automatically calculate the gain setting by instructing it to constrain the measured fluorescence to 90% of maximum. Use the same gain setting for both excitation wavelengths.

References

1. Di Virgilio F, Steinberg TH, Silverstein SC (1990) Inhibition of Fura-2 sequestration and secretion with organic anion transport blockers. *Cell Calcium* 11:57–62
2. Grynkiewicz G, Poenie M, Tsien RY (1985) A new generation of Ca^{2+} indicators with greatly improved fluorescence properties. *J Biol Chem* 260:3440–3450
3. Roe MW, Lemasters JJ, Herman B (1990) Assessment of Fura-2 for measurements of cytosolic free calcium. *Cell Calcium* 11:63–73

Part III

Measurement of Ca²⁺ Channel Activity

Chapter 7

Whole-Cell Patch-Clamp Recording of Voltage-Sensitive Ca²⁺ Channel Currents in Single Cells: Heterologous Expression Systems and Neurones

**Jon Brown, Atticus H. Hainsworth, Alessandro Stefani,
and Andrew D. Randall**

Abstract

Voltage-sensitive calcium channels (VSCC) are vital to the normal physiology of many cell types, including neurones, skeletal, cardiac and smooth muscle cells, heart pacemaker tissue and endocrine cells. Whole-cell recording is a functional electrophysiological assay that allows real-time measurement of macroscopic VSCC activity at the level of single cells. Using this technique, it is possible to probe the molecular physiology, pharmacology, and biophysics of VSCC proteins with a level of precision rarely surpassed in cell biological studies. With best practice voltage-dependent gating behaviors of VSCCs can be interrogated with temporal resolution <100 µs. These advantages have commonly been exploited using recombinant channels heterologously expressed in cell-lines, where the molecular identity of the channel under study can be precisely defined, and also in native cell types freshly isolated from intact tissue using enzymes. The latter approach is especially valuable for study of adult brain neurons as these cells are not amenable to primary culture. We also describe a method with which VSCCs can be studied in nucleated macropatches derived from neurons without the use of enzymes. Although automated patch-clamp systems are now available they have limitations, and manual whole-cell recording of VSCC currents remains an expert technique requiring intelligent, conative experimentation.

Key words: Calcium channel, Calcium current, HVA, LVA, CaV, Calcium channel antagonist, Calcium channel alpha1 subunit, Whole-cell patch clamp

1. Introduction

Voltage-sensitive Ca²⁺ channels (VSCC) play a central role in an extensive array of physiological processes. Their importance in cellular function arises from their ability both to sense membrane voltage and to conduct Ca²⁺ ions across the cell membrane; two features, that when combined, couple membrane excitability to a key intracellular second messenger. Through this relationship,

Table 1
Classification of VSCC alpha1 subunits (see ref. 1)

Group	Other group names	Alpha subunit	Previous nomenclature	Cellular counterpart
CaV1	L-type Ca ²⁺ channels, Dihydropyridine receptors	CaV1.1 CaV1.2 CaV1.3 CaV1.4	α1S α1C α1D α1F	L-type L-type L-type L-type
CaV2	Presynaptic Ca ²⁺ channels	CaV2.1 CaV2.2 CaV2.3	α1A α1B α1E	P/Q-type N-type R-type
CaV3	Low voltage activated, LVA, Low threshold Ca ²⁺ channels	CaV3.1 CaV3.2 CaV3.3	α1G α1H α1I	T-type T-type T-type

activation of VSCCs is tightly coupled to the gamut of cellular functions which are dependent on intracellular Ca²⁺, including muscle contraction, energy metabolism, gene expression and exocytotic/endocytotic cycling.

VSCCs are formed from a core α1 subunit which comprises the Ca²⁺ selective pore, the voltage sensor, and most drug binding sites. Accessory subunits α2δ, β, and γ modulate channel function by altering biophysical properties and cell surface expression. The primary level of VSCC diversity results from the differing functional and pharmacological properties of α1 subunits (Table 1). For a description of VSCC subtype classification, see ref. (1).

Whole-cell (tight seal) recording is a form of patch-clamp technique utilizing a glass microelectrode (“pipette”) connected to a sensitive voltage clamp amplifier that can record picoamp currents (pA, 10⁻¹² A). Under the control of a micromanipulator, a recording pipette filled with the desired intracellular solution is gently pressed against the surface of a single cell. Typically light microscopy is used both to select the cell for examination and to monitor electrode placement. However, in certain preparations, for example tissue slices or neurones *in vivo*, so-called “blind” patch-clamp is sometimes performed; in this case the interaction between the pipette and the cell is not directly observed, but is instead inferred from electrical changes. Once an electrode is in contact with a cell gentle suction is applied and a tight seal forms between the pipette glass and plasma membrane, giving electrical resistance in excess of 1 GΩ (the “gigaseal”). From this “cell-attached” mode, additional stronger suction is used to rupture the patch of cell membrane delimited by the pipette mouth thereby generating electrical access to the cytoplasm. In this “whole-cell” mode, the transmembrane voltage can be controlled (“clamped”) and the net current flow

across the cell membrane measured, with well-defined external and internal solutions. This level of control over membrane transport parameters at the single cell level has earned whole-cell recording its deserved popularity as a reporter of ion channel function. Changes in current produced by voltage pulses, variation in ion concentrations, or drug application can then be monitored. For further details of patch-clamp methods, see refs. (2–6).

1.1. Whole-Cell Recordings of Calcium Currents: The Foundations

Whole-cell recordings of calcium channel currents were first performed in cultured bovine adrenal chromaffin cells (7) and snail neurons (8). Similar techniques were later validated in various cell types acutely isolated from adult animals, for example rat sympathetic ganglia (9). Recording conditions were refined and demonstration of channel blockade by divalent ions (e.g., cadmium, cobalt, and nickel) became routine. In addition, using a combination of whole-cell and single channel recordings several groups began dissecting the biophysical properties of VSCCs, in terms of their activation, deactivation, and inactivation properties (10, 11) and the first studies of pharmacological modulation of whole-cell calcium currents appeared (e.g., (12); see ref. 13). On the basis of gating kinetics, VSCC types were classified as transient (T), sustained or long (S, L), or N (neither T nor L/S) (14–16). As years passed similar approaches were used to uncover additional pharmacologically and biophysically distinct classes (P, Q, and R-type) of native VSCC (17–19). Furthermore, significant progress was made in understanding the molecular basis of VSCC diversity, aligning the properties of various recombinant channel subunit combinations with those of native channels in neurones and other cells.

Some 10 years after patch-clamp methods were first described methods allowing application of patch-clamp recording to brain slices were first described. Brain slices potentially have advantages over acutely dissociated neurones in that they have not been treated with proteolytic enzymes or subjected to the mechanical dissociation procedure. Whole-cell recording from neurones in brain slices has been used to characterize Ca^{2+} currents in neurones, although the extensive branching geometry of largely intact neurones combined with the large amplitude currents they possess can present substantial technical problems largely related to space clamp issues. Furthermore, using slice preparations, Ca^{2+} currents have been characterized with whole-cell recordings direct from presynaptic terminals (20, 21). We have also found that it is possible to record Ca^{2+} currents from nucleated macropatches isolated from the cell bodies of neurons in brain slices (see below).

Here we summarize the whole-cell recording methods generally used to characterize macroscopic currents mediated by VSCCs. We describe approaches used to study recombinant VSCCs expressed in cell-lines, native VSCCs in brain neurons isolated by enzymatic treatment and VSCCs in nucleated macropatches isolated from neurones in acute brain slices.

2. Materials

2.1. Recording Recombinant VSCC Currents in Cell-Lines

1. Maintain in cell culture a suitable cell-line expressing the desired recombinant VSCC subunits (see Note 1). It is convenient to grow cells on glass coverslips (see Note 2), which can be transferred to the recording chamber. Alternatively cells can be grown in standard plastic cell culture dishes.
2. HEPES-buffered saline (HBS) is composed of 130 mM NaCl, 5 mM KCl, 2 mM CaCl₂, 1 mM MgCl₂, 30 mM glucose, 10 or 20 mM HEPES acid pH 7.3 with NaOH, 310–315 mOsm/l.
3. Extracellular solution for VSCC recordings: 140 mM tetraethyl ammonium (TEA) chloride, 10 mM HEPES acid, 2.5 (range 2–5) mM CaCl₂ or BaCl₂ (or occasionally SrCl₂), 5 mM CsCl, 10 mM glucose, and 1 mM MgCl₂, pH 7.3 with TEA-OH, osmolarity 310–315 mOsm/l. Make up 200–500 ml; this can be used for a few days if kept in the fridge. See Notes 3–6.
4. Internal solution: 108 mM Cs Me-sulfonate, 24 mM HEPES acid, 10 mM EGTA, 4.5 mM MgCl₂, 0.1 mM CaCl₂, 4 mM Na-ATP, 0.3 mM Na-GTP, 5 mM creatine, 5 mM Na-phosphocreatine, 5 mM pyruvate, 5 mM oxalacetate, 5 µg/ml Calpain Inhibitor peptide. Make up aliquots of 2–5 ml and freeze them. See Notes 7 and 8.

2.2. Recording Whole-Cell VSCC in Acutely Isolated Neurons

1. The process of enzymatically dissociating neurons from adult brain is given in Note 9. We have studied neurons from diverse brain areas (striatum, sensorimotor cortex, globus pallidus) using the basic protocol given here (e.g., (22–24)). Points to note in regard to this preparation are given below (see Notes 10–12).
2. HEPES-buffered Hank's balanced salt solution (HBSS): 10 mM HEPES free acid, 138 mM NaCl, 3 mM KCl, 1 mM MgCl₂, and 2 mM CaCl₂, pH 7.3 adjusted with NaOH, 300 mOsm/l.
3. Na *isethionate* solution: 140 mM Na isethionate, 2 mM KCl, 1 mM MgCl₂, 23 mM glucose, 15 mM HEPES acid, 1 mM kynurenic acid, 1 mM pyruvic acid, 0.1 mM nitroarginine, and 0.05 mM glutathione (pH 7.3; 310 mOsm/l).
4. The pipette solution: 185 mM N-methyl-D-glucamine, 40 mM HEPES acid, 11 mM EGTA acid (or BAPTA), 4 mM MgCl₂, adjusted to pH 7.2–7.3 with AR grade phosphoric or sulfuric acid. Aliquots of this solution can be stored in the freezer. On the day of use add the following: 20 mM phosphocreatine, 2–3 mM ATP, 0.2 mM GTP, 0.1–0.2 mM leupeptin; final osmolarity 270–280 mOsm/l. Solutions containing BAPTA should be protected from light. See Notes 12 and 13.
5. The external recording solution: 165 mM TEA-Cl, 5 mM CsCl₂, 10 mM HEPES acid, 10 mM glucose, and 2.5 or 5 mM

BaCl_2 (as the charge carrier); pH adjusted to 7.35 with CsOH or TEA-OH. If necessary, sucrose is added to bring the osmolality to 305 mOsm. See Notes 3, 5–8.

6. If desired, NaCl can be substituted for TEA as the major cation in external recording solution: 125 mM NaCl, 20 mM CsCl, 1 mM MgCl_2 , 10 mM HEPES acid, 5 mM BaCl_2 , 0.001 mM TTX, and 10 mM glucose (pH 7.3 with TEA-OH; 300–305 mOsm/l).
1. Brain slices are prepared by standard methods from the brain of rodents aged 14 days or older. We have made successful macropatch recordings of voltage-gated currents from brain slices obtained from multiple brain areas of rodents aged up to 25 months (see ref. 25 for example).
2. A bicarbonate buffered artificial cerebrospinal fluid (aCSF) gassed with 95% O_2 :5% CO_2 is used as the extracellular recording for brain slices. The composition of the standard aCSF we use is (mM): NaCl, 124; KCl, 3; NaHCO_3 , 26; CaCl_2 , 2; NaH_2PO_4 , 1.25; MgSO_4 , 1; D-glucose, 10. The Ca^{2+} concentration of this solution can be raised to around 4–5 mM to increase Ca^{2+} current amplitude, but no further due to precipitation of Ca^{2+} salts.
3. Pipette solution we have used for Ca^{2+} current recordings in macropatches is Cs-Methanesulfonate, 130; NaCl, 20; Cs-HEPES, 10; EGTA, 0.2; Na-GTP, 0.3; Mg-ATP, 4; pH 7.3, 285–290 mOsm.

2.4. The Recording Setup

Assemble a standard patch-clamp apparatus, for both cell-lines and dissociated neurons. The core components are as follows.

1. For standard visualized patch-clamp methods a light microscope is required. An inverted style microscope is usual for culture/dissociated cells although these can also be studied on a fixed stage upright microscope. Fixed stage upright microscopes are typically used for visualizing cells in brain slices this can be more effective when the microscope is equipped with infrared differential interference contrast optics. Microscopes can also be equipped with simple fluorescence optics if required (i.e., for visualizing GFP transfected cells).
2. Mounting the microscope on an antivibration air table or employing other means to reduce transmitted vibrations (e.g., steel plate on tennis balls) will greatly increase success rates.
3. Some form of recording chamber mounted on the microscope stage. This can be as simple as a plastic culture dish although we favor commercially available solutions that facilitate perfusion of the chamber (e.g., RC series chambers from Warner instruments).

4. A patch-clamp amplifier (e.g., Molecular Devices Multiclamp 700 or Axopatch, HEKA EPC10)—it is also possible to use a switch-clamp amplifier such as the SEC-05X made by NPI, these are somewhat more technically demanding to use but may be advantageous if very large currents are to be studied.
5. A suitable low-drift micromanipulator (e.g., Burleigh, Narishige, Scientifica) onto which the amplifier headstage is mounted and/or pipette holder is mounted.
6. Some form of analog–digital interface (e.g., 1401 from CED, Digidata from Molecular Devices, ITC 18 from Intratech or various National Instruments boards) linked to a personal computer with software to acquire data and control experiments (e.g., pClamp from Molecular Devices, Pulse from HEKA, Strathclyde freeware from Dr J. Dempster, ref. 26).
7. An electrode puller will be required to fabricate pipettes. These come in vertical and horizontal configurations and a broad range of price levels. Many labs seem to do fine with quite simple, relatively inexpensive vertical pullers like the PB-7 made by Narishige.
8. In addition to the above, the following should be considered: a Faraday cage surrounding the microscope (these are commonly used but may not be absolutely required for most whole-cell studies), an oscilloscope (not always essential when using with modern fast A to D boards but useful for troubleshooting and other “old school” tricks), some form of temperature controller (if experiments are to be performed away from ambient temperature, see Note 14) and equipment to perfuse the recording chamber and/or perform solution exchanges (see Note 15). For external solution exchange, we favor a local change in extracellular perfusion. To achieve this we use a gravity-fed multibarrel “liquid filament” approach, whereby parallel streams of solutions are translated across the recorded cell in order to produce rapid solution changes (time to completion 30–100 ms). A number of such systems are available commercially (e.g., the relatively inexpensive systems sold by Warner Instruments). A microforge of some description will be needed if pipettes are to be fire polished prior to use. This manipulation is rarely essential but can significantly improve the quality or success rate of gigaseal formation.

3. Methods

3.1. General Points

As with much electrophysiology, preparation prior to starting VSCC recording will yield dividends, whereas diving in unprepared may lead to disaster—poor electrophysiology data can be worse than

no electrophysiology data. Keep your mind on the goals: beautiful, clean well clamped currents, the clearest test of your hypothesis and the paper in your favorite high impact journal.

1. Assemble your setup, such that patch-clamp amplifier talks to the data acquisition system, that the computer runs the software smoothly, and that you can play back recorded currents. Check this by filling a pipette and recording the current response to a 5 mV step voltage first in air, then in bath solution.
2. Carefully plan your extracellular and internal solutions (see Notes 3–8, 12, and 13). A major concern for VSCC recording is “rundown” of the current with time (see Note 16). You may need to modify your internal solution in the light of preliminary experiments, or even consider perforated patch recording (see Note 17).
3. Plan the voltage protocols that you will use to answer your question (see Note 18). You will likely need more than one protocol in any given recording. Consider the temperature you will work at. If this is not ambient temperature ensure that your setup will achieve your desired temperature and maintain it with minimal fluctuations.
4. Learn as much as possible about your cell type and its complement of calcium channels before you begin. Do a literature search, talk to the people who gave you the cells, and ask your Biochemist friend. For example, does expression begin only at 2 days after plating out? What bath solution is best for gigaseal formation? Are the cells densely packed with Ca-activated anion or K channels? Do the cells form gap junctions when next each other (if so avoid recording from cells touching each other).

3.2. The Basic Process of Recording Whole-Cell VSCC Currents

1. Choose a suitable smooth, healthy-looking, debris-free cell before you fill the pipette.
2. Pull a pipette and fill with filtered internal solution to around half full.
3. Patch-clamp amplifier should be in voltage clamp mode, whole-cell capacity compensation and series resistance compensation turned off. The recording software (or the inherent seal test setting of the amplifier) should be set to regularly (e.g., 1–10 Hz) deliver small voltage steps, ~1–5 mV, these are used to test pipette resistance and monitor seal formation.
4. Mount filled patch pipette on electrode holder such that the silver chloride wire of the holder makes contact with the pipette solution. (The electrode holder is in turn attached to headstage which is attached to micromanipulator (see Note 19)).
5. Apply positive pressure to pipette lumen (see Note 20).
6. Lower pipette into bath solution, approximately remove current offsets using the pipette offset control, check pipette

resistance and, if suitable, use your micromanipulator to position the pipette tip close to your chosen cell. In necessary re-zero current using pipette offset control.

7. Gently touch cell surface, remove positive pressure and then apply gentle suction; monitor gigaseal formation by observing current response to small voltage step command, e.g., 5 mV (see Notes 21 and 22).
8. If a gigaseal is formed, neutralize fast capacitance transients with appropriate controls. Once a gigaseal is formed place the pipette potential at -70 mV (if not previously done so, see Note 22) then enter whole-cell configuration by brief application of further suction and/or high voltage “zaps” (see Note 23).
9. If the whole-cell configuration is successfully achieved (this will be apparent by the large whole-cell capacitance transients that appear) then neutralize capacitance transients; this will establish the initial series resistance value (see Note 24).
10. If series resistance is sufficiently low for the proposed experimental purposes, apply series resistance compensation (typically 70–90%). See Note 25.
11. After obtaining whole-cell access, the cell is bathed in appropriate external solution for VSCC current recording, this can be done by exchanging the entire bath solution or by using a more local exchange for example using multibarrel fast extracellular perfusion (see Note 13). Recordings typically last for 5–15 min, but can last much longer than this.
12. Start data acquisition. Initially apply a simple square-wave depolarizing test pulse to around 0 mV see how much VSCC current is present (e.g., Fig. 1).
13. You may then apply your chosen voltage protocol (see Note 17) and/or expose the cell to the drugs of interest. It is usual to record a few (**3–20**) currents predrug, then exchange the external solution to apply the drug (see Note 13) and again record a few traces, ideally until a steady-state response is seen. Then wash off the drug and record current responses, ideally showing a near-complete recovery to predrug levels, although this may not be realized with drugs with a high affinity such as toxins.

3.3. The Basic Process of Making Nucleated Macropatch Recordings from Brain Slices

1. Brain slices are mounted and held down in the chamber of a standard slice recording setup. The chamber is constantly perfused with aCSF at the chosen temperature (see Note 26). A cell of healthy appearance is visually identified using the microscope. For brain slices is typically done with infrared differential interference contrast optics or alternatively with the oblique illumination methods.
2. Using similar methods to those described above the cell is approached with an electrode and a gigaseal formed using gentle

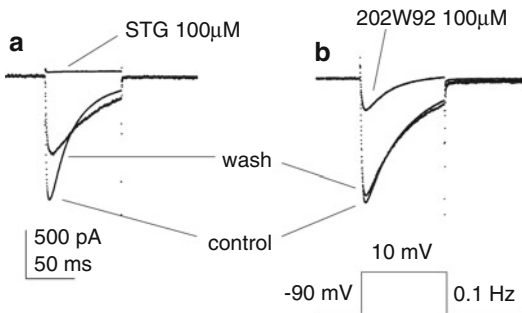


Fig. 1. R-type voltage-sensitive calcium channel currents mediated by human $\alpha 1E + \beta 3$ subunits expressed in HEK293 cells (see ref. (33)). The currents are induced by 100 mV square pulses of duration 100 ms, applied every 10 s, with 2.5 mM Ba²⁺ as the charge carrier. The control currents exhibit clear voltage-dependent inactivation. Application of the lamotrigine analogs sipatrigine (STG) or 202 W92 (each at 100 μ M) inhibits the VSCC-mediated currents (panels a and b, respectively). The peak current amplitude is inhibited >95% by sipatrigine, and approximately 70% by 202 W92. After washing out sipatrigine, the current recovers partially but the recording shows signs of poor voltage control, possible due to declining gigaseal resistance. In the example shown for 202W92, the recording shows almost complete recovery following removal of the drug. A.H. Hainsworth, unpublished data.

suction. We usually then set the pipette potential to around -70 mV before obtaining whole-cell access by applying an additional bout of suction. At this stage, prior to making the nucleated macropatch one might chose to record some data from the cell in whole-cell mode (for example the presence and properties of spontaneous synaptic responses).

3. To generate the nucleated macropatch from a whole-cell recording the first step is to apply suction to the cell in whole-cell mode. This causes the nucleus to move under the pipette tip—which can be seen on the microscope image. Following this the suction is maintained and the pipette slowly backed away from the cell body. The formation of a macropatch is indicated by the loss of the whole-cell capacity transients that are diagnostic of the whole-cell mode (do not cancel these if you are planning to make macropatches). The large (~5 μ m diameter) spherical patch enclosing the nucleus can also be observed forming on the pipette tip as it is moved away. We usually pull the macropatch completely out of the brain slice. Doing this means solution exchanges occur more rapidly and also electrical events (for example action potentials) occurring in nearby neurones (or the nucleus-free remnants of the “macropatched” cell) are not picked up in the recording.
4. The capacitance of a typical nucleated patch from a hippocampal or cortical neurone is 1.5–2.5 pF, we usually obtain series resistance values below 10 M Ω . This capacitance can be neutralized and series resistance compensated as for conventional whole-cell recordings (see above). With the recording solutions

described we usually observe input resistances above 1 G Ω in successful macropatches.

5. Not all whole-cell recordings will yield a viable macropatch, however, after a short period of practice success rates >50% are realizable by most experienced patch clampers. As with conventional recordings if you fail just fill another pipette and try another cell. Persistence is a key virtue for the neurophysiologist.
6. Once the macropatch is obtained it is treated experimentally very like a conventional whole recording, which voltage steps/ramps being applied to examine current properties. Recording durations seem similar to those in conventional whole-cell studies. In our experience Ca²⁺ current amplitudes are usually quite modest in macropatches, particularly in comparison with the size of Na⁺ and K⁺ currents (see Note 27). Although currents are small they consist of biophysically distinct components (see Note 28).

4. Notes

Recombinant VSCCs in host cell lines and other heterologous expression systems

1. Cell types typically chosen for VSCC expression are those lacking endogenous Ca²⁺ currents and regarded as “good” transfection hosts. Most commonly used are epithelial cells such as HEK-293, CHO and COS-7 cells, all of which express very low levels of voltage-gated channels. It must be noted, however, that cell-lines from the same original source (i.e., with the same name) can vary considerably in their membrane properties and channel complement. For example there are reports of HEK293 cells that express, albeit quite small, endogenous VSCC (27, 28), though we have never observed them. An alternative, widely used, host for VSCC expression is the Xenopus oocyte which can be injected with either cDNA or mRNA for VSCC subunits. These are too large for whole-cell methods and require two electrode voltage clamp or the cut-open oocyte technique.

Recombinant VSCCs subunit combinations can be either transiently or stably expressed in host cell lines. With the exception of the CaV3 family, where expression of an $\alpha 1$ subunit alone produces robust VSCC-mediated currents, it is usually necessary to co-express at least a β subunit—and often a β and $\alpha 2\delta$ —along with an $\alpha 1$ subunit to generate suitable currents. This requirement to express two or three different subunits has made the generation of stable cell-lines for CaV1 and CaV2 family channels a substantial although not insurmountable

challenge, examples are reported in refs. (29) (alpha1B) (30) (alpha1A) and (31) (alpha1E). The inclusion of a visible marker (e.g., green fluorescent protein) to identify transfected cells in studies using transient gene expression permits a much greater number of successful recordings to be made per working day.

2. Other considerations with respect to host cells involve the level of VSCC expression and the cell-culture substrate used when plating cells out. The major reason for controlling expression level is to set the size of the VSCC-mediated currents to a level that is suitable for whole-cell recording. An ideal range to aim for would be a current, at the peak of the *I*-*V* relationship, of 300–1,500 pA in 2 mM Ca²⁺, when stepping from a hyperpolarized holding potential (e.g., -100 mV). Current amplitudes can be manipulated in additional ways, including varying nature of concentration of the permeating divalent ion species (see below) and altering the test and/or holding potentials employed. Regarding plating of cells we typically use glass coverslips coated with poly-D-Lysine and maintained within standard 35 mm plastic petri dishes. A range of other substrates, including direct plating onto tissue culture plastic, are also suitable. One advantage of using glass coverslips is they can be readily broken into numerous shards. These can then individually be transferred to the recording chamber, giving numerous “individual” preparations from a single 35 mm petri dish.

With stable VSCC cell-lines, expression levels can change with passage number and it is prudent to monitor this and work with passage numbers within a defined window. In addition we have found that expression levels change with time after the final plating. Even with cells that generally have a very high average level of VSCC expression we found a proportion of cells with no Ca²⁺ current whatsoever; this may reflect a stage in the cell cycle. Expression levels in both transient and stable expression systems can be further altered by changing culture conditions. For example the addition of butyrate to culture media increases expression of some cell surface proteins. Changes in culture temperature can also be utilized to promote functional expression of certain VSCCs (e.g., (30)).

Recording solutions

3. There is considerable diversity in the solutions used for whole-cell studies of VSCC function. Usually, the primary goal driving decisions on solution composition reflect the need to eliminate current flow through other ion channels whilst sparing (or augmenting) current through VSCCs. Consequently, these decisions will reflect the ion channel complement of the cell used as an expression host and the level of VSCC expression achieved. Secondary considerations may reflect specific

experimental demands, such as a desire to be as close to the physiological condition as possible or a desire to limit intracellular processes triggered by Ca^{2+} entry, for example Ca^{2+} -dependent VSCC inactivation or activation of Ca^{2+} -dependent channels.

4. For recombinant VSCCs we have used a very simple extracellular solution based on 140 mM tetraethyl ammonium (TEA) chloride and 10 mM HEPES buffer (e.g., (32, 33)). In some studies this is only supplemented with the chloride salt of the permeating divalent species, usually CaCl_2 or BaCl_2 (occasionally SrCl_2). To generate currents of a suitable amplitude for study the concentration of the permeating divalent ion is set between 1 and 20 mM (most usually 2 or 5 mM). For CaV1 and CaV2 families Ba^{2+} and Sr^{2+} give currents two to three times larger than equimolar Ca^{2+} , whereas for CaV3 channels currents are of a broadly similar amplitude in all three ions. Over and above the three components described above we have at various times and for various reasons added CsCl (5 mM), glucose (10 mM), and MgCl_2 (1 mM) to the bathing solution. Whatever the precise composition of the extracellular solution, we adjust the pH to 7.3 with TEA-OH and aim for a final extracellular osmolarity of 310–315 mOsm. To achieve the latter target makeup we adjust the TEA-Cl concentration as required by the particular solution composition. Other large cations can be used in place of TEA as the majority extracellular ion, for example N-methyl-D-glucamine and choline, indeed, in many systems the more physiological Na^+ ion would also be acceptable. Our standard recording method (described below) involves gigaseal formation to be carried out in a simple pseudo-physiological HEPES-buffered saline (HBS) which is also used to constantly perfuse the recording chamber. This solution is also used to maintain cells after they have been removed from the cell culture incubator.
5. At very low concentrations of divalent cations VSCCs effectively conduct monovalent ions such as K^+ , Na^+ , Li^+ , and protons (e.g., (34)). Workers wishing to study such currents should ensure that the extracellular Ca^{2+} concentration is sufficiently low by using a Ca^{2+} chelator such as EGTA or BAPTA. This is because divalent ion contamination is significant in both double distilled water and commercial NaCl and LiCl (for example 140 mM NaCl made with standard lab chemicals and completely divalent free water, would be expected to contain around 3 μM Ca^{2+} and 1.5 μM Ba^{2+}).
6. Junction potentials. The combination of bath and electrode solutions used in many VSCC experiments produce significant liquid junction potentials (for example, 14 mV between a Cs Me-sulfonate-based electrode solution and a TEA-Cl-based

bath solution). If uncorrected, these potentials can produce significant voltage errors. We usually calculate our junction potentials using the utility included in the pClamp software suite. It is also possible to measure junction potentials electrically (35).

7. Pipette (internal) solutions should be filtered (0.2 μm) to remove dust/debris. In whole-cell experiments, pipette solution rapidly replaces the intracellular ionic milieu. Pipette solutions for recording VSCCs typically contain Cs^+ as their predominant cation, as this eliminates most current through potassium channels. As for the major anion a number of species have been adopted. These include Cl^- , methanesulfonate, gluconate, aspartate, and glutamate; a significant advantage of the use of the former is that it results in small junction potentials when used with the common bath solutions. The other main features of pipette solutions are the provision of suitably buffered levels of Ca^{2+} and pH along with some additional provisions to sustain intracellular signalling and limit Ca^{2+} current rundown. Ca^{2+} is usually buffered with either EGTA or BAPTA. If a defined intracellular Ca^{2+} concentration is required a set amount of Ca^{2+} is included along with the chelators and the actual concentration calculated with appropriate software.
8. Osmolarity. For cell-lines, we aim for pipette solutions with a value of 295–300 mOsm for use with bath solutions of 310–315 mOsm. For dissociated neurons, we strongly suggest a greater difference in osmolarity, with external around a “physiological” 305 mOsm and the internal 270–275 mM (including the addition of all final constituents—leupeptin, GTP, ATP, phosphocreatine, etc.).

Dissociation of central neurons

9. Brain slices (300–400 μM thick) are cut on a Vibrotome and maintained in aCSF at room temperature for up to 6 h. When required the desired brain area is dissected out under a stereomicroscope using a scalpel, to give a microslice. Usually, only one microslice is then incubated in HBSS at 35°C, bubbled with 100% O_2 . In order to minimize hypoxic damage, the incubation and dissociation media can be supplemented with kynurenic acid (1 mM), pyruvic acid (1 mM), nitroarginine (0.1 mM, and glutathione (0.05 mM) (see Subheading 2, also ref. 36). From 30 to 60 min later, 1 micro-slice is incubated in HBSS containing 0.5 mg/ml protease pronase E (Sigma protease type XIV, 1.0 mg/ml at 32–35°C). See Note 11. The tissue is washed three times with HBSS, then mechanically triturated using three glass Pasteur pipettes, flame-polished to successively narrower tip diameter. Alternatively, the tissue may be rinsed in an antioxidant Na isethionate solution. The cell

suspension supernatant is then placed in a Petri dish mounted on the stage of an inverted microscope. Cells are allowed to settle for about 10 min, following which a background flow of HBSS is initiated through the bath (~1 ml/min).

10. General notes on dissociation of central neurons. Acute preparations of isolated cells are somewhat variable. Some degree of hypoxia is unavoidable. We have studied the survival of dissociated pallidal neurons and found a dramatic loss of viable cells when preparation are made from rats aged > 2 months. We routinely use animals < 7–8 weeks of age, ideally in the 20–35 days postnatal range (assuming they represent fully developed neurons).
11. We have found the nonspecific protease type XIV (pronase E, Sigma) to be most effective (instead of trypsin or papain). This usually gives acutely isolated somata with “enzymatically chopped” long dendrites. The ability to isolate neurons without extensive arborizations is important for adequate voltage clamp control of the whole-cell surface (“space clamp”), at least for quite slow, sustained conductances such as VSCC. We have used pronase E in the concentration range 0.5–1.0 mg/ml at 32–35°C. Enzyme incubation times are between 25 and 40 min. Mody and co-authors were probably the first to suggest pronase E for central neurons (37), although the enzyme had a previous long history for different preparations (e.g., retina). It should be noted that substantial effects of Pronase E on ion channel function have been reported, including loss of sodium channel inactivation, reduction of low-threshold calcium current and shifts of voltage-dependence. Some scientists have tried to minimize the effects of proteolysis by means of a “mixed” or purely mechanical mode of dissociation (e.g., (38)).
12. General rules for whole-cell recordings of VSCCs in isolated central neurons. We perform whole-cell recordings utilizing pipettes (glass capillaries from WPI, PG52165-4) pulled on a Flaming-Brown puller and fire polished just prior to use. Pipette resistance is 3–8 MΩ when filled with internal solution. We aim to limit potential Ca-dependent inactivation of VSCCs, and thus entirely replace all external Ca^{2+} with Ba^{2+} , but maintain some free intracellular calcium (< 20–50 nM) using EGTA or BAPTA (unless the assessment of calcium-dependent calcium release is a priority). Minimize VSCC current rundown (39). As a rule, internal 3 mM ATP significantly prolongs VSCC survival (40). Consider the possible permeability of VSCC by monovalent cations, e.g., potassium or protons (34).
13. In dissociated neurons we favor the impermeant cation N-methyl D-glucamine (NMG) as the main internal cation, in order to impede outward currents. On the others hand, whole-cell recordings from neurons in “intact tissue” such as intra-slice

patch recording, usually utilize potassium salts as sulfonates. Powers and Binders (41), studying spinal motoneurons in 300 μm slices, are a typical example. To study the full ensemble of physiological currents, they used a pipette solution containing (in mM): 146 KCH_3SO_4 , 5 KCl, 2 MgCl_2 , 2 EGTA, 10 MOPS, 2 Na_2ATP , and 0.2 Na_3GTP , pH 7.3. For recording inward currents in isolation, the pipette solution was (in mM): 100 CsCl, 20 TEA-Cl, 5 MgCl_2 , 2 BAPTA, 10 HEPES, 5 Na_2ATP , 0.5 Na_3GTP , pH 7.3.

General whole-cell recording methods

14. Temperature. The majority of patch-clamp studies of channel properties are still performed at room (“ambient”) temperature, for experimental simplicity. Anyone wanting to draw parallels between the physiological condition and a recombinant preparation, however, may be advised to consider a series of recordings at physiological temperature. Those taking this route should check the pH of all solutions at experimental temperature and correct for altered junction potentials (for example a combination of intracellular CsMeSO₄ 140, TEA-Cl 10 and extracellular TEA-Cl 140, CsMeSO₄ 10—all mM—will change junction potential by ~6 mV between 20 and 37°C). In addition, at higher temperature currents will exhibit faster kinetics (Fig. 2) and may well be larger. This can affect voltage clamp fidelity and series resistance.
15. External solution exchange. Some VSCC experiments can be performed in static bath preparations, however, any manipulation that requires changing solutions or adding drugs will require some form of bath perfusion or cell perfusion device. Although a fairly straightforward approach, completely exchanging the bath solution carries certain disadvantages. Firstly with bath perfusion it can take some time to effect the desired solution exchange, particularly if there is significant dead-space in the perfusion system. This can be minimized by using small volume chambers (or laminar flow chambers) and placing a solution manifold as close as possible to the perfusion entry to the bath. A second disadvantage is that bath exchange can use significant solution volumes, which although not a generally problem for simple salt solutions, can have implications when expensive drugs or toxins are applied. Our favored approach is to use a fast perfusion device (see above) to effect local cell perfusion. Here the cell is locally perfused from 200 to 500 μm diameter glass barrels at flow rates of about 100–200 $\mu\text{l}/\text{min}$, in addition the bath is perfused with a single solution at 1–2 ml/min. In many of our experiments the bath is perfusate is a simple HEPES-buffered saline consisting mainly of NaCl supplemented with glucose and chloride salts of Ca^{2+} .

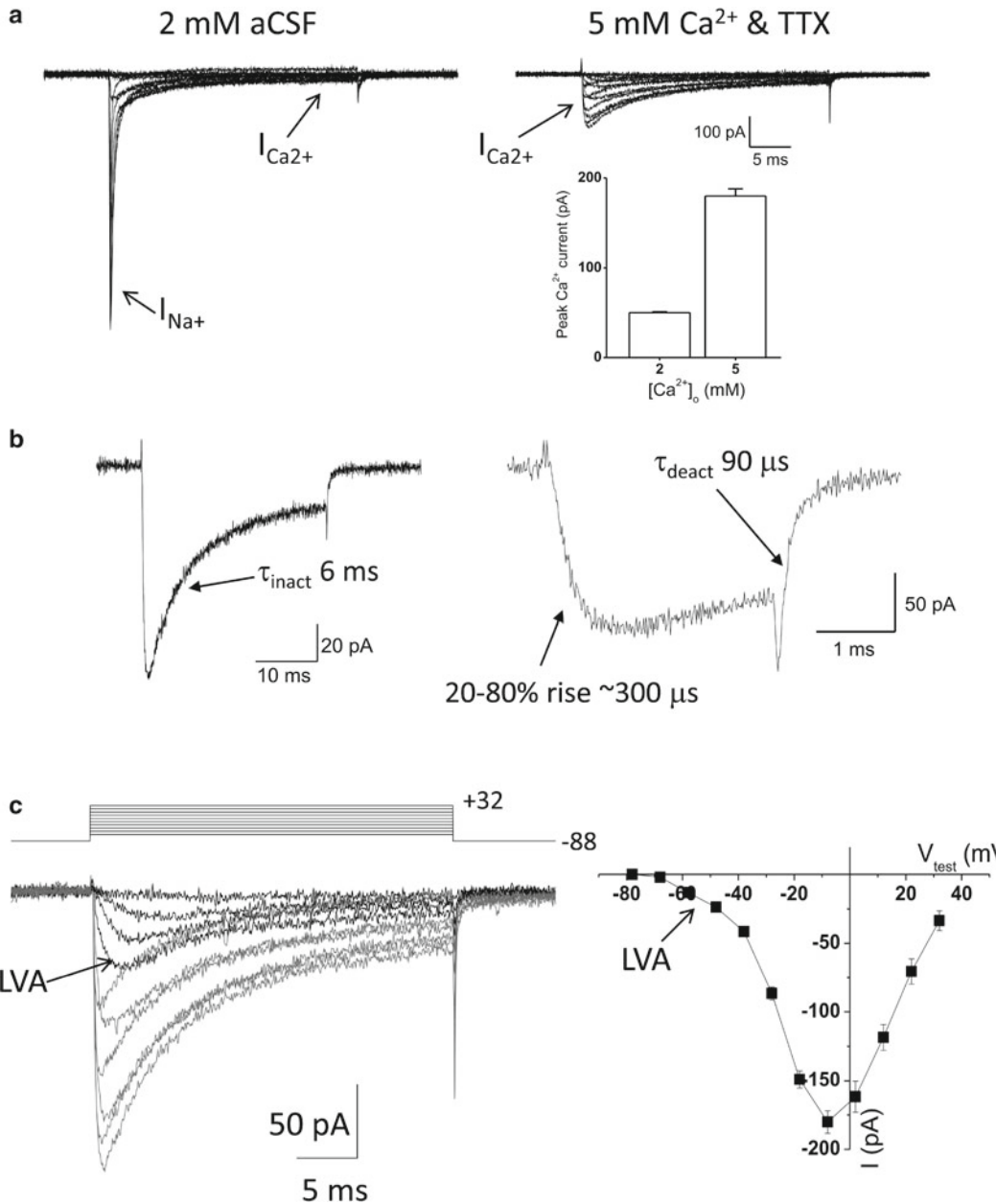


Fig. 2. Voltage-sensitive Ca^{2+} currents in macropatches isolated from acute brain slices. All data shown are from nucleated macropatches isolated from the cell bodies of hippocampal CA3 pyramidal cells in brain slices prepared from 2 to 3 week old rats. Recordings were all made at room temperature. (a) Traces from an example current versus voltage series gathered from a holding potential of -88 mV and utilizing 30 ms depolarizing test stimuli spaced at 10 mV intervals. *Left*, currents recorded in normal artificial cerebrospinal fluid (aCSF), containing 2 mM Ca^{2+} . Note the initial large fast activating, fast inactivating inward Na^+ current (I_{Na^+}) and the much smaller maintained currents. *Right*, Ca^{2+} currents ($I_{\text{Ca}^{2+}}$) recorded from the same macropatch in the presence of TTX (1 μM) to abolish I_{Na^+} and elevated extracellular Ca^{2+} ions, in the presence of TTX (error bars, where visible represent the S.E.M.) (b) Gating kinetics of Ca^{2+} currents in nucleated macropatches. Currents recorded in TTX and 5 mM Ca^{2+} in response to test depolarizations to -8 mV from a holding potential of -88 mV . *Left*, a long depolarization (30 ms) to illustrate inactivation kinetics. *Right*, a brief depolarization (3 ms) to illustrate activation and deactivation. (c) *Left*, an example full current–voltage series from a macropatch in 5 mM Ca^{2+} illustrating the presence of both low voltage-activated (LVA; black traces, current in response to $V_{\text{test}} = -58, -48, -38 \text{ mV}$) and high voltage-activated Ca^{2+} currents (pale traces: $V_{\text{test}} = -28, -18, -8, 2, 12, 22, 32 \text{ mV}$). *Right*, peak current versus voltage relationships pooled from multiple records like that shown on the left. J.T. Brown and A.D. Randall, unpublished data.

and Mg^{2+} . We typically form our gigaseals in this NaCl based solution before turning on the local perifusion (with applies the TEA-based VSCC bath solution described above) and entering the whole-cell configuration.

16. Rundown of VSCC currents. Time-dependent rundown of VSCC-mediated currents is a common problem in whole-cell experiments, one way to reduce this is to use perforated patch methods (see below). Alternatively pipette solutions can be supplemented with biochemical reagents proposed to prolong recording lifetime. Most commonly included are ATP and GTP (which also require inclusion of Mg^{2+} to produce any benefit). Some workers include phosphocreatine (and sometimes creatine phosphokinase). Other additions include calpain inhibitor peptide, cAMP, pyruvate and oxaloacetate, and the peptidase inhibitor leupeptin. To limit current rundown in recordings of recombinant human CaV2.3, we have used the pipette solution listed in Subheading 2 (above).

For dissociated neurons, with 0.1 mM EGTA in the pipette, the addition of 3 mM ATP significantly prolongs I_{Ca} survival, whilst no further improvement obtained by increasing the ATP to 10 mM or replacing ATP with creatine phosphate (40).

17. Perforated patch recording. See reference (42). Starting from the cell-attached configuration, this method of recording uses antibiotic/antifungal agents (e.g., nystatin, amphotericin) to “perforate” the cell membrane beneath the tip of the patch electrode. This process generates electrical continuity between the pipette and the cytoplasm, thus allowing the macroscopic currents of the entire cell membrane to be recorded. The degree and rate at which the pipette contents exchange with the cell’s interior during perforated patch recordings depend on the perforating agent used and how extensively the membrane is perforated. Furthermore, certain perforating agents exhibit selectivity in their ionic permeabilities and consequently can be used to preserve the physiological concentrations of certain ions (e.g., gramicidin is used to preserve physiological Cl^- gradients, ref. (43)). The key feature of perforated patch recording is that it preserves the intracellular biochemistry of the cell. This can prove valuable in: (1) reducing the rundown of VSCCs; (2) studying regulation of VSCC function by intracellular signalling cascades. Because Ca^{2+} chelators such as EGTA and BAPTA do not pass through most perforating ionophores, perforated patch recording does not allow the investigator to control the level of intracellular Ca^{2+} buffering. Thus VSCC activation can produce very large internal Ca^{2+} rises that may be poorly controlled - particularly in the epithelial cells frequently used as expression hosts, which are not “designed” to cope with such Ca^{2+} loads, having no voltage-gated channels of their own.

To an aliquot of standard electrode solution, the perforating agent is added at a suitable concentration (usually from a stock solution in DMSO). Many workers report that the perforating efficacy of agents such as nystatin declines with time in solution. Consequently, a new aliquot of electrode solution containing the perforating agent should be prepared every 2 h.

Having prepared solutions, the very tip of the recording pipette is filled with internal solution devoid of perforating agent. It is important not to fill too much of the tip in this way. To achieve this, we fabricate our pipettes from microfilament-containing glass (e.g., Clark Electromedical GC120F10). We then immerse the back (i.e., unpulled) end of the pipette in electrode solution (this fills the tip by capillary action) for about 5 s, before removing and rapidly blotting the immersed end dry on filter paper. Using a 1 ml syringe and flexible microfilament (WPI microfil) the rest of the pipette is then filled to about half full with pipette solution containing perforating agent. After this the cell-attached configuration is entered in the standard way and fast capacitance neutralization performed. The process of perforation is then monitored by observing the appearance of whole-cell capacitance transients. These will grow in amplitude and narrow in width as the access resistance decreases. When these changes to the capacity transient have stabilized, and if the series resistance has reached a sufficiently low value, recording of whole-cell responses can be initiated.

18. Voltage protocols. The components of a VSCC response to a square voltage command of 100 mV amplitude from a holding potential of -90 mV is shown in Fig. 1. The response rapidly rises to a peak through a process of time-dependent activation. Whilst the command potential is maintained a decline from the initial peak is observed for most, if not all, VSCCs. This is a consequence of the process of inactivation (which can be either voltage- or Ca^{2+} -dependent).

The multiple phases of the Ca^{2+} current response to a simple voltage step allows one to measure a range of parameters. The most commonly made measurement is the peak current amplitude during the command pulse, in addition the amplitude of the tail current can be characterized. The kinetics of activation, inactivation and deactivation can also be quantified, as can recovery from inactivation. Furthermore, all of the above parameters are voltage-dependent and can also exhibit dependencies on each other.

For a simple first pharmacological experiment with any compound many workers will simply track the time course of the peak Ca^{2+} channel current amplitude measured at a single test potential applied from a fixed holding potential. The test potential used will often be close to that which produces

maximum current amplitude, typically around 0 mV for an HVA channel and -15 mV for an LVA channel. The holding potential would usually be set at a level which elicits little steady-state inactivation. To know where the test and holding potentials lie on the activation and inactivation curves an initial series of *I*-*V* relationships and steady-state inactivation curves can be gathered (for protocols see below). When using such a protocol we would utilize a P-over-4 leak subtraction method and would store both leak-subtracted and raw data to the computer. It can also be useful to include a “passive” voltage step (e.g., -80 to -90 or -70 mV) in the acquired data trace. The purpose of this is to allow both an assessment of the effectiveness of the P-over-4 leak subtraction and to provide a means to calculate and subtract leak from the raw data if there are concerns about the outcome of the chosen P-over-4 paradigm.

Although many workers use such a protocol simply to measure peak current amplitude versus time, the current trace will also provide information on activation rate, tail current amplitude and deactivation rate. Furthermore, if the test pulse is long enough the rate of macroscopic inactivation can be estimated. Given that compounds can alter all of these parameters it is suggested that they are at least “eyeballed” for change during an experiment, and better still, analyzed quantitatively. It is also worth noting that changes in these parameters with time, particularly deactivation kinetics, can be good indicators of changes in the fidelity of the voltage clamp and consequently of recording quality.

For many VSCCs expressed in common host cells (e.g., HEK293, CHO, and COS) it is likely that all, or nearly all, the VSCCs will be inactivated in the culture dish prior to obtaining whole-cell access. This is because the resting membrane potential of such host cells is typically very depolarized (e.g., -35 to -5 mV). Consequently, when recordings are started with standard protocols the current will often run up for a short time as the entire channel population slowly shifts to a new equilibrium in which most channels are in noninactivated closed states at rest. After this initial period of run-up the current amplitude may for a while become steady with respect to time. In most recording scenarios the current will begin to rundown at some finite rate, although under the right conditions this rundown can be very slow (see Note 16).

The next most common protocol to be used for VSCC analysis is the current–voltage relationship (e.g., Fig. 2a, c). In its most common form, this consists of a series of depolarizing steps of incrementally increasing amplitude applied from a negative holding potential. For example, 10 mV test potential increments from -80 mV to +60 mV, all applied from a holding potential of -80 mV. The standard readout is a plot of

peak current amplitude versus test potential. With the right protocol the voltage-dependence of activation and inactivation rates and conductance-voltage plots can also be obtained.

Firstly, it is well worth including a zero amplitude step as the first pulse (e.g., -80 “to” -80 mV). The main reason for this is in subsequent analysis where the measured “peak” during such a zero amplitude test pulse can be subtracted from all subsequent peaks as a means to remove the effect of background current noise on measured peak current. Indeed it may also be worth including a single hyperpolarizing step at the start or the end of the data set, this can be used to judge the effectiveness of leak subtraction, or as a basis for an ohmic leak subtraction method.

Secondly, to define the shape of the voltage-dependence of activation, which realistically only spans about 30 mV for most VSCCs, we often include smaller increments in test potential (5 mV or even 3 mV) in the area of the rising phase of the I - V (the downstroke of the U-shape of a typical I - V). For example, for an HVA current, we may include additional test pulses to -35 , -25 , -15 and -5 mV. In order to keep protocols short we may then leave out test pulses to, -70 and -50 , $+20$ and $+40$ mV, where there is either no channel activation or channel activation is close to maximal and thus current amplitude is only a consequence of electrochemical driving force.

Thirdly, some consideration must be given to the length of the test pulses employed. For small depolarizations channel opening may be very slow, so to obtain a good estimate of the peak current a long pulse will be required. Contrarywise, for strong depolarizations peak current will be reached in a few milliseconds and longer pulses will usually produce some degree of channel inactivation. If one is only interested in studying current activation, the length of the test pulse can be set so that it is just longer than the time required to reach peak macroscopic current. Indeed, this is the best method to use if one is trying to determine peak conductance-voltage relationships from tail current measurements. If one wishes to assess the kinetics of macroscopic inactivation at various test potentials, pulses long enough to induce a reasonable degree of inactivation will be required. As for activation studies these test pulses may need to be of different durations for different test potentials, since the rate of inactivation is voltage-dependent. Furthermore, when eliciting significant inactivation during test pulses, sufficient time must be left between test pulses to allow recovery from inactivation to occur (this can be estimated using a standard recovery from inactivation protocol).

Inactivation of VSCCs is another important parameter and one that is often relevant to pharmacology, as many compounds preferentially bind to inactivated states. As mentioned above

macroscopic inactivation kinetics can be measured during the depolarizing voltage pulses used to characterize channel activation. However, inactivation (albeit much slower) also occurs at potentials that fail to activate VSCCs significantly. This is easily demonstrated in experiments designed to characterize steady-state inactivation relationships. Put simply, to gather such data one varies the holding potential employed before applying a brief test pulse to activate the VSCCs. This test pulse is of invariant amplitude, typically to the around the peak of the I-V relationship, and is usually brief (just long enough to produce peak current). Commonly steady-state inactivation protocols use a conditioning prepulse of incremental amplitude applied for a few seconds before the test pulse. Alternatively, after the test pulse the cell is repolarized to the next holding potential which is then maintained until the next test pulse applied. Notably, as the rate of inactivation is faster at more depolarized levels there is a tendency with such methods, to fail to reach a steady-state level of inactivation at the more hyperpolarised holding potentials employed, however this rarely has a highly significant effect on the final curve if sufficient points around the mid-point of inactivation are gathered. The output of such experiments is plotted as peak current response in the test pulse versus pretest pulse holding potential. The data are typically normalized to current amplitude produced during the maximally effective test pulse. For steady-state inactivation measurements we would recommend that leak subtraction sweeps are gathered after the test pulse, rather than before.

Ca^{2+} -dependent inactivation (i.e., channel inactivation caused by cytoplasmic Ca^{2+}) is often studied with paired test pulse protocols. Here the first test pulse amplitude is varied, such that the level of Ca^{2+} entry changes, and the degree of inactivation thus produced is studied by applying an invariant second test pulse. Having said this, using such protocols it is very difficult to entirely separate Ca^{2+} -dependent inactivation from voltage-dependent inactivation, whereas the reverse separation can be achieved by studying the flux of monovalent cations in the absence of Ca^{2+} . At extreme depolarizations relatively little Ca^{2+} -dependent inactivation is produced (because little Ca^{2+} enters the cell due to driving force considerations) but voltage-dependent inactivation is maximal due to the strong depolarization.

Inactivated VSCCs recover from voltage-dependent inactivation with a rate that depends on the membrane potential. To characterize recovery from inactivation a paired pulse protocol is typically used. Here a series of paired pulses are applied in which a first test pulse that substantially inactivates the VSCC population is followed, at a varied latency, by a brief, second test pulse. The response to the second pulse is used to monitor

what proportion of the channels have recovered from the inactivation produced in the first pulse to a state that allows them to be reactivated by the second pulse. It is good practice to leave sufficient time between individual paired pulse stimuli to allow near-complete recovery from inactivation. Furthermore, we recommend that the change in inter-pulse interval is made in a logarithmic fashion rather than a linear one as the process of recovery from inactivation typically follows an exponential (or often multi-exponential) time course. The voltage-dependence of the rate of recovery from inactivation can be determined by performing a series of such experiments in which the holding potential employed between the paired pulses is systematically varied.

The last major biophysical hallmark we shall consider is deactivation, the process through which VSCCs close upon membrane repolarization. Like activation and inactivation deactivation is a voltage-dependent process which is speeded at more hyperpolarized potentials. To characterize this voltage-dependence a protocol in which a fixed amplitude test pulse is followed by repolarization to a range of different potentials is employed. Repolarization to potentials at which VSCCs exhibit no measurable opening in activation protocols will produce a large inward tail current. This large current will then decline rapidly to the zero current level. The decline in this current represents the process of deactivation and can be fit with exponential functions, the time constant of which will depend on voltage. The key factor to note here is that deactivation is very fast. At room temperature CaV3 family channels (i.e., LVA T-type channels) deactivate with time constants of the order of 1 ms at -80 mV. HVA channels (CaV1 and CaV2) deactivate perhaps ten times faster (Fig. 2). Indeed, to characterize the rapid deactivation of these channels faithfully the very best patch-clamp practice must be employed to elicit a suitably fast voltage clamp (e.g., large electrodes, very low series resistance, and accurate capacitance compensation). For example in the past we have measured CaV2.2 channel deactivation time constants of around 60 μ s, using 0.6 M Ω electrodes and ~1 M Ω series resistances compensated by ~90% (44). Due to the speed and voltage-dependence of deactivation, the best tip for tail current measurements, for example to create conductance-voltage curves, is to use the most depolarized repolarization potential possible (e.g., around -50 or -60 mV).

Above we have summarized a range of standard voltage-step protocols for making simple biophysical measurements. Review of the literature will uncover a range of other voltage-step protocols including, for example, triple pulse measurements favored by some laboratories for inactivation studies.

Of course in the physiological situation VSCC opening and closing is not triggered by square-wave voltage changes, but instead by physiological membrane potential changes. These will include, depending on the VSCC type, action potentials, synaptic potentials, and pacemaker currents. Analysis of how VSCCs are activated by such voltage changes can be revealing when considering how biophysical parameters relate to physiological role. To achieve this goal, recorded real or digitally synthesized physiological voltage transients can be used as voltage commands (e.g., (45–47)). Alternatively models of channel gating produced from the sorts of experiments described above can be used to simulate the physiological behavior of VSCCs under various conditions. It is often advisable to complement studies of recombinant channels with analysis of native VSCCs which of course may exhibit somewhat different behaviors due to their environment or post-translational modifications.

The basic process of recording whole-cell VSCC currents

19. Operator should hold an earthed (grounded) lead when touching the headstage. The sensitive amplifier in the headstage input can be damaged by static electricity.
20. Pressure and suction can be applied using a syringe (e.g., 10 ml) or by mouth (through the body of a 1 ml syringe). The pressure applying line is connected to suction port of the electrode holder via a three way stopcock and suitable tubing. This allows applied pressure (or suction) to be locked in. We prefer to leave positive pressure on the pipette lumen until we touch the surface of the cell.
21. We visually observe the occurrence of contact between the pipette and the cell surface. You can also detect this by watching the current response of the electrode.
22. In cells that form gigaseals slowly (or with difficulty) we find that seals of 50–500 M Ω can be encouraged to convert to gigaseals by placing the pipette potential at a negative value, e.g., -70 mV and by applying the VSCC bath solution.
23. Certain amplifiers provide a “zap” button which delivers a short duration high amplitude electrical pulse which dielectrically perturbs the membrane with the intent of aiding breaking through to the whole-cell configuration. We have used this at times, although rarely resort to it presently. We find it is most effective when combined with suction rather than used alone.
24. Prior to neutralizing capacity transients and compensating for series resistance it can be useful to check whether the current under study is present in the cell (e.g., by using a single voltage step to a potential where a good-sized current would be expected or, if appropriate, by applying a brief agonist application). There is little point in optimizing recording parameters

if there is no current to record. This is particularly applicable when working with transiently transfected cells.

25. Series resistance. In terms of the fidelity of the voltage clamp and lack of voltage errors the best recordings are made with the lowest access resistances. Thus, if there is no reason to work with higher series resistance levels (for example to reduce rundown), aim low. The best way to achieve this is to use as low a resistance electrode as is commensurate with getting a decent number of gigaseals that can be converted to whole-cell recordings. For the common host cells such as HEK293s and CHOs we would generally have series resistance values in the range of 2–5 MΩ and have worked at <1 MΩ. Generally in such systems we would not work with recordings with an access resistance >10 MΩ and certainly never more than 20 MΩ. Having said this, the most important factor is to marry the level of uncompensated series resistance with the amplitude of the current under study, for example for a slowly activating current of 100 pA amplitude an uncompensated series resistance of 15 MΩ may not cause any significant errors for most experiments. Whereas a 5 MΩ series resistance and a fast gating 15 nA current could combine to produce substantial recording errors.

Macropatch recordings

26. In the original descriptions of nucleated macropatch methods, both in cultured neurones (48) and brain slices (49), recordings were only made at room temperature. However, almost all of our own work to date on VSCCs in macropatches has been performed at ~33°C (Fig. 2), a temperature employed in many neurophysiological brain slice studies. Our methods also are effective for recordings both room temperature and 37°C. Notably the kinetics of Ca²⁺ currents, in particular inactivation kinetics are quite fast at near physiological temperatures (Fig. 2b).
27. Peak Ca²⁺ current amplitude in macropatches from P14 CA3 pyramidal cells average 180 pA in 5 mM Ca²⁺ and rarely exceed 200 pA (Fig. 2a, c). Currents in 2 mM Ca²⁺ aCSF average only around 50 pA. In contrast, voltage-gated Na⁺ and K⁺ currents can be very much larger (see Fig. 2 and also ref. 25). For this reason it is prudent to use TTX to block voltage-gated Na⁺ currents when studying Ca²⁺ currents in macropatches.
28. As in conventional whole-cell recordings from dissociated neurones multiple current components are clearly present in nucleated macropatches isolated from rodent hippocampal neurones. As shown in Fig. 2c high and low-voltage activated components can be observed, based both on activation voltage range and kinetics.

References

1. Ertel EA, Campbell KP, Harpold MM, Hofmann F, Mori Y, Perez-Reyes E, Schwartz A, Snutch TP, Tanabe T, Birnbaumer L, Tsien RW, Catterall WA (2000) Nomenclature of voltage-gated calcium channels. *Neuron* 25:533–535
2. Sakmann B, Neher E (1983) Single-channel recording. Plenum, New York, NY
3. Hamill OP, Marty A, Neher E, Sakmann B, Sigworth FJ (1981) Improved patch-clamp techniques for high-resolution current recording from cells and cell-free membrane patches. *Pflugers Arch* 391:85–100
4. Levis RA, Rae JL (1992) Constructing a patch clamp setup. *Methods Enzymol* 207:14–66
5. Levis RA, Rae JL (1998) Low-noise patch-clamp techniques. *Methods Enzymol* 293:218–266
6. The Axon Guide. http://www.axon.com/MR_Axon_Guide.html
7. Fenwick EM, Marty A, Neher E (1982) Sodium and calcium channels in bovine chromaffin cells. *J Physiol* 331:599–635
8. Lux HD, Brown AM (1984) Patch and whole cell calcium currents recorded simultaneously in snail neurons. *J Gen Physiol* 83:727–750
9. Ikeda SR, Schofield GG, Weight FF (1986) Na⁺ and Ca²⁺ currents of acutely isolated adult rat nodose ganglion cells. *J Neurophysiol* 55:527–539
10. Matteson DR, Armstrong CM (1984) Na and Ca channels in a transformed line of anterior pituitary cells. *J Gen Physiol* 83:371–394
11. Carbone E, Lux HD (1987) Kinetics and selectivity of a low-voltage-activated calcium current in chick and rat sensory neurones. *J Physiol* 396:547–570
12. Tsien RW, Bean BP, Hess P, Lansman JB, Nilius B, Nowycky MC (1986) Mechanisms of calcium channel modulation by beta-adrenergic calcium agonists. *J Mol Cell Cardiol* 18: 691–710
13. Hille B (2001) Ion channels of excitable membranes. Sinauer, Sunderland, MA
14. Hess P, Lansman JB, Tsien RW (1984) Different modes of Ca channel gating behaviour favoured by dihydropyridine Ca agonists and antagonists. *Nature* 311:538–544
15. Bossu JL, Feltz A, Thomann JM (1985) Depolarization elicits two distinct calcium currents in vertebrate sensory neurones. *Pflugers Arch* 403:360–368
16. Dupont JL, Bossu JL, Feltz A (1986) Effect of internal calcium concentration on calcium currents in rat sensory neurones. *Pflugers Arch* 406:433–435
17. Llinás R, Sugimori M, Hillman DE, Cherksey B (1992) Distribution and functional significance of the P-type, voltage-dependent Ca²⁺ channels in the mammalian central nervous system. *Trends Neurosci* 15:351–355
18. Randall A, Tsien RW (1995) Pharmacological dissection of multiple types of Ca²⁺ channel currents in rat cerebellar granule neurons. *J Neurosci* 15:2995–3012
19. Zhang JF, Randall AD, Ellinor PT, Horne WA, Sather WA, Tanabe T, Schwarz TL, Tsien RW (1993) Distinctive pharmacology and kinetics of cloned neuronal Ca²⁺ channels and their possible counterparts in mammalian CNS neurons. *Neuropharmacology* 32:1075–1088
20. Takahashi T, Forsythe ID, Tsujimoto T, Barnes-Davies M, Onodera K (1996) Presynaptic calcium current modulation by a metabotropic glutamate receptor. *Science* 274:594–597
21. Bischofberger J, Geiger JR, Jonas P (2002) Timing and efficacy of Ca²⁺ channel activation in hippocampal mossy fiber boutons. *J Neurosci* 22:10593–10602
22. Stefani A, Pisani A, Mercuri NB, Bernardi G, Calabresi P (1994) Activation of metabotropic glutamate receptors inhibits calcium currents and GABA-mediated synaptic potentials in striatal neurons. *J Neurosci* 14:6734–6743
23. Stefani A, Spadoni F, Bernardi G (1997) Differential inhibition by riluzole, lamotrigine, and phenytoin of sodium and calcium currents in cortical neurons: implications for neuroprotective strategies. *Exp Neurol* 147:115–122
24. Hainsworth AH, Spadoni F, Lavaroni F, Bernardi G, Stefani A (2001) Effects of extracellular pH on the interaction of sipatrigine and lamotrigine with high-voltage-activated (HVA) calcium channels in dissociated neurones of rat cortex. *Neuropharmacology* 40:784–791
25. Brown JT, Chin J, Leiser SC, Pangalos MN, Randall AD (2011) Altered intrinsic neuronal excitability and reduced Na⁽⁺⁾ currents in a mouse model of Alzheimer's disease. *Neurobiol Aging* 32:2109.e1–2109.e14
26. Dempster J. Strathclyde software. <http://innovol.sibs.strath.ac.uk/physpharm/ses.shtml>
27. Vasquez C, Navarro-Polanco RA, Huerta M, Trujillo X, Andrade F, Trujillo-Hernandez B, Hernandez L (2003) Effects of cannabinoids on endogenous K⁺ and Ca²⁺ currents in HEK293 cells. *Can J Physiol Pharmacol* 81:436–442
28. Berjukow S, Doring F, Froschmayr M, Grabner M, Glossmann H, Hering S (1996) Endogenous calcium channels in human embryonic kidney (HEK293) cells. *Br J Pharmacol* 118:748–754

29. Bleakman D, Bowman D, Bath CP, Brust PF, Johnson EC, Deal CR, Miller RJ, Ellis SB, Harpold MM, Hans M (1995) Characteristics of a human N-type calcium channel expressed in HEK293 cells. *Neuropharmacology* 34: 753–765
30. McCool BA, Pin JP, Harpold MM, Brust PF, Stauderman KA, Lovinger DM (1998) Rat group I metabotropic glutamate receptors inhibit neuronal Ca²⁺ channels via multiple signal transduction pathways in HEK 293 cells. *J Neurophysiol* 79:379–391
31. Pereverzev A, Klockner U, Henry M, Grabsch H, Vajna R, Olyschlager S, Viatchenko-Karpinski S, Schroder R, Hescheler J, Schneider T (1998) Structural diversity of the voltage-dependent Ca²⁺ channel alpha1E-subunit. *Eur J Neurosci* 10:916–925
32. McNaughton NC, Hainsworth AH, Green PJ, Randall AD (2000) Inhibition of recombinant low-voltage-activated Ca(2+) channels by the neuroprotective agent BW619C89 (Sipatrigine). *Neuropharmacology* 39:1247–1253
33. Hainsworth AH, McNaughton NC, Pereverzev A, Schneider T, Randall AD (2003) Actions of sipatrigine, 202 W92 and lamotrigine on R-type and T-type Ca²⁺ channel currents. *Eur J Pharmacol* 467:77–80
34. Zeilhofer HU, Swandulla D, Reeh PW, Kress M (1996) Ca²⁺ permeability of the sustained proton-induced cation current in adult rat dorsal root ganglion neurons. *J Neurophysiol* 76: 2834–2840
35. Neher E (1992) Correction for liquid junction potentials in patch clamp experiments. *Methods Enzymol* 207:123–131
36. Song WJ, Surmeier DJ (1996) Voltage-dependent facilitation of calcium channels in rat neostriatal neurons. *J Neurophysiol* 76:2290–2306
37. Mody I, Salter MW, MacDonald JF (1989) Whole-cell voltage-clamp recordings in granule cells acutely isolated from hippocampal slices of adult or aged rats. *Neurosci Lett* 96:70–75
38. Matsuo S, Jang IS, Nabekura J, Akaike N (2003) Alpha 2-Adrenoceptor-mediated presynaptic modulation of GABAergic transmission in mechanically dissociated rat ventrolateral preoptic neurons. *J Neurophysiol* 89:1640–1648
39. Kameyama A, Yazawa K, Kaibara M, Ozono K, Kameyama M (1997) Run-down of the cardiac Ca²⁺ channel: characterization and restoration of channel activity by cytoplasmic factors. *J Neurophysiol* 433:547–556
40. Belles B, Malecot CO, Hescheler J, Trautwein W (1988) “Run-down” of the Ca current during long whole-cell recordings in guinea pig heart cells: role of phosphorylation and intracellular calcium. *Pflugers Arch* 411:353–360
41. Powers RK, Binder MD (2003) Persistent sodium and calcium currents in rat hypoglossal motoneurons. *J Neurophysiol* 89:615–624
42. Horn R, Marty A (1988) Muscarinic activation of ionic currents measured by a new whole-cell recording method. *J Gen Physiol* 92:145–159
43. Akaike N (1994) Glycine responses in rat CNS neurons studied with gramicidin perforated patch recording. *Jpn J Physiol* 44:S113–S118
44. McNaughton NC, Randall AD (1997) Electrophysiological properties of the human N-type Ca²⁺ channel: I. Channel gating in Ca²⁺, Ba²⁺ and Sr²⁺ containing solutions. *Neuropharmacology* 36:895–915
45. Scroggs RS, Fox AP (1992) Multiple Ca²⁺ currents elicited by action potential waveforms in acutely isolated adult rat dorsal root ganglion neurons. *J Neurosci* 12:1789–1801
46. McNaughton NC, Bleakman D, Randall AD (1998) Electrophysiological characterisation of the human N-type Ca²⁺ channel II: activation and inactivation by physiological patterns of activity. *Neuropharmacology* 37:67–81
47. Warre RC, McNaughton NC, Randall AD (2002) Differential discrimination of fast and slow synaptic waveforms by two low-voltage-activated calcium channels. *Neuroscience* 110:375–388
48. Sather W, Dieudonné S, MacDonald JF, Ascher P (1992) Activation and desensitization of N-methyl-D-aspartate receptors in nucleated outside-out patches from mouse neurones. *J Physiol* 450:643–672
49. Martina M, Jonas P (1997) Functional differences in Na⁺ channel gating between fast-spiking interneurones and principal neurones of rat hippocampus. *J Physiol* 505:593–603

Chapter 8

Combined Calcium Fluorescence Recording with Ionic Currents in Contractile Cells

Richard D. Rainbow

Abstract

Measurement of calcium (Ca^{2+}) fluorescence in conjunction with ionic currents is of particular importance in contractile cells, such as cardiac ventricular myocytes and vascular smooth muscle. The interplay between membrane potential and intracellular calcium ($[\text{Ca}^{2+}]_i$) is fundamental to the regulation of contractile function and cell signalling. Here the loading of cells either with an esterified fluorescence indicator prior to patch clamp recording, or dye loading via the patch pipette with “free” indicator, is described to allow simultaneous measurement of fluorescence and electrical signals.

Key words: Fluorescence, Ion currents, Dual measurements, Electrophysiology

1. Introduction

In any muscle cell type the depolarization of the cell membrane will generally lead to a contraction. Such depolarization generally causes an opening of voltage-gated channels including Na^+ and Ca^{2+} where in the influx of the latter leads to an increase in $[\text{Ca}^{2+}]_i$. The increase in $[\text{Ca}^{2+}]_i$ occurs as a consequence of the Ca^{2+} influx through the voltage-gated channel and corresponding Ca^{2+} -induced Ca^{2+} release (CICR) from the ryanodine receptors (RyR) on the sarcoplasmic reticulum (SR) store (1–4). The result of such an increase in $[\text{Ca}^{2+}]_i$ is to cause contractile protein activation triggering rapid contraction in skeletal and cardiac muscle, or a slower sustained contraction in smooth muscle.

For this chapter isolated cardiac ventricular myocytes and isolated portal vein smooth muscle cells will be the focus. Cardiac ventricular myocytes are large cells in both dimension (often more than $100 \mu\text{m} \times 10 \mu\text{m} \times 10 \mu\text{m}$) and in terms of the amount of membrane (as measured by capacitance often being greater than

100 pF) (see Note 1). The dimensions give both advantage and disadvantage in patch clamp recording; they are easy to use in terms of manipulating the patch electrode on to the cell, however more problematic in terms of actually clamping the membrane for fast changes in holding potential. For Ca^{2+} fluorescence recording they are rather nice to work with as they will load readily with esterified indicators and can be easily paced to contract by either electric field stimulation (EFS) or via the patch electrode. Ideally, when working with a contractile cell, a ratiometric dye would be used due to the fact that the cell changes shape considerably during each contraction. Fura-2 works very well in isolated ventricular myocytes as its K_d is approximately 220 nM which is well above the normal resting $[\text{Ca}^{2+}]_i$ which is around 100 nM. The $[\text{Ca}^{2+}]_i$ may rise up as high as 600 nM during the contractile cycle and so fluorescence changes can be readily resolved (3). In quiescent cells, i.e., not stimulated to contract in any way, a nonratiometric dye such as Fluo-3 or Fluo-4 can be used to resolve Ca^{2+} sparks in these cells.

Isolated portal vein smooth muscle cells are often used as model of vascular smooth muscle. These cells, as in nearly all smooth muscle cells, show a slower sustained elevation of $[\text{Ca}^{2+}]_i$ in response to depolarization or Gq-mediated vasoconstrictor activity. Again, ratiometric indicators such as Fura-2 are preferable as any morphological changes in the cell during the elevated $[\text{Ca}^{2+}]_i$ are compensated for by using the ratio of the 340 and 380 nm signals.

The image acquisition rate is perhaps less important for global Ca^{2+} measurements in smooth muscle cells due to the more prolonged changes in $[\text{Ca}^{2+}]_i$ seen in these cells; however, at least 10 frames per second is useful in order to get accurate information regarding the rates of change in $[\text{Ca}^{2+}]_i$. For ventricular myocytes where the changes in $[\text{Ca}^{2+}]_i$ are much more rapid and pronounced then a faster acquisition rate is required. Provided that the imaging system used is able to record 8–10 ratios per second (16–20 frames a second) then full Ca^{2+} transients can be resolved at a pacing rate of 1–2 Hz.

2. Materials

2.1. Cell Isolation; Ventricular Myocytes (5, 6)

1. Adult male Wistar rats were humanely killed in accordance with Home Office regulations (1986).
2. Hearts were rapidly excised, placed in a cold Ca^{2+} -free Tyrode solution (see Subheading 2.3) to arrest the contractions.
3. The excised heart was mounted via the aorta on a Langendorff cannula and the heart perfused in a retrograde fashion with warmed Ca^{2+} -free Tyrode to clear residual blood.

4. The solution was swapped for Ca^{2+} -free Tyrode solution containing an enzyme mix (Protease, collagenase and BSA) for 6–15 min (until the heart becomes soft and rod-shaped cells appear in the perfusate).
5. The solution was then exchanged for a 2 mM Ca^{2+} containing Tyrode (NT) for 3 min.
6. The digested heart was cut down into a flask containing NT and the tissue shaken in a 37 °C water bath to liberate the cells from the tissue.
7. After 5 min the NT containing cells was drained off of the residual tissue, sieved to remove residual tissue and washed. The remaining tissue was then resuspended in NT and the process repeated until the tissue had almost completely dispersed.
8. Cells were allowed to settle for 20 min, the supernatant removed, and then resuspended in NT. This wash was repeated. The isolation protocol typically yields 70–90 % rod-shaped myocytes that can be used 30 min to 36 h after isolation. Cells were stored at room temperature for 24–36 h.

**2.2. Cell Isolation;
Portal Vein
Myocytes (7)**

1. Adult male guinea pigs were humanely killed in accordance with UK Home Office Regulations 1986.
2. The hepatic portal vein was quickly excised and placed into a Krebs solution (see Subheading 2.3, item 2).
3. The vein was cut open and placed lumen side down and the adventitial layer removed.
4. The tissue was then turned over and cleaned, cut into strips, and incubated at 35 °C in isolation buffer (see Subheading 2.3, item 3) containing 1.64 mg/ml BSA (Sigma), 1.7 mg/ml Papain (Sigma), and 0.7 mg/ml dithioerythritol (Sigma) for 14–15 min.
5. The tissue was washed with BSA containing isolation buffer three times and then incubated for a further 12–14 min in BSA containing isolation buffer containing 2.2 mg/ml F-type blend collagenase (Sigma) and 1 mg/ml hyaluronidase (Sigma).
6. Digested tissue was then gently washed and the cells were released from the tissue by gentle trituration.
7. Cells were stored at 4 °C and used 30 min to 6 h after isolation.

2.3. Buffers

1. Ca^{2+} -free Tyrode solution contains: 135 mM NaCl, 6 mM KCl, 0.33 mM NaH_2PO_4 , 10 mM glucose, 10 mM HEPES, 1 mM MgCl_2 , pH 7.4 with NaOH. NT solution has 2 mM CaCl_2 added. Ventricular myocyte recordings are all done in NT solution.
2. Krebs solution for dissecting portal vein myocytes contains: 118.4 mM NaCl, 4.7 mM KCl, 25 mM NaHCO_3 , 1.13 mM

NaH_2PO_4 , 11.2 mM glucose, 1.13 mM MgCl_2 , 2.56 mM CaCl_2 , pH by bubbling solution.

3. Isolation buffer for portal vein myocytes contains: 55 mM NaCl, 6 mM KCl, 80 mM Na Glutamate, 0.2 mM EDTA, 10 mM glucose, 10 mM HEPES, 1 mM MgCl_2 , 0.1 mM CaCl_2 , pH 7.3 with NaOH.
4. Recording solution for Ca^{2+} currents in portal vein smooth muscle cells: 40 mM NaCl, 80 mM Na glutamate, 20 mM TEA, 30 mM glucose, 10 mM HEPES, 1.1 mM MgCl_2 , 3 mM CaCl_2 , pH 7.4 with NaOH.
5. Pipette solution for ventricular myocyte electrophysiology: 30 mM KOH, 110 mM KCl, 5 mM EGTA (see Note 2), 10 mM HEPES, 0.61 mM CaCl_2 , 1 mM MgCl_2 , 1 mM ATP, 0.1 mM ADP, 0.1 mM GTP, pH to 7.2 with HCl (see Notes 3 and 4).
6. Pipette solution for portal vein smooth muscle electrophysiology: 85 mM CsSO_4 , 20 mM CsCl , 10 mM sodium Pyruvate, 30 mM HEPES, 3 mM ATP, 2.5 mM (L)-Malic acid, 2.5 mM NaH_2PO_4 , 5 mM Phosphocreatine, 0.5 mM GTP, 1 mM MgCl_2 , pH to 7.2 with CsOH.

2.4. Reagents

1. Fura-2/Fura-2-AM (Invitrogen) is made up as a 1 mM stock in dimethylsulfoxide (DMSO).
2. Fluo-3(AM) and Fluo-4(AM) (Invitrogen) are both also made up as 1 mM DMSO stock.
3. All stocks should be maintained at -20°C and freeze–thawed a minimal number of times. Ideally stocks should be aliquoted to minimize freezing–thawing.

3. Methods

3.1. “AM”-Dye Loading of Isolated Ventricular, or Portal Vein, Myocytes

The protocol used by the author for loading of isolated ventricular (8) and portal vein (7) myocytes with the esterified dyes is identical and so will not be differentiated here. Additionally this protocol has also been used in isolated mesenteric and aortic arterial myocytes, colonic myocytes (9), and HEK293 cells. 1–5 μM of “AM”-dye have been used successfully by the author, in each new cell type a higher concentration was used as a first test and so this will be described below:

1. 200 μl of cell suspension is added to 795 μl of the recording solution to be used
2. The 1 mM “AM”-dye stock is defrosted and agitated to ensure that the dye is fully dissolved in the DMSO.

3. 5 µl of the stock is added to the 995 µl cell suspension to make a final volume of 1 ml.
4. The loading suspension is then wrapped in foil to ensure that the sample is as dark as possible and then placed on a rocking platform for 15 min (ventricular myocytes) or 25 min (smooth muscle cells).
5. The cell suspension is then placed for a further 10 min in the recording chamber (2 ml total volume) to allow the cells to settle and adhere to the glass coverslip lining the base of the system. Again, this is maintained as light-free as possible.
6. The perfusion system is then started where the perfusion flow acts to remove nonadhered cells and also serves to wash the cells removing residual dye and so reducing background fluorescence.
7. Once the perfusion is at the desired temperature or after a few minutes of perfusion if the experiments are to be conducted at room temperature, a cell is chosen and the appropriate configuration of the patch clamp technique is used (see Note 5).
 - (a) In most cases whole-cell recording is used. In this configuration a high resistance (gigaohm) seal is made between the tip of the electrode and the cells membrane, which is then ruptured to make the pipette solution and the cytoplasm a continuous solution. From this the membrane potential of the cell can be controlled to activate membrane currents (voltage clamp), or the membrane potential can be measured (current clamp).
8. Once the cell is clamped by the electrode in the appropriate patch configuration the fluorescence signals and acquisition rate can be adjusted appropriately for the type of recording being undertaken.
 - (a) For recording of Ca^{2+} -transients in response to electrical stimulation (e.g., action potentials in cardiac myocytes) then a fast acquisition rate is required. (see Note 6)
 - (b) For recording of global $[\text{Ca}^{2+}]_i$ changes over minutes then a sampling frequency of 1 ratio/image per second may be sufficient.

3.2. Patch Electrode Loading of Fluorescent Indicator

If the fluorescent indicator is loaded via the patch pipette rather than by esterified dye loading this can be advantageous in terms of amounts of indicator used and in terms of rate of experiments!

1. Around 200 µl of cell suspension is placed into the perfusion chamber for approximately 10 min to allow the cells to adhere to the glass coverslip.
2. The 1 mM frozen stock of free-acid indicator is defrosted, mixed thoroughly, and a volume added to the intracellular

recording solution (pipette solution) to give 5–10 μM final concentration of the indicator.

- The perfusion should be started and the protocol followed as outlined in Subheading 3.1, steps 6–8.

3.3. Examples of Electrophysiological Recordings Together with Changes in $[\text{Ca}^{2+}]_i$

3.3.1. Simultaneous Recording of Cardiac Action Potentials and Calcium Signals

Cardiac cells are constantly working in a cycle of contraction and relaxation in order to allow the heart to efficiently work to move blood around the body. This cycle can be examined at the single cell level using a combination of patch clamp electrophysiology, calcium imaging and edge detection. In the example recording (Fig. 1.) the cell under investigation has been patch electrode loaded with dye so that corresponding changes in $[\text{Ca}^{2+}]_i$ with the stimulation of action potential can be measured. Additionally the edges of the cell can be measured to allow the contractile function of the cell to be determined too.

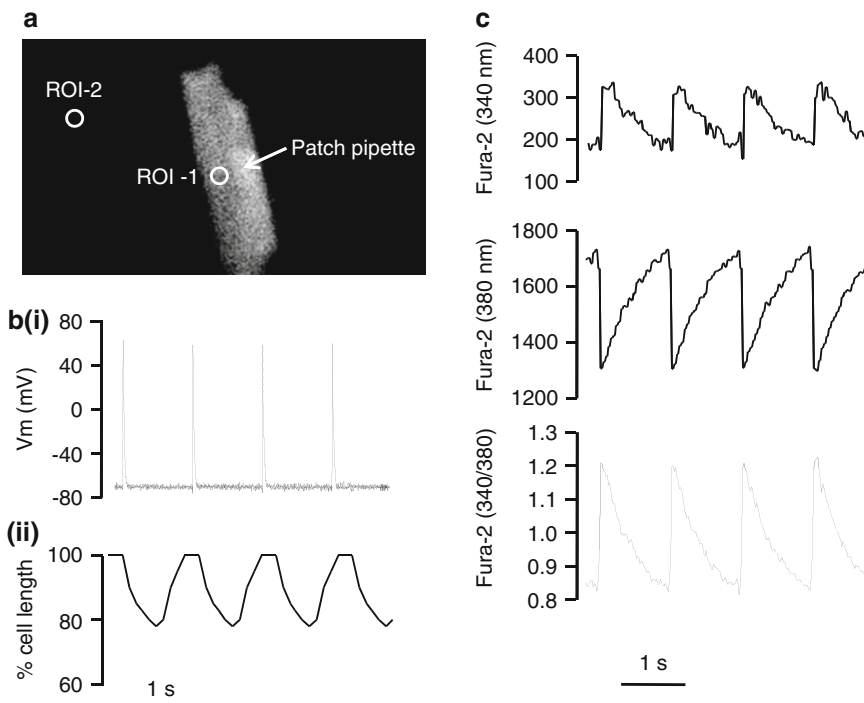


Fig. 1. Simultaneous action potential, calcium fluorescence and contractile function measurement from an rat isolated ventricular myocyte. Electrophysiology recorded using an Axopatch 200B amplifier, digitized using an nation instruments interface, fluorescence was excited using a Cairn monochromator and recorded using an Andor iXon camera. Data recorded and analyzed using Winfluor software developed by Dr. John Dempster (University of Strathclyde, UK). (a) 380 nm fluorescent image of the ventricular myocyte. Fluorescent indicator (Fura-2) introduced via the patch pipette. Circle “ROI-1” indicates the region that the fluorescence measurements were made. This region was analyzed as it moves the least during contraction. (b) (1) Action potentials recorded under current-clamp conditions. Action potentials were stimulated at a frequency of 1 Hz via the patch pipette. (2) Video-edge detection recording of cardiomyocyte length. (c) Fluorescence recording from Fura-2 excited at 340 nm, 380 nm and the 340:380 ratio recorded at ROI-1 and background subtracted using ROI-2.

1. Rat ventricular myocytes are isolated as outlined
2. Myocytes are pipette loaded with free-acid Fura-2 rather than ester loaded.
3. Recordings are made in the whole-cell current-clamp mode in order to measure action potentials rather than membrane currents (see Note 7).
4. Myocytes are stimulated to contract by a 5 ms depolarizing pulse via the patch pipette at a frequency of 1 Hz (somewhat slower than the native rat heart rate).
5. Data acquisition rate is around 20 ratio images per second (40 frames per second)
6. The action potential and calcium fluorescence data are recorded simultaneously using the WinFluor software (Dr. John Dempster, University of Strathclyde), and analyzed offline. Figure 1 shows an example recording in which action potential, calcium fluorescence and contractile function data have been measured in the same cell.

3.3.2. Simultaneous Recording of Depolarizing Currents and $[Ca^{2+}]_i$

Recording ionic currents on the plasma membrane of muscle cells does not significantly differ from the description of recording the action potential outlined in Subheading 3.3.1, and is similar in both cardiac and vascular smooth muscle cell types.

1. Cells are isolated as outlined in Subheadings 2.1 and 2.2.
2. In the example shown in Fig. 2 ventricular myocytes are loaded with the cell permeant Fura-2-AM form of the dye.
3. Electrophysiological recordings are made in voltage-clamp mode. The membrane potential is clamped at -70 mV and a depolarizing pulse to 0 mV applied.
4. Data acquisition rate for the ventricular myocyte recording is around 20 ratio images a second (40 frames per second).
5. Figure 2 shows the fast inward currents recorded from an isolated ventricular myocyte depolarized to 0 mV for 200 ms and the corresponding increase in $[Ca^{2+}]_i$.

3.3.3. Recording of Ca^{2+} -Activated Ionic Currents

In vascular smooth muscle cells two main types of calcium-activated channels exist: the calcium-activated chloride current (Cl_{Ca}) and the calcium-activated potassium channel (K_{Ca}). These channels are involved in opposing activities in vascular smooth muscle where Cl_{Ca} currents generally depolarize whilst K_{Ca} cause a hyperpolarization. The spontaneous activity of RyR releasing Ca^{2+} from the sarcoplasmic reticulum (SR) to cause elevations in $[Ca^{2+}]_i$ influences membrane potential of these cells by activating these Ca^{2+} -sensing currents. Spontaneous transient outward currents (STIC) and spontaneous transient inward currents (STOC) have been demonstrated to be due to Ca^{2+} -induced activation of Cl_{Ca} and BK_{Ca} , respectively.

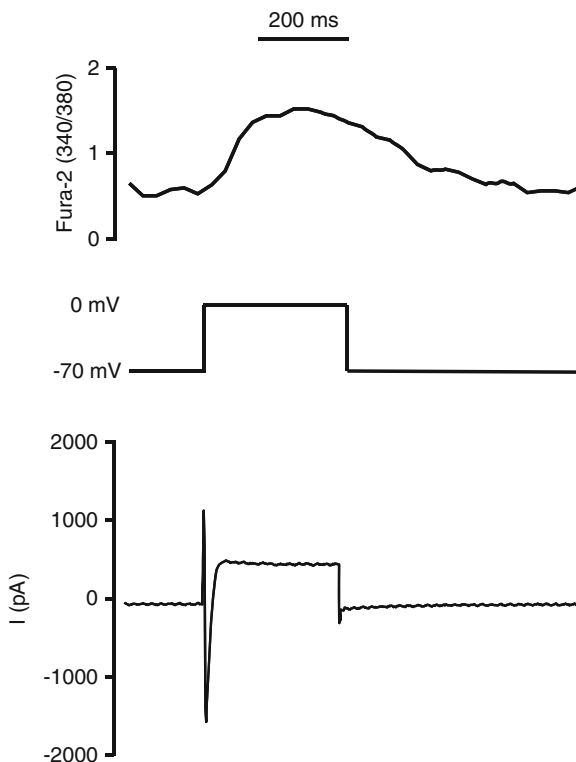


Fig. 2. Simultaneous measurement of ionic currents and $[Ca^{2+}]$, from a rat isolated ventricular myocyte. As indicated the holding potential was stepped from -70 mV to 0 mV for 300 ms during which a large inward current was seen. Following this inward current a substantial change in $[Ca^{2+}]$, occurred as indicated by the change in the $340/380$ ratio which recovered after the membrane potential was stepped back to -70 mV . The outward current seen during the depolarization is most likely to be due to voltage-gated potassium channels as there was no TEA or Cs to block their activity.

Both of the channel types can be readily recorded in vascular smooth muscle cells (neither of which are present in cardiac muscle). The K_{Ca} current can be activated by depolarizing to anything more positive than about -40 mV and can be further enhanced with caffeine to stimulate spark activity at the SR. Cl_{Ca} currents can be distinguished from BK_{Ca} by holding the membrane potential at more negative, for example -70 mV . At this potential the Cl driving force is quite large as E_{Cl} is around -20 mV ; however, BK_{Ca} channels, due to their voltage and Ca^{2+} dependence, are not active. In this example recording the SR Ca^{2+} release will be triggered by using a caged- IP_3 which is released by flash photolysis (7).

1. Portal vein smooth muscle cells are isolated as described (7) (Subheading 2.2).
2. Fluo-4-AM (see Note 8) is used to load the cells as described (Subheading 3.1) with the addition of $10\text{ }\mu\text{M}$ wortmannin to limit contraction (7) (see Note 9).

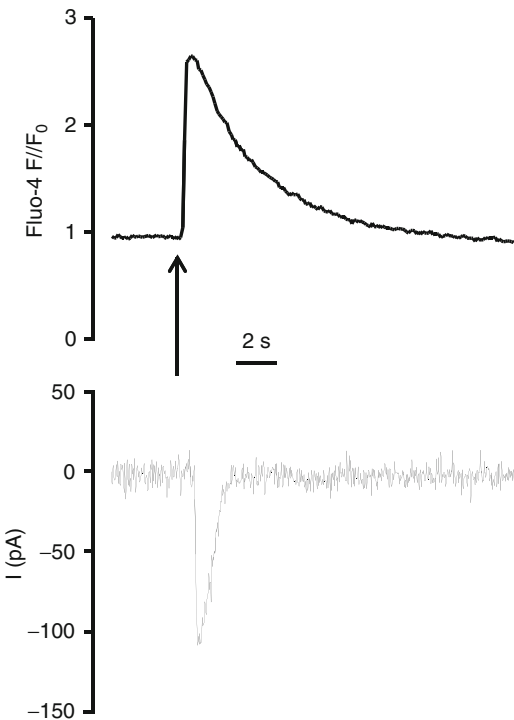


Fig. 3. Simultaneous measurement of Cl_{ca} currents and $[\text{Ca}^{2+}]$ from an isolated portal vein myocyte. The membrane potential of the isolated cell was voltage-clamped at -70 mV and the cell loaded with caged- IP_3 via the patch pipette. Free IP_3 was liberated by photolysis with UV light (*indicated by the arrow*) and the corresponding $[\text{Ca}^{2+}]_i$ change and Cl_{ca} current recorded. In this example trace the recording was carried out at room temperature. Recorded in Prof. John McCarron's laboratory, University of Strathclyde.

3. Caged- IP_3 ($10 \mu\text{M}$) is added to the pipette solution (Subheading 2.3, item 6).
4. The whole-cell recording technique is achieved and the membrane potential clamped at -70 mV .
5. 5–10 min should be given to dialyze the cell with the caged- IP_3 .
6. Photolysing the caged- IP_3 with a 5 ms flash of UV light should release enough IP_3 to see a substantial inward chloride current (see Fig. 3).

4. Notes

1. The large size of ventricular cells (membrane capacitance) makes them rather difficult to easily voltage clamp. The membrane of the ventricular myocytes also traverses the cells in the t-tubule network so hugely increasing the “surface” membrane

that must be charged and discharged during each voltage step. This is not an issue for current-clamp recordings of action potentials, but is a limitation when doing voltage-clamp experiments. For potassium currents this isn't so much of a problem as the current measurements can be taken from the end of the voltage pulse where you can be sure that the membrane is at the potential expected. This is more problematic for fast inward currents such as Na^+ and Ca^{2+} currents. Some amplifiers (such as the Axon Axopatch 200B) partially get around this by having a 0.1β gain function; however, care should be taken when measuring such fast currents.

2. EGTA can be difficult to get into solution. Use the 30 mM KOH to dissolve the EGTA then add the rest of the constituents.
3. The pipette solution will be slightly alkali and so use HCl to pH to 7.2.
4. If pipette loading with Ca^{2+} indicators consider leaving out the EGTA. Too much Ca^{2+} buffering may limit the ventricular myocyte contractions. However, if you want to completely prevent contractions of the ventricular cell you may choose to increase the EGTA to 10 mM, or increase the indicator concentration.
5. Typically electrodes of 3–6 $M\Omega$ are suitable for patching both ventricular myocytes and vascular smooth muscle cells. Sealing onto a ventricular myocyte is usually easy if the cells are of reasonable quality, often no suction on the pipette is required to achieve a gigaohm seal. No positive pressure should be put onto the pipette (see Note 7) and the electrode should be placed near the center of the cell. Ventricular and smooth muscle myocytes tend to contract towards the center of the cell so this is the region that moves the least during contraction and so is the most stable to patch. The electrode should be slowly moved down on to the cell and when the electrode touches the cell the pipette resistance will at least double (e.g., 5 $M\Omega$ to $>10 M\Omega$). At this point, if the seal isn't already forming on its own, a very gentle suction can be applied to the cell and the holding potential should be changed, as soon as the electrode resistance is over 100 $M\Omega$, from 0 mV to -70 mV. In eight out of ten ventricular myocytes this will give a gigaohm seal within 5–10 s. Once the leak current is less than 25 pA, further suction can be applied to achieve the whole-cell configuration. Vascular smooth muscle cells can be patch clamped in the same way as outlined above; however, their rate of sealing is significantly slower, always requires some gentle suction, and takes more patience!
6. For a camera based imaging system the rate limiting step will be the amount of information that the camera is trying to process.

The acquisition rate can be improved by “pixel binning” so instead of recording the information for every single pixel merging data with neighboring pixels. For example 2×2 binning will merge the data from 4 pixels, 3×3 from 9 pixels etc. This will increase the acquisition rate, but will also decrease the fidelity of the image. Alternatively using a smaller region of the camera chip may be advantageous. For example, a camera with a 1028×1028 chip will acquire images at a faster rate if only 512×512 is selected in the software, combined with pixel binning this rate will be further increased. Additionally, keeping the exposure time to a minimum will increase the rate of acquisition for most imaging systems.

7. Microelectrode resistances between 3 and $5\text{ M}\Omega$ should be used where possible to facilitate diffusion of fluorescent indicators, or other large cell-impermeant molecules, into the cytoplasm. Additionally, positive pressure should not be applied to the pipette when entering the solution. Firstly, this will send dye from the pipette into the bath and occasionally this can increase the background fluorescence. Secondly, with contractile cells such as ventricular myocytes and smooth muscle cells if the pipette solution is K^+ based then spraying the cells with this solution will increase extracellular K^+ around the cell which will change E_{K} and so may depolarize the cell causing contraction. Finally, ATP in the patch pipette may also trigger contraction in vascular smooth muscle due to stimulation of P_2X and P_2Y receptors.
8. Fluo-3 (excitation at around 488 nm) rather than Fura-2 (dual excitation at 340 and 380 nM) is used in this experiment as the photolysis of Caged- IP_3 uses UV light.
9. Wortmannin is used in this experiment to disrupt contraction of the vascular smooth muscle (one such action is to inhibit myosin light chain kinase); however, it should be used with caution in cell signalling type experiments as it has effects on Phosphoinositide-3-kinases (PI3Ks) and other PI3K related enzymes such as mTOR, DNA-PK, some phosphatidylinositol 4-kinases and mitogen-activated protein kinase (MAPK) at high concentrations.

Acknowledgments

The author would like to thank Sean Brennan (University of Manchester) for his help with the recording shown in Fig. 1. The author would also like to thank Prof. John McCarron (University of Strathclyde) for allowing the recording of the Cl_{Ca} current shown in Fig. 3 to be used in this chapter.

References

1. Chalmers S et al (2007) Ion channels in smooth muscle: regulation by the sarcoplasmic reticulum and mitochondria. *Cell Calcium* 42:447–466
2. Kentish JC et al (1990) Calcium release from cardiac sarcoplasmic reticulum induced by photorelease of calcium or ins(1,4,5)p3. *Am J Physiol* 258:H610–H615
3. Bers DM (2002) Cardiac excitation-contraction coupling. *Nature* 415:198–205
4. Sanders KM (2008) Regulation of smooth muscle excitation and contraction. *Neurogastroenterol Motil* 20(Suppl 1):39–53
5. Lawrence C, Rodrigo GC (1999) A Na^+ -activated K^+ current (IK_{Na}) is present in guinea-pig but not rat ventricular myocytes. *Pflugers Arch* 437:831–838
6. Rainbow RD et al (2005) Reduced effectiveness of hmr 1098 in blocking cardiac sarcolemmal K_{ATP} channels during metabolic stress. *J Mol Cell Cardiol* 39:637–646
7. Rainbow RD, Macmillan D, McCarron JG (2009) The sarcoplasmic reticulum Ca^{2+} store arrangement in vascular smooth muscle. *Cell Calcium* 46:313–322
8. Rainbow RD et al (2004) SUR2A C-terminal fragments reduce K_{ATP} currents and ischaemic tolerance of rat cardiac myocytes. *J Physiol* 557:785–794
9. McCarron JG, Olson ML (2008) A single luminally continuous sarcoplasmic reticulum with apparently separate Ca^{2+} stores in smooth muscle. *J Biol Chem* 283:7206–7218

Part IV

Measurement of Ins(1,4,5)P₃ and Ca²⁺ Release from Intracellular Stores

Chapter 9

Measurement of Phospholipase C by Monitoring Inositol Phosphates Using [³H]Inositol Labeling Protocols in Permeabilized Cells

Alison Skippen, Philip Swigart, and Shamshad Cockcroft

Abstract

Data on the production of inositol phosphates is a useful complement to measurements of intracellular Ca^{2+} . The basic principle is labeling of the inositol lipids by growing the appropriate cell line in culture in the presence of [³H]inositol for 2–3 days to reach labeling equilibrium. Lithium ions at 10 mM inhibits the degradation of inositol phosphates to free inositol and is used to trap the inositol in the inositol polyphosphate forms. Inositol phosphates can be separated with ease from free inositol by using anion exchange chromatography. A method capable of easily processing approximately 40–60 samples in a single day is presented.

Key words: Phospholipase C, [³H]Inositol phosphates, Permeabilized cells

1. Introduction

Hormones, neurotransmitters, chemoattractants, and growth factors all elicit intracellular responses, on binding to cell surface receptors, by activating inositol phospholipid-specific phospholipase C (PLC). Activated PLC catalyzes the hydrolysis of phosphatidylinositol bisphosphate (PIP_2), a minor membrane phospholipid, to form two second messengers, diacylglycerol (DAG) and inositol (1,4,5)trisphosphate [$\text{Ins}(1,4,5)\text{P}_3$]. DAG is a direct activator of protein kinase C isozymes, and $\text{Ins}(1,4,5)\text{P}_3$ mobilizes intracellular Ca^{2+} . G protein-coupled receptors couple to the PLC- β family via G proteins, and tyrosine kinase receptors activate PLC γ isozymes (1, 2). Regardless of the PLC isozyme activated, the product is invariably $\text{Ins}(1,4,5)\text{P}_3$.

To monitor the activation of PLC enzymes, the authors have established, in their laboratory, methods of using permeabilized cells.

Permeabilized cells are useful for examining the regulatory components that are essential for $\text{Ins}(1,4,5)\text{P}_3$ production. Calcium levels can be rigorously controlled as well as appropriate regulatory proteins such as phosphatidylinositol transfer protein (PITP) (3–5). Permeabilized cells can be used under conditions in which the cytosolic proteins are still present (“acutely permeabilized”) and in which the cytosolic proteins have been allowed to leak out of cells. The loss of cytosolic proteins leads to the phenomenon of “run-down” in which the ability of GTP γ S or a receptor agonist to stimulate PLC is diminished. The response can be “reconstituted” by addition of exogenously added cytosolic proteins (3). A major reconstituting factor in the cytosol is PITP (3–6).

$\text{Ins}(1,4,5)\text{P}_3$ is rapidly metabolized by phosphatases, and therefore the authors assay for the production of inositol (poly)phosphates. The stimulus for PLC activation can be a direct activator of G proteins, e.g., GTP γ S or an agonist that interacts with an appropriate cell-surface receptor (3–6). The protocols can be applied to most cell lines. Commonly used cell lines in the authors’ laboratory are HL60 cells (both undifferentiated and differentiated) and RBL-2H3, but other cell lines have also been used (3–6).

The basic principle is the labeling of the inositol lipids by growing the appropriate cell line in culture in the presence of [^3H]inositol for 2–3 days. This ensures that the inositol-containing lipids are prelabeled to near equilibrium prior to the experiment. Lithium ions at 10 mM inhibits the degradation of inositol phosphates to free inositol and is used to trap the inositol in the inositol polyphosphate forms. Inositol phosphates can be separated with ease from free inositol by using anion exchange chromatography. Approximately 40–60 samples can be easily processed in a single day.

2. Materials

1. Mammalian cells: HL60 available from American Type Culture Collection (ATCC), Rockville, MD.
2. [^3H]inositol is the myo [1,2- ^3H]inositol in sterile water and is obtained from American Radiolabeled Chemicals, Inc, (product code ART 0261A) (<http://www.arc-inc.com>).
3. Growth medium: RPMI-1640 available from Sigma-Aldrich (cat. no. R-0883).
 - (a) The growth medium can be stored at 4°C and supplemented with 12.5% heat-inactivated fetal calf serum (FCS) (see Note 1).
 - (b) 12 ml penicillin/streptomycin (Sigma P-0906) and 25 ml glutamine solution (Sigma G-7513)/L when the medium is to be used (see Note 2).

- (c) The supplemented medium can be stored at 4°C for 1–2 weeks.
4. Labeling medium: Medium 199 (M199) is available from Sigma-Aldrich (M-2154) (see Notes 3 and 4).
 - (a) The M199 is supplemented with 12 ml of penicillin/streptomycin and 25 ml of glutamine/L.
 - (b) Because FCS is excluded, the labeling medium is supplemented with either
 - Insulin (Sigma I-5500) (5 µg/ml final) and transferrin (Sigma T-2252) (5 µg/ml final) as growth factors at the time of labeling or
 - 12.5% heat-inactivated dialyzed FCS (Invitrogen 26400-036).
 5. PIPES buffer: 20 mM PIPES, 137 mM NaCl, and 3 mM KCl, pH 6.8.
 - (a) Made from stock solutions, 1 M PIPES:
 - Dissolve 302.4 g of PIPES (Sigma P6757) in 600 ml of H₂O and adjust the pH to approximately 6.0 with concentrated NaOH (see Note 5).
 - When the PIPES is fully dissolved, adjust to pH 6.8 and make up the volume to 1 L. The PIPES can be aliquoted and stored at –20°C for several months.
 6. 20× NaCl/KCl solution: Dissolve 159 g of NaCl and 4 g of KCl in 1 L of H₂O and store at 4°C, stable for months.
 - (a) For 100 ml PIPES buffer, take 5 ml of 20× NaCl/KCl stock plus 2 ml of 1 M PIPES stock to 100 ml with H₂O checking that the pH is still 6.8.
 7. Permeabilization buffer: PIPES buffer supplemented with 1 mg/ml glucose and 1 mg/ml bovine serum albumin (BSA).
 8. Streptolysin O (SLO) is obtained from Sigma (product no. S-140).
 - (a) Each bottle contains 40 IU equivalents and is dissolved in 2 ml of H₂O to make a stock solution of 20 IU/ml.
 - (b) The stock solution is stored at 4°C for 1–2 weeks and is used at 0.4–0.6 IU/ml in experiments (see Note 6).
 9. 0.1 M MgATP stock solution: Dissolve 605 mg of disodium trihydrate ATP (Roche, Lewes, East Sussex, UK, product no. 127531) in a 10-ml solution containing 2 ml of 1 M Tris and 1 ml of 1 M MgCl₂ (see Note 7). The solution is stable at –20°C for 1–2 years at neutral pH.
 10. Calcium buffers: Required stock solutions are as follows:
 - (a) 100 mM EGTA prepared in 20 mM PIPES, 137 mM NaCl, 3 mM KCl, pH 6.8.

Table 1
Preparation of Ca²⁺ buffer stock solution

pCa	Vol. (ml) Ca ²⁺ .EGTA	Vol. (ml) EGTA
7 (100 nM)	0.996	7.004
6 (1 μM)	4.698	3.302

- (b) 100 mM Ca²⁺.EGTA (100 mM EGTA, 100 mM CaCl₂ [see Note 8]) prepared in 20 mM PIPES, 137 mM NaCl, 3 mM KCl, pH 6.8. These stocks can be stored at -20°C for several months.
- (c) To prepare Ca²⁺ buffer (pCa 7 and pCa 6) stock solutions, combine stock solutions of 100 mM Ca²⁺.EGTA and 100 mM EGTA to achieve the desired free Ca²⁺ (see Table 1 and Note 9).

These quantities are calculated for a final (EGTA)_{total} = 3 mM, (MgCl₂) = 2 mM, and pH 6.8. Eight milliliters of each buffer stock solution are prepared by mixing the Ca²⁺.EGTA and EGTA solutions (100 mM) in the proportions indicated in Table 1. For use the buffer stocks (100 mM) (which do not contain Mg) are diluted to 3 mM (EGTA)_{total}.

11. Dimethyl sulfoxide (DMSO) from Sigma (D-5879).
12. 60 mM Dibutyryl cAMP (DbcAMP) (Sigma (D-0627)):
 - (a) Dissolve 100 mg of the powder in 3.08 ml of DMSO.
 - (b) The DbcAMP is used at a final concentration of 300 μM (1 ml stock to 200 ml cells) to differentiate HL60 cells.
13. 1 M LiCl stored at -20°C for several months.
14. Preparation of Dowex 1-X8 anion exchange resin (see Note 10):
 - (a) Place 100 g of Dowex resin in a beaker.
 - (b) Add 400 ml of 1 M NaOH and stir with a glass rod.
 - (c) Allow the resin to settle (1–2 h).
 - (d) Carefully decant the NaOH solution, add 400 ml of 1 M formic acid, and stir with a glass rod.
 - (e) Allow the resin to settle and decant the formic acid.
 - (f) Wash the resin five times with 400 ml of H₂O. The resin can be left as a 50% slurry in H₂O at 4°C. One ml of the slurry is used per column and either Pasteur pipets or purchased columns (Poly-Prep columns, product no. 731-1550 Bio-Rad, Hercules, CA) can be used (see Note 11).

3. Methods

3.1. Maintenance of HL60 Cell Cultures

1. Dilute HL60 cells to between 0.3 and 0.5×10^6 cells/ml. Generally, use 50 ml in 75-cm² tissue culture flasks with a 5% CO₂ atmosphere.
2. Grow the cells to confluence (usually takes 2–3 days) and dilute to between 0.3 and 0.5×10^6 cells again (see Note 12).
3. Use one flask to label, keeping one flask as a seed culture.

3.2. Differentiation of HL60 Cells (See Note 13)

1. Differentiate a confluent flask of cells in the presence of 300 μM DbcAMP; the cells will be differentiated by 36–40 h.
2. Cells can be prelabeled with [³H]inositol, by transferring them to M199 and labeling as described in Subheading 3.3 with the addition of the DbcAMP (1 ml of stock DbcAMP to 200 ml of cells).

3.3. Preparation of [³H]Inositol-Labeled HL60 Cells (See Note 14)

1. HL60 cells can be labeled with [³H]inositol with one of the two methods:
 - (a) Procedure 1
 - Pellet 50 ml of confluent (2×10^6 cells/ml) cells by centrifugation at $1,000 \times g$ for 5 min at room temperature (Heraeus Megafuge 1.0, Brentwood, Essex, UK).
 - Resuspend the cells in 10 ml of M199 without FCS but with glutamine and penicillin/streptomycin.
 - Add the 10 ml of cells to 40 ml of M199 without FCS containing glutamine and penicillin/streptomycin, to which has been added 0.25 ml of a 1 mg/ml sterile solution of insulin and 0.25 ml of a 1 mg/ml sterile solution of transferrin (final concentrations of 5 μg/ml each).
 - Add 50 μCi (1 μCi/ml final) [³H]inositol.
 - Grow cells for 48 h.
 - 50-ml cells are sufficient for 50 incubations.
 - (b) Procedure 2
 - Pellet 20 ml of confluent (2×10^6 cells/ml) cells by centrifugation at $1,000 \times g$ for 5 min at room temperature (Heraeus Megafuge 1.0, Brentwood, Essex, UK) (see Note 15).
 - Resuspend the cells in 10 ml of M199 containing glutamine and penicillin/streptomycin with 12.5% heat-inactivated dialyzed FCS.
 - Add the 10 ml of cells to 40 ml of M199 with 12.5% dialyzed FCS containing glutamine and penicillin/streptomycin.
 - Add 50 μCi (1 μCi/ml final) [³H]inositol.

- Grow cells for 48 h.
- 50-ml cells are sufficient for 50 incubations.

**3.4. PLC Activity
in “Acutely
Permeabilized”
HL60 Cells**

1. Centrifuge 50 ml of [³H]inositol-labeled cells at $1,000 \times g$ for 5 min at room temperature.
2. Discard the supernatant, which contains most of the radioactivity, and gently resuspend the cells in 40 ml of permeabilization buffer (PIPES buffer plus 1 mg/ml of glucose and 1 mg/ml of BSA).
3. Pellet the cells and wash once more with the permeabilization buffer.
4. After the final centrifugation, resuspend the cells in 2–3 ml of the permeabilization buffer.
5. Equilibrate the washed radiolabeled cells at 37°C for 10–25 min.
6. In a 1.5-ml Eppendorf tube (see Note 16), add 50 µL of labeled cells to the equivalent volume of permeabilization buffer supplemented with the following:
 - (a) SLO (0.4 IU/ml final).
 - (b) MgATP (1 mM final).
 - (c) MgCl₂ (2 mM final).
 - (d) Ca²⁺ buffered with 3 mM EGTA (pCa6).
 - (e) LiCl (10 mM final) (see Note 17).
 - (f) GTPγS (10 µM final).
7. Incubate the mixture at 37°C for 20 min.
8. Place the reactions in an ice bath and terminate the reactions with one of the two methods:
 - (a) Procedure 1
 - Quench the assay with 500 µL of (chloroform:methanol [1:1 by vol/vol]) and vortex.
 - Add 250 µL of H₂O and vortex.
 - Centrifuge the samples for 5 min at $1,000 \times g$ at 4°C (see Note 18).
 - Use 400 µL of the aqueous phase for inositol phosphate analysis.
 - (b) Alternative procedure:
 - Quench the assay with 500 µL of ice-cold saline (0.9% NaCl).
 - Centrifuge at $2,000 \times g$ to sediment the permeabilized cells.
 - Use 400 µL of the supernatant for inositol phosphate analysis.

**3.5. Separation
of Inositol Phosphates
by Dowex
(See Note 19)**

1. Load the 400- μ L sample containing the radiolabeled inositol phosphates onto the prepared Dowex columns.
2. Allow the sample to gravity flow through the column.
3. Wash the columns with 6 ml of H₂O (see Note 20).
4. Wash the columns with 6 ml of 5 mM sodium tetraborate/60 mM sodium formate (see Note 21).
5. Elute total inositol phosphate with 3 ml of 1 M ammonium formate/0.1 M formic acid directly into scintillation vials.
6. Alternatively, if inositol monophosphate (IP1), inositol bisphosphate (IP2), and inositol trisphosphate (IP3) are to be separated, elute stepwise into scintillation vials:
 - (a) 3 ml of 0.2 M ammonium formate/0.1 M formic acid (IP1).
 - (b) 3 ml of 0.4 M ammonium formate/0.1 M formic acid (IP2).
 - (c) 3 ml of 1 M ammonium formate/0.1 M formic acid (IP3 and inositol tetrakisphosphate [IP4] if present in the sample) (see Fig. 1a, See Note 22).
7. Add scintillant and measure radioactivity (see Note 23).
8. Regenerate the columns by washing with 6 ml of 2 M ammonium formate/0.1 M formic acid followed by extensive washing with H₂O (10–15 ml) (see Note 24).

**3.6. Data Handling
(See Note 25)**

The dpm in inositol phosphates provides the level of PLC activity in individual experiments. The amount of dpm found in inositol phosphates is ultimately dependent on the amount of label incorporated by the cells, which can vary from experiment to experiment. The increase in inositol phosphates can also be expressed as a function of the total radioactivity (dpm) incorporated into the inositol lipids. This allows results to be calculated as a percentage of the total lipids.

**3.7. Determination
of Radioactivity
Incorporated into
the Inositol Lipids**

1. Carefully remove the total lipid chloroform extract obtained from the first procedure and transfer it to a clean scintillation vial.
2. Allow the chloroform to evaporate by leaving the vials open in a fume hood overnight.
3. Add 500 μ L of methanol to the dried lipids followed by 2 ml of scintillation cocktail and measure dpm.

**3.8. Establishing
Conditions for
Rundown of PLC
Activity**

1. Use 4.5 ml of washed [³H]inositol-labeled cells in the permeabilization buffer.
2. Add cocktail (0.5 ml) of SLO (0.4 IU/ml final), MgATP (1 mM final), and Ca²⁺, pCa 7 (100 nM buffered with 100 mM EGTA final) to the cells.

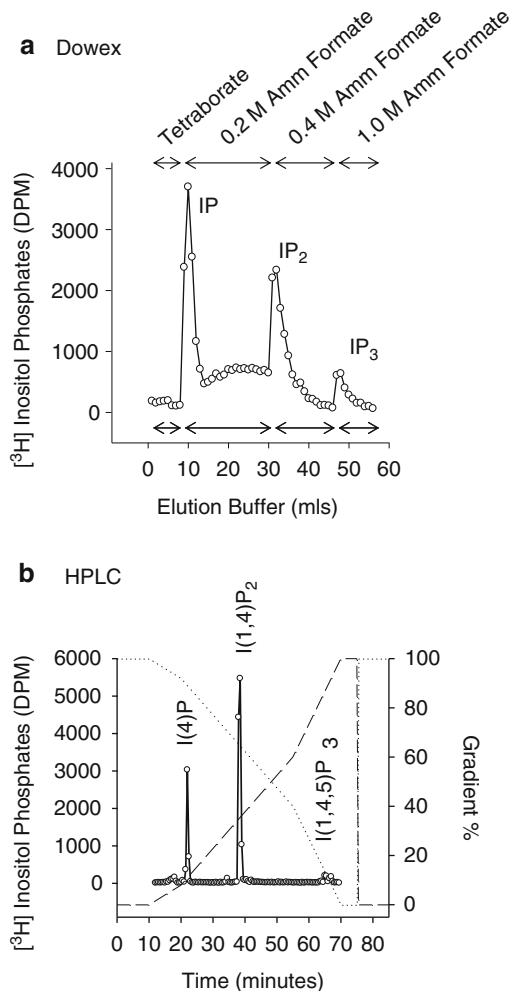


Fig. 1. Comparison of two identical samples analyzed on (a) Dowex anion exchange resin and (b) anion exchange HPLC. HL60 cells were radiolabeled for 48 h with [^3H]inositol and were permeabilized for 10 min with SLO as described in Subheading 3.9. Cells were washed and incubated at 37°C with PI $\text{T}\alpha$ (5 μM) and GTP γS (10 μM). After 20 min the samples were quenched and the aqueous phase containing the inositol phosphates was analyzed by (a) Dowex or (b) HPLC. In (a) the sample was loaded onto the Dowex anion exchange resin and the inositol phosphates were eluted in 1 ml fractions using the solutions indicated. In (b) the inositol phosphates were analyzed on a Partisil 10 SAX column using a gradient of 1.4 M monobasic ammonium phosphate buffer adjusted to pH 3.7 with orthophosphoric acid, and fractions were collected every 0.5 min (see Note 26).

3. At timed intervals, remove $4 \times 50 \mu\text{L}$ aliquots of cells and transfer to duplicate assay tubes containing 50 μL of a cocktail containing Ca^{2+} , pCa 6 (1 μM buffered with 3 mM EGTA final), LiCl (10 mM final), MgCl_2 (2 mM final) \pm GTP γS (10 μM final).
4. Incubate the samples at 37°C for 20 min.
5. Quench the reaction using one of the two methods previously described in Subheading 3.4 and analyze [^3H]inositol phosphates as described in Subheading 3.5 (see Note 27).

3.9. Reconstitution of G Protein-Stimulated PLC by Cytosolic Factors in Rundown Cells

- Incubate 4.5 ml of washed [³H]inositol-labeled HL60 cells in permeabilization buffer with 0.5 ml of cocktail containing SLO (0.4 IU/ml final), MgATP (1 mM final), and Ca²⁺, pCa 7 (100 nM buffered with 3 mM EGTA final) for 10 min (see Notes 28 and 29).
- After permeabilization, dilute the cells to 35 ml with ice-cold permeabilization buffer.
- Centrifuge the cells at 2,000×*g* for 5 min to pellet the cells (see Note 30).
- Resuspend the cell pellet in 2× assay buffer (permeabilization buffer supplemented with Ca²⁺, pCa 6 with 6 mM EGTA final), LiCl (20 mM final), MgATP (4 mM final), and MgCl₂ (4 mM final) (see Note 31).
- Prepare tubes in advance that contain 25 µL of cytosol, or other reconstituting factors (e.g., PIPIP)±GTPγS at 20 µM.
- Transfer 25 µL of permeabilized cells to assay tubes on ice (see Note 32).
- Transfer the assay tubes to a 37°C water bath and incubate the samples for 20 min.
- Quench the assay as described in Subheading 3.4, step 8, and Subheading 3.5 and assay for inositol phosphates.

3.10. Assaying for PLC Activity Using a Receptor-Directed Agonist in Differentiated HL60 Cells That Express the FMetLeuPhe Receptor

- Incubate 4 ml of washed differentiated [³H]inositol-labeled HL60 cells in permeabilization buffer with 1 ml of cocktail containing SLO (0.4 IU/ml final), MgATP (1 mM final), and Ca²⁺, pCa 7 (100 nM buffered with 3 mM EGTA final) for 10 min.
- After permeabilization, dilute the cells to 35 ml with ice-cold permeabilization buffer.
- Centrifuge the cells at 2,000×*g* for 5 min to pellet the cells.
- Resuspend the cell pellet in 2× assay buffer (permeabilization buffer supplemented with pCa 6 [6 mM EGTA], LiCl [20 mM], MgATP [4 mM], and MgCl₂ [4 mM]).
- Prepare tubes in advance that contain 25 µL of cytosol, or other reconstituting factors±FMLP at 1 µM final and GTP at 100 µM final.
- Transfer 25 µL of permeabilized cells per assay tube on ice.
- Transfer the assay tubes to a 37°C water bath and incubate the samples for 20 min.
- Quench the assay as described in Subheading 3.4, step 8, and Subheading 3.5 and assay for inositol phosphates (see Note 33).

4. Notes

1. FCS from Sera Laboratories International Ltd (EU-000-F): Heat inactivate before use by immersing a thawed bottle in a 56°C bath for 1 h.
2. Batches of RPMI-1640 can be stored with FCS added; however, the glutamine and penicillin/streptomycin must be added only as each bottle is needed.
3. Because RPMI-1640 medium contains relatively high levels of inositol, cells are labeled in M199. Concentration of inositol in different media are as follows: M199, 0.05 mg/ml; RPMI-1640, 35 mg/ml; and DMEM, 7.2 mg/ml.
4. FCS is also excluded owing to high levels of inositol.
5. The solution will start out at approximately pH 2.5–3.0 and will fluctuate as NaOH is added and the PIPES dissolves. Generally the PIPES is fully dissolved by pH 6.0–6.2.
6. The solution will become cloudy after a couple of days, but this will not affect permeabilization and can be partially cleared by warming to 37°C before use. Alternatively the SLO can be aliquoted and stored at –20°C for several months.
7. The use of 200 mM Tris (final) effectively gives a neutral final solution (pH 7.0). This should be checked and adjusted accordingly.
8. High-quality EGTA is required from Fluka Chemie AG, Gillingham, Dorset, UK (product no. 03779). CaCl₂ is analytical grade from BDH.
9. Values have been obtained using the program “Chelate” for a pH of 6.8 (8).
10. The Dowex resin (1×8 and mesh size 100–200) is purchased from Sigma-Aldrich in the chloride form and must be converted to the formate form.
11. The Dowex is transferred to Pasteur pipets (0.5 ml bed volume) equipped with a glass wool plug (gloves should be worn when making the glass wool plugs).
12. HL60 cells are generally passed for 50–60 passages, and then fresh cells are thawed from liquid nitrogen. Always make sure that you have stocks from early passages saved for future use.
13. HL60 cells can be differentiated toward neutrophils by the addition of DbcAMP or DMSO. DMSO is flammable and must be kept from open flames.
14. Other cell lines can be used. The authors have successfully labeled and reconstituted RBL-2H3 cells. Cells are labeled with 1 µCi of [³H]inositol/ml being added directly to the medium (Dulbecco's modified Eagle's medium + 5% FCS), and

the cells are grown for 48 h. It is preferable to add the label when the cells have just been split.

15. If HL60 cells are to be differentiated with DbcAMP at the same time as labeling with [³H]inositol using Procedure 2, then 30 ml of confluent (2×10^6 cells/ml) cells should be pelleted by centrifugation at $1,000 \times g$ for 5 min at room temperature.
16. Prepare the Eppendorf tubes with the appropriate reagents in an ice bath and transfer to a 37°C water bath 5 min prior to the addition of 50 µL cells.
17. LiCl inhibits the conversion of inositol phosphates back to free inositol. It can be kept as a 1 M stock at -20°C.
18. The lipids are present in the lower chloroform phase, and the upper aqueous phase contains the water-soluble components including the inositol phosphates.
19. Inositol phosphates can also be analyzed on High-Performance Liquid Chromatography (HPLC) (7). This technique is able to identify the individual inositol phosphate isomers (Fig. 1b).
20. This step washes out the [³H]inositol.
21. This step elutes glycerophosphoinositol.
22. Two identical samples were analyzed on Dowex and HPLC for comparison in Fig. 1.
23. The scintillation cocktail should be able to accommodate 1 M salt. (Use Ultima-Flo (from Packard Bioscience, Pangbourne, Berkshire, UK)).
24. The Dowex columns can be used and reused indefinitely if they are regenerated with 2 M ammonium formate/0.1 M formic acid after each use.
25. The increase in inositol phosphate can be expressed as a function of the total radioactivity (dpm) incorporated into the inositol lipids. This allows results to be calculated as a percentage of the total lipids.
26. The sample (Fig. 1b) was analyzed by anion exchange, HPLC on a Partisil 10 SAX column (250 mm × 4.6 mm (from Hichrom, Reading, UK)) (with a Partisil 10 SAX guard cartridge (Hichrom)) (7). The method used was taken from (9). Briefly, the gradient program was set up using a flow rate of 1.25 ml/min and the fraction collector was set up to collect fractions at 0.5-min intervals (750 µL per fraction). The gradient was as follows:

0–1.4 M ammonium phosphate/orthophosphoric acid, pH 3.7							
Time (minutes)	0	10	55	70	75	75.5	85
% buffer	0	0	35	100	100	0	0

27. Data can be plotted as the extent of GTP γ S-stimulated PLC activity and a function of the permeabilization interval. Total rundown is typically 80–90% for GTP γ S-stimulated PLC activity.
28. The permeabilization cocktail can be made up from stocks as follows: pCa 7, 150 μ L; SLO solution, 150 μ L; MgATP, 50 μ L; and permeabilization buffer (PIPES+glucose and BSA), 150 μ L.
29. Longer permeabilization times (i.e., 40 min) allow many more cytosolic factors to leak out.
30. Care should be taken because the permeabilized cell pellet is quite loose and some cells may be lost when decanting the buffer.
31. 2 \times Assay buffer can be made up as follows: pCa 6, 62.5 μ L; MgATP (0.1 M), 40 μ L; MgCl₂ (0.4 M), 10 μ L; LiCl (1 M), 20 μ L; and permeabilization buffer, 865 μ L.
32. The final concentrations during the incubation will be as follows: Ca²⁺, pCa 6 (1 μ M final buffered with 3 mM EGTA final), LiCl (10 mM final), MgATP (2 mM final), MgCl₂ (2 mM final), and GTP γ S (10 μ M final).
33. The FMLP receptor-driven response can be much weaker than the GTP γ S response.

References

1. Rhee SG (2001) Regulation of phosphoinositide-specific phospholipase C. *Annu Rev Biochem* 70:281–312
2. Rebecchi MJ, Pentyala SN (2000) Structure, function, and control of phosphoinositide-specific phospholipase C. *Physiol Revs* 80:1291–1335
3. Thomas GMH, Cunningham E, Fensome A, Ball A, Totty NF, Troung O, Hsuan JJ, Cockcroft S (1993) An essential role for phosphatidylinositol transfer protein in phospholipase C-mediated inositol lipid signalling. *Cell* 74:919–928
4. Kauffmann-Zeh A, Thomas GMH, Ball A, Prosser S, Cunningham E, Cockcroft S, Hsuan JJ (1995) Requirement for phosphatidylinositol transfer protein in epidermal growth factor signalling. *Science* 268:1188–1190
5. Allen V, Swigart P, Cheung R, Cockcroft S, Katan M (1997) Regulation of inositol lipid-specific phospholipase C δ by changes in Ca²⁺ ion concentrations. *Biochem J* 327:545–552
6. Cunningham E, Tan SW, Swigart P, Hsuan J, Bankaitis V, Cockcroft S (1996) The yeast and mammalian isoforms of phosphatidylinositol transfer protein can all restore phospholipase C-mediated inositol lipid signalling in cytosol-depleted RBL-2H3 and HL60 cells. *Proc Natl Acad Sci U S A* 93:6589–6593
7. Skippen A, Jones DH, Morgan CP, Li M, Cockcroft S (2002) Mechanism of ADP ribosylation-factor-stimulated phosphatidylinositol 4,5-bisphosphate synthesis in HL60 cells. *J Biol Chem* 277:5823–5831
8. Tatham PER, Gomperts BD (1990) Cell permeabilisation. In: Siddle K, Hutton JC (eds) Peptide hormones—a practical approach. IRL, Oxford, England, pp 257–269
9. Bird IM (1998) Phosphoinositidase C activation assay III. Methods in molecular biology 105: phospholipid signalling protocols. Bird IM (ed) Humana Press Inc, Totowa, NJ, pp 25–45.

Chapter 10

Single-Cell Imaging Techniques for the Real-Time Detection of IP₃ in Live Cells

Carl P. Nelson

Abstract

Inositol 1,4,5-trisphosphate (IP₃) is a ubiquitous second messenger, derived from the hydrolysis of phosphatidylinositol 4,5-bisphosphate (PIP₂) by enzymes of the phospholipase C (PLC) family. Binding of IP₃ to its cognate receptor in the endoplasmic reticulum membrane leads to release of Ca²⁺ into the cytoplasm, which is involved in the regulation of an array of cellular functions. Traditional techniques for the detection of IP₃ have required the extraction of a large number of cells, with limitations in the time resolution of changes in IP₃ and an inability to obtain detailed information on the dynamics of this second messenger in single cells. Recent progress in this field has led to the development of a number of genetically encoded fluorescent biosensors, which upon recombinant expression are able selectively to detect real-time changes in IP₃ in single live cells. In this chapter, I detail protocols for the expression, visualization (by confocal or fluorescence microscopy), and interpretation of data obtained with such biosensors expressed in mammalian cells.

Key words: Inositol 1,4,5-trisphosphate, Fluorescent biosensor, Cell signaling, Phospholipase C, Fluorescent microscopy, Fluorescence resonance energy transfer

1. Introduction

1.1. Techniques for the Detection of Inositol 1,4,5-Trisphosphate

The generation of inositol 1,4,5-trisphosphate (IP₃) and 1,2-diacylglycerol (DAG) from phospholipase C (PLC)-mediated hydrolysis of phosphatidylinositol 4,5-bisphosphate (PIP₂) is a key signal transduction pathway, utilized by a wide range of cell-surface receptors. DAG recruits and activates protein kinase C (PKC) isoforms at the plasma membrane, while the hydrophilic messenger IP₃ mediates Ca²⁺ release from intracellular stores. Traditional techniques for measuring changes in intracellular IP₃ include [³H]-inositol labeling followed by separation of the [³H]-IP₃ fraction (1), HPLC separation of endogenous IP₃ (2, 3), and enzymatic fluorometric assays (4). These techniques are laborious, slow,

expensive, and in many cases involve purification of IP₃ prior to detection. The development of sensitive and selective mass assays for IP₃ (5, 6) facilitated the measurement of endogenous levels of IP₃ with little requirement for purification. These assays have been widely used and detailed protocols have previously been described (7, 8). However, in common with all biochemical measurements of IP₃, these techniques rely on the use of a large number of cell (typically > 10⁴ cells per reaction) and fail to provide information either on distinct response profiles across a heterogeneous cell population or spatially and/or temporally encoded signals.

These limitations were at least to some degree overcome by the development of a biosensor based on a fusion of the pleckstrin homology (PH) domain of phospholipase C δ and the fluorescent protein eGFP (eGFP-PH (9, 10)). The PH domain binds with high affinity and selectivity to the polar head group of PIP₂, which is responsible for the enrichment of eGFP-PH to the plasma membrane at rest. Upon PLC activation, as PIP₂ levels fall and cytosolic IP₃ levels increase, eGFP-PH translocates from plasma membrane, into the cytosol, with the extent of this translocation reflecting PLC activity and IP₃ generation (9, 10). eGFP-PH has been used extensively in the measurement of IP₃ generation (11), although doubts remain as to whether it detects changes in IP₃ or PIP₂, or in fact reflects the composite effects of alterations in these two inversely related signaling molecules (11–13). Nonetheless, this biosensor permits real-time measurement of PLC activity in single live cells and has been used to analyze asynchronously responding cells and localized PLC signaling (14–16), which was previously not possible.

More recently, a new generation of IP₃ biosensors has been developed, utilizing the fluorescence resonance energy transfer (FRET) technique. FRET involves the non-radiative transfer of energy from an initially excited “donor” fluorophore (excited by exposure to light of a characteristic wavelength) to an “acceptor” fluorophore. This process is highly dependent on the proximity of the donor and acceptor fluorophores (with FRET efficiency being inversely proportional to the sixth power of the distance between donor and acceptor) and relies on overlapping donor emission and acceptor excitation spectra. A number of biosensors for signaling intermediates have been developed, utilizing FRET between CFP (donor) and YFP (acceptor) variants (17). Most share a common strategy of a tandem fusion protein between a binding domain, which is suitably selective for the signaling intermediate of interest, and CFP and YFP fluorophores (17). Several groups have independently developed IP₃ biosensors, exploiting the high affinity and selectivity of the IP₃ receptor (IP₃R) family for IP₃, by incorporating binding domains from IP₃Rs into CFP-YFP tandem fusions (18–21). Binding of IP₃ to these biosensors causes a conformational change, which alters the FRET between CFP and YFP

fluorophores. By measuring CFP and YFP fluorescence levels, a FRET ratio may be obtained, changes in which provide an index of alterations in IP₃ levels experienced by the biosensor. FRET-based IP₃ biosensors have been used to study spatiotemporal aspects of IP₃ signaling in live cells in the cytosol (18, 20–23), as well as in neuronal dendrites and even in the nucleus (19).

In this chapter, I describe detailed protocols for the expression and visualization of both the eGFP-PH translocating biosensor and IRIS-1, an example of the new generation of IP₃ biosensors utilizing the FRET technique. Far from providing a definitive protocol, I hope that these methods, along with the guidance provided in the Notes section, will allow users to adapt these approaches to suit the equipment available in their laboratory and the biological questions they wish to pose. In the following section, I outline the benefits and limitations of each of the two distinct approaches (translocating eGFP-PH and FRET-based IRIS-1 biosensors) to allow the users to choose the technique most suited to their research.

1.2. Criteria to Be Considered in the Choice of IP₃ Biosensor

1.2.1. Selectivity for IP₃

Since eGFP-PH binds to both IP₃ and PIP₂, the extent to which eGFP-PH translocation represents changes in these two second messengers has been widely debated (11, 12). eGFP-PH exhibits a higher in vitro affinity for IP₃ than PIP₂ (14) (and is also >60-fold selective for IP₃ over IP₂ and IP₄ (24)) and evidence has been presented that in live cells, eGFP-PH translocation in response to PLC activation might reflect changes in cytosolic IP₃ (13, 16, 25–27). In contrast, a number of studies have provided evidence that dynamic changes in PIP₂ levels might be the predominant driving force for eGFP-PH translocation (9, 28, 29). It is therefore possible that the relative contributions of IP₃ and PIP₂ to eGFP-PH dynamics may vary under different cellular conditions and/or cell backgrounds. For this reason, it is advisable to address this question in your system of choice, perhaps by the over-expression of IP₃-metabolizing enzymes, such as IP₃ 3-kinase (13, 16, 26) and IP₃ 5-phosphatase (25). Sensitivity of eGFP-PH translocation to the over-expression of these enzymes is a good indication of the IP₃ dependency of the response, although the potential role of a loss of Ca²⁺-dependent potentiation of PLC activity following expression of IP₃-metabolizing enzymes must also be considered (13).

In contrast, the binding domain within IRIS-1 (and other FRET-based IP₃ biosensors) consists of the IP₃-binding domain of the IP₃ (type 1) receptor (21) and would therefore be anticipated selectively to bind IP₃. Indeed, the affinity of IRIS-1 for IP₃ is >50-fold higher than for IP₄ and >400-fold greater than for IP₂ (21). IRIS-1 is therefore a highly selective IP₃ biosensor.

1.2.2. Signal:Noise Ratio and Sensitivity to Changes in IP₃

The magnitude of response observed to maximal PLC stimulation is much greater for eGFP-PH than for IRIS-1. In common with many FRET biosensors, maximal changes in IRIS-1 FRET ratio

are typically <10%, while my estimates of the baseline noise indicate a standard deviation of approx. 1.5% around the baseline. In contrast, cytosolic eGFP-PH fluorescence typically increased by 300–500% in the same system, above a baseline noise level of <5%. Given the similar potency of MCh in SH-SY5Y cells measured using IRIS-1 ($pEC_{50} = 5.38 \pm 0.43$) and eGFP-PH ($pEC_{50} = 5.19 \pm 0.11$ (13)), as well as using the IP₃ mass assay ($pEC_{50} = 4.96 \pm 0.03$ (30)), both biosensors appear suitably sensitive to changes in intracellular IP₃. However, in terms of signal:noise ratio, eGFP-PH may be the superior biosensor.

1.2.3. Requirement for Specialized Equipment

Visualization of cells expressing either biosensor requires specialized imaging equipment. Clear resolution of the localization of eGFP-PH requires confocal microscopy (see Note 10), whereas FRET measurements can be performed with an epifluorescence microscope. Although this might make the IRIS-1 biosensor slightly more accessible, the requirement for dual-emission wavelengths to be measured means that significant adaptation might be required to allow FRET measurements to be performed with standard Ca²⁺ imaging microscopy equipment.

1.2.4. Interference with Endogenous Signaling Pathways

Over-expression of any protein may influence cellular behavior, but this may be of particular concern for those proteins with high affinity for inositol phospholipids (such as eGFP-PH), as this could preclude hydrolysis of the lipid target. Indeed, this has been previously reported for eGFP-PH (9), and in SH-SY5Y cells we found that eGFP-PH expression caused a modest, but statistically significant attenuation of PLC signaling, as determined by Ca²⁺ imaging (13). IRIS-1 is unlikely to bind inositol phospholipids; however if expressed at high levels, it could “buffer” significant amounts of IP₃, but this has yet to be investigated. As discussed in Note 6, it is therefore advisable to ensure that fluorescent biosensors are expressed at levels appropriate for “sampling” not buffering changes in [IP₃].

1.2.5. Susceptibility to Artifacts

Given the smaller signal:noise ratio and the relatively small magnitude of alterations in fluorescence involved in IRIS-1 responses (see Fig. 1), care must be taken to ensure that the observed responses are genuine. Although YFP fluorescence is relatively sensitive to alterations in pH (31, 32), the use of Venus (a modified YFP, showing less pH sensitivity (33)) in IRIS-1 minimizes the risk of pH-mediated artifacts. Nonetheless, it is advisable to undertake control experiments (detailed in Note 13) to ensure that apparent changes in FRET ratio truly result from alterations in CFP–YFP FRET, rather than direct effects on the emission from either/both fluorophore(s).

Artifacts are less commonly observed when using the eGFP-PH biosensor, since responses are only registered by increases in

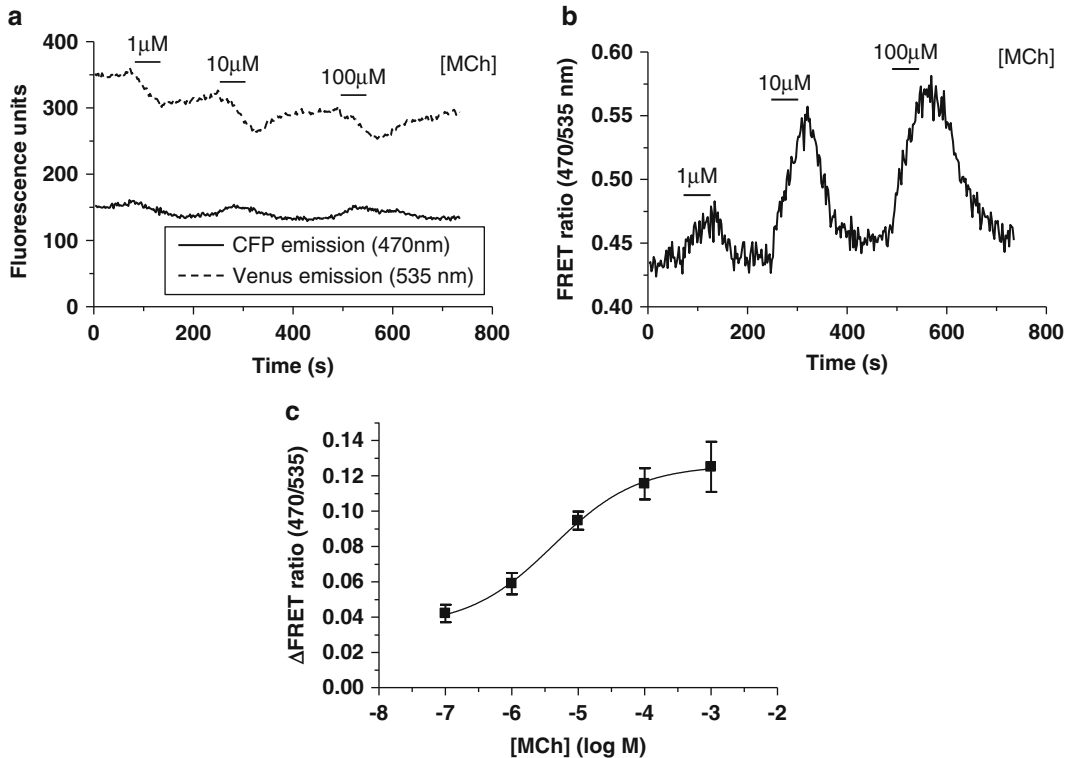


Fig. 1. Analysis of muscarinic acetylcholine receptor-mediated IP₃ signaling in SH-SY5Y cells by IRIS-1 FRET. (a) CFP (470 nm; solid trace) and Venus (535 nm; dashed trace) fluorescence emissions, recorded from SH-SY5Y cells transiently expressing the IRIS-1 biosensor. Cells were stimulated with the indicated concentrations of MCh for the period shown by the horizontal bars. Data are expressed as raw fluorescence units. (b) FRET ratio trace corresponding to the CFP and Venus fluorescence data illustrated in (a). MCh was applied in the concentrations indicated and for the period denoted by the horizontal bars. Data are expressed as FRET ratio, defined as emission at 470 nm/emission at 535 nm. (c) Mean MCh concentration-response curve for FRET changes in IRIS-1-expressing cells. Data are represented as mean \pm s.e.m. from between 5 and 13 different cells and are expressed as Δ FRET ratio, defined as (peak FRET ratio following MCh stimulation) – (baseline FRET ratio).

cytosolic fluorescence. If there is any doubt that an increased cytosolic signal results from a genuine response, it may be verified by ensuring that a concomitant decrease in plasma membrane fluorescence is also observed.

1.2.6. Kinetic Resolution

eGFP-PH translocation has been found to correlate well with the time-course of changes in IP₃ (13, 27, 34) and has been used extensively to measure real-time changes in PLC signaling (11). The ability to visualize the dynamic changes in PLC activity, occurring in live cells, is one of the major advances provided by the eGFP-PH biosensor. Although the FRET-based IP₃ biosensors have also been used to investigate real-time cytosolic IP₃ dynamics over a similar timescale (21), I have found that IRIS-1 responses were significantly slower to develop than eGFP-PH responses to the same stimulus (see Fig. 1b vs. 2b). Similarly slow kinetics were

also reported for the membrane-targeted LIBRA biosensor, with peak responses to muscarinic acetylcholine receptor stimulation in SH-SY5Y cells only being achieved 2–5 min after stimulation (18). The reason for the slower kinetics observed for these IP_3 biosensors is unclear. If devising an approach to measure IP_3 signaling kinetics using these biosensors, a preliminary investigation of biosensor kinetics in your cell system of choice might therefore be prudent.

1.2.7. Visual Representation of Responses

Although the most informative use of fluorescent biosensors comes from a quantitative analysis of changes in biosensor signal (see Subheading 3.4), for illustrative purposes it is often desirable to display representative images of the responses. eGFP-PH-expressing cells are often suitable for such a visual representation (see Fig. 2a), with a clear change in biosensor localization upon agonist

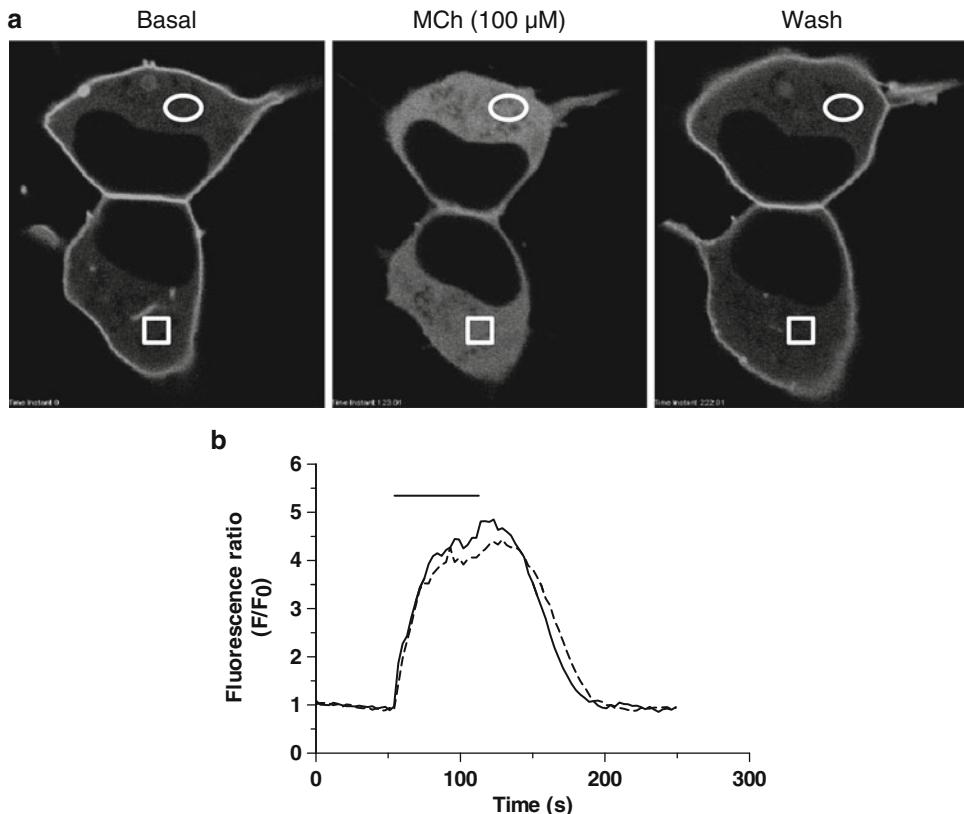


Fig. 2. Analysis of muscarinic acetylcholine receptor-mediated PLC activation in SH-SY5Y cells by eGFP-PH translocation. **(a)** Confocal images of SH-SY5Y neuroblastoma cells transiently expressing eGFP-PH before stimulation (Basal), during stimulation with MCh (100 μM , 60 s) and following agonist washout (Wash). **(b)** Traces illustrating changes in fluorescence intensity within the regions of interest (white ellipse corresponding to solid trace and white square corresponding to dashed trace) indicated on the images shown in **(a)**, upon stimulation with MCh (100 μM) for the period denoted by the horizontal bar. Data are displayed as normalized fluorescence values (relative to initial fluorescence) expressed as a self-ratio of F/F_0 , where F_0 is the initial fluorescence intensity and F is the fluorescence intensity at a given time.

stimulation. In contrast, as a result of the relatively small changes in fluorescence signal even in response to maximal agonist stimulation, FRET biosensors are less amenable to a clear visual representation. It is possible to display scaled pseudocolor images to illustrate changes in FRET ratio (21), but they are rarely as striking as the images representing translocating biosensor responses (26).

1.2.8. Measuring Localized Changes in IP₃

Biosensors based on the FRET principle have the benefit of being able to report changes in their target molecule in the local environment. This means that it is possible to specifically target the biosensor to subcellular domains, as has been done with the LIBRA (plasma membrane localized (18)) and Fretino (nuclear localized (19)) biosensors, allowing measurement of IP₃ levels within those regions. Such targeting is not possible with eGFP-PH if it is to be used as a translocating biosensor to report changes in IP₃ levels. However, a modified approach based on measuring FRET between CFP- and YFP-labeled versions of the PH domain of PLCδ (28) provides a sensitive readout for PLC activity without the requirement for optical sectioning. This facilitates a robust quantification of PLC activity even in very flat cells or in subcellular regions such as neurites (28), which is otherwise impossible with the PH domain biosensor.

2. Materials

2.1. Preparation and Transfection of Cells

1. SH-SY5Y human neuroblastoma cells.
2. Minimum essential medium, 2 mM L-glutamine and 10% newborn calf serum, supplemented with 100 U/mL penicillin, 100 µg/mL streptomycin, 2.5 µg/mL amphotericin (all from Invitrogen, Paisley, UK).
3. 25 mm glass coverslips (thickness 1.5 (160–190 µm), VWR, Lutterworth, UK).
4. LipofectAMINE2000 (Invitrogen, Paisley, UK).
5. Basal minimum essential medium (Invitrogen, Paisley, UK), without supplements.
6. Mammalian expression plasmid containing the fluorescent biosensor of choice (IRIS-1 (based upon the IP₃-binding domain of IP₃R1 fused with Venus and eCFP) in pcDNA3.1 or the pleckstrin homology domain of PLCδ1 in peGFP-C1 (eGFP-PH)), in maxiprep quantities.

2.2. Fluorescence Resonance Energy Transfer Imaging

1. Krebs-Henseleit buffer (KHB: NaCl 118 mM, KCl 4.7 mM, CaCl₂ 1.3 mM, KH₂PO₄ 1.2 mM, MgSO₄ 1.2 mM, NaHCO₃ 25 mM, HEPES 5 mM, glucose 10 mM; pH 7.4).

2. Teflon coverslip dish (V.MSC-TD, Harvard Apparatus, Kent, UK).
3. Peltier unit (PDMI-2 open perfusion micro-incubator, controlled by TC 202A temperature controller, Harvard Apparatus, Kent, UK).
4. Peristaltic pump perfusion system (Gilson Minipuls peristaltic pump, Anachem, Luton, UK).
5. Zeiss Axiovert 200 epifluorescence microscope (Carl Zeiss, Welwyn Garden City, UK).
6. Cooled CCD camera (Orca ER, Hamamatsu Photonics, Welwyn Garden City, UK).
7. MetaFluor software (Molecular Devices, Berkshire, UK).
8. 100 W xenon arc lamp (Hamamatsu Photonics, Welwyn Garden City, UK).
9. Zeiss FLUAR 40× (NA 1.30) oil-immersion objective lens (Carl Zeiss, Welwyn Garden City, UK).
10. 440 ± 20 nm excitation filter and 470 ± 20 nm and 535 ± 20 nm emission filters, fitted to filter wheels (all from PerkinElmer, Bucks, UK).
11. Methacholine (MCh, Sigma, Poole, UK), 10 mM stock solution in KHB.

2.3. Confocal Imaging of Fluorescent Biosensors

1. KHB (NaCl 118 mM, KCl 4.7 mM, CaCl₂ 1.3 mM, KH₂PO₄ 1.2 mM, MgSO₄ 1.2 mM, NaHCO₃ 25 mM, HEPES 5 mM, glucose 10 mM; pH 7.4).
2. Teflon coverslip dish (V.MSC-TD, Harvard Apparatus, Kent, UK).
3. Peltier unit (PDMI-2 open perfusion micro-incubator, controlled by TC 202A temperature controller, Harvard Apparatus, Kent, UK).
4. Peristaltic pump perfusion system (Gilson Minipuls peristaltic pump, Anachem, Luton, UK).
5. Olympus FV500 laser scanning confocal system (with three photomultiplier tube (PMT) detectors), with Olympus IX70 inverted microscope (Olympus Europa, Hamburg, Germany).
6. Olympus Fluoview TIEMPO v.5.0 software.
7. 100 W mercury lamp (Olympus Europa, Hamburg, Germany).
8. 60× oil-immersion objective lens (PLAPO60xOI, NA 1.40, Olympus Europa, Hamburg, Germany).
9. 10 mW argon laser (458 nm, 488 nm, 514 nm).
10. 560 nm dichroic beam splitter, BA 505IF long-pass filter.
11. MCh (Sigma, Poole, UK), 10 mM stock solution in KHB.

2.4. Analysis of Experimental Data

1. MetaFluor software (Molecular Devices, Berkshire, UK).
2. Olympus Fluoview v.5.0 software (Olympus Europa, Hamburg, Germany).
3. Prism v.5 (GraphPad Software, San Diego, CA, USA) and Excel (Microsoft, Redmond, Washington, USA) analysis software.

3. Methods

The following section describes a standard protocol for the transfection of SH-SY5Y cells, followed by detailed methods for both epifluorescence measurements of the FRET-based IP₃ biosensor IRIS-1 and confocal imaging of the translocating biosensor eGFP-PH. However, it is anticipated that these specific protocols may be easily adapted for the imaging of a wide variety of similar biosensors (see Note 1) and can be applied to a range of model cell lines (e.g., HEK, CHO), as well as certain primary cells.

3.1. Preparation and Transfection of Cells

1. 48–72 h prior to experimentation, seed cells onto sterile 25 mm glass coverslips such that they are 40–60% confluent 24 h later.
2. Transfect cells 24 h later with 0.5 µg cDNA (either IRIS-1 or eGFP-PH) per coverslip using 1.5 µL LipofectAMINE2000 (i.e., in a 1:3 ratio with cDNA) in 100 µL basal minimum essential medium, according to the manufacturer's instructions (see Note 2).
3. 4–6 h later, remove medium and replace with fresh, fully supplemented medium.
4. 24–48 h post-transfection cells are ready to be imaged (see Note 3).

3.2. Fluorescence Resonance Energy Transfer Imaging

Prior to experimentation, it will be necessary to set up a FRET imaging protocol, which may then be employed in all subsequent experiments. At each time-point throughout the course of the experiment, the FRET construct should be excited at 440 nm and emissions sequentially measured at 470 and 535 nm, respectively, allowing a FRET ratio to be calculated (see Note 4).

1. Remove coverslip containing cells and wash with pre-warmed KHB (1 mL).
2. Mount coverslip in a Teflon coverslip dish and carefully add pre-warmed KHB (1 mL).
3. Maintain cells at 37°C in a Peltier unit under continual perfusion (5 mL/min) with KHB (see Note 5).

4. Under brightfield illumination, focus cells using a 40 \times oil immersion objective lens on an inverted epifluorescence microscope.
5. Identify transfected cells under fluorescence illumination and select an appropriate field of view, ideally containing ≥ 2 transfected cells (see Note 6).
6. Mark a region of interest (ROI) within the cytosol of each cell (see Note 7) and begin recording, typically every 2–3 s (depending on the speed of the response in question) (see Note 8).
7. Where possible, drug additions should be made via the continual perfusion system (see Note 9). Note the timings of the additions made and how long the cells were exposed to the drug(s). Stimulation of the endogenous M₃ mACh receptor population in SH-SY5Y cells with MCh (100 μ M), perfused onto the cells for 60 s, is adequate to observe a maximal change in 470/535 FRET ratio, which is fully reversible on agonist washout (see Fig. 1b).

3.3. Confocal Imaging of eGFP-PH

Set up an eGFP excitation protocol, utilizing the 488 nm argon laser to excite eGFP and a long-pass filter (BA 505IF) to collect emissions above 505 nm.

- 1–3. As in Subheading 3.2, steps 1–3.
4. Using a 60 \times oil immersion objective lens, focus cells under brightfield illumination on a laser-scanning confocal inverted microscope (see Note 10).
- 5 and 6. As in Subheading 3.2, steps 5 and 6. Also, see Note 11.
7. Add drug treatments via the continual perfusion system where possible (see Note 9), noting when and for how long the cells are exposed to the drug(s). Stimulation of the endogenous M₃ mACh receptor population with MCh (100 μ M), for 60 s, generates a maximal, transient translocation of the eGFP-PH biosensor from plasma membrane to cytosol (see Fig. 2).

3.4. Analysis of Experimental Data

1. Once the experiment is complete, ensure that the image stack is saved to the hard drive. Analysis of these data can then be revisited at a later date or performed immediately.
2. We routinely analyze both IRIS-1 and eGFP-PH imaging experiments by positioning ROIs within the cytoplasm of each cell being studied (see Note 12). Playback of the experiment allows a suitable size and position of ROI to be chosen (see Note 7). The mean (or integrated) fluorescence value for the area enclosed by the ROI can then be calculated for each frame of the experiment and can usually be exported as a data file and viewed in Microsoft Excel, GraphPad Prism, or other suitable data analysis packages.

3. Data can then be plotted as raw or normalized fluorescence values against time to provide an indication of the time-course and extent of biosensor translocation (in the case of eGFP-PH) or CFP and YFP fluorescence changes (in the case of IRIS-1) (see Note 13).
4. The concentration dependency of a response may also be determined by measuring the normalized peak responses to a range of agonist concentrations (see Fig. 1b, c). Both translocating and FRET biosensors can therefore provide quantitative measures of dynamic changes in IP₃, as well as kinetic data relating to rates of onset and offset of responses (13, 35) (see Note 14).

4. Notes

1. The IRIS-1 biosensor is one of several similar probes, independently developed, but based around the principle of a tandem fusion between an IP₃-binding domain (from an IP₃ receptor subtype) and two compatible fluorophores (usually CFP and YFP variants), which transduce changes in binding domain conformation upon IP₃ binding into changes in FRET between the two fluorophores (18–21). The protocol we describe here can therefore be adopted for any such CFP–YFP FRET biosensors designed to measure IP₃ (or indeed for a range of similar biosensors for a variety of other intracellular signaling intermediates, such as cAMP (36)). Similarly, additional translocating GFP-labeled biosensors can be studied in the same way as the eGFP-PH probe, including those which translocate from cytosol to plasma membrane (i.e., in the opposite direction to eGFP-PH) upon stimulation (e.g., the DAG sensor, eGFP-PKC γ -C1₂ (37)). In the latter case, experiments may be performed using the protocol described in this chapter, with the understanding that an increase in the target molecule (at the membrane) will be represented by a decrease in cytosolic fluorescence signal.
2. We routinely use LipofectAMINE2000 (Invitrogen, Paisley, UK), but alternative lipofection reagents, including Fugene (Roche Diagnostics, Burgess Hill, UK) and GeneJuice (Merck Biosciences, Nottingham, UK), are similarly effective in most cell types. However, I would recommend that the transfection conditions are optimized for each biosensor/cell type combination. The conditions which may be varied include the choice of lipofection reagent, the quantity of cDNA transfected, and the ratio of cDNA:lipofection reagent employed. 0.5 μ g cDNA is typically optimal for fluorescent biosensors in our chosen cell

systems, providing a balance between sufficient levels of expression and the potential for cytotoxicity, which may be associated with the use of high levels of lipofection reagent. The latter point must also be taken into consideration when optimizing the ratio of cDNA:lipofection reagent. Ratios of between 1:2 and 1:4 are routinely used, but since all such reagents are to some extent cytotoxic, the amount to which cells are exposed should be minimized. Removing antibiotics from the medium for the period in which the cells are exposed to the cDNA/lipofection reagent may also reduce the potential for cell death following transfection, since cells are known to be particularly susceptible to antibiotic damage during this process.

The success (or otherwise) of the transfection process is often judged not only by the level of expression within cells but also by the proportion of cells that are visibly expressing the biosensor (i.e., the transfection efficiency). While relatively high transfection efficiencies (in some cases >50% in cell lines) can be achieved using lipofection, primary cells are often considerably more resistant to transfection, yielding very low levels of transfection efficiency (perhaps as low as 1 or 2%). Although larger proportions of the cell population may be transfected using alternative techniques (such as nucleofection (Lonza, Cologne, Germany)), this is often not necessary for biosensor imaging experiments, where imaging 1 or 2 cells per experiment may still be achieved with a low transfection efficiency.

3. It is usually possible to image biosensor-transfected cells either 24 or 48 h post-transfection. In our experience, there is little difference between these two time-points, but we would recommend that this is optimized for each biosensor/cell type pairing to ensure that enough time is allowed for protein expression and trafficking.
4. The requirement for single-excitation (440 nm) and dual-emission (470 and 535 nm) recordings necessitates the use of an emission filter wheel to allow rapid switching between the 470 ± 20 nm and 535 ± 20 nm filters during the recording period. Since the rate of recording will be limited, to some extent, by the time taken to switch between filters, we recommend that the exposure time for each measurement be minimized. We routinely use 50 ms exposures, but depending on the level of signal achieved with this, it may be necessary to extend this exposure time to 100–150 ms. Longer exposure times will not only slow the rate of recording but may also exacerbate the bleaching of one or both of the fluorophores. It is advisable to optimize the experimental setup, to minimize the exposure time, while allowing a reasonable level of signal (perhaps 100–500 fluorescence intensity units) to be detected through both 470 and 535 nm channels.

When using the IRIS-1 IP₃ biosensor, it is advisable to express changes in FRET as 470/535 FRET ratios (i.e., emission at 470 nm/emission at 535 nm), since an increase in IP₃ will lead to a decrease in CFP-to-YFP FRET (and therefore a decrease in 535 nm signal and an increase in 470 nm signal), such that the 470/535 nm ratio will increase. This ensures a more straightforward interpretation of the data, with an increase in ratio being indicative of an increase in [IP₃].

It should be noted that due to the nature of the excitation and emission spectra of CFP and YFP, alternative combinations of excitation and emission filters may still allow an accurate detection of CFP-YFP FRET. The main considerations are that CFP is selectively excited (with minimal direct excitation of YFP) and that, as much as possible, the signals detected through the two emission channels represent distinct CFP and YFP components, respectively. The most convenient way of determining this is to visualize the respective spectra alongside each other, as can be done using Invitrogen's Fluorescence SpectraViewer (<http://www.invitrogen.com/site/us/en/home/support/Research-Tools/Fluorescence-SpectraViewer.html>).

5. I routinely perform these experiments at physiological temperatures, but it is possible to work at lower temperatures if desired. In order to work at a temperature greater than room temperature, it is advisable to pre-warm the KHB solution in a water bath, rather than rely entirely on the Peltier unit to warm the solution. In this case, the “dead space” in the perfusion system should also be minimized in order to reduce heat loss from the buffer during perfusion. It is also necessary to monitor the coverslip bath temperature independently of the Peltier unit, as this can differ by 2–3°C.
6. Identification of transfected cells is best achieved by viewing the cells through the microscope eyepiece, under fluorescence illumination (illuminating Venus and/or CFP fluorophores in the case of the IRIS-1 biosensor). The individual cell(s) to be used in the experiment should be chosen carefully. Amongst the available transfected cells, it is important to select one which appears healthy and of a typical morphology for that cell type (this can be verified by comparison under brightfield illumination with un-transfected cells on the same coverslip, as well as the user’s prior knowledge of the cell type). The level of expression of the biosensor within the cell should also be considered. While it is necessary to ensure that the expression level is high enough to yield a detectable level of fluorescence through all channels, very highly expressing cells should be avoided. High levels of over-expression of any protein may adversely impact on cellular function, but this is of particular concern for constructs such as IRIS-1 and eGFP-PH, since

these biosensors may perturb normal PIP₂/IP₃ dynamics through their affinity for binding to IP₃ and/or PIP₂. Ideally, cells expressing an intermediate level of biosensor (i.e., cells exhibiting an intermediate level of fluorescence) should be selected for experimentation. It is often possible to image more than one cell per experiment, depending on the confluence of the cells and the transfection efficiency. While this is clearly preferable to single-cell imaging, the other considerations outlined above should not be compromised in return for a larger number of cells per experiment.

7. Selecting an ROI within the cell(s) allows measurement of the fluorescence intensity within that region alone. Although not possible with all software systems, many, including Fluoview (Olympus) and Metafluor (Molecular Devices), have the capability to do this during the live experiment, providing an online indication of changes in biosensor fluorescence/localization. In general, larger ROIs will provide a better signal-to-noise ratio, but care must be taken to ensure that the region stays within the boundary of the cell throughout the experiment. If the cells being imaged remain relatively static during stimulation, larger ROIs may be used, but if the cells are motile, it is advisable to minimize the size of the ROIs. In most cases, ROIs can be redrawn/positioned after the experiment to ensure that a suitable area is covered.
8. In most cases, biochemically determined peak IP₃ responses are generated within 10–30 s (38, 39). This timescale may therefore dictate the desired rate of sampling for an IP₃ biosensor. Indeed, eGFP-PH translocation reaches a peak within 20–40 s (9, 13, 34). Sampling at a rate of 1 image every 2 s (0.5 Hz) is therefore sufficient to accurately record eGFP-PH translocation. Our experience with the IRIS-1 biosensor is that responses develop comparatively slowly, only reaching a peak within approx. 60 s. A sampling rate of <1 Hz is therefore sufficient for IRIS-1 imaging.
9. The continual perfusion system provides the most convenient means of applying drugs to the cells. However, when using lipophilic compounds it is advisable to apply these directly into the bath so as to avoid contaminating the perfusion system for future experiments. Run the experiment with a static bath (of known volume) and carefully apply the reagent (from a concentrated stock solution) into the bath by pipette. Movement artifacts (resulting from movement of the stage/coverslip) may occur if recording whilst making such additions, but with care these can be minimized.
10. Although a wide-field fluorescence microscope is capable of visualizing fluorescent protein expression within cells, it is not suitable for imaging changes in the subcellular localization of fluorescent biosensors such as eGFP-PH. Images seen through

a conventional microscope represent the sum of the in-focus region (determined by the depth of field of the objective lens, typically around 1 μm) plus that of the out-of-focus regions. As a result, for a typical cell, around 80% of the light making up the image may be out of focus (40). When visualizing a cell expressing a fluorescent protein localized to the plasma membrane (such as eGFP-PH), this out-of-focus light yields a blurry and undefined image, unsuitable for accurately measuring changes in localization of the biosensor. In contrast, confocal microscopy eliminates the out-of-focus light using a pinhole aperture to restrict the light paths entering the detector to only those coming from the in-focus region. This allows resolution of finer structures within the specimen, greatly enhances the contrast, and effectively provides an “optical section” through the cell, such as those shown in Fig. 10.2a. With respect to the eGFP-PH biosensor, this degree of resolution allows the clear visualization of eGFP-PH translocation between membrane and cytosolic compartments.

11. When setting up the experiment, the aim should be to maximize image quality, while minimizing the potential for photo-bleaching or saturation of the response, while allowing image acquisition to occur at an appropriate rate (see Note 8). In our experience, eGFP-PH translocations in most cell types yield a maximal change in cytosolic fluorescence of <10-fold. To avoid problems with saturation, it is advisable to set the basal cytosolic fluorescence level to $\leq 10\%$ of the maximum detectable fluorescence level. On a 12-bit system (with a total of 4,096 fluorescence intensity units), this requires an initial cytosolic fluorescence of ≤ 400 units. In order to maximize the image quality/signal size while avoiding photo-bleaching, we recommend predominantly using the gain settings on the PMT to maximize the signal detection and using the laser at the lowest strength at which it is possible to obtain a sufficiently clear image. It may also be necessary to sacrifice some image quality for scanning speed if photo-bleaching becomes a problem, but with eGFP this is rarely the case.
12. For translocating biosensors such as eGFP-PH (41) and eGFP-labeled PKC isoenzymes (42), it may sometimes be appropriate to use line-scans to measure fluorescence intensity across the cell. Line-scans may provide more information about the localization of the probe, since they profile the expression at the membrane and within the cytosol, while cytosolic ROIs only profile changes occurring in cytosolic fluorescence. However, ROIs are better suited to measuring dynamic changes, such as those occurring in response to PLC activation and for this reason they are widely used in the analysis of eGFP-PH data.
13. Although it is likely that most data will ultimately be expressed in terms of FRET ratio, it is important to initially examine the

individual CFP and YFP emission traces, primarily to ensure that apparent responses are not artifactual. A genuine change in CFP–YFP FRET should be reflected in both CFP and YFP traces, with a decrease in FRET (as occurs in IRIS-1 following IP₃ binding) resulting in not only a decrease in YFP emission but also a small increase in CFP emission (as a result of the decreased energy transfer to YFP leading to a larger fluorescence emission from the CFP) (see Fig. 1a). The change in CFP is often very subtle, but is usually apparent, even in relatively small responses. If the change in FRET ratio does not correspond with some change in both CFP and YFP emissions (in opposing directions), it may well be artifactual. A major source of FRET artifacts is the relatively high pH sensitivity of YFP (31, 32). This is largely overcome by the use of less pH-sensitive modified YFPs, such as the Venus fluorophore (33) used in IRIS-1 (21). However, the validity of an apparent FRET response may be confirmed by performing the experiment under conditions where the YFP fluorophore alone is directly stimulated (thus removing any element of energy transfer from CFP to YFP). Under such conditions a treatment which acts only through a change in FRET would not alter the YFP fluorescence, but if the apparent FRET response is due to (for instance) pH-dependent changes in YFP fluorescence, the directly excited YFP will exhibit an altered emission.

14. The eGFP-PH biosensor has been used to determine quantitative estimates of agonist potency and to profile the kinetics of single-cell IP₃ dynamics. Where these values have been compared in the same system with traditional biochemical estimates of IP₃ levels, a good agreement has generally been reported (9, 34, 43, 44). The various FRET-based IP₃ biosensors, including IRIS-1, have been less extensively studied. However, my estimate of MCh potency in SH-SY5Y cells determined using IRIS-1 is similar to that determined using eGFP-PH (13) and the IP₃ mass assay (30) (see Subheading 1.2). Given the well-established IP₃ selectivity of IRIS-1 (21), the FRET probe would therefore seem to be a reliable index of IP₃ levels, even though the rate of onset of the FRET response appears slower than the generation of IP₃ (see Note 8).

Acknowledgements

I gratefully acknowledge Prof. Tobias Meyer (Stanford University, USA) for making the eGFP-PH biosensor available to us and Prof. Katsuhiko Mikoshiba (RIKEN, Japan) for providing us with the IRIS-1 biosensor. I also thank Prof. John Challiss (University of Leicester, UK) for his critical reading of the manuscript.

References

1. Berridge MJ et al (1983) Changes in the levels of inositol phosphates after agonist-dependent hydrolysis of membrane phosphoinositides. *Biochem J* 212:473–482
2. Irvine RF et al (1985) Metabolism of inositol 1,4,5-trisphosphate and inositol 1,3,4-trisphosphate in rat parotid glands. *Biochem J* 229:505–511
3. Kennedy ED et al (1989) A simple enzymic method to separate [³H]inositol 1,4,5- and 1,3,4-trisphosphate isomers in tissue extracts. *Biochem J* 260:283–286
4. Shayman JA, Morrison AR, Lowry OH (1987) Enzymatic fluorometric assay for myo-inositol trisphosphate. *Anal Biochem* 162:562–568
5. Challiss RA, Batty IH, Nahorski SR (1988) Mass measurements of inositol(1,4,5)trisphosphate in rat cerebral cortex slices using a radioreceptor assay: effects of neurotransmitters and depolarization. *Biochem Biophys Res Commun* 157:684–691
6. Bredt DS, Mourey RJ, Snyder SH (1989) A simple, sensitive, and specific radioreceptor assay for inositol 1,4,5-trisphosphate in biological tissues. *Biochem Biophys Res Commun* 159:976–982
7. Batty IH et al (1997) Receptor-linked phosphoinositide metabolism. In: Turner AJ, Bachelard HS (eds) *Neurochemistry: a practical approach*, 2nd edn. Oxford University Press, Oxford, pp 229–268
8. Zhang L (1998) Inositol 1,4,5-trisphosphate mass assay. *Methods Mol Biol* 105:77–87
9. Varnai P, Balla T (1998) Visualization of phosphoinositides that bind pleckstrin homology domains: calcium- and agonist-induced dynamic changes and relationship to myo-[³H] inositol-labeled phosphoinositide pools. *J Cell Biol* 143:501–510
10. Stauffer TP, Ahn S, Meyer T (1998) Receptor-induced transient reduction in plasma membrane PtdIns(4,5)P₂ concentration monitored in living cells. *Curr Biol* 8:343–346
11. Nahorski SR et al (2003) Visualizing phosphoinositide signalling in single neurons gets a green light. *Trends Neurosci* 26:444–452
12. Varnai P, Balla T (2006) Live cell imaging of phosphoinositide dynamics with fluorescent protein domains. *Biochim Biophys Acta* 1761:957–967
13. Nelson CP, Nahorski SR, Challiss RAJ (2008) Temporal profiling of changes in phosphatidylinositol 4,5-bisphosphate, inositol 1,4,5-trisphosphate and diacylglycerol allows comprehensive analysis of phospholipase C-initiated signalling in single neurons. *J Neurochem* 107:602–615
14. Hirose K et al (1999) Spatiotemporal dynamics of inositol 1,4,5-trisphosphate that underlies complex Ca²⁺ mobilization patterns. *Science* 284:1527–1530
15. Micheva KD, Holz RW, Smith SJ (2001) Regulation of presynaptic phosphatidylinositol 4,5-bisphosphate by neuronal activity. *J Cell Biol* 154:355–368
16. Nash MS et al (2002) Determinants of metabotropic glutamate receptor-5-mediated Ca²⁺ and inositol 1,4,5-trisphosphate oscillation frequency. Receptor density versus agonist concentration. *J Biol Chem* 277:35947–35960
17. Miyawaki A (in press) Development of probes for cellular functions using fluorescent proteins and fluorescence resonance energy transfer. *Annu Rev Biochem* [in press]
18. Tanimura A et al (2004) Fluorescent biosensor for quantitative real-time measurements of inositol 1,4,5-trisphosphate in single living cells. *J Biol Chem* 279:38095–38098
19. Sato M et al (2005) Locating inositol 1,4,5-trisphosphate in the nucleus and neuronal dendrites with genetically encoded fluorescent indicators. *Anal Chem* 77:4751–4758
20. Remus TP et al (2006) Biosensors to measure inositol 1,4,5-trisphosphate concentration in living cells with spatiotemporal resolution. *J Biol Chem* 281:608–616
21. Matsuya T et al (2006) Cytosolic inositol 1,4,5-trisphosphate dynamics during intracellular calcium oscillations in living cells. *J Cell Biol* 173:755–765
22. Tanimura A et al (2009) Monitoring of IP₃ dynamics during Ca²⁺ oscillations in HSY human parotid cell line with FRET-based IP₃ biosensors. *J Med Invest* 56(Suppl):357–361
23. Shirakawa H et al (2006) Measurement of intracellular IP₃ during Ca²⁺ oscillations in mouse eggs with GFP-based FRET probe. *Biochem Biophys Res Commun* 345:781–788
24. Lemmon MA et al (1995) Specific and high-affinity binding of inositol phosphates to an isolated pleckstrin homology domain. *Proc Natl Acad Sci USA* 92:10472–10476
25. Okubo Y et al (2001) Visualization of IP₃ dynamics reveals a novel AMPA receptor-triggered IP₃ production pathway mediated by voltage-dependent Ca²⁺ influx in Purkinje cells. *Neuron* 32:113–122
26. Nash MS et al (2004) Synaptic activity augments muscarinic acetylcholine receptor-stimulated inositol 1,4,5-trisphosphate production

- to facilitate Ca^{2+} release in hippocampal neurons. *J Biol Chem* 279:49036–49044
27. Xu C, Watras J, Loew LM (2003) Kinetic analysis of receptor-activated phosphoinositide turnover. *J Cell Biol* 161:779–791
 28. van der Wal J et al (2001) Monitoring agonist-induced phospholipase C activation in live cells by fluorescence resonance energy transfer. *J Biol Chem* 276:15337–15344
 29. Winks JS et al (2005) Relationship between membrane phosphatidylinositol-4,5-bisphosphate and receptor-mediated inhibition of native neuronal M channels. *J Neurosci* 25:3400–3413
 30. Martin AK, Nahorski SR, Willars GB (1999) Complex relationship between $\text{Ins}(1,4,5)\text{P}_3$ accumulation and Ca^{2+} -signalling in a human neuroblastoma revealed by cellular differentiation. *Br J Pharmacol* 126:1559–1566
 31. Llopis J et al (1998) Measurement of cytosolic, mitochondrial, and Golgi pH in single living cells with green fluorescent proteins. *Proc Natl Acad Sci USA* 95:6803–6808
 32. Elsliger MA et al (1999) Structural and spectral response of green fluorescent protein variants to changes in pH. *Biochemistry* 38:5296–5301
 33. Nagai T et al (2002) A variant of yellow fluorescent protein with fast and efficient maturation for cell-biological applications. *Nat Biotechnol* 20:87–90
 34. Nash MS et al (2001) Single-cell imaging of graded $\text{Ins}(1,4,5)\text{P}_3$ production following G-protein-coupled-receptor activation. *Biochem J* 356:137–142
 35. Jensen JB et al (2009) Fluorescence changes reveal kinetic steps of muscarinic receptor-mediated modulation of phosphoinositides and Kv7.2/7.3 K^+ channels. *J Gen Physiol* 133:347–359
 36. Willoughby D, Cooper DM (2008) Live-cell imaging of cAMP dynamics. *Nat Methods* 5:29–36
 37. Oancea E et al (1998) Green fluorescent protein (GFP)-tagged cysteine-rich domains from protein kinase C as fluorescent indicators for diacylglycerol signaling in living cells. *J Cell Biol* 140:485–498
 38. Tobin AB, Lambert DG, Nahorski SR (1992) Rapid desensitization of muscarinic m3 receptor-stimulated polyphosphoinositide responses. *Mol Pharmacol* 42:1042–1048
 39. Willars GB, Nahorski SR, Challiss RA (1998) Differential regulation of muscarinic acetylcholine receptor-sensitive polyphosphoinositide pools and consequences for signaling in human neuroblastoma cells. *J Biol Chem* 273:5037–5046
 40. Murray JM (2006) Confocal microscopy, deconvolution and structured illumination methods. In: Spector DL, Goldman RD (eds) *Basic methods in microscopy*. Cold Spring Harbor Laboratory Press, pp 43–81
 41. Nelson CP, Challiss RA (2011) The use of translocating fluorescent biosensors for real-time monitoring of GPCR-mediated signaling events. *Methods Mol Biol* 746:329–343
 42. Nelson CP et al (2008) Visualizing the temporal effects of vasoconstrictors on PKC translocation and Ca^{2+} signaling in single resistance arterial smooth muscle cells. *Am J Physiol Cell Physiol* 295:C1590–C1601
 43. Bartlett PJ et al (2005) Single cell analysis and temporal profiling of agonist-mediated inositol 1,4,5-trisphosphate, Ca^{2+} , diacylglycerol, and protein kinase C signaling using fluorescent biosensors. *J Biol Chem* 280:21837–21846
 44. Balla A et al (2008) Maintenance of hormone-sensitive phosphoinositide pools in the plasma membrane requires phosphatidylinositol 4-kinase III α . *Mol Biol Cell* 19:711–721

Chapter 11

Measurement of Inositol(1,4,5)Trisphosphate Using a Stereospecific Radioreceptor Mass Assay

Darren Smart

Abstract

Inositol(1,4,5)trisphosphate [$\text{Ins}(1,4,5)\text{P}_3$] is an important second messenger that activates its cognate $\text{Ins}(1,4,5)\text{P}_3$ receptor to release Ca^{2+} from intracellular stores. The assay described in this chapter uses the $\text{Ins}(1,4,5)\text{P}_3$ receptor (essentially as a binding protein) to measure the biologically active trisphosphate (specifically from other trisphosphates). The binding protein ($\text{Ins}(1,4,5)\text{P}_3$ receptor) is prepared from Bovine adrenal glands and this is mixed with [^3H]-labeled and unlabeled (generated from biological samples or standards) $\text{Ins}(1,4,5)\text{P}_3$. Using the same principles as for radioimmunoassay/ELISA the mass of $\text{Ins}(1,4,5)\text{P}_3$ in biological samples can be estimated.

Key words: Inositol phosphates, Inositol(1,4,5)trisphosphate, Radioreceptor assay

1. Introduction

Inositol(1,4,5)trisphosphate [$\text{Ins}(1,4,5)\text{P}_3$] is an intracellular second messenger that plays an important role in calcium homeostasis and, thus, many diverse cellular processes including neuronal signaling, smooth muscle contraction, fertilization, and sensory perception (1). $\text{Ins}(1,4,5)\text{P}_3$ formation is triggered by the activation of a wide variety of seven-transmembrane, G protein-linked receptors, e.g., muscarinic, glutamate, dopamine, and opioid receptors (1–3), as well as by the activation of the tyrosine kinase-linked growth factor receptors (1). $\text{Ins}(1,4,5)\text{P}_3$ is produced by the phospholipase C (PLC)-mediated hydrolysis of phosphatidylinositol 4,5-bisphosphate (1, 4), and is metabolized by 3-kinase and 5-phosphatase (5), with the actual intracellular concentration of $\text{Ins}(1,4,5)\text{P}_3$ being dependent on the balance between formation and metabolism. $\text{Ins}(1,4,5)\text{P}_3$ in turn binds to the $\text{Ins}(1,4,5)\text{P}_3$ receptor on the smooth endoplasmic reticulum, causing a conformational

change that opens the intrinsic calcium channel in the receptor, thus allowing the efflux of calcium ions from the intracellular stores (4). For further details, see the reviews by Berridge (1) and Furuichi and Mikoshiba (4).

Historically, $\text{Ins}(1,4,5,\text{P}_3)$ was measured in terms of total inositol polyphosphate turnover in the presence of lithium in cells that had been “loaded” with [^3H]inositol (6, 7). This technique was subsequently refined by using separation columns or high-pressure liquid chromatography to separate the various inositol polyphosphates and, even to some degree, their isomers (7–9). However, there are several significant disadvantages associated with these [^3H]inositol loading techniques. First, the main assumption of these techniques is that all pools of phosphoinositides are labeled to equilibrium under the assay conditions, yet there is very little experimental evidence for this (9). Second, it is almost inevitable that in [^3H]inositol-loaded cells, there would be some degree of agonist-induced changes in the specific radioactivity of the inositol trisphosphates (9). Third, these [^3H]inositol loading techniques do not take into account changes in the metabolism of $\text{Ins}(1,4,5,\text{P}_3)$. For example, in rat acinar cells depolarization with K^+ stimulates polyphosphoinositide hydrolysis without affecting $\text{Ins}(1,4,5,\text{P}_3)$ levels because of a simultaneous enhancement of 3-kinase-mediated $\text{Ins}(1,4,5,\text{P}_3)$ metabolism (10, 11). Finally, the [^3H]inositol-loading techniques are less likely to detect small, transient changes in $\text{Ins}(1,4,5,\text{P}_3)$ formation because they make only a minute contribution to total polyphosphate turnover, and this is masked by basal accumulation in the presence of lithium (2, 3, 11).

In 1988 Challiss et al. (9) published a paper that described a stereospecific radioreceptor assay for $\text{Ins}(1,4,5,\text{P}_3)$ mass. This assay was superior to the [^3H]inositol-loading protocols because it made no assumptions about the establishment of equilibrium of label in various pools of polyphosphoinositides, nor was it susceptible to agonist-induced changes in specific radioactivity (9). Furthermore, subsequent studies have shown that the radioreceptor assay also takes into account changes in $\text{Ins}(1,4,5,\text{P}_3)$ metabolism (10, 11), and is able to detect small, transient changes in $\text{Ins}(1,4,5,\text{P}_3)$ levels (2, 3, 11). This radioreceptor assay is based on the same simple principles as any other radioreceptor assay. The unlabeled $\text{Ins}(1,4,5,\text{P}_3)$ in the sample competes with a fixed amount of [^3H]-labeled $\text{Ins}(1,4,5,\text{P}_3)$ for a limited amount of a specific binding protein. The bound and free $\text{Ins}(1,4,5,\text{P}_3)$ are separated by rapid vacuum filtration, and subsequent measurement of the radioactivity in the assay tube enables the amount of unlabeled $\text{Ins}(1,4,5,\text{P}_3)$ in the sample to be determined by interpolation from a standard curve. The fundamental step in developing such an assay is the identification and purification of a suitable binding protein. Challiss et al. (9) used a relatively crude extract of the $\text{Ins}(1,4,5,\text{P}_3)$ receptor prepared from bovine adrenal cortex. This was a suitable binding protein

because the Ins(1,4,5)P₃ receptor displays the necessary high affinity and stereoselectivity for Ins(1,4,5)P₃, especially compared to Ins(1,3,4)P₃ (4, 9), and it is both abundant in and easily extracted from bovine adrenal cortex (9). Rat cerebellum was also tested as a potential source of the binding protein, but was found to give smaller yields with lower affinity (9).

In the remainder of this chapter we describe how the binding protein is prepared, how the Ins(1,4,5)P₃ is extracted from the samples, how the radioreceptor assay is performed, and how the data are processed. Furthermore, the common pitfalls and how to avoid or deal with them are described.

2. Materials

1. Ins(1,4,5)P₃ binding protein buffer (BP buffer): 20 mM NaHCO₃ and 1 mM dithiothreitol (DTT; see Note 1) in distilled water, pH 8.0 (see Note 2). Store at 4°C (see Note 3). Two liters of this buffer is sufficient to prepare ~100 mL of binding protein from 10 to 12 adrenal glands.
2. 10–12 fresh bovine adrenal glands (see Note 4).
3. 1 M trichloroacetic acid (TCA). This should be stored in a glass-stoppered bottle at 4°C for no longer than 3 months.
4. 10 mM EDTA in distilled water, pH 7.4. This should be stored at 4°C for no longer than 3 months.
5. Freon/Octylamine (F/O): 1:1 (v/v) mixture of 1,1,2-trichlorofluoroethane (Freon) and tri-*n*-octylamine, both of which are available from Aldrich, Poole, UK (see Note 5).
6. 25 mM sodium bicarbonate (NaHCO₃) in distilled water. This should be stored at 4°C for no longer than 3 months.
7. Stock Ins(1,4,5)P₃ standard: 1 mM d-myo-inositol-1,4,5-triphosphate hexasodium monohydrate (Research Biochemicals International, MA) in distilled water. Store in 20-μL aliquots at -20°C (see Note 6).
8. Stock [³H]Ins(1,4,5)P₃: This is obtained from Amersham (Braunschweig, Germany) at 10 μCi/mL. Store at -20°C for no longer than 4 weeks past the activity date.
9. Tris-EDTA (TE) buffer: 100 mM Tris-HCl and 4 mM EDTA in distilled water at pH 8.0. Store at 4°C; keeps virtually indefinitely.
10. Diluent: Mix 3 mL of Krebs/HEPES buffer (see Note 7), 3 mL of TCA, 1.25 mL of EDTA, and 3 mL of F/O. Vortex well and then centrifuge at 500 × *g* for 2 min at 4°C. This mixture will now have separated into two distinct phases (layers).

Take 5 mL of the upper phase and neutralize with 2.5 mL of NaHCO₃. The remainder of the upper phase as well as the lower phase should be discarded. The diluent should be made fresh on the day of use and then kept at 4°C.

11. Wash buffer: 25 mM Tris-HCl, 1 mM EDTA, 5 mM NaHCO₃ in distilled water, pH 7.8. This must be made fresh on the day of use and kept at 4°C. Two liter is sufficient for a 72-tube assay.
12. A Brandell cell harvester and Whatman GF/B filters (Fisons, Loughborough, UK).

3. Methods

3.1. Preparation of the Ins(1,4,5)P₃ Binding Protein

1. Take the adrenal glands, halve longitudinally, remove the medulla (see Note 8), and then scrape the cortex from the capsule (see Note 9).
2. Pool the cortex tissue in a 500-mL glass beaker, dilute 1 in 6 with ice-cold BP buffer, and homogenize thoroughly, taking care that there are no lumps of cortex left intact.
3. Centrifuge the homogenate at 2,000×*g* for 10 min at 4°C (see Note 10).
4. Carefully decant (see Note 11) and keep the supernatant. Store the supernatant at 4°C.
5. Rehomogenize the pellet in a minimum volume of BP buffer (see Note 12) and then centrifuge at 2,000×*g* for 10 min at 4°C. Decant (see Note 11) the supernatant and pool it with the supernatant from step 4. Discard the pellet.
6. Centrifuge the pooled supernatant at 20,000×*g* for 30 min at 4°C (see Note 13). A soft pellet will form at the bottom of the tube.
7. Carefully decant (see Note 11) the supernatant into fresh centrifugation tubes and store the pellet at 4°C. Recentrifuge the supernatant at 20,000×*g* for 30 min at 4°C (see Note 13). A smaller soft pellet will form at the bottom of the tube.
8. Repeat step 7.
9. Pool all the pellets and resuspend in BP buffer at ~30 mg/mL (see Note 14).
10. Then dispense the binding protein into 1-mL aliquots and store at -20°C until needed (see Note 15).

3.2. Sample Preparation

1. Incubate the relevant cells with the appropriate agonist for the required time (e.g., see ref. 3), in a final volume of 0.3 mL in polypropylene tubes (12×75 mm; Sarstedt, UK). Terminate

reactions by the addition of an equal volume (0.3 mL) of ice-cold 1 M TCA (see Note 16).

2. Next vortex the samples and centrifuge at $500 \times g$ for 10 min at 4°C.
3. Carefully decant the uppermost 500 μ L of the supernatant (see Note 17) into fresh polypropylene tubes. Discard the remaining supernatant and “pellet.”
4. Add 125 μ L of EDTA and 500 μ L of F/O to the supernatant, cap the tubes, vortex, and then centrifuge at $500 \times g$ for 2 min at 4°C. At the end of this process, the samples will have separated into two clearly delineated phases (layers).
5. Take 200 μ L of the upper phase, which contains the Ins(1,4,5) P₃, and place into fresh tubes. Neutralize this with 100 μ L of 25 mM NaHCO₃, cap, and vortex the tubes. Discard the remaining upper, as well as the lower, phase. The samples should be stored at 4°C for no longer than 1 week, and must not be frozen.

3.3. Radioreceptor Ins(1,4,5)P₃ Mass Assay

1. It is essential that the entire assay is carried out on ice. At the start of the assay, make up fresh wash buffer (see Subheading 2, item 11) and place in a refrigerator to cool.
2. Label the appropriate number of polypropylene tubes (12 \times 75 mm; Sarstedt), i.e., the relevant number of samples (single or in duplicate) and the standard curve, consisting of total counts (TOT), nonspecific binding (NSB), and six standards (std. 0.036, 0.12, 0.36, 1.2, 3.6, and 12 pmol tube) in duplicate. These labeled tubes should be placed in a Brandell harvester rack on ice at the start of the assay.
3. Thaw out the correct amount (1 mL/30 tubes) of binding protein (see Note 18).
4. Make up fresh diluent (see Subheading 2, item 10) and store on ice.
5. Dilute the stock Ins(1,4,5)P₃ standard with diluent in the following manner (see Note 19):
 - (a) NSB: 20 μ L of stock + 480 μ L of diluent.
 - (b) 12 pmol std: 10 μ L of NSB + 990 μ L of diluent.
 - (c) 3.6 pmol std: 100 μ L of 12 pmol std. + 200 μ L of diluent.
 - (d) 1.2 pmol std: 20 μ L of 12 pmol std. + 180 μ L of diluent.
 - (e) 0.36 pmol std: 20 μ L of 3.6 pmol std. + 180 μ L of diluent.
 - (f) 0.12 pmol std: 20 μ L of 1.2 pmol std. + 180 μ L of diluent.
 - (g) 0.036 pmol std: 20 μ L of 0.36 pmol std. + 180 μ L of diluent.

These standards should be stored on ice until pipetted into the relevant tubes, as described in step 9.

6. Prepare the working concentration of the tracer $\{[^3\text{H}]\text{Ins}(1,4,5)\text{P}_3\}$ by adding stock $[^3\text{H}]\text{Ins}(1,4,5)\text{P}_3$ to TE buffer at 15 $\mu\text{L}/\text{mL}$ (see Note 20). Allow 1 mL of tracer/30 tubes. Store on ice until used.
7. Pipet 30 μL of TE buffer into each of the labeled tubes in the Brandell harvester rack (see Note 21).
8. Pipet 30 μL of diluent into the two TOT tubes (see Note 21).
9. Pipet 30 μL of standard/sample into the appropriate tubes (see Notes 21 and 22).
10. Pipet 30 μL of the working concentration of $[^3\text{H}]\text{Ins}(1,4,5)\text{P}_3$ into each tube (see Notes 21 and 23).
11. Gently vortex all the tubes for a few seconds (see Note 24).
12. Pipet 30 μL of the binding protein into each tube (see Note 25).
13. Gently vortex all the tubes for a few seconds, and allow to incubate on ice for 40 min (see Note 26). At this point the total assay volume is 120 μL .
14. Filter on a Brandell cell harvester (Whatman GF/B filters) with the ice-cold wash buffer (see Note 27) to separate the bound and free $[^3\text{H}]\text{Ins}(1,4,5)\text{P}_3$. Each tube should receive two washes of ~3 mL, each in quick succession (see Note 28). The bound material will be clearly visible as a brown deposit on the filter (see Note 29).
15. The filters should be extracted overnight in a suitable scintillant, e.g., Optiphase Safe (Wallac, UK), and then counted in a β -counter for 3 min/tube.

3.4. Data Processing (See Note 30)

1. Calculate the average cpm for each standard, and sample if assayed in duplicate (see Note 31).
2. Calculate the percent bound for each standard and sample as follows:

$$\% \text{ Bound} = \frac{(\text{Standard or sample dpm} - \text{NSB dpm}) \times 100}{\text{TOT dpm} - \text{NSB dpm}}$$

3. The percent bound for the standards can then be plotted [against the relevant concentration of $\text{Ins}(1,4,5)\text{P}_3$] to generate a standard curve, using a suitable curve-fitting program (i.e., GraphPad Prism, CA) or by hand on semilog graph paper. Then, using the relevant percent bound values, the concentrations of $\text{Ins}(1,4,5)\text{P}_3$ in the samples can be “read off” this curve.

4. Notes

1. DTT is harmful and should therefore be handled with all due care. However, its inclusion is essential or the binding protein will rapidly become degraded.
2. Although ideally this buffer should be at pH 8.0, any pH in the range 7.9–8.1 is acceptable.
3. This buffer should be prepared on the day of use, but can be used on the following day if stored at 4°C. Do not store for longer than 24 h prior to use.
4. These are obtained from an abattoir and can come from cattle of any age or either sex. Most abattoirs will allow direct dissection of the adrenal gland, and many will cut out the glands for a small fee. However, it should be borne in mind that the vast majority of abattoir workers do not know what the adrenal gland looks like or where it is located and, therefore, are likely to provide the wrong material. It is preferable to collect intact glands, but “bits” of gland, when the gland has been damaged during the butchery of the cattle, can still be used. The glands must be “fresh,” i.e., collected as soon as possible after the cattle have been slaughtered, and must not be frozen. It is best to minimize the delay between the removal of the glands and the preparation of the binding protein, but if this delay is likely to exceed 2 h, the glands (wrapped in a plastic bag) need to be transported on ice.
5. Care should be taken when handling these chemicals and their mixture, as they are potent irritants. The F/O mixture should be made up just prior to use and, being somewhat unstable, cannot be stored for more than a couple of hours. Furthermore, exposure to the F/O mixture does cause some plastics to become extremely brittle, hence the reason that sample preparation and the assay are conducted in polypropylene tubes.
6. The stock $\text{Ins}(1,4,5)\text{P}_3$ standard must not be thawed and then refrozen, as this causes significant breakdown of the standard, leading to high NSB values and a poor-quality standard curve. The stock standard still degenerates slowly even when frozen and thus should be discarded after 2 months.
7. Or, whatever physiological buffer the cell incubations were performed in can be used.
8. The medulla is the “off-white” material in the center of the adrenal gland, and is best removed by pulling it gently upward with a pair of forceps while cutting it away from the underlying cortex using a pair of fine-dissecting scissors. It is essential to remove as much of the medulla as possible to minimize NSB.

9. The cortex is the reddish-brown material that surrounds the medulla, and is easily scrapped from the semitransparent, tough outer membrane or capsule, using a small metal spatula.
10. It is essential from this moment on that the crude binding protein is kept at 4°C. If all the material in a given step cannot be handled at once, then store any excess on ice or in the refrigerator, until the material can be dealt with.
11. This is best done using a long, fine-pointed, disposable glass pipet, and care must be taken not to suck up any of the pellet. If any of the pellet is decanted, then the pipet and its contents should be discarded, rather than risk contaminating the rest of the supernatant.
12. If there is still material from step 2 waiting to be rehomogenized, then use this, rather than the BP buffer, to resuspend the pellet. However, note that if this is done then the subsequent pellet will still need to undergo step 5, as part of this pellet has not been washed twice.
13. Alternatively, centrifuge at $40,000 \times g$ for 20 min at 4°C.
14. The protein content of the combined pellets resuspended in a minimum volume of BP buffer should be measured using a suitable assay (e.g., Folin-Lowry) prior to the full resuspension. In general, 10–12 adrenal glands should yield ~80 mL of binding protein.
15. The binding protein can be thawed and refrozen once, but repeated freeze/thaw cycles should be avoided. The binding protein will keep for ~6 months at -20°C, although it should be noted that the binding protein will gradually degrade over this period, causing the total binding to fall and the NSB values to rise.
16. Once the TCA has been added, the sample can be stored at 4°C for up to 1 h prior to undergoing the rest of the extraction procedure. This allows “batching” of the samples and thus more effective time management.
17. If using a Gilson pipet to decant the supernatant, it is advisable to first remove the waste tip dispeller.
18. Allow the binding protein to thaw slowly. Do not heat the frozen binding protein in a water bath or by other means, as this causes considerable degradation of the binding protein, leading to high NSB values.
19. The standards and NSB are made at these concentrations to obtain the correct final concentrations in the assay, in which there is a 1 in 4 dilution factor.
20. The appropriate procedures for handling radioactivity should be used at all times. The dilution of 15 µL of stock/mL of TE buffer is based on the assumption that the specific activity of

the stock [^3H]Ins(1,4,5)P₃ is ~40 Ci/mmol. If the specific activity is significantly higher, add proportionally less stock/mL; if the specific activity is significantly lower, then add proportionally more stock/mL.

21. Remember to do all pipetting into the tubes while the tubes are still on ice. Furthermore, care must be taken when pipetting as the volumes involved are very small. The most common problem is drops of the assay components sticking to the sides of the tube. These can be brought down by gently tapping the base of the tube, or by using a fine disposable pipet to blow the drops down.
22. NSB tubes receive 30 μL of the NSB “standard” made in step 5 of Subheading 3.3.
23. All due care should be maintained when pipetting radioactive material.
24. This step is essential for obtaining a smooth standard curve (see Note 31). If there are any drops on the sides of the tubes, then these must be brought down prior to vortexing (see Note 21).
25. Particular care must be taken when pipetting out the binding protein. The aliquot of binding protein being used must be vortexed frequently (approximately every minute) to keep the binding protein uniform. Furthermore, as the binding protein is very viscose, it is particularly prone to sticking to the sides of the assay tubes (see Note 21).
26. Timing of this step is crucial. If the incubation is too short, equilibrium will not have been achieved and there will be a far greater degree of intra-assay variability. On the other hand, if the incubation is too long, there is a tendency toward increased NSB values. Forty minutes is optimal, but anywhere between 38 and 50 min is acceptable.
27. It is advisable to wash the first filter with the wash buffer prior to harvesting the samples. Care must be taken to ensure that the filters are fitted properly to avoid leaking.
28. Do not overfill (more than 3/4) the tubes, or there will be a risk of overflow and the associated loss of material. Be aware that not all tubes will fill at the same rate.
29. If the deposit is somewhat “faded” (i.e., sandy rather than brown) in color, this indicates that the binding protein is not concentrated enough. This is inevitably associated with low total counts (see Note 31). If this occurs, concentrate the remaining binding protein prior to its use by centrifuging the thawed binding protein at $5,000 \times g$ for 15 min at 4°C and then pipetting off 250 μL of the “clear” supernatant. Vortex vigorously to resuspend the binding protein.
30. Most modern counters have packages on them that will automatically plot the standard curve and calculate the sample values.

Table 1
Common assay problems and their causes

Problem	Possible cause
High NSB (>10%)	<ul style="list-style-type: none"> The stock [³H]Ins(1,4,5)P₃ may have degraded. This is usually associated with a low TOT cpm The stock standard may have degraded. This is usually associated with a distorted standard curve Binding protein may have degraded. This is usually associated with all tubes having low cpm
All tubes have low cpm	<ul style="list-style-type: none"> The binding protein has degraded (associated with high NSB) or is too dilute (see Note 29) The tracer is too dilute (see Note 20) or has degraded (usually associated with high NSB)
Standard curve is distorted	<ul style="list-style-type: none"> Stock standard has degraded (associated with high NSB) or has been diluted incorrectly Step 11 of Subheading 3.3 has not been performed
Standards have low cpm, but samples are normal TOT > 2,500 dpm	<ul style="list-style-type: none"> Standards were incorrectly diluted, or have degraded (associated with high NSB) This is often associated with a shallow standard curve Tracer has been incorrectly diluted (see Note 20)

31. Ideally TOT should lie in the range of 1,000–2,500 dpm and the NSB should be 5–10%. This is the stage at which most assay problems will become apparent. Table 1 describes the most common problems and their usual causes. However, it should be borne in mind that other factors will also affect assay performance, most notably temperature and pH. Therefore, at all times it is essential to ensure that the assay is performed on ice, that dilutions are made correctly, and that all the buffers are at the optimal pH.

References

- Berridge MJ (1993) Inositol trisphosphate and calcium signalling. *Nature* 361:315–325
- Smart D, Smith G, Lambert DG (1994) Halothane and isoflurane enhance basal and carbachol-stimulated inositol(1,4,5)triphosphate formation in SH-SY5Y human neuroblastoma cells. *Biochem Pharmacol* 47:939–945
- Smart D, Smith G, Lambert DG (1994) μ -Opioid receptor stimulation of inositol(1,4,5)trisphosphate formation via a pertussis toxin-sensitive G protein. *J Neurochem* 62: 1009–1014
- Furuichi T, Mikoshiba K (1995) Inositol 1,4,5-trisphosphate receptor-mediated Ca²⁺ signaling in the brain. *J Neurochem* 64:953–960
- Shears SB (1989) Metabolism of the inositol phosphates upon receptor activation. *Biochem J* 260:313–324
- Kendall DA, Nahorski SR (1984) Inositol phospholipid hydrolysis in rat cerebral cortical slices: II. Calcium requirement. *J Neurochem* 42:1388–1394
- Wojcikiewicz RJH, Lambert DG, Nahorski SR (1990) Regulation of muscarinic agonist-induced

- activation of phosphoinositidase C in electrically permeabilized SH-SY5Y human neuroblastoma cells by guanine nucleotides. *J Neurochem* 54: 676–685
8. Yu VC, Sadee W (1986) Phosphatidylinositol turnover in neuroblastoma cells: regulation by bradykinin, acetylcholine, but not μ and δ opioid receptors. *Neurosci Lett* 71:219–223
9. Challiss RAJ, Batty IH, Nahorski SR (1988) Mass measurements of inositol(1,4,5)trisphosphate in rat cerebral cortex slices using a radioreceptor assay: effects of neurotransmitters and depolarization. *Biochem Biophys Res Commun* 157:684–691
10. Zhang GH, Melvin JE (1993) Membrane potential regulates Ca^{2+} uptake and inositol phosphate generation in rat sublingual mucous acini. *Cell Calcium* 14:551–562
11. Smart D, Wandless A, Lambert DG (1995) Activation of phospholipase C in SH-SY5Y neuroblastoma cells by potassium-induced calcium entry. *Br J Pharmacol* 116:1797–1800

Part V

Specialist Measurement Techniques

Chapter 12

Measurement of $[Ca^{2+}]_i$ in Smooth Muscle Strips Using Front-Surface Fluorimetry

Hideo Kanaide and Katsuya Hirano

Abstract

Changes in the cytosolic Ca^{2+} concentrations ($[Ca^{2+}]_i$) play a primary role in the regulation of the contraction of smooth muscle cells. However, the relationship between $[Ca^{2+}]_i$ and tension exhibits a temporal change during the time course of contraction or relaxation. The extent of the tension development for a given change in $[Ca^{2+}]_i$ also varies depending on the type of contraction and relaxation. Therefore, it is essential to measure $[Ca^{2+}]_i$ and tension simultaneously in order to determine the molecular and cellular mechanisms in both the regulation of contraction and relaxation of smooth muscle. This chapter provides the basic principles of the technique of front-surface fluorimetry as well as the protocols and tips for the simultaneous measurement of $[Ca^{2+}]_i$ and tension in the smooth muscle tissues with use of fura-2 or Fura-PE3 as fluorescent Ca^{2+} indicators. The loading of sufficient amount of the Ca^{2+} indicators in smooth muscles is essential for the successful measurement of $[Ca^{2+}]_i$ with minimum optical artifacts. The protocol gives our practice for the loading of the Ca^{2+} indicators in various smooth muscle tissues.

Key words: Calcium, Contraction, Front-surface fluorimetry, Smooth muscle

1. Introduction

In regulating the contraction of smooth muscle cells, changes in the cytosolic concentrations of Ca^{2+} ($[Ca^{2+}]_i$) play a primary role as the initiation of contraction is associated with Ca^{2+} binding to calmodulin with the subsequent activation of myosin light chain kinase. During the contraction induced by receptor-mediated stimulation, however, there are temporal changes in the relationship between $[Ca^{2+}]_i$ and the developed tension. Furthermore, the receptor-mediated stimulation also produces a proportionately greater tension for a given change in $[Ca^{2+}]_i$ than does K^+ depolarization. Therefore, it is important to measure $[Ca^{2+}]_i$ and tension simultaneously in order to determine the molecular and cellular mechanisms in both the regulation of contraction and relaxation

of smooth muscle. For this purpose, front-surface fluorimetry of fura-2, a $[Ca^{2+}]_i$ indicator dye (1), has been performed on small smooth muscle strips (2, 3).

The technique of front-surface fluorimetry is commonly used for measuring tissue fluorescence. The first and, so far, the only successful technique known to monitor the naturally occurring fluorescence of intact tissue in surface fluorimetry was developed by Chance et al. (4). Using surface fluorimetry and a perfused rat heart, they reported the depth of penetration of excitation light (366 nm), and hence the detection of fluorescence (460 nm), to be 0.4 mm, and studied the kinetics of mitochondrial flavoprotein and the reduced form of pyridine nucleotide in the myocardium. They also developed a front-surface fluorimeter utilizing a bifurcated fiber-optic light source to perform surface fluorimetry of the kidney (5). The underlying principle of front-surface fluorimetry is simple: the closer the distance between the excitation light source (and also the detector) and the object, the easier and more accurate the detection of the emission light becomes.

In the author's front-surface fluorimeter, concentric optic fibers are used: the excitation light is guided through quartz optic fibers arranged in an inner circle, and emission light is collected by glass optic fibers arranged in an outer circle. By preparing small-sized specimens of smooth muscle strips, the entire front surface of the sample can be illuminated, and almost the whole fluorescence signal from the front surface can be detected by the use of concentric optic fibers placed close to the sample.

One of the advantages of using a fura-2 signal is the ratiometric measurement of two excitation wavelengths, which cancels the parallel changes in the intensities of the two emitted light signals induced by the moving artifact produced by the contraction, shortening, or torsion of the sample, and changing or bubbling of the solutions. In addition, since the emitted light from the entire front surface of the sample strip is detected by these confronted optical fibers, the amount of the observed fura-2 dye is thus kept constant, while any possible artifact owing to the movement or changing shape of the strips during contraction is eliminated as far as possible. Therefore, the signals obtained of front-surface fura-2 fluorescence simply indicate the changes in $[Ca^{2+}]_i$ of the smooth muscle cells and not the artifacts owing to either the contraction or movement of the smooth muscle strips.

2. Materials

1. $[Ca^{2+}]_i$ indicator dyes: These dyes are all directly purchased in special packaging from the manufacturers. Fura-2/AM (mol wt = 1,002; an acetoxyethyl [AM] form of fura-2) is from

Invitrogen (Carlsbad, CA) and Dojindo Laboratory (Kumamoto, Japan), and fura-PE3/AM (mol wt=1,258) is from TEFLABS (Austin, TX). Small plastic tubes in special packaging contain either fura-2/AM or fura-PE3/AM dry powder, 50 µg each, and are stored at -20°C.

2. Fura-2 loading buffer: Oxygenated (bubbling with a mixture of 95% O₂ and 5% CO₂), Dulbecco's modified Eagle's medium (Invitrogen) containing fura-2/AM (or fura-PE3/AM), 5% inactivated fetal bovine serum (FBS) (Invitrogen), and whenever necessary, pluronic F127 (TEFLABS), cremophor EL (Sigma, St. Louis, MO), and/or probenecid (Sigma), as shown in Table 1.
3. Normal physiological salt solution (PSS): 123 mM NaCl, 4.7 mM KCl, 15.5 mM NaHCO₃, 1.2 mM KH₂PO₄, 1.2 mM MgCl₂, 1.25 mM CaCl₂, and 11.5 mM d-glucose. Ca²⁺-free PSS contains 2 mM EGTA instead of CaCl₂. High-K⁺ PSS is of the same composition as normal PSS, except for the equimolar substitution of KCl for NaCl.
4. Quartz organ bath: A quartz cuvette (5 mL; 1×1×5 cm) is used. Three faces of the cuvette are covered with a quartz water jacket to maintain the experimental temperature, whereas one free face of the cuvette is used for surface fluorimetry.
5. Force transducer: TB-612 T (Nihon Koden, Tokyo, Japan).
6. Front-surface fluorimeter (CAM-OF-3) (2, 3, 6):
 - (a) Fluorimeter: In collaboration with the Japan Spectroscopic Co. (JASCO, Tokyo, Japan) dual-wavelength excitation microscopic fluorimeter on the market, a CAM-230 2-λ Microscopic fluorimeter (JASCO) is remodeled into the front-surface fluorimeter, CAM-OF-3. The remodeling involves the conversion of the connection of dual-wavelength excitation fluorimeter to a fluorescence microscope to a configuration with a fiber-optic light guide.
 - (b) Optic fibers: In collaboration with FUJITOK Co. (Tokyo, Japan), the fiber-optic light guide Optical Assy 800 (FUJITOK) is specifically designed and made for front-surface fluorimetry. The light guide utilizes a bifurcated fiber-optic light source with quartz fibers (95 fibers [330–340-µm diameter × 500-mm length, ST200D-S]) in one branch and glass fibers (250 fibers [300–310-µm diameter × 800-mm length, S0-230/250-50FE]) in the other branch. Fibers are concentrically arranged at the common end, which faces the samples. The quartz fibers are arranged in an inner circle (3 mm diameter) whereas the glass fibers are arranged in an outer circle (7 mm diameter) at the common end.
 - (c) Photomultiplier, R-268 (Hamamatsu Photonics, Shizuoka, Japan) is utilized.

Table 1
Conditions for fura-2 loading on smooth muscle cells^a

Species	Smooth muscle	Concentrations of fura-2/AM (μM)	Incubation time (h)	Other additions
Human	Umbilical artery	50	4	–
	Urinary bladder	25	6	–
	Cultured coronary cells	10	1	–
Bovine	Mid-cerebral artery	50	4	–
	Ophthalmic artery	50	4	–
	Coronary artery	50	4	–
	Pedal artery	50	4	–
Pig	Coronary artery	25	4	–
	Pulmonary artery	25	4	–
	Pulmonary vein	25	4	–
	Renal artery	50	4	–
	Trachea	50	4	–
	Urinary bladder	40 ^b	6	0.1% Pluronic F127
	Cultured coronary cells	10	1	–
Rabbit	Basilar artery	10	3	–
	Ear artery	40 ^b	4	–
	Femoral artery	50	4	–
	Saphenous vein	40 ^b	6	0.1% Pluronic F127
	Vein graft	40 ^b	6	0.1% Pluronic F127
	Urinary bladder	50 ^b	7	–
	Corpus cavernosum	50 ^b	7	–
Rat	Basilar artery	25	3	–
	Aorta	25	3	0.08% Cremophor EL, 1 mM probenecid
	Myometrium	40 ^b	6	0.1% Pluronic F127
	Cultured aortic cells	10	1	–
Mouse	Aorta	50 ^b	3	1 mM Probenecid
Guinea pig	Taenia coli	50 ^b	8	0.02% Pluronic F127

^aFBS (5%) is added to all loading solutions and temperature is 37°C

^bInstead of fura-2/AM, fura-PE3 is utilized

- (d) A block diagram of front-surface fluorimetry using CAM-OF-3 is shown in Fig. 1. Dual-excitation light (340 nm, 380 nm) is obtained using two spectrometers from a 150-W Xenon light source. Using a chopper wheel, the excitation light is then alternately (400 Hz) guided through quartz optic fibers and directly illuminates the sample strip (5 mm length \times 1 mm width \times 0.1 mm thickness). The fluorescence of the entire front surface is

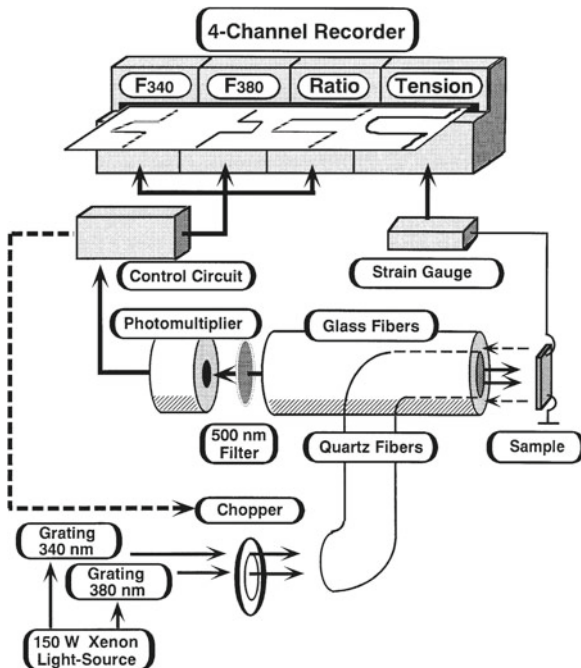


Fig. 1. A block diagram of the front-surface fluorimetry for fura-2 using CAM-OF-3.

collected by glass fibers and introduced through a 500-nm band-pass filter into a photomultiplier. The ratio of the fluorescence intensities at 340 nm (F340) and 380 nm (F380) excitation, F340/F380, is monitored.

7. Recordings: All data (F340, F380, F340/F380, and tension) are recorded using a computerized data acquisition system (MacLab, Analog Digital Instruments, Castle Hill, Australia; Macintosh, Apple computer, Cupertino, CA), which enables the $[Ca^{2+}]_i$ -tension relationship of smooth muscle contraction and relaxation to be studied.
8. To take fluorescent microphotographs of the smooth muscle strips stained with fura-2, a fluorescence microscope (Axioskop, Zeiss, Germany), equipped with a water-immersion objective system (Plan-Neofluor 40, Zeiss) and appropriate combinations of filters (BP 340 for excitation light and BP 500–530 for fluorescence), is utilized.

3. Methods

3.1. Fura-2 Loading

1. Prior to each measurement, dissolve either 50 µg of fura-2/AM or fura-PE3/AM powder in 50 µL of dimethyl sulfoxide (DMSO), then dilute with fura-2 loading solution (with the

final concentration of DMSO ranging from 1 to 5%), and utilize only once.

2. Incubate smooth muscle strips in oxygenated fura-2 loading buffer using the conditions shown in Table 1. Fura-2 (or fura-PE3) loading for smooth muscle cells varies depending on the species and organ.
 3. After loading with fura-2, incubate the smooth muscle strips in normal PSS for at least 1 h before starting the measurements in order to remove the dye in the extracellular space and for the purpose of equilibration (see Notes 1 and 2).
- 3.2. Measurement of Isometric Tension Development**
1. Perform the simultaneous determination of the tension and $[Ca^{2+}]_i$ of the smooth muscle strips at 37°C.
 2. At the beginning of the fura-2 equilibration period, mount the strip vertically and connect to a force transducer in a quartz organ bath.
 3. During this period, stimulate the strip with 118 mM K⁺ PSS every 15 min and increase the resting tension in a stepwise manner until levels that will induce the maximal tension development are reached (see Note 3).
 4. Record the responsiveness to 118 mM K⁺ PSS before the start of each experimental protocol. The developed tension is expressed in percentages, assuming the values in normal PSS (5.9 mM K⁺) to be 0%, and in 118 mM K⁺ PSS to be 100%.

3.3. Front-Surface Fluorimetry

1. To minimize background fluorescence owing to any possible extraneous signals, fluorimetry must be performed in a dark-room (see Notes 4 and 5).
2. Using front-surface fluorimetry, simultaneously monitor changes in the fluorescence emission (F340, F380, and their ratio, F340/F380) from the entire front surface and tension development of fura-2-loaded smooth muscle strips (see Note 6).
3. The fluorescence ratio (F340/F380) is utilized as an index of $[Ca^{2+}]_i$, and is expressed as a percentage, assuming the values in normal (5.9 mM K⁺) and 118 mM K⁺ PSS to be 0% and 100%, respectively. The determination of the 100% levels of tension and fluorescence ratios is performed at the same time just prior to the start of the experimental protocol (see Note 7).
4. Estimate the absolute values of $[Ca^{2+}]_i$ for the 0% (5.9 mM K⁺) and 100% levels (at the steady state of the contraction induced by 118 mM K⁺ depolarization) of the fluorescence ratio (F340/F380) using separate measurements as follows: After recording the 100% levels of F340/F380 induced by the depolarization with 118 mM K⁺ PSS, apply ionomycin (final concentration: 5 μM for rat aorta, and 25 μM for the porcine coronary artery).

Thereafter, F340 further increases until reaching plateau levels ($F_{340_{max}}$). The solution is then changed to Ca^{2+} -free PSS, and F340 gradually decreases until reaching a steady state ($F_{340_{min}}$). $[Ca^{2+}]_i$ is calculated according to the following equation, which is the calibration equation for fura-2 using intensity values (F340) at only one wavelength:

$$[Ca^{2+}]_i = K_d(F - F_{min}) / (F_{max} - F), \quad (1)$$

in which K_d is the apparent dissociation constant for Ca^{2+} at 37°C and is assumed to be 224 nM (1), F is the fluorescence signal of F340 expressed in percent, and F_{min} and F_{max} are $F_{340_{min}}$ and $F_{340_{max}}$, respectively. F at 5.9 mM K^+ and at 118 mM K^+ depolarization are assigned to be 0 and 100%, respectively. Thus, the $[Ca^{2+}]_i$ levels at $F=0\%$ and $F=100\%$ are assigned to be those at the fluorescence ratios (R ; F340/F380) of 0 and 100%, respectively (see Note 8).

4. Notes

1. To show evidence that fura-2 is almost exclusively and homogeneously loaded in smooth muscle cells, it is recommended that fluorescence photomicrographs be taken of the sample using a fluorescence microscope (Axioskop).
2. The incubation time and the concentration of fura-2/AM for fura-2 loading appear to be long and excessive in comparison to those reported by other workers (Table 1). However, these are the most appropriate conditions to obtain reliable recordings. Under these conditions, the intracellular fura-2 concentration is expected to be approx 13 μM , and the inhibition of tension development owing to Ca^{2+} -buffering action of fura-2 is not recognized (6). The exclusive and homogeneous staining of smooth muscle cells with fura-2 can be confirmed by taking fluorescence photomicrographs. The insufficient loading of smooth muscles with fura-2/AM at its lower concentration or shorter incubation time frequently induces a smaller fluorescence signal with greater optical artifacts during measurements. For easier and homogeneous loading of fura-2, FBS, pluronic F127, cremophor EL, or probenecid (7) are used either alone or in various combinations (8) (Table 1).
3. In proximal coronary arterial strips ($5 \times 1 \times 0.1$ mm) of the pig, an appropriate resting tension is approx 250 mg.
4. Background fluorescence: To avoid possible extraneous contamination of the signal the strip is suspended in a quartz organ

bath and the measurements are performed in a darkroom. In addition, ratiometry continuously negates parallel changes in intensities of F340 and F380. Background fluorescence, if any, is always subtracted.

5. The nature of the autofluorescence of the tissue is pyridine nucleotide (reduced form), flavoproteins, or cytochromes, and is essentially related to energy metabolism. The population of mitochondria is so small that the absorbance of excitation light or the fluorescence by these naturally occurring pigments is negligible in smooth muscle cells. In addition, the extinction coefficient and fluorescence quantum yield of fura-2 are so high that autofluorescence of the tissue is easily overcome.
6. With concentric optic fibers, which have a 3-mm quartz inner circle and a 7-mm glass outer circle at the common end, the most suitable distance between the optical fibers and the strip is approx 8 mm. The shorter the distance, the greater the excitation light and, hence, the emission signal. However, it must be noted that a greater intensity of excitation (ultraviolet) light may also cause a greater degree of tissue injury and photobleaching of the fluorescence dye, which will disturb the experiments over a long time course. Furthermore, if the distance is too close and the common end comes into contact with the strip, the emission from the area of the strip overridden by the inner circle cannot be detected by the outer circle. Thus, the distance and the angle between the common end of the optical fibers and the strip are adjusted to the most appropriate for each measurement. This is one of the most important principles regarding front-surface fluorimetry.
7. The absolute values of the fluorescence ratio, F340/F380, for the fura-2–Ca²⁺ complex cannot be obtained when CAM 230 is utilized, because this fluorimeter is essentially designed for use in microscopic fluorimetry. The fluorescence intensities are not normalized by the intensity of the excitation light, which directly correlate with the intensities of the 340 or 380 nm signal of the xenon light source. The spectrum of the xenon light source indicates that the intensity of excitation light at 380 nm is much greater (approximately three times) than that at 340 nm. To perform ratiometry with a good balance of excitation between 340 and 380 nm, i.e., to make the F340/F380 reach approx 1 at rest (0%), a combination of appropriately sized metal-optical slits placed in both excitation light paths, in front of and after the grating spectrometers, is used. To estimate the changes in [Ca²⁺]_i in the experimental protocols, it is not essential to obtain the absolute values of F340/F380.
8. Estimation of the absolute values of [Ca²⁺]_i:
 - (a) The absolute values of [Ca²⁺]_i are estimated in separate measurements: In prolonged experimental protocols,

although the changes in fluorescence ratio to certain stimulations (such as to high K^+ depolarization) are well maintained, the responsiveness of the strips to ionomycin varies depending on the time course of the experimental protocols, and, thus, great variations in the calculated absolute values of $[Ca^{2+}]_i$ are observed. Therefore, it is not recommended to express the $[Ca^{2+}]_i$ levels with absolute $[Ca^{2+}]_i$ values calculated at the end of each experiment. Only for approximation purposes are the absolute values of $[Ca^{2+}]_i$ at the 0 and at 100% levels of the fluorescence ratio determined in separate measurements. In porcine coronary arterial smooth muscle cells, $[Ca^{2+}]_i$ at the 0 and 100% levels correspond to approx 100 and 900 nM, respectively.

- (b) Ionomycin induces an increase in the fluorescence signal in a concentration-dependent manner. The maximum response is obtained with 5 and 25 μM ionomycin in rat aorta (9) and porcine coronary artery, respectively.
- (c) Grynkiewicz et al. (1) described the following equation to determine the absolute values of $[Ca^{2+}]_i$ in ratiometry:

$$[Ca^{2+}]_i = K_d(R - R_{\min}) / (R_{\max} - R)(S_{f2} / S_{b2}), \quad (2)$$

where K_d is a dissociation constant and R is the fluorescence ratio ($F340/F380$). R_{\max} is obtained by the addition of ionomycin in normal PSS (saturating Ca^{2+}), and R_{\min} is obtained in Ca^{2+} -free PSS (zero Ca^{2+}). S_{f2}/S_{b2} is the ratio of proportionality coefficients of free fura-2 and Ca^{2+} -bound fura-2 at 380 nm, which is influenced by various optical factors, including excitation intensity, path length, and instrumental efficiency. Therefore, in front-surface fluorimetry using optic fibers, the S_{f2}/S_{b2} values vary depending on the relation between the optic fibers and strips, even though they can be kept constant for each measurement. Since F380 is not stable at the time when F340 reaches $F340_{\max}$ and $F340_{\min}$, the recordings of R_{\max} and/or R_{\min} often appear to be difficult, and hence $[Ca^{2+}]_i$ cannot be determined. Equation 1 is thus considered to be the most appropriate for determining the absolute values of $[Ca^{2+}]_i$.

- (d) Equation 2 is closely analogous to Eq. 1. From these two equations, the following form is obtained:

$$(F - F_{\min}) / (F_{\max} - F) = (R - R_{\min}) / (R_{\max} - R)(S_{f2} / S_{b2}).$$

The S_{f2}/S_{b2} value can be adjusted to 1 by changing the optical slits in the light paths and/or by changing the relative

positioning between the common end of the optic fibers and the strip. Empirically, in the range between $F=0\%$ ($R=0\%$) and $F=100\%$ ($R=100\%$), the following equation is obtained:

$$(F - F_{\min}) / (F_{\max} - F) \approx (R - R_{\min}) / (R_{\max} - R).$$

Thus, in the physiological range of changes in $[Ca^{2+}]_i$, one can employ the following equation to calculate the absolute values of $[Ca^{2+}]_i$:

$$[Ca^{2+}]_i \approx K_d (R - R_{\min}) / (R_{\max} - R). \quad (3)$$

It has been noted, however, that the $[Ca^{2+}]_i$ values obtained are only an approximation of true $[Ca^{2+}]_i$ values.

References

- Grynkiewicz G, Poenie M, Tsien RY (1985) A new generation of Ca^{2+} indicators with greatly improved fluorescence properties. *J Biol Chem* 269:3440–3450
- Hirano K, Kanaide H, Abe S, Nakamura M (1990) Effects of diltiazem on calcium concentrations in the cytosol and on force of contractions in porcine coronary arterial strips. *Br J Pharmacol* 101:273–280
- Abe S, Kanaide H, Nakamura M (1990) Front-surface fluorometry with fura-2 and effects of nitroglycerin on cytosolic calcium concentration and on tension in the coronary artery of the pig. *Br J Pharmacol* 101:545–552
- Chance B, Salkovitz IA, Kovach AGB (1972) Kinetics of mitochondrial flavoprotein and pyridine nucleotide in perfused heart. *Am J Physiol* 223:207–218
- Frank H, Barlow CH, Chance B (1976) Oxygen delivery in perfused rat kidney: NADH fluorescence and renal function state. *Am J Physiol* 231:1082–1089
- Miyagi Y, Kobayashi S, Nishimura J, Fukui M, Kanaide H (1995) Resting load regulates vascular sensitivity by a cytosolic Ca^{2+} -insensitive mechanism. *Am J Physiol* 268:C1332–C1341
- Di Virgilio F, Steinberg TH, Swanson JA, Silverstein SC (1988) Fura-2 secretion and sequestration in macrophages: a blocker of organic anion transport reveals that these processes occur via a membrane transport system for organic anions. *J Immunol* 140:915–920
- Watanabe C, Yamamoto H, Hirano K, Kobayashi S, Kanaide H (1992) Mechanisms of caffeine-induced contraction and relaxation of rat aortic smooth muscle. *J Physiol* 456:193–213
- Watanabe C, Yamamoto H, Kobayashi S, Kanaide H (1993) Extracellular Ca^{2+} -dependent potentiation by cocaine of serotonin- and norepinephrine-induced contractions in rat vascular smooth muscle. *Circ Res* 72:1191–1201

Chapter 13

Calcium Measurements from Whole Heart Using Rhod-2

Bum-Rak Choi

Abstract

Calcium recording from whole heart is an important technique to investigate role of calcium in cardiac arrhythmias. Intracellular calcium can be recorded from multiple locations using imaging devices and organic dyes or genetic probe (Tallini et al. PNAS 103(12):4753–4758, 2006) from whole heart. Here, we describe the optical apparatus and the method to record intracellular calcium transients.

Key words: Optical mapping, Calcium transients, Action potentials, Rhod-2, RH237, Whole heart, Calibration

1. Introduction

Anomalies in calcium handling have been linked to many pathological conditions and cardiac arrhythmias such as atrial fibrillation (1, 2), ventricular fibrillation (3, 4), heart failure (5, 6), myocardial infarction (7, 8), and ischemia/reperfusion (9). Spontaneous calcium release can directly cause triggered activity such as early/delayed afterdepolarizations (10–13) and calcium alternans (14–20) can cause action potential alternans, increasing the risk of conduction blocks and reentry formation. It is important to point out that heart in nature has complex 3D structure and heterogeneous calcium handling can be a major source of arrhythmia. Calcium measurement from whole heart is, therefore, a necessary step to investigate arrhythmia mechanisms in many pathological cases. It is often required to measure action potentials simultaneously to understand relationship between calcium and action potentials and recent progresses in high-speed high-sensitive cameras make it possible to record superior quality of calcium and action potentials from multiple locations and map their propagations and dynamic features of calcium and voltage interactions.

Several calcium dyes have been used to record calcium transients from intact hearts, Indo-1 (20, 21), Fura-Red (22), and Rhod-2 (3, 12, 23–25). Each dye has advantages and disadvantages and should be used based on experimental goals. Among those, Rhod-2 has relatively higher K_d value (~720 nM), and can be excited at 540 nm, which is visible range and has less tissue scattering and absorption by tissue than UV excitation. Unlike ratiometric dyes, the calibration of single-wavelength dye such as Rhod-2 needs greater caution to consider background changes and dye leaks. This chapter introduces calibration procedure of calcium recording and analysis routines, and describes two important parts of calcium measurements from whole heart, perfusion system, and optical apparatus.

2. Materials

2.1. General Reagents

1. Rhod-2/AM, 1 mg, cell-permeable (Invitrogen, Carlsbad, CA). Make a stock solution of Rhod-2 by dissolving 1 mg of Rhod-2 in 1 ml of dimethylsulfoxide and store in a freezer (-20°C).
2. RH237, 5 mg (Invitrogen, Carlsbad, CA). Make a stock solution of RH237 by dissolving 1 mg of RH237 in 1 ml of dimethylsulfoxide and store in a freezer (-20°C).
3. (\pm) Blebbistatin 5 mg (EMD Biosciences) in 50 mM package (in 342 μ L dimethylsulfoxide). Make a stock solution of Blebbistatin by adding 1 ml of dimethylsulfoxide.
4. Tyrode's solution in mM: 130 NaCl, 24 NaHCO₃, 1.0 MgCl₂, 4.0 KCl, 1.2 NaH₂PO₄, 5 Dextrose, gassed with 95% O₂ and 5% CO₂ for 5 min at pH 7.4 and add 1.25 CaCl₂ to eliminate precipitation of CaCO₃.

2.2. Heart Chamber

The chamber is an important component of the calcium recording system to maintain the temperature at 35°C and reduce the light reflection from the curvature of the heart. Figure 1 shows a schematics of heart chamber optimized for adult rabbit hearts (> 5-month-old). The size of heart chamber can be modified easily for smaller hearts such as rats and guinea pigs (see Note 1).

2.3. Optical Apparatus

The optical apparatus should allow 0.5–3× magnification to image sufficiently large region of the heart. Figure 2 shows a schematic diagram with two lens combination and two dichroic mirrors.

1. Fluorescence from calcium dyes can be imaged on the image sensor at various magnifications. The front lens (50 mm f1.2 Nikon lens) is mounted on the first dichroic box (Beam splitter holder #78150, Newport, Irvine, CA) with excitation light housing (520±20 nm, Dolan-Jenner MH-100 Metal Halide

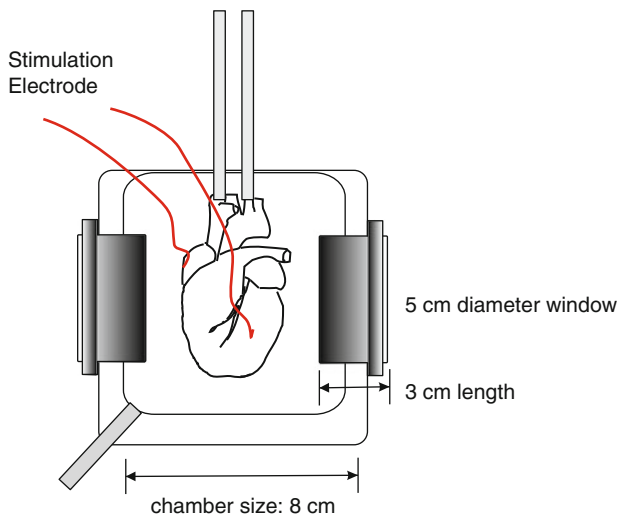


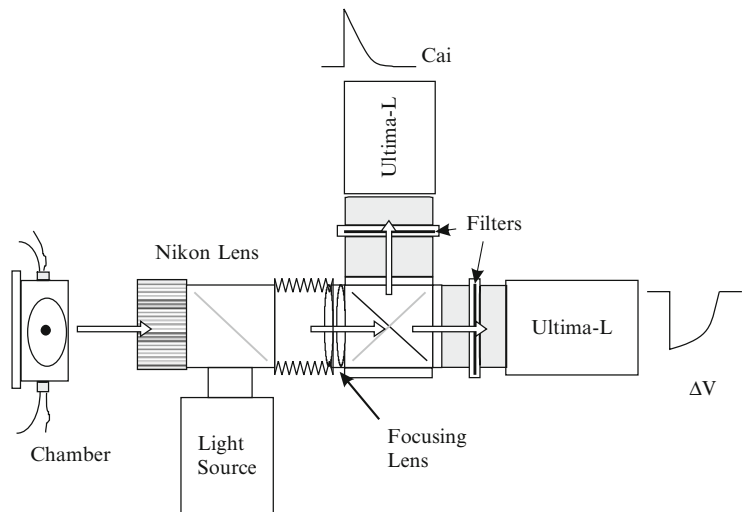
Fig. 1. Heart chamber. The chamber (Radnoti LLC, Monrovia, CA) has two windows for imaging and stimulation/ECG electrodes. The dimensions are for rabbit hearts.

Fiber Optic Illuminator). The front lens can give 0.4–1× magnification to CCD sensors (see Note 2).

2. The secondary lens (75 mm focal length) is mounted on the second dichroic box to refocus calumniated light to the camera sensors. Excitation, beam splitter, and emission filters can be ordered from Omega Filters, Brattleboro, VT 05301.
3. V_m camera is fixed on the rail and Ca_i camera is mounted on the xyz manipulator for fine alignment. Two cameras can be aligned by putting a ruler and moving Ca_i camera until the correlation between two images is maximum.
4. The fluorescence signal from single pixel represents the sum of fluorescence from many cells in focus. The depth resolution is determined by pixel size, magnification, numerical aperture of camera lens, and wavelength of the fluorescence light. The depth resolution can be estimated with the following equation,

$$d = \frac{\lambda \cdot n}{NA^2} + \frac{n \cdot e}{M \cdot NA}$$
, where d is depth of focus, NA is a numerical aperture of camera lens, M is magnification, e is the dimension of single pixel, n is a refractive index (water~1.3), and λ is emission wavelength. Typical depth resolution with $100 \times 100 \mu\text{m}^2$ pixel size, 1:1 magnification, and 0.3 NA will be $500 \mu\text{m}$. Therefore, signals should be interpreted appropriately when highly complex, inhomogeneous tissue will be mapped such as surviving layer of myocardial infarction, SA or AV node, and endocardial surface with Purkinje fibers attached.
5. To avoid photobleaching, heart should be exposed to the excitation light only during the recording briefly.

a Schematics of Optical Apparatus



b Schematics of Optical Apparatus

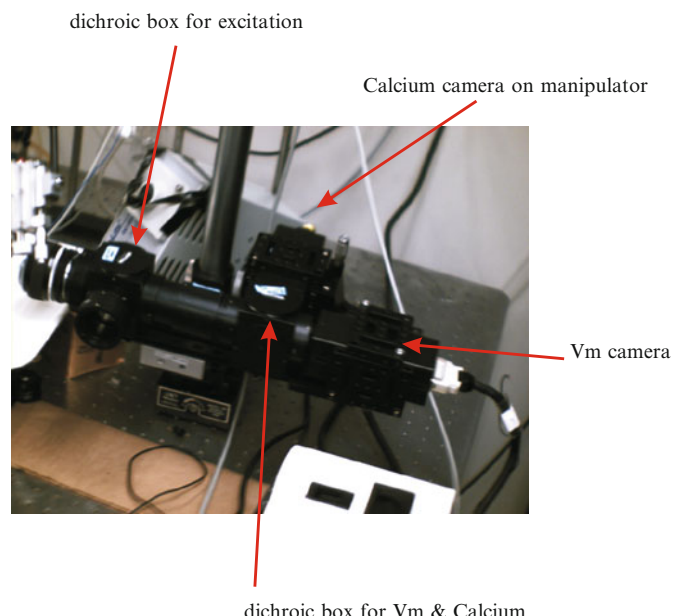


Fig. 2. Optical apparatus. (a) Schematic diagram of optical apparatus. Light from 150 W tungsten-halogen lamp is collimated, passed through 520 ± 20 nm interference filters, and focused on the heart. Fluorescence from the stained heart is collected by a camera lens and passed through a dichroic mirror to split the emission wavelength below and above 630 nm. Wavelengths below 645 nm are passed through a 585 ± 20 nm interference filter (Rhod-2) and those above through a 715 nm cutoff filter (RH237), and the two images of the heart were focused on two CMOS camera (100 \times 100 pixels, Ultima-L, Scimidia). (b) Actual picture of the system. Two cameras and two dichroic boxes are mounted on a rail to accommodate different magnification from 2×2 mm 2 to 25×25 mm 2 field of view (see the text for detail). Ca $^{2+}$ camera is mounted on the xyz Calibration manipulator for easy alignment of two cameras.

3. Methods

3.1. Heart Harvest and Perfusion

It is critical to harvest hearts from live animal to record electrical activity from Langendorff perfusion system. High dose of anesthesia often halts heart contraction, which results in ischemic condition. Even several minutes of ischemia may cause significant physiological changes and heart cannot be used for the study proposed here. For this reason, the following surgical procedures are generally used to harvest hearts from animal.

1. Rabbits can be anesthetized with buprenorphene (0.03 mg/kg IM), acepromazine (0.5 mg/kg IM), xylazene (15 mg/kg IM), and ketamine (60 mg/kg IM).
2. Wait about 5 min and inject pentothal (35 mg/kg, IV) and heparin (200 U/kg, IV) through ear vein.
3. The following methods are typically used to assess pain and the effectiveness of anesthesia: (1) eye reflex and its dilation status and (2) pain/reflex from toes.
4. After animal is in deep anesthesia assessed by above two criteria, the abdominal part right below the diaphragm is opened and hearts can be excised immediately within 30 s.
5. The heart needs to be immediately transported to the cold Tyrode's solution with ice to stop contraction and eliminate further ischemia/energy loss by contraction. Within 1 min, the heart can be transported to the Langendorff perfusion system where hearts are retrogradely perfused through aorta with a Tyrode's solution described above.

3.2. Staining Procedure

The staining procedure includes (1) perfusion with a contraction blocker (Blebbistatin, 2–10 μ M) to stop motion artifact (see Note 3), (2) RH237 (300 μ L from the stock solution), and (3) Rhod-2/AM (300 μ L from the stock solution).

1. Reduction of motion artifact with Blebbistatin: Blebbistatin stock solution in DMSO can be directly added to the bubble traps or added to the reservoir to make the final concentration of 2–10 μ M. Blebbistatin gradually reduces the heart contraction in 10–15 min (see Note 4).
2. RH237 for V_m : Record one background fluorescence before and after staining RH237. This background fluorescence will be used for dye calibration and $\Delta F/F_0$. RH237 can be injected to the bubble trap and can be stained within a minute.
3. Rhod-2/AM for C_{ai} : Add Rhod-2/AM (300 μ L for adult rabbit, 100–150 μ L for guinea pig or rat, 50 μ L for mouse heart) to the bubble trap slowly (about 2 min). Continuously monitor ECG recordings (see Note 5). Since Rhod-2/AM needs to enter into the cytosol and catalyzed into Rhod-2, the staining procedure typically takes about 10 min.

3.3. Rhod-2 Calibration

Investigation of heterogeneous Ca^{2+} cycling requires comparison of Ca^{2+} amplitude, rise time, rate of rise, and decay of Ca^{2+} transients (Fig. 3a) from different regions of hearts. The major advantage of Rhod2 is its superior fluorescence characteristics and the absence of spectral overlap with the V_m -sensitive dye, RH237. However, rhod-2 is a single-wavelength dye, making ratiometric calibration impossible. This limitation can be overcome by calibration method developed by Del Nido et al. (24, 25) using the following equation:

$$[\text{Ca}^{2+}]_i = K'_d (F - F_{\min}) / (F_{\max} - F),$$

where $K_d' = 710 \text{ nM}$, F_{\min} is a baseline fluorescence from unstained tissue, and F_{\max} can be obtained at the end of the experiment by flushing dyes with high- Ca^{2+} solutions and the addition of 2,2'-DTDP to release Ca^{2+} from SR (Fig. 3b) (25, 26).

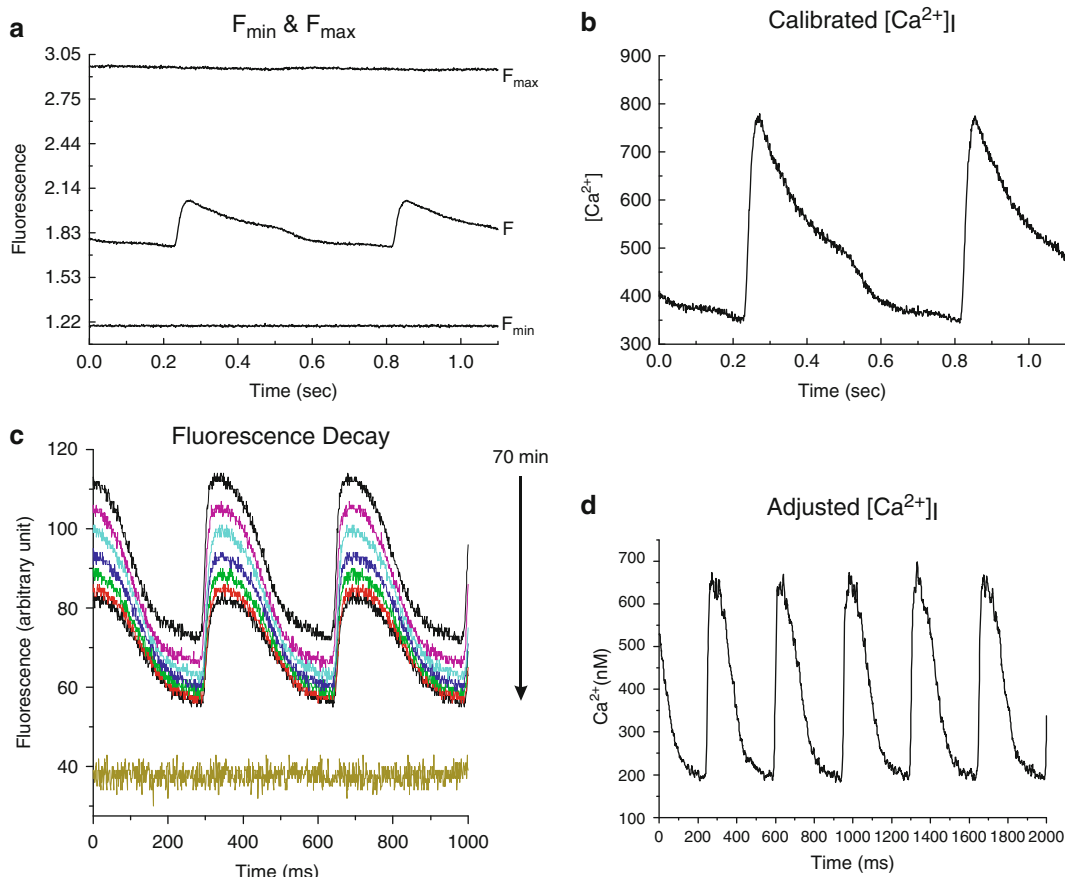


Fig. 3. Rhod-2/AM calibration. (a) Typical example of F_{\min} and F_{\max} . (b) Calibrated Ca_i . F_{\min} and F_{\max} were obtained within 30 min of Rhod-2 staining. (c) Fluorescence decay due to bleaching and dye leak. F_{\min} is shown below Ca^{2+} transients for reference. (d) Ca_i after adjusting fluorescence decay in F_{\max} .

1. The first step is to record the baseline fluorescence from unstained tissue (F_{\min}). After 15–20 min of settling in the perfusion system, Blebbistatin can be added to stop the contraction. Before adding rhod-2, take a quick scan (2–4 s) at the same sampling rate (typically 1,000 frames/s) from unstained heart with excitation light on.
2. Add rhod-2 as described in the previous section.
3. F_{\max} can be obtained by 3 mM Ca^{2+} and 100 μM 2,2'-DTDP mixed in Tyrode's solution, which produces rapid saturation of intracellular rhod-2 with Ca^{2+} from extracellular space and SR. Typically 5-min perfusion of F_{\max} calibration solution will be sufficient to record F_{\max} .
4. This method assumes that rhod-2 retention in the cell is stable until F_{\max} is obtained. We determined rhod-2 fluorescence changes with time by recording rhod-2 signals every 5 min for up to 2 h after single injection of 200 μL of stock solution (1 mg of rhod-2 in 1 ml of DMSO). Figure 3c shows changes in the rhod2 fluorescence signal with time. Fluorescence from rhod2 decays slowly ($\tau_{1/2}=70$ min). Since typical experiments including the proposed programmed stimulation protocol and isoproterenol experiments need 40- to approximately 60-min recordings, fluorescence decay due to photobleaching and dye washout needs adjustment. A single exponential decay curve fitting can be used to estimate correct F_{\max} value in time. Figure 3d shows an example of calibration of the rhod-2 signal, suggesting the feasibility of Ca^{2+} calibration. Note that the diastolic Ca_i is around 200–350 nM range higher than typical diastolic Ca_i measurement (~100 nM) from isolated single myocyte. This high fluorescence is mostly due to dye uptake from different cell types such as fibroblasts, smooth muscle cells, and endothelial cells, and needs special attention near myocardial infarction.

3.4. Data Analysis

3.4.1. Ca^{2+} Transient Analysis

Typical analyses of calcium transients include time delay between action potential and calcium transients, rise time (time to peak), rate of rise, amplitude, duration (typically 50, 75, or 90% recovery), and decay fitted to a single exponential decay curve. These parameters can be mapped to investigate heterogeneities in calcium handling such as apex vs. base, endo to epi, and border zone vs. remote zone in myocardial infarction. Figure 4 shows typical maps of activation, recovery, and duration. Amplitude and duration of Ca^{2+} transients can be measured at different cycle lengths to investigate their restitution kinetics.

3.4.2. Detection of Spontaneous Ca^{2+} Release

The time delay between action potential and calcium transient can be measured at pixel resolution and detect spontaneous Ca^{2+} release. Phase plots of Ca_i vs. V_m can be used to better illustrate the

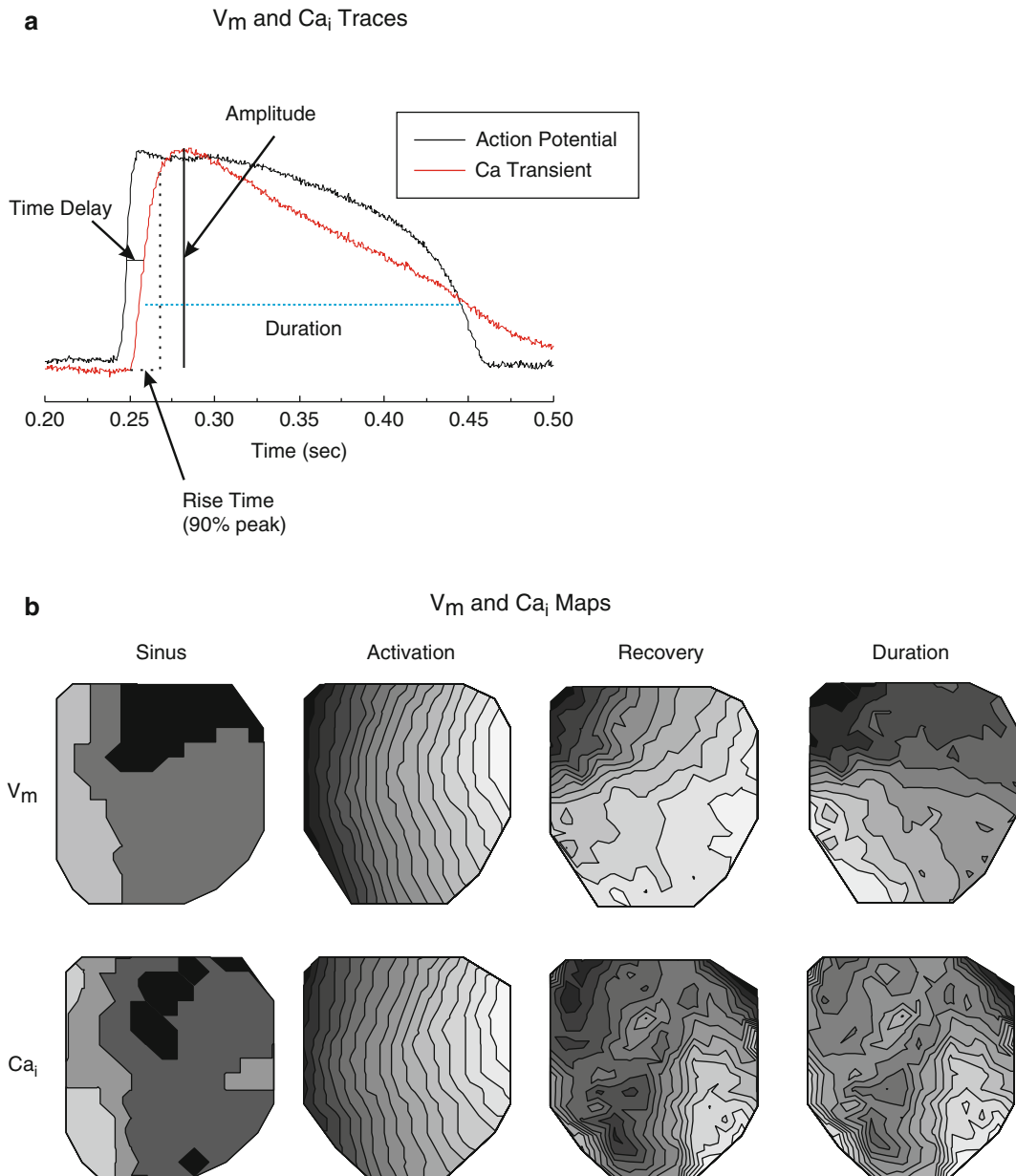


Fig. 4. Ca^{2+} transient analysis. (a) Typical example of V_m and Ca_i recorded from the same location using RH237 and Rhod-2. (b) Maps of activation, recovery, and duration. Ca_i follows action potential activation and recovery, suggesting tight relationship between action potentials and calcium transients (modified from ref. 24).

temporal relationship between V_m and Ca_i (12, 27, 28). Figure 5a superimposes optical recordings of APs and Ca_i transients and plots the phase map generated by a normal cardiac beat. Ca_i vs. V_m phase maps had a counterclockwise trajectory, the action potential upstroke fires first preceding the rise of Ca_i . Later during repolarization, the downstroke of action potentials becomes steeper than

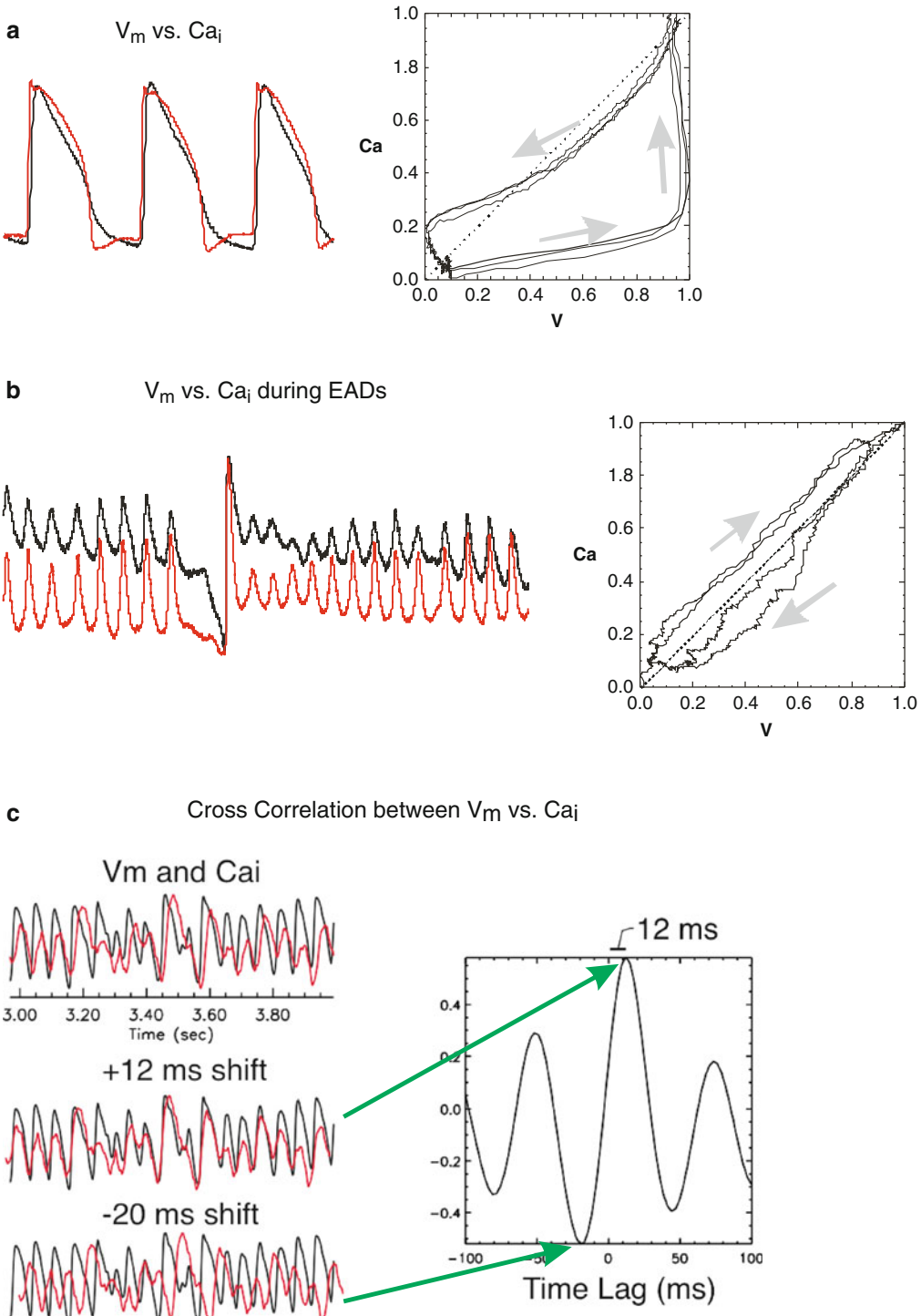


Fig. 5. Phase plot of V_m and Ca_i . V_m and Ca_i are normalized for each set of diodes and phase maps of Ca_i versus V_m are plotted. Phase maps of Ca_i versus V_m for a heart under sinus rhythm. (b) Phase maps of V_m and Ca_i during spontaneous Ca^{2+} release. During spontaneous Ca^{2+} release, phase maps have elliptical densely packed trajectories near the center-line. The direction of rotation is clockwise or opposite to the trajectory during sinus rhythm (panel a). The trajectories of the phase maps indicate that Ca_i precedes V_m at the origins of EADs (modified from ref. 12). (c) Correlation Analysis of V_m and Ca_i in VF. Sample traces of V_m and Ca_i are shown on the left and cross correlation with time lag is shown on the right panel. Cross correlation reaches maximum at the average time delay (12 ms) between V_m and Ca_i (modified from ref. 23).

the recovery of Ca_i , forming a “boomerang” shape. Panel B shows phase plot during spontaneous calcium release. The phase maps had a clockwise elliptical trajectory.

3.4.3. Correlation Analysis of Action Potential and Ca^{2+} Transient

The relationship between Ca_i and action potential during ischemia, alternans, and VF can be quantitatively analyzed using cross correlation analysis. Cross correlation (CC) calculates correlation coefficient between two signals after shifting time lag. The cross correlation of two signals, X and Y , and time lag (L) is defined as

$$R_{XY}(L) = \begin{cases} \frac{\sum_{k=0}^{N-L-1} (X_{k+L} - \bar{X})(Y_k - \bar{Y})}{\sqrt{\sum_{k=0}^{N-1} (X_k - \bar{X})^2} \sqrt{\sum_{k=0}^{N-1} (Y_k - \bar{Y})^2}} & \text{For } L < 0 \\ \frac{\sum_{k=0}^{N-L-1} (X_k - \bar{X})(Y_{k+L} - \bar{Y})}{\sqrt{\sum_{k=0}^{N-1} (X_k - \bar{X})^2} \sqrt{\sum_{k=0}^{N-1} (Y_k - \bar{Y})^2}} & \text{For } L \geq 0 \end{cases},$$

where \bar{X} and \bar{Y} are means of corresponding series and N is the number of points in the series. The maximum correlation between two occurs when two signals are nicely overlapped and can be used to estimate time delay between action potential and Ca_i .

Figure 5c is a typical example of V_m and Ca_i recordings. VF was induced by burst stimulation and V_m and Ca_i were simultaneously recorded as described above. Ca_i oscillations were still in synchrony with V_m oscillations as shown in Fig. 5c. The average time delay between action potential and Ca_i was 12 ms, which can be confirmed by overlapping two traces of V_m and Ca_i in the middle panel in Fig. 5c. The time delay can be estimated from cross correlation plot (right panel). Cross correlation reaches at maximum when two traces are overlapped each other with time lag of 12 ms. The positive time lag indicates that V_m still triggers Ca_i release in VF.

4. Notes

1. For mouse hearts, the heart chamber can be as small as 2 cm in diameter and it is recommended to have additional heater or additional pump to superfuse to exchange solution in the chamber at higher rate to maintain the temperature.
2. For higher magnification, the lens can be mounted in a reverse direction with a reverse ring coupler (Nikon BR-2A—Reverse ring), which can give up to 2× magnification for smaller hearts such as mouse hearts.

3. Blebbistatin is a small molecule inhibitor which has high affinity and selectivity to myosin II. By interfering with interactions with actin it reduces, and can arrest, cardiac contractions.
4. Blebbistatin is light sensitive and therefore the solution reservoir needs to be wrapped with aluminum foil to prevent photodamage.
5. Heart rate should be monitored, and it may drop slightly during dye perfusion and staining procedure.

Acknowledgement

This work was supported by NIH grant R01 HL096669-01 to BRC.

References

1. Wongcharoen W et al (2007) Aging increases pulmonary veins arrhythmogenesis and susceptibility to calcium regulation agents. *Heart Rhythm* 4(10):1338–1349
2. Ono N et al (2007) Spontaneous atrial fibrillation initiated by triggered activity near the pulmonary veins in aged rats subjected to glycolytic inhibition. *Am J Physiol Heart Circ Physiol* 292(1):H639–H648
3. Omichi C et al (2004) Intracellular Ca dynamics in ventricular fibrillation. *Am J Physiol Heart Circ Physiol* 286(5):H1836–H1844
4. Chudin E et al (1999) Intracellular Ca(2+) dynamics and the stability of ventricular tachycardia. *Biophys J* 77(6):2930–2941
5. Hoeker GS et al (2009) Spontaneous calcium release in tissue from the failing canine heart. *Am J Physiol Heart Circ Physiol* 297(4): H1235–H1242
6. Curran J et al (2010) Spontaneous Ca waves in ventricular myocytes from failing hearts depend on Ca(2+)-calmodulin-dependent protein kinase II. *J Mol Cell Cardiol* 49(1):25–32
7. Belevych AE et al (2009) Redox modification of ryanodine receptors underlies calcium alternans in a canine model of sudden cardiac death. *Cardiovasc Res* 84(3):387–395
8. Chou CC et al (2007) Remodelling of action potential and intracellular calcium cycling dynamics during subacute myocardial infarction promotes ventricular arrhythmias in Langendorff-perfused rabbit hearts. *J Physiol* 580(Pt. 3):895–906
9. Clusin WT (2008) Mechanisms of calcium transient and action potential alternans in cardiac cells and tissues. *Am J Physiol Heart Circ Physiol* 294(1):H1–H10
10. Szabo B, Kovacs T, Lazzara R (1995) Role of calcium loading in early afterdepolarizations generated by Cs+ in canine and guinea pig Purkinje fibers. *J Cardiovasc Electrophysiol* 6(10 Pt 1):796–812
11. Verduyn SC et al (1995) The effect of flunarizine and ryanodine on acquired torsades de pointes arrhythmias in the intact canine heart. *J Cardiovasc Electrophysiol* 6(3): 189–200
12. Choi BR, Burton F, Salama G (2002) Cytosolic Ca2+ triggers early afterdepolarizations and Torsade de Pointes in rabbit hearts with type 2 long QT syndrome. *J Physiol* 543(Pt 2): 615–631
13. Volders PG et al (1997) Similarities between early and delayed afterdepolarizations induced by isoproterenol in canine ventricular myocytes. *Cardiovasc Res* 34(2):348–359
14. Saitoh H, Bailey JC, Surawicz B (1989) Action potential duration alternans in dog Purkinje and ventricular muscle fibers. Further evidence in support of two different mechanisms. *Circulation* 80(5):1421–1431
15. Shimizu W, Antzelevitch C (1999) Cellular and ionic basis for T-wave alternans under long-QT conditions. *Circulation* 99(11):1499–1507
16. Sato D et al (2006) Spatially discordant alternans in cardiac tissue: role of calcium cycling. *Circ Res* 99(5):520–527
17. Hayashi H et al (2007) Dynamic origin of spatially discordant alternans in cardiac tissue. *Biophys J* 92(2):448–460

18. Bao M et al (2007) Abnormal intracellular calcium handling underlying T-wave alternans and its hysteresis. *Cardiology* 108(3): 147–156
19. Sato D et al (2007) Inferring the cellular origin of voltage and calcium alternans from the spatial scales of phase reversal during discordant alternans. *Biophys J* 92(4):L33–L35
20. Pruvot EJ et al (2004) Role of calcium cycling versus restitution in the mechanism of repolarization alternans. *Circ Res* 94(8):1083–1090
21. Lee HC et al (1987) Cytosolic calcium transients from the beating mammalian heart. *Proc Natl Acad Sci USA* 84(21):7793–7797
22. Wu Y, Clusin WT (1997) Calcium transient alternans in blood-perfused ischemic hearts: observations with fluorescent indicator fura red. *Am J Physiol* 273(5 Pt 2):H2161–H2169
23. Choi BR, Liu T, Salama G (2006) Calcium transients modulate action potential repolarizations in ventricular fibrillation. *Conf Proc IEEE Eng Med Biol Soc* 1:2264–2267
24. Choi BR, Salama G (2000) Simultaneous maps of optical action potentials and calcium transients in guinea-pig hearts: mechanisms underlying concordant alternans. *J Physiol* 529(Pt 1): 171–188
25. Del Nido PJ et al (1998) Fluorescence measurement of calcium transients in perfused rabbit heart using rhod 2. *Am J Physiol* 274(2 Pt 2): H728–H741
26. Choi BR, Salama G (2000) Simultaneous maps of optical action potentials and calcium transients in guinea-pig hearts: mechanisms underlying concordant alternans. *J Physiol* 529 (Pt 1):171–188
27. duBell WH et al (1991) The cytosolic calcium transient modulates the action potential of rat ventricular myocytes. *J Physiol* 436:347–369
28. Schlotthauer K, Bers DM (2000) Sarcoplasmic reticulum Ca(2+) release causes myocyte depolarization. Underlying mechanism and threshold for triggered action potentials. *Circ Res* 87(9):774–780

Chapter 14

Measurement of Changes in Endothelial and Smooth Muscle Ca²⁺ in Pressurized Arteries

Kim A. Dora and Michael A. Hill

Abstract

The use of single- and dual-wavelength Ca²⁺-sensitive fluorescent dyes to monitor changes in endothelial and/or smooth muscle intracellular Ca²⁺ levels has provided information linking Ca²⁺ events to changes in arterial function. Here we describe the *in vitro* techniques used to selectively load Ca²⁺ indicators into either the endothelium or the smooth muscle of cannulated rat cremaster arteries. These vessels normally develop spontaneous myogenic tone that is largely unaffected by the loading of Ca²⁺ indicators or the subsequent imaging procedures. This suggests that there is minimal Ca²⁺ buffering or damage, and that the fluorescent indicator-loaded vessels behave similarly to unloaded preparations. Importantly, these approaches are applicable to both isobaric and isometric preparations and have been also used for the study of a number of vascular beds including cerebral, mesenteric, coronary, and skeletal muscle vasculatures.

Key words: Arteries, Endothelial cells, Imaging

1. Introduction

An ability to measure changes in cellular Ca²⁺ in freshly dissected, cannulated, and pressurized arteries has provided insight into the signaling pathways linking changes in endothelial and smooth muscle Ca²⁺ to changes in diameter. This has provided substantial information as to how agonist and physical stimuli lead to changes in the mechanical state of arteries. Such studies have also contributed to our understanding that changes in Ca²⁺ not only affect interaction of the contractile proteins via Ca²⁺-calmodulin-mediated activation but also concomitantly participate in other processes from regulation of ion channels to remodeling.

An important recent development in the study of small artery function has been the capability of selectively imaging the thin endothelial cell layer using confocal microscopy (1). Further, with the aid of highly sensitive digital cameras and non-linescan confocal

microscopes such as Nipkow disk confocal systems (2) this can be done with high temporal and spatial resolution. Similarly, imaging changes in smooth muscle cell Ca^{2+} has advantages with high-speed imaging systems. In both cell types rapid, spontaneous, Ca^{2+} events (including sparks, waves, puffs, and pulsars) can be imaged and compared to agonist-mediated responses in isolated and cannulated arteries pressurized to the physiological range. Importantly, the enhanced spatiotemporal resolution of these approaches extends and complements ratiometric Ca^{2+} measurements that, while typically reporting averaged cellular ion concentrations, retain an advantage in situations where absolute calibration is required.

This chapter describes the materials, equipment, and protocols used for measuring changes in intracellular Ca^{2+} in either endothelial or vascular smooth muscle cells of arterioles held under isobaric conditions. The information is limited to fluorescence-based measurements using acutely loaded Ca^{2+} indicators including fluo-4, Oregon green 488 BAPTA-1, and fura-2. For alternate approaches such as genetically encoded Ca^{2+} sensors, readers are referred elsewhere (3, 4).

2. Materials

Prepare all solutions using ultrapure water (prepared by purifying deionized water to attain a sensitivity of $18 \text{ M}\Omega \text{ cm}$ at 25°C) and analytical grade reagents.

2.1. Imaging Equipment

- When using fluo-4 or Oregon green 488 BAPTA-1 for Ca^{2+} measurements, where fast acquisition of multicellular fields is required, a system as typified by Nipkow disk-based confocal systems is used (see Figs. 1 and 2 and Note 1). If lower acquisition rates are required, conventional linescan confocal systems can be used. The laser line is 488 nm, and either a back-lit electron multiplied (EM) CCD or intensified (I) CCD camera is used (see Note 2). The emission wavelength is 515 nm for both indicator dyes.
- When using fura-2 for Ca^{2+} measurements, the microscope should be equipped with optics suitable for UV illumination and switching excitation wavelengths (see Fig. 3). This includes an illumination light source (typically a 75 W xenon lamp), and switching filter or monochromator, to allow alternating 340 and 380 nm illumination. Fluorescence emission (510 nm) is detected using either an EMCCD/ICCD camera as above.
- For each Ca^{2+} indicator, the speed of acquisition can be improved by using a photomultiplier tube for acquisition of average emitted fluorescence intensity. The disadvantage of this approach is the lack of spatial resolution of Ca^{2+} events.

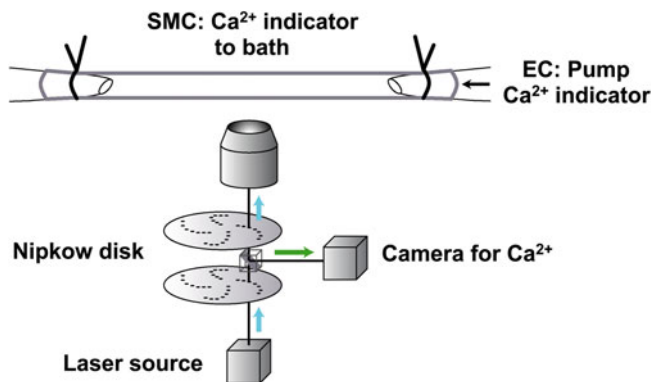


Fig. 1. Experimental setup for measuring changes in endothelial and smooth muscle cell fluorescence intensity using a Nipkow disk confocal system. Either endothelial or smooth muscle cells are loaded with Ca²⁺ indicator (OGB-1/AM or fluo-4/AM) as described in the methods. Endothelial cells are loaded for 30 min via the lumen, whereas smooth muscle by addition to the bath for 60 min. A 488 nm laser is used to excite the Ca²⁺ indicator and emitted light passes back through the Nipkow disk and dichroic mirror to the sensitive EMCCD or ICCD camera. Cells are imaged using a high NA, >100 μm working distance 40 \times or 60 \times water immersion objective.

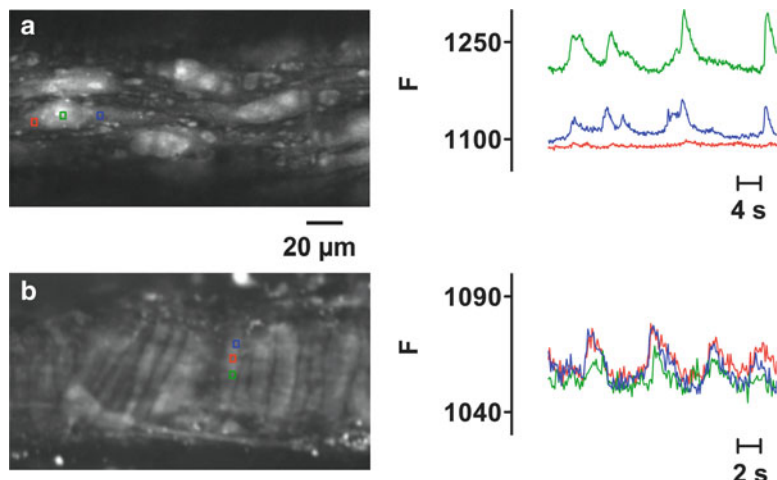


Fig. 2. Spontaneous changes in endothelial and smooth muscle cell fluorescence intensity. Micrographs of loaded endothelial cells (a) and smooth muscle cells (b) loaded with OGB-1. The micrographs have been cropped to 248 \times 135 pixels. The original images were 512 \times 279 pixels (EC) and 512 \times 201 pixels (SMC) and were acquired at 11 and 8.6 Hz, respectively, using a 40 \times /0.9 NA objective. The average fluorescence intensities (F) in the colored regions over a single endothelial or smooth muscle cell are shown on the right, with corresponding colored lines. Using these acquisition speeds it is possible to monitor movement of Ca²⁺ events along single cells, as well as between cells.

4. It is imperative that the laser power should be kept to a minimum to avoid damaging cells and minimizing photobleaching of the indicators. To achieve this an extremely sensitive detection system should be used for collecting fluorescence intensity (see Note 3).

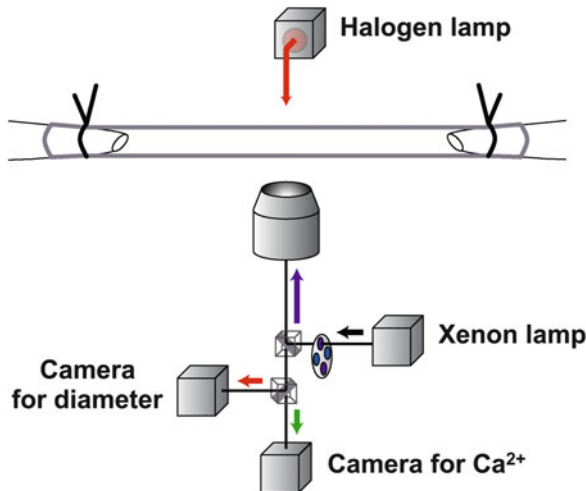


Fig. 3. Experimental setup for simultaneously measuring changes in arteriolar diameter together with endothelial and/or smooth muscle cell fluorescence intensity using a conventional fluorescence microscope. Either endothelial and/or smooth muscle cells are loaded with Ca^{2+} indicator (in this case fura-2/AM) as described in the methods. The excitation light from a xenon lamp passes via a dichroic mirror to the artery, and for fura-2 must also pass through a wavelength switching system to enable excitation at 340 and 380 nm. The emitted light passes back through the dichroic mirror and a beam splitter to the sensitive EMCCD or ICCD camera. A red filter in the halogen lamp path restricts light to wavelengths above 650 nm, which can be used to generate brightfield images for simultaneous diameter measurements using a camera attached to the second port of the beam splitter (see Subheading 2.1, item 5).

5. If required, simultaneous measurements of arteriolar diameter and endothelial and/or smooth muscle cell Ca^{2+} can be obtained by focusing at the midplane of arteries (see Note 4). Conventional linescan confocal microscopes equipped with a transmitted light channel will allow the excitation wavelength to generate and acquire a brightfield image separate from, but simultaneously to, the emitted fluorescence specific to the Ca^{2+} indicator. Similarly, with mercury or xenon lamp-based systems, transillumination can be directed through a red filter (>650 nm) before reaching the artery and the transmitted light split to a black and white CCD video or digital camera. The excitation of the Ca^{2+} indicator remains unaffected and the emitted fluorescence is directed through the beam splitter with dichroic mirror to the EMCCD/ICCD camera as outlined above.

2.2. Buffer

1. MOPS buffer: 145 mM NaCl, 4.7 mM KCl, 2.0 mM CaCl_2 , 1.17 mM MgSO_4 , 2.0 mM MOPS, 1.2 mM NaH_2PO_4 , 5.0 mM glucose, 2.0 mM pyruvate, 20 μM EDTA, 2.75 mM NaOH. It is recommended that a fatty acid and endotoxin-free bovine serum albumin (1%, for example USB No. 10856) be added to

the MOPS-buffered solution and used for the dissection and the luminal perfusion solution (see Note 5). In all cases, adjust pH to 7.40 ± 0.02 .

2.3. General Reagents

1. Oregon Green 488 BAPTA-1/AM (OGB-1/AM, Invitrogen, Paisley, UK). Make up as a stock (2 mM) solution by dissolving in dimethylsulfoxide (DMSO) and store aliquots (10 μ L) at -20°C until required.
2. Fluo-4/AM (Invitrogen, Paisley, UK). Make up as stock (2.3 mM) solution by dissolving in DMSO.
3. Fura-2/AM (Invitrogen, Paisley, UK). Make up as stock (0.5 mM) solution by dissolving in DMSO.
4. Pluronic F-127 (20% in DMSO, Invitrogen, Paisley, UK). Prepare 0.02% Pluronic in MOPS buffer. Add dissolved stock to make a final concentration of either 10 μM OGB-1/AM and fluo-4/AM or 2 μM fura-2/AM. Filter (0.2 μm pore) all Ca^{2+} indicator solutions.
5. As for many applications using fluorescence all solutions should be protected from stray/room light when possible.

3. Methods

3.1. Isolation and Cannulation of Vessels

1. For isolation of cremaster arteries, animals are anesthetized, the cremaster muscles exteriorized, excised from the rat, and placed in ice-cold MOPS buffer (see Note 6). Segments of the main intramuscular artery or its branches (1A and 2A) are dissected from the muscle as previously described (1, 5). In brief, a segment (approximately 2 mm in length) is microdissected from between the two obliquely arranged layers of skeletal muscle. Dissection requires a high-quality stereomicroscope and cooled conditions ($<4^{\circ}\text{C}$). Microdissection is performed using ultrafine iris spring scissors (for example Fine Science Tools No. 15000-00) and high-quality fine forceps (for example, Fine Science Tools No. 11252-23). Artery segments are cannulated at each end with fire-polished glass micropipettes (external diameter $\sim 75 \mu\text{m}$) and secured with 11-0 monofilament suture (see Note 7). Cannulation is performed in cold MOPS buffer as described above.
2. The authors use chamber setups (see Note 8) with cannulation pipettes held by micromanipulators positioned on the movable stage of inverted microscopes. Quality micromanipulator systems allow precise alignment of cannulation pipette tips. Thin coverslips (25 mm \times 50 mm; thickness 0.15 mm) are used for the base of the temperature-regulated chamber (Warner

Instruments, Hamden, CT, USA), with volume ~2–5 mL. The combination of the thin coverslips and precision micromanipulators enables the arteries to be carefully positioned near the base of the chamber and the use of high numerical aperture, short working distance water immersion objectives (usually 40 \times or 60 \times ; N.A. ~1.2; working distance >100 μ m; for fura-2 20 \times or 40 \times objectives with enhanced UV transmission are required). Each pipette is independently connected a length of polyethylene tubing (internal diameter 1.14 mm), each of which is connected to a 5 mL syringe that can be easily raised to the desired working pressure.

3. Once cannulated, the arteries are continuously superfused (2 mL/min) with a buffered physiological salt solution such as the MOPS buffer and warmed to 34–35°C over 20 min while still at low pressure. The luminal pressure (see Note 9) is increased in 10–15 mmHg increments and the vessel is straightened at each pressure using the micromanipulators. Pressure is increased until the artery does not longitudinally lengthen further (<90 mmHg) and pressure then reduced to the working pressure (usually 70–80 mmHg). At this stage it is also important to ensure that both ends of the artery are vertically aligned and the vessel remains close to the coverslip (see Note 10).
 4. Following an equilibration period (~30 min), arteries develop myogenic tone. In all experiments it is a prerequisite that all vessels are free of pressure leaks, show spontaneous myogenic tone, and are responsive to agonists to be considered viable for further experimentation. Viability of the endothelium is tested by full dilatation (>95% passive maximal diameter) to 1 μ M acetylcholine.
1. OGB-1 remains within endothelial cells for significantly longer periods than fluo-4 and fura-2 and can therefore be more convenient to use for endothelial cell Ca²⁺ imaging experiments (see Note 11).
 2. Lower the pressure to 5 mmHg, disconnect the tubing at the end of one pipette, attach tubing connected to a pump (peristaltic or syringe) containing the filtered OGB-1/AM solution, and pump at 50 μ L/min for 2–3 min. Stop the pump and allow the dye to load into the endothelial cells for a total of 30 min at 34°C.
 3. It is often useful to image the endothelium during the loading period, setting the laser power and camera gain to faintly detect the internal elastic lamina autofluorescence. If possible, this should be done at the acquisition speed required for Ca²⁺ imaging (see Note 12). The endothelial cells will usually not be visible for at least 10–15 min, and will not be bright even after

3.2. Oregon Green BAPTA-1 Loading of Endothelial Cells

a 30-min loading. However, to avoid loading of smooth muscle cells, the authors find that 30 min is the maximum time for loading.

4. After ~25 min of loading, change the tubing back to MOPS buffer ready to start the pump at 30 min to wash out the indicator dye. Let the dye de-esterify for a further 30 min, and then raise the pressure back to the working pressure.
5. Experimental protocols can then be performed. The responses to agonists should remain consistent for at least 2 h, and usually up to 6 h, with minimal bleaching or damage.
6. Note that both fluo-4 and fura-2 can be used to measure endothelial cell Ca^{2+} , but the indicators readily move to the smooth muscle cells, so the length of experiments is limited to approximately 30 min.

3.3. Oregon Green BAPTA-1, Fluo-4, and Fura-2 Loading of Smooth Muscle Cells

1. OGB-1/AM, fluo-4/AM, or fura-2/AM can be used for smooth muscle cell Ca^{2+} imaging.
2. The cells can be loaded at the working pressure, and can be loaded at room temperature to reduce compartmentalization of the dye and extrusion from cells during the loading period.
3. The filtered indicator dye is added to the vessel chamber, and allowed to load into the smooth muscle cells for 60 min at 70 mmHg. The cells can be imaged over this period to monitor the uptake of dye, again using the autofluorescence as a starting position (see Subheading 3.2, step 3). In this case, the smooth muscle cells will not be visible for at least 30 min, and again allow 30 min of de-esterification following washout of dye at 34–35°C.
4. At 34–35°C the vessels should regain their original levels of myogenic tone (see Note 13).

3.4. Use of the Ratiometric Indicator Fura-2 for Global Estimates of Cytosolic Ca^{2+}

1. In some situations it may be more desirable to perform global cytosolic Ca^{2+} measurements using a ratiometric indicator, for example, when it is important to be able to provide a calibration and report Ca^{2+} changes in terms of actual concentrations. In this situation a ratiometric dye provides the advantages of minimizing artifacts due to vessel contraction and variation in indicator loading. As this technique has been widely used in the study of isolated arteries and arterioles (see, for example, ref. 5) it will only be briefly described here to contrast it with the methods used for the single-wavelength indicators. The discussion will be limited to the dual excitation wavelength indicator, fura-2.
2. To load arteriolar endothelial or smooth muscle cells with fura-2, see Subheadings 3.2 or 3.3 above.

3. At the end of experiments, the maximum range of fura-2 fluorescence intensity at each wavelength (340 and 380 nm) is measured. Minimum levels of fluorescence (F_{\min}) are obtained following superfusion with 0 mM Ca²⁺ buffer containing 4 mM EGTA. Maximum levels of fluorescence (F_{\max}) are obtained after superfusion with 2 mM Ca²⁺ buffer in the presence of an ionophore such as bromo-A23187 (15 µM) or ionomycin.

3.5. Data Handling and Interpretation

Image stacks are analyzed off-line using various software programs (for example ImageJ, NIH, Bethesda, MD, USA; Image SXM, Steve Barrett, Liverpool, UK; MetaMorph, Molecular Devices, Sunnyvale, CA, USA; Imaris, Bitplane AG, Zurich, Switzerland). Depending on the aim of the experiment, global or subcellular changes in average fluorescence intensity can be measured by carefully positioning regions of interest. Image SXM has the advantage of tracking regions of interest whilst measuring average intensity, which is useful if cells move during agonist responses, as commonly occurs under isobaric conditions in cannulated vessels.

With single-wavelength Ca²⁺ indicators, data are usually presented as a fractional fluorescence increase (F/F_0), determined by dividing the fluorescence of an area (F) by a baseline average F_0 . Depending on the system, background fluorescence may be subtracted before determining F/F_0 , and serves to improve the amplitude of the ratio. To measure temporal and spatial characteristics of Ca²⁺ events across or between cells, multiple adjacent regions of interest can be analyzed, or off-line “linescans” can be obtained by positioning lines across/between cells and measuring fluorescence intensity of each pixel over time. Performing this off-line has the advantage of analyzing multiple linescans in a single image stack, but is limited to the acquisition rate of the original full image field.

In the case of fura-2 measurements, data are often reported in terms of the ratio of fluorescence emission at excitation of 340 and 380 nm ($R = F_{340}/F_{380}$) (see Note 14). The advantage of this approach is that the ratio value is largely unaffected by factors such as vessel movement and variation in indicator loading.

In situ calibration of fura-2 measurements can be performed by collecting F_{\min} and F_{\max} values as described above and applying the calibration equation developed by Grynkiewicz et al. (6):

$$[\text{Ca}^{2+}] = K_d [(R - R_{\min}) / (R_{\max} - R)] \beta,$$

where the dissociation constant $K_d = 224$; $\beta = (F_{\min_{380}}) / (F_{\max_{380}})$; and R_{\min} and R_{\max} are calculated from the fluorescence intensity measurements collected under the appropriate conditions.

As there are a number of assumptions in applying this equation (for example indicator homogeneity within areas of data collection—see ref. 7) such data should be interpreted cautiously.

4. Notes

1. The authors use Olympus inverted microscopes (models IX 71 and 81). However, all research grade microscopes (for example Leica, Nikon, and Zeiss) equipped for fluorescence can be used.
2. The authors use Andor iXon DV887 back illuminated EMCCD and Stanford Photonics XR Mega-10EX S30 cameras.
3. Damage is typically seen as uneven vessel diameter in areas that have been subjected to laser illumination. Photobleaching is evident as a rapid loss of fluorescence signal following illumination. Both these issues can be avoided by using low laser intensity combined with the most sensitive camera available (for examples see Note 2).
4. Vessel diameter can be measured online (or off-line if the image is recorded) using either edge tracking systems or electronic calipers.
5. Inclusion of albumin in the luminal solutions is particularly important for maintaining consistent endothelial function during an experiment.
6. Removal of the cremaster muscle under anesthesia tends to cause blood to be retained in the vessels making them more easy to be visualized during dissection.
7. The authors use suture from suppliers such as Alcon and Ethicon. A more economical alternative is to unwind larger and less expensive multi-strand sutures. Care should be taken, however, to use a suture that grips and does not slip on the cannulation pipettes.
8. The authors use custom-made cannulation systems; however, commercial systems are available from suppliers such as Living Systems and Danish Myo Technologies.
9. Luminal pressure can be applied through a hydrostatic pressure head or a purpose-built peristaltic pump (for example available from Living Systems and Danish Myo Technologies).
10. The distance of the vessel from the coverslip will be dependent on the working distance of the objective lens.
11. Luminal loading of OGB-1 more selectively loads endothelial cells, with minimal loss of fluorescence signal from the endothelium over a few hours. Despite washout from the lumen, within an hour other indicators (especially fluo-3 and fluo-4) reduce fluorescence intensity in endothelial cells, and load smooth muscle cells, perhaps due to passage via gap junctions.
12. Before loading, the acquisition settings can be altered (e.g., longer exposure) to visualize the autofluorescence from the internal elastic lamina, and as the OGB-1 loads the endothelial

cells the settings can be altered to those used during the experiment. This helps ensure that the correct focal plane is imaged to observe the loading of cells.

13. As a general rule decreased tone is suggestive of excessive Ca^{2+} buffering. If this occurs, check indicator concentrations or decrease the concentration if fluorescence signal is adequate.
14. These values can be corrected for background fluorescence and autofluorescence, if appropriate. If all data are presented as normalized ratios consideration should also be given to showing example raw fluorescence data.

References

1. McSherry IN, Sandow SL, Campbell WB, Falck JR, Hill MA, Dora KA (2006) A role for heterocellular coupling and EETs in dilation of rat cremaster arteries. *Microcirculation* 13:119–130
2. Kansui Y, Garland CJ, Dora KA (2008) Enhanced spontaneous Ca^{2+} events in endothelial cells reflects signalling through myoendothelial gap junctions in pressurized mesenteric arteries. *Cell Calcium* 44:135–146
3. Ledoux J, Taylor MS, Bonev AD, Hannah RM, Solodushko V, Shui B, Tallini Y, Kotlikoff MI, Nelson MT (2008) Functional architecture of inositol 1,4,5-trisphosphate signaling in restricted spaces of myoendothelial projections. *Proc Natl Acad Sci U S A* 105:9627–9632
4. Tallini Y, Brekke J, Shui B, Doran R, Hwang SM, Nakai J, Salama G, Segal S, Kotlikoff M (2007) Propagated endothelial Ca^{2+} waves and arteriolar dilation in vivo. Measurements in $\text{Cx}40^{\text{BAC}}$ GCaMP2 transgenic mice. *Circ Res* 101:1300–1309
5. Meininger GA, Zawieja DC, Falcone JC, Hill MA, Davey JP (1991) Calcium measurement in isolated arterioles during myogenic and agonist stimulation. *Am J Physiol Heart Circ Physiol* 261:H950–H959
6. Grynkiewicz G, Poenie M, Tsien RY (1985) A new generation of Ca^{2+} indicators with greatly improved fluorescence properties. *J Biol Chem* 260:3440–3450
7. Hyrc KL, Rzeszotnik Z, Kennedy BR, Goldberg MP (2007) Determining calcium concentration in heterogeneous model systems using multiple indicators. *Cell Calcium* 42:576–589

Chapter 15

Single Cell and Subcellular Measurements of Intracellular Ca^{2+} Concentration

John G. McCarron, Marnie L. Olson, Susan Chalmers, and John M. Girkin

Abstract

Increases in bulk average cytoplasmic Ca^{2+} concentration ($[\text{Ca}^{2+}]_c$) are derived from the combined activities of many Ca^{2+} channels. Near (<100 nm) the mouth of each of these channels the local $[\text{Ca}^{2+}]_c$ rises and falls more quickly and reaches much greater values than occurs in the bulk cytoplasm. Even during apparently uniform, steady-state $[\text{Ca}^{2+}]$ increases large local inhomogeneities exist near channels. These local increases modulate processes that are sensitive to rapid and large changes in $[\text{Ca}^{2+}]$ but they cannot easily be visualized with conventional imaging approaches. The $[\text{Ca}^{2+}]$ changes near channels can be examined using total internal reflection fluorescence microscopy (TIRF) to excite fluorophores that lie within 100 nm of the plasma membrane. TIRF is particularly powerful when combined with electrophysiology so that ion channel activity can be related simultaneously to the local subplasma membrane and bulk average $[\text{Ca}^{2+}]_c$. Together these techniques provide a better understanding of the local modulation and control of Ca^{2+} signals.

Key words: TIRF, $[\text{Ca}^{2+}]$, Fluorescence imaging, Smooth muscle cell isolation, Patch clamp, Image analysis

1. Introduction

Total internal reflection fluorescence microscopy (TIRF) provides a method of selectively exciting molecules close to an interface (1–3). Total internal reflection occurs when light traveling in a material of high refractive index meets a material of lower refractive index. If the light hits the interface at normal incidence (zero degrees) it will pass through un-deviated. However as the angle of incidence increases light will be refracted according to Snell's law until eventually a critical angle is reached at which light is totally reflected, i.e., the surface acts like a perfect mirror (Fig. 1). Although the light is totally reflected an electric field (known as an evanescent field) is present on the other side of the interface which

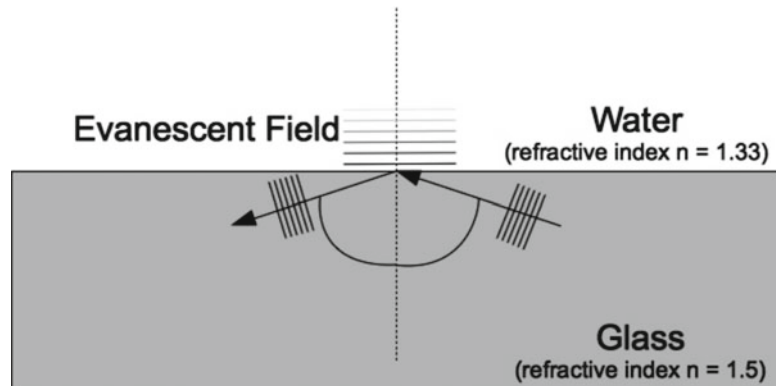


Fig. 1. Total internal reflection generates an evanescent wave. This figure shows the evanescent field propagating from a glass/water interface when the angle of incidence exceeds the critical angle. The evanescent field intensity declines exponentially with distance from the interface.

can excite fluorophores (Fig. 1) (4). This evanescent field decays rapidly with distance from the interface following an exponential falloff so that only fluorescent molecules close to the interface are excited. In this way it is possible to excite fluorophores and so obtain fluorescent images exclusively from very close to the surface. Typically TIRF will excite fluorophores within 200 nm of the surface, and in certain cases, using a low excitation power, less than 100 nm—significantly better than the diffraction limit in the axial direction (~350 nm). TIRF used in combination with small synthetic molecule Ca^{2+} indicators, e.g., fura-2 or fluo dyes, which are considerably faster in detecting Ca^{2+} and have wider dynamic ranges than the fluorescent protein Ca^{2+} indicators, enables subcellular $[\text{Ca}^{2+}]$ to be measured.

Our system, described below, combines TIRF and conventional wide-field epi-fluorescence and electrophysiology. The method enables measurement of subplasma membrane Ca^{2+} ($[\text{Ca}^{2+}]_{\text{PM}}$) signals and comparison of bulk average $[\text{Ca}^{2+}]_{\text{c}}$ (global signals) so that an understanding to the initiation (5) and propagation of the signals (6, 7) is possible.

2. Materials

2.1. Smooth Muscle Tissue

1. A segment of distal colon (~5 cm) excised from a male guinea pig (300–500 g) (8) (see Note 1).

2.2. Buffers

1. Oxygenated KREBS (physiological saline solution) for dissection (mM): 118.4 NaCl, 25 NaHCO_3 , 4.7 KCl, 1.13 NaH_2PO_4 , 1.3 MgCl_2 , 2.7 CaCl_2 , and 11 glucose; pH 7.4.

2. Cell isolation buffer (mM): 80 Na-glutamate, 55 NaCl, 6 KCl, 10 glucose, 10 Hepes, 1 MgCl₂, 1 CaCl₂, and 0.2 EDTA; pH 7.3 titrated with NaOH.
3. Cell isolation solution #1: Isolation buffer (item 2) which contains (mg/ml) 2.0 bovine serum albumin, 1.0 papain, and 0.7 dithioerythritol.
4. Cell isolation solution #2: Isolation buffer (item 2) contains (mg/ml) 2.0 bovine serum albumin, 1.5–3.5 collagenase type 1,2,3, or 4 (Worthington, USA) (see Note 2).
5. Extracellular bath solution (mM): 80 Na-glutamate, 40 NaCl, 20 tetraethylammonium chloride (TEA), 1.1 MgCl₂, 3 CaCl₂, 10 Hepes, and 30 glucose; pH 7.4 titrated with NaOH.
6. Pipette solution (mM): 85 (Cs)₂SO₄, 20 CsCl, 1 MgCl₂, 30 Hepes, 3 MgATP, 2.5 pyruvic acid, 2.5 malic acid, 1 NaH₂PO₄, 5 creatine phosphate, and 0.5 guanosine phosphate; pH 7.2.

2.3. General Reagents

1. Fluo-5F acetoxymethylester (AM) (Invitrogen, Paisley, UK). Made up as a stock (5 mM) solution by dissolving in dimethylsulfoxide and stored at -20°C until required (see Note 3).
2. Wortmannin (Sigma, Poole, UK). Made up as a 10 mM stock solution and stored as aliquots (5 µL) at -20°C until required.

2.4. Optical Instrumentation

1. The complete optical system is shown in Fig. 2. This system is based upon a conventional Nikon TE2000 inverted microscope and TIRF lens (×60, 1.49NA Nikon Plan Apo) (see Note 4).
2. The microscope has two filter turrets for dichroic mirrors on a dual epi-illuminator before the objective lens, enabling both conventional fluorescence excitation and TIRF excitation without moving any components on the microscope.
3. The TIRF light is provided by a frequency-doubled diode-pumped laser operating at 473 nm (Laser 2000, Northampton, UK) with a noise of less than 0.01% rms from 1 Hz to 10 MHz. The TEM₀₀ output is coupled using a homebuilt system into a single-mode optical fiber with a numerical aperture (N.A.) of 0.1 and a core diameter of 3 µm. The laser excitation has ~1.5 mW of light emerging from the end of the optical fiber.
4. The fiber is connected into the Nikon TIRF attachment at the rear of the TE2000 and the laser excitation is directed to the objective by a custom designed dichroic mirror (Z473RDC, Chroma, Vermont, USA) present in the top turret (Fig. 2a).
5. The objective lens allows the laser beam to be introduced at the outer edge of the objective aperture to achieve a high angle of incidence of the beam on the coverslip surface. The angle of incidence of illumination is adjusted to exceed the critical angle to generate TIRF and an evanescent excitation field giving a penetration ~100 nm (see Notes 5–7).

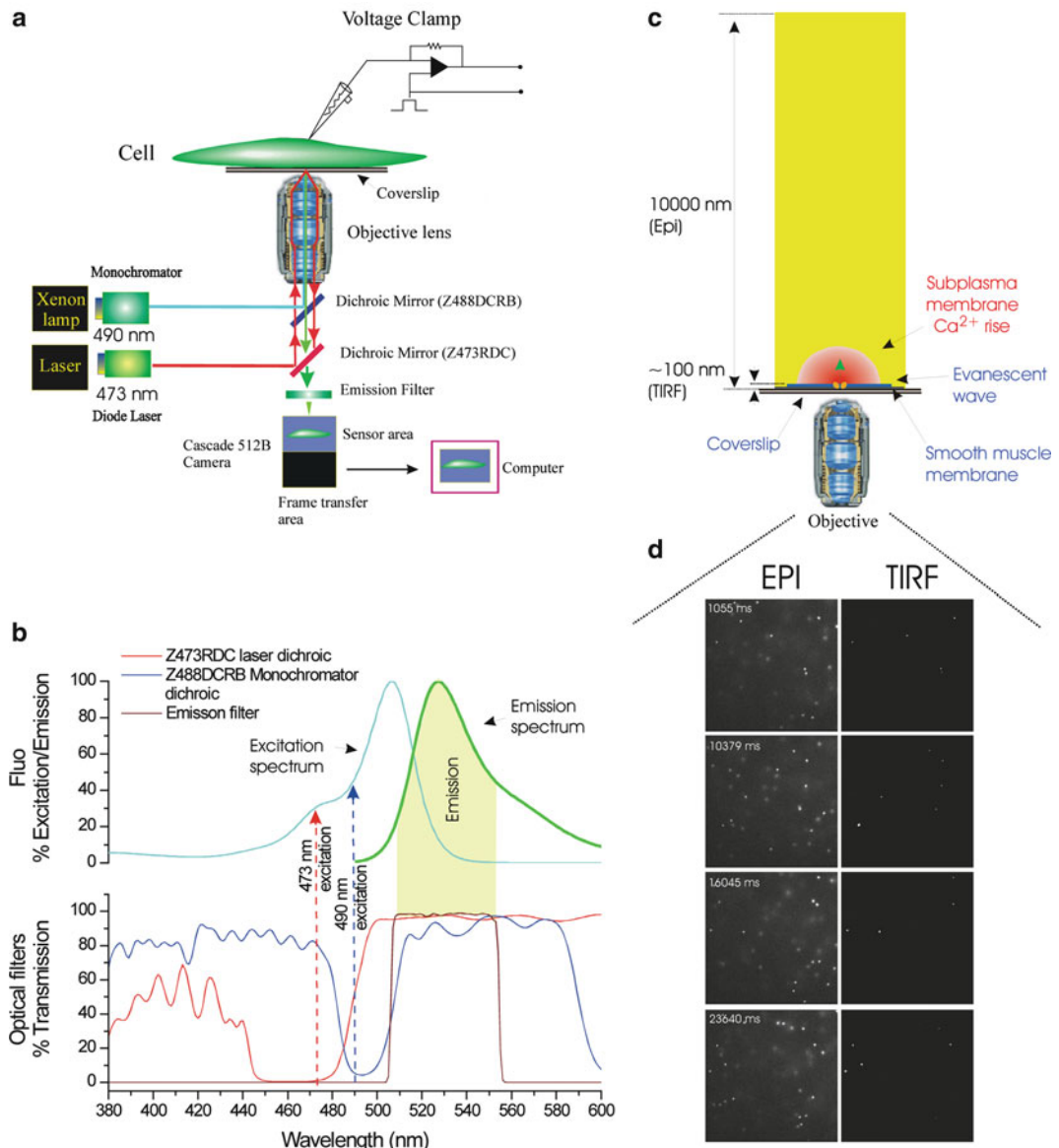


Fig. 2. Schematic of the TIRF and wide-field epi-fluorescence system. (a) The experimental system was constructed around a Nikon TE2000U microscope; excitation and emission light paths are shown. Single cells were voltage clamped in whole cell configuration. Cells were loaded with fluo-5F and illuminated by two separate excitation sources (at 490 and 473 nm) via a dual epi-illuminator. The first wavelength (490 nm, bandpass 5 nm; blue) was provided by a monochromator and guided via a fiber optic guide through a field stop diaphragm, a neutral density filter, and HQ480/40 excitation filter (not shown) before being reflected off a custom-made long-pass dichroic mirror (Z488DCRB). The latter was transmissive in the ranges 380–480 nm and 506–589 nm and reflective from 485 to 499 nm (b). The second excitation wavelength (473 nm; red), for TIRF illumination, was provided by a blue diode-pumped laser and guided via a fiber optic coupling through an iris and 10 \times beam expander. The 473 nm light was then reflected off a dichroic mirror (Z473RDC) and transmitted through the upper dichroic (Z488DCRB) (a, b) and focused to a spot on the back focal plane of the objective lens (Nikon 60 \times , oil immersion, NA 1.49). The laser focusing lens was mounted on a micrometer-driven translation system so that the laser beam could be adjusted to enter the periphery of the objective aperture to achieve total internal reflection at the interface between the cover glass and the aqueous bathing medium. Fluorescence excited in the specimen by the evanescent wave or wide-field epi-illumination was collected through the objective lens, passed through the dichroic mirrors and a

6. Wide-field epi-fluorescence excitation illumination is provided by an arc lamp (PTI Inc, West Sussex, UK) with the wavelength controlled via a monochromator to give 490 nm (band-pass 5 nm) coupled via a liquid light guide.
7. The monochromator light is directed to the objective by a custom designed dichroic interference filter (Z488DCRB, Chroma, USA) on the lower epi-illuminator (Fig. 2a). This light passes through the dichroic in the top epi-illuminator and onto the sample.
8. Rapid switching between TIRF and wide-field illumination is achieved by triggering the laser shutter open using a TTL pulse which simultaneously drives the monochromator to 250 nm (a wavelength that is optically blocked in the system). Terminating the TTL pulse shuts the laser closed and moves the monochromator to 490 nm (see Note 8).

3. Methods

3.1. Dissection and Smooth Muscle Cell Isolation

1. Excise distal colon and open the vessel with a longitudinal incision and pin on a Sylgard (Dow-Corning)-coated Petri dish.
2. Bath the tissue in oxygenated (95% O_2 –5% CO_2) physiological saline solution.
3. Remove the mucosa, connective tissue, and fat and use the circular smooth muscle layer to isolate single smooth muscle myocytes by a two-stage enzymatic dissociation (see Note 9).
4. To isolate single smooth muscle cells, incubate the tissue first for 25 min in isolation buffer #1, wash with isolation buffer (2 mg/ml BSA), and then incubate for 25 min in isolation buffer #2. Wash the tissue again in isolation buffer (2 mg/ml BSA) (see Note 10).
5. Triturate the tissue gently using a fire-polished Pasteur pipette to release single myocytes.
6. Store cells at 4°C and use within 24 h of isolation. Experiments are carried out at room temperature ($20 \pm 2^\circ\text{C}$).

Fig. 2. (continued) barrier filter, and imaged by a Photometrics Cascade 512B camera (Roper Scientific). The camera uses a back-illuminated frame transfer CCD with on-chip electron. (c) Enlarged view illustrating the imaging of near-membrane Ca^{2+} from the microdomain (red) around a single open channel by evanescent wave (blue) formed by the TIRF objective lens and the simultaneously measured wide-field epi-fluorescence depth of field. The depth of the TIRF field was ~100 nm and that of the wide-field epi-fluorescent field ~10,000 nm. (d) Single image frames of sub-resolution (100 nm) fluorescent latex beads floating in solution obtained in TIRF (right) and wide-field epi-fluorescence (left). Under wide-field epi-illumination (EPI, (d), left) sub-resolution fluorescent latex beads floating in solution are illuminated through the field. Individual beads drift through Brownian motion. In TIRF illumination (d, TIRF, right) beads are illuminated only when they are within the evanescent field, i.e., within ~100 nm of the coverslip. Beads diffusing in and out of the evanescent field appear and disappear suddenly (from McCarron et al. (2009) J Gen Physiol 133:439–457).

3.2. Fluo 5F AM Loading of Cells

1. Load cells with fluo 5F acetoxymethyl ester (AM) (5 μ M) together with wortmannin (10 μ M; to prevent contraction) for at least 20 min prior to the beginning of the experiment in the dark on a rocking platform (see Note 11).
2. Place cell suspension in a custom-built Perspex chamber (volume ~2 ml) with a No. 1 coverslip attached to the bottom (removable; sealed with vacuum grease) to allow imaging using an inverted microscope.
3. Allow cells to settle for at least 10 min.
4. Superfuse extracellular bath solution (~10 ml) slowly across the cell chamber to wash away any extracellular fluo 5F AM and introduce extracellular Ca^{2+} .

3.3. Electrophysiology

1. Patch clamp cells in the tight-seal, whole-cell configuration (9, 10) (see Note 12).
2. Lower the patch clamp electrode into the bath while maintaining positive pressure to prevent bath solution from being drawn up into the electrode.
3. Bring the electrode near to the cell and zero the liquid junction potential.
4. Apply a 5 mV repetitive pulse via the amplifier and monitor current as a measure of seal resistance.
5. Attach the electrode to the cell (cell-attached mode) by gentle suction at a holding potential of -30 mV; the current amplitude will gradually decline from a stepwise change to a flat line broken with small capacitance spikes.
6. Further gentle suction creates a small hole in the cell membrane (whole-cell mode); capacitance spikes increase in amplitude.
7. Slowly decrease the holding potential to -70 mV before switching from seal-test to external control.
8. Measure whole-cell currents using an Axopatch 200B (Axon Instruments, Union City, CA, USA), low-pass filter at 500 Hz, digitally sample at 1.5 kHz using a Digidata interface and pClamp (version 10; Axon Instruments), and store for analysis.
9. Trigger membrane depolarization using a protocol created in pClamp where the holding potential is increased from -70 mV to +10 mV for 500 ms to transiently depolarize the cell, and trigger Ca^{2+} entry and increase in $[\text{Ca}^{2+}]_c$.

3.4. Measurement of Intracellular Ca^{2+} in Wide-Field and TIRF

1. Measure bulk average $[\text{Ca}^{2+}]_c$ using conventional wide-field epi-fluorescence and subplasma membrane $[\text{Ca}^{2+}]_{PM}$ using TIRF (see Note 13).
2. Collect fluorescence emission from the smooth muscle cell by the objective lens. Select emission wavelength using a barrier

filter (D535-40 m; Fig. 2). Transmitted fluorescence is captured by a cooled, back-illuminated frame transfer CCD camera with on-chip electron multiplication (Cascade 512B; Photometrics Tuscan, AZ, USA).

3. Acquire images sequentially with alternating laser and monochromator illumination at a frequency of up to 300 Hz (see Note 14).
4. Synchronize electrophysiological measurements and imaging data by recording, on pClamp, a transistor-transistor logic (TTL) output from the CCD camera, which reports both its frame capture and readout status together with the electrophysiological information.

3.5. Data Analysis

1. Analyze $[\text{Ca}^{2+}]$ images using the program Metamorph 7.5 (Molecular Devices Ltd., Wokingham, England) (see Note 15).
2. To compensate for variations in fluorescence across the imaging field, e.g., from interference patterns from the glass coverslip and the coherent laser beam and irregularities in distance between the smooth muscle membrane and coverslip, express fluorescence signals as ratios (F/F_0 or $\Delta F/F_0$) of fluorescence counts (F) relative to baseline (control) values (taken as 1) before stimulation (F_0) after background subtraction. Do not filter, smooth, or average original fluorescence recordings (see Note 16).

3.6. Examples of $[\text{Ca}^{2+}]_{\text{PM}}$ and $[\text{Ca}^{2+}]_c$ Measurements from Single Colonic Smooth Muscle Cells

3.6.1. Depolarization-Evoked $[\text{Ca}^{2+}]_{\text{PM}}$ and $[\text{Ca}^{2+}]_c$ Increases

The authors have shown that depolarization of the plasma membrane (-70 to $+10$ mV) activates a voltage-dependent Ca^{2+} current and increases $[\text{Ca}^{2+}]_c$ (Fig. 3). The $[\text{Ca}^{2+}]_c$ increase, measured in the bulk cytoplasm, by wide-field epi-fluorescence, occurs approximately uniformly and simultaneously throughout the cell. In contrast, the increase in $[\text{Ca}^{2+}]_{\text{PM}}$ measured by TIRF was, in some regions, neither uniform nor simultaneous in either transient (Fig. 3) or prolonged (Fig. 4) depolarizations.

1. Isolate cells (see Subheading 3.1, steps 1–9).
2. Load an aliquot of the cell suspension with fluo 5F AM (see Subheading 3.2).
3. Settle the loaded cells on a glass coverslip bottomed chamber and wash.
4. Patch clamp a single cell in whole-cell configuration and maintain at a holding potential of -70 mV.
5. Measure $[\text{Ca}^{2+}]_{\text{PM}}$ changes near simultaneously in epi-fluorescence and TIRF (see Note 17).
6. Figure 3 shows that the time course of the rise, the peak amplitude, and the rate of recovery of $[\text{Ca}^{2+}]_c$ to baseline values, after the end of depolarization, in different regions of the cell,

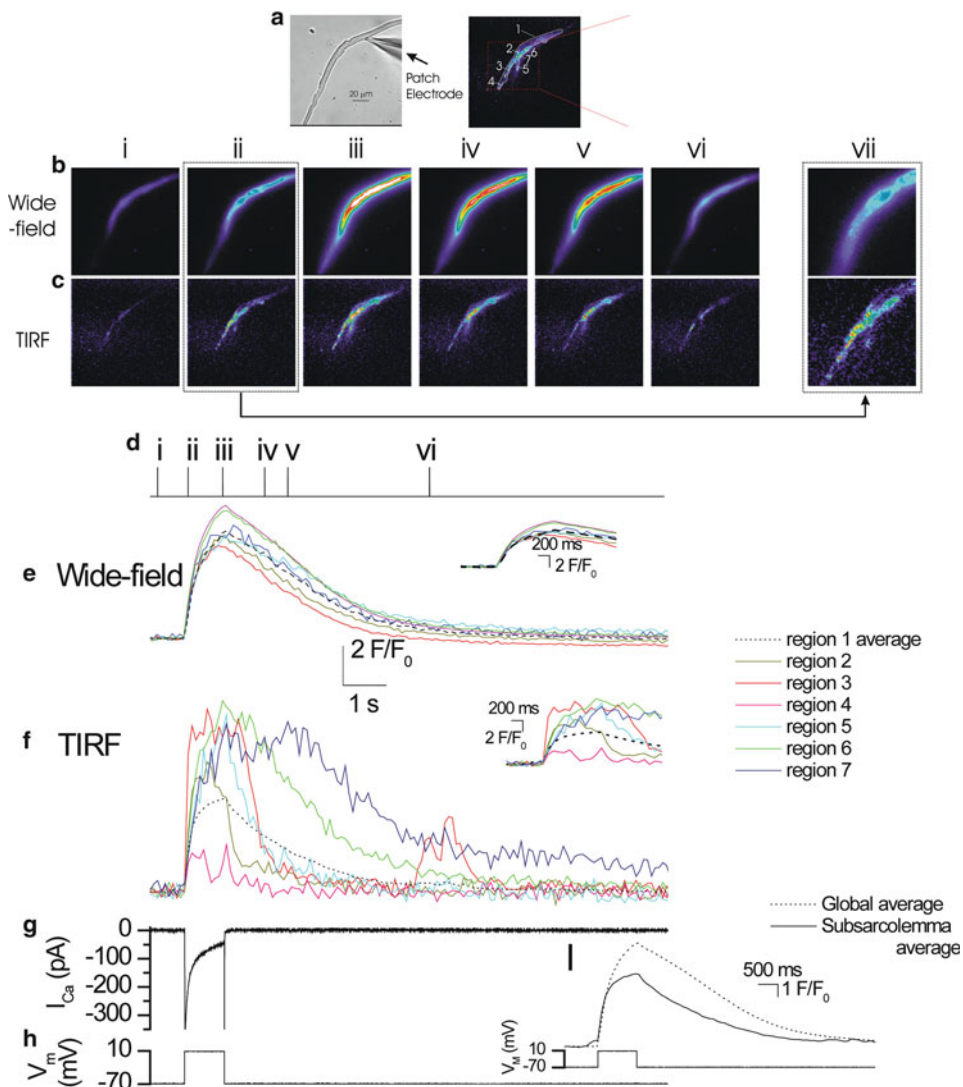


Fig. 3. Simultaneous wide-field epi-fluorescence and TIRF $[Ca^{2+}]$ measurements in voltage-clamped single colonic myocytes. Depolarization (-70 mV to $+10\text{ mV}$; H) activated a voltage-dependent Ca^{2+} current (I_{Ca} ; G) to evoke a rise in $[Ca^{2+}]$ (b, c, e, f). The rise in $[Ca^{2+}]$ which occurred in the subplasma membrane space (measured by TIRF) (c, f) was more rapid in onset than that seen in the bulk cytoplasm (measured by wide-field epi-fluorescence) (b, e). The $[Ca^{2+}]$ images (b, c) are derived from the time points indicated by the corresponding numerals in (d). $[Ca^{2+}]$ changes in (b, c) are represented by color: blue low and red/white high $[Ca^{2+}]$. The images (b, c) were taken before (i), during (ii-iii), and after (iv-vi) depolarization and show the resulting $[Ca^{2+}]$ changes. Changes in the fluorescence ratio with time (e, f) are derived from 2×2 pixel boxes (regions 1–6 in a, middle and right (expanded) panel; drawn at a 3×3 pixel size to facilitate visualization) and from a larger region encompassing the entire TIRF region (region 7). The latter was used to obtain an average subplasma membrane and bulk average $[Ca^{2+}]_c$ increase (i). Significantly, while the $[Ca^{2+}]_c$ increase which occurred in the bulk cytoplasm (b, e) was approximately uniform and simultaneous throughout the cell, those in subplasma membrane space (c, f) had a wide range of amplitudes and various time courses. Note the spark-like events in region 3 towards the end of the recording. (a) Left panel shows a bright field image of the cell; see also whole cell electrode (right side). Insets in (e, f) show the rising phase of the transients on an expanded time base. For comparison, (i) shows the average subplasma membrane and bulk average $[Ca^{2+}]_c$ rise as measured in region 7 (a, right-hand panel). (b, c) (vii) shows an enlargement of (ii) to illustrate the localized nature of the rise in $[Ca^{2+}]$ in the subplasma membrane space (from McCarron et al. (2009) J Gen Physiol 133:439–457).

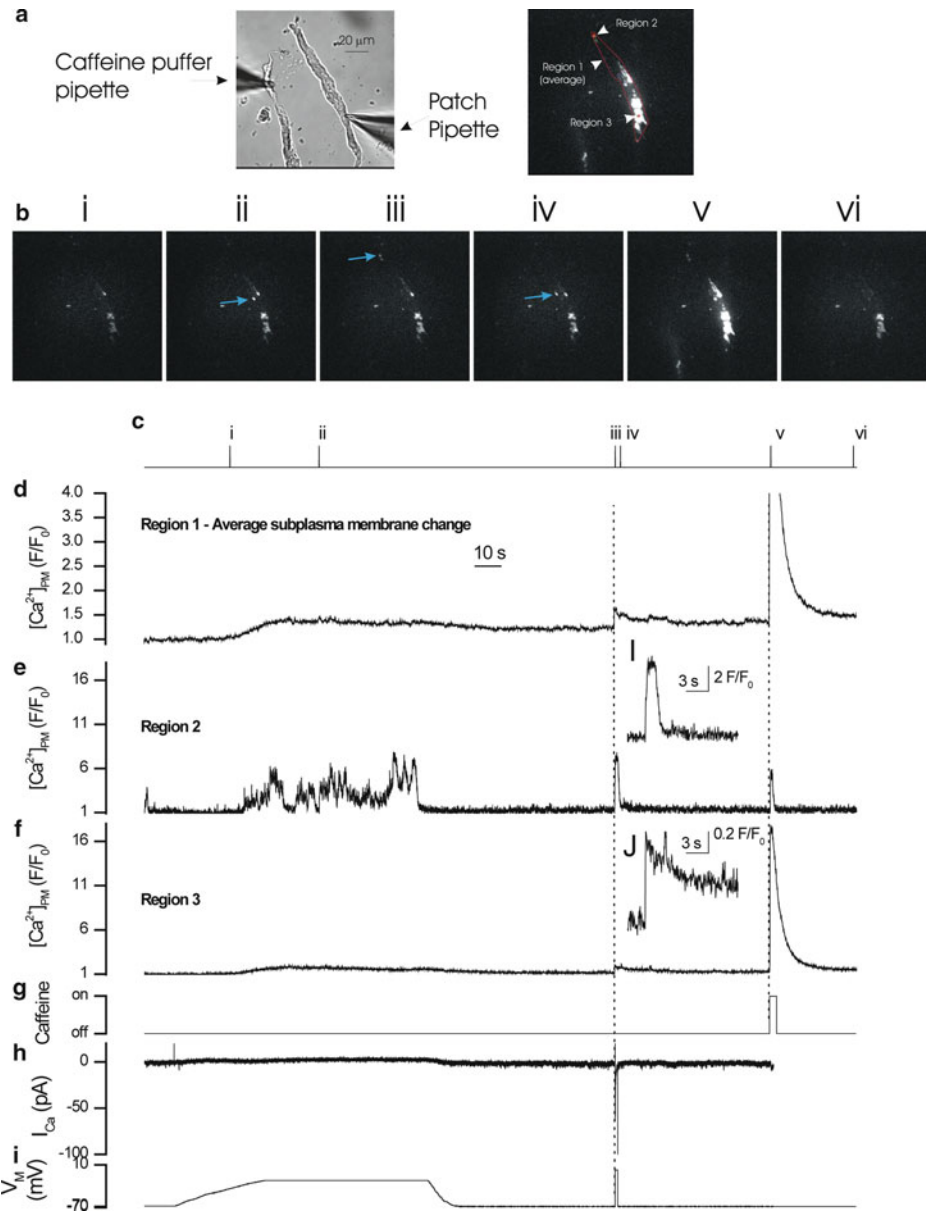


Fig. 4. Local subplasma membrane Ca^{2+} transients in response to plasma membrane depolarization and caffeine in a voltage-clamped single colonic myocyte. Gradual depolarization from -70 mV to -20 mV (i) elevated $[\text{Ca}^{2+}]$ in the subplasma membrane space as measured in TIRF (d–f). The $[\text{Ca}^{2+}]$ increase was more localized and substantially larger in some regions than others (compare e and f). Two example regions (regions 2 and 3) are shown (panels e and f); localized rises occurred in region 2 but not region 3. Blue arrows in the frames in (b) (ii–iv) show examples of the localized rises in $[\text{Ca}^{2+}]$. The $[\text{Ca}^{2+}]$ increase which occurred in region 3 (f) was slow and of smaller magnitude than that of region 2 (e). When the membrane potential was restored to -70 mV (i) $[\text{Ca}^{2+}]$ was returned towards resting levels. A subsequent transient depolarization to 0 mV (h) activated voltage-dependent Ca^{2+} current (I_{Ca} ; h) and increased $[\text{Ca}^{2+}]$ (d–f). The increase was larger and declined more rapidly in region 2 (d and inset i) than region 3 (e and inset j). Those regions (region 2, e) which showed large responses to depolarization had small responses to RyR activation by caffeine (g). Conversely, a large response (region 3, f) to caffeine (g) occurred in regions with small responses to depolarization. Region 1 (d) is a subplasma membrane average change. Numerals in images (b) correspond to those in (c). Changes in the fluorescence ratio with time (d–f) are derived from 1 pixel boxes (regions 2 and 3; shown at 3×3 pixels to facilitate visualization) and from a larger region the entire TIRF image (region 1) to obtain an average subplasma membrane $[\text{Ca}^{2+}]$ change (d). The position of the regions from which the transients (d–f) were obtained is shown in (a) (right-hand panel). A bright field image of the cell is shown in (a; left panel); see also whole cell electrode (right side) and puffer pipette which contained caffeine (10 mM; left side) (from McCarron et al. (2009) J Gen Physiol 133:439–457).

did not differ significantly from each other (as measured by epi-fluorescence). In TIRF, the time course of the rise, the peak amplitude, and the rate of recovery of $[Ca^{2+}]_{PM}$ to baseline values, after the end of depolarization, in certain regions differed significantly from the average $[Ca^{2+}]_{PM}$ values and those in identical regions of the bulk cytoplasm.

3.6.2. Caffeine-Evoked $[Ca^{2+}]_{PM}$ Increases

The authors have shown that activation of RyR with caffeine evokes $[Ca^{2+}]_{PM}$ increases. Although there was a large global $[Ca^{2+}]_{PM}$ increase the magnitude of Ca^{2+} increase varied at different subplasma membrane locations (Fig. 4).

1. Isolate cells (see Subheading 3.1, steps 1–9).
2. Load an aliquot of the cell suspension with fluo 5F AM (see Subheading 3.2).
3. Settle loaded cells on a glass coverslip bottomed chamber and wash.
4. Patch clamp a single cell in whole-cell configuration and maintain at a holding potential of -70 mV.
5. Puff caffeine onto the cell using hydrostatic pressure ejection.
6. Measure $[Ca^{2+}]_{PM}$ changes in TIRF.
7. Figure 3 shows that region 2 produces a relatively small caffeine-evoked $[Ca^{2+}]_{PM}$ increase as compared to region 3 (note the scale difference for the average subplasma membrane change). Interestingly, region 2 shows a much greater $[Ca^{2+}]_{PM}$ increase during V_M depolarization as compared to region 3.

4. Notes

1. Male guinea pigs (300–500 g) are humanely killed in accordance with the guidelines of the Animal (Scientific Procedures) Act UK 1986.
2. The collagenase type and concentration are determined empirically for each enzyme lot used. When purchasing a new collagenase we batch test several types (1–4) of collagenase to determine the optimal type and concentration. Although expensive and time consuming, once determined, in our hands, the parameters are kept with little variation for 1–2 years or until the lot is consumed.
3. Fluo 5F has reportedly faster Ca^{2+} binding kinetics and lower affinity as compared to fluo 4, which is advantageous when measuring $[Ca^{2+}]_c$ at the plasma membrane near channel openings.
4. In basic terms (specific systems can vary slightly) an annular ring of light is directed into the back aperture of a very high

numerical aperture lens (Fig. 2b). The numerical aperture is such that this light is totally internally reflected when it tries to exit the sample slide to create the required evanescent field. The same objective lens then observes fluorescence emitted from the sample in a conventional epi-configuration using the central portion of the lens. The advantage of this method is that the light annulus can be controlled at the rear of the microscope enabling a simple adjustment of the angle of the light to be made to set the TIRF angle through the objective. Thus no optical coupling (except the normal oil for a high NA objective) is required near the sample and all the illumination optics can be kept away from the wet (physiological solutions), and less than ideally clean, biological area. In addition the laser beams can be fully enclosed, reducing the laser safety concerns that exist with exposed beams.

5. To determine optimal imaging conditions, a test sample which consists of sub-resolution fluorescent beads bathed in fluorescein is imaged. This sample allows imaging parameters (illumination angle and intensity) which produce maximum image contrast to be determined and an illumination field that is generally even to be generated (Fig. 2d).
6. Even though TIRF imaging exceeds the diffraction limit in the axial direction, the limit of resolution in the lateral direction remains at the diffraction limit.
7. The electromagnetic field has a frequency identical to that of the incident light and an exponential intensity profile which is maximum at the glass–liquid interface.
8. One unexpected issue which arose in establishing these methods came from the relatively slow (2 ms) movement of the monochromator between 250 and 470 nm when compared to the CCD camera’s rapid frame switch (~2 µs) in frame transfer mode. As a result a small amount of light from the “wrong” wavelength initially was recorded during the 2-ms monochromator switch which created an increased background fluorescence. After exploring several possibilities the simplest solution was to add a 490 nm narrow bandpass excitation filter to the monochromator excitation light path. Imaging was achieved using EMCCD cameras (a photometrics Evolve 128 (full frame rate ~300 frames/s) or cascade 512B (full frame rate ~30 frames/s)) (Fig. 2).
9. The smooth muscle is cut into 1 cm strips. Two strips were used for each collagenase concentration and typically three collagenase concentrations were used in each isolation procedure.
10. It is possible to modify the protocol (enzyme concentration and time of incubation) for other smooth muscle tissues.
11. Choose a density of cells that allows individual cells to be imaged.

12. Fire-polished glass electrodes (tip diameter ~2–5 μm) are filled with pipette solution (see Subheading 2.2, step 7).
13. One difficulty which arises when using freshly isolated smooth muscle cells comes from their crenulated structure which may result in the cells not lying completely flat on the coverslip. The evanescent wave extends only ~100 nm from the coverslip (Fig. 2c) and if the cells are not flat there is only a small footprint of cell that can be viewed.
14. In TIRF the imaging speed limitation is not determined by the kinetics of the excitation source (as in confocal microscopy, STED, STORM, PALM, and SIM) but only by the acquisition rate of the imaging camera and speed and brightness of the indicators to enable imaging rates of ~300 frames per second with adequate signal intensity.
15. Any suitable off-line image analysis software should work (i.e., ImagePro, ImageJ, Velocity). Metamorph works well for our purposes because it allows real-time evaluation of individual regions of interest (ROI) as a function of time.
16. An issue which may limit the full analysis of results is that the Ca^{2+} signals measured in the evanescent field are a complex sum of signals from saturated fluorophore near the channel reducing to signal from infrequent binding events at a small distance from the channel. Fluorophore saturation will mean that the gradient cannot easily be de-convolved so that the fluorescent signal is likely to be an especially nonlinear representation of Ca^{2+} changes. Even if the dye did not saturate, converting the fluorescent signal to a Ca^{2+} concentration relies on calibration carried out in steady-state conditions. Such conditions are unlikely to be valid in the rapidly changing micro-domains in the subplasma membrane space during Ca^{2+} influx. Indeed it is likely that the assumption that the dye equilibrates instantly with Ca^{2+} will not be correct during influx near a Ca^{2+} channel which is rapid (~0.6 million ions per second), i.e., there is local nonequilibrium within the system (11). Even the rapid small molecule Ca^{2+} indicators are too slow to follow these fast Ca^{2+} increases.
17. Many (~30%) cells that had been voltage clamped were rejected because they failed to show fluorescence in TIRF, even though fluorescence occurred in wide-field epi-fluorescence. The absence of fluorescence in TIRF suggests that those cells had not come into contact with the glass coverslip sufficiently well to bring the cytosol within the evanescent field. In cells where TIRF fluorescence was evident, fluorescence did not occur throughout but over restricted regions (20–100 μm) of the cell presumably because the cell had uneven contact with the coverslip.

Acknowledgements

This work was funded by the Wellcome Trust (092292/Z/10/Z) and British Heart Foundation (PG/08/066 and BHF Research Excellence Award); their support is gratefully acknowledged.

References

1. Demuro A, Parker I (2005) "Optical patch-clamping": single-channel recording by imaging Ca²⁺ flux through individual muscle acetylcholine receptor channels. *J Gen Physiol* 126:179–192
2. Navedo MF, Amberg GC, Votaw VS, Santana LF (2005) Constitutively active L-type Ca²⁺ channels. *Proc Natl Acad Sci U S A* 102:11112–11117
3. McCarron JG, Olson ML, Currie S, Wright AJ, Anderson KI, Girkin JM (2009) Elevations of intracellular calcium reflect normal voltage-dependent behavior, and not constitutive activity, of voltage-dependent calcium channels in gastrointestinal and vascular smooth muscle. *J Gen Physiol* 133:439–457
4. Hecht E (2002) Optics, 4th edn. Addison-Wesley, Boston
5. Olson ML, Chalmers S, McCarron JG (2010) Mitochondrial Ca²⁺ uptake increases Ca²⁺ release from inositol 1,4,5-trisphosphate receptor clusters in smooth muscle cells. *J Biol Chem* 285:2040–2050
6. McCarron JG, Bradley KN, MacMillan D, Muir TC (2003) Sarcolemma agonist-induced interactions between InsP₃ and ryanodine receptors in Ca²⁺ oscillations and waves in smooth muscle. *Biochem Soc Trans* 31:920–924
7. McCarron JG, Chalmers S, MacMillan D, Olson ML (2010) Agonist-evoked Ca²⁺ wave progression requires Ca²⁺ and IP₃. *J Cell Physiol* 224:334–344
8. Chalmers S, McCarron JG (2008) The mitochondrial membrane potential and Ca²⁺ oscillations in smooth muscle. *J Cell Sci* 121:75–85
9. McCarron JG, Olson ML (2008) A single luminally continuous sarcoplasmic reticulum with apparently separate Ca²⁺ stores in smooth muscle. *J Biol Chem* 283:7206–7218
10. Bradley KN, Currie S, MacMillan D, Muir TC, McCarron JG (2003) Cyclic ADP-ribose increases Ca²⁺ removal in smooth muscle. *J Cell Sci* 116:4291–4306
11. Bortolozzi M, Lelli A, Mammano F (2008) Calcium microdomains at presynaptic active zones of vertebrate hair cells unmasked by stochastic deconvolution. *Cell Calcium* 44:158–168

Chapter 16

Simultaneous Analysis of Intracellular pH and Ca²⁺ from Cell Populations

Raul Martinez-Zaguilan, Linda S. Tompkins, Robert J. Gillies, and Ronald M. Lynch

Abstract

Although changes in both pH_{in} and $[\text{Ca}^{2+}]_{\text{i}}$ have been observed in response to a variety of agonists, it is not clear whether these ionic events work independently or are coordinated to lead to a specific physiological response. One of the fundamental problems in studying these ionic events is that changes in pH_{in} modify Ca^{2+} regulatory mechanisms and changes in Ca^{2+} may modify pH regulation. It is desirable to use a technique that allows concomitant monitoring of these two ions in cell populations with high time resolution. Furthermore, like many Ca^{2+} binding proteins, all Ca^{2+} -sensitive fluoroprobes are inherently sensitive to pH owing to competition of H^{+} for the Ca^{2+} -binding sites. This chapter describes experimental paradigms that provide optimum conditions for simultaneous measurement of pH from the fluorescence emission of snarf-1, and Ca^{2+} using fura-2. The fluorescence spectra of these compounds are sufficiently different to allow simultaneous measurement of pH and Ca^{2+} both in vitro and in vivo. Moreover, the ratio of the H^{+} -sensitive wavelengths of snarf-1 is unaffected by Ca^{2+} , or the concomitant presence of fura-2 in cells. Although the fluorescence ratio of fura-2 is insensitive to the presence of snarf-1, it is affected by pH, as indicated above. We describe procedures to correct for this effect and to obtain calibration parameters for fura-2 and snarf-1 required to facilitate analysis of pH and Ca^{2+} concentrations within cell populations.

Key words: Intracellular Ca^{2+} , Intracellular pH, Snarf-1

1. Introduction

Manipulation of cell function through stable transfection of agonist-specific receptors, components of second messenger cascades, or proteins with specific functional activities (enzymes, transporters, and channels) has provided the tools to study intra- and intercellular signaling phenomena at a molecular level (1–3). In addition, cotransfection of cells with sequences coding for fluorescent markers such as green fluorescent protein has facilitated the selection and analysis of transfected cells (4, 5). Techniques are

also required to screen for and to monitor the functional changes associated with the genetic manipulation in order to investigate the physiological role of a component within a complex system such as a cell. Hormones and other agonists often elicit changes in intracellular pH (pH_{in}) (6, 7) and/or calcium ($[\text{Ca}^{2+}]_{\text{i}}$) (8, 9) that modulate cell responses. Thus, methods for comparing steady-state ion concentrations and the regulation of these ions between cell populations in which signaling pathways have been modified can provide an approach to screen for functional changes in signal transduction for selective agonists.

There are several fluorescent indicators for measuring pH and Ca^{2+} (10). These probes are commercially available in acetoxyethyl (AM) ester forms, which allow passive loading of cells with minimal effect on cell physiology (10). Optimally, these probes should be specific for the ion of interest and have a high quantum efficiency, and the affinity of the probe (K_d) for the ion of interest should be within the physiological range. To simultaneously monitor pH_{in} and $[\text{Ca}^{2+}]_{\text{i}}$, the probes need to have distinct excitation or emission characteristics. An additional feature required for accurate analyses is that each probe exhibit at least two excitation or emission wavelengths reciprocally sensitive to the ion of interest. The ratio of ion-sensitive wavelengths provides a precise measure of ion levels that is relatively independent of dye concentration. An excitation or emission wavelength that is ion insensitive is also desirable, since analysis of signal intensity at this wavelength allows for simultaneous determination of the efficiency of dye loading, dye leakage from cells, as well as possible interactions between probes including quenching (11).

Two probes that meet the described criteria for simultaneous pH/ Ca^{2+} measurements are snarf-1 and fura-2 (11, 12). The ratio of fluorescence emission intensities at 644/584 nm for snarf-1, and the ratio of fura-2 fluorescence excited alternately at 340/380 nm can be used to generate calibration curves for pH and Ca^{2+} , respectively. The isoexcitation wavelength (ion insensitive) for fura-2 at 360 nm and the isoemission wavelength of snarf-1 at 600 nm are monitored to determine the stability of dye loading and to alert one to other potential artifacts.

Although changes in both pH_{in} and $[\text{Ca}^{2+}]_{\text{i}}$ have been observed in response to a variety of agonists, it is not clear whether these ionic events work independently or are coordinated to lead to a specific physiological response. One of the fundamental problems in studying these ionic events is that changes in pH_{in} modify Ca^{2+} regulatory mechanisms (e.g., Ca^{2+} -binding proteins, Ca^{2+} ATPase (11) Ca^{2+} channels (13)) and changes in Ca^{2+} may modify pH regulation (e.g., $\text{Na}^{+}/\text{H}^{+}$ exchanger (14), H^{+} -ATPase (15)). Therefore, it is desirable to use a technique that allows concomitant monitoring of these two ions in cell populations with high time resolution. Furthermore, like many Ca^{2+} binding proteins, all Ca^{2+} -sensitive

fluoroprobes are inherently sensitive to pH owing to competition of H⁺ for the Ca²⁺-binding sites (12, 16). Thus, changes in pH induced by an agonist can complicate analysis of the activated Ca²⁺ response when using Ca²⁺ fluoroprobes. Similarly, analysis of differences in steady-state Ca²⁺ between unique cell populations can be influenced by differences in resting cell pH. For example, resting pH in neoplastic cells is generally higher compared to normal controls (17). For most Ca²⁺ fluoroprobes, the sensitivity to H⁺ is most prevalent at relatively acidic pH values (12, 16). However, many cell lines do exhibit resting pH lower than 7.0, and some perturbations can lower pH into the sensitive range. Fortunately, the effect of pH on the Ca²⁺-binding parameters can be predicted and used to correct the Ca²⁺ signal (12, 16).

This chapter describes experimental paradigms that provide optimum conditions for simultaneous measurement of pH from the fluorescence emission of snarf-1, and Ca²⁺ using fura-2. The fluorescence spectra of these compounds are sufficiently different to allow simultaneous measurement of pH and Ca²⁺ both in vitro and in vivo. Moreover, the ratio of the H⁺-sensitive wavelengths of snarf-1 is unaffected by Ca²⁺, or the concomitant presence of fura-2 in cells (16). Although the fluorescence ratio of fura-2 is insensitive to the presence of snarf-1, it is affected by pH, as indicated above. Therefore, the authors will describe procedures to correct for this effect and to obtain the calibration parameters (K_d or p K_a , R_{min} and R_{max}) for fura-2 and snarf-1 required to facilitate analysis of pH and Ca²⁺ concentrations within cell populations.

2. Materials

1. Three cell lines are used in the studies described:
 - (a) RIN-38 are an insulin-secreting transformed β cell line (18).
 - (b) Endothelial cells were isolated from human umbilical vein endothelium (HUVE) (19).
 - (c) HSF cells are fibroblasts isolated from human skin.
2. Cell culture media is Dulbecco's modified Eagle's medium supplemented with 5.6 mM glucose, 10% fetal bovine serum (FBS), 1 U penicillin/mL, and 0.1 mg/mL streptomycin sulfate.
3. Cells are cultured for experiments on glass coverslips (9×22 mm) contained in 10-cm dishes at initial plating densities of approx 5×10^4 cells/dish. Cells are grown to near confluence for fluorescence experiments.
4. 0 Ca²⁺ buffer (KEGTA): 110 mM KCl, 20 mM MOPS, 20 mM NaCl, and 10 mM K₂H₂EGTA. The K₂H₂EGTA is obtained by

mixing equimolar concentrations of EGTA and K₂CO₃. pH is adjusted using KOH.

5. Calcium-saturated buffer (CaEGTA): 110 mM KCl, 20 mM MOPS, 20 mM NaCl, and 10 mM K₂CaEGTA obtained by mixing equimolar concentrations of EGTA and CaCO₃. The most critical requirement for this buffer is to contain equimolar concentrations of calcium and EGTA in order to achieve a stoichiometric balance. Because EGTA is rarely 100% pure, these buffers normally contain a 5% excess of EGTA by weight (see Note 1). This excess EGTA in K₂EGTA buffer is not likely to cause problems because the performance of calcium buffers is not very sensitive to total calcium concentration.
6. Standard experimental buffer (EB): 1.3 mM CaCl₂, 1 mM MgSO₄, 5.4 mM KCl, 0.44 mM KH₂PO₄, 110 mM NaCl, 0.35 mM NaH₂PO₄, 1 mM NaHCO₃, 5 mM glucose, 2 mM glutamine, and 25 mM HEPES, pH 7.15, at 37°C. Experiments can be performed under 5% CO₂/95% air if the EB contains HCO₃⁻ at a concentration set by its equilibrium with CO₂ at the desired pH value using Eq. 1

$$[\text{HCO}_3^-] = pK_a (1.52 \text{ mM}) \times 10 (\text{pH} - 6.24) \quad (1)$$

in which 1.52 mM is the concentration of CO₂ in Hank's balanced salt solution at 37°C, and 5% ambient CO₂ (e.g., pCO₂ = 38 mmHg); and 6.24 is the pK for the process of CO₂ hydration (20).

7. In vitro pH values used for calibration are obtained with a pH meter using a standard gel-filled combination electrode. The electrode is calibrated at two known pH values using commercially prepared standards from VWR Scientific (San Francisco, CA).
8. Fluorescence measurements are performed in a temperature-controlled cuvette housed in an SLM 8000C fluorometer (SLM, Urbana, IL) using 4-nm band-pass slits and an external rhodamine standard as a reference. Sample temperature is maintained at 37°C by keeping both the water jacket and the buffer at 37°C using a circulating water bath. Spectral data for fura-2 are acquired by scanning the excitation monochromator between 300 and 500 nm with the emission monochromator set at 510 nm. Spectra from snarf-1 are acquired by setting the excitation monochromator at 534 nm and scanning the emission monochromator between 540 and 700 nm.
9. Cell holder for fluorometric measurements: Two coverslips containing cells are placed back to back (cells on the outside surface), and transferred to the quartz fluorometer cuvette using a holder/perfusion device as described previously (21). The holder maintains the coverslips upright in the fluorescence light

path at an angle of 30° allowing for illumination of a spot at the same position on both coverslips. The use of quartz cuvettes is essential when monitoring fluorescence in the ultraviolet region, as with fura-2. Tubing from a dual line peristaltic pump is used to introduce fresh media into the bottom of the chamber while removing an equal volume from the chamber top. Small bore tubing (Masterflex #13, Fluid Metering Inc., Syosset, NY) is used as the inlet and larger bore tubing (#14) for the outlet line. The cells are continuously perfused at a rate of 3.0 mL/min (see Note 2). Prototypes of this device with modifications have been published elsewhere (21, 22). A commercially available coverslip holder for fluorescence measurements is also available (Spectronics Instruments, Rochester, NY).

10. Fluorometric data collection for simultaneous pH and Ca²⁺ measurements: Continuous data collection occurs while the emission and excitation modes are alternated as follows. Emission at 510 nm with sequential scanning to excitation wavelengths of 340, 360, and 380 nm (fura-2 conditions), followed by excitation at 534 nm with the emission monochromator sequentially scanned to 584, 600, and 644 nm (snarf-1 conditions). An individual cycle requires 15 s. Temporal resolution is limited primarily by the slew rate of the monochromator, and not integration time of the phototube. Data are translated to ASCII format for manipulation and analysis (16).
11. Data analysis: Conversions of ratio values to both pH_{in} and Ca²⁺ are performed using Eqs. 2, 3, and 6 (Subheading 3.1), and plotted using a commercial software (see Note 3; SigmaPlot, Statistical Product and Service Solutions, Chicago, IL). Analysis of both in vitro and in situ calibration curves, as well as estimation of the pK_as, R_{max}, and R_{min} values for snarf-1 and fura-2, is obtained from Eqs. 1–5 using a simplex method and by least-squares regression analysis (MINSQ, MicroMath Scientific Software, Salt Lake UT, or SigmaPlot).
12. Fluoroprobes can be obtained from several sources from including Molecular Probes (Eugene, OR), and Teflabs (Austin, TX). For each day of experiments, a fresh batch of dye is used. AM dyes are prepared using anhydrous methylsulfoxide (MSO) as a solubilizing agent. The fluorescent probes can be obtained in 50-μg or 1-mg portions. MSO is removed from its container using a syringe equipped with an appropriate gauge needle, or, for the small volumes required for the 50-μg containers, a Hamilton syringe can be used. If 1-mg quantities are prepared, the stock solution should be aliquoted into smaller portions (10 μL) and stored at –80°C until use. Freeze thawing of probes should be avoided.
13. Unless otherwise stated, all other chemicals of commercial grade were from Sigma (St. Louis, MO).

3. Methods

3.1. Calculation of pH and Ca²⁺ from the Ratio of Ion-Sensitive Wavelengths

Excitation or emission wavelengths that increase or decrease on cation binding are monitored. The ratio of fluorescence at the ion-sensitive wavelengths is used to determine the extent of ion-bound dye, and hence the free ion concentration by the following equations:

$$\text{pH} = pK_a + \log(S_{f2} / S_{b2}) + \log[(R - R_{\min}) / (R_{\max} - R)] \quad (2)$$

$$[\text{Ca}^{2+}] = K_d (S_{f2} / S_{b2}) [(R - R_{\min}) / (R_{\max} - R)] \quad (3)$$

in which R , R_{\min} , and R_{\max} are the measured, minimum, and maximum ratios, respectively. For snarf-1, R increases with pH; hence R_{\max} represents the ratio of fluorescence intensity of ion-sensitive wavelengths under fully deprotonated conditions, whereas R_{\min} is the ratio for the dye when it is fully protonated. In the case of fura-2, R increases with increasing Ca^{2+} ; hence R_{\min} represents fura-2 in the absence of Ca^{2+} ($\text{Ca}^{2+} < 1 \text{ nM}$) whereas R_{\max} represents the Ca^{2+} -fura-2 chelate. S_{f2} and S_{b2} are the fluorescence values at the denominator wavelengths for the free and bound forms of the dye, respectively. These values are used to correct the titration curve for the fact that denominator and numerator wavelengths are independently sensitive to ion binding. If an ion-insensitive wavelength is used as the denominator, S_{f2}/S_{b2} becomes 1 and the term is eliminated.

Since the ratio of fluorescence at the ion-sensitive wavelengths for fura-2 is affected by pH (at pH values > 7.0), corrections for changes in pH during an experiment, or when comparing steady-state values between populations is often warranted. The pH sensitivity of fura-2 can be described by the following equations which rely on data acquired from the calibrations described in Subheading 3.2. The effect of pH on the K_d is described by # (pH corrected):

$$K_d \# = (K_{d\max} + \log 10(\text{pH}_{\text{in}} - pK_a) \times K_{d\min}) / \log 10(\text{pH}_{\text{in}} - pK_a) + 1 \quad (4)$$

whereas the effect of pH on the R_{\min} and R_{\max} of fura-2 is determined by

$$R^{\#} = k1 \times (\text{pH})^3 + k2 \times (\text{pH})^2 + k3 \times (\text{pH}) + k4 \quad (5)$$

Equation 5 is empirically derived by fitting data acquired from the in vitro calibration curves generated for fura-2 as pH is varied. Thus, pH-corrected $[\text{Ca}^{2+}]$ ($[\text{Ca}^{2+}]^{\#}$) can be estimated by using the following equation and fitting these parameters into the equation:

$$[\text{Ca}^{2+}]^{\#} = K_d \# \times (R - R_{\min}^{\#}) / (R_{\max}^{\#} - R) \quad (6)$$

The accuracy of the $[\text{Ca}^{2+}]$ estimate relies on the accuracy of in situ and in vitro titrations (16). It also relies heavily on appropriate

estimations of pH. In many cases, the K_d of fura-2 for Ca^{2+} in vitro is similar to that measured in situ, so this parameter may not be cell-type dependent (12, 16). However, other investigators have reported differences between the in vitro and in situ estimated K_d values (23, 24). Moreover, the R_{\max} and R_{\min} values are likely to be cell-type dependent because the dynamic range of the dyes is determined by viscosity and interactions of dye with intracellular proteins. Thus, the authors emphasize the need for determining the calibration parameters in individual cell types if accurate quantification of $[\text{Ca}^{2+}]$ is required.

3.2. In Vitro Calibration of Snarf-1 and Fura-2

In vitro calibration of dyes allows estimation of pH and Ca^{2+} concentrations from the measured ratio values (Fig. 1). However, this calibration is also important to determine the dynamic range of the equipment and which R_{\min} and R_{\max} ratio values are reasonable. To calibrate the probes, Ca^{2+} concentration is varied at a set pH by combining fixed amounts of KEGTA and CaEGTA buffers that are held at constant and equal pH by strong buffers that do not bind Ca^{2+} , such as MOPS. A set of EGTA buffers are prepared between pH 5.5 and 8.0. Equal amounts of fura-2 and snarf-1 are added to each of the initial stock solutions. By serially diluting the KEGTA solution with CaEGTA at a given pH, calibration solutions are prepared with good precision. The magnitude of the increment in Ca^{2+} is determined by the effect of pH on the K_d EGTA; specifically, smaller (tenths of nanomolar increments) are obtained at alkaline

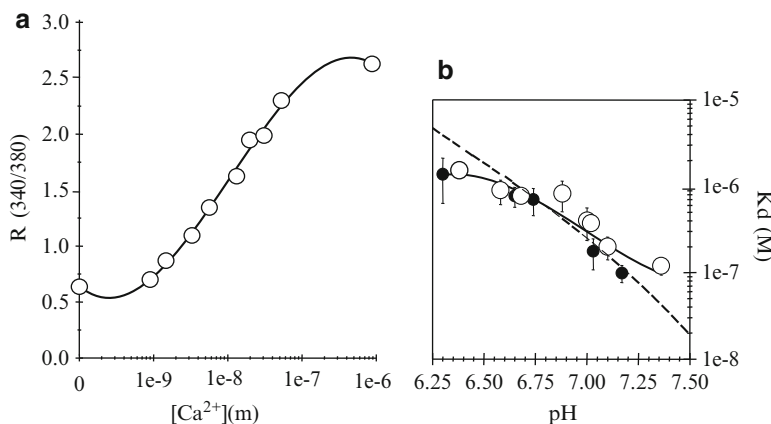


Fig. 1. In situ calibration of fura-2 in 3T3 cells (a). The 340/380 ratio for fura-2 increases as Ca^{2+} is increased at fixed pH. Similar calibrations were repeated over a range of pH values as indicated in (b). Panel (b) shows the effect of pH on the apparent affinity of fura-2 for Ca^{2+} estimated in vitro (i.e., free acid forms of the dyes in solution; open circles) and in 3T3 cells (closed circles). Each point represents the mean \pm SD of 9–11 different Ca^{2+} concentrations per pH value. H^+ and Ca^{2+} dissociation constants were calculated as described earlier. The dashed line indicates the effect of pH on the K_d of EGTA (16).

Table 1
Estimated concentration of Ca²⁺ at 37°C for three sequential dilutions as described in Subheading 3.2

Dilution	1	2	3	4	5	6	7	8	9	10	11
pH 7.2	0	1.0e-8	2.11e-8	3.35e-8	4.73e-8	6.25e-8	7.94e-8	9.83e-8	1.19e-7	1.42e-7	1.68e-7
pH 7.0	0	3.73e-8	7.88e-8	1.25e-7	1.76e-7	2.33e-7	2.96e-7	3.66e-7	4.45e-7	5.31e-7	6.28e-7
pH 6.3	0	4.69e-7	9.9e-7	1.57e-6	2.22e-6	2.93e-6	3.72e-6	4.6e-6	5.58e-6	6.67e-6	7.88e-6

pH, whereas larger increments (i.e., hundredths of nanomolar to micromolar) are obtained at acidic pH (25) (see Note 4).

1. Fura-2 and snarf-1 in their free acid forms are dissolved to final concentrations of 2 μM and 1 μM, respectively, into 30 mL of the KEGTA buffer held at 37°C and a specific pH between 5.5 and 8.0. pH is titrated using KOH.
2. A 3-mL aliquot is placed into a quartz cuvette, and the initial fura-2 excitation and snarf-1 emission data are acquired (zero Ca²⁺).
3. Three milliliters of CaEGTA (at the same pH) containing 2 μM fura-2- and 1 μM snarf-1-free acids is added to the remaining 27 mL with stirring; e.g., 9 mmol KEGTA added to 1 mmol CaEGTA. Again, a 3-mL aliquot is taken to acquire fura-2 excitation and snarf-1 emission data.
4. Each 3-mL aliquot removed for fluorescence analysis is replaced with an equal volume of the CaEGTA to provide a continuous variation in Ca²⁺. This procedure provides incremental changes in “cell” Ca²⁺, as described previously (12, 16). The estimated Ca²⁺ concentrations for each of 11 iterations at three distinct pH settings are provided in Table 1 as an example.
5. Another set of 30-mL starting solutions of KEGTA and CaEGTA are titrated to a unique pH, and the procedure is repeated. Increments of 0.25 pH units are reasonable for the initial titration. However, subsequent calibrations can be performed using 0.5 pH unit increments.

3.3. Loading of Ion-Sensitive Indicators into Cells

The ion-sensitive probes in their AM forms are lipophilic and cell permeant. Cellular esterases cleave the ester groups to yield free acids that are relatively impermeant and, therefore, “trapped” within cells (10). See Note 5 regarding sequestration of probes into sub-cellular compartments, and Note 6 regarding cell viability issues.

1. Two coverslips containing confluent or near confluent cell cultures are incubated for 30 min at 37°C in 3 mL of EB containing 7 μM snarf-1/AM and 2 μM fura-2/AM. This can be

performed in a single well of a six-well cell culture dish, and all wash solutions can occupy other wells (see Note 7).

2. After the 30-min loading period, the cells are washed three times with EB containing 0.2% (v/v) FBS, followed by a second incubation in FBS containing EB for 30 min, to allow for the complete hydrolysis of the esters, and leakage of uncleaved dyes from the cells.
3. The two coverslips are placed back to back into the holder/perfusion device, which is subsequently inserted into the fluorometer cuvette for pH/Ca²⁺ measurements.

3.4. In Situ Calibration of Snarf-1 and Fura-2

In situ calibrations are important to compare absolute steady-state concentrations of the ions in different cell populations. This is particularly important when cells are transfected with vectors that influence growth rate, which often is associated with changes in steady-state pH (3, 26). In addition, biological variability between cells must be recognized. By incubating cells in an “intracellular” buffer in the presence of selective ionophores for H⁺, K⁺, and Ca²⁺, intracellular ion concentration can be manipulated by changing media concentrations, and therefore, the probes trapped within the cytosolic compartment can be adequately calibrated. 4Br-A23187, a nonfluorescent Ca²⁺ ionophore is used in combination with nigericin/valinomycin in high K⁺/EGTA buffers to generate physiologically relevant calibration curves for intracellularly trapped fura-2 and snarf-1 (see Note 8). By varying pH_{ex} between pH 6.0 and 8.0 at 0.25 unit increments, one can obtain the pK_a of snarf-1 from the in situ calibration curves. Sequential incubation with media containing incrementally increasing Ca²⁺ concentration ranging from 0 to submicromolar or low micromolar to 250 μM provides a full analysis of K_d, R_{min}, and R_{max} for fura-2 at each pH.

1. 300 mL of KEGTA containing 2 μM 4Br-A23187, 2 μM valinomycin, and 5 μM nigericin is prepared.
2. Dye-loaded cells on coverslips are transferred to the fluorometer cuvette and perfused in KEGTA buffer at selected pH values. Fluorescence is then continuously recorded until equilibration of extracellular ions with the intracellular space is reached typically 3–5 min.
3. Fura-2 excitation and snarf-1 emission spectra are acquired (see Note 9).
4. Sequential dilutions: Steps 3–5 are identical to those carried out for in vitro calibrations (Subheading 3.2). However, a minimum of 3 min is required for equilibration of ions between media and intracellular space at the new Ca²⁺/pH setting (see Note 10).

3.5. Comparison of Steady-State Ion Concentrations Between Unique Cell Populations

To evaluate the validity of using *in situ* calibration parameters for estimating pH and Ca^{2+} in each specific experiment, the *in situ* R_{\min} and R_{\max} for both probes needs to be assessed. For simplicity and reliability, cells are perfused with KEGTA and CaEGTA buffers (containing ionophores) at three distinct pH values (i.e., 6.0, 7.0, and 7.5) to obtain the corresponding R values, thereby allowing comparison of the *in situ* titration parameters from a discrete number of points versus those generated from a complete *in situ* titration (see Note 10).

1. Dye-loaded cells on coverslips are transferred to the fluorometer cuvette and perfused in EB for 2–3 min prior to data acquisition. Full emission and excitation spectra are acquired to evaluate the quality of the spectra (see Note 11).
2. Fluorescence data at ion-sensitive wavelengths are then acquired, and ion-insensitive wavelengths are followed to determine if dye loading is stable or if dye is quenched (see Notes 12 and 13).
3. The resting ion concentrations are evaluated after a stable signal is obtained (see Note 14).
4. Full emission and excitation spectra of snarf-1 and fura-2 are acquired to confirm that the spectral characteristics are comparable to the calibration spectra.
5. The perfusion media are changed to KEGTA buffer containing ionophores at a selected pH value (e.g., 6.3; Table 1, see Note 9), and fluorescence is continuously recorded until equilibration of extracellular ions with the intracellular space is achieved—typically 3–5 min.
6. The perfusion media are changed to KEGTA diluted with CaEGTA held at equal pH to obtain a midrange Ca^{2+} concentration (e.g., approx 3 μM , dilution 5; see Note 9, Table 1).
7. The perfusion media are changed to KEGTA diluted with CaEGTA held at equal pH to obtain the maximal Ca^{2+} concentration (dilution 11; see Note 9, Table 1).
8. Sequence 5–7 is repeated at two additional pH values (e.g., see Note 4).
9. Spectra obtained at each pH/ Ca^{2+} value are compared to those obtained during the *in situ* calibrations at the same pH/ Ca^{2+} values, to determine the validity of the limited calibration.

3.6. Experimental Protocols for Analyzing Ion Homeostasis

Alterations in expression of many specific proteins are translated into differences in cell function. Specific experimental protocols can be designed to test directly for the associated changes in handling of H^+ and Ca^{2+} . Analyses of these effects are simplified if each cell is used as its own control. However, as we will demonstrate, accurate *in situ* calibration can be crucial for determining the

accuracy of a response under specific conditions. Provided in this section are examples that describe methods for testing some specific pathways important for ion homeostasis. In addition, methods for standardizing responses between experiments are described.

3.6.1. Na⁺/Ca²⁺ Exchanger

The effect of Na⁺ removal on [Ca²⁺]_i can be used to evaluate the activity of the Na⁺/Ca²⁺ exchanger (19, 27, 28). If the Na⁺/Ca²⁺ exchanger is present, Na⁺ removal results in a rapid increase in [Ca²⁺]_i owing to reversal of the exchanger. Na⁺ removal can also result in a decrease in pH owing to inactivation of the Na⁺/H⁺ exchanger, although other pH regulatory mechanisms can compensate to maintain pH constant (i.e., activation of HCO₃⁻ transport or H⁺-ATPases).

1. Dye-loaded cells are incubated in EB, and the ion-sensitive ratio for both probes is monitored to determine when a stable signal is attained.
2. Perfusion media are changed to media in which NaCl has been replaced with 140 mM of N-methylglucamine-Cl, and the ion-sensitive ratios are monitored continuously.
3. At the end of the experiment, 25 mM NH₄Cl is added to the perfusion media to elicit a rapid alkalinization.
4. The perfusion media is replaced with NH₄Cl-free EB to allow recovery of pH (see Note 15).

As shown in Fig. 2, removal of Na⁺ resulted in a decrease in pH due to inhibition of the Na⁺/H⁺ exchanger in both human umbilical vein endothelial cells (HUVEC) and in human skin fibroblasts (HSF). Removal of Na⁺ also resulted in an increase in the Fura-2 ratio and thereby in apparent changes in Ca²⁺. However, correction for the fura-2 signal response for the change in pH induced by Na⁺ removal indicates that the increase in Ca²⁺ in HUVEC, which could be interpreted as increase in Na⁺/Ca²⁺ exchanger activity, is actually an artifact; i.e., correction of the Fura-2 signal response for changes in pH indicates that there are no significant changes in Ca²⁺ following Na⁺ removal in HUVEC. Similar artifactual increases in the fura-2 ratio owing to decreasing pH following Na⁺ replacement have been observed in ovarian luteal cells (28). Importantly, Na⁺ removal in HSF results in apparent increase in Ca²⁺ that is persistent, even after correction for pH effects on Fura-2, indicating that HSF exhibit significant Na⁺/Ca²⁺ exchanger activity. The relevance of pH corrections on fura-2 data is difficult to evaluate a priori. However, the magnitude of these corrections is clearly larger for acidic than for alkaline pH excursions (12, 16).

3.6.2. Normalization of Agonist-Stimulated Responses

Insulin secretion from pancreatic β -cells is primarily activated by increased metabolism of nutrients and, in particular, glucose with a K_m of approx 15 mM. Ca²⁺ is the second messenger that couples

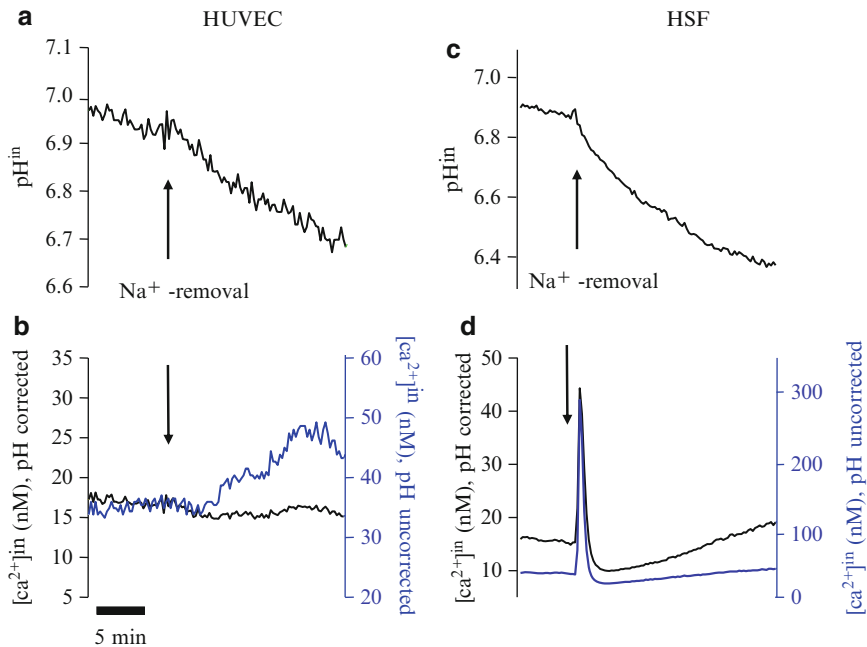


Fig. 2. Effects of Na⁺ removal on pH and Ca²⁺ in HUVEC (a, b) and HSF (c, d) cells. Cells were perfused at a rate of 3 mL/min with HBSS, pH 7.15 at 37°C. At the time indicated (arrow), the Na⁺ in the media was exchanged for N-methyl glucamine; isosmotically substituted. The bottom panels show the Ca concentration calculated from a standard calibration curve without correction for the observed changes in pH (black lines), and with correction (blue lines), as described in Eq. 6.

secretion to cell activation. Unlike normal β -cells, the RIN-38 cells are excited maximally at 1–5 mM glucose. Described is a protocol used to evaluate the effects of modulators of secretion on the glucose-activated response.

1. Dye-loaded cells are incubated in EB containing 0.1 mM glucose, and the ion-sensitive ratio for both probes is monitored to determine when a stable signal is attained.
2. The perfusion media is changed to media containing 5 mM glucose, and the ion-sensitive ratios are monitored continuously (Fig. 3).
3. After the cell response has peaked, the cells are perfused with low-glucose media to wash out the response.
4. After ion concentrations return to baseline, either a second response is initiated (control), or a modulator is added.
5. In the case for testing the effect of a modulator on a subsequent response, the second agonist (glucose) response is initiated by changing the perfusion media to one containing both glucose and the modulator.
6. At the termination of the experiment, 40–60 mM KCl can be added to the perfusion media to elicit a maximal signal response in many, but not all, cell types (see Fig. 3b).

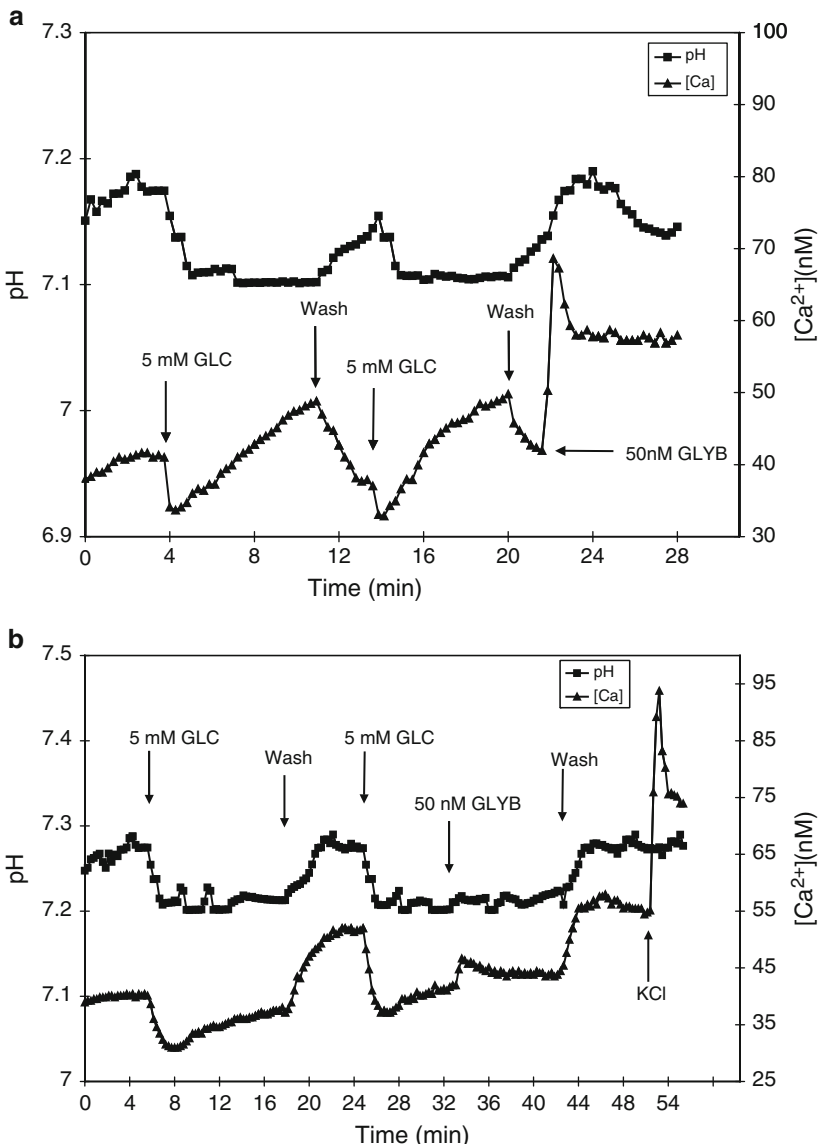


Fig. 3. Glucose induced changes in Ca^{2+} and pH in the insulin secreting beta cell line RIN-38. (a) Responses of wild-type RIN-38 cells to repetitive challenges with glucose. Cells were incubated in media containing 0.1 mM glucose under resting conditions, and were returned to this media to “wash out” the response. After Ca^{2+} returned to baseline, a second response was elicited. The magnitude and rate of response and recovery between the two responses are compared to determine the variability between repetitive activation by the agonist. The effect of a modulator on the agonist-initiated response can be precisely determined by comparing its effect on signaling with that observed in the initial modulator-free response. Also shown is the effect of Glyburide (10^{-7} M) on cell Ca^{2+} . Glyburide closes nucleotide-sensitive K^{+} channels (K_{ATP}), leading to cell depolarization and enhanced Ca^{2+} influx via voltage dependent channels. (b) Effect of knockdown of the sulfonylurea receptor SUR1 in RIN-38 cell signaling. The ability of glucose to elicit an increase in Ca^{2+} is lost in RIN-38 which express limited SUR1, although the initial decrease in cell Ca^{2+} and pH remain indicating that these effects are independent of K_{ATP} channel activity. The response to glyburide also is greatly attenuated as expected. The absence of an elevation in Ca^{2+} could be due to loss of dye sensitivity or saturation, which can easily be tested by subsequent addition of KCl, i.e., KCl can be added at the end of an experiment to fully depolarize the membrane in order to estimate the maximal (peak) signal response. See Note 16.

The second response to elevated glucose is compared to the initial response (% initial) to analyze the effect of a modulator. This approach normalizes the effect of a modulator among different experiments independent of differences in absolute signal responses between individual experiments. Comparison among repetitive glucose responses without modulator evaluates the variability of the control response (shown in Fig. 3a). Also shown is the effect of the sulfonylurea (SU) compound glyburide on cell Ca^{2+} . Glyburide by binding to the SU receptor closes the K_{ATP} channel leading to membrane depolarization and a rapid influx of Ca^{2+} from the extracellular space.

3.6.3. Knockout of the Sulfonylurea Receptor (Isoform 1 [SUR1]) in RIN-38 Cells

In response to increasing glucose from 0.05 to 5 mM, the initial decrease in Ca^{2+} observed in the parental line is maintained, but the secondary elevation in Ca^{2+} that activates the secretory response is absent (Fig. 3b). As expected, treatment with glyburide elicits only a small change in Ca^{2+} , since SUR expression is low. Addition of KCl at the end of the experiment demonstrates that the dynamic range of fura-2 is not limiting the observation of the secondary rise in Ca^{2+} following either glucose stimulation or glyburide treatment. Absence of a response to KCl would be indicative of a problem with dye loading or responsiveness, explaining a similar absence of response to the test agonist. Furthermore, the response after KCl may be used to normalize the original agonist response; i.e., data are analyzed as a percentage of the maximal (KCl) response. However, there are some specific caveats using this approach (see Note 16).

4. Notes

1. Methods to assess the extent of EGTA impurity have been published (29). The impact of this lack of purity in estimating $[\text{Ca}^{2+}]$ is larger at high buffer ratios. A simple empirical method for preparing solutions with stoichiometric balance is to assume that EGTA is approx 5% impure. Thus, a 5% excess EGTA is added to the buffer to compensate for the lack of purity (29).
2. All cells within the population will leak dye into the cuvette medium over time. Therefore, perfusion of the chamber to remove leaked dye is absolutely essential. Buildup of active probe in the medium will obviously lead to spurious results owing to profound differences in extracellular and intracellular ion levels and volumes.
3. Data obtained from simultaneous measurements are further analyzed using SigmaPlot. An advantage of using this system is that data obtained (from either SLM or PTI instruments) can be imported into the SigmaPlot spreadsheet. The equations

needed to estimate pH and Ca²⁺ (i.e., Eqs. 1–6) can be written into this format and iteratively solved using built-in algorithms. Then, graph templates can be extracted and used to instantly plot the data. Thus, a plot can be generated in <1 min provided that there are only minor changes in the legends of the figure.

4. Because pH affects the K_d of EGTA for Ca²⁺, i.e., K_d is larger at acidic than alkaline pH (see Fig. 1), it follows that the magnitude of the Ca²⁺ change for a given titration step is larger at acidic than at alkaline pH. The expected Ca²⁺ concentrations at three distinct pH values (using temperature- and pH-corrected K_d values for Ca²⁺ binding on EGTA) for typical calibration curves outlined in Subheading 3.2 (steps 2 and 3) are indicated in Table 1. The EGTA K_d values used for estimating free Ca²⁺ are 4.22 μM, 336 nM, and 90 nM for pH values of 6.3, 7.0, and 7.2, respectively.
5. A general assumption related to dye loading is that the probes become localized within the compartment of interest, which, in this case, is the cell cytosol. Access to a fluorescence microscope facilitates the analysis of probe distribution. Unfortunately, depending on exact loading conditions, the ion-sensitive probes can become sequestered into subcellular compartments. One relatively quick approach is to permeabilize the cell membrane with a detergent (saponin, 0.1%; 1 min), and to measure the level of fluorescence that remains in the cells. Normally >80% of the signal should be lost with this maneuver unless significant compartmentation or autofluorescence is present. Factors that can influence compartmentation of dye are concentration of AM dye in the loading media, the time of loading, and temperature at which loading is carried out. Approaches to specifically load probes into the cytosol have been described in detail (30), and should be consulted if unwanted compartmentalization of the probes occurs.
6. Dye toxicity: The effect of AM dyes on cell viability and proliferation should be evaluated. In the author's experience, when snarf-1 and fura-2/AM are used at concentrations of <15 μM, there are only minimal effects on cell viability in the more than 40 different cell types they have used. Cell viability can easily be evaluated by trypan blue exclusion. If loss of viability occurs, the time required for cell loading, the temperature at which loading is carried out, or the dye concentration in the loading media can be decreased. On the other hand, even at concentrations as low as 1 μM with incubation times of 5–10 min, followed by washout of the dye, cell proliferation is decreased without any apparent cytotoxic effect (16). The mechanisms underlying the inhibition in cell division are not apparent but may be related to ATP depletion or to aldehyde formation on cleavage of the AM form of these dyes (31).

7. To ensure homogeneous loading, the authors recommend the use of a rocker platform (Bellco, Vineland, NJ) or a belly dancer (Sorvall, Greenville, NC), which can be placed in the 5% CO₂ incubator, at 37°C. In addition, pluronic acid can be used to assist in dye loading, if problems with limited dye loading occur. Addition of 1 µL of a 20% stock solution of pluronic acid to 1 mL of loading media often facilitates enhanced levels and more uniform loading of AM dyes.
8. Use of nigericin plus valinomycin is essential to fully collapse the pH gradient and, therefore, to adequately calibrate fura-2 *in situ* because in many cells, varying Ca²⁺ levels can affect pH, which, in turn, affects fura-2 fluorescence (16).
9. If both signals are similar to those observed from *in vitro* experiments in terms of spectral shape, proceed with the experiment. If anomalous spectra are obtained, investigate whether the aberrant profiles are due to inherent properties of the cell (i.e., autofluorescence). This can be overcome by ensuring proper loading of the cells. Thus, load another set using higher fura-2 or snarf-1 concentrations. In addition, it is critical that the relative fluorescence intensities of fura-2 and snarf-1 are equivalent (<50% difference in either dye is acceptable). Failure to ensure equivalent loading results in the intensity of one dye overwhelming the other due to inevitable spectral overlap, which will preclude correct measurement of both ions. Equal loading can be achieved by increasing/decreasing the concentration of the AM conjugates in the loading.
10. To obtain reliable *in situ* calibration parameters (i.e., K_d /pK, R_{max} , R_{min}) for estimating pH or Ca²⁺, the authors recommend analyses from at least six different pH and Ca²⁺ concentrations (each in triplicate). For Ca²⁺, titrations should be performed at a minimum of five different pH values because the goodness of the fit with Eqs. 1–6 using nonlinear minimization routines is determined by the number of observations. In some cell types, it is problematic to perform complete *in situ* titrations for Ca²⁺, because high Ca²⁺ levels can induce contractility and/or cell detachment. Similarly, it is often difficult to perform complete titrations at high pH, because most cells do not tolerate prolonged alkaline pH. Thus, it is difficult to obtain reliable ratio values at alkaline pH or high Ca²⁺. Consequently, there is much error in estimates of *in situ* R_{max} values for both Ca²⁺ and pH indicators. One common solution to this problem is the use of the *in vitro* R_{max} , which can be generated to a high degree of accuracy. This phenomenon does not have a significant effect on characterizing the effect of pH on the K_d of Ca²⁺ indicators, because the pK of this effect is quite low, and thus the K_d is relatively insensitive at alkaline pH values. Although it is theoretically possible to partially overcome this problem by linearizing

the data (requiring fewer points at high Ca²⁺ or high pH), in the authors' experience, both linear and nonlinear methods provide similar K_d/pK and R_{\min} values, and more reproducible *in situ* R_{\max} values are obtained from nonlinear methods.

11. If the calculated R_{\min} or R_{\max} values are distinct (>10%) from those obtained from the complete calibrations, it may indicate that the intracellular environment of the cell population has changed, and therefore new titrations are required. In the authors' experience with 3T3 cells, thawing of new cell cultures and complete *in situ* titrations are generally required every 12 passages. However, this must be tested for every batch and for each individual cell type.
12. Online analyses of all useful wavelengths are important for correct interpretation of data. The behavior of these wavelengths, and not only ratios, should be continuously monitored during an experiment. Specifically, treatments that elicit increases in pH should elicit distinct increases and decreases in the signal at 644 and 584 without changes in the isoemissive wavelength. Similarly, increases in Ca²⁺ should be associated with increases and decreases in the fluorescence signals at 340 and 380 nm, respectively. This is particularly important when analyzing R_{\min} and R_{\max} for assessment of absolute ion concentrations.
13. Dye behavior at isoemissive/isoexcitation wavelengths should be assessed throughout an experiment. A drastic drift in the fluorescence signal may indicate that cells are detaching or exhibiting changes in cell volume. The ratio method partially corrects for this; however, if the changes are not symmetric, then the ratio values also are modified. The signals at the iso-excitation and isoemissive point of fura-2 and snarf-1, respectively, are particularly useful for monitoring dye leakage. It is normal to observe a decrease in signal owing to dye leakage/extrusion or photobleaching of the probe. In the ratio mode, this will typically be corrected, and the resulting ratio should be stable.
14. Individual cells within a population of cultured cells can have very heterogeneous resting ion levels, which may be due to many factors, including their state of differentiation. A consideration when attempting to analyze "normal resting" levels is developing an approach to bring all cells to a similar level of activation. For example, RIN-38 cells are mildly activated by amino acids and other nutrient factors. The authors have found that treating these cells with alanine during the AM wash period stabilizes the subsequent responses of cells within the population to glucose, which results in a significant decrease in the variability of response to many agonists, and normalizes resting Ca²⁺ levels.

15. Addition of activators such as KCl or NH₄Cl at the end of an experiment provides general information regarding dye responsiveness. However, the signal response of the dye exhibits a nonlinear response at high ion concentrations, making such a maneuver difficult to interpret with respect to absolute ion concentration.
16. In cells that express voltage-activated Ca²⁺ channels, KCl can be used to elicit membrane depolarization at the end of an experiment to evaluate absolute maximal Ca²⁺ signal responses for an individual experiment. In the absence of voltage-activated Ca²⁺-dependent channels, or lack of a response to KCl treatment, ionomycin or A23187 can be used to determine the maximal signal response.

References

1. Becker TC, Noel RJ, Lynch RM, Johnson JH, Takeda J, Bell GI, Newgard CB (1996) Adenovirus mediated overexpression of glucokinase isoforms in islets: minimal secretory and metabolic effects relative to hexokinase overexpression. *J Biol Chem* 271:390–394
2. Gillies RJ, Martinez-Zaguilan R, Martinez GM, Serano R, Perona R (1990) Tumorigenic 3T3 cells maintain an alkaline intracellular pH under physiological conditions. *Proc Natl Acad Sci USA* 87:7414–7418
3. Tompkins LS, Murphy SM, Nullmeyer KD, Weber C, Lynch RM (2002) Regulation of secretory granule pH in insulin secreting cell lines. *Am J Physiol Cell Physiol* 283: C429–C437
4. Patterson GH, Knobel SM, Sharif WD, Kain SR, Piston DW (1997) Use of green fluorescent protein and its mutants in quantitative fluorescence microscopy. *Biophys J* 73:2782–2790
5. Hanson GT, McAnaney TB, Park ES, Rendell ME, Yarbrough DK, Chu S, Xi L, Boxer SG, Montrose MH, Remington SJ (2002) Green fluorescent protein variants as ratiometric dual emission pH sensors. I. Structural characterization and preliminary application. *Biochemistry* 41:15477–15488
6. Putney LK, Denker SP, Barber DL (2002) The changing face of the Na⁺/H⁺ exchanger, NHE1: structure, regulation, and cellular actions. *Annu Rev Pharmacol Toxicol* 42:527–552
7. Putnam RW (2001) Intracellular pH regulation. In: Speralakis N (ed) *Cell physiology source book*, 3rd edn. A Molecular Approach, pp 357–376
8. Clapham DE (1995) Calcium signaling. *Cell* 80:259–268
9. Berridge MJ, Bootman MD, Roderick HL (2003) Calcium signaling: dynamics, homeostasis and remodelling. [Review]. *Nat Rev Mol Cell Biol* 4:517–529
10. Opas M (1997) Measurement of intracellular pH and pCa with a confocal microscope. *Trends Cell Biol* 7:75–80
11. Martinez-Zaguilan R, Gurule M, Lynch RM (1996) Simultaneous measurement of pH and Ca²⁺ in single insulin secreting cells by microscopic spectral imaging. *Am J Physiol* 270:C1438–C1446
12. Martinez-Zaguilan R, Parnami G, Lynch RM (1996) Selection of ion indicators for simultaneous measurement of pH and Ca²⁺. *Cell Calcium* 19:337–349
13. Orchard CH, Kentish JC (1990) Effects of changes of pH on the contractile function of cardiac muscle. *Am J Physiol* 258: C967–C981
14. Sanchez-Armass S, Martinez-Zaguilan R, Martinez G, Gillies RJ (1994) Regulation of pH in rat synaptosomes. I. Role of sodium, bicarbonate, and potassium. *J Neurophysiol* 71:2236–2248
15. Van Adelsberg J, Al-Awqati Q (1986) Regulation of cell pH by Ca²⁺-mediated exocytotic insertion of H⁺-ATPases. *J Cell Biol* 102:1638–1645
16. Martinez-Zaguilan R, Martinez GM, Lattanzio F, Gillies RJ (1991) Simultaneous measurements of intracellular pH and Ca²⁺ using the fluorescence of snarf-1 and fura-2. *Am J Physiol* 260:C297–C307
17. Perona R, Serrano R (1988) Increased pH and tumorigenicity of fibroblasts expressing a yeast H⁺ pump. *Nature* 334:438–440
18. Clark SA, Quaade C, Constandy H, Hansen P, Halban P, Ferber S, Newgard CB, Normington K (1997) Novel insulinoma cell lines produced by iterative engineering of GLUT2,

- glucokinase, and human insulin expression. *Diabetes* 46(6):958–967
19. Martinez-Zaguilan R, Chinnock BF, Wald-Hopkins S, Bernas M, Way D, Weinand M, Witte MH, Gillies RJ (1996) [Ca²⁺]_i and pH in homeostasis in Kaposi sarcoma cells. *Cell Physiol Biochem* 6:169–184
20. Gillies RJ, Martinez-Zaguilan R (1991) Regulation of intracellular pH in BALB/c-3T3 cells: bicarbonate raises pH via NaHCO₃/HCl exchange and attenuates the activation of Na⁺/H⁺ exchange by serum. *J Biol Chem* 266: 1551–1559
21. Ohkuma S, Poole B (1978) Fluorescence probe measurement of the intralysosomal pH in living cells and the perturbation of pH by various agents. *Proc Natl Acad Sci USA* 75:3327–3331
22. Iredale PA, Dickenson JM (1995) Measurement of intracellular free calcium ion concentration in cell populations using Fura-2. *Methods Mol Biol* 41:203–213
23. Konishi M, Olson A, Hollingworth S, Baylor SM (1988) Myoplasmic binding of fura-2 investigated by steady-state fluorescence and absorbance measurements. *Biophys J* 54:1089–1104
24. Bassani JWM, Bassani RA, Bers DM (1995) Calibration on indo-1 and resting intracellular [Ca²⁺]_i in intact rabbit cardiac myocytes. *Biophys J* 68:1453–1460
25. Harrison SM, Bers DM (1989) Correction of proton and Ca²⁺ association constants of EGTA for temperature and ionic strength. *Am J Physiol* 256:C1250–C1256
26. Martinez GM, Martinez-Zaguilan R, Gillies RJ (1994) Effect of glucose on pH and Ca²⁺ in NIH-3T3 cells transfected with the yeast p-type H⁺-ATPase. *J Cell Physiol* 161:129–141
27. Lax D, Martinez-Zaguilan R, Gillies RJ (1994) Furazolidone increases thapsigargin-sensitive Ca²⁺-ATPase in chick cardiac myocytes. *Am J Physiol* 36:H734–H741
28. Martinez-Zaguilan R, Wegner JA, Gillies RJ, Hoyer PB (1994) Differential regulation of Ca²⁺ homeostasis in ovine large and small luteal cells. *Endocrinology* 135:2099–2108
29. Klabusay M, Blinks JR (1996) Some commonly overlooked properties of calcium buffer systems: a simple method for detecting and correcting stoichiometric imbalance in Ca²⁺ EGTA solutions. *Cell Calcium* 20: 227–234
30. Roe MW, Lemasters MM, Herman B (1990) Assessment of Fura-2 for measurements of cytosolic free calcium. *Cell Calcium* 11:63–74
31. Tiffert T, Garcia-Sancho J, Lew V (1984) ATP depletion caused by low concentrations of formaldehyde and/or Ca²⁺-chelator esters in human red cells. *Biochim Biophys Acta* 773: 143–156
32. Tsien RY (1989) Fluorescent indicators of ion concentration. *Methods Cell Biol* 30:127–156
33. Dixon DA, Haynes DH (1990) The pH dependence of the cardiac sarcolemmal Ca²⁺-transporting ATPase: evidence that the Ca²⁺ translocator bears a doubly negative charge. *Biochim Biophys Acta* 1029:274–284

Chapter 17

Measurements of Ca^{2+} Concentration with Recombinant Targeted Luminescent Probes

Denis Ottolini, Tito Calì, and Marisa Brini

Abstract

In the last two decades the study of Ca^{2+} homeostasis in living cells has been enhanced by the explosive development of genetically encoded Ca^{2+} -indicators. The cloning of the Ca^{2+} -sensitive photoprotein aequorin and of the green fluorescent protein (GFP) from the jellyfish *Aequorea victoria* has been enormously advantageous. As polypeptides, aequorin and GFP allow their endogenous production in cell systems as diverse as bacteria, yeast, slime molds, plants, and mammalian cells. Moreover, it is possible to specifically localize them within the cell by including defined targeting signals in the amino acid sequence. These two proteins have been extensively engineered to obtain several recombinant probes for different biological parameters, among which Ca^{2+} concentration reporters are probably the most relevant. The GFP-based Ca^{2+} probes and aequorin are widely employed in the study of intracellular Ca^{2+} homeostasis. The new generation of bioluminescent probes that couple the Ca^{2+} sensitivity of aequorin to GFP fluorescence emission allows real-time measurements of subcellular Ca^{2+} changes in single cell imaging experiments and the video-imaging of Ca^{2+} concentrations changes in live transgenic animals that express GFP-aequorin bifunctional probes.

Key words: Bioluminescence, Aequorin, Ca^{2+} signaling, Organelles, Targeting, Recombinant Ca^{2+} probes, PMCA and SERCA activity measurements, Whole cells

1. Introduction

Ca^{2+} signals can be detected using different Ca^{2+} reporters, i.e., molecules sensitive to Ca^{2+} which undergo physicochemical changes after ion binding. Usually these variations are sufficiently prominent to be monitored and converted in Ca^{2+} concentration ($[\text{Ca}^{2+}]$) values. Significant developments in Ca^{2+} imaging and the suitability of different techniques and indicators have permitted the monitoring of local Ca^{2+} signals in different cell types and the acquisition of fine spatiotemporal detail.

Fluorescent chemical probes, as small organic molecules trapable in the cytoplasm with high dynamic range, ease of use, and

calibration, are widely employed. In recent years, the molecular cloning and subsequent engineering of aequorin and green fluorescent protein (GFP) from the bioluminescent jellyfish *Aequorea victoria* have permitted a strong contribution to the development of new Ca^{2+} sensors particularly useful in the study of Ca^{2+} signaling in specific cell regions (1–4).

All Ca^{2+} indicators show some advantages and disadvantages and the choice of one or the other depends on the biological problem to be investigated. In this chapter we discuss choice of bioluminescent proteins to monitor Ca^{2+} concentration. We also provide a comprehensive overview of principles, applications, and the more recent developments in field of Ca^{2+} monitoring based on the detection of bioluminescence of the recombinant Ca^{2+} sensitive photoprotein aequorin.

1.1. Aequorin as a Ca^{2+} Probe

Aequorin is a 21 kDa protein and, as produced by various *Aequorea* species, includes an apoprotein and a covalently bound prosthetic group (coelenterazine). The Ca^{2+} -dependent luminous reaction requires both the protein and the prosthetic group (Fig. 1a). Since recombinant expression yields only the polypeptide, the prosthetic group must be added exogenously. This process (the “reconstitution” of the active protein) is a critical step in the use of the photoprotein. It requires diffusion of the prosthetic group across the cell membrane and incorporation into the recombinant polypeptide. In our experience, both events occur quite easily in a wide variety of cell types, albeit relatively slowly. Thus, it is sufficient to add coelenterazine to the cell culture medium, and provided aequorin is exposed to low Ca^{2+} and thus consumption is limited, enough active photoprotein is formed in 1–2 h to carry out the experiment.

When Ca^{2+} ions bind to three high-affinity binding sites (EF-hand type), aequorin undergoes an irreversible reaction, in which a photon is emitted. For $[\text{Ca}^{2+}]$ between 10^{-7} and 10^{-5} M there is a relationship between the fractional rate of consumption (i.e., L/L_{\max} , where L_{\max} is the maximal rate of discharge at saturating Ca^{2+} concentrations) and $[\text{Ca}^{2+}]$. Due to the cooperativity between the three binding sites, light emission is proportional to the 2nd–3rd power of $[\text{Ca}^{2+}]$ (Fig. 1b); this property on the one hand accounts for the excellent signal-to-noise ratio of aequorin and on the other may significantly affect the measurements (see below).

Given that the probe (different from fluorescent indicators) is gradually consumed throughout the experiment, the signal tends to decrease and the conversion into Ca^{2+} concentration can be obtained only at the end of the experiment, when total aequorin content is estimated and L/L_{\max} can be backcalculated for each data point. Photoprotein consumption that occurs when aequorin is exposed to high Ca^{2+} concentration can become a problem in two instances: (a) when the compartment or cell domain is endowed with high Ca^{2+} concentrations at rest and extensive Ca^{2+} -dependent

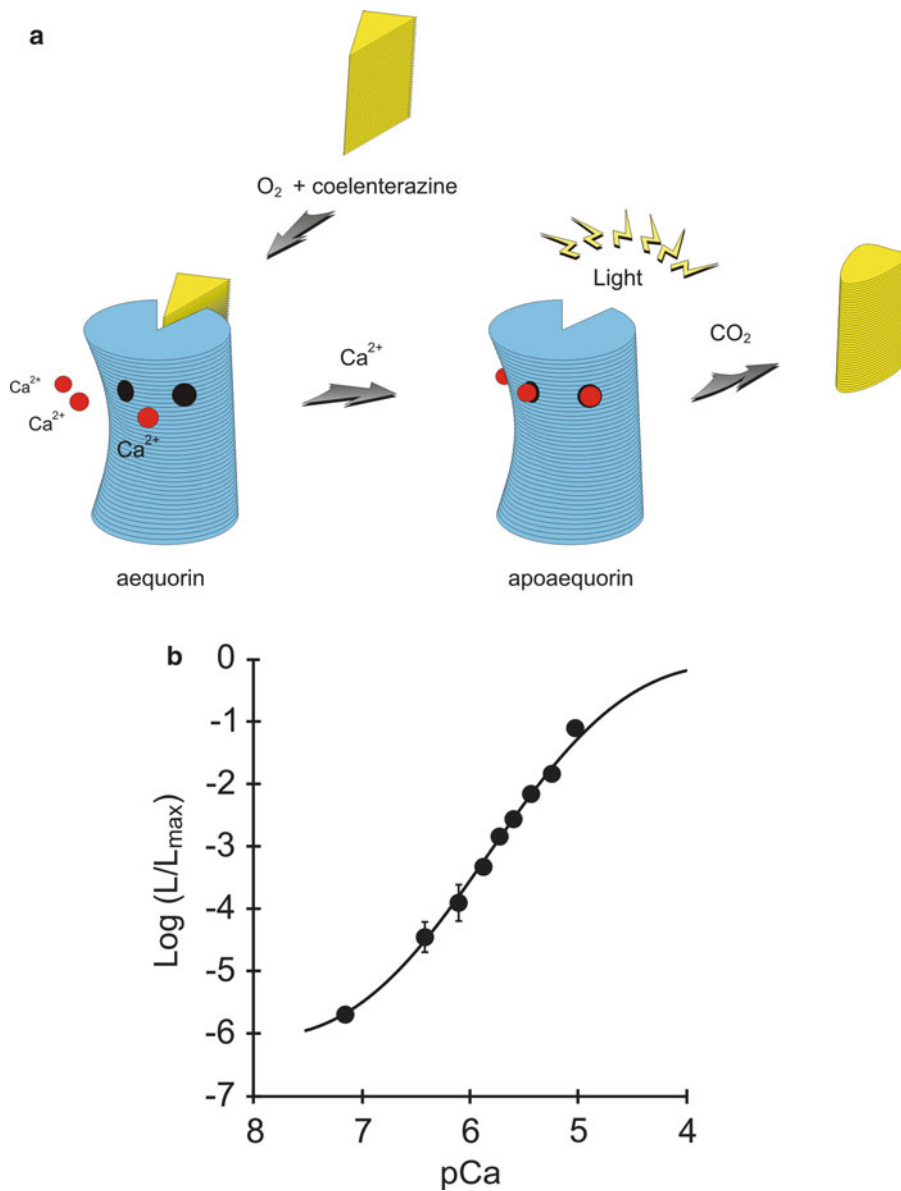


Fig. 1. (a) Schematic model of the irreversible reaction of aequorin. When Ca^{2+} ions bind to the EF-hand binding sites of the reconstituted aequorin a photon is emitted and that molecule of aequorin is irreversibly discharged. (b) $[\text{Ca}^{2+}]$ response curve of recombinant expressed aequorin. L Light emission immediately after adding the buffer Ca^{2+} solution, L_{max} integral of aequorin counts from mixing to the end of the experiment, i.e., after aequorin consumption with excess Ca^{2+} .

consumption parallels the process of reconstitution, and thus little, or negligible, functional aequorin is available at the beginning of the experiment; (b) when the compartment is endowed with low resting $[\text{Ca}^{2+}]$ (and thus effective reconstitution takes place), but after stimulation large increases in $[\text{Ca}^{2+}]$ concentration and thus quantitative aequorin discharge occur.

1.2. Advantages of Aequorin

1. Selective intracellular distribution. The main advantage of aequorin is that being a protein it can be engineered to induce specific localization to a cellular region of interest. This approach is favored by the advances in cell biology obtained in the past years, which have revealed the minimal targeting sequences driving endogenous proteins to their correct intracellular location. Indeed, the sequences as well as details of the molecular machinery involved have been identified for organelles, such as the mitochondria (5) and the nucleus (6, 7). In other cases, less information is available, and thus it is necessary to fuse the heterologous protein to the entire resident polypeptide. Using this targeting strategy it is possible, in principle, to monitor Ca^{2+} concentration not only in specific cell regions but also in the proximity of a protein of interest.
2. Wide dynamic range. With respect to sensitivity range, aequorin is well suited for measuring $[\text{Ca}^{2+}]$ between 0.5 and 10 μM . The wide dynamic range, together with the low buffering effect (see below), makes the photoprotein the tool of choice when it is desirable to quantitatively estimate the large $[\text{Ca}^{2+}]$ rises that occur in some cell types (e.g., those occurring in neuronal cells). Also this wide dynamic range is insufficient when (thanks to specifically targeted chimeras) the photoprotein is addressed to a compartment endowed with high $[\text{Ca}^{2+}]$ such as the organelle acting as intracellular store of agonist-releasable Ca^{2+} . In this case strategies can be devised to reduce the affinity of the photoprotein. The first is to act on the Ca^{2+} -binding sites of the photoprotein. The Asp119 Ala mutation reduces the affinity of the photoprotein approx. 50-fold (8) and has been instrumental in the development of aequorin probes targeted to the endoplasmic reticulum (ER) (9), the sarcoplasmic reticulum (SR) (10), the Golgi apparatus (11), and the subplasmalemmal space (12). Mutated aequorin directed to the mitochondrial matrix has also been generated to better report high micromolar Ca^{2+} levels documented in the mitochondrial matrix (13). The second point of action is the prosthetic group. Numerous chemical modifications of the prosthetic group have been carried out, which modify, in different ways, the Ca^{2+} -triggered reaction of the photoprotein (14). Among these particularly useful modifications have been those (coelenterazine i and n) that reduce light emission at high $[\text{Ca}^{2+}]$ and thus in combination with the apoprotein mutation have made feasible the direct measurement of Ca^{2+} in organelles approaching the millimolar range (15). A final solution to this experimental problem is substituting Ca^{2+} in the cells with a cation with similar physiological behavior but less effective in eliciting the luminous reaction of aequorin. Such a cation is a classical surrogate of Ca^{2+} in physiology studies; Sr^{2+} permeates across Ca^{2+}

channels and is transported by Ca²⁺ ATPases. Indeed, the approx. 100-fold lower sensitivity of aequorin for Sr²⁺ accounts for the drastically lower rate of photoprotein consumption in the intracellular stores and thus prolonged and reliable monitoring of these key cell domains can be achieved (9).

3. High signal-to-noise ratio. Mammalian cells are not endowed with chemiluminescent proteins, so background in aequorin measurement is very low (typically 4–6 cps from a 13 mm coverslip of transfected cells). Moreover, the steep relationship between the increases in light emission and Ca²⁺ concentration (see above) accounts for the very large luminescence peaks observed upon cell stimulation. For an average level of transfection, the total number of detectable photons from 10³ to 10⁴ cells is approx. 10⁷ to 10⁸, and peak increases of >10³ and 10⁴ cps, i.e., >100–1,000-fold over background, can be detected with cytosolic and mitochondrial aequorin, respectively.
4. Low Ca²⁺ buffering effect. Thank to the excellent signal-to-noise ratio, reliable aequorin measurements can be obtained with moderate levels of expression (i.e., <1 μM). Thus, though in principle all Ca²⁺ probes perturb Ca²⁺ homeostasis because they bind Ca²⁺ and thus act as Ca²⁺ buffers, this effect is much less relevant for aequorin than for the trappable fluorescent dyes (typically loaded at concentrations of >50 μM, i.e., >100 times higher than recombinant aequorin) (16).
5. Possibility of co-expressing the Ca²⁺ probe with a protein of interest. The possibility of modifying the molecular repertoire of a cell is today one of the most powerful tools for dissecting complex signaling pathways and unraveling the relative contribution of the different components. This is certainly true also for calcium signaling and one of the experimental tasks we often face is that of measuring Ca²⁺ concentration specifically in cells expressing a normal or mutated signaling component. With dyes, given that it is not possible to load the indicator in the subset of transfected cells, this is usually accomplished by either using clones stably expressing the transgene (with the problems deriving from the natural variability of cell clones) or using laborious single cell analysis of transfected cell populations. Aequorin gives an easy solution to the problem, because it can be co-expressed with the protein of interest. In transient expression studies, the Ca²⁺ probe is exclusively localized to the fraction of transfected cells (depending on the cell type 3–70% of the total population), which are thus very representative of the behavior of the parental population (17, 18).

1.3. Disadvantages of Aequorin

1. Low light emission. The major disadvantage in the use of aequorin is the low amount of light emitted by the photoprotein. Each aequorin molecule emits only one photon, and only

a very small fraction of the photoprotein pool ($<10^{-3}$) emits light throughout the experiment. This is not a major problem when total recordings from a coverslip of transfected cells are carried out as described above. However, it is often desirable to carry out single cell imaging experiments, similar to the imaging of cytoplasmic Ca^{2+} concentration with dyes (that revealed phenomena of particular interest such as waves, localized rises, etc.). With aequorin, this is quite difficult. Special imaging systems are needed, with enhanced sensitivity at the cost of lower spatial resolution. Thus, although single cell imaging experiments with recombinant aequorin have been carried out and provided interesting biological information (19), this approach is technically difficult and possibly disappointing if an image quality similar to those of conventional dyes is expected. Recently new bioluminescent Ca^{2+} probes have been developed by combining the fluorescent properties of GFP with the Ca^{2+} sensitivity of aequorin (20). In these reporters the two proteins were fused: the aequorin moiety acts as Ca^{2+} sensor which delivers emission energy to the GFP acceptor in a bioluminescence resonance energy transfer (BRET): process similar to that observed in natural conditions in the medusa. Optimization of the energy transfer between the two molecules was obtained by insertion of a covalent link which was designed after the evaluation of different ratios of green over blue light emission. Using the same approach adopted for the aequorin chimeras, several GFP-aequorins have been targeted to specific cell regions, including the mitochondrial matrix, endoplasmic reticulum and to microdomains important in synaptic transmission such as synaptic vesicles and the postsynaptic density. The stability and high signal-to-noise ratio of these new reporters are important properties that enable real-time measurements of subcellular Ca^{2+} changes in single mammalian neurons (20). GFP fluorescence allows visualization and choice of the appropriate neuronal area in transfected cells. Ca^{2+} signal can be recorded using a modified epifluorescence microscope where the intensities of BRET activity were translated in pseudo color or using a luminometer according to a protocol similar to that used for the detection of aequorin alone (see below).

2. Overestimation of the average rise in cells (or compartments) with heterogeneous behavior. Due to the steep Ca^{2+} response curve of aequorin, if the probe is distributed between a high and a low Ca^{2+} domain, the former will undergo a much larger discharge. The total signal will be calibrated as an “average” $[\text{Ca}^{2+}]$ increase that will be substantially biased by the region at high Ca^{2+} . In other words, given that an increase in 1 pCa unit causes a 100–1,000-fold increase in light emission, a tiny volume undergoing a very large $[\text{Ca}^{2+}]$ increase will drastically

increase total light output and thus be “interpreted” by the calibration algorithms as a moderate Ca²⁺ rise throughout the cells. Conditions can be envisaged in which this effect can become very significant: for example, a Ca²⁺ rise of 3 μM detected in neurons could in fact be lower but severely biased by hotspots occurring throughout the dendritic tree.

3. The loading procedure. The obvious requirement of this approach is that a cell is amenable to transfection. The significant improvement of transfection techniques and the development of virus based gene delivery have made this problem less severe. In our experience, all cell types can be transfected, with either the simple calcium phosphate procedure (which proves effective in most cell types) or other techniques (liposomes, gene gun, electroporation, viral infection). Conversely, the need to maintain the cells in culture for enough time to produce the recombinant protein can be an important limitation, rendering the extension of the approach to interesting cell types (e.g., pancreatic acinar cells, spermatozoa, etc.) quite difficult.

2. Materials

2.1. Available Aequorin Constructs

1. Cytosol (cytAEQ): recombinantly expressed wild-type aequorin is exclusively cytosolic and, therefore, it does not require any modification to measure [Ca²⁺] in this compartment. The only modification made has been at the 5' end of the coding region to include the HA1 epitope tag in order to verify the correct localization of the probe (16).
2. Nucleus (nu/cytAEQ): the chimeric cDNA encodes a fusion protein composed by a portion of the glucocorticoid receptor GR, including the nuclear localization signal (NLS), the hormone binding domain and the HA1 epitope tagged aequorin. This polypeptide is localized in the cytosol in the absence of glucocorticoids, and translocated to the nucleus upon hormone treatment (21).
3. Mitochondria (mtAEQ): a mitochondrially targeted aequorin was constructed by fusing (in-frame cDNA) the HA1-aequorin (HA1/AEQ) to the cDNA of the mitochondrial presequence derived from subunit VIII of the human cytochrome c oxidase (22). The encoded polypeptide is composed of the cleavable mitochondrial presequence, six amino acids of the mature mitochondrial polypeptide plus the whole photoprotein.
4. Mitochondrial intermembrane space (mimsAEQ): the cDNA encoding HA1-tagged aequorin was fused with that encoding glycerol phosphate dehydrogenase (GPD), an integral protein

of the inner mitochondrial membrane with a large C-terminal tail protruding on the outer side of the membrane, i.e., the intermembrane space (23).

5. Plasma membrane (pmAEQ): the chimeric cDNA was constructed by fusing the cDNA encoding SNAP-25 and HA1-tagged aequorin (12). The targeting of aequorin to the subplasmalemmal space was based on the fusion with SNAP-25, a protein which is synthesized on free ribosomes and recruited to the inner surface of the plasma membrane after palmitoylation of specific cysteine residues.
6. Endoplasmic reticulum (erAEQ): in our chimera retention in the endoplasmic reticulum (ER) does not depend on the typical C-terminal sequence KDEL but on the presence at the N-terminus of aequorin of the CH1 domain. The encoded polypeptide includes the leader sequence (L), the VDJ and CH1 domains of an IgY2b heavy chain and aequorin at the C-terminus. The chimera is retained in the ER because of the binding of the CH1 domain to the resident endogenous ER protein BiP (24). This binding is displaced only by the light chain, while in the absence of this (i.e., not in plasma cells) the CH1 domain is expected to be selectively retained in the ER. The aequorin used to measure $[Ca^{2+}]$ in this compartment was also modified by introducing an epitope tag and a point mutation (Asp119 → Ala), which reduces the Ca^{2+} affinity of the photoprotein (9).
7. Sarcoplasmic reticulum (srAEQ): this chimera results from the fusion of HA1-tagged aequorin with the C-terminus of the endogenous SR protein calsequestrin (CS) (10).
8. Golgi apparatus (goAEQ): the chimeric cDNA was constructed by fusing the cDNA encoding the transmembrane portion of sialyltransferase (ST) and HA1-tagged aequorin. The fusion polypeptide is retained in the Golgi apparatus because of a 17 amino acid membrane-spanning domain of sialyltransferase, a resident protein of the lumen of the *trans*-Golgi and *trans*-Golgi network (TGN) (11).

A summary of available AEQ constructs is shown in Fig. 2.

2.2. Cell Cultures

Cell culture media and reagents according to the specific cell types to be analyzed.

2.3. Reconstitution

Wt and mutated Coelenterazine (coelenterazine n) are commercially available.

2.4. Reagents

Most substances required to perform the techniques described are available from common suppliers of laboratory reagents. According to the cell types, it is necessary to have agonists able to mobilize Ca^{2+} .

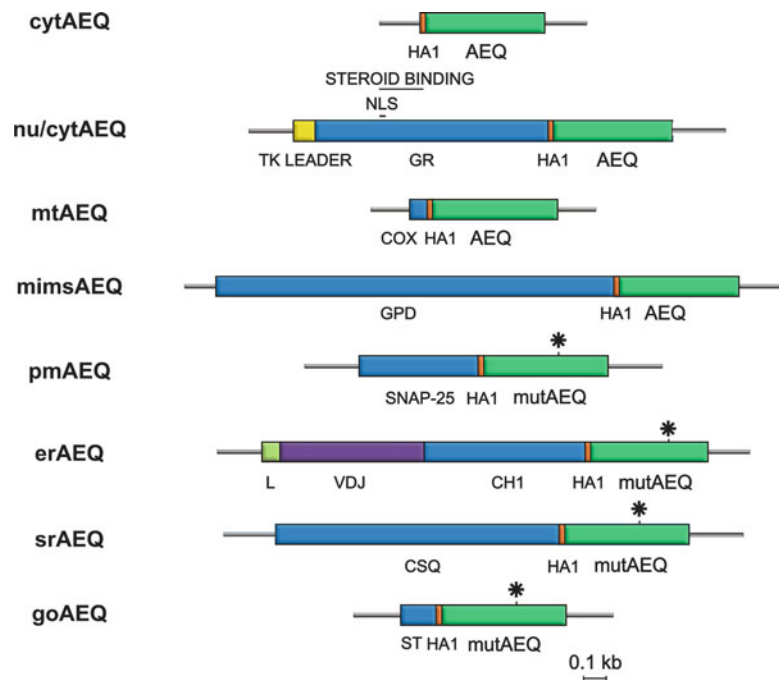


Fig. 2. Schematic representation of different HA1-targeted aequorin (AEQ) chimeras. The strategy for the specific targeting of the chimeras in the different cellular compartments is described in the text. Asterisk shows the position of the (Asp → 119Ala) mutation in the second “EF-hand” Ca²⁺ binding site of aequorin. *mutAEQ* mutated aequorin, *cytAEQ* cytosolic aequorin, *nu/cytAEQ* nucleus/cytosol shuttling aequorin, *mtAEQ* mitochondrial aequorin, *mimsAEQ* mitochondrial intermembrane space aequorin, *pmAEQ* plasma membrane aequorin, *erAEQ* endoplasmic reticulum aequorin, *srAEQ* sarcoplasmic reticulum aequorin, *goAEQ* Golgi apparatus aequorin.

from the intracellular stores or promoting Ca²⁺ entry from the extracellular space. Anti-HA1 antibodies are useful to perform immunocytochemistry analysis of recombinantly expressed aequorin since all the available constructs are tagged with HA1 epitope.

3. Methods

A schematic representation of a typical experiment is shown in Fig. 3.

3.1. Aequorin Expression in Living Cells

We currently employ in the lab mainly two procedures to deliver aequorin into cells: standard transfection with calcium phosphate coprecipitation or using commercial cationic lipids and viral infection (i.e., lentiviral transduction). Other groups have used other standard

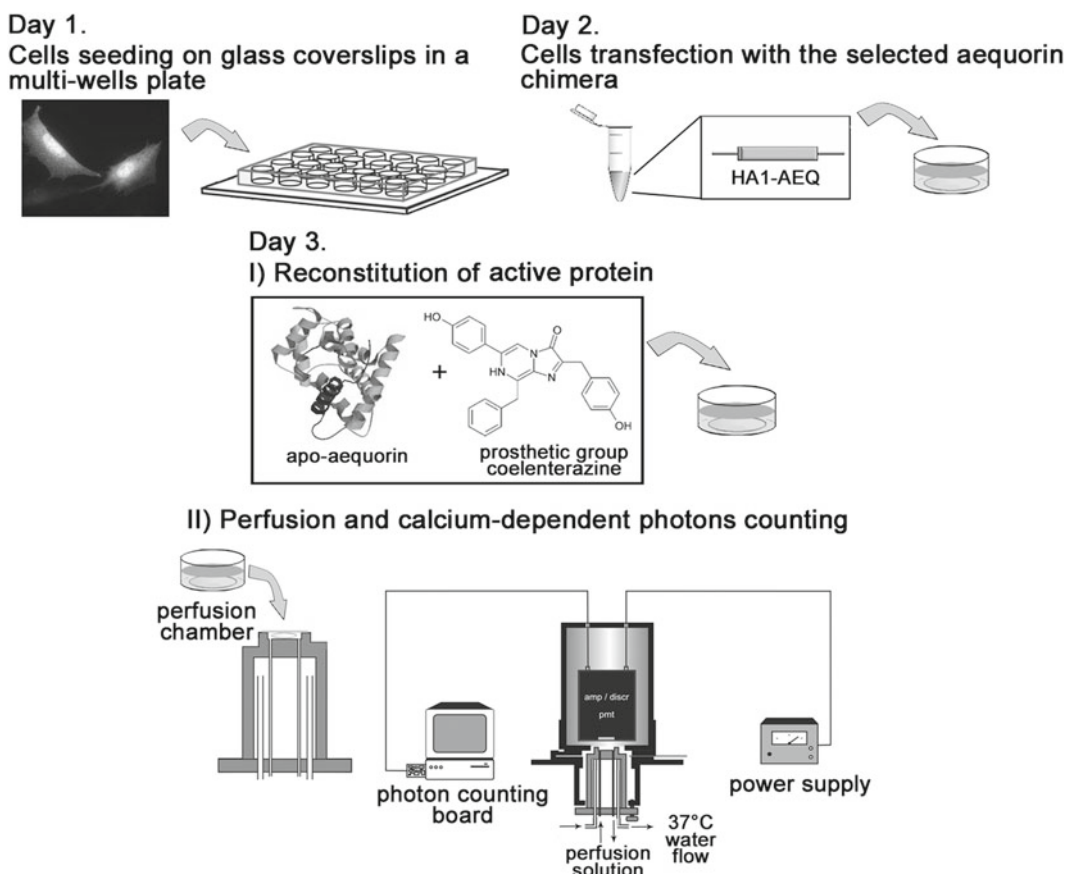


Fig. 3. Schematic representation of a typical experiment and of the aequorin measuring system. *Pmt* photomultiplier, *amp/discr* amplifier/discriminator.

procedures for loading aequorin cDNA into cells, including electroporation and particle gun delivery. Both transient transfection and stable clones can be generated. Overall, recombinant expression of aequorin has proven so far totally innocuous, independent of subcellular localization of the protein and of cell type.

3.2. Calcium Phosphate Procedure

The cells are trypsinized and plated the day before transfection onto a 13 mm round diameter coverslip at 30–50% of confluence (see Note 1). For each aequorin measurement we normally use $2\text{--}3 \times 10^5$ cells seeded onto a 13 mm coverslip in 1 ml of appropriate growth medium supplemented with serum. The following protocol refers to the transfection of 1 coverslip and should be scaled up according to the experimental need.

1. Dilute 4 µg of plasmid DNA, purified either by CsCl gradient or by anion exchange columns, in 45 µl of 1× TE sterile (Tris EDTA) and add 5 µl of a 2.5 M CaCl₂ solution.

2. In another Eppendorf tube put 50 µl of 2× HBS (NaCl 280 mM, Hepes 50 mM, Na₂HPO₄ 1.5 mM, pH 7.12 with NaOH 0.5 M) sterilized by 0.22 µM filter.
3. Under sterile hood add dropwise the content of the first tube (DNA plus CaCl₂) to the second one (2× HBS) under vortexing.
4. A cloudy precipitate should be visible (see Note 2), incubate 30 min at room temperature.
5. Change the cell culture medium with fresh medium.
6. Add dropwise the Ca-phosphate-DNA precipitate to the well with the coverslip.
7. Incubate overnight in the cell incubator.
8. The following day wash the cells with fresh medium in order to remove the excess of Ca-phosphate precipitate.
9. 24–36 h after transfection perform aequorin measurement.

3.3. Cationic Lipids: Lipofectamine 2000/ Transfectin Reagents

1. The day before transfection mammalian cells are trypsinized, washed, and diluted at the density of 1–3 × 10⁵ cells/ml of growth medium without antibiotics.
2. A final volume of 0.5 ml/well is plated onto 13 mm glass coverslips seeded at the bottom of a 24 wells plate.
3. The day of transfection the cells should reach approximately 85–90% of confluence.
4. For most cell lines a DNA (µg) to Lipofectamine2000/ Transfectin (µl) ratio of 1:2 to 1:3 is used.
5. The day of transfection 0.8–1 µg/well of plasmid DNA is diluted in 50 µl/well of Opti-MEM without serum (Gibco, Invitrogen); in parallel 2 µl/well of lipofectamine2000/ Transfectin are diluted in 50 µl of Opti-MEM and incubated 5 min at room temperature.
6. At the end of the 5 min incubation time the diluted DNA is combined with the hydrated lipofectamine2000/Transfectin to reach a final volume of 100 µl/well and incubated 20 min at room temperature to obtain the DNA-Lipofectamine/ Transfectin complex formation.
7. The 100 µl of complexes are then added dropwise to each well by rocking the plate back and forth.
8. Cells are incubated at 37°C and 5% CO₂ for 16–48 h before testing transgene expression. If toxicity occurs, the medium can be changed after 3–6 h from the DNA-Lipofectamine/ Transfectin complex addition.

This protocol could be applied for transfection of adherent as well as suspension cells. Suggested reagent quantities for different sizes of plates/wells are depicted in the Table 1.

Table 1
Transfection procedure for different culture sizes

Culture vessel	Surface area per well (cm ²)	Relative surface area (vs. 24-well)	Volume of plating medium	DNA (μg) and dilution volume (μl)	Lipofectamine™ 2000 (μl) and dilution volume (μl)
96-well	0.3	0.2	100 μl	0.2 μg in 25 μl	0.5 μl in 25 μl
24-well	2	1	500 μl	0.8 μg in 50 μl	2.0 μl in 50 μl
12-well	4	2	1 ml	1.6 μg in 100 μl	4.0 μl in 100 μl
35-mm	10	5	2 ml	4.0 μg in 250 μl	10 μl in 250 μl
6-well	10	5	2 ml	4.0 μg in 250 μl	10 μl in 250 μl
60-mm	20	10	5 ml	8.0 μg in 0.5 μl	20 μl in 0.5 μl
10-cm	60	30	15 ml	24 μg in 1.5 μl	60 μl in 1.5 μl

3.4. Lentiviral Transduction

1. This protocol is mainly used to transduce primary cell cultures, i.e., cerebellar granule cells or neurons. Vector production and gene delivery must be performed in a biosafety level-2 environment.
2. Lentiviral particles can be produced as described in ref. (25). Briefly, HEK293T packaging cells (15×10^6 cells in 150 mm culture plates), cultured in Dulbecco's modified Eagle's medium supplemented with 10% fetal calf serum, 2 mM L-glutamine, 40 μg/ml penicillin/streptomycin, were co-transfected (24 h after plating) with three packaging plasmids pMDLg/pRRE, pMD2.VSVG, pRSV-Rev and the third generation lentiviral backbone vector (pRRLsin.PPTs.hCMV.AEQ.pre, where the aequorin cDNA of interest has been cloned) (26), by means of the calcium-phosphate transfection method.
3. After 10 h, the transfection medium was replaced with fresh culture medium, and cells were grown for 72 h.
4. The medium was then collected and filtered through a 0.45 μm PES filter (Millipore Corporation).
5. Viral particles were harvested by ultracentrifugation ($50,000 \times g$, 2 h), resuspended in 0.2 ml of phosphate-buffered saline (PBS), and stored at -80°C until use.
6. Primary cultures were generally treated with lentiviral particles (diluted in culture medium) 24 h after plating, and, after additional 24 h, added with an equal volume of culture medium.
7. Quantification of lentiviral stock infectivity can be estimated by anti-HA immunocytochemistry on cells infected with serial lentiviral dilutions. Maximal dilution that allowed >70% cells infection is generally used.

3.5. Aequorin Reconstitution (See Note 3)

Recombinantly expressed aequorin is only the polypeptide portion of the photoprotein. In order to measure $[\text{Ca}^{2+}]$ changes it is necessary to reconstitute it in the active form. To do this it is sufficient to add the prosthetic group, coelenterazine, to the incubation medium for few hours in order to allow the diffusion of coelenterazine through the cellular membranes. Coelenterazine employed in our experiments is a synthetic hydrophobic prosthetic group (see Note 4).

1. Reconstitution of cytosolic, nuclear and mitochondrially targeted aequorin: the coverslip with the transfected cells is incubated with 5 μM coelenterazine for 2 h in DMEM supplemented with 1% FCS at 37°C in 5% CO_2 atmosphere. Then, the coverslip is directly transferred to the luminometer chamber, where it is perfused with KRB saline solution (Krebs-Ringer modified buffer: 125 mM NaCl, 5 mM KCl, 1 mM Na_3PO_4 , 1 mM MgSO_4 , 5.5 mM glucose, 20 mM HEPES, pH 7.4, 37°C).
2. Reconstitution of ER, SR and Golgi apparatus targeted aequorin: in order to obtain a sufficient amount of active protein, it is necessary to make a drastic reduction of the luminal Ca^{2+} before the reconstitution. Otherwise the high rate of aequorin consumption strongly counteracts the process. To this end, the cells are incubated for 1 h at 4°C, in KRB supplemented with coelenterazine (5 μM), the Ca^{2+} ionophore ionomycin (5 μM), and 600 μM EGTA. After this incubation, cells are extensively washed with KRB supplemented with 2% BSA and 1 mM EGTA before being transferred to the luminometer chamber.

Alternatively, to discharge the ER/SR Ca^{2+} content the cells can be incubated for 5 min with the SERCA inhibitor 2,5 di (tert-butyl)-1,4-benzohydroquinone (tBuBHQ, 10 μM) and an agonist inducing Ca^{2+} mobilization from the intracellular stores in KRB supplemented with 3 mM EGTA, followed by washing in KRB containing 100 μM EGTA, 2% bovine serum albumin (BSA) and 10 μM tBuBHQ. Aequorin reconstitution is then carried out by incubating the cells with 5 μM coelenterazine for 1 h in KRB containing 100 μM EGTA and 10 μM tBuBHQ at 25°C.

After this incubation, cells are extensively washed with KRB supplemented with 2% BSA and 1 mM EGTA before being transferred to the luminometer chamber.

3. Reconstitution of the subplasmamembrane region targeted aequorin may be performed in the same conditions described for cytosolic aequorin; however, the efficiency is reduced drastically in media containing physiological Ca^{2+} concentrations (1 mM). In order to increase the amount of active pmAEQ the transfected cells are transferred to modified KRB supplemented with 100 μM EGTA and 5 μM coelenterazine. After 45 min of incubation at 37°C, the coverslip is transferred to the luminometer chamber.

3.6. The Aequorin Measuring System

1. The aequorin measuring apparatus is schematically shown in Fig. 3 and was built on the model of that described in ref. (27). Therefore, only the principles are hereinafter described, referring to the above article for any technical detail.
2. The 13 mm coverslips with the cells are placed inside a 37°C thermostated perfusion chamber (diameter 15 mm, height 2 mm). During aequorin measurement, the cell chamber is held in close proximity to a photomultiplier, which is kept in a dark refrigerated box (4°C).
3. An amplifier discriminator is built in the photomultiplier housing; the pulses generated by the discriminator are captured by a Thorn EMI photon counting board, installed on an IBM-compatible computer. The board allows the storing of the data for further analyses.
4. During the experiment, the thermostated chamber is continuously perfused with buffer via a Gilson peristaltic pump (see Note 5). In order to obtain a more rapid equilibration of the perfusing medium inside the chamber, during the changes of medium the flow rate can be increased.
5. At the end of each experiment the cells are lysed by perfusing them with a hyposmotic medium containing 10 mM CaCl₂ and a detergent (100 μM digitonin) in order to discharge all the aequorin that was not consumed during the experiment. This allowed estimation of the total aequorin content which is required to convert the luminescence data into [Ca²⁺] values.
6. At the end of the experiment the luminescence data can be directly converted into free [Ca²⁺] by means of a program which, based on the calculated fractional rate of consumption of aequorin and the Ca²⁺ response curve at physiological conditions of pH, ionic strength and [Mg²⁺], estimates the [Ca²⁺] to which the photoprotein is exposed (16).

3.7. Calibration

As discussed above, the irreversible Ca²⁺ dependent luminescent reaction of aequorin allows prolonged measurements of a dynamic parameter such as the variation of Ca²⁺ concentration in response to different stimuli because of the existence of a relationship between the fractional rate consumption of the photoprotein and the Ca²⁺ concentration in the medium. This relationship has been thoroughly investigated for the native protein and verified to be maintained for the recombinantly expressed photoprotein.

1. To transform luminescence values into [Ca²⁺] values we used essentially the method described by Allen and Blinks, which relies on the relationship between [Ca²⁺] and L/L_{\max} , where L is the light intensity at a given moment and L_{\max} is that which would have been recorded if, at the same moment, all the

aequorin present in the cell had been suddenly exposed to a saturating $[\text{Ca}^{2+}]$.

2. The rate constant of aequorin consumption at saturating $[\text{Ca}^{2+}]$ is 1.0 s^{-1} and a good estimate of the L_{\max} can be obtained by estimating the total aequorin content by discharging all the aequorin content at the end of the experiment (by adding excess of Ca^{2+} and detergents) and collecting all the total amount of aequorin light output.
3. As aequorin is being consumed continuously, the value of L_{\max} is not constant and decreases steadily during the experiment. The value of L_{\max} to be used for $[\text{Ca}^{2+}]$ calculation at every point along the experiment should be calculated as the total light output of the whole experiment minus the light output recorded before the point.
4. The relationship between the ratio L/L_{\max} and $[\text{Ca}^{2+}]$ has been modelled (28). Given that in this model the values of the parameters of the algorithm were obtained with native aequorin (a mixture of several protein isoforms bound to natural coelenterazine) we determined the values of these parameters from recombinantly expressed photoprotein (which represents a single isoform, modified at the amino terminus and reconstituted with a chemically synthesized coelenterazine).
5. Experimental data were obtained by mixing a solution containing cytosolic aequorin (cytAEQ, cell lysate) with a solution containing different $[\text{Ca}^{2+}]$, prepared to give defined pCa values in the final solution (29).
6. The count number obtained immediately after the mixing and the total number of counts in the sample were measured to obtain L/L_{\max} ratios.
7. The values obtained by fitting final pCa and L/L_{\max} ratio in the theoretical curve based on the model mentioned above are very similar to those of Allen and coworkers (16, 28). This protocol has been applied to calibrate the other aequorin chimeras and to calibrate the signal of aequorin reconstituted with coelenterazines n.
8. Figure 4 shows the calibration of cytAEQ and mutated erAEQ reconstituted with wt coelenterazine, and that of mutated erAEQ reconstituted with low affinity coelenterazine n.
9. Various physiological parameters may affect the Ca^{2+} sensitivity of aequorin, such as $[\text{Mg}^{2+}]$, which reduces the sensitivity of aequorin and thus must be known for an accurate $[\text{Ca}^{2+}]$ estimation in the cell and/or compartment of interest; the ionic strength and pH (although the effect of this parameter is very modest in the physiological range, i.e., 6.6–7.4). For physiological pH, temperature and ionic strength a 2nd–3rd power

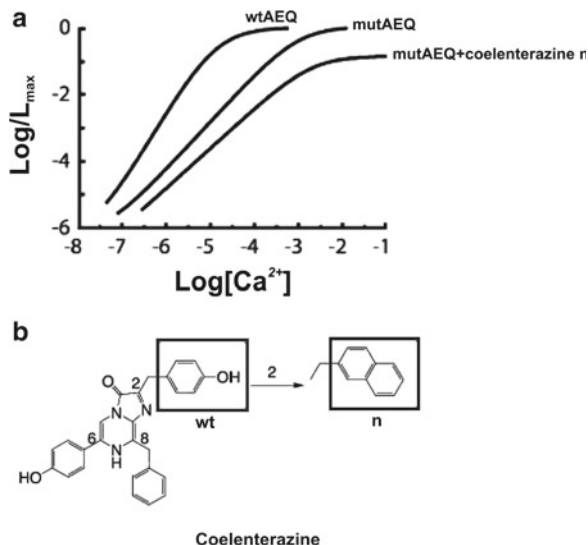


Fig. 4. [Ca²⁺] response curves of recombinantly expressed aequorins (a) and chemical structures of coelenterazines (b). L Light emission immediately after adding the buffer Ca²⁺ solution, L_{\max} integral of aequorin counts from mixing to the end of the experiment, i.e., after aequorin consumption with excess Ca²⁺.

relationship between the rate of consumption and pCa²⁺ can be observed in the pCa²⁺ range of 5–7; the presence of three Ca²⁺ binding sites in the aequorin molecules is responsible for the high degree of cooperativity and for the steep relationship between photon emission rate and [Ca²⁺].

3.8. Applications to Measure SERCA and PMCA Activity in Living Cells

A powerful approach for investigating the role and properties of a protein is its heterologous overexpression followed by the study of the modified cell. The heterologous expression of proteins and the consequent analysis of their effects in living cells has the major advantage of preserving the intact physiological environment and the native regulators which are inevitably lost during protein purification procedures. Several biological parameters can be explored through this strategy: in particular, the Ca²⁺ sensitive photoprotein aequorin co-transfected with genes of interest permits exploration of [Ca²⁺] a key parameter in the different cell compartments. As already mentioned aequorin can be recombinantly produced in different cell systems and targeted to specific locations within the cell by including defined localization signals. This strategy has been successfully employed to perform a functional analysis of membrane Ca²⁺ transporters in living cells. The plasma membrane calcium pump (PMCA) and the sarco(endo)plasmic reticulum calcium pump (SERCA) are essential components of the Ca²⁺ homeostasis system: they are present in all animal tissues. In eukaryotic cells Ca²⁺ is extruded through the plasma membrane or sequestered

into the sarco(endo)plasmic reticulum. Although reports have appeared on the interdependence between PMCA and SERCA pump expression in various cell lines, the relative contribution of the two systems to Ca²⁺ homeostasis has remained elusive. To evaluate the respective roles of the PMCA and SERCA pumps in Ca²⁺ homeostasis we have carried out experiments in which two ubiquitous pump isoforms, PMCA4 and SERCA2b, have been overexpressed in CHO cells using targeted recombinant aequorin to monitor the Ca²⁺ concentration in the cytosol, in the lumen of the endoplasmic reticulum and in the mitochondrial matrix of cells at rest and upon stimulation with an inositol 1,4,5-trisphosphate generating agonist. The effects of their overexpression on cytosolic [Ca²⁺] and, most interestingly, on organellar Ca²⁺ were pump-specific: the PMCA pump was more effective than the SERCA pump in rapidly reversing the [Ca²⁺] rise induced by the IP₃-generating stimulus both in the cytosol and in the mitochondria. A direct relationship was observed between PMCA and SERCA overexpression and ER free [Ca²⁺] levels: the overexpression of the former caused a reduction in ER [Ca²⁺] levels, of the latter an increase. Despite the overexpression of either pump (about threefold their endogenous content) no drastic changes were detected in the overall process of Ca²⁺ homeostasis, suggesting that the different systems involved became mutually adapted to maintain constant Ca²⁺ signaling (30). The approach has been extended to perform a comparative analysis of the different PMCA isoforms (31) and the analysis of mutant PMCAAs responsible for genetic disease.

4. Notes

1. Cell confluency must be seriously taken into account when transfecting with Ca-P procedure since low cell confluency will ensure an optimal transfection but a low light signal during measurement. In contrast high cell confluency may affect the transfection efficiency of the Ca-P precipitates.
2. The solution should appear cloudy but as homogeneous as possible, the presence of large floating aggregates will strongly reduce the transfection efficiency.
3. It is important to add the coelenterazine solution directly onto each 13 mm glass coverslips, adding it well by well. Preparation of a working solution containing coelenterazine diluted at the final concentration of 5 µM in DMEM 1% FCS and the subsequent addition after removing the tissue culture medium will strongly impair the reconstitution process.
4. The coelenterazine stock solution must be prepared on ice under low light condition, aliquoted in glass tubes and stored

at -80°C. This will ensure optimal storage conditions of the prosthetic group.

5. The plastic tubes used for the perfusion of lipophilic compounds must be extensively washed before each set of experiments in order to eliminate any residual trace of contaminants. 70% ethanol as well as 2% BSA or 5% Sodium hypochlorite solutions are useful to this purpose.

Acknowledgments

The authors are indebted to past and present collaborators and thank the University of Padova (local funding and Ateneo Project 2008 CPDA082825), the Telethon Foundation (Project GGP04169), the Italian Ministry of University and Research (PRIN 2003, 2005, 2008), and the Italian National Research Council (CNR, Agency 2000) for financial support.

References

1. Demaurex N (2005) Calcium measurements in organelles with Ca²⁺-sensitive fluorescent proteins. *Cell Calcium* 38:213–222
2. Giepmans BN, Adams SR, Ellisman MH, Tsien RY (2006) The fluorescent toolbox for assessing protein location and function. *Science* 312:217–224
3. Brini M (2008) Calcium-sensitive photoproteins. *Methods* 46:160–166
4. Paredes RM, Etzler JC, Watts LT, Zheng W, Lechleiter JD (2008) Chemical calcium indicators. *Methods* 46:143–151
5. Hartl FU, Pfanner N, Nicholson DW, Neupert W (1989) Mitochondrial protein import. *Biochim Biophys Acta* 988:1–45
6. Kalderon D, Roberts BL, Richardson WD, Smith AE (1984) A short amino acid sequence able to specify nuclear location. *Cell* 39:499–509
7. Dingwall C, Laskey RA (1991) Nuclear targeting sequences – a consensus? *Trends Biochem Sci* 16:478–481
8. Kendall JM, Sala-Newby G, Ghilaut V, Dormer RL, Campbell AK (1992) Engineering the CA(2+)-activated photoprotein aequorin with reduced affinity for calcium. *Biochem Biophys Res Commun* 187:1091–1097
9. Montero M, Brini M, Marsault R, Alvarez J, Sitia R, Pozzan T, Rizzuto R (1995) Monitoring dynamic changes in free Ca²⁺ concentration in the endoplasmic reticulum of intact cells. *EMBO J* 14:5467–5475
10. Brini M, De Giorgi F, Murgia M, Marsault R, Massimino ML, Cantini M, Rizzuto R, Pozzan T (1997) Subcellular analysis of Ca²⁺ homeostasis in primary cultures of skeletal muscle myotubes. *Mol Biol Cell* 8:129–143
11. Pinton P, Pozzan T, Rizzuto R (1998) The Golgi apparatus is an inositol 1,4,5-trisphosphate-sensitive Ca²⁺ store, with functional properties distinct from those of the endoplasmic reticulum. *EMBO J* 17:5298–5308
12. Marsault R, Murgia M, Pozzan T, Rizzuto R (1997) Domains of high Ca²⁺ beneath the plasma membrane of living A7r5 cells. *EMBO J* 16:1575–1581
13. Montero M, Alonso MT, Carnicer E, Cuchillo-Ibanez I, Albilllos A, Garcia AG, Garcia-Sancho J, Alvarez J (2000) Chromaffin-cell stimulation triggers fast millimolar mitochondrial Ca²⁺ transients that modulate secretion. *Nat Cell Biol* 2:57–61
14. Shimomura O, Musicki B, Kishi Y (1989) Semisynthetic aequorins with improved sensitivity to Ca²⁺ ions. *Biochem J* 261:913–920
15. Barrero MJ, Montero M, Alvarez J (1997) Dynamics of [Ca²⁺] in the endoplasmic reticulum and cytoplasm of intact HeLa cells. A comparative study. *J Biol Chem* 272:27694–27699
16. Brini M, Marsault R, Bastianutto C, Alvarez J, Pozzan T, Rizzuto R (1995) Transfected aequorin in the measurement of cytosolic Ca²⁺ concentration ([Ca²⁺]_c). A critical evaluation. *J Biol Chem* 270:9896–9903

17. Bastianutto C, Clementi E, Codazzi F, Podini P, De Giorgi F, Rizzuto R, Meldolesi J, Pozzan T (1995) Overexpression of calreticulin increases the Ca²⁺ capacity of rapidly exchanging Ca²⁺ stores and reveals aspects of their luminal microenvironment and function. *J Cell Biol* 130:847–855
18. Lievremont JP, Rizzuto R, Hendershot L, Meldolesi J (1997) BiP, a major chaperone protein of the endoplasmic reticulum lumen, plays a direct and important role in the storage of the rapidly exchanging pool of Ca²⁺. *J Biol Chem* 272:30873–30879
19. Rutter GA, Burnett P, Rizzuto R, Brini M, Murgia M, Pozzan T, Tavare JM, Denton RM (1996) Subcellular imaging of intramitochondrial Ca²⁺ with recombinant targeted aequorin: significance for the regulation of pyruvate dehydrogenase activity. *Proc Natl Acad Sci USA* 93:5489–5494
20. Baubet V, Le Mouellic H, Campbell AK, Lucas-Meunier E, Fossier P, Brulet P (2000) Chimeric green fluorescent protein-aequorin as bioluminescent Ca²⁺ reporters at the single-cell level. *Proc Natl Acad Sci USA* 97:7260–7265
21. Brini M, Marsault R, Bastianutto C, Pozzan T, Rizzuto R (1994) Nuclear targeting of aequorin. A new approach for measuring nuclear Ca²⁺ concentration in intact cells. *Cell Calcium* 16:259–268
22. Rizzuto R, Simpson AW, Brini M, Pozzan T (1992) Rapid changes of mitochondrial Ca²⁺ revealed by specifically targeted recombinant aequorin. *Nature* 358:325–327
23. Rizzuto R, Pinton P, Carrington W, Fay FS, Fogarty KE, Lifshitz LM, Tuft RA, Pozzan T (1998) Close contacts with the endoplasmic reticulum as determinants of mitochondrial Ca²⁺ responses. *Science* 280:1763–1766
24. Sitia R, Meldolesi J (1992) Endoplasmic reticulum: a dynamic patchwork of specialized subregions. *Mol Biol Cell* 3:1067–1072
25. Follenzi A, Naldini L (2002) HIV-based vectors. Preparation and use. *Methods Mol Med* 69:259–274
26. Zufferey R, Dull T, Mandel RJ, Bukovsky A, Quiroz D, Naldini L, Trono D (1998) Self-inactivating lentivirus vector for safe and efficient in vivo gene delivery. *J Virol* 72:9873–9880
27. Cobbold P L J (1991) In: McCormack JG, Cobbold PH (eds) *Cellular calcium: a practical approach*. Oxford University Press, New York, pp 55–81
28. Allen D, Blinks JR, Prendergast FG (1976) Aequorin luminescence: relation of light emission to calcium concentration. A calcium-independent component. *Science* 195:996–998
29. Fabiato A (1991) In: Cobbold PH, McCormack JG (eds) *Cellular calcium: a practical approach*. Oxford University Press, Oxford UK, pp 159–176
30. Brini M, Bano D, Manni S, Rizzuto R, Carafoli E (2000) Effects of PMCA and SERCA pump overexpression on the kinetics of cell Ca(2+) signalling. *EMBO J* 19:4926–4935
31. Brini M, Coletto L, Pierobon N, Kraev N, Guerini D, Carafoli E (2003) A comparative functional analysis of plasma membrane Ca²⁺ pump isoforms in intact cells. *J Biol Chem* 278:24500–24508

Chapter 18

Chimeric G Proteins in Fluorimetric Calcium Assays: Experience with Opioid Receptors

Valeria Camarda and Girolamo Calo¹

Abstract

High throughput calcium mobilization assays are extensively used for pharmacological characterization of GPCR ligands. These approaches, initially developed for G_q -coupled receptors, can be extended to G_i coupled GPCRs using chimeric G proteins. Here we used the $G\alpha_{q5}$ protein to force the nociceptin/orphanin FQ (N/OFQ) peptide (NOP) receptor, as well as the classical opioid receptors to signal through the PLC-IP₃-Ca²⁺ pathway in CHO cells. Calcium levels were monitored using the fluorometric imaging plate reader FlexStation II and the Ca²⁺ dye Fluo 4 AM. For investigating the pharmacology of the NOP receptor a panel of full and partial agonists and antagonists were assessed, while a small panel of agonists and antagonists was used for evaluating the pharmacological profile of opioid receptors. Some limitations of this assay and differences in the results obtained in comparison with those with G_i based biochemical assays are described. Overall, the present results confirm that the chimeric G protein strategy is useful for studying the pharmacological activity of G_i coupled receptor ligands and that the aberrant signaling does not produce any measurable change in the pharmacological profile of the receptor under study. Thus, this G protein strategy is extremely useful for setting up primary screening assays for NOP and classical opioid receptors and likely for other members of the GPCR family.

Key words: Chimeric G proteins, Nociceptin/orphanin FQ, Opioid receptors, Calcium signaling, Ligand efficacy and potency

1. Introduction

Calcium mobilization assays are extensively used for investigating the pharmacological profile of receptors, particularly in the G protein coupled receptor (GPCR) field. Since the middle 1990 the identification of novel GPCR ligands particularly in industrial laboratories are mainly based on the use of automated fluorometers and calcium dyes. These approaches, initially developed for G_q coupled receptors, were subsequently extended to G_i coupled receptors using several strategies including the use of chimeric G proteins. Conklin and colleagues (1) demonstrated that replacement

of between three and nine amino acids of the C-terminal $G\alpha_q$ sequence with the corresponding $G\alpha_i$ sequence enabled G_i coupled GPCRs to stimulate the modified $G\alpha_q$ subunit and hence activate phospholipase C (PLC). Kostenis et al. (2) showed that single-point replacement of the highly conserved glycine residue in position 66 with other amino acids (i.e., aspartate) confers to $G\alpha_q$ the ability to link various non- G_q -coupled receptors to the PLC-IP₃-Ca²⁺ pathway. Combination of the G66D mutation with the C-terminal alteration ($G\alpha_{qG66D15}$) gave rise to a mutant protein which is superior to the individual mutants with respect to stimulation of PLC (3).

Thus chimeric G proteins represent a helpful strategy for forcing G_i coupled receptors to couple with the PLC-IP₃-calcium pathway and this approach has been validated with a large panel of G_i coupled GPCRs (2) including classical opioid and the nociceptin/orphanin FQ (N/OFQ) peptide (NOP) receptors (4).

In this chapter the authors present, as example, the successful use of chimeric proteins to force the classical opioid and NOP receptor to signal through the Ca²⁺ pathway in CHO cells. The classical opioid receptors (μ or MOP, δ or DOP, κ or KOP) as well as the NOP receptor are coupled to G proteins of the $G_{i/0}$ type; therefore their activation produces inhibition of adenylyl cyclase and calcium channels, and activation of potassium channels. This pattern of cellular actions is responsible for the inhibition of neurotransmitter release (presynaptic localization) and cellular excitability (postsynaptic localization).

2. Materials

2.1. Cell Culture

1. CHO cells stably expressing the human recombinant NOP (CHO_{NOP}) were a generous gift from Dr. Maïthe Corbani, Institut de Pharmacologie et de Biologie Structurale, Toulouse, France, CHO_{DOP} were supplied by Dr. Eva Varga, Department of Medical Pharmacology, The University of Arizona, Tucson, USA, CHO_{MOP} and CHO_{KOP} were both provided by Prof. Larry Toll SRI International, Menlo Park, CA, USA.
2. Culture medium for CHO_{NOP} , CHO_{DOP} , CHO_{MOP} , and CHO_{KOP} cells: DMEM and Ham F-12 (1:1), 2 mM L-glutamine, 10% FBS, 200 µg/ml geneticin, 100 IU/ml penicillin, 100 IU/ml streptomycin (see Note 1).
3. CHO_{NOP} , CHO_{DOP} , CHO_{MOP} , and CHO_{KOP} cells expressing the $G\alpha_{qi5}$ chimeric protein and CHO_{DOP} cells expressing the $G\alpha_{qG66D15}$ chimeric protein were generated in the laboratory of Prof. Tommaso Costa, Istituto Superiore di Sanità, Rome, Italy.

4. Culture Medium for CHO_{NOP}, CHO_{DOP}, CHO_{MOP} and CHO_{KOP} cells expressing the G α_{q5} chimeric protein and CHO_{hDOP} cells expressing the G $\alpha_{qG66Di5}$ chimeric protein: DMEM and Ham F-12 (1:1), 2 mM L-glutamine, 10% FBS, 100 IU/ml penicillin, 100 IU/ml streptomycin, 200 μ g/ml geneticin, 100 μ g/ml hygromycin B.

2.2. Transfection Procedures

CHO cells lines permanently co-expressing NOP or opioid receptors and the C-terminally modified G α_{q5} were prepared by infecting the CHO lines described above with a recombinant retrovirus expressing the chimeric α subunit and the hygromycin resistance gene. Similarly CHO cells lines permanently co-expressing the DOP receptor and the C-terminally modified G $\alpha_{qG66Di5}$ were prepared by infecting the CHO lines described above with a recombinant retrovirus expressing the chimeric α subunit and the hygromycin resistance gene. Polyclonal cell lines were generated using the pantropic retroviral expression system from BD-Clontech, as described previously (5). Stable lines were selected under hygromycin B (100 μ g/ml) and geneticin (600 μ g/ml) for 2–3 weeks after infection.

2.3. Buffers

1. Serial dilution of ligands are made in Hank's Balanced Salt Solution (HBSS) buffer (137 mM NaCl, 5.4 mM KCl, 0.25 mM Na₂HPO₄, 0.44 mM KH₂PO₄, 1.3 mM CaCl₂, 1.0 mM MgSO₄, 4.2 mM NaHCO₃, 5 mM glucose), supplemented with 20 mM HEPES, and 0.005% BSA fraction V (see Note 2).
2. Cells are loaded using medium supplemented with 2.5 mM probenecid (see Note 3), 3 μ M of the calcium sensitive fluorescent dye Fluo-4 AM and 0.01% pluronic acid (see Note 4).
3. After 30 min at 37°C the loading solution is substituted with HBSS buffer added with 20 mM HEPES, 2.5 mM probenecid, and 500 μ M Brilliant Black (see Note 5).

2.4. Drugs

1. The standard compounds used in this study were as follows: naltrindole and nor-binaltorphimine from Tocris Bioscience, DPDPE and dynorphin A from Neosystem; dermorphin, N/OFQ, and N/OFQ related peptides were prepared and purified in house as previously described in ref. 6.
2. All other reagents were from Sigma Chemical Co. (Poole, U.K.) or E. Merck (Darmstadt, Germany) and were of the highest purity available.
3. Stock solutions (1 mM) of peptides were made in distilled water and kept at -20°C until use. The other compounds were solubilized in saline at 30 μ M. Successive dilutions of ligands were made in saline.

2.5. General Reagents

1. Fluo-4 AM make up as a stock (2 mM) solution by dissolving in dimethylsulfoxide and storing aliquots (20 µL) at -20°C.
2. Probenecid (Sigma). Dissolve fresh at 250 mM in 50% NaOH 1 M and 50% HBSS. Use at 2.5 mM in buffer.
3. Brilliant Black (Aldrich). Make 50 mM in water and keep at room temperature. Dilute to 500 µM with HBSS added with 20 mM HEPES, 2.5 mM probenecid.

3. Methods

3.1. Multiwell Plating of Cells

1. When the cells reach confluence, split the confluent monolayer using trypsin (0.5 g/L)-EDTA (0.2 g/L, 5 ml).
2. Transfer 10 µl of the medium containing the cells in suspension in the hemocytometer chamber in order to calculate the number of the cells/ml of solution.
3. Centrifuge the solution at 1,000× g for 5 min, aspirate the supernatant and resuspend the pellet in Xml of medium in order to produce 0.5×10^6 cells/ml.
4. Using a multichannel pipette add 100 µl of the medium containing the cells in 96-well black clear bottom plate (see Note 6) in order to seed 50,000 cells/well and incubate overnight at 37°C, 5% CO₂ (see Note 7).

3.2. Fluo-4 Loading and Measurement of Intracellular Calcium

1. Calcium mobilization studies were performed using the fluorometer FlexStation II (Molecular Device, Union City, CA 94587, US).
2. The day after plating the cells, incubate the cells with the loading solution for 30 min at 37°C, 5% CO₂. Aspirate the loading solution and replace with 100 µl buffer added with 20 mM HEPES, 2.5 mM probenecid, and 500 µM Brilliant Black.
3. Leave the plate 10 min at room temperature in the reading chamber of FlexStation II to allow equilibration of the basal fluorescence (see Note 8). Read the basal fluorescence (excitation wavelength 485 nm, emission wavelength 520 nm) simultaneously in the 96 wells and assess the Coefficient of Variation (CV) (see Note 9).
4. Set the protocol and run the experiment.
5. For antagonist experiments the integrated 8-channel pipettor adds 50 µl of 3× antagonist solution in 100 µl of buffer in every well and then instrument records the fluorescence at 2 s intervals for 2 min in every row. Every row is incubated with the antagonist for 24 min.

6. When the first addition is complete, the agonist challenge occurs by addition of 50 μ l of 4x agonist (every well contains now 150 μ l). The fluorescence is recorded again for 2 min.
7. The SoftMax software then calculated for each well the difference between max and min fluorescence intensity units (FIU) and expressed this value as percent over the baseline fluorescence. These data are then cut and paste into the sheet of Graph Pad 5.0 software in order to be analyzed by non linear curve fitting equations.
8. All data are expressed as means \pm standard error of the mean (SEM) of n experiments. For potency values 95% confidence limits were indicated.
9. Agonist potencies are given as pEC_{50} (the negative logarithm to base 10 of the molar concentration of an agonist that produces 50% of the maximal possible effect, E_{max}). Concentration response curve to agonists are fitted with the following equation:

$$\text{Effect} = \text{baseline} + (E_{max} - \text{baseline}) / \left(1 + 10^{((\text{Log}EC_{50} - X) \times \text{HillSlope})} \right)$$

where X is the agonist concentration.

Assuming a competitive interaction, antagonist potencies derived from inhibition experiments are expressed as pK_B , calculated from the following equation:

$$K_B = IC_{50} / \left(\left[2 + ([A]/EC_{50})^n \right]^{1/n} \right) - 1$$

where IC_{50} is the concentration of antagonist that produces 50% inhibition of the agonist response, $[A]$ is the concentration of agonist, EC_{50} is the concentration of agonist producing a 50% maximal response and n is the Hill coefficient of the concentration response curve to the agonist. For non competitive antagonists $pIC_{50} \approx pK_B$ (see Note 10).

10. For investigating the type of antagonism concentration response curves to the agonist should be performed in the presence of increasing concentrations of antagonist (i.e., classical Schild protocol). In the case of competitive interaction the antagonist potency can be expressed as pA_2 (7).

3.3. $[Ca^{2+}]_i$ Measurements in CHO Cells Co-expressing Gi Coupled Receptors and Chimeric G Proteins

3.3.1. NOP Receptors

1. N/OFQ was completely inactive up to 1 μ M concentrations in CHO stably expressing the $G\alpha_{q5}$ but not the NOP receptor. In CHO_{NOP} cells (not expressing the $G\alpha_{q5}$ protein), N/OFQ produced a modest stimulatory effect ($\approx 50\%$ over the basal values) only at highest concentration tested, i.e., 1 μ M. In contrast the peptide produced a robust and concentration dependent stimulatory effect in cells expressing both the NOP receptor and the chimeric G protein. Raw data from a single representative N/OFQ concentration response curve experiment are shown in Fig. 1.

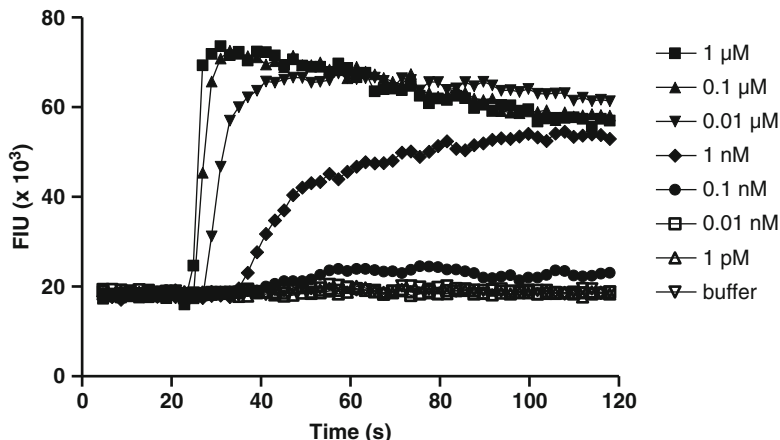


Fig. 1. Raw data from a single representative N/OFQ concentration–response curve experiment in CHO_{NOP} cells expressing the $\text{G}\alpha_{q/11}$ chimeric protein.

N/OFQ displayed high potency (pEC_{50} 9.09 ($\text{CL}_{95\%}$: 8.84–9.34)) and maximal effects of $222 \pm 14\%$ over the basal values. Similar maximal effects were obtained with a series of NOP full agonists including the peptides N/OFQ(1-13) NH_2 and UFP-112, and the non peptide Ro 64-6198, NNC-63-0532, and Ro 65-6570 ((8) and Camarda V., unpublished data). The order of potency of agonists was similar to that previously obtained in classical assays for G_i coupled receptors ($[^{35}\text{S}]GTP\gamma S$ stimulation and cAMP level inhibition). A detailed analysis of these results demonstrated however that the potency of UFP-112 and the Roche compounds is somewhat underestimated in the calcium assay. This may likely derive from the slow kinetic of action of these ligands recorded in isolated tissue experiments (9, 10). In fact the long time required to obtain full activation of NOP receptors by these agonists might be an issue when receptor activation is measured via the transient calcium response which is characterized by a rapid kinetic. For a detailed discussion of this topic see ref. 8.

- As shown in Fig. 2, the NOP partial agonists [F/G]N/OFQ(1-13) NH_2 and Ac-RYYRIK-NH₂ produced a concentration dependent stimulation of calcium levels. In line with previous findings both compounds were found less potent than N/OFQ (by approximately 30-fold). The maximal effect elicited by these ligands was a fraction of that of the natural ligand however this difference did not reach the statistical level of significance. Thus ligand efficacy tends to be overestimated in the calcium assay. This is not unexpected considering that the calcium assay is characterized by amplification of the signal/response coupling (11).

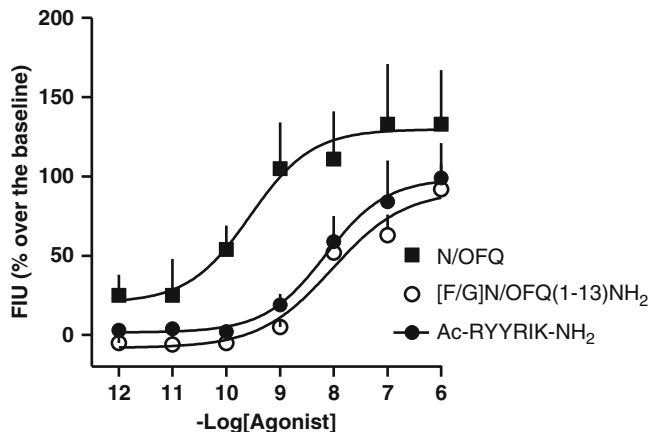


Fig. 2. Concentration–response curve to NOP receptor partial agonists in calcium mobilization experiments performed in CHO_{NOP} cells stably expressing the G α_{q5} protein. Ligand effects were expressed as percent over the baseline. Data are the mean of four separate experiments performed in duplicate.

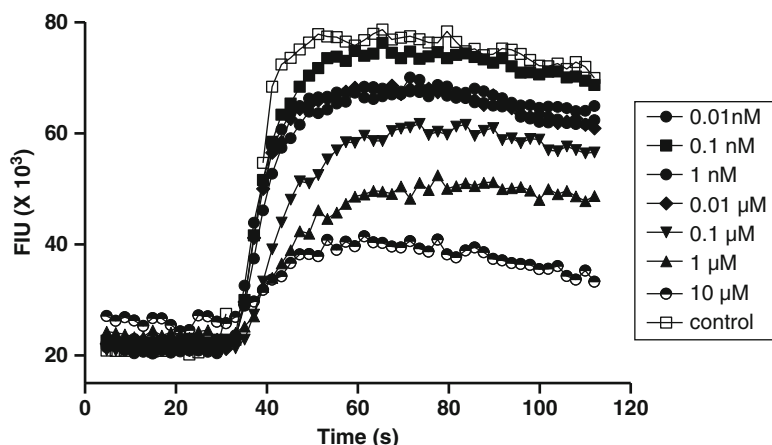


Fig. 3. Raw data from a single representative experiment of the inhibition curve to UFP-101 against N/OFQ 10 nM in CHO cells expressing the G α_{q5} chimeric protein.

3. Finally the NOP receptor coupled to the calcium pathway was characterized with the use of receptor antagonists in inhibition response curves. These experiments are performed by testing increasing concentration of antagonist against the stimulatory effect elicited by a fixed concentration of agonist approximately corresponding to its EC₈₀. Figure 3 displays an example of raw data obtained in this kind of experiments using UFP-101 as NOP antagonist.

A panel of NOP receptor antagonists, including the peptides [Nphe¹]N/OFQ(1-13)NH₂ and UFP-101, and the non peptide J-113397, Trap-101, SB-612111, compound 24, and

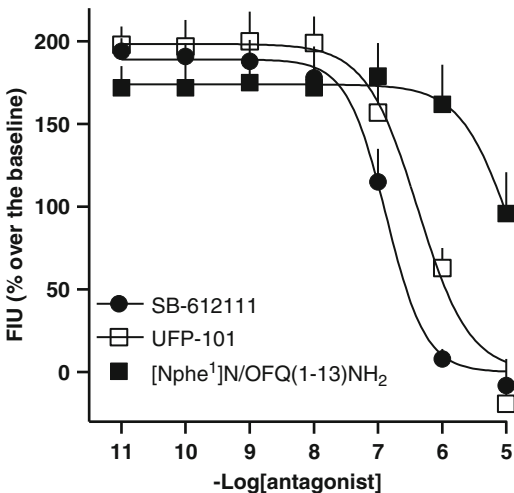


Fig. 4. Inhibition response curves obtained by challenging 10 nM N/OFQ with increasing concentrations of $[Nphe^1]N/OFQ(1-13)NH_2$, UFP-101, and SB-612111 in the calcium mobilization assay performed in CHO_{NOP} cells stably expressing the $G\alpha_{q5}$ protein. Data are the mean \pm sem of four separate experiments performed in duplicate.

compound 35, was assessed in inhibition response experiments (8, 12, 13). As an example inhibition response curve to some NOP antagonists are displayed in Fig. 4.

pK_B values were calculated assuming a competitive type of interaction and the following rank order of antagonist potency was derived: compound 24 > compound 35 > SB-612111 > J-113397 = Trap-101 > UFP-101 > $[Nphe^1]N/OFQ(1-13)NH_2$. This is superimposable to the rank order of potency obtained at both recombinant human NOP investigated with classical assay for G_i coupled receptors and native NOP receptors expressed in animal tissues investigated with bioassay techniques (14).

The type of antagonism must be evaluated experimentally in Schild plot experiments (see Note 11). This has been done for J-113397 (8) and compound 24 (12); in both cases the competitive nature of the interaction has been confirmed and the relative pA_2 perfectly matched the pK_B values obtained in inhibition response curves.

3.3.2. Opioid Receptors

1. The pharmacological profile of human recombinant opioid receptors was evaluated in CHO cells expressing the chimeric protein $G\alpha_{q5}$. Results obtained with a small panel of opioid receptor agonists are summarized in Table 1.
2. Finally, in all the three cell lines ATP concentration dependently stimulated calcium mobilization via activation of endogenously expressed purinergic receptors showing similar potencies (pEC_{50} range 5.80–6.18) and maximal effects. In CHO cells expressing

Table 1

Effects of standard opioid receptor agonists and ATP in CHO cells expressing $\text{G}\alpha_{q5}$ and recombinant human opioid receptors in the calcium mobilization assay

	DOP		MOP		KOP	
	$p\text{EC}_{50}$	E_{max}	$p\text{EC}_{50}$	E_{max}	$p\text{EC}_{50}$	E_{max}
Morphine	crc incomplete		6.61 ± 0.17	$130 \pm 17\%$	crc incomplete	
DPDPE	8.89 ± 0.23	$76 \pm 2\%$	Inactive		Inactive	
Dermorphin	6.43 ± 0.48	$78 \pm 3\%$	7.89 ± 0.36	$146 \pm 29\%$	Inactive	
Dynorphin A	7.73 ± 0.27	$75 \pm 4\%$	6.67 ± 0.50	$121 \pm 37\%$	8.95 ± 0.31	$222 \pm 16\%$
N/OFQ	Inactive		Inactive		Inactive	
ATP	5.80 ± 0.35	$176 \pm 17\%$	6.18 ± 0.17	$270 \pm 42\%$	5.91 ± 0.15	$252 \pm 20\%$

Morphine produced incomplete concentration response curves in KOP and DOP cells and displayed moderate potency at MOP receptors. DPDPE displayed high potency ($p\text{EC}_{50} 8.89$) at DOP being inactive at the other receptors. Dermorphin was inactive at KOP and displayed 30-fold higher potency for MOP than DOP. Dynorphin A displayed the following order of potency: KOP > DOP > MOP. In summary, the following order of potency of agonists was measured in the different cell lines:

MOP: dermorphin > morphine = dynorphin A (DPDPE inactive), DOP: DPDPE > dynorphin A > dermorphin > morphine, KOP: dynorphin A >> morphine (DPDPE and dermorphin inactive)

the $\text{G}\alpha_{q5}$ protein but not opioid receptors ATP produced similar results while none of the opioid receptor agonists was able to stimulated calcium mobilization (data not shown).

3. As far as the signal to noise ratio is concerned, this was good in CHO_{KOP} cells (≈ 3), acceptable in CHO_{MOP} cells (2–2.5), while rather low in CHO_{DOP} cells (<2). This low signal in DOP cells is barely sufficient for performing agonist studies but not for investigating the effects of antagonists. This prompted us to generate a novel CHO cell line expressing the DOP receptor together with the $\text{G}\alpha_{q\text{G66D}5}$ chimeric protein whose efficiency in coupling non-G_q-coupled GPCR to the PLC-IP₃-Ca²⁺ pathway was reported to be superior to that $\text{G}\alpha_{q5}$ (3). This has been confirmed by the present results obtained by comparing the concentration response curve to DPDPE in CHO_{DOP} cells expressing the $\text{G}\alpha_{q5}$ or the $\text{G}\alpha_{q\text{G66D}5}$ chimeric protein (Fig. 5). In fact the potency of the DOP selective agonist DPDPE was similar in the two cell lines ($p\text{EC}_{50} 8.67$ and 8.60) while its maximal effects were significantly higher in $\text{G}\alpha_{q\text{G66D}5}$ ($146 \pm 23\%$ over the basal) compared to $\text{G}\alpha_{q5}$ expressing cells ($70 \pm 10\%$ over the basal). In parallel experiments ATP showed superimposable results in the two cell lines ($p\text{EC}_{50} 6.44$ and 6.30; $E_{\text{max}} 199 \pm 9\%$ and $217 \pm 16\%$).

4. Standard antagonists for classical opioid receptors were evaluated in the calcium assay; naltrindole was used for the DOP

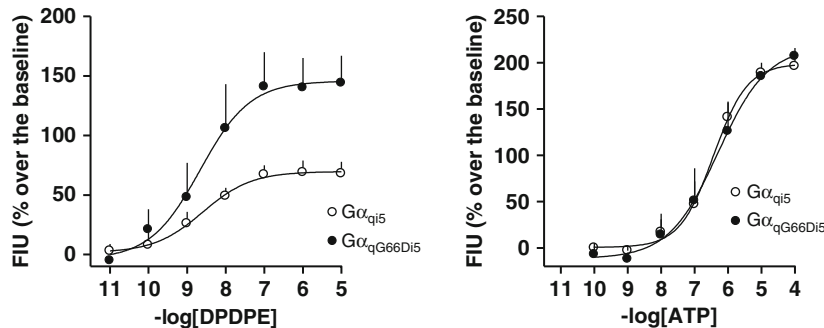


Fig. 5. Concentration response curve to DPDPE (left panel) and ATP (right panel) in calcium mobilization experiments performed in CHO_{DOP} cells stably expressing $G\alpha_{q5}$ or $G\alpha_{qG66D15}$ chimeric G proteins. Agonist effects were expressed as % over the baseline. Data are the mean of three separate experiments performed in duplicate.

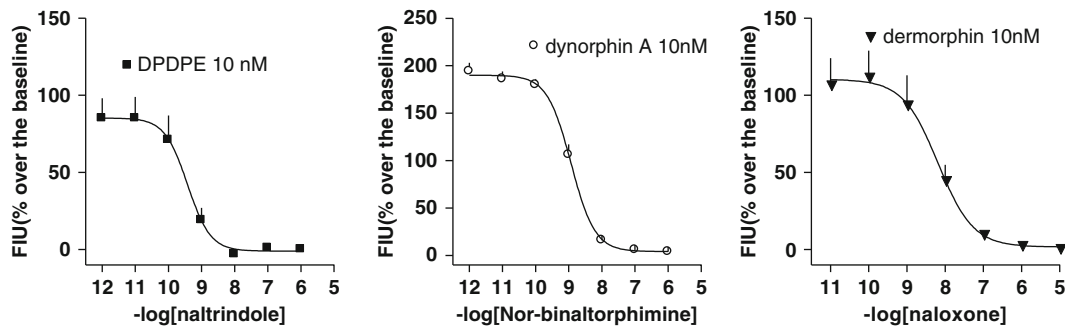


Fig. 6. Inhibition response curves obtained by challenging 10 nM DPDPE, Dynorphin A and Dermorphin with increasing concentrations of Naltrindole, Nor-binaltorphimine and Naloxone in the calcium mobilization assay performed in CHO_{DOP} cells stably expressing the $G\alpha_{qG66D15}$ protein (left panel), and CHO_{KOP} and CHO_{MOP} cells stably expressing the $G\alpha_{q5}$ protein (middle and right panel). Data are the mean \pm sem of four separate experiments performed in duplicate.

receptor, Nor-binaltorphimine for the KOP, and naloxone for the MOP. As reported in Fig. 6 these antagonists were able to inhibit in a concentration dependent manner the stimulatory effect elicited by selective agonists (DPDPE, dynorphin A, and dermorphin for the DOP, KOP, and MOP receptors, respectively). Assuming a competitive type of antagonism the following pK_B values were derived: 10.00 for naltrindole, 10.17 for Nor-binaltorphimine, and 8.50 for naloxone.

3.3.3. Conclusions

1. The present results demonstrated that the use of chimeric G proteins represents a useful and reliable strategy to force classical opioid and the NOP receptor to couple with the calcium signaling pathway.
2. Detailed studies performed with full and partial agonists and pure antagonists suggest that the aberrant coupling does not produce any measurable bias to the pharmacological profile of the NOP

receptor. The same can be said for classical opioid receptors although these have been investigated to a lesser extent.

3. This assay can be successfully used for pharmacological studies in particular for screening investigations. The most interesting ligands selected with this assay should be always reinvestigated using tests based on the physiological receptor coupling.
4. The ability of the calcium assay to correctly determine the pharmacological behavior of a given ligand depends on its pharmacological activity. In our experience the following limitations have been detected:
 - (a) Results obtained with pure antagonists are perfectly superimposable to those collected to G_i based biochemical assays in terms of potency. Investigation of the type of antagonism (surmountable vs insurmountable) can be demanding (see Note 11 for details).
 - (b) The efficacy of partial agonists tends to be overestimated in this assay.
 - (c) The potency of agonists characterized by slow kinetics of action is possibly underestimated.
5. Despite these limitations, there is no doubt that the chimeric G protein strategy is extremely useful for setting up primary screening assays not only for opioid receptors but also for other members of the GPCR family as summarized in Table 2.

Table 2
Examples of successful use of chimeric G proteins for the functional activity of various G_i/G_o coupled receptors by assessing the Ca^{2+} mobilization

Receptor	Chimeric G protein	References
NPY-Y ₂	$G\alpha_{q5}$	(15)
Cannabinoid CB ₂	$G\alpha_{q05}$ and $G\alpha_{q5}$	(16)
Adrenergic α_{2c}	$G\alpha_{q5}$	(17)
Dopamine D _{2s}	$G\alpha_{q05}$	(18)
Histamine H ₃	$G\alpha_{q5}$	(19)
mGluR ₂ ; mGluR ₄	$G\alpha_{q5}$	(20)
Melatonin	$G\alpha_{q5}$	(21)
5-HT ₆	$G\alpha_{q5}$	(22)
GABA B	$G\alpha_{q5}$	(23)

4. Notes

1. All tissue culture media and reagents are supplied by Invitrogen (San Diego, CA, US) and from Cambrex Bioscience (Walkersville, Maryland, USA).
2. The addition of the buffer containing BSA produces, in some type of cells, a fluorescence signal. Thus, the authors suggest minimizing the amount of BSA.
3. Probenecid is an inhibitor of organic anion transporter expressed by the cells. Fluo-4 is a membrane permeable acetoxyethyl (AM) ester. Once inside cells, it is hydrolyzed in its anionic form that binds Ca^{2+} . Probenecid prevents the export of this anion and the lowering of the signal. Probenecid is prepared in a basic solution. Add always the same amount of 1 M HEPES to keep the physiological PH.
4. Add pluronic acid, a nonionic surfactant, in the same amount of Fluo-4 AM to improve its water solubility.
5. Brilliant Black is a food dye added with the purpose of quenching the extracellular background fluorescence. In the presence of Brilliant Black the wash step is not needed.
6. For cells that do not perfectly adhere to the bottom of the wells (i.e., HEK293 cells), a coating with poly-D-lysine (PDL) is required. PDL (average MW 30,000–70,000) is dissolved in sterile water to a final concentration of 10 $\mu\text{g}/\text{ml}$. The 96-well plates are coated with PDL solution for 30 min at room temperature. After removing the coating by aspiration and washing the wells a couple of times, leave the plates to dry at room temperature then store them in the fridge.
7. Adhesion of cells to the edge of wells (“edge effects”) is a phenomenon well known in the HTS screening literature and it can cause well-to-well variations. The adequate mixing of the cells to avoid seeding in clumps, can minimize the edge effects. One of the causes of the edge effect can be the thermal gradient in the incubator, therefore after plating the cells it is helpful to leave them from 30 to 60 min to settle at room temperature before placing the plate in the incubator.
8. Repeated records of the basal fluorescence units straight after the substitution of the loading solution with the buffer containing Brilliant Black provide unstable values within 5–10 min. After that time the values became constant.
9. CV is equal to the standard deviation of the fluorescence basal values in the 96 wells divided by the mean. It is expressed as a percent and a low value (3–5%) reflects the homogeneity of both the loading through the wells and the growing of the cells.

10. For details about the calculation of surmountable vs. insurmountable antagonist potency in inhibition response curve experiments see the discussion contained in Chap. 10 “A pharmacology primer: theory, applications, and methods, 2006” (11).
11. The lack of stirring and consequent slow diffusion of the drugs into the well associated with the transient nature of the calcium response may cause hemiequilibrium conditions. This can be the reason for recording a depression of the agonist maximal effects (insurmountable behavior) in the calcium assay using a compound which behaves as a competitive antagonist in other tests. An example of this can be found in ref. 24. Hemiequilibrium conditions can be minimized by facilitating drug diffusion in the well. This can be done by increasing temperature and/or by introducing three cycles of mixing after antagonist injection. For instance, the neuropeptide S receptor antagonist SHA 68 caused a strong depression of neuropeptide S elicited maximal effects in cells expressing the murine receptor when the experiment was performed at room temperature while it behaved as a competitive antagonist in experiments performed at 37°C and introducing the mixing step (25).

References

1. Conklin BR, Farfel Z, Lustig KD, Julius D, Bourne HR (1993) Substitution of three amino acids switches receptor specificity of Gq alpha to that of Gi alpha. *Nature* 363:274–276
2. Kostenis E, Waelbroeck M, Milligan G (2005) Techniques: promiscuous Galphalpha proteins in basic research and drug discovery. *Trends Pharmacol Sci* 26:595–602
3. Kostenis E, Martini L, Ellis J, Waldhoer M, Heydorn A, Rosenkilde MM, Norregaard PK, Jorgensen R, Whistler JL, Milligan G (2005) A highly conserved glycine within linker I and the extreme C terminus of G protein alpha subunits interact cooperatively in switching G protein-coupled receptor-to-effector specificity. *J Pharmacol Exp Ther* 313:78–87
4. Coward P, Chan SD, Wada HG, Humphries GM, Conklin BR (1999) Chimeric G proteins allow a high-throughput signaling assay of Gi-coupled receptors. *Anal Biochem* 270: 242–248
5. Molinari P, Casella I, Costa T (2008) Functional complementation of high-efficiency resonance energy transfer: a new tool for the study of protein binding interactions in living cells. *Biochem J* 409:251–261
6. Guerrini R, Calo G, Rizzi A, Bianchi C, Lazarus LH, Salvadori S, Temussi PA, Regoli D (1997) Address and message sequences for the nociceptin receptor: a structure-activity study of nociceptin-(1-13)-peptide amide. *J Med Chem* 40:1789–1793
7. Schild HO (1947) pA, a new scale for the measurement of drug antagonism. *Br J Pharmacol Chemother* 2:189–206
8. Camarda V, Fischetti C, Anzellotti N, Molinari P, Ambrosio C, Kostenis E, Regoli D, Trapella C, Guerrini R, Severo S, Calo G (2009) Pharmacological profile of NOP receptors coupled with calcium signaling via the chimeric protein G alpha q5. *Naunyn Schmiedebergs Arch Pharmacol* 379:599–607
9. Rizzi D, Bigoni R, Rizzi A, Jenck F, Wichmann J, Guerrini R, Regoli D, Calo G (2001) Effects of Ro 64-6198 in nociceptin/orphanin FQ-sensitive isolated tissues. *Naunyn Schmiedebergs Arch Pharmacol* 363:551–555
10. Rizzi A, Spagnolo B, Wainford RD, Fischetti C, Guerrini R, Marzola G, Baldissarotto A, Salvadori S, Regoli D, Kapusta DR, Calo G (2007) In vitro and in vivo studies on UFP-112, a novel potent and long lasting agonist selective for the nociceptin/orphanin FQ receptor. *Peptides* 28:1240–1251
11. Kenakin TP (ed) (2006) A pharmacology primer. Academic Press

12. Fischetti C, Camarda V, Rizzi A, Pela M, Trapella C, Guerrini R, McDonald J, Lambert DG, Salvadori S, Regoli D, Calo G (2009) Pharmacological characterization of the nociceptin/orphanin FQ receptor non peptide antagonist Compound 24. *Eur J Pharmacol* 614: 50–57
13. Trapella C, Fischetti C, Pela M, Lazzari I, Guerrini R, Calo G, Rizzi A, Camarda V, Lambert DG, McDonald J, Regoli D, Salvadori S (2009) Structure-activity studies on the nociceptin/orphanin FQ receptor antagonist 1-benzyl-N-[3-[spiroisobenzofuran-1(3H),4'-piperidin-1-yl]propyl] pyrrolidine-2-carboxamide. *Bioorg Med Chem* 17:5080–5095
14. Lambert DG (2008) The nociceptin/orphanin FQ receptor: a target with broad therapeutic potential. *Nat Rev Drug Discov* 7:694–710
15. Shoblock JR, Welty N, Nepomuceno D, Lord B, Aluisio L, Fraser I, Motley ST, Sutton SW, Morton K, Galici R, Attack JR, Dvorak L, Swanson DM, Carruthers NI, Dvorak C, Lovenberg TW, Bonaventure P (2010) In vitro and in vivo characterization of JNJ-31020028 (N-(4-{4-[2-(diethylamino)-2-oxo-1-phenylethyl]piperazin-1-yl}-3-fluorophenyl)-2-pyridin-3-ylbenzamide), a selective brain penetrant small molecule antagonist of the neuropeptide YY(2) receptor. *Psychopharmacology (Berl)* 208:265–277
16. Malysz J, Daza AV, Kage K, Grayson GK, Yao BB, Meyer MD, Gopalakrishnan M (2009) Characterization of human cannabinoid CB2 receptor coupled to chimeric Galphai(q5) and Galphai(qo5) proteins. *Eur J Pharmacol* 603: 12–21
17. Kurko D, Békes Z, Gere A, Baki A, Boros A, Kolok S, Bugovics G, Nagy J, Szombathelyi Z, Ignacz-Szendrei G (2009) Comparative pharmacology of adrenergic alpha(2C) receptors coupled to Ca(2+) signaling through different Galphai proteins. *Neurochem Int* 55:467–475
18. Heinrich JN, Brennan J, Lai MH, Sullivan K, Hornby G, Popiolek M, Jiang LX, Pausch MH, Stack G, Marquis KL, Andree TH (2006) Aplindore (DAB-452), a high affinity selective dopamine D2 receptor partial agonist. *Eur J Pharmacol* 552:36–45
19. Krueger KM, Witte DG, Ireland-Denny L, Miller TR, Baranowski JL, Buckner S, Milicic I, Esbenshade TA, Hancock AA (2005) G protein-dependent pharmacology of histamine H3 receptor ligands: evidence for heterogeneous active state receptor conformations. *J Pharmacol Exp Ther* 314:271–281
20. Kowal D, Nawoschik S, Ochalski R, Dunlop J (2003) Functional calcium coupling with the human metabotropic glutamate receptor subtypes 2 and 4 by stable co-expression with a calcium pathway facilitating G-protein chimera in Chinese hamster ovary cells. *Biochem Pharmacol* 66:785–790
21. Yokoyama T, Kato N, Yamada N (2003) Development of a high-throughput bioassay to screen melatonin receptor agonists using human melatonin receptor expressing CHO cells. *Neurosci Lett* 344:45–48
22. Zhang JY, Nawoschik S, Kowal D, Smith D, Spangler T, Ochalski R, Schechter L, Dunlop J (2003) Characterization of the 5-HT6 receptor coupled to Ca2+ signaling using an enabling chimeric G-protein. *Eur J Pharmacol* 472: 33–38
23. Wood MD, Murkitt KL, Rice SQ, Testa T, Punia PK, Stammers M, Jenkins O, Elshourbagy NA, Shabon U, Taylor SJ, Gager TL, Minton J, Hirst WD, Price GW, Pangalos M (2000) The human GABA(B1b) and GABA(B2) heterodimeric recombinant receptor shows low sensitivity to phaclofen and saclofen. *Br J Pharmacol* 131:1050–1054
24. Camarda V, Spagnol M, Song W, Vergura R, Roth AL, Thompson JP, Rowbotham DJ, Guerrini R, Marzola E, Salvadori S, Cavanni P, Regoli D, Douglas SA, Lambert DG, Calo G (2006) In vitro and in vivo pharmacological characterization of the novel UT receptor ligand [Pen5, DTrp7, Dab8]urotensin II(4–11) (UFP-803). *Br J Pharmacol* 147:92–100
25. Ruzza C, Rizzi A, Trapella C, Pela M, Camarda V, Ruggieri V, Filaferro M, Cifani C, Reinscheid RK, Vitale G, Ciccocioppo R, Salvadori S, Guerrini R, Calo G (2010) Further studies on the pharmacological profile of the neuropeptide S receptor antagonist SHA 68. *Peptides* 31:915–925

Chapter 19

Compartmentalizing Genetically Encoded Calcium Sensors

David A. Williams, Mastura Monif, and Kate L. Richardson

Abstract

Within single cells there is a complex myriad of signaling which controls physiological process many of which are modulated, or signaled directly, by intracellular calcium ions. Understanding the exquisitely sensitive, and spatially restricted, changes in calcium has been of interest to the researcher for a number of years. Recent advances in this field have been driven by the development of genetically encoded calcium probes for detecting calcium changes within the cells specifically targeting organelles such as mitochondria, endoplasmic reticulum, and the nucleus. In this chapter the authors outline some of the available fluorescent probes, with particular emphasis on an endoplasmic reticulum targeted calcium biosensor in cell signaling studies with astrocytes, detailing experimental protocols and the interpretation of data from such probes.

Key words: Calcium biosensor, D1-ER cameleon, Astrocytes, Endoplasmic reticulum, Transfection, Confocal microscopy

1. Introduction

Calcium is a ubiquitous cellular messenger controlling a diverse array of physiological processes from fertilization through to gene transcription, muscle contraction, cell proliferation and migration, cell differentiation, and ultimately cell death (1, 2). Within a single cell, calcium can have multiple and contrasting effects. The accomplishment of such exquisite control of a myriad of often parallel processes is an extreme example of multitasking, ultimately dependent on spatial and temporal compartmentalization of intracellular ionized calcium concentrations ($[Ca^{2+}]_i$) (3). Localized calcium signals are “spatially restricted” microdomains of calcium (diameter ~10–100 nm) at the opening of channels (4), or larger subcellular volumes ranging up to several micrometers (2). These brief pulses of calcium occur near the mouth of the membrane ion channels (plasmalemma, endoplasmic reticulum) before calcium diffuses away or becomes bound to calcium buffers (5). These signals can

stay transiently localized and activate effectors within close proximity to the channels; they can conscript other effectors or can be summated to produce global increases in calcium that can propagate throughout and between cells (6).

Until the last decade the majority of investigations of intracellular Ca^{2+} signaling dynamics have utilized organically synthesized Ca^{2+} -sensitive dyes such as fura-2, indo-1, fluo-3, and fluo-4. These synthetic calcium indicators display rapid response kinetics to changes in Ca^{2+} levels and are available with a range of (off-the-shelf) Ca^{2+} affinities. Dyes can be loaded into cells with very high efficiencies with the majority of the cells containing the indicator of interest after a simple loading protocol ((7); see Note 1). This most commonly involves incubation with an esterified (uncharged, inactive) form of the dye with the final location of active dye molecules determined by the intracellular compartment in which they are cleaved progressively by esterases. With this loading promiscuity comes the difficulty of resolving signaling contributions that may arise in restricted volumes of the cells (e.g., near membranes, within organelles). Hence, the intricacies of “localized” signals are difficult to resolve (8).

An important new direction of the last decade has been the evolving design of genetically encoded probes that incorporate green fluorescent protein or its variants (9), as molecular tools for detecting calcium (and other ion) dynamics in cells. This is such a rapidly progressing field that many of the latest developments are best followed through various social media that avidly discuss new developments and applications (e.g., *OpenOptogenetics*, *Brain Windows*; see Note 2). Invariably, these intelligently designed molecules are fusions of natural fluorophores (GFP or the like) and endogenous Ca^{2+} sensors or fragments (calmodulin or troponin-C: (10)).

Miyawaki and colleagues fused Cyan Fluorescent Protein (CFP; a derivative of GFP) to the N terminus of calmodulin, (CaM) and Yellow Fluorescent Protein to the C terminus of M13 (a 26-residue peptide derived from the CaM-binding region of the skeletal muscle myosin light chain kinase) (11) to create the “cameleons”. Absorption of light by the CFP moiety can lead to fluorescence resonance energy transfer (FRET) to the YFP, by a molecular rearrangement that is increased with elevations in intracellular calcium levels. Pericams were developed by Nagai and colleagues (12). Whereas FRET utilizes two GFP mutants, pericams consist of single a GFP variant sensitive to physiologically relevant substrates such as calcium ions. To construct the pericams, circularly permuted enhanced yellow fluorescent proteins (cpEYFP) were used in which the amino and carboxyl portions were reconnected by a short spacer between the original termini. Calmodulin was fused to the C terminus of cpEYFP, and its target peptide, M13 to the N terminus. By mutating several amino acids near the chromophore, three types of pericams were obtained; “flash-pericam” that became

brighter with calcium binding, “inverse pericam” that dimmed upon calcium binding, and “ratiometric pericam” that displayed a shift in the excitation wavelength maximum.

While current genetically encoded Ca^{2+} sensors are not without their experimental limitations (limited dynamic range and relatively slow binding kinetics compared to organic sensors), the benefits of genetic encoding (having cells make their own sensors), and the capacity for targeting to specific cell locations, balance these disadvantages. The ability to detect changes in the levels of cytosolic and compartmentalized Ca^{2+} in living cells is fundamental to understanding the complexities of Ca^{2+} signaling. It is clear that the ER, as a major cellular storage of Ca^{2+} , and an important contributor to a diverse array of signaling cascades, should be the subject of considerable research focus (13). In this chapter the authors will discuss practical elements of this type of focus.

To target genetically encoded calcium sensors to particular locations in the cell, signaling sequences or target peptides derived from endogenous proteins normally resident in these locations can be used for specific targeting (Fig. 1). We have found these to be effective in trafficking calcium sensors to a variety of locations including the nucleus (14), mitochondria and endoplasmic reticulum (15).

In this chapter the authors describe the use of an endoplasmic reticulum (ER) targeted Ca^{2+} -biosensor, D1-ER cameleon (16) in cell signaling studies with astrocytes. These approaches require an understanding of the general strategies employed with synthetic calcium indicators and a solid foundation in molecular techniques for recombinant DNA technology. In addition, it is essential to

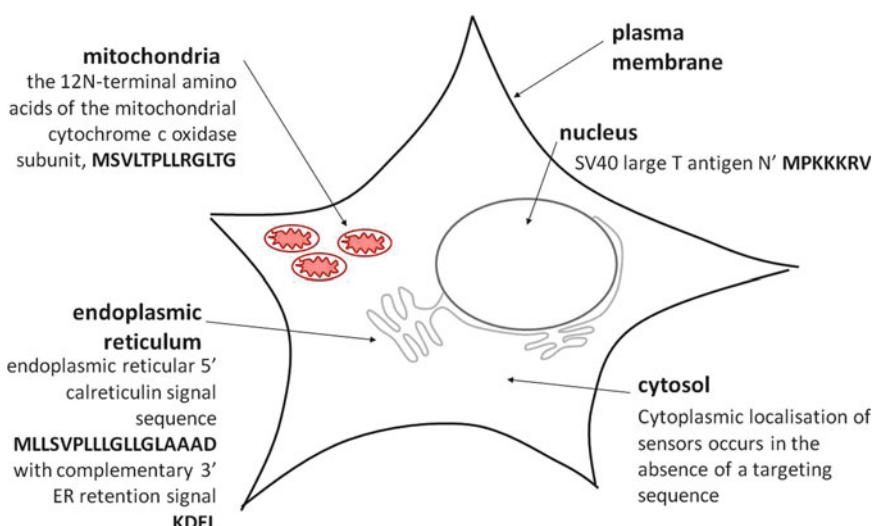


Fig. 1. The intracellular organelles most commonly targeted with localized genetically encoded Ca^{2+} sensors. Also shown are examples of targeting sequences used by endogenous proteins that normally localize to these organelles and intracellular sites.

develop a new frame of reference for data interpretation as in many instances fluorescence data represent the *reduction* in a Ca^{2+} -dependent signal (e.g., Ca^{2+} being *released* from the compartment where the Ca^{2+} sensor is localized). The protocols will complement a number of excellent methodological compendia that have been described in recent years (17–20).

2. Materials

2.1. Molecular Biology

1. Mammalian expression plasmid containing the genetically encoded Ca^{2+} sensor (construct DNA) (see Note 3).
2. Competent *E. coli* cells (see Note 4)—commercially available (One Shot® TOP10F' Invitrogen; cat# C3030-03, C3030-06).
3. Luria broth (Miller's LB broth)—commercially available. Some laboratories do make their own stock solutions (see Note 5).
4. Ampicillin-containing agar plates—commercially available (Invitrogen, cat# 11593-019).
5. Maxi-prep DNA purification kit—commercially available (HiSpeed, QIAGEN, cat# 12662).
6. 1 kb DNA step ladder (New England Biolabs, Genesearch, cat# N3232L).
7. DNA loading dye (Promega, cat# G1881).

2.2. Cell Culture

1. Halothane anesthetic (Ellar Laboratories).
2. Earle's Balanced Salt Solution (BSS); (GIBCO, Invitrogen cat# 14155-063).
3. Enzyme solution (10 mL Earle's BSS; 100 μL of 50 mM EDTA, sterile, pH to 7 with NaOH; 150 μL of 100 mM CaCl_2 ; 1.5–2 mg cysteine; 200 units of papain suspension—425 μL ; Sigma, cat #P3125).
4. Culture medium (Minimum Essential Medium—MEM; GIBCO, Invitrogen; supplemented with: 1 mM glucose; Penicillin-Streptomycin—5,000 units/mL; Invitrogen; 10% heat-inactivated Fetal Bovine Serum GIBCO, Invitrogen; MITO+™ Serum Extender—Becton Dickinson; 2 mM L-glutamine—GIBCO, Invitrogen).
5. 12-Well cell culture plates (JRH Biosciences).
6. 18 mm poly-D-lysine (Sigma) coated coverslips (SDR Clinical Technology).
7. Hemocytometer for cell density calculations.

2.3. Transfection

1. CalPhos™ mammalian transfection kit (Becton Dickinson Biosciences, Scientifix).
2. Transfection medium (culture medium without FBS and serum extender) (Minimum Essential Medium—MEM; GIBCO, Invitrogen; supplemented with: 1 mM glucose; Penicillin–Streptomycin—5,000 units/mL; Invitrogen; 2 mM L-glutamine—GIBCO, Invitrogen).
3. Ca-phosphate mixing solutions (*Solution A*: 1–2 µg Plasmid DNA, 6.2 µL 2 M Calcium Solution, Sterile Water to 50 µL total volume; *Solution B*: 50 µL 2× HBS) (see Note 6).

2.4. Fluorescence Imaging

1. HEPES buffer (mM: NaCl 135, KCl 5, HEPES 10, Glucose 10, CaCl₂ 1, MgCl₂ pH: 7.4) at room temperature (~25°C).
2. Organically synthesized Ca²⁺ indicators (50 µg dry aliquots)—dissolved in ~50 µL of dry DMSO (Sigma) to create working stock solutions. Larger stock volumes can be generated (1 mg/mL) and subdivided into smaller aliquots for storage (~20°C).
3. Synthetic calcium indicators were all purchased from Molecular Probes (Invitrogen).

3. Methods**3.1. Bacterial Transformation for Construct Amplification**

1. Two microliters of midi quality DNA (0.5–1.5 µg/µL) are used to transform competent *E. coli* cells. The bacterial cells are removed from the -70°C freezer and placed on ice for 10–15 min.
2. The DNA sample for each construct is added to an individual pre-labeled tube containing competent cells. After gentle mixing, the tube of bacterial cells/DNA should be incubated on ice for 15 min.
3. To initiate optimal uptake of DNA, the cells are then heat shocked at 42°C for 1 min using a water bath, before being returned to ice. The transformed cells are transferred to a sterile 10 mL plastic tube containing 0.5 mL of Luria Broth (LB).
4. To rescue the transformed bacterial cells the 10 mL tube is then placed in a Ratek shaker incubator for 1 h at 37°C and 255 rpm.
5. The solution is spread on to two pre-prepared ampicillin-containing agar plates, one low density (spread with ~50 µL of the LB/bacterial solution) and one high density (spread with ~500 µL of the LB/bacterial solution).
6. The agar plates are incubated at 37°C overnight (~16 h) to generate bacterial colonies.

3.2. MAXI-prep (Large Scale Plasmid DNA Purification)

1. Maxi-prep DNA for the calcium biosensor construct is prepared in order for use in transfection.
2. A single bacterial colony is used to inoculate 200 mL of LB (see Note 7). For selection, 200 µL of ampicillin (50 mg/µL) was added to the mixture. This LB/bacterial mixture was incubated overnight (18–22 h) in a Ratek shaker incubator set at 240 rpm and 37°C.
3. Plasmid DNA was purified using the Maxi-prep DNA purification kit. At the end of the procedure the amplified and purified DNA constructs were dissolved in 500 µL of Tris-EDTA (pH 8.0) which was included in the Maxi kit.
4. For confirmation of appropriate size DNA, Maxi-prep DNA fragments were run on an agarose gel.
5. 1 µL of the Maxi-prep sample is diluted with 99 µL of ddH₂O.
6. The yield and purity of Maxi-prep DNA is assessed by spectrophotometric (BioPhotometer, Eppendorf) analysis at 260 and 280 nm.
7. A control solution of 1 µL TrisEDTA and 99 µL of ddH₂O is used as a reference.

3.3. Restriction Enzyme Digestion and Agarose Gel Electrophoresis

1. For confirmation of a successful Maxi-prep DNA preparation, the amplified and purified DNA constructs are digested with appropriate restriction enzymes (see Note 8) and the digested fragments are run on agarose gel to confirm the presence of DNA fragments of expected size.
2. All enzymes are used in accordance with the guidelines set by the manufacturer (New England Biolabs). The total volume of restriction enzyme reactions is typically set at 40 µL with ddH₂O.
3. In general, digestions are assembled with 4 µL of Maxi-prep DNA, 4 µL of appropriate 10× buffer (supplied by New England Biolabs), and if required, 0.4 µL of 100× BSA (Bovine Serum Albumin; also supplied by New England Biolabs), and 1 µL of each restriction enzyme. The contents are mixed and centrifuged briefly (~5 s, at 500 rpm).
4. All restriction enzyme reactions are incubated at 37°C overnight (18–22 h), and then heat inactivated at 65°C for 20 min before agarose gel electrophoresis.
5. To visualize the digested DNA and to confirm the presence of expected bands, DNA loading dye is added to the DNA sample at 1/5 of the total volume.
6. Samples are electrophoresed on a pre-prepared agarose gel at 120 V, 500A for 35 min using a Propak-100 power supply (Australian Chromatography Company).

7. To provide a size reference, 1 μ L (500 μ g/mL) of 1 kb DNA step ladder is utilized and made up to 10 μ L with loading dye and ddH₂O.
8. DNA bands are visualized using an ultraviolet light source transilluminator.

3.4. Primary Hippocampal Neuron-Glia Mixed Cultures

1. Protocols for handling animals are reviewed and approved by the Animal Ethics Committee at The University of Melbourne, Australia (see Note 9).
2. Primary hippocampal neuron-glia mixed cultures are prepared from P2-5 Sprague-Dawley rats.
3. The animals are anesthetized by halothane (~1 mL) inhalation in an air-tight chamber (see Note 9).
4. The brains are removed under laminar flow and the hippocampi are dissected out and finely chopped.
5. The dissection solution consists of Earle's BSS warmed to 37°C prior to the culture process.
6. The hippocampal pieces are placed in a previously prepared and warmed (37°C) enzyme solution.
7. The enzyme solution containing the dissected and roughly chopped hippocampal pieces is then heated to 37°C for 35 min to allow papain to digest the extracellular matrices.
8. The hippocampal tissue is washed three times with culture medium to remove all traces of papain, and the mixture is triturated with flame sterilized and polished Pasteur pipettes to create a suspension of single cells.
9. The cells are plated into 12-well cell culture plates containing 18 mm poly-D-lysine coated coverslips at a density of 1.8×10^5 cells/well (as determined by a hemocytometer).
10. Cultures are maintained in supplemented culture medium.
11. For 1 well of a 12-well tissue culture plate, 1 mL of culture medium is used.
12. Cells are then grown (cultured) at 37°C in an incubator with a humidified atmosphere of 5% CO₂/95% O₂.
13. The culture medium is changed 4 days post culturing and cells are ready for transfection 7 days after commencing culture.

3.5. Transfection

1. The exogenous plasmid DNA biosensor construct is introduced into cultured cells using a modified calcium phosphate transfection technique (21).
2. This process used a calcium phosphate mammalian transfection kit according to the manufacturer's protocols, but with some steps optimized further.

3. The DNA concentration used is 2 µg/well of a 12-well culture plate (1.8×10^5 cells/well).
4. Pre-warmed (37°C) transfection medium is added to a new 12-well plate (1 mL medium/well). This is done for all wells containing coverslips and cells.
5. The DNA/Ca²⁺ phosphate precipitate is prepared by mixing solution A and B.
6. Solution A is mixed with solution B by adding approximately 1/8th volume of solution A at a time into solution B and then pipette mixing the mixture several times (see Note 6).
7. The mixture is vortexed (Ratek vortex mixer) for 2–3 s (low speed). Mixing of solution A with B is repeated until no solution a remains.
8. The mixed solution is left to rest at room temperature for 20 min to form fine particles of precipitate.
9. During this incubation period, coverslips are transferred from their original plate to the new plate containing the transfection medium (the specific well for each coverslip is noted so that each coverslip can be returned to the same original well later). Both plates are then returned to the incubator.
10. After a 20 min incubation time for formation of the calcium phosphate precipitate the plate containing the transfection medium with the newly placed coverslips of cells is removed from the incubator.
11. The DNA/Ca²⁺ phosphate suspension is added drop-wise to each coverslip (100 µL/coverslip).
12. The plate is rocked gently back and forth to distribute the transfection solution evenly over the coverslip of cells (see Note 10).
13. The cells are incubated in the presence of the precipitate for 2 h in a 5% CO₂/95% O₂ humidified incubator at 37°C. At the end of the incubation period, the precipitate forms a homogenous “snow like” cover over the field of cells.
14. After incubation the precipitate needs to be dissolved to reduce cell toxicity. This is done by removing the precipitate solution from each well, and replacing it with transfection medium (1 mL/well) pre-equilibrated in a 10% CO₂/90% O₂ incubator for at least 4 h.
15. After adding the 10% CO₂ equilibrated transfection medium, the transfection plate is returned to the 5% CO₂/95% O₂ culture incubator for a further 1.25 h.
16. The coverslips are transferred with sterile, fine forceps from the transfection plate back to their original wells containing the original (“old”) culture medium.
17. At 72 h post-transfection the expression of the exogenous constructs can be imaged (see Note 11).

3.6. Confocal Microscopy

1. Primary hippocampal cultures are viewed 72 h post-transfection, with a Zeiss LSM 510 META multiphoton/confocal microscope.
2. Images are acquired with a 40× IR-Achromat (numerical aperture: 0.80), water immersion objective (see Note 12).
3. For live cell imaging, the cells are bathed in HEPES buffer.

3.7. Calcium Imaging Using Synthetic Calcium Indicators

1. A field of cells expressing the exogenous construct is selected and control images are taken to identify transfected cells (see Notes 11–13).
2. Fluo-4 is previously prepared in a concentrated form (1 mM) in anhydrous DMSO in aliquots and was stored at -20°C.
3. The DMSO stock solution was then diluted in a suitable experimental solution to a final concentration of 1–5 μM. Cells are initially washed with 1 mL of HEPES buffer, then loaded with 2 μL of fluo-4 AM (in a total volume of 1 mL of HEPES buffer) and left at room temperature (~25°C) for 25 min.
4. Cells are washed twice and then mounted in a cell bath. Recordings are made in HEPES buffer.
5. Time-course experiments for measurement of dynamic changes in Ca²⁺ concentration (fluo-4 and D1-ER cameleon) involve the collection of an average of two to four consecutive 512 × 512 pixel confocal images every 5 s for 10 min (120 images total) (see Note 14). These long term imaging protocols utilize a time controlled acquisition module of the specific confocal software (these are very similar for all types of image acquisition systems).
6. Specific agonists (e.g., glutamate, 20 μM) or calcium ionophores such as ionomycin (Sigma; concentration 1 μM) are applied at designated time points after commencement of data collection.
7. Background corrected fluo-4 fluorescence (F) is determined for defined regions of interest and converted to relative fluorescence intensities ($F - F_0/F_0$), where F_0 represents the average initial (pre-agonist) fluorescence level (see Note 15).
8. This is a commonly applied normalization procedure for fluorescence sensors that exhibit only a change in fluorescence intensity and not spectral characteristics (e.g., peak excitation or emission wavelength) with the binding of Ca²⁺. This normalization largely adjusts for variations in the absolute fluorescence levels between cells in individual experiments and between different experiments, which are due to normal experimental variations in the concentration of internalized sensors.

3.8. Image Acquisition for Genetically Encoded Ca^{2+} -Sensors

1. Transfected hippocampal cultures adherent on poly-L-lysine coated coverslips are prepared for imaging by aspiration of the growth media, and a wash with 1 mL of HEPES buffer.
2. Coverslips are mounted into a coverslip holder, specifically designed for bathing cells in appropriate buffers during the confocal microscopy experiments (see Note 16).
3. We use a purpose built observation chamber with inlet and outlet valves for perfusion of solutions and drug application. The lines connecting to bath inlet are reliant upon gravity feed for perfusion with a stop valve for interchange between perfused solutions. Bath outlet is controlled via an adjustable flow-rate, pump system (Scintilla EpiPump).
4. Changes in the external Ca^{2+} concentration (Ca^{2+} -HBS, zero Ca^{2+} -HBS) are achieved by selecting from alternative bath solution reservoirs with stopcock control.
5. For more precise delivery of drugs to selected cells or groups of cells, a Picospritzer II (General Valve Co. USA) is used to provide pressure ejection of small volumes (10–100 μL) of selected drugs (glutamate, thapsigargin) through glass micro-electrodes. Electrodes are positioned adjacent to target cells with a stage-mounted, fine-control (X-Y-Z) micromanipulator (Burleigh PCS series-5000).
6. A laser-controlled programmable pipette puller (Sutter Model P-2000) was used for electrode manufacture and employed predetermined pull programs controlling heat intensity, time-course and duration of the pull.
7. An IR-Achromat 40 \times N.A 0.80 W, immersion objective lens was used for all image acquisition procedures. Sensors and dyes were excited with the 488 nm and 458 nm lines of a 100 mW argon ion laser. In addition, the 543 nm line of a 100 mW Green Helium Neon laser was utilized for some protocols.
8. High spatial resolution images for assessment of fluorescence distribution patterns (D1-ER cameleon, ER Tracker Red) are obtained by averaging four to eight consecutive 512 \times 512 pixel scans.
9. “Lambda mode” images are acquired to optimize selection of emission wavelengths for quantitative studies (fluo-4 and D1-ER cameleon). This involves use of fixed excitation wavelength (458 or 488 nm) while varying the emission wavelength in 10 nm increments over the predicted range distribution to generate an emission spectrum.
10. Every image, and the Meta data associated with it, is recorded to computer hard disk.
11. The confocal parameters (confocal aperture, and PMT gain and black level) are adjusted to obtain distinguishable fluorescence

(high signal-to-noise ratios) values and these parameters are kept constant throughout each individual time-course experiment.

12. Laser intensity is set to minimize the level of photobleaching of fluorophores. In any given field of cells several regions of interest (ROI) are defined, within the cytosol or contained within the organelles of interest. For some experiments multiple cells (four to eight), and for others only individual cells, are examined.
13. Not all cells in a field of view are fluorescent because of heterogeneity in transfection efficiency for genetically encoded calcium sensors with any transfection protocol. These non-fluorescent cells can serve as controls for autofluorescence, and are also selected as regions of interest (ROI) during response monitoring.
14. Regions of Interest (ROIs) are defined on images interactively using a mouse driven cursor. Average fluorescence intensity values are calculated automatically and corrected for background intensity levels of defined, adjacent (noncellular) regions (Zeiss Time Series software). Data files can be exported to Excel (Microsoft Office) spreadsheets for any further data calculations.
15. During experiments images were collected concurrently at dual emission wavelength ranges centered on 480 and 535 nm. These ranges equate to the optimized emission ranges for the CFP and citrine components of D1-ER cameleon, representing fluorescence output from the Ca^{2+} -free and Ca^{2+} -bound forms of the sensor, respectively.
16. Ratio (535 nm/480 nm) images were calculated by direct division of the component fluorescence images (each subject to background correction; (see Note 15)). Data are presented for D1-ER cameleon as average ratio (535/480) values for selected ROIs.

3.9. Examples of Subcellular Localization of D1-ER Cameleon

D1-ER cameleon was almost exclusively expressed in protoplasmic glial cells of primary hippocampal cultures. While the incidence of transfected neurons was almost nonexistent (well below 1%), ~20% of astrocytes exhibited distinctive, nonuniform fluorescence patterns following transfection with D1-ER cameleon (Fig. 2). High spatial resolution images illustrated the specific subcellular distribution pattern of this biosensor. D1-ER cameleon displayed a reticular fluorescence pattern that was consistent with the localization of the ER and enclosed a large, non-fluorescent region of each cell that was consistent with the size and location of the nucleus (*nuc*, Fig. 2b). A continuous fluorescence pattern that surrounded the nucleus is evident, a pattern consistent with the structure of the nuclear envelop (*ne*, Fig. 2b) which is known to be contiguous with the ER.

Confirmation of the organelle identity for D1-ER cameleon fluorescence in primary hippocampal cultures is provided by co-labeling experiments where cells expressing D1-ER cameleon

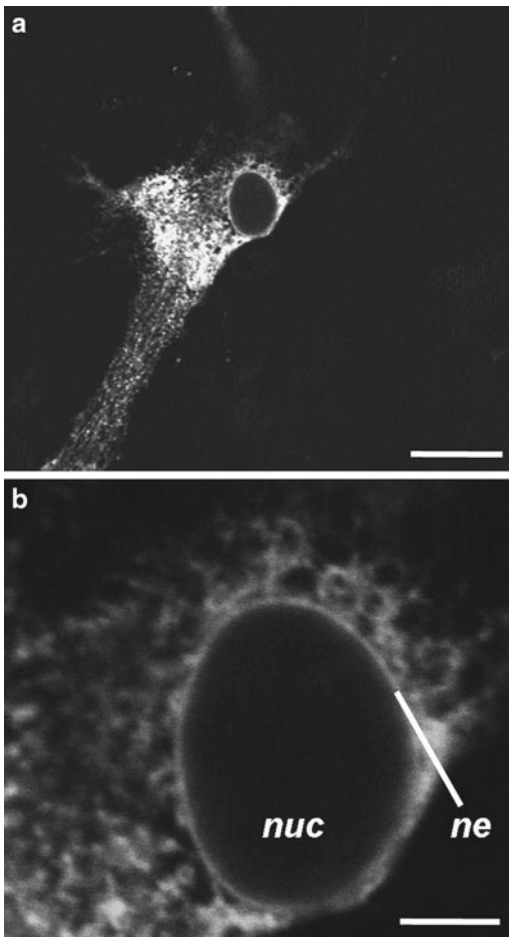


Fig. 2. Localization of D1ER in an astrocyte. (a) Reticular fluorescence is apparent throughout the cell, but is more highly concentrated in the central core of the cell as shown in panel (b). Reticular structures are clearly continuous with the double membrane (*ne*) known to envelop the cell nucleus (*nuc*). Scale bars—(a): 20 μm ; (b): 5 μm .

are then treated with ER Tracker Red, an organic stain that preferentially labels the ER (Fig. 3). These co-labeled astrocytes exhibit identical fluorescence patterns when D1-ER cameleon (a, c) and ER Tracker Red (b, d) are specifically excited. These observations confirm the source of D1-ER cameleon fluorescence as the ER.

**3.10. Examples
of ER Ca^{2+}
Measurements Made
in Rat Hippocampal
Astrocytes:
Glutamate-Induced
Cytosolic Ca^{2+}
Responses**

Primary hippocampal cultures loaded with the cytosolic Ca^{2+} sensor, fluo-4 are exposed to glutamate (20 μM) via Picopipette application during acquisition of a series of images (Fig. 4; time-course analysis). In the presence of normal extracellular Ca^{2+} levels ($\text{Ca}^{2+}\text{-HBS}$), glutamate causes marked fluctuations in normalized fluorescence values ($\Delta F/F_0$) (Fig. 4b) for all defined intracellular regions of interest (Fig. 4a). These complex, multicomponent responses represent oscillations of astrocyte $[\text{Ca}^{2+}]$. Removal of

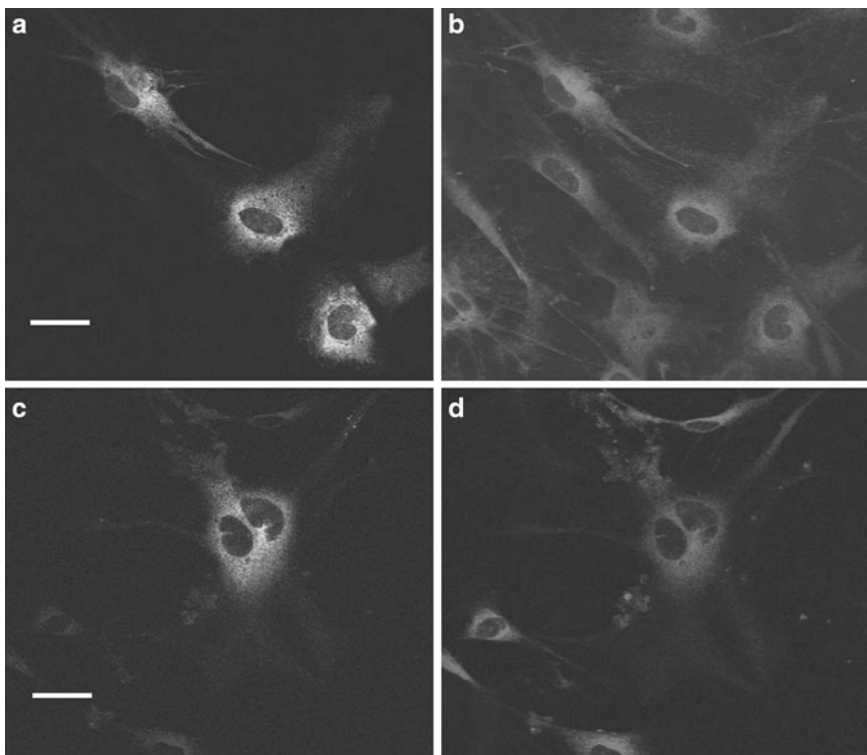


Fig. 3. Colocalization of the ER Ca^{2+} biosensor, D1-ER cameleon, and specific ER probe ER Tracker Red. **(a, c)**: Astrocytes expressing D1ER cameleon (citrine component of the cameleon excited—488 nm excitation/535 nm emission). Scale Bars: 20 μm . **(b, d)**: Identical field following staining of astrocytes with the specific endoplasmic reticulum dye, ER Tracker Red (543 nm excitation/630 nm emission). Identical fluorescence patterns result from both procedures indicating common organelle signal sources. Note, while ER Tracker Red stains all cells, only a subset of astrocytes within the field is transfected with D1ER. Scale bars: **(a)**: 20 μm , **(c)**: 20 μm .

extracellular Ca^{2+} results in the marked reduction in the amplitude of the glutamate-induced oscillations (Fig. 4c), indicating a significant, but not exclusive, dependence on Ca^{2+} influx for the generation of these Ca^{2+} signals. The residual component (Fig. 4c) is likely to represent Ca^{2+} released from intracellular storage.

3.11. Examples of the Response of D1-ER Cameleon to Glutamate Application

A similar experimental protocol can be used to assess the potential contribution to these responses of Ca^{2+} released from the ER. Figure 5 illustrates that the fluorescence ratio (535 nm/480 nm) shows repeatable, reversible reductions in response to glutamate application (20 μM), in both the presence (Fig. 5c) and absence (Fig. 5d) of external Ca^{2+} . The magnitude of these ratio reductions is found, when considering pooled data ($n=5$ experiments), not to be statistically significantly different in both situations. These responses suggest that released ER Ca^{2+} contributes to the Ca^{2+} oscillations reported by the cytosolic Ca^{2+} sensor, fluo-4 (Fig. 4).

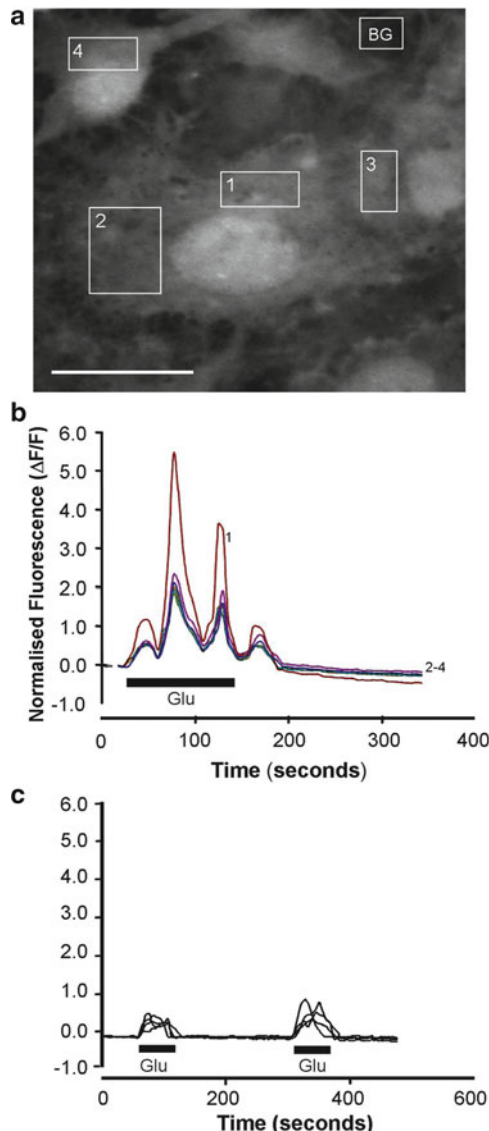


Fig. 4. Effect of glutamate on cytosolic Ca^{2+} levels in astrocytes. (a) Image indicating selected regions of interest for fluorescence recordings. BG denotes background (noncellular) region. Scale bar 20 μm . Changes in normalized fluorescence response of fluo-4, indicative of the change in cytosolic $[\text{Ca}^{2+}]$, in response to glutamate (20 μM) applications (horizontal bars) recorded in the presence (b) or absence (c) of extracellular Ca^{2+} in the perfusate (HBS) ($n=5$).

In both Ca^{2+} and Ca^{2+} -free conditions the ER shows a similar initial level of Ca^{2+} loading (i.e., similar initial ratio value), and prolonged (second) applications of glutamate cause larger ER Ca^{2+} depletions. Interestingly, the ER Ca^{2+} level appears to rundown in the maintained absence of extracellular Ca^{2+} (Fig. 5d), suggesting a generalized progressive depletion of cellular Ca^{2+} supplies.

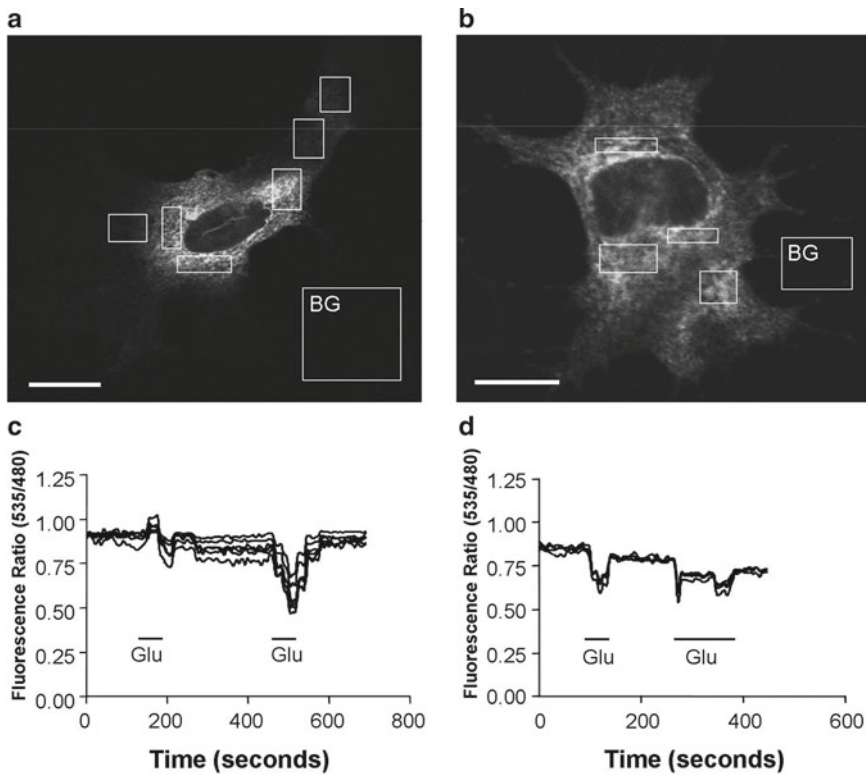


Fig. 5. Effect of glutamate on endoplasmic reticulum (ER) Ca^{2+} levels in astrocytes. (a, b) Images indicating selected regions of interest for fluorescence recordings. BG denotes background (noncellular) region. Scale bars (a): 20 μm , (b): 10 μm . Changes in ratio fluorescence response of D1-ER cameleon in ROIs, indicative of the change in ER $[\text{Ca}^{2+}]$, in response to glutamate (20 μM) applications (horizontal bars) recorded in the presence (c) or absence (d) of extracellular Ca^{2+} in the perfusate (HBS).

3.12. Effects of ER Ca^{2+} Depletion on Glutamate-Induced Ca^{2+} Oscillations

Further evaluation of the potential importance of the ER in contributing Ca^{2+} for these astrocyte cytoplasmic Ca^{2+} oscillations requires direct manipulation of the ER Ca^{2+} store, and this can be achieved by use of thapsigargin (TG), an inhibitor of the smooth endoplasmic reticulum ATPase pump. The effect of TG application to D1-ER cameleon fluorescence is shown in Fig. 6. It is clear from assessment of average ratio values of selected ROIs (Fig. 6a), that TG causes a marked and largely irreversible (in this time frame) depletion of ER Ca^{2+} level (Fig. 6b). This depletion is still evident well after withdrawal of TG application supporting a practical role for TG in chronic depletion of astrocyte ER Ca^{2+} stores.

TG application causes statistically significant reductions in astrocyte glutamate-induced Ca^{2+} signals recorded with fluo-4 (Fig. 7). The marked TG-induced elevation in cytosolic Ca^{2+} (Fig. 7, second peak) would result from the ER Ca^{2+} -depletion shown in Fig. 6 which is likely to be the primary cause of the diminished Ca^{2+} -responses to subsequent glutamate application. This is strong evidence for the importance of ER Ca^{2+} contributions to glutamate-induced Ca^{2+} oscillations.

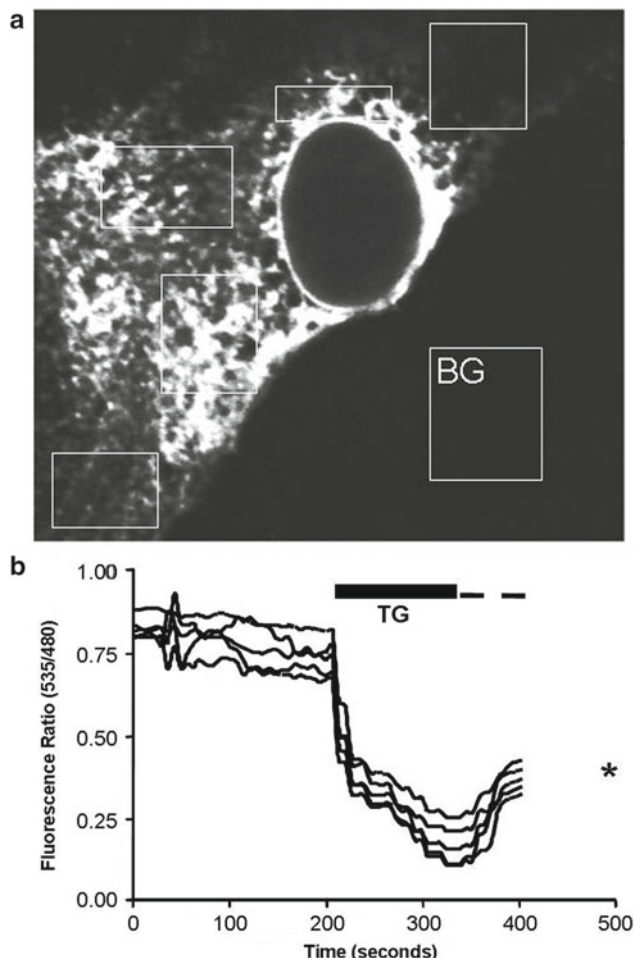


Fig. 6. Effect of Thapsigargin on astrocyte ER- Ca^{2+} levels. (a): Ratio image immediately prior to application of Thapsigargin (TG 1 μM) indicating regions-of-interest (ROI) for measurement. BG denotes background (noncellular) region. (b): Time-course of change of fluorescence ratio (535/480) for ROIs. TG application indicated by *solid horizontal bar*. *Dotted line* emphasizes that TG is known to be difficult to remove from cells during wash-out (*average ROI ratio still reduced at $t=500$ s). ($n=5$).

4. Notes

1. Cells are incubated in HEPES buffer to which 1–5 μM of fluorescent Ca^{2+} indicator (from 1 mM stock in dry DMSO) is added. 25 min at 25°C is allowed for dye internalization. Cells are then washed in fresh buffer to allow for completion of the de-esterification of internalized indicator. This process should be optimized for the cell type that is selected for experiments. Variables that can be modified include the following: initial dye concentration, cell density, loading time, temperature (cold load,

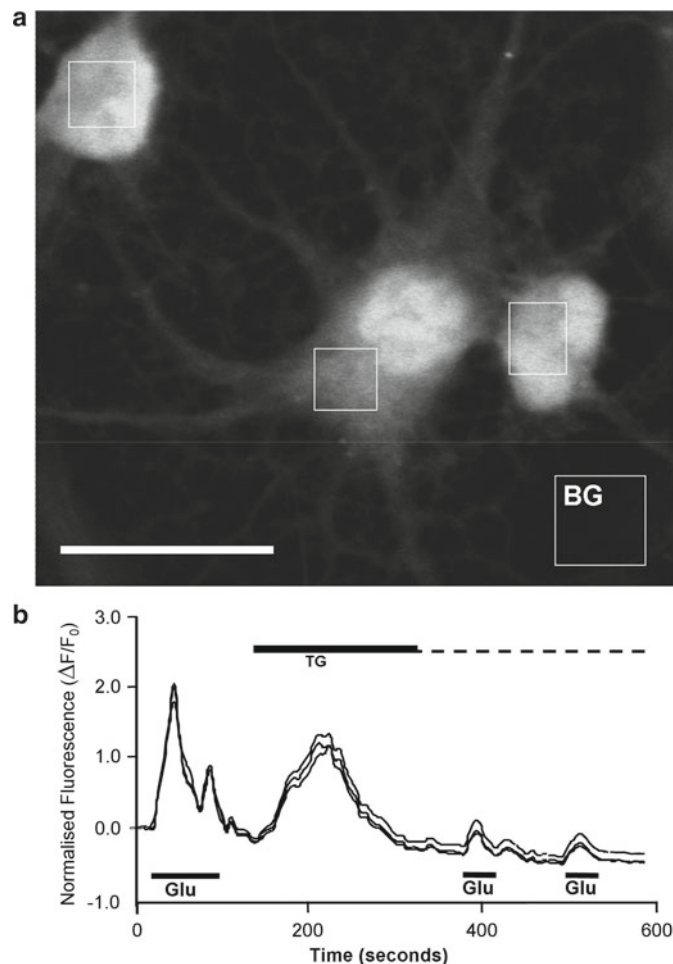


Fig. 7. Effect of thapsigargin application on glutamate-induced Ca^{2+} responses in astrocytes. **(a)** Image indicating selected ROIs for fluo-4 fluorescence recordings. BG denotes background (noncellular) region. Scale bar 20 μm . **(b)** Normalized fluorescence responses ($\Delta F/F$) for ROIs. Cells were continually perfused with Ca^{2+} -HBS. Glutamate (20 μM) was applied via Picospritzer at times indicated by lower horizontal bars. Thapsigargin (TG—1 μM) was added directly to the bathing solution (indicated by *upper solid horizontal bars*) and remained present throughout the remainder of the acquisition period.

warm de-esterification; 25, 30, or 37°C), solution agitation, and number and duration of washes.

2. *OpenOptogenetics*: a collaborative project aiming at promoting, facilitating and democratizing the use of optogenetic approaches in biological research.

<http://www.openoptogenetics.org/>.

Brain Windows: <http://brainwindows.wordpress.com/>.

3. Plasmid DNA of particular constructs can often be sourced by contacting research groups that have generated the original

materials. These samples are generally shipped in a desiccated form (adhered to paper).

4. Competent cells (*E. coli* are generally used) are those that had had their cell walls modified (heat shock, electroporation, chemical treatment) to allow for ready passage and incorporation of foreign DNA (e.g., biosensor constructs).
5. For 1 L of LB, dissolve 10 g Tryptone, 5 g yeast extract, and 10 g NaCl in 950 mL deionized water. If necessary adjust the pH of the solution to 7.0 with NaOH. Use additional deionized water to a final volume of 1 L. The mixture should be autoclaved for 20 min at 15–20 psi. Allow to cool and add antibiotic (optional). Store refrigerated or at room temperature until required. There are LB broth variants with different NaCl levels—optimized for different bacterial strains.
6. This volume is sufficient for the transfection of a single well of cell. The volumes can be scaled up for transfection of multiple cell wells.
7. A single bacterial colony can be scraped from the plate using a sterile pipette tip. The tip (and colony) can then be dropped directly into the broth vessel.
8. Restriction Enzymes (restriction endonucleases) are enzymes that cut DNA (double- or single-stranded) at specific recognition sites (specific nucleotide sequences) termed restriction sites. It is essential to know the nucleotide sequence of the plasmid vector in use (a restriction map is usually supplied with the construct). The choice of cleavage points will determine the fragment size expected for gel electrophoresis. There are a number of useful Web tools to assist in the selection of restriction enzymes (e.g., <http://www.colorado.edu/chemistry/bioinfo/RestrictionEnzymeMapping.htm>).
9. The Animal Ethics guidelines for animal handling, euthanasia and disposal will vary between Research Institutions. The local guidelines should be followed. In particular, there may be alternative guidelines with respect to animal anesthesia.
10. It is important not to rotate the plates as this concentrates transfection precipitate in the center of the well.
11. We most commonly use a Zeiss LSM 510-Meta multiphoton/confocal microscope equipped with 488 nm argon, 543 nm Green, 633 nm Red Helium/Neon and 800 nm Chameleon lasers. This confocal is coupled to a Zeiss upright microscope (Axioskop 2).
12. The choice of objective lenses for confocal imaging depends on available microscopes (inverted or upright configuration). In general, lenses with a high numerical aperture provide the highest spatial resolution and this is accentuated by accurate matching of the lens and immersion medium. Invariably, with

upright microscopes water immersion objectives are the preferred choice. The working distance of the objective will influence the ease with which ancillary equipment such as perfusion inlets/outlets and spritzing electrodes can be positioned.

13. The choice of laser lines and filter sets for confocal imaging is governed by the spectral characteristics of the fluorophore in use. Lambda stack images (Zeiss Meta confocal) allow for optimization of filter selections.
14. A priori knowledge of the physiological Ca^{2+} response to an agonist is useful in setting the data acquisition rate. As a working rule sampling frequency should be set at a rate that is at least twice as high as the greatest frequency of data change expected in the physiological response.
15. While all cells have a level of endogenous fluorescence (autofluorescence) at the wavelength combinations (excitation, emission) commonly used in Ca^{2+} -imaging experiments, this is generally low compared to the fluorescence introduced by exogenous fluorophores. To obtain the highest precision quantitative data autofluorescence should be determined and subtracted from the total fluorescence levels determined experimentally. The fluorescence- $[\text{Ca}^{2+}]$ relationship is steep in the $[\text{Ca}^{2+}]$ range around the dissociation constant (K_d) for Ca^{2+} binding, and for many most commonly used organically synthesized indicators this coincides with the resting levels of Ca^{2+} . Autofluorescence for monolayer cultures can be collected by imaging collections or individual unloaded cells. These measures can be achieved prior to dye loading of the culture, or in a separate collection of cells. It is essential that autofluorescence values (absolute fluorescence intensities) are collected at the same confocal aperture, PMT gain and black level settings as will be used for collection of fluorescence data. In practice these settings are often interactively optimized for a particular level of cell dye loading and, therefore, autofluorescence reading are best recorded after data collection. Following transfection with genetically encoded Ca^{2+} sensors there are sufficient nontransfected cells within the microscope field of view to dedicate several regions of interest for data collection to these cells for autofluorescence monitoring.
16. We commonly use bespoke cell perfusion baths that we have designed to allow for all requirements of an experiment. The important features include the ability to reversibly mount the circular coverslips used to culture cells, physical access (above) for microelectrodes accounting for the profile of the selected objective lenses, and inlet and outlet ports for solution exchange (if required). There are a number of sources of commercially available cell baths that may suit your specific imaging requirements (For example: <http://www.microscopyu.com/articles/livecellimaging/culturechambers.html>).

References

1. Berridge MJ, Bootman MD, Lipp P (1998) Calcium – a life and death signal. *Nature* 395(6703):645–648
2. Bootman MD, Lipp P, Berridge MJ (2001) The organisation and functions of local Ca^{2+} signals. *J Cell Sci* 114(Pt 12):2213–2222
3. Berridge MJ (1997) The AM and FM of calcium signalling. *Nature* 386(6627):759–760
4. Matveev V, Bertram R, Sherman A (2011) Calcium cooperativity of exocytosis as a measure of Ca^{2+} channel domain overlap. *Brain Res* 1398:126–138
5. Berridge MJ (1998) Neuronal calcium signalling. *Neuron* 21(1):13–26
6. Bootman MD, Berridge MJ, Lipp P (1997) Cooking with calcium: the recipes for composing global signals from elementary events. *Cell* 91(3):367–373
7. Hirst RA et al (2006) Measurement of $[\text{Ca}^{2+}]_i$ in whole cell suspensions using fura-2. *Methods Mol Biol* 312:37–45
8. Llinás R, Sugimori M, Silver RB (1992) Presynaptic calcium concentration microdomains and transmitter release. *J Physiol Paris* 86(1–3):135–138
9. Chudakov DM et al (2010) Fluorescent proteins and their applications in imaging living cells and tissues. *Physiol Rev* 90:1103–1163
10. Heim N, Griesbeck O (2004) Genetically encoded indicators of cellular calcium dynamics based on troponin-C and green fluorescent protein. *J Biol Chem* 279:14280–14286
11. Miyawaki A et al (1997) Fluorescent indicators for Ca^{2+} based on green fluorescent proteins and calmodulin. *Nature* 388(6645):882–887
12. Nagai T et al (2001) Circularly permuted green fluorescent proteins engineered to sense Ca^{2+} . *Proc Natl Acad Sci USA* 98(6):3197–3202
13. Sobie EA, Lederer WJ (2011) Dynamic local changes in sarcoplasmic reticulum calcium: physiological and pathophysiological roles. *J Mol Cell Cardiol* 52(2):304–311
14. Petrou S et al (2000) Genetically targeted calcium sensors enhance the study of organelle function in living cells. *Clin Exp Pharmacol Physiol* 27(9):738–744
15. Bowser DN et al (2002) Release of mitochondrial Ca^{2+} via the permeability transition activates endoplasmic reticulum Ca^{2+} uptake. *FASEB J* 16(9):1105–1107
16. Palmer AE et al (2004) Bcl-2 mediated alterations in endoplasmic reticulum Ca^{2+} analysed with an improved genetically encoded fluorescent sensor. *Proc Natl Acad Sci USA* 101:17404–17409
17. Palmer AE, Tsien RY (2006) Measuring calcium signalling using genetically targetable fluorescent indicators. *Nat Protoc* 1(3):1057–1065
18. Knopfel T, Diez-Garcia J, Akemann W (2006) Optical probing of neuronal circuit dynamics: genetically encoded versus classical fluorescent sensors. *Trends Neurosci* 29:160–166
19. Kotlikoff MI (2007) Genetically encoded Ca^{2+} indicators: using genetics and molecular design to understand complex physiology. *J Physiol* 578:55–67
20. McCombs JE, Palmer AE (2008) Measuring calcium dynamics in living cells with genetically encodable calcium indicators. *Methods* 46(3):152–159
21. Jiang M, Deng L, Chen G (2004) High Ca^{2+} -phosphate transfection efficiency enables single neuron gene analysis. *Gene Ther* 11(17):1303–1311

Chapter 20

Measurement of Cytosolic-Free Ca²⁺ in Plant Tissue

Martin R. McAinsh and Carl K.-Y. Ng

Abstract

A range of techniques have been used to measure the concentration of cytosolic-free Ca²⁺ ($[Ca^{2+}]_{cyt}$) in plant cells. Fluorescent Ca²⁺-sensitive indicators have been used extensively to measure plant $[Ca^{2+}]_{cyt}$ and a number of techniques are available for loading these into plant cells. Here we describe a method for measuring $[Ca^{2+}]_{cyt}$ in the guard cells of the model plant species *Commelina communis* by ratio photometry and imaging techniques using the ratiometric fluorescent Ca²⁺-sensitive indicator fura-2.

Key words: *Commelina communis*, Guard cells, Fura-2, Microinjection, Ratiometric measurements

1. Introduction

Several techniques have been used to measure the concentration of cytosolic-free Ca²⁺ ($[Ca^{2+}]_{cyt}$) in plants including Ca²⁺-sensitive microelectrodes, Ca²⁺-sensitive photoproteins, fluorescence resonance energy transfer (FRET)-based cameleon reporters, and fluorescent Ca²⁺ indicators (1, 2). Ca²⁺-sensitive microelectrodes (3) can be used only in cells that are able to withstand impalement with two electrodes or a double-barreled electrode. In addition, microelectrodes suffer from slow response times and difficulties with calibration. These problems are particularly acute in plant cells in which the high turgor often results in partial displacement of the sensor, and the subsequent loss of sensitivity, following impalement. Consequently, the use of Ca²⁺-sensitive electrodes has been limited to only a few studies in plants and algae (for example, see refs. 4, 5).

Calcium-sensitive photoproteins, such as aequorin (6), emit light on binding Ca²⁺. The luminescence is directly proportional to $[Ca^{2+}]_{cyt}$ and can be measured by either luminometry or imaging techniques. Initially, measurements of plant $[Ca^{2+}]_{cyt}$ using aequorin

were restricted to a limited number of cell types due to the need to microinject this high-molecular-weight protein into cells using pressure (see below) (7). Aequorin has subsequently been introduced into plants by stable transformation techniques (8), allowing the protein to be targeted specifically to the cytosol (8, 9) or to organelles (9, 10) and to specific cell types (10), including guard cells (11). This provides a noninvasive method for monitoring whole-plant $[Ca^{2+}]_{cyt}$ and organelar-free Ca^{2+} . However, potential limitations with this technique include differences in the stability, distribution or localization of aequorin in cells, and differences in the permeability of cells to the luminophore coelenterazine. In addition, this technique has so far been restricted to a number of transformable cell types and species such as tobacco and *Arabidopsis*.

Cameleons are green fluorescent protein (GFP)-based Ca^{2+} sensor (12) consisting of a fusion protein comprising a cyan-emitting version of GFP (CFP) linked to calmodulin and a calmodulin-binding peptide (M13) and an enhanced yellow-emitting GFP (YFP). Binding of Ca^{2+} to the calmodulin domain induces a conformational change that can be detected by FRET between the component cyan and yellow fluorescent protein domains. $[Ca^{2+}]_{cyt}$ can therefore be measured by determining the efficiency of FRET. Like aequorin, cameleons can be introduced into plants by stable transformation techniques and have the potential to be targeted to specific cell types or organelles (12, 13). However, to date as with aequorin their use has been restricted to plant species including *Arabidopsis* (14, 15) and *Medicago truncatula* (16, 17).

Fluorescent Ca^{2+} -sensitive indicators have been used extensively to measure plant $[Ca^{2+}]_{cyt}$ (1, 2). These fall into two main categories: (1) non-ratiometric indicators, which exhibit an increase in fluorescence across the whole of the emission spectra on binding Ca^{2+} (e.g., calcium green) and (2) ratiometric indicators, which exhibit a shift in either their excitation or emission spectra when they bind Ca^{2+} (e.g., fura-2). Fura-2 exhibits a shift in its excitation maximum (510-nm emission) on binding Ca^{2+} , so the fluorescence at 340 nm increases and the fluorescence at 380 nm decreases with increasing $[Ca^{2+}]_{cyt}$; the 340/380 nm fluorescence ratio is proportional to $[Ca^{2+}]_{cyt}$ (18). Quantification of $[Ca^{2+}]_{cyt}$ using non-ratiometric indicators is complicated by cell-to-cell variations in the concentration and distribution of indicators within cells, together with indicator loss during experiments (18). Therefore, ratiometric measurements of $[Ca^{2+}]_{cyt}$ obtained using either a ratiometric Ca^{2+} -sensitive indicator or a combination of non-ratiometric Ca^{2+} -sensitive indicator co-loaded into cells with a Ca^{2+} -insensitive dye such as Texas Red are preferred.

A number of techniques are available for loading fluorescent Ca^{2+} -sensitive indicators into plant cells, including low-pH loading, ester loading, electroporation, digitonin permeabilization, and microinjection (1, 2). Of these, microinjection has proved the most

successful method in plants (19, 20). In addition, patch-clamp techniques have also been used to introduce compounds into plant cell protoplasts in the whole-cell configuration (21, 22). Recently, a biolistic method using microscopic gold particles has been developed for loading Ca^{2+} -sensitive indicators into plant and algal cells in a similar approach to that used to transform undifferentiated plant material (23). Biolistic delivery has the advantage of being faster and technically less demanding than microinjection, may be used on a wider range of cell types than microinjection including those which are too small or delicate to be efficiently microinjected, and may be used in species which have hitherto not been amenable to transformation (24, 25).

The Ca^{2+} -dependent fluorescence signal of cells loaded with Ca^{2+} -sensitive indicators can be quantified using either photometric or imaging techniques. The equipment required for each of these techniques differs markedly, although there are four common components. These are (1) an excitation light source that allows the selection of excitation wavelengths, (2) a specimen holder for the isolation and perfusion of cells, (3) a detector that enables the emission wavelengths to be specified, and (4) signal processing for amplification, recording, and analysis of data. Ratio photometry detects total fluorescence emissions. This provides quantitative and temporal information about changes in whole-cell $[\text{Ca}^{2+}]_{\text{cyt}}$. Ratio imaging, employing conventional imaging techniques, uses a video camera to detect the fluorescence emissions, providing additional information about the spatial distribution of $[\text{Ca}^{2+}]_{\text{cyt}}$. Furthermore, three-dimensional spatial resolution can be achieved using confocal scanning laser microscopy and/or two-photon laser microscopy (26).

There are two important factors that must be taken into account when using fluorescent Ca^{2+} indicators to measure $[\text{Ca}^{2+}]_{\text{cyt}}$ in plants: (1) cell autofluorescence and (2) signal-to-noise ratio (SNR). Plant cells are highly autofluorescent at the excitation wavelengths of many of the Ca^{2+} -sensitive indicators. Therefore, it is essential to correct for the contribution this makes to the total fluorescence signal at excitation or emission wavelengths. Following autofluorescence correction, the signal from cells loaded with Ca^{2+} -sensitive indicators is often low, making measurements extremely noisy. The noise can be reduced by integrating successive fluorescence measurements, increasing the SNR ratio.

Many of the techniques required for the measurement of $[\text{Ca}^{2+}]_{\text{cyt}}$ in plant tissue, including the introduction of calcium reporters into cells, quantification of the Ca^{2+} -dependent signals (typically fluorescence), and calibration of such signals, are illustrated clearly in studies of $[\text{Ca}^{2+}]_{\text{cyt}}$ in stomatal guard cells (for reviews, see refs. 27–29). These studies also highlight many of the problems, and their solutions, which are encountered during measurements of plant $[\text{Ca}^{2+}]_{\text{cyt}}$. In this chapter, the authors describe a

method for measuring $[Ca^{2+}]_{cyt}$ in guard cells of the model species *Commelina communis* by ratio photometry and conventional imaging techniques using the ratiometric fluorescent Ca^{2+} -sensitive indicator fura-2.

2. Materials

1. Plant material: *C. communis* L. is grown from seed in Levington M3 potting compost in a temperature-controlled growth room (day/night temperature of $24/19 \pm 1^\circ C$, 16-h day, photon flux density of $150 \mu mol/m^2/s$). Maintain the plant free from H_2O stress at all stages of development (30) (see Note 1).
2. Isolation buffer: 10 mM 2-(*N*-morpholino)ethanesulfonic acid (MES) in distilled H_2O . Adjust to pH 6.2 with KOH. Store at $4^\circ C$ (see Notes 2 and 3).
3. Perfusion buffer: 10 mM MES and 10 mM KCl in distilled H_2O . Adjust pH 6.2 with KOH. Store at $4^\circ C$ (see Notes 2 and 3).
4. Opening buffer: 10 mM MES and 50 mM KCl in distilled H_2O . Adjust pH 6.2 with KOH. Store at $4^\circ C$ (see Notes 2 and 3).
5. Fura-2: Prepare a 10 mM stock solution of fura-2 pentapotassium salt (see Notes 4 and 5) in double-distilled H_2O . The stock solution of fura-2 should be made up in a 0.5-mL microfuge tube. Check that the pH is approximately 7.0 by spotting a small aliquot of the solution onto pH paper. Adjust the pH using very small volumes of pH reagents (see Note 6). Store at $-20^\circ C$. Prepare a fresh injection solution of 0.5 mM fura-2 daily by diluting the stock solution with 50 mM KCl made up in double-distilled H_2O (see Note 7). Immediately prior to use, centrifuge the fura-2 stock solution at $13,000 \times g$ for 10 min in a microfuge.
6. Coverslips: 18×18 and 22×64 mm.
7. Low melting point wax (e.g., from Agar Scientific).
8. Petroleum jelly.
9. Low-power soldering iron.
10. Perfusion system: Perfusion can routinely be provided under gravity from a temperature-controlled reservoir mounted approximately 50 cm above the specimen (see Note 8). The reservoir consists of a small (6 L) heated water bath and a purpose-built cooling coil. Perfusion media are delivered to the specimen along an insulated pipe. Excess media are removed from the specimen under vacuum (19, 20). A schematic representation of

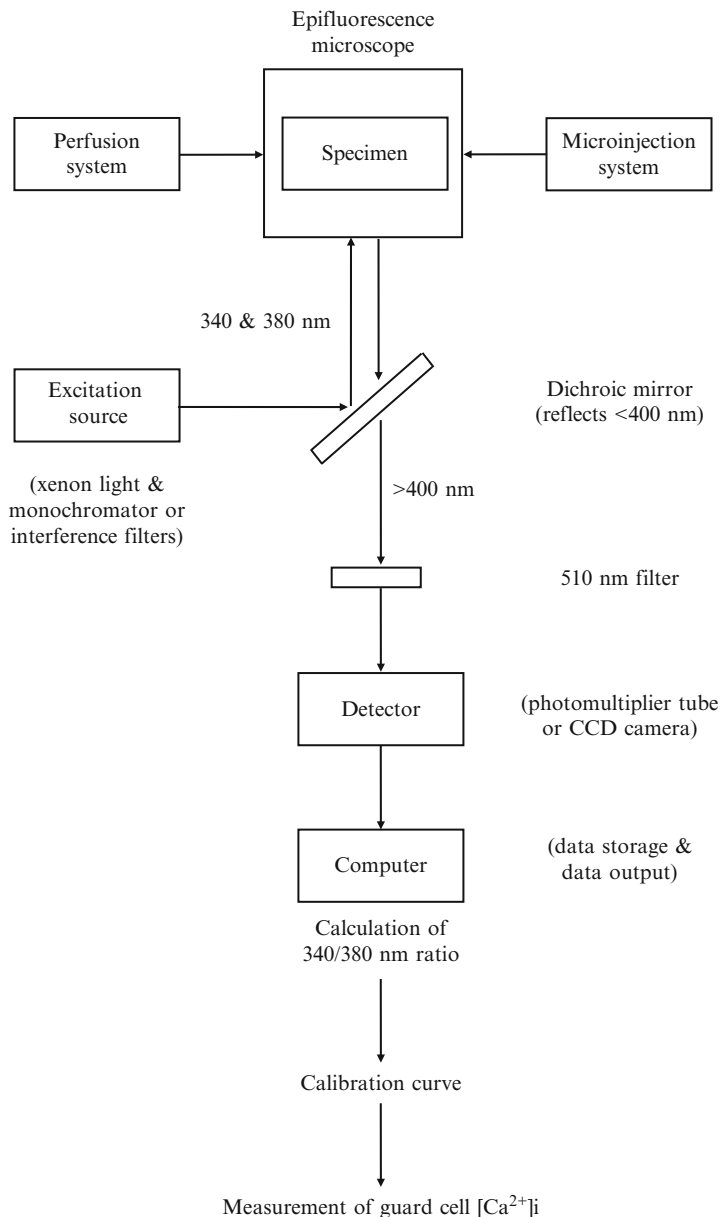


Fig. 1. A schematic representation of the photometric and/or conventional imaging equipment required for measurements of $[\text{Ca}^{2+}]_{\text{cyt}}$ in stomatal guard cells using fura-2.

the perfusion system used during measurements of guard cell $[\text{Ca}^{2+}]_{\text{cyt}}$ is shown in Fig. 1 (see Note 9).

11. **Microinjection of fura-2:** Micropipettes are best fabricated from quartz glass capillaries (1.0-mm outside diameter, Sutter Instruments, Novato, CA) using a laser-based microelectrode puller (Sutter Instruments, Novato, CA; Model P-2000 Micropipette Puller) (see Note 10). Micropipettes are positioned using a precision micromanipulator. Fura-2 is microinjected by

pressure using a modified pressure probe (31) and using an average pressure of 1.2 MPa. A schematic representation of the system used to microinject guard cells is shown in Fig. 1 (see Note 11).

12. Fluorescence microscopy: Specimens are viewed using an inverted epifluorescence microscope with ultraviolet (UV) optics (see Note 12). Additional stage illumination is from a halogen cold light source (e.g., Schott, Germany). Fluorescence excitation is from a xenon light source and is transmitted to the microscope via a liquid light guide with excitation wavelengths (340 and 380 nm, 10-nm bandwidth) selected using a monochromator or interference filters (e.g., Cairn Research, UK). Emission (510 nm, 20-nm bandwidth) wavelengths are specified using together with a 400 nm dichroic mirror (see Note 13). Typically, a 40 \times oil immersion (UV) lens and non-fluorescent immersion oil are used for all measurements. A schematic representation of the epifluorescence microscope used in the measurement of guard cell $[Ca^{2+}]_{cyt}$ is shown in Fig. 1.
13. Measurement of $[Ca^{2+}]_{cyt}$: Fluorescence emissions (510 nm) are quantified using either ratio photometry (19–21, 23) or ratio imaging (32–34) techniques. A schematic representation of the photometric and imaging systems used to quantify the Ca^{2+} -dependent fluorescence of fura-2 in guard cells is shown in Fig. 1 (see Note 14).

3. Methods

3.1. Preparation of Leaf Epidermis

1. Detach the leaf to be peeled immediately prior to each experiment (32).
2. Place the leaf on a glass plate and cut it into lamina strips of manageable widths (5–8 mm) with a razor blade or a scalpel (see Notes 15–18).
3. Cut through the upper epidermis near one end, without damaging the lower epidermis, to form a tab in the lamina strip to obtain the abaxial epidermis (see Notes 19 and 20).
4. Turn the lamina strip over and pull the tab formed in step 3 gently back with forceps for a few millimeters to separate the tissues.
5. Peel the remaining epidermis off by pulling the tab vertically away from the rest of the lamina, holding the latter in position with a mounted needle (see Notes 21–23).
6. Float the detached epidermis (cuticle up) on CO_2 -free isolation buffer at 25°C. Remove the remaining leaf tissue from both ends of the epidermal strip using sharp scissors.

3.2. Perfusion System

1. Cut the freshly prepared epidermis in pieces 2 cm in length (32) (see Notes 24 and 25).
2. Mount the epidermal strip cuticle side down in the middle of a long no. 1.5 coverslip (see Notes 26 and 27).
3. Pipe a ring of petroleum jelly around the epidermal strip using a 1-mL syringe.
4. Secure the epidermal strip around the edge with four smaller coverslips. Press these down firmly on the petroleum jelly (see Note 28).
5. Attach the securing coverslips to the bottom coverslip using low melting point wax (see Note 29) creating a small open perfusion chamber, approximately 0.5×1.0 cm and the one coverslip deep, over the center of the strip (see Note 30).
6. Place a drop of CO₂-free perfusion buffer at 25°C in the perfusion chamber to prevent the epidermis from drying out.
7. Mount the perfusion system on the microscope stage, with the exposed epidermis upward, as if it were a standard microscope slide.
8. Place the inlet and outlet of the perfusion system at the front and rear of the perfusion chamber, respectively.
9. Perfuse the specimen continuously (6 mL/min) with CO₂-free perfusion buffer at 25°C in the dark (see Note 31).

3.3. Microinjection of Fura-2

1. Pull injection micropipette (see Notes 10, 32, and 33).
2. Fill the tip of the micropipette with fura-2 using a MicroFil non-metallic syringe needle (World Precision Instruments, Hertfordshire, UK) (see Note 34).
3. Backfill the micropipette with hydraulic fluid used in the pressure injection system and insert the microelectrode into the pipette holder (see Note 35).
4. Position the micropipette in the perfusion chamber close to the guard cell to be microinjected (see Note 36).
5. Determine the autofluorescence of each guard cell at 340 and 380 nm prior to microinjection as described below in Subheadings 3.4 and 3.5.
6. Impale the guard cell with the injection micropipette (see Note 37).
7. Load the fura-2 in the tip of the injection micropipette into the cytosol of the guard cell using 1.2 MPa for up to 1 min (20). Monitor the progress of injection at either 340 or 380 nm excitation (see Notes 38 and 39).
8. Remove the injection micropipette from the cell following microinjection (see Note 40).

9. Perfuse the fura-2-loaded guard cells in opening buffer at 25°C under conditions of continuous illumination (photon flux density of 1,000 $\mu\text{mol}/\text{m}^2/\text{s}$) from a halogen cold light source for 1 h to promote stomatal opening (see Note 41).
10. Select stomata that open to the same aperture as those on the rest of the epidermal strip (6–10 μm) and in which both the injected and non-injected cells of a single stoma exhibit the same increase in turgor for measurements of $[\text{Ca}^{2+}]_{\text{cyt}}$ (see Notes 25, 40, 42, and 43).

3.4. Ratio Photometry

1. Use ratio photometry to monitor whole-cell $[\text{Ca}^{2+}]_{\text{cyt}}$ from a single guard cell (see Note 44).
2. Sample both the 340- and 380-nm excitation (510-nm emission) Ca^{2+} -dependent fura-2 fluorescence.
3. Integrate the signal following autofluorescence subtraction online (Subheading 3.3, step 5) (see Note 45).
4. Calculate the 340/380-nm ratio online (19–21, 23).

3.5. Ratio Imaging

1. Use ratio imaging to monitor spatially localized changes in $[\text{Ca}^{2+}]_{\text{cyt}}$ (see Note 44).
2. Measure the camera dark signal prior to each experiment. Subtract this from images online.
3. Record alternate 340- and 380-nm excitation (510-nm emission) images.
4. Integrate both signals over individual frames (see Note 45).
5. Calculate the mean autofluorescence from the cytoplasmic region of an unloaded guard cell at both excitation wavelengths (see Note 46).
6. Subtract the mean autofluorescence values from each pair of averaged 340- and 380-nm images, pixel by pixel, at the end of the experiment.
7. Divide the autofluorescence-subtracted 340-nm image by the corresponding autofluorescence-subtracted 380-nm image, on a pixel-by-pixel basis, to produce a series of 340/380-nm ratio images (32–34).

3.6. Calibration

1. Perform an in vitro (external) calibration of the 340/380-nm fluorescence ratio versus $[\text{Ca}^{2+}]_{\text{cyt}}$ using Ca^{2+} calibration buffers (World Precision Instruments, Hertfordshire, UK) (10, 100, and 1,000 nM of free Ca^{2+}) containing 0.5 μM fura-2 (see Notes 47 and 48).
2. Determine the autofluorescence of a 20- μL drop of distilled H_2O on a glass coverslip (Subheadings 3.4 and 3.5).
3. Pipette 20- μL aliquots of each of the calibration buffers onto a glass coverslip.

4. Calculate the 340/380-nm fluorescence ratio for each of the calibration buffers using either ratio photometry (Subheading 3.4) or ratio imaging (Subheading 3.5).
5. Construct a standard curve of the 340/380-nm fluorescence ratio against the concentration of free Ca²⁺ (19, 20, 23, 32–34).

4. Notes

1. Growth conditions vary depending on the plant species.
2. Always use tissue culture grade MES (e.g., from Sigma-Aldrich). MES buffers should be aerated with CO₂-free air for 1 h before use and during experiments. CO₂-free air can be obtained by pumping air through a 15-cm column of soda lime (19).
3. MES buffers tend to become contaminated even when stored at 4°C. This can cause problems with perfusion systems and the microinjection of cells. Therefore, unused buffers should be discarded regularly.
4. The Molecular Probes Handbook (35) is an invaluable source of reference for researchers. The Invitrogen Web site provides up-to-date information on all Molecular Probes products (<http://www.invitrogen.com>).
5. This is the maximum concentration to which fura-2 will dissolve in aqueous solution.
6. The pH of the stock solution seldom requires adjustment. If the pH differs markedly from pH 7.0, it should be adjusted using very small volumes of either 5 M KOH or HCl.
7. Refreeze the fura-2 stock solution after use. Fura-2 solutions can be subjected to repeated freeze–thaw cycles without any detrimental effects. However, the fura-2 stock solution should be aliquoted into smaller volumes to minimize the number of times it is thawed and refrozen.
8. The perfusion rate can be adjusted by altering the height of the reservoir and/or the diameter of the perfusion tubing although alterations in the rate of delivery of plant hormones such as abscisic acid have been shown to affect stomatal responses (36). Typically, a perfusion rate of 6 mL/min is used (19, 20, 23, 32–34).
9. Alternative perfusion systems used in studies of guard cell [Ca²⁺]_{cyt} include perfusion of guard cell protoplasts in the cell-attached configuration and the exchange of perfusion media using low-noise peristaltic pumps (21, 22).

10. Rigid, extremely sharp micropipettes with a small tip diameter are required for the microinjection of plant cells. Micropipettes with these characteristics are most frequently obtained from quartz glass capillaries although aluminosilicate and borosilicate glass capillaries with a larger outside diameter and thicker walls (i.e., smaller inside diameter) can also be used. The harder quartz glass capillaries require a specialized laser-based micropipette puller (Sutter Instruments, Novato, CA; Model P-2000 Micropipette Puller), whereas aluminosilicate or borosilicate capillaries can be used with conventional vertical and horizontal micropipette pullers. Glass capillaries can be obtained with an outside diameter of 1.0, 1.2, or 1.5 mm, although larger sizes are available, and with a range of inside diameters. The use of filamented glass capillaries can help with the filling of micropipettes.
11. Fura-2 has also been iontophoretically microinjected into guard cells (19, 20, 32, 33).
12. A range of inverted epifluorescence microscopes have been used in Ca^{2+} measuring systems (19–23, 32, 34).
13. Fura-2 suffers from photobleaching during prolonged exposure to high-intensity 340- and 380-nm light. This can be reduced by the inclusion of neutral density filters in the light path. In addition, liquid light guides attenuate the excitation light reducing the intensity of excitation.
14. Ratiometric fluorescent Ca^{2+} -sensitive indicators have been employed to measure guard cell $[\text{Ca}^{2+}]_{\text{cyt}}$ using commercial and purpose-built photometric (19–21, 23) and imaging, both conventional (32–34) and CSLM (22), techniques.
15. In the case of *C. communis*, the epidermis is typically peeled from the youngest fully expanded leaf of 4-week-old plants although this may vary among species.
16. Lamina strips are normally used immediately. If not, they are floated on CO_2 -free isolation buffer at 25°C to avoid desiccation.
17. Turgid leaves are easier to peel than flaccid ones.
18. All experiments are conducted during the middle of the photoperiod, between 10 am and 6 pm, to minimize the effects of diurnal changes in stomatal responses.
19. Great care should be taken to cut through the leaf only as far as the lower epidermis. This requires practice.
20. Adaxial epidermis can be obtained by cutting through the lower epidermis.
21. Leaving the final few millimeters of leaf tissue attached to the epidermis aids handling.
22. Maximum viability is achieved if the epidermis is peeled from the lamina strip at an even, slow speed, taking care to be consistent in the angle of peeling.

23. Peeling is best performed in a pool of CO₂-free isolation buffer at 25°C on a glass plate.
24. Guard cells with a low turgor are more easily microinjected than those with a high turgor. Therefore, it is important to use only epidermal strips in which stomata are open to <1 μm. This can be achieved by maintaining plants in the dark for 1 h before use. Stomatal apertures can be determined by mounting a small piece of epidermis from the epidermal strip in a drop of CO₂-free isolation buffer at 25°C on a glass slide. Cover the epidermis with a glass coverslip. Press the coverslip down gently with a mounted needle to expel all the air. The epidermis can then be viewed under the microscope and the stomatal apertures measured using an eyepiece graticule (32).
25. The use of epidermis in which stomata are open to <1 μm allows the stomata to be opened in CO₂-free opening buffer at 25°C following microinjection of fura-2. This provides an indicator of guard cell viability (32).
26. Transfer the epidermis to a long coverslip by holding one end with a pair of forceps while supporting the other with a mounted needle. If the strip rolls up, it is relatively simple to unroll it on the coverslip.
27. It is essential that the epidermal strip is completely flat on the coverslip. This can be achieved by carefully smoothing the strip with a mounted needle and then blotting it gently with a small piece of tissue.
28. The securing coverslips are fabricated from 18 × 18 mm coverslips. Cut into convenient sizes using a diamond-tipped knife. Typically whole coverslips are used to secure the ends of the strip while the sides are secured with half coverslips.
29. The perfusion chamber is fabricated by using 2-mm strips of low melting point wax and a low-power soldering iron to solder the coverslips together.
30. Large-volume perfusion chambers introduce a lag period in the changeover of perfusion media during which mixing occurs. This can affect the kinetics of stimulus-induced changes in [Ca²⁺]_{cyt}. The small volume of the perfusion chamber allows rapid, almost instantaneous changeover of the perfusion media.
31. Specimens should be perfused with CO₂-free perfusion buffer at 25°C in the dark for at least 10 min before use to determine whether they will retain focus.
32. Micropipettes with tip diameters ranging from 0.1 to 1.0 μm have been used to microinject plant cells (1). Typically micro-electrodes with a tip diameter of <0.25 μm fabricated from either filamented borosilicate (1.2-mm outside diameter, 0.68-mm inside diameter) (19, 32, 33) or 1.0-mm quartz

outside diameter (21, 34) glass capillaries are used for the microinjection of guard cells. The tip diameter of a representative sample of microelectrodes is measured by scanning electron microscopy (37).

33. Glass micropipettes tend to go blunt overnight. Therefore, fresh micropipettes should be pulled at the start of each experiment.
34. Concentrations of Ca^{2+} indicators that have been used to fill microelectrodes range from 50 μM to 10 mM (1). Increasing the concentration of fura-2 reduces volume required for injection to achieve a given cytosolic concentration of fura-2. In turn, this reduces the potential damage caused by injection.
35. Take care to exclude air bubbles by tapping the micropipette with the tip pointed downward before inserting it into the pipette holder.
36. Positioning the micropipette in the perfusion chamber is a highly exacting task and requires practice. It is often impractical to locate the micropipette down the microscope using low magnifications because of the presence of immersion oil on the coverslip. However, by reducing the level of bright-field illumination using the field diaphragm, the micropipette can normally be located by its shadow at high magnification.
37. Gentle tapping of the injection micromanipulator is often required to achieve penetration of guard cells.
38. Fura-2 loaded into the cytosol of guard cells gives a discrete pattern of fluorescence around the edge of cells and in the region of the nucleus (19). Cells should not be overloaded as this will buffer changes in $[\text{Ca}^{2+}]_{\text{cyt}}$.
39. Limit the illumination of the specimen with 340- and 380-nm light to the center of the specimen, using the excitation diaphragm of the microscope, to reduce the potential damage to non-injected guard cells from high-intensity UV excitation.
40. The success rate for microinjection is <10 %. Epidermal strips should be discarded after 30–60 min if microinjection is unsuccessful.
41. It is important to use a cold light source such as the Schott KL 1500 to provide continuous illumination of the perfusion chamber to prevent heating of the specimen.
42. Fura-2-loaded cells should meet all the criteria for estimating guard cell viability before use in measurements of $[\text{Ca}^{2+}]_{\text{cyt}}$ (32).
43. Occasionally microinjected guard cells lose some or all of the fura-2 from the cytosol during the opening protocol (Subheading 3.3, step 9). These cells should be discarded.
44. Limit the area from which the fluorescence is recorded to a single guard cell using the emission diaphragm of the microscope.

45. The signal from fura-2-loaded cells is often quite low following autofluorescence correction, making measurements extremely noisy. The noise can be reduced by integrating both the 340- and 380-nm Ca²⁺-dependent fura-2 fluorescence (510-nm emission) over a number of measurements, increasing the SNR.
46. In imaging studies of guard cell [Ca²⁺]_{cyt}, autofluorescence subtraction is complicated by cell movements owing to stomatal closure making it impossible to subtract the initial image of the unloaded cell from all subsequent images. Therefore, a mean autofluorescence calculated from the cytoplasmic region of an unloaded guard cell at both excitation wavelengths is subtracted from images, pixel by pixel, at the end of each experiment (32–34).
47. Similar results are obtained for both in vitro and in vivo calibrations of the 340/380-nm fluorescence ratio in guard cells (32). Consequently, an in vitro calibration can be used routinely.
48. In vivo calibration is performed by perfusing fura-2-loaded guard cells with buffers containing different concentrations of free Ca²⁺ in the presence of a Ca²⁺ ionophore (10 nM–10 μM Br-A23187). It is assumed that the [Ca²⁺]_{cyt} reaches equilibrium with the external concentration of free Ca²⁺ within 10 min. Calibrations can be performed by either (1) constructing a standard curve of the 340/380-nm fluorescence ratio against the concentration of free Ca²⁺ or (2) using the following equation:

$$[\text{Ca}^{2+}] = bK_d[(R - R_{\min}) / (R_{\max} - R)],$$

where R = any cell ratio value, $b = \text{Ca}_{\text{free}}^{2+}/\text{Ca}_{\text{bound}}^{2+}$ fluorescence (380 nm), R_{\min} = ratio in Ca²⁺-free conditions, and R_{\max} = ratio value in the presence of high (saturating) external Ca²⁺. Practical difficulties are often encountered during in vivo calibration due to loss of fura-2 from cells following treatment with ionophore, inability to reach a steady R_{\min} or R_{\max} , or extremely slow or zero response to the ionophore.

Acknowledgments

The authors thank the European Community, The Royal Society, the Natural Environment Research Council (UK), the Biotechnology and Biological Sciences Research Council (UK), Science Foundation Ireland (Republic of Ireland), and the Irish Research Council for Science, Engineering and Technology (Republic of Ireland) for funding.

References

1. Rudd JJ, Franklin-Tong VE (2001) Unravelling response-specificity in Ca^{2+} signalling pathways in plant cells. *New Phytol* 151:7–33
2. McAinsh MR (2007) Calcium oscillations in guard cell adaptive responses to the environment. In: Mancuso S, Shabala S (eds) *Rhythms in plants: phenomenology, mechanisms, and adaptive significance*. Springer, Berlin
3. Volkov AG (2006) *Plant electrophysiology: theory and methods*. Springer, Berlin
4. Miller AJ, Sanders D (1987) Depletion of cytosolic free calcium induced by photosynthesis. *Nature* 326:397–400
5. Felle H (1988) Auxin causes oscillations of cytosolic free calcium and pH in *Zea mays* coleoptiles. *Planta* 174:495–499
6. Brini M (2008) Calcium-sensitive photoproteins. *Methods* 46:160–166
7. Williamson RE, Ashley CC (1982) Free Ca^{2+} and cytoplasmic streaming in the alga, *Chara*. *Nature* 296:647–651
8. Knight MR et al (1991) Transgenic plant aequorin reports the effects of touch and cold-shock and elicitors on cytoplasmic calcium. *Nature* 352:524–526
9. Knight H, Trewavas AJ, Knight MR (1996) Cold calcium signalling in *Arabidopsis* involves two cellular pools and a change in calcium signature after acclimation. *Plant Cell* 8:489–503
10. Kiegle E et al (2000) Cell-type-specific calcium responses to drought, salt and cold in the *Arabidopsis* root. *Plant J* 23:267–278
11. Dodd AN et al (2006) Time of day modulates low-temperature Ca^{2+} signals in *Arabidopsis*. *Plant J* 48:962–973
12. Miyawaki A et al (1997) Fluorescent indicators for Ca^{2+} based on green fluorescent proteins and calmodulin. *Nature* 388:882–887
13. Emmanouilidou E et al (1999) Imaging Ca^{2+} concentration changes at the secretory vesicle surface with a recombinant targeted cameleon. *Curr Biol* 9:915–918
14. Allen GJ et al (1999) Cameleon calcium indicator reports cytoplasmic calcium dynamics in *Arabidopsis* guard cells. *Plant J* 19:735–747
15. Allen GJ et al (2001) A defined range of guard cell calcium oscillation parameters encodes stomatal movements. *Nature* 411:1053–1057
16. Kosuta S et al (2008) Differential and chaotic calcium signatures in the symbiosis signaling pathway of legumes. *Proc Natl Acad Sci U S A* 105:9823–9828
17. Canato M et al (2011) Arbuscular mycorrhizal hyphopodia and germinated spore exudates trigger Ca^{2+} spiking in the legume and nonlegume root epidermis. *New Phytol* 189:347–355
18. Grynkiewicz G, Poenie M, Tsien RY (1985) A new generation of Ca^{2+} indicators with greatly improved fluorescence characteristics. *J Biol Chem* 260:3440–3450
19. McAinsh MR, Brownlee C, Hetherington AM (1990) Abscisic acid-induced elevation of guard cell cytosolic Ca^{2+} precedes stomatal closure. *Nature* 343:186–188
20. Ng CK-Y et al (2001) Drought-induced guard cell signal transduction involves sphingosine-1-phosphate. *Nature* 410:596–599
21. Schroeder JI, Hagiwara S (1990) Repetitive increases in cytosolic Ca^{2+} of guard cells by abscisic acid activation of nonselective Ca^{2+} permeable channels. *Proc Natl Acad Sci U S A* 87:9305–9309
22. Lemtiri-Chlieh F et al (2003) Inositol hexakisphosphate mobilizes an endomembrane store of calcium in guard cells. *Proc Natl Acad Sci U S A* 100:10091–10095
23. Bothwell JHF et al (2006) Biolistic delivery of Ca^{2+} dyes into plant and algal cells. *Plant J* 46:327–335
24. Bothwell JHF et al (2008) Ca^{2+} signals coordinate zygotic polarization and cell cycle progression in the brown alga *Fucus serratus*. *Development* 135:2173–2181
25. Wheeler GL, Joint I, Brownlee C (2008) Rapid spatiotemporal patterning of cytosolic Ca^{2+} underlies flagellar excision in *Chlamydomonas reinhardtii*. *Plant J* 53:401–413
26. Fricker M, Runions J, Moore I (2006) Quantitative fluorescence microscopy: from art to science. *Annu Rev Plant Biol* 57:79–107
27. Dodd AN, Kudla J, Sanders D (2010) The language of calcium signalling. *Annu Rev Plant Biol* 61:593–620
28. Kim T-H et al (2010) Guard cell signal transduction network: advances in understanding abscisic acid, CO_2 , and Ca^{2+} signaling. *Annu Rev Plant Biol* 61:561–591
29. Kudla J, Batistic O, Hashimoto K (2010) Calcium signals: the lead currency of plant information processing. *Plant Cell* 22:541–563
30. McAinsh MR, Brownlee C, Hetherington AM (1991) Partial inhibition of ABA-induced stomatal closure by calcium-channel blockers. *Proc R Soc Lond B* 243:195–201
31. Oparka KJ et al (1991) Modification of the pressure-probe technique permits controlled intracellular microinjection of fluorescent-probes. *J Cell Sci* 98:539–544
32. McAinsh MR, Brownlee C, Hetherington AM (1992) Visualizing changes in cytosolic-free Ca^{2+} during the response of stomatal guard cells to abscisic acid. *Plant Cell* 4:1113–1122

33. McAinsh MR et al (1995) Stimulus-induced oscillations in guard cell cytosolic free calcium. *Plant Cell* 7:1207–1219
34. Webb AAR et al (2001) The role of calcium in ABA-induced gene expression and stomatal movements. *Plant J* 26:351–362
35. Iain Johnson I, Spence MTZ (2010) Molecular probes handbook: a guide to fluorescent probes and labeling technologies, 11th edn. Molecular Probes, Eugene, OR
36. Trejo CL, Clephan AL, Davies WJ (1995) How do stomata read abscisic acid-signals. *Plant Physiol* 109:803–811
37. Brown KT, Flaming DG (1986) Advanced micropipette techniques for cell physiology. Wiley, Chichester, UK

Chapter 21

Measurement of Ca^{2+} -ATPase Activity (in PMCA and SERCA1)

Danuta Kosk-Kosicka

Abstract

Ca^{2+} -ATP pumps (those on the plasma membrane; PMCA and sarcoplasmic reticulum; SERCA1) have an important role to play in the regulation of intracellular calcium concentrations. In this chapter, three preparations, two membranes and a purified enzyme, best suited for studies of Ca^{2+} -ATPase activity are described. The two selected membranes are the human red blood cell (RBC) ghosts, a representative of plasma membranes (PM), and the rabbit skeletal muscle SR, an intracellular membrane. In this protocol, Pi released during the ATPase reaction is subsequently measured colorimetrically as a complex of molyb-dovanadate. The method is simple (one-step), fast, sensitive, and reliable.

Key words: Ca^{2+} -ATP pumps, PMCA, SERCA1

1. Introduction

Ca^{2+} -ATP pumps play a vital role in intracellular calcium homeostasis and signaling. They remove excess Ca^{2+} from the cytoplasm, either into the lumen of the intracellular sarcoplasmic reticulum/endoplasmic reticulum (SR/ER) network or out of the cell, and fine-tune local calcium concentrations allowing for proper functioning of a variety of Ca^{2+} -dependent reactions. They are also integral components of Ca^{2+} -dependent cellular events and cascades that are regulated by precisely controlled Ca^{2+} concentrations.

Although Ca^{2+} transport is a physiological function of Ca^{2+} pumps, their Ca^{2+} -ATPase activity is so well characterized that it is used as an indicator of their function. In this chapter, three preparations—two membranes and a purified enzyme—best suited for studies of Ca^{2+} -ATPase activity are described. The two selected membranes are the human red blood cell (RBC) ghosts, a representative of plasma membranes (PM), and the rabbit skeletal muscle SR, an intracellular membrane. These contain the respective Ca^{2+} -ATPase forms: plasma membrane Ca^{2+} -ATPase

(PMCA; PMCA 4 and 1) and SR Ca^{2+} -ATPase (SERCA; SERCA1). These preparations are the simplest, most commonly used, and well characterized in which Ca^{2+} -ATPases have been extensively studied. They are easy to prepare without contamination from other membrane types; thus, they contain a single specific Ca^{2+} -ATPase activity. In addition, these preparations are devoid of other Ca^{2+} -transporting systems, such as $\text{Na}^+/\text{Ca}^{2+}$ exchanger. Moreover, the Na^+,K^+ -ATPase activity in RBC membranes is very low, as compared to other plasma membranes. The only enzymatic activity that needs to be considered in the described P_i measurements is that of the Mg^{2+} -ATPase, which is also low and easily subtractable.

Ghost membranes are prepared in hypotonic solutions, and calmodulin (CaM) is removed by EDTA washing (1, 2). Because the resulting ghosts are depleted of endogenous CaM, they are suitable for studies of the calcium-dependent CaM activation of PMCA. The strong interaction of CaM with PMCA has made possible its purification by affinity chromatography following detergent solubilization (1, 2). Preparation of CaM-Sepharose-4B columns is included in the procedure (see Note 1). The author has extensively modified the originally published purification procedures, and the protocol allows for purification of PMCA soluble in C_{12}E_8 , which is very stable on storage at -80°C in the presence of 20% glycerol and is easily activated by addition of phospholipids (3). The preparation is suitable for various studies, including spectroscopic measurements that cannot be conducted on the membranous enzyme owing to its low abundance (0.1% of membrane proteins) and the effects of various phospholipids (4). Slight modifications allow for application of this procedure to other plasma membranes, as has been recently described for the synaptosomal membranes of rat cerebellum (5). SERCA1 is conveniently studied in SR, in which it comprises up to 80% of SR membrane protein.

Biochemical characterization of the enzyme in the membrane and at different stages of purification from the membrane always includes determination of its steady-state Ca^{2+} -ATPase activity. The assay is especially useful for the purified, soluble PMCA as a rapid functional test to complement structural studies. Ca^{2+} -ATPase activity in combination with fluorescence resonance energy transfer, fluorescence polarization, and equilibrium centrifugation measurements performed on such preparations allowed the author to establish that enzyme concentration-dependent dimerization is a mechanism of PMCA activation (6–8). The enzymatic hydrolysis rate of ATP is determined by quantitation of the inorganic phosphate (P_i) resulting from ATP hydrolysis by the pump as a function of time. In the described protocol, P_i released during the ATPase reaction is subsequently measured colorimetrically as a complex of molybdoavanadate (9, 10). The method is simple (one-step), fast, sensitive, and reliable (see Note 2).

2. Materials

2.1. Reagents

1. Outdated packed human RBCs for preparation of ghost membranes are obtained from the local Red Cross or blood donation center.
2. Skeletal muscle SR is prepared from hind legs of the rabbit (New Zealand White).
3. Unless specified otherwise, the reagents, including egg yolk phosphatidylcholine (PC) (P5763), CNBr-activated Sepharose-4B, aprotinin, bovine brain CaM for affinity chromatography, and divalent cation ionophore A23187 were purchased from Sigma (St. Louis, MO).
4. CaM for Ca²⁺-ATPase activity assays was from Calbiochem (San Diego, CA); standard solution was prepared by dissolving 1 mg of CaM in 1 mL of water and stored at -20°C.
5. 0.2-mM ionophore solution is made with ethanol.
6. Glycerol was from Serva (Boehringer Ingelheim Bioproducts Partnership, Heidelberg, Germany) (see Note 3).
7. Protein microassay and sodium dodecyl sulfate (SDS) were from Bio-Rad (Hercules, CA).
8. Octaethylene glycol mono-n-dodecyl ether, C₁₂E₈ (see Note 4), was from Nikkol (Tokyo, Japan). To prepare 0.1 M aqueous solution, pour the detergent (melted in a warm water bath) into warm deionized water (do not boil), and stir gently. Store at -4°C in a dark glass bottle.
9. Pellicon Cassette System used in preparation of RBC ghost membranes by molecular filtration is from Millipore (Bedford, MA) (2). The Cassette contains Millipore Pellicon HVLP filters (pore size 0.5 μm) in 20 sheets and it lasts for approximately 15 preparations.
10. All solutions are prepared with deionized water.

2.2. Plasma Membranes: Human RBC Ghost Membranes

1. Washing solution: 130 mM KCl, 20 mM Tris-maleate, pH 7.4 (total volume 7 L).
2. Lysis solution: 5 mM Tris-maleate, 1 mM EDTA, pH 7.4 (23 L).
3. Ghost storage solution: 10 mM Tris-maleate, pH 7.4 (15 L).

2.3. Rabbit Skeletal Muscle SR Membranes

1. Solution 1: 10 mM MOPS, 10% sucrose, 0.1 mM EDTA, pH 7.0 (1 L).
2. Solution 2: 10 mM MOPS, 0.6 M KCl, pH 7.0 (0.5 L).
3. Solution 3: 10 mM MOPS, 30% sucrose, pH 7.0 (0.5 L).

**2.4. Preparation
of CaM-Sepharose-4B
for Affinity
Chromatography (11)**

1. 1 mM HCl for swelling (200 mL).
2. Coupling solution: 100 mM sodium borate, 100 mM NaCl, 50 μ M CaCl₂, pH 8.2 (10 mL, freshly prepared).
3. Blocking solution: 500 mM ethanolamine/HCl (10 mL, freshly prepared).
4. Washing solution: 130 mM KCl, 10 mM Tris-HCl, pH 7.4 (150 mL).
5. Solution A for column regeneration: 0.1 M Trizma, 0.5 M NaCl, 0.755 mM C₁₂E₈, pH 8.5 (100 mL).
6. Solution B for column regeneration: 0.1 M CH₃COONa, ten-fold diluted acetic acid, 0.5 M NaCl, 0.755 mM C₁₂E₈, pH 4.5 (100 mL).

**2.5. Purification
of PMCA**

1. Solubilization solution (2×): 40 mM Tris-maleate, pH 7.4, 1 mM MgCl₂, 260 mM KCl, 1.5 mM C₁₂E₈ (to be added separately), 0.1 mM CaCl₂, 40% glycerol, 4 mM dithiothreitol (DTT) (70 mL).
2. Equilibration solution: 10 mM Tris-maleate, pH 7.4, 0.5 mM MgCl₂, 130 mM KCl, 7.55 mM C₁₂E₈, 0.05 mM CaCl₂, 20% glycerol, 2 mM DTT (250 mL).
3. Washing solution: 10 mM Tris-maleate, pH 7.4, 0.5 mM MgCl₂, 130 mM KCl, 0.755 mM C₁₂E₈, 0.05 mM CaCl₂, 20% glycerol, 2 mM DTT (150 mL).
4. Elution solution: 10 mM Tris-maleate, pH 7.4, 0.5 mM MgCl₂, 130 mM KCl, 0.755 mM C₁₂E₈, 5 mM EGTA, 20% glycerol, 2 mM DTT (50 mL). PC suspension: Pipet 30 μ L of PC solution (100 mg/mL) into a small glass tube and immediately place under a stream of nitrogen delivered slowly through a Pasteur pipet. Blow dry while turning the tube to achieve an even layer of PC on the bottom. Add 300 μ L of elution solution and sonicate using a small probe, periodically placing the tube on ice to avoid overheating, until the solution clears (see Note 5).

**2.6. Ca²⁺-ATPase
Activity Standard
Assay Buffers**

1. For ghost membranes: 50 mM Tris-maleate, pH 7.4, 8 mM MgCl₂, 120 mM KCl, 1 mM EGTA, 1.008 mM CaCl₂ to yield the required 17.5 μ M free calcium (see Note 6). CaCl₂ is omitted from the buffer used for Mg²⁺-ATPase activity.
2. For SR membranes: 50 mM Tris-maleate, pH 7.4, 8 mM MgCl₂, 120 mM KCl, 1 mM EGTA, 10 μ M ionophore A23187, 1.008 mM CaCl₂ to yield the required 17.5 μ M free calcium (see Note 7). CaCl₂ is omitted from the buffer used for Mg²⁺-ATPase activity.
3. For purified PMCA: 50 mM Tris-maleate, pH 7.4, 8 mM MgCl₂, 120 mM KCl, 1 mM EGTA, 0.150 mM C₁₂E₈,

1.008 mM CaCl₂ to yield the required 17.5 µM free calcium. When preparing this assay buffer, take into account the composition of the elution solution in which PMCA is stored (see Notes 8 and 9).

2.7. P_i Measurement

1. Ammonium molybdate: Dissolve 5 g of (NH₄)₆Mo₇O₂₄·4H₂O in water and add 0.5 mL of ammonia (sp gr 0.90) to make 50 mL.
2. Ammonium metavanadate: Dissolve 0.1175 g of NH₄VO₃ in 20 mL of boiling water, and cool under tap water immediately after vanadate dissolves; follow with addition of 0.305 mL of concentrated (sp gr 1.42) nitric acid that has been diluted with 0.7 mL of water. Add water up to 50 mL total volume.
3. 20% SDS solution: Dissolve 10 g of SDS in water to make 50 mL.
4. Mixed Lin–Morales reagent: Mix the solutions in items 1–3 with 17.5 mL of concentrated nitric acid and make up to 0.5 L with water. Store in a dark glass bottle. This solution will keep for 1–2 mo; discard when a significant amount of precipitate forms on the bottom. For the assays described in Subheading 3.3, use Lin–Morales solution diluted threefold with water.

3. Methods

3.1. Preparation of Membranes Containing Either PMCA (RBC Ghosts) or SERCA1 (SR)

3.1.1. RBC Ghosts

All steps are carried out at 4°C either in the cold room or on ice. The solutions can be prepared up to 1 week ahead of time and kept refrigerated. All glassware is chilled before use.

The preparation takes 8–10 h.

1. Start with 3 U of packed erythrocytes (750 mL): Divide them among six 250-mL centrifuge bottles, fill with washing solution, and centrifuge at 4,000×*g* for 10 min. Remove the supernatant and the fluffy coat of white blood cells. (Use a Pasteur pipet connected to an aspirator water pump.)
2. Wash two more times with 5 vol of washing solution using 12 centrifuge bottles.
3. Pour the washed cells into an Erlenmeyer flask containing 2 L of the lysis solution while continuously stirring gently by hand. Add lysis solution to a total volume of up to 4 L (the desired volume ratio of lysis solution to the washed erythrocytes is 8–10:1). Leave in a cold room for 15 min.

4. In the meantime, wash the Pellicon with 2 L of lysis solution and subsequently fill with lysate. Wash the RBCs by continuous application of fresh lysis solution (up to 12–15 L total volume), followed by 10–15 L of storage solution until the membranes are light pink (see Note 10).
5. Transfer the membranes to 40-mL centrifuge tubes (16 tubes). If necessary, fill up with washing solution. Centrifuge at $20,000 \times g$ for 30 min. Aspirate supernatants.
6. Vortex the tubes and transfer the pellets with a Pasteur pipet into a beaker kept on ice. Wash the tubes with small aliquots of storage solution, and by transferring to consecutive tubes recover all material (see Notes 11 and 12).
7. Measure the total volume and set aside small aliquots for protein and preliminary Ca^{2+} -ATPase activity assays. Divide the ghosts into plastic tubes and place in a freezer at -80°C , where they can be stored for a prolonged time (see Notes 13–15).

3.1.2. Light SR Membranes (12)

The preparation takes approximately 8 h.

1. Remove muscle from both hind legs of the rabbit and place in a large beaker of 0.1 mM EDTA.
2. Cut off the unwanted material and wash once in distilled water.
3. Weigh 170 g of muscle and add 510 mL of solution 1 (see Note 16). Blend for 15 s every 5 min for 1 h. Check pH every 10–20 min; add 10% NaOH solution to maintain pH between 6.5 and 7.0.
4. Divide into four parts and centrifuge in 250-mL centrifuge bottles at $15,000 \times g$ for 20 min.
5. Collect supernatant and filter through 1–2 in. of gauze. There should be about 320 mL of filtrate. Divide the filtrate into eight 40-mL tubes, and centrifuge at $40,000 \times g$ for 90 min.
6. Discard supernatant and suspend sediments of alternate tubes in 10 mL of solution 2. Scrape off pellet with a glass rod and pour into next tube; scrape off second pellet and pour suspension into the homogenizer. Repeat with 5 mL of solution 2 again in alternate tubes. Use a total of 60–70 mL of solution 2.
7. Disperse aggregates with a glass homogenizer (40 mL Dounce). Homogenize in portions until uniform, avoiding foam. Incubate in a cold room for 40 min.
8. Divide the suspension into five to six 15-mL Corex tubes and centrifuge at $15,000 \times g$ for 20 min.
9. Collect approximately 10 mL of supernatant into each of five to six polycarbonate tubes. Do not take the very top layer or the very thick bottom layer. Centrifuge at $40,000 \times g$ for 90 min.

10. Discard supernatant and dissolve pellet in 18 mL of solution 3 as described in step 6. Homogenize and divide into small polypropylene tubes. Quick freeze in liquid nitrogen or by placing in a -80°C freezer (see Notes 17 and 18).

3.2. Purification of PMCA from RBC Ghosts

3.2.1. Preparation of CaM-Sepharose-4B Affinity Chromatography Columns

For preparation of three affinity chromatography columns, use 2.8 g of dry Sepharose-4B (which will swell to 9.8 mL) and 8 mg of CaM.

1. Place 1.4 g of CNBr-activated Sepharose-4B in each of the two 15-mL Corex tubes. Slowly add 14 mL of 1 mM HCl, stirring gently with a thin glass rod. Let this swell for 15 min at room temperature.
2. Spin down at low speed for 5–10 min. Aspirate HCl, taking care not to remove any Sepharose. Repeat five times more.
3. To each tube add 2 mL of coupling solution, hand mix end to end, and quickly follow with addition of 2 mL of coupling solution containing CaM at 2 mg/mL (see Note 19). Mix gently overnight in a cold room using a rotation apparatus (see Note 20).
4. Spin down at low speed for 10 min. To each tube add 4 mL of blocking solution and incubate for 2 h at room temperature. Determine the amount of unbound CaM (spectrophotometrically, with E_1 mg/mL at 276 nm) in the collected supernatant to calculate the coupling efficiency.
5. Wash the resin six times by alternating distilled water and washing solution. Suspend in washing solution with 0.02% merthiolate for storage at 4°C.
6. Prepare chromatography columns by slowly pouring the resin suspension into 10-mL plastic syringes fitted with plastic tubing and stoppers so that the flow rate can be easily controlled (see Notes 21 and 22).

3.2.2. Purification of PMCA

Two 3-mL columns are used in this 8- to 9-h-long purification procedure. All steps are carried out at 4°C, either in a cold room or on ice. Use cold solutions. Include aprotinin in all solutions in steps 1–4 (see Note 23).

1. Thaw 500 mg of ghosts by placing them in a water bath at room temperature. In the meantime, cool the centrifuge.
2. Vortex the thawed ghosts and divide into four 40-mL centrifuge tubes. Add the 2× solubilization solution without C₁₂E₈, vortex, and pipet C₁₂E₈ slowly in, while constantly vortexing the tube, to the final concentration of 0.755 mM. Add aprotinin. Keep protein concentration at 8–10 mg/mL (see Note 24).
3. After a 10-min incubation on ice, centrifuge at 40,000 $\times g$ for 45 min. Collect the supernatant containing solubilized membrane

proteins. Measure the volume, divide into two portions, and load onto two CaM-Sepharose columns at a flow rate of 0.25 mL/1 min. The loading step takes approximately 2 h.

4. Wash each column with 30–40 mL of washing solution at a flow rate of 0.25 mL/min until no protein is coming out of the column (absorbance reading at 280 nm equals that of the washing solution).
5. Start adding elution solution and immediately change the flow rate to 0.5 mL/min. Collect 0.8–1-mL fractions, recording absorbance at 280 nm (see Note 25). Combine fractions with high protein concentration; these are usually fractions 3–5. Perform protein assay (see Note 26).
6. Supplement the eluted PMCA with PC suspension: 30 μ L/1 mL eluent (see Note 27). Store the preparation in small aliquots (0.2–1 mL, see Note 28) at –80°C. At this point, 30–40 min have elapsed since initiation of PMCA elution from the column.
7. Run the rest of the elution solution through the column (total volume of 20 mL), and follow with 20 mL of equilibration solution with 0.02% merthiolate (see Note 29). To regenerate the columns, run 10 bed volumes (30 mL) of solutions A and B. Equilibrate with equilibration solution. Add 0.02% merthiolate if being stored.

3.3. Determination of Ca^{2+} -ATPase Activity

Ca^{2+} -ATPase activity is determined through measurements of P_i resulting from ATP hydrolysis by the Ca^{2+} pump.

1. Prepare 1.7-mL polypropylene tubes with appropriate assay buffer (see Note 30). Additionally, for determination of the CaM-dependent Ca^{2+} -ATPase activity, add 5 μ L of CaM solution of appropriate concentration (see Note 31).
2. Add 2–10 μ L membrane or purified enzyme preparation (see Note 32) to enough appropriate assay buffer and water to a total of 95 μ L. Start the Ca^{2+} -ATPase reaction 15 s later by adding 5 μ L of 60 mM ATP, cap the tube, vortex, and place in the rack in the water bath at 37°C (see Note 33). Start the stopwatch at the moment ATP is added. Repeat the procedure for each tube at 1-min intervals. Perform each data point in duplicates (see Note 34).
3. Stop the Ca^{2+} -ATPase reaction at 15 or 30 min (see Note 35) by adding 300 μ L of the diluted Lin–Morales reagent to consecutive tubes at 1-min intervals. Vortex and transfer the whole aliquot to a Cuvette, and read the absorbance at 350 nm at 30 s as timed from the addition of the Lin–Morales reagent (see Notes 36 and 37).
4. To quantify the amount of P_i present in the Ca^{2+} -ATPase assay, use a calibration curve obtained by this procedure (no incubation

necessary) using K₂HPO₄ solutions of known concentrations as standards (see Note 38).

5. The Ca²⁺-ATPase activity in the membranes is calculated as a difference between the activity determined in the appropriate standard assay buffer and the assay buffer in which calcium is omitted. By contrast, the purified PMCA has no Ca²⁺-independent activity (see Note 39). The CaM-dependent activation is determined as a difference in Ca²⁺-ATPase activity in the presence and absence of CaM (see Notes 40 and 41).

4. Notes

1. Commercially available CaM-Sepharose-4B sometimes produces enzyme that is not CaM sensitive, suggesting CaM bleaching.
2. The only drawback to this method is that the solubility of SDS is sensitive to its ionic environment. SDS present in the Lin-Morales solution effectively denatures the assayed protein, thus stopping the reaction and dissolving the protein. Using a threefold-diluted Lin-Morales solution, we seldom encounter problems. Trace amounts of precipitation were observed only with some membranes, such as microvessels, and these could be removed by sedimentation in a countertop centrifuge without affecting the P_i measurement. On some occasions, such as studying the effects of solutes containing phosphate on Ca²⁺-ATPase activity, instead of colorimetric measurement the released P_i may be determined by ³²P_i radioactivity measurement (13, 14). In this procedure, ³²P-ATP is used to start the Ca²⁺-ATPase reaction. Then, after the reaction is terminated with perchloric acid, ³²P_i is extracted with charcoal and, following a filtration through Millipore filters, extracted into a 2-methyl-1-propanol/benzene mixture. An aliquot of the organic phase is counted in a scintillation counter.
3. Enzyme purified in the presence of glycerol bought from other companies is often less active.
4. Substitution of C₁₂E₈ for Triton X-100 and addition of glycerol result in a stable PMCA preparation. Another advantage of C₁₂E₈ over Triton X-100 is lack of interference with protein absorbance at 280 nm, making it easy to monitor protein elution from the column.
5. PC suspension does not totally clarify. It takes some practice to reach exactly the desired point and not further. For future use write down your conditions.
6. Total calcium in solutions needs to be measured by atomic absorption for precise calculations of CaCl₂ to be added. This is

especially important when Ca^{2+} -ATPase activity is measured as a function of free calcium concentration. Our experience shows that 16 μM calcium contamination (from reagents, water, glassware, and so on) should be taken into account. Free Ca^{2+} concentrations are calculated based on the constants given by Schwartzenbach et al. (15), pH, and competitive effects of Mg^{2+} , K^+ , and nucleotide as described by Fabiato and Fabiato (16).

7. The composition of this assay buffer has been modified as compared to buffers used by other investigators. The author wanted it to be as close as possible to the assay buffer used for PMCA activity for the purpose of comparative studies on the two Ca^{2+} pumps. The specific activity of SERCA1 obtained using the author's conditions does not differ from the activity reported in other laboratories.
8. Depending on the volume of PMCA that is added, calculate how much C_{12}E_8 and EGTA will be delivered with the enzyme, and add appropriately less of each while preparing the assay buffer. For example, addition of 5 μL of PMCA per assay tube results in 0.0375 mM C_{12}E_8 and 0.25 mM EGTA, i.e., 25% of the desired final concentrations of both components. To assure good reproducibility, the author prepares separate stock solutions of reaction mixture (RM) for experiments in which various amounts of PMCA are added (such as determination of Ca^{2+} -ATPase activity as a function of PMCA concentration, which reflects enzyme activation by self-association (6, 7, 16)). Thus, for an experiment in which 5 μL of PMCA will be added to the assay tube, prepare 6.5 mL of RM (an amount adequate for 2 days of experiments) comprising the following: 1 mL of 0.5 M Tris-maleate, pH 7.4; 1.5 mL of 0.9 M KCl; 0.8 mL of 0.1 M MgCl_2 ; 0.075 mL of 0.1 M EGTA, pH 7.4; 1.125 mL of 1 mM C_{12}E_8 ; 1.2595 mL of 8 mM CaCl_2 ; and 0.7405 mL water. Then to each tube, pipet in the following order: 65 μL of RM, 18–23 μL of water, 5 μL of CaM (if necessary), 2–7 μL of PMCA, and 5 μL of ATP. RM can be refrigerated for several days.
9. When Ca^{2+} -ATPase activity is measured as a function of free calcium concentration, prepare RM without calcium and pipet CaCl_2 separately to each tube. Since the commercially available standard CaCl_2 solutions have a low pH, dilute them with a Tris buffer to keep the pH reproducible in all assay tubes. Titrate calcium solution against EGTA solution.
10. An alternative way to remove hemoglobin after RBC lysis is repetitive centrifugation (1). This is performed at first in 250-mL centrifuge bottles at $11,000 \times g$ for 20 min. When the pellet becomes fluffy, the material has to be transferred to 40-mL tubes for centrifugation at $20,000 \times g$ for 20 min. A total of five washes with lysis solution are usually followed by four

washes with storage solution until the supernatant is no longer red. Having compared the two methods, the author prefers to use the Pellicon because it is less tedious than repetitive centrifugation.

11. The pellet does not have to be white. Some reddish coloration does not interfere with the activity assays. Sometimes a red core is present in the pellets; make sure not to include it in the collected material.
12. At this stage, be very careful to recover all material; it is pure, concentrated ghost membrane.
13. The expected volume is 90–120 mL.
14. In the author's experience, preparations kept for 2 years were still fully active without loss of Ca²⁺-ATPase activity.
15. The preparation yields 600–800 µg of PMCA protein.
16. One 5–6-lb rabbit yields approximately 150–200 g of muscle.
17. SR preparation stored at –80°C remains active for many years.
18. The preparation yields approximately 100 mg SR protein.
19. Reactive groups hydrolyze at high pH at which coupling of CaM is performed; thus, perform this step quickly to ensure maximal coupling of CaM. Calculate the efficiency of coupling by comparing the absorbance at 276 nm for CaM solution in the coupling buffer before addition to the Sepharose, and in the supernatant after the coupling (see step 4). In the author's experience, the coupling efficiency is between 88 and 95%.
20. Alternatively, the coupling could be performed for 2 h at room temperature. We find the overnight incubation more convenient. Also, step 4 (blocking) could be performed overnight in a cold room.
21. Place a small amount of glass wool on the bottom of the syringe. After packing the column, test different flow rates and make sure that the eluent is clear (if the resin is coming out, one will see it on the wall of the glass tube in which the eluent is collected).
22. The author has used a variety of chromatography columns, including commercially available ones, in different sizes; the described small-scale procedure using syringe columns provides consistently reproducible, active, and CaM-stimulated PMCA preparation. The columns last for 15–20 purifications.
23. Add 100 Kallikrein IU of aprotinin/mL of solution, right before using them. It is especially important at the beginning of the purification procedure when other proteins are still present. There is no need to add aprotinin to the elution solution.
24. For a final protein concentration of 10 mg/mL, the total volume is 12.5 mL. Add 6.25 mL of 2× solubilization solution

and 0.95 mL of 10 mM C₁₂E₈. The volume of ghosts should be 5.3 mL. Ghost preparation is usually less concentrated than 23 mg/mL; thus, centrifuge the thawed ghosts in the four tubes (after filling them with the storage solution) at 20,000×*g* for 20 min. Have the desired volume of 5.3 mL marked on the tube so that you will know when to stop aspirating the supernatant.

25. The UV₂₈₀ absorbance of washing and elution solutions needs to be alike in order to observe the elution of the Ca²⁺-ATPase protein. For this reason, we always prepare these solutions at the same time.
26. Before adding PC, determine protein concentration of the combined eluent, using Bio-Rad Protein Micro-assay, based on the Bradford dye-binding procedure. Add 10–20 µL to 790–780 µL of water (total volume 800 µL), and 200 µL of the reagent. The values (80–140 µg protein/mL) are usually close to the expected concentration based on UV readings. PC interferes with the assay. In the first preparation, before combining all fractions, collect small volumes of the eluted PMCA and perform the protein and Ca²⁺-ATPase activity assay. This way the elution profile of the column will be known. One can also keep separately, if desired, the most active PMCA fractions.
27. It is recommended to initially divide the eluted enzyme into small aliquots and add to each of them different amounts of PC. Then, determine Ca²⁺-ATPase activity in the presence and absence of CaM for each to establish optimal PC:enzyme molar ratio for activation of the preparation.
28. The author freezes PMCA in aliquots that can be used in 1-day experiments. It is not advisable to thaw a tube more than two to three times because significant loss of activity may occur.
29. It is safe to leave columns in elution solution until the next day. The columns are usually regenerated the next day while performing the preliminary characterization of purified PMCA (Ca²⁺-ATPase activity and purity by gel electrophoresis).
30. The reaction can be performed in small glass tubes of appropriate volume that would allow for good mixing of the reaction mixture and the Lin–Morales reagent. The author chose to perform the assay in sealed polypropylene tubes because they are suitable for studies on the effect of volatile anesthetics on the Ca²⁺-ATPase activity.
31. In a typical assay, the author uses 2 µM CaM (final concentration in the reaction is 100 nM).
32. The optimal amounts of protein in the assay at 37°C/25°C usually are 10–12/16–20 µg of ghost membranes,

- 0.20/0.36 µg of SR, and 0.2–0.3/0.4–0.65 µg (i.e., 30–50 nM final concentration in the assay) for the CaM-independent dimeric PMCA.
33. When the reaction is performed at a different temperature, the correct range of absorbance readings will be assured by either changing the amount of protein in the assay (an example is shown in Note 32 for 25 vs. 37°C) or the reaction time.
 34. Reproducibility of the assay is very good. For some plasma membrane preparations, such as microvessels, there is significant scatter; in such cases, triplicates should be used.
 35. The reaction is linear for at least 30–40 min. It is advisable to check first the linearity for your particular preparation before settling on performing the reaction for either 15 or 30 min. The author usually selects a 30-min reaction time, which allows for 30 tubes in one assay performed by one person.
 36. Alternatively, the reading could be made at 30–60 min after the addition of the Lin–Morales reagent. In this case, the 1-min intervals between readings do not need to be made.
 37. The absorbance of the samples is read against a blank prepared and treated the same way as the samples, with the exclusion of the studied protein. For membranous preparations, it is advisable to double-check that they are not contributing to the reading (at higher protein concentration some plasma membranes do—in such cases subtract the absorbance).
 38. The calibration curve that expresses the sensitivity of the method shows linearity in the range of final P_i concentrations up to 1.75×10^{-4} M. 10 nmol of P_i in the tube gives an absorbance reading of 0.25. If desired, the sensitivity can be increased by using the nondiluted Lin–Morales reagent.
 39. Specific activities for the Ca²⁺-ATPase in the three preparations at 37°C are 0.8–1.4 µmol P_i/(mg protein h) in ghost membranes, 300 µmol P_i/(mg protein h) for SERCA1 in skeletal SR, and 180–300 µmol P_i/(mg protein h) for the purified PMCA.
 40. In a typical CaM-dependent Ca²⁺-ATPase activity assay, CaM is added at 100 nM concentration to assure a molar ratio of CaM to PMCA of 2:1 (**6, 17, 18**).
 41. By dividing the CaM-dependent by the CaM-independent activity, the CaM stimulation factor is derived. CaM stimulates the PM Ca²⁺-ATPase activity up to five to sevenfold, depending on the particular membrane preparation and calcium as well as potassium concentrations. In the purified PMCA preparations, CaM stimulates only Ca²⁺-ATPase activity of the monomeric enzyme whereas the dimers are fully activated through enzyme self-association (**6–8, 17**).

References

1. Niggli V, Penniston JT, Carafoli E (1979) Purification of the (Ca^{2+} + Mg^{2+})-ATPase from human erythrocyte membranes using a calmodulin affinity column. *J Biol Chem* 254: 9955–9958
2. Gietzen K, Tejcka M, Wolf HV (1980) Calmodulin affinity chromatography yields a functional purified erythrocyte (Ca^{2+} + Mg^{2+})-dependent adenosine triphosphatase. *Biochem J* 189:81–88
3. Kosk-Kosicka D, Scaillet S, Inesi G (1986) The partial reactions in the catalytic cycle of the calcium-dependent adenosine triphosphatase purified from erythrocyte membranes. *J Biol Chem* 261:3333–3338
4. Missiaen L, Raeymaekers L, Wuytack F, Vrolix M, DeSmedt H, Casteels R (1989) Phospholipid-protein interactions of the plasma-membrane Ca^{2+} -transporting ATPase. *Biochem J* 263:687–694
5. Kosk-Kosicka D, Zylinska L (1997) Protein kinase and calmodulin effects on the plasma membrane Ca^{2+} -ATPase from excitable and non-excitable cells. *Mol Cell Biochem* 173:79–87
6. Kosk-Kosicka D, Bzdega T (1988) Activation of the erythrocyte Ca^{2+} -ATPase by either self-association or interaction with calmodulin. *J Biol Chem* 263:18,184–18,189
7. Kosk-Kosicka D, Bzdega T, Wawrzynow A (1989) Fluorescence energy transfer studies of purified erythrocyte Ca^{2+} -ATPase. *J Biol Chem* 264:19,495–19,499
8. Sackett DL, Kosk-Kosicka D (1996) The active species of plasma membrane Ca^{2+} -ATPase are a dimer and a monomer-calmodulin complex. *J Biol Chem* 271:9987–9991
9. Lecocq J, Inesi G (1966) Determination of inorganic phosphate in the presence of adenosine triphosphate by the molybdo-vanadate method. *Anal Biochem* 15:160–163
10. Lin T-I, Morales MF (1977) Application of a one-step procedure for measuring inorganic phosphate in the presence of proteins: The actomyosin ATPase system. *Anal Biochem* 77:10–17
11. Pharmacia LKB Biotechnology, Affinity Chromatography, Principles and Methods, Pharmacia LKB Biotechnology, 1993
12. Eletr S, Inesi G (1972) Phospholipid orientation in sarcoplasmic membranes: spin-label ESR and proton NMR studies. *Biochim Biophys Acta* 282:174–179
13. Carvalho MGC, Souza DG, deMeis L (1976) On a possible mechanism of energy conservation in sarcoplasmic reticulum membrane. *J Biol Chem* 251:3629–3636
14. Kosk-Kosicka D, Kurzmack M, Inesi G (1983) Kinetic characterization of detergent-solubilized sarcoplasmic reticulum adenosinetriphosphatase. *Biochemistry* 22:2559–2567
15. Schwartzenbach G, Senn H, Andereff G (1957) *Helvetica Chimica Acta* 40:1886–1900
16. Fabiato A, Fabiato F (1979) *J Physiol (Paris)* 75:463–464
17. Kosk-Kosicka D, Bzdega T, Johnson JD (1990) Fluorescence studies on calmodulin binding to erythrocyte Ca^{2+} -ATPase in different oligomerization states. *Biochemistry* 29:1875–1879
18. Kosk-Kosicka D (1990) Comparison of the red blood cell Ca^{2+} -ATPase in ghost membranes and after purification. *Mol Cell Biochem* 99:75–81

INDEX

A

- Acetoxymethylester (AM) 3, 4, 6, 8, 13–14, 36–38, 52, 65, 70, 79–80, 102, 105, 109, 198–203, 208, 211, 212, 221–225, 244, 247, 250, 257–259, 294
Action potential 125, 139, 147–149, 152, 207, 213–216
Adherent cells 20, 35, 38, 66–72, 96, 104, 107–115
Adrenal gland 187, 188, 191
AEQ. *See* Aequorin (AEQ)
Aequorea victoria 54–55, 264
Aequorin (AEQ) 2, 24, 101, 264–278, 317
 cytosol (cytAEQ) 267, 269, 271, 275, 277, 279, 318
 endoplasmic reticulum (erAEQ) 23, 54, 266, 268, 270, 271, 279
 golgi apparatus (goAEQ) 266, 270, 271, 275
 mitochondria (mtAEQ) 23, 266–271, 275, 279
 mitochondrial intermembrane space (mimsAEQ) 269, 271
 nucleus (nu/cytAEQ) 23, 266, 269, 271
 plasma membrane (pmAEQ) 23, 270, 271, 275, 278–279
 sarcoplasmic reticulum (srAEQ) 266, 270, 271
Affinity chromatography 334, 336, 339
Agonists 11, 13, 19, 21, 35, 61, 80, 81, 82, 94–95, 97, 101–104, 156, 163, 172, 176, 177, 182, 188, 219, 226, 245, 254, 255, 256, 275, 279, 287, 289, 291, 292, 295, 315
AM. *See* Acetoxymethylester (AM)
Antagonist 81, 94–95, 99–104, 286, 287, 289–293, 295
Apoptosis 178, 297
Aprotinin 335, 339, 343
Asante calcium green 3
Astrocytes 299, 307–312
ATPase 244, 266–267, 311, 333–345
Autofluorescence 10, 19, 21, 23, 29, 40, 44–45, 91, 110, 111, 113, 204, 224, 225, 227–228, 257, 258, 307, 315, 319, 323, 324, 329

B

- Background 15, 19, 21, 67, 79, 101, 130, 147, 148, 153, 169, 202–204, 208, 211, 226, 228, 235, 239, 267, 294, 305, 310–313
Bioluminescent probes 268

- Biosensors 47–48, 58–60, 71–72, 168–182, 302, 303, 307, 309, 314
Bleaching 178, 212, 225, 341
Blebbistatin 208, 211, 213, 217
Brilliant Black 285, 286, 294
- C**
- Ca^{2+} currents (I_{Ca}) 119, 121, 126, 127, 129, 132, 134, 140, 146, 152
Caffeine 237, 238
Caged compounds 10
Caged-IP₃ 151
Calcium (Ca^{2+}) 35, 53, 148, 156, 185, 207, 244, 267, 283, 297, 319, 333
 activated chloride current (Cl_{Ca}) 149
 channel 14, 41, 77, 100, 117–140, 149, 150, 185–186, 219, 222, 233, 238, 240, 244, 255, 260, 266–267, 284, 297
 crimsonTM 3
 green-1 3, 101
 greenC₁₈TM 3, 17
 orangeTM 3
 transients 69–71, 81, 93, 101, 108, 119, 144, 147, 208, 212–214, 216, 234–237, 267, 295
Calibration 9, 11, 18–21, 24, 40, 44, 65, 66, 92, 111–114, 203, 211–213, 220, 226, 240, 244–254, 257–259, 263–264, 268–269, 276–278, 317, 319, 324–325, 329, 340–341, 345
Calmodulin (CaM) 24–27, 55–56, 197, 298, 318, 334, 335, 339, 341–345
CaM. *See* Calmodulin (CaM)
Cameleons 25, 26, 55, 56, 298, 318
Cardiac ventricular myocytes
 (Cardiomyocytes) 143–144, 148
CCD camera. *See* Charge coupled device (CCD) camera
CFP. *See* Cyan fluorescent protein (CFP)
Charge coupled device (CCD) camera 51, 68, 101, 103, 105, 174, 220, 222, 233, 235
Chimeric G-protein 101, 283–295
Chinese hamster ovary (CHO) cells 37, 41–42, 44–45, 94, 101, 102, 109, 110, 113–115, 279, 284, 285, 287–293
CHO cells. *See* Chinese hamster ovary (CHO) cells
Coelenterazine 23, 264, 266, 270, 275, 277–280, 318

- Commelina communis* 319–320
 Compartmentalization 15, 19, 54, 79, 80, 225, 257, 297–315
 Confocal microscopy 10, 12–13, 16, 17, 21, 28, 36, 47–85, 170, 181, 219, 222, 240, 305, 306, 314
 Coverslips 63, 64, 66–70, 72–75, 80, 82, 120, 127, 147, 173–175, 179, 180, 223, 224, 227, 231, 233–235, 238, 240, 245–247, 250–252, 268, 272, 273, 275, 276, 279, 300, 303, 304, 306, 315, 320, 323, 324, 327, 328
 Cuvette 20, 38, 39, 40, 44, 199, 246, 247, 250, 251, 252, 256
 Cyan fluorescent protein (CFP) 24, 55–58, 60, 75–77, 84, 168–169, 171, 173, 177, 179, 181–182, 298, 307, 318
- D**
- DAG. *See* Diacylglycerol (DAG)
 D1-ER Cameleon biosensor 299, 307, 309
 Detection 1, 18, 22, 23, 27–30, 48–50, 53–54, 60, 66, 68, 69, 71, 72, 81, 139, 148, 167–182, 186, 198, 204, 213–216, 220, 221, 230, 263, 264, 268, 269, 318, 319
 Dextran-conjugated indicators 14, 17, 18, 22–23
 Diacylglycerol (DAG) 58, 59, 60, 71, 81, 155, 167, 177
 Dichroic 50, 78, 174, 208–210, 221, 222, 231–233, 322
 Dowex 158, 161, 162, 164, 165
 Dual emission indicators 8, 12–13
- E**
- eGFP. *See* Enhanced GFP (eGFP)
 eGFP-PH biosensor 168–173, 176, 177, 179–182
 eGFP-PH_{PLC81} 58, 59, 81
 eGFP-PKCγ(C1₂) 59, 60, 81
 EGTA 2, 11, 18, 20, 21, 37, 38, 52, 65, 71, 77, 96, 109, 112, 120, 121, 128, 129, 130, 131, 133, 146, 152, 157, 158, 160, 161, 162, 163, 166, 199, 226, 245–246, 249, 256, 257, 275, 336–337, 342
 Electrophysiology 122–123, 146, 148–151, 230, 234, 235
 Endothelial cells 16, 213, 219, 221, 224–225, 227–228, 245
 Enhanced GFP (eGFP) 54, 58, 60, 62, 72, 74, 176, 181
 Enhanced YFP (EYFP) 25–26, 60, 318
 Esterase 14, 36, 79, 109, 250, 298
 Esterified indicator. *See* Acetoxymethyl ester (AM)
 Evanescent wave 230, 232, 233, 240
- F**
- FCS. *See* Fluorescence correlation spectroscopy (FCS)
 Flash photolysis 10, 150
 FlexStation 91–97, 286
 FLIM. *See* Fluorescence lifetime imaging (FLIM)
- FLIPR®. *See* Fluorometric imaging plate reader (FLIPR®)
 Fluo-3 4, 16, 20, 103, 144, 146, 153
 Fluo-4 3, 9, 103, 144, 146, 223, 225, 285–287, 294, 305
 Fluo 5F Acetoxymethyl ester (AM) 231, 234
 Fluo-5N 5
 Fluorescence correlation spectroscopy (FCS) 36, 37, 60, 156, 157, 159, 164–165, 275, 279
 Fluorescence lifetime imaging (FLIM) 60
 Fluorescence recovery after photobleaching (FRAP) 60
 Fluorescence resonance energy transfer (FRET) 24, 25, 55–58, 60, 75–77, 84, 85, 168–171, 173–177, 179, 181–182, 298, 318
 Fluorescent biosensor 174
 Fluorometric imaging plate reader (FLIPR®) 91, 93, 99–105
 Force transducer 199, 202
 FRAP. *See* Fluorescence recovery after photobleaching (FRAP)
 FRET. *See* Fluorescence resonance energy transfer (FRET)
 Front-surface fluorimetry 197–206
 Fura-2 2, 35, 52, 92, 109, 144, 198, 220, 230, 244, 298, 318
 Fura-2 (AM) 36, 37, 38, 80, 109, 146, 149, 198–200, 203, 222, 223, 225, 250, 257
 Fura-C₁₈ 6, 17
 Fura red 6, 9–10, 52–54, 57, 208
- G**
- Genetically encoded sensor 52, 56, 220, 297–315
 Geneticin 37, 43, 63, 284, 285
 GFP. *See* Green fluorescent protein (GFP)
 G Protein coupled receptor (GPCR) internalization 60–65, 72–74, 83–84
 Green fluorescent protein (GFP) 24, 25, 54–56, 58, 61, 121, 127, 243, 264, 268, 298, 318
 Gryniewicz (equation) 36, 39, 109, 113
 Guard cells 318–329
- H**
- HEK cells 42–43, 175
 [³H]Inositol 155–167, 186
 HL60 cells 156, 158–160, 162–165
 HSF cells. *See* Human skin fibroblasts (HSF) cells
 Human skin fibroblasts (HSF) cells 245, 253
 Hygromycin 285
- I**
- Imaging 11, 36, 48, 93, 103, 125, 144, 170, 208, 219, 230, 263, 304, 317
 Immunofluorescence 47–48, 64, 66–69, 79
 Indo-1 2–9, 12, 13, 16, 25, 29, 52–53, 208, 298
 Inositol 1,4,5-Triphosphate (IP₃) 58, 155, 167, 185
 Inositol phosphates 155–166
 Inositol polyphosphate 186

- Ins(1,4,5)P₃ binding protein 187, 188
 Intracellular pH 108, 243–260
 Ionomycin 21, 65, 71, 77, 85, 96, 110,
 112, 115, 202, 205, 226, 260, 275, 305
 Ionophore 11, 19–21, 71, 77, 112, 115,
 133, 226, 251, 252, 275, 329, 335, 336
- L**
- Langendorff technique 144, 211
 Laser 2, 3, 28, 29, 49–53, 58, 62,
 66–70, 72, 74, 77, 78, 82–84, 101, 103, 174, 176,
 181, 220, 221, 224, 227, 231–233, 235, 239, 306,
 307, 314, 315, 319
 Leaf epidermis 322, 326
 Lentiviral 271, 274
 Ligand internalization 61–63, 73–74
 Lithium 156, 186
 Loading 3, 36, 52, 92, 101, 108, 133, 144,
 161, 186, 200, 220, 232, 244, 267, 285, 298, 318, 340
- M**
- Macropatch 119, 121, 124–126, 132, 140
 MagFura-2 7
 Magfura-5 7
 Methoxyquin2MF 3
 Microdomain 17, 18, 233, 268, 297
 Microinjection 14, 317–319, 321–328
 Muscle contraction 35, 143, 152, 153, 185,
 197–198, 201, 297
 Muscle strips 197–206, 239
- N**
- NA. *See* Numerical aperture (NA)
 Neurones 117–140
 NG108-15 cells 36, 39–41, 44
 Non-ratiometric 52, 101, 144, 318
 NOVOstar microplate reader 107–115
 Numerical aperture (NA) 28, 84, 174, 209,
 221, 224, 231, 232, 238–239, 314
- O**
- Optical mapping 209
 Optimization of loading 14–16, 101
 Oregon green 488 BAPTA-1 3, 220, 223–225
 Organelle 14–17, 21, 23, 26, 53, 54,
 56–57, 65–66, 74–77, 266, 298, 307–309, 318
 Organelle targeting 16–17, 23, 26, 54,
 266, 299, 318
- P**
- ³²P 341
 Patch clamp 14, 117–140, 144, 147,
 148, 152, 234, 235, 238, 319
- Patch Pipet 14, 80, 123, 147–149, 151, 153
PC. *See* Phosphatidylcholine (PC)
 PDL. *See* Poly-D-lysine (PDL)
 Perforated patch recording 123, 133
 Perfusion 70–75, 77, 80, 82, 85, 122, 124,
 128, 131–132, 147, 148, 174, 176, 179, 180, 208,
 211, 213, 217, 223, 240, 251–254, 256, 276, 280,
 306, 315, 319–321, 323–325, 327, 328
 Permeabilised cells 12, 17, 22, 66, 67,
 78–79, 85, 130, 133, 155–166, 257, 318
 Phosphatidylcholine (PC) 104, 335, 336,
 340, 341, 344
 Phosphatidylinositol 4,5-bisphosphate
 (PIP₂) 155, 167–169, 179–180, 185
 Phospholipase C (PLC) 39, 48, 58–60, 71–72, 100,
 155–156, 160–163, 166–173, 181, 185, 284, 291
 Photobleaching 10–12, 16, 18, 29, 49,
 52–54, 56, 62, 68, 69, 73, 78, 82–84, 91–93, 115,
 178, 181, 204, 209, 213, 221, 227, 259, 307, 326
 Photodiode 49
 PIP₂. *See* Phosphatidylinositol 4,5-bisphosphate (PIP₂)
 Plant tissue 317–329
 Plasma membrane calcium pump (PMCA) 278–279,
 333–345
 PLC. *See* Phospholipase C (PLC)
 Pleckstrin homology (PH) domain 58, 168, 173, 294
 Pluronic 15, 70, 79, 94–96, 102, 103, 105, 109, 110, 115,
 199, 200, 203, 223, 258, 285, 294
 PMCA. *See* Plasma membrane calcium pump (PMCA)
 Poly-D-lysine (PDL) 64, 66, 70, 71, 73, 82,
 94, 96, 102, 104, 127, 294, 300, 303, 306
 Portal vein smooth muscle cells 143, 144, 146, 150
 Pressurized arteries 219–228
 Probenecid 16, 37, 41–43, 80,
 94–96, 102–105, 108, 110, 199, 200, 203, 285,
 286, 294
 Purification 65, 167–168, 186, 220,
 256, 272, 278, 285, 300, 302, 333, 334, 336,
 339–341, 343–345
- Q**
- Quin2 2–9, 53
- R**
- Radioreceptor 185–194
 Rat cremaster arteries 223
 Ratiometric indicator 2, 7–10, 12, 20, 52,
 53, 55, 56, 59–60, 225–226, 318–320, 326
 RBC. *See* Red blood cells (RBC)
 Receptor internalization 48, 61, 62, 72–74, 81–84
 Recombinant 23, 24, 27, 29–30, 37, 41–43,
 57, 63, 72, 80, 83, 100–101, 113–115, 119, 120, 126,
 128, 131, 133, 139, 263–280, 284, 285, 290, 299
 Red blood cells (RBC) 333–335, 337–340, 342

- Regions of interest (ROI)..... 75, 83, 84, 148, 176, 180, 226, 240, 266, 305, 307, 308, 310–312, 315
 Reversible permeabilization..... 15
 Rhod-2..... 2–9, 16, 53, 54, 207–217
 Rin38 cells 245, 254,–256, 259
 ROI. *See* Regions of interest (ROI)
 Run-down 123, 129, 130, 133, 135, 140, 156, 161–163, 166, 310
 Ryanodine 69
- S**
- Sarco(endo)plasmic reticulum calcium pump (SERCA)..... 85, 275, 278–279, 333–334
 Second messenger..... 10, 58, 71, 117, 155, 169, 185, 243, 253–254
 SERCA. *See* Sarco(endo)plasmic reticulum calcium pump (SERCA)
 SH-SY5Y cells 36, 39, 40, 43–45, 170–173, 175, 176, 182
 Signal-to-noise..... 23, 51, 91, 92, 101, 103, 112, 169–170, 180, 264, 267–268, 291, 306–307, 319
 Single cell 2, 28, 35, 44, 54, 61, 64–65, 69–71, 75, 82, 117–140, 148, 167–182, 221, 229–240, 267, 268, 297, 303, 314, 324
 Single channel 14, 28, 119
 Single excitation indicators..... 6, 9–10, 12, 20
 Smooth muscle cells 143, 144, 146, 147, 149, 150, 152, 153, 197–206, 213, 220–222, 225, 227, 233–238, 240
 Solubilisation..... 15, 79, 247, 285, 294, 334, 336, 339–341, 343–344
 Subcellular localization..... 15, 36, 57, 61, 68, 69, 73, 173, 180–181, 272, 307–308
 Subcellular measurements 229–240
 Suspension..... 19, 20, 22, 35–45, 96, 104, 129–130, 145, 146, 147, 203, 234, 235, 238, 300, 303, 304, 336, 338–340

T

- TG. *See* Thapsigargin (TG)
 Thapsigargin (TG)..... 21, 76, 306, 311, 312, 313
 TIRF. *See* Total internal reflection fluorescence (TIRF)
 TIRFM. *See* Total internal reflection fluorescence microscopy (TIRFM)
 Tissue culture 29, 37–38, 43, 66, 127, 159, 279, 294, 303, 325

- Total internal reflection fluorescence (TIRF)..... 28, 229–240

- Total internal reflection fluorescence microscopy (TIRFM)..... 28, 60, 239

- Triton X..... 37, 39, 44, 64, 67, 341

V

- Vascular smooth muscle cells (VSM) 144, 149, 150, 152, 153, 220

- Vascular tone 224, 225

- Visible excitation indicators..... 7, 9–10, 28, 49, 52, 53

- Voltage-clamp 130, 131, 135, 138, 140, 147, 149, 151, 152, 232, 236, 237, 240

- Voltage-gated calcium current 121, 126, 140, 143

- Voltage-sensitive Ca^{2+} channels (VS CC)..... 41, 117–140

- VS CC . *See* Voltage-sensitive Ca^{2+} channels (VS CC)

- VSM. *See* Vascular smooth muscle cells (VSM)

W

- Whole-cell configuration 14, 124, 133, 139, 147, 152, 232, 234, 235, 238, 319

- Whole heart 207–217

- Wortmannin 150, 153, 231, 234

Y

- Yellow fluorescent protein (YFP) 24–26, 54–55, 58, 60, 77, 84–85, 168–170, 173, 177, 179, 181–182, 298, 318

- YFP. *See* Yellow fluorescent protein (YFP)